PIERS 2006-TOKYO

Progress In Electromagnetics Research Symposium

Abstracts

August 2–5, 2006

Tokyo, Japan

www.emacademy.org
www.piers.org

PIERS 2006-TOKYO Abstracts

Published by

The Electromagnetics Academy
777 Concord Avenue, Suite 207
Cambridge, MA 02138
www.emacademy.org

Printed in Tokyo, Japan

ISBN: 1-933077-10-7

Progress in Electromagnetics Research Symposium

August 2-5, 2006
Tokyo, Japan

PIERS 2006-TOKYO ORGANIZATION

PIERS Chairman

J. A. Kong, Massachusetts Institute of Technology, Cambridge, Massachusetts, USA

PIERS 2006-Tokyo General Chairman

M. Tateiba, Kyushu University, Fukuoka, Japan

PIERS 2006-Tokyo General Vice-Chairmen

M. Koshiba, Hokkaido University, Sapporo, Japan

Y. Kotsuka, Tokai Universtiy, Hiratsuka, Japan

PIERS 2006-Tokyo Technical Chairman

K. Kobayashi, Chuo University, Tokyo, Japan

PIERS 2006-Tokyo Organizing Committee

M. Aikawa	M. Ando	I. Awai	Y. Furuhama
M. Geshiro	M. Hashimoto	M. Hayakawa	T. Hinata
A. Hirose	T. Hori	Y. Horikawa	H. Ikuno
T. Ishihara	K. Ito	M. Izutsu	K. Kagosima
T. Kashiwa	H. Kawakami	K. Kobayashi	A. Komiyama
K. Komiyama	Y. Kotsuka	M. Kuroda	M. Kosiba
S. Kubota	H. Matsumoto	S. Makino	S. Mano
M. Matsumoto	Y. Miyazaki	T. Miyoshi	I. Nagano
J. Nakayama	M. Nishimoto	S. Nomoto	H .Ogura
K. Ouchi	M. Sato	T. Sato	K. Sawaya
T. Shiozawa	H. Shirai	K. Shogen	T. Takenaka
M. Taki	K. Tanaka	M. Tanaka	M. Tateiba (Chairman)
M. Tsuji	K. Uchida	T. Uno	O. Wada
Y. Yamaguchi	T. Yamasaki	K. Yasumoto	

PIERS 2006-Tokyo International Steering Committee

J. M. Arnold	W.-M. Boerner	K.-S. Chen	W. C. Chew
V. Freilikher	I. Hajnsek	M. Idemen	A. Ishimaru
T. Itoh	L.-W. Li	L. P. Ligthart	K. M. Luk
G. Manara	R. C. McPhedran	A. I. Nosich	C. Pichot
A. Priou	P. Pampaloni	J. W. Ra	R. Raugi
P. Russer	A. B. Samokhin	Y. Rahmat-Samii	T. Sengor
Yu. V. Shestopalov	P. D. Smith	L. Tsang	S. Tretyakov
W. X. Zhang			

PIERS 2006-Tokyo Symposium Committee

A. Komiyama, M. Nishimoto, M. Sato, T. Sato, H. Shirai, T. Yamasaki

PIERS 2006-Tokyo Administrative Committee

Y. Ando, S. Furukawa, N. Goto, Y. Hara, A. Ito, M. Lai, S. Ohnuki, B.-I. Wu, T. Yamasaki (Chairman)

PIERS 2006-Tokyo Technical Program Committee

A. Andrenko, Q. Jiang, K. Kobayashi (Chairman), J. Lu, Y. Okuno, T. M. Grzegorczyk (Vice-Chairman), R. L. King, M. Kuroda, J. Nyenhuis

PIERS 2006-Tokyo Local Arrangements Committee

A. Hirata, S. Koshikawa, R. Sato, H. Hosono, H. Sato, H. Shirai (Chairman)

PIERS 2006-Tokyo Finance Committee

M. Geshiro, M. Matsumoto, A. Komiyama (Chairman), K. Morishita

PIERS 2006-Tokyo Publicity Committee

K. Cho, Y. Naka, M. Yokota, A. Matsushima, M. Nishimoto (Chairman)

PIERS 2006-Tokyo Registration Committee

T. Miwa, M. Sato (Chairman), J. Sonoda

PIERS 2006-Tokyo Planning Committee

H. Arai, M. Geshiro, A. Hirose, T. Hori, T. Ishihara, K. Kobayashi, A. Komiyama, M. Koshiba, Y. Kotsuka, M. Nishimoto, S. Nomoto, M. Sato, T. Sato (Chairman), H. Shirai, M. Tateiba, M. Tsuji, T. Uno, T. Yamasaki

PIERS 2006-Tokyo Session Organizers

M. Agu	S. Barmada	W. M. Boerner	T. Brown
H. C. Chang	F. Costen	T. Endo	N. Engheta
M. Fujimoto	O. Fujiwara	O. Hashimoto	K. Hatakeyama
M. Hayakawa	A. Hirata	A. Hirose	K. Honjo
I. Hosako	T. Ishihara	K. Ito	M. Kagami
T. Kawanishi	H. Kikuchi	K. Kobayashi	Y. Konishi
Y. Kotsuka	S. K. Koul	M. Kuroda	N. Kuster
A. A. Lestari	H. Luce	A. Maeda	Y. Maekawa
E. Marx	A. Massa	Y. Miyazaki	M. Mukaida
Y. Nikawa	R. Nishii	Y. Okuno	T. Onishi
A. Osipov	K. Ouchi	C. Pichot	M. Saillard
K. Saitoh	A. Sanada	M. Sato	Y. Shestopalov
T. Takuma	R. Talhi	D. P. Tsai	A. Viitanen
O. Wada	S. Watanabe	G. Q. Xie	Y. Yamaguchi
T. Yamasaki	J. Yang	A. G. Yarovoy	M. Yokota
Y. Yun	S. Zouhdi		

PIERS 2006-TOKYO SPONSORSHIP

Sponsorship

- ☐ The Electromagnetics Academy

Co-sponsorship

- ☐ MIT Center for Electromagnetic Theory and Application, Research Laboratory of Electronics
- ☐ The Electromagnetics Academy at Zhejiang University
- ☐ The Institute of Electrical Engineers of Japan (IEEJ)

Technical Co-sponsorship

- ☐ Electronics Society, The Institute of Electronics, Information and Communication Engineers (IEICE)

Cooperation

- ☐ The Radiation Science Society of Japan

Financial Supporters

- ☐ Chuo University
- ☐ International Communications Foundation
- ☐ Support Center for Advanced Telecommunications Technology Research
- ☐ The Telecommunications Advancement Foundation

PIERS 2006 SESSIONS

Session 1A1
Waveguides and Transmission-Lines Based on Metamaterials

Electromagnetic Waves Guided by Magnetic Metastructures

N. V. Ilin, I. G. Kondratiev, and **A. I. Smirnov**

Institute of Applied Physics, Russia

Studying unusual properties of metastructures at which magnetic permeability and dielectric permittivity can accept negative values both together, and separately, gets recently the increasing urgency in connection with occurrence and prompt increase ways of realization of such media. In the given work we shall consider the electromagnetic waves guided by magnetic layers out of metamaterials, in the macroscopic description, without going into particulars of realization.

Let we have a free metamaterial layer as first case (see Fig. 1a) and metamaterial layer surrounded by metal planes - as second case (see Fig. 1b). Note, that last situation has complete concordance with layer in waveguide for TE modes.

a) b)

Figure 1: Magnetic layer(a) and magnetic layer surrounded by metal planes(b).

The electromagnetic waves for various types of permeability tensor (1) have been studied.

$$\bar{\bar{\mu}}_1 = \left\| \begin{array}{ccc} \mu_{xx} = \mu_{eff} & 0 & 0 \\ 0 & \mu_{yy} = 1 & 0 \\ 0 & 0 & \mu_{zz} = 1 \end{array} \right\|; \ \bar{\bar{\mu}}_2 = \left\| \begin{array}{ccc} \mu_{xx} = 1 & 0 & 0 \\ 0 & \mu_{yy} = 1 & 0 \\ 0 & 0 & \mu_{zz} = \mu_{eff} \end{array} \right\|; \quad (1)$$

$$\bar{\bar{\mu}}_3 = \left\| \begin{array}{ccc} \mu_{xx} = \mu_{eff} & 0 & 0 \\ 0 & \mu_{zz} = 1 & 0 \\ 0 & 0 & \mu_{zz} = \mu_{eff} \end{array} \right\|.$$

Here μ_{eff} is effective magnetic permeability at which typical frequency dependence for metamaterials made of resonant elements has following view(see Fig. 2):

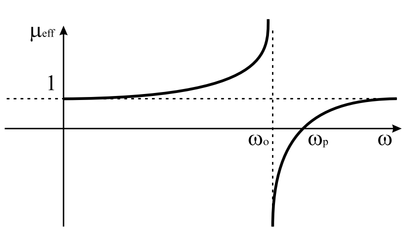

Figure 2: Effective permeability

Dispersive characteristics and field structures of waves guided by mentioned patterns have been in detail investigated. It has been shown that both direct and backward waves are available in similar systems. At that decelerating coefficient can change in the great limits. With help of such waves, it is possible to explain experimentally observable effect of propagation modes below cutoff in loaded waveguide.

Present properties show perspectivity of use examined structures for miniaturization of waveguides, as effectivity decelerating systems, etc.

Analysis, Design and Construction of a New Power Sampler with Small Size

A. A. L. Neyestanak
Jahad Daneshgahi, Iran
M. Mirhossaini
Eslamic Azad University, Iran
N. Ahmidi
Amir Kabir University of Technology, Iran

This paper describes the theory of the operation of directional coupler and presents some information about designing a very flat coefficient coupling. A power monitor is designed and then optimized for UHF band. In this paper, a transformer element is used to obtain a very flat coupling factor and then it is fabricated and compared with experimental results. Using two elements an outstanding result in size and coupling factor has been achieved. The measured results of the optimized power monitor validate a high compatibility between the simulation and the real experience. There are a lot of ways to design a wideband directional coupler, calculations of which are very difficult; but in this paper, with the information found in other papers about directional couplers, a directional coupler with multi element is designed to obtain a flat-coupled factor and a weak coupling factor. Some methods, which have been recognized in the past years by a number of authors, have been employed [1], [2], [3]. In this directional coupler, two elements are used, calculations of which are in the related section. Dimensions of this directional coupler are related according to the impedances of each element and calculations of odd and even mode impedances, which are renormalized with 50Ω. Figure 1 show that the power sampler.

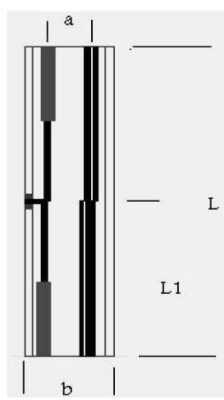

Figure 1: Two-element power monitor

REFERENCES

1. R. Levy, "General synthesis of asymmetric multi-element coupled-transmission-line directional coupler," *IEEE Trans .on Microwave Theory and Techniques*, vol .MTT -11, July 1963, pp. 226-237.
2. B.M. Oliver, "Directional electromagnetic couplers," *Proc IRE*, vol.42, November 1954, pp.1688-1692.
3. . L Matthaei, L. Young, and E. M. T. Jones, "Microwave Filters, Impedance- Matching Networks and Coupling Structures". New York: McGraw Hill, 1988.

Emprical Studies on Electyromagnetic Fields around Two Thin Wires

H. Echigo and **K. Sato**

Tohoku Gakuin University, Japan

It is well known that two thin wires is fundamental one for the radio-frequency (RF) signal and energy transmission systems since they give the basic concept and knowledge about the RF transmission and radiation phenomena. They are the main issues of EMC research field. In this paper, experimental measurements of magnetic fields around two thin wires are described. Measured data was obtained as complex numbers (amplitude and phase) those lead to give motion pictures of virtual wave propagations using the Phase Injection Method. The results obtained give the evidence that the waves are radiating mainly out of the feeding point, the line end and curved portion of the line.

The Influence of Metal Type on Split Ring Resonator (SRR) Resonant Features in the Near Infra Red

N. P. Johnson [1], **A. Z Khokhar** [1], **S. McMeekin** [2], **C. Jin** [3]
H. M Chong [1] and **R. M De La Rue** [1]

[1]University of Glasgow, UK
[2]Glasgow Caledonian University, UK
[2]University of Toronto, Canada

To incre a s e the functionali ty of metama t e r i al s it is desi r able to chang e eithe r individual or groups of element s forming the metama t e r i al- for instanc e to actively open and close the gaps in Split Ring Resona to r s (SRRs). Sever al groups have fabrica t e d SRRs from gold on insulating subst r a t e s such as silica. Here we have fabrica t e d several sets of SRRs on silicon, a potent ially active mate r i al, using gold, silver and aluminum. Qualitative compa r i sons show that the metals behave in a similar manor , with the position of TM and TE peaks giving a reson an t wavelength ratio of approxima t ely 2.6:1. The depa r tu r e from this behaviour observed with silver SRRs is att ribut ed to diffusion of the silver and shor ting of the rings at small lattice cons tan t s . The reson an t featur e s have been measu r e d down to 2.3 microns with simulations showing good agre eme n t with experime n t . Aluminum is an impor t an t metal in silicon foundries and unlike gold is compa t ible with silicon in that it does not introduc e deep levels. Aluminium on silicon could form the basis of actively cont rolled metama t e r i al s in the infra read region and beyond.

Metamaterial Transmission Lines Based on Complementary Split Ring Resonators: a Review

I. Gil [1], **J. Bonache** [1], **M. Gil** [1], **J. G. García** [1], **F. Martín** [1] **J. D. Baena** [2], **M. Freire** [2], **R. Marqués** [2], **F. Falcone** [3],**T. Lopetegi** [3],**M. A. G. Laso** [3] and **M. Sorolla** [3]

[1]Universitat Autònoma de Barcelona, Spain
[2]Universidad de Sevilla, Spain
[3]Universidad Pública de Navarra, Spain

In this work, an exhaustive study of the behaviour of left handed microstrip lines based on complementary split rings resonators (CSRRs) is carried out. This particle, which is the dual image of SRRs, allows for the design of negative effective permittivity microstrip lines by periodically etching CSRRs in the ground plane, underneath the conductor strip. The resulting device generates a deep rejection frequency band with sharp cutoff. In order to achieve left handedness it is necessary to introduce an effective negative valued permeability to the structure. This can be achieved by means of series (capacitive) gaps etched in the conductor strip. In this case, a narrow transmission band with backward wave propagation arises. Both structures are of interest to the design of compact microwave circuits, such as filters and diplexers. An accurate circuit model which includes all the physical effects (inter-resonator's coupling and transmission line parameters) for this kind of structures has been proposed, including a method to extract the electrical parameters from measurement or electromagnetic simulation. A thorough analysis of inter-resonator's coupling has been also carried out. To this end a study in terms of CSRRs separation and shape (rectangular or circular) has been done. It is concluded that electric coupling between CSRRs can be significant only if these resonators are rectangular and they are tiny spaced (see Fig.1). Nevertheless, it has been found that this coupling does not affect the behaviour of these structures as onedimensional metamaterials. Reconfigurability is one of the key aspects to study in next future. This means the design of tunable filters and resonators by combining CSRRs with RF-MEMS. Work is in progress in this direction.

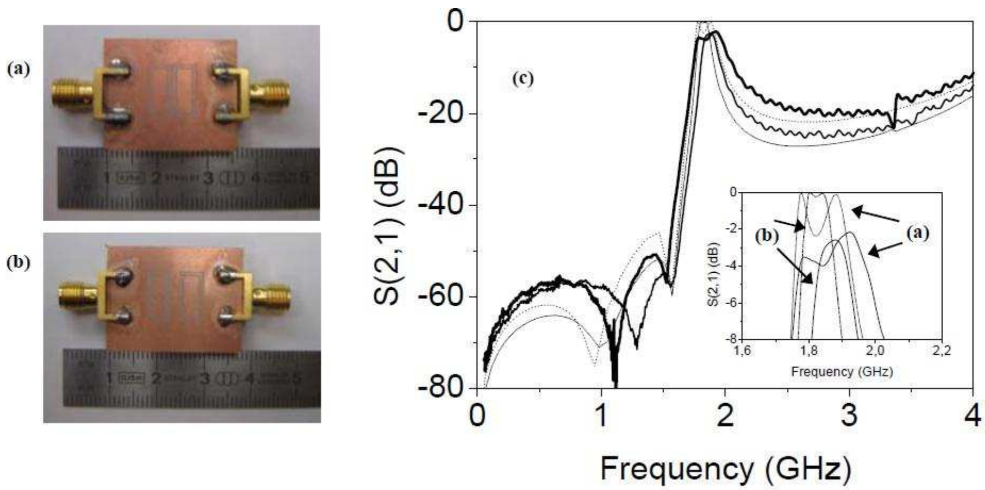

Figure 1: Fabricated two-stage CSRR-based structure with rectangular CSRRs separated 0.1mm (a) and 2.0mm (b). Measured frequency response (bold line) of both structures and electromagnetic simulation (dotted line) are depicted in (c).

Waveguiding by Dichroic Filters Metamaterial

M. Beruete [1], **M. Sorolla** [1], and **I. Campillo** [2]

[1]Public University of Navarre, Spain
[2]Labein Centro Tecnológico, Spain

The use of Dichroic filters operating in the Millimeter Waves, made of a metallic plate drilled with a two dimensional hole-array, help to the design of a Photonic Crystal consisting of stacking several plates separated by air. In spite of the fact that the longitudinal periodicity predicts a band-gap around 85 GHz, a lower band-gap is also present at 57 GHz due to transversal periodicity. Several configurations have been explored both in simulation and measurement. Interesting waveguiding phenomena have been observed for potential applications.

REFERENCES

1. P.F. Goldsmith, Quasioptical Systems-Gaussian Beam, Quasioptical Propagation, and Applications, IEEE Press, 1998.
2. J. D. Joannopoulos, R. D. Meade, and J. N. Winn, gPhotonic Crystals: Molding the Flow of Lighth, Princeton, NJ, Princeton Univ. Press, 1995.

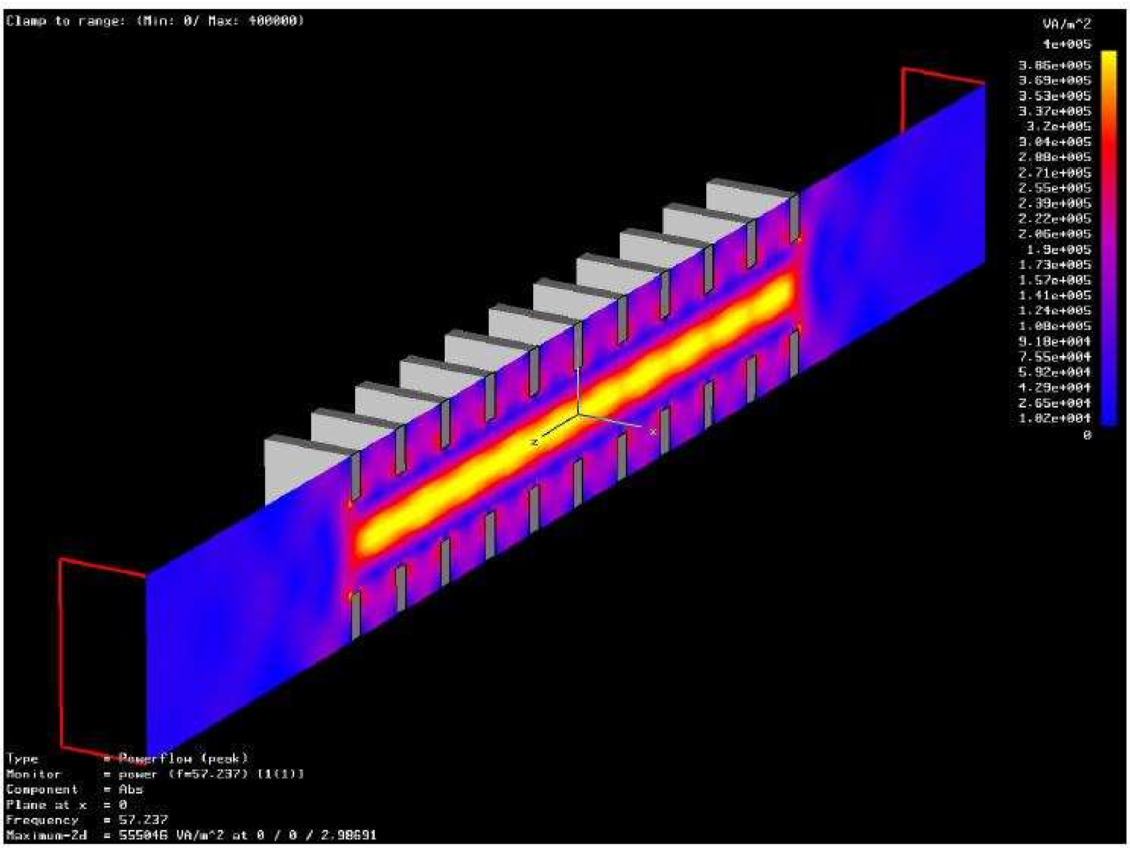

Miniaturization of Microwave Circuits by Using Artificial Transmission Lines

J. P. Kim
Chung-Ang University, Korea

Development of the wireless communication system leads to the increasing demand on the miniaturization and integration of microwave circuit elements. Artificial transmission line (ATL), transmission line which is periodically loaded with series or shunt elements, has been used for size reduction of microwave circuits[1]. It can also be applied to make a transimission line width be proper for easy fabrication.

An approximate design method based on lumped element modeling has been proposed and applied to design branch line hybrids[2], but design error becomes larger as the number of ATL sections decreases. In this paper, a distributed circuit modeling with the help of ABCD parameter formulation is proposed to derive a much more accurate design method. The developed design equations are then applied to design a lowpass filter (LPF), 3 dB and 10 dB brach line hybrid and coupler.

A 3rd-order Chebyshev type microstrip LPF with 0.2 dB ripple and a cut-oR frequency of 2 GHz is considered. At first, a conventional LPF is obtained after applying the Richard's transformation and Kuroda's identity. In this case, line widths of connecting lines and parallel stubs are generally narrow and wide, respectively. Now narrow lines are replaced by ATL sections with series inductive element, and wide lines by ATL sections with parallel susceptive elements. Series inductive elements can be implemented with slot-cuts on a ground plane or meandered lines, and parallel susceptive elements with microstrip open stubs. The amount of reduction mainly depends on the ratio of related line impedances. A LPF was designed, where slot-cuts on a ground plane were adopted for implementing series inductive elements, and the size was reduced to 60 % of that of the conventional LPF without ATLs. Fig 1(a) shows measured electrical characteristics of a fabricated LPF along with the design specifications and FDTD simulation data3, and reasonable agreements were observed.

For further validation check, design examples of 3 dB and 10 dB branch line hybrid were considered. In designing a 10 dB coupler, meander lines were chosen for implementing series inductive elements. Fig. 1(b) and (c) show the design results. Even the bandwidth becomes slightly narrower compared to the that of the conventional ones, agreements were also reasonable. The size of the proposed hybrids were reduced to 45 % and 30 % for the 3 dB hybrid and 10 dB coupler, respectively, compared with the conventional ones. Finally, the reasonable agreements of electrical characteristics and circuit miniaturizatio

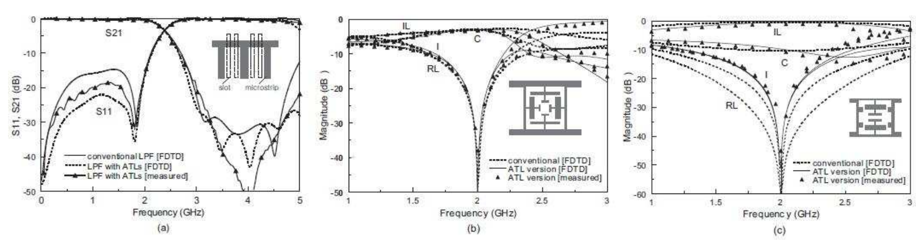

Figure 1: Measured and simulation data; (a) LPF, (b) 3 dB hybrid, and (c) 10 dB coupler

REFERENCES

1. M. C. Scardelletti, G. E. Ponchak, and T. M. Weller, "Miniaturized Wilkinson power dividers utilizing capacitive loading," *IEEE Microwave Wireless Comp. Lett.*, vol. 12, pp. 6-8, Jan., 2002.
2. K. W. Eccleston and S. H. M. Ong, "Compact planar microstripline branch-line and rat-race couplers," *IEEE Trans. Microwave Theory Tech.*, vol. 51, pp. 2119-2125, Oct., 2003.
3. CST MICROWAVE STUDIO, Ver. 4.2, Computer Simulation Technology(CST), Germany.

Metawaveguides and Antennas Formed by Chains of Resonating Particles

A. Viitanen
Helsinki University of Technology, Finland

For designing small-scaled waveguides with desired properties a periodic arrangement of longitudinally directed resonant dipole particles over perfect electric or perfect magnetic conductor plane are considered. The waveguiding and radiation properties of these struc- tures are studied. Depending on the frequency range the dipoles may be small loaded wire antennas in microwave frequencies or plasmon resonant particles, for example metal ellip- soids, in optical region. The particles are close to each other forming a coupled dipole array and the mirror image array due to the conductor boundary. Analytical solutions for waves propagating along this meta-waveguide are presented. Conditions for guided wave solutions as well as those for leaky waves are given. The electromagnetic properties of this kind of waveguides depend strongly on the frequency properties of the inclusions near the particle resonance. In this example very simple resonating loads, series and parallel resonant circuits, are used. In the analytical expressions of the eigenvalue equation the infinite summations are evaluated in fast converging form to get effciently dispersion curves near the eigenres- onances of the inclusions. Fast converging algorithms are necessary since near the resonant frequencies the electromagnetic properties of the structure change drastically. It is found that either forward or backward wave exists in the presence of electric wall. In the presence of a perfect magnetic wall with some proper resonant loads both forward and backward waves exist. These structures may be used as waveguides at very narrow frequency bands for forward and backward waves. In radiation regime these structures behave as antennas with superdirective properties.

Magnetic Current Line Source in a Medium with Strong Spatial Dispersion

I. S. Nefedov, A. Viitanen, and **S. A. Tretyakov**
Helsinki University of Technology, Finland

Spatial dispersive materials have recently received attention because of interesting elec- tromagnetic phenomena and possible new applications. Examples of such media are wire media, single, double or triple wire media, which are also called as artificial plasma. The single wire medium, is effectively characterized by a uniaxial permittivity dyadic in which the permittivity component parallel to the direction of wires depends on the correspond- ing wave vector. Presence of spatial dispersion causes existence of additional waves and a necessity to use additional boundary conditions for solution of boundary-value problem for such media. For the same reason the standard expressions for fields, excited by sources in unbounded anisotropic media are not applicable for media with spatial dispersion.

In this paper we have obtained Green's function for magnetic current line inside a single wire medium. This expression contains three parts, describing excitation of the TEM mode, the TM mode, and a contribution caused by their interaction. The near field is calculated numerically and the field in a far zone (which is non-trivial only above plasma resonance frequency, because below plasma resonance TEM mode only exists in the far zone) is found analytically using saddle-point method. Developed approach can be used for more compli- cated problems for sources in plane-stratified media.

Session 1A2
Recent Advances on Metamaterials

Transmission Properties Of Metal Hole Arrays In terahertz Region

M. Hangyo
Osaka University, Japan

F. Miyamaru
Institute of Physical and Chemical Research (RIKEN), Japan

Extraordinary transmission phenomenon of electromagnetic waves (from visible to microwave) through metal hole arrays (MHA's) has attracted much attention in recent years. We have investigated transmission properties of thin metal slabs periodically perforated with holes in the terahertz (THz) region. The transmission spectra show characteristic resonant peak depending on the structure of the samples. Dependence of the spectra on the incident angle, spacing between holes, thickness of a thin dielectric film attached on the surface, etc. indicates that the surface plasmon polarition (SPP) plays an important role in the transmission mechanism. In the double layer system, the transmission spectra show anomalous dependence on the relative lateral displacement of the two layers, which is explained by the near-field coupling of the SPP's on the two surfaces of the layers.

The MHA's also show interesting polarization properties. The linearly polarized THz waves show large polarization change after transmitted through the MHA by tilting the incident angle only slightly from the normal. From the independence of the ellipticity and polarization rotation angle on the slab thickness, it is confirmed that this phenomenon occurs at surfaces. The incident angle dependence of the ellipticity and polarization rotation spectra indicates the participation of the SPP in this phenomenon. The polarization characteristics of the elliptic hole arrays and screw hole arrays also show quite interesting polarization characteristics.

Finally, we made the hole arrays with doped-Si and $SrTiO_3$ in order to investigate the role of the surface mode in the transmission more generally. For doped Si, the dielectric constant of the material changes from metallic to dielectric in the THz region with decreasing temperature from 300 K to 10 K and both real and imaginary parts of the dielectric constant of $SrTiO_3$ are large positive values. The experimental results indicate that the SPP is not the only origin of the characteristic resonant transmission spectra, but any surface waves can contribute to such a phenomenon.

A Possible Route for Left-Handed Meta-Materials using Ferromagnetic-Metal Nanocomposite Films

S. Tomita
Nara Instituteof Science and Technology (NAIST), Japan

The electromagnetic responses of materials are determined by the electric permittivity (ϵ) and magnetic permeability (μ). Materials with both ϵ and μ negative are called left-handed (LH) materials. They are theoretically predicted to show extraordinary electromagnetic responses, e.g., a reversed Doppler shift and negative refraction of electromagnetic waves. However, the LH materials have not yet been found in nature. Only artificial LH meta-materials consisting of metallic split-ring resonators and wires have been reported in the region of microwaves. Recently, a novel route to LH meta-materials in the microwave region using nanocomposites containing ferromagnetic-metal nanoparticles has been proposed. This is based on the fact that the μ of the particles in the nanocomposites can be negative in the vicinity of electron magnetic resonance (EMR) frequency. In this work, we prepare nanocomposite films consisting of metallic Ni nanoparticles several nanometers in diameter embedded in polymer matrices as a possible candidate for LH meta-materials and study their electromagnetic properties in the microwave region.

Nanocomposite films were prepared by using chemical techniques. Transmission electron microscopic (TEM) studies were carried out. We have found that the diameter and volume fraction of the Ni particles in the composite can be controlled independently and precisely. These structural parameters strongly affected the EMR condition for microwaves. This suggests that the control of the film microstructures is important to tune the frequency where the LH meta-materials may be obtained in this route. Experimental results of microwave transmission measurements will be shown.

Linear and Nonlinear Electromagnetic Responses of Metamaterials in Optical Regime

T. Ishihara
Tohoku University, Japan

In optical frequencies, elctromagntic wave can be generated by lasers, which provides large controllability on pulse shape, polarization as well as intensity.We report linear and nonlinear optical responses of periodic artificial structures fabricated by vacuum sputtering and/or electron beam lithography.

First we discuss metal-dielectric short-period multi-layers, which can be treated as prototypes of metamaterial. By designing the ratio of metal and dielectric, plasma frequency is artificially controlled. Effective response functions in such structure are investigated by analyzing transmission and reflection spectra. Measurements on Ag/SiO_2 multi-layers are compared with numerical calculation, based on the scattering matrix formalism.

Secondly we discuss second order nonlinear responses (second harmonic generation and optical rectification) in metallic photonic crystal slabs, which are composed of centrosymmetric materials with asymmetric photonic unit cell. The samples are fabricated with electron-beam lithography and dry-etching technique. The origin of experimentally observed nonlinearity will be scrutinized.

Negative Refraction of Guided Wave Mode in Ferrite Based Periodic Layered composites

R. X. Wu, T. Zhao, F. Yang, and **P. Chen**
Nanjing University, China

Recently, there is an increasing interesting in ferromagnetic magnetic materials based negative refraction [1-5]. It has been proved that ferrite based layered composite could be a negative refraction materials or even a left-handed materials, which depends on the structure and the component materials [2]. In this work, we have proposed a composite with periodic layered ferrite-dielectric film, and analyzed and calculated its dispersion using the equivalent transmission line model. We have found that the composite may have negative effective refraction index only for TE guided wave. For TM mode guided wave, the composite always has the positive refraction index. We have simulated the wave propagation in the composite by FEM method, and observed back wave propagation for the TE guided wave.

The existence of negative refraction index depends not only on the negative permeability of the ferrite but also the loss of the dielectric. However, the loss of the composite is closely related to that of the dielectric layers in the composite. Using the lower loss dielectric can reduce the loss of the composites greatly, but too small dielectric loss will result in the disappearing of the negative refraction index. Therefore, find the balance between the negative index and loss is very important.

* This work is supported by the National Natural Science Foundation of China under Project No. 60471020 and theNational Basic Research Program 973 of China under Project No. 2004CB719805.

REFERENCES

1. S. T. Chui and L. Hu, Phys. Rev. B 65, 144407 (2002)
2. R.X. Wu, J. Appl. Phys. 97, 076105, (2005)
3. T. Zhao, R.X. Wu, F.Yang, and P. Chen, Acta Physica Sinica 55, 179, (2006)
4. T. Ueda and M. Tsutsumi, *IEEE Trans.* Magnetics 41 (10): 3532, (2005)
5. S. Tomita, K. Akamatsu, H. Shinkai, et al., *Phys. Rev.* B 71, 180414, (2005)

Three-Dimensional Negative-Refractive-Index Metamaterials Composed of Spherical Dielectric Resonators

T. Ueda and **T. Itoh**
University of California, U.S.A.

Left-handed (LH) metamaterials have been intensively studied for applications to perfect lens, near field imaging, and so forth [1],[2]. LH materials have negative effective permittivity and permeability simultaneously, and support backward wave propagation. Most of the artificial materials are classified into two structures; the first one is a combination of split ring resonators and thin wires, and the second one is a transmission line loaded with series capacitances and shunt inductances. It is noted that they are made of metals especially in the resonant sections, and have been demonstrated in the microwave, millimeter-wave, and terahertz frequency regions. However, for higher frequencies up to optical regions, metals are no longer a good conductor, but can be treated as plasma having a negative epsilon as well as a relatively large imaginary part. Therefore, it is necessary to propose and design new configurations of LH materials beyond the terahertz region. Of course, it is desirable to construct it without metals, especially in the resonant sections, in order to prevent the loss effect.

So far, certain types of LH metamaterials have been proposed without metals by using dielectric resonators (DRs). One is the two-DR scheme, which is composed of both TE and TM resonances of DRs, the operations of which correspond to split ring resonators and thin wires, respectively [3]. However, from the point of view of the fabrication tolerance, it is difficult to adjust both the TE and TM resonant frequencies of DRs because of the narrow operational band. The other type is the one-DR scheme [4]. It is constructed based on the mutual coupling between DRs, as is well-known in designing the conventional microwave band pass filters using DRs [5]. They can have a wide operational band due to the coupling between DRs.

In this work, propagation characteristics have been numerically investigated in the three-dimensional lattice structures which are composed of dielectric spheres in a host dielectric medium in an attempt to obtain the isotropic negative-refractive index near the resonant frequency of the spheres. For simplicity, we have assumed that they have the periodicity in the calculation but this is not essential for the operation. In the numerical simulation, we have investigated various types of lattice structures such as simple cubic, body-centered cubic, and face-centered cubic (FCC) lattices, and so forth. The left handed characteristics are confirmed in the dispersion diagrams for the FCC lattice in any propagation directions in the vicinity of point around at spherical TE resonant frequencies. The behavior of the EM wave propagation is mainly governed by the resonant conditions of spheres, but not by Bragg scattering in the periodic structure that is used for designing band gaps in photonic crystals [6]. It is found that there are still some problems of anisotropy, polarization dependence of the EM wave, and undesired secondary scattering modes. In addition, we have also investigated the cases where additional spheres are doped or some components are subtracted in the unit cell of the FCC lattice to attempt to improve the dependence of propagation direction and polarization. As a result, it is found that the isotropic characteristics can be obtained near the Γ point for a reduced FCC lattice structure although it still has the multi-mode problem.

REFERENCES

1. V. G. Veselago, *Sov. Phys. Usp.*, 10, 509, 1968.
2. D. R. Smith, W. J. Padilla, D. C. Vier, S. C. Nemat-Nasser, S. Schultz, *Phys. Rev. Lett.*, 84, 4184, 2000.
3. C. L. Holloway, E. Kuester, J. Baker-Javis, P. Kabos, *IEEE Trans. Antennas Propagation.*, 51, 2596, 2003.
4. E. A. Semouchkina, G. B. Semouchkin, M. Lanagan, C. A. Randall, *IEEE Trans. Microwave Theory Tech.*, 53, 1477, 2005.
5. S. B. Cohn, *IEEE Trans. Microwave Theory Tech.*, MTT-16, 218, 1968.
6. M. Notomi, *Phys. Rev. B*, 62, 10696, 2000.

Dielectric Resonator Made of Artificial Molecules

I. Awai, A. K. Saha, and **Q. Wei**
Ryukoku University, Japan

A dielectric resonator is made of molecules each of which is essentially a tiny resonator. The resonance of each molecule couples to those of others, which splits the resonant frequencies. Vast numbers of molecules combine the split discrete frequencies into a continuum. The combined resonance results a high permittivity and it elongates the tail down to the microwave frequency band. This remaining high permittivity realizes a small-sized microwave dielectric resonator. An artificial dielectric

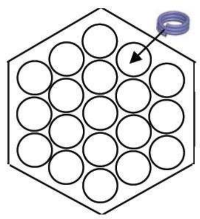

Figure 1: Helices and honey- comb frame, helix dimension; 0.5ϕ copper wire, 4 mm outer dia, 0.5mm pitch, 3 turns

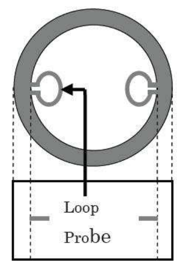

Figure 2: Metal shield for exciting $TE_{01n+\delta}$ modes

resonator is made of metal unit particles whose resonant frequency depends basically on their size. The similar reasoning for sufficiently many particles will predict a miniaturized microwave resonator fabricated with artificial material.

We have prepared helices made of copper as shown in Fig.1. Each resonant frequency ranges from 2.0-2.3 GHz mainly due to the fluctuation of pitch of a helix. They are arranged in a honeycomb acrylic resin frame with thickness 3.0mm, and piled to make a resonator. It will behave as a dielectric disk resonator macroscopically.

The resonator is inserted in a circular cylindrical metal shield intended for TE01 modes excitation of a disk dielectric resonator shown in Fig.2. A measured result, Fig.3, suggests that the expected resonance is occurring. The extracted equivalent specific permittivity is 80, being inversely calculated from the resonant frequency 1.75 GHz. The confirmation should be followed for other important modes, such as HE11, EH11, and TM01 modes.

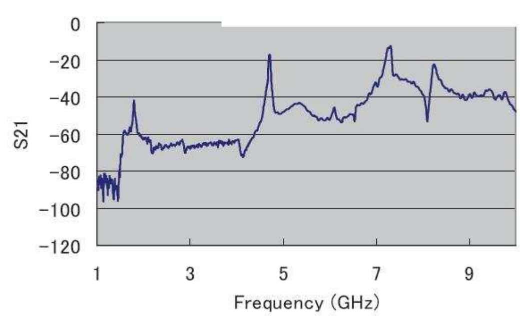

Figure 3: Measured result for 7 layers of honeycomb sheet

We have shown the preliminary evidence for correspondence of an artificial molecule to natural counterpart in fabricating dielectric resonators. Unit particles of different shape could realize a similar disk resonator. Miniaturization, higher unloaded Q and good spurious property will be attained for microwave resonators by knowing the behavior of artificial molecules,

Novel Ultra Wideband (UWB) Metamaterial (MTM) Passive Components

C. Caloz and **H. V. Nguyen**
École Polytechnique, Canada
A. Sanada
Yamaguchi University, Japan

Ultra wideband (UWB) is an emerging technology, somewhat reminiscent to the first "wireless" experiments by Hertz, where the electromagnetic signal is directly modulated onto a time-domain pulse without any carrier. Due to the subsequent huge bandwidth of the spectrum (typically from 25% to 120% or more), UWB systems exhibit super-high data rates and excellent immunity to multipath interference; in addition, they provide fine-resolution ranging for radar positioning and tracking applications. After nearly a hundred year supremacy of narrow-band wireless technology, from the invention of the heterodyne mixer by Armstrong in 1918, new solutions are thus needed to address the new challenges posed by UWB. All of the RF front-end philosophy, from the modulator to the antenna, has to be rethought in different terms. In particular, novel microwave devices supporting such huge bandwidth need to be developed.

Recently, metamaterial (MTM) structures, more specifically composite right/left-handed (CRLH) transmission line (TL) MTM structures [C. Caloz and T. Itoh, *Electromagnetic Metamaterials, Transmission Line Theory and Microwave Applications*, Wiley-IEEE Press, November 2005], were shown to offer interesting solutions in terms of UWB hardware. In particular, we developed novel CRLHbased couplers [H. V. Nguyen and C. Caloz, hSimple-design and compact MIM CRLH microstrip 3-dB coupled-line coupler,h*IEEE MTT-S Int. Microwave Symp.*, June 2006, to be published], filters [H. V. Nguyen and C. Caloz, hBroadband highly selective bandpass filter based on a tapered coupled-resonator (TCR) CRLH structure,h *Proc. of the European Microwave Association*, 2006, to be published] and 6-port front-ends [H. V. Nguyen and C. Caloz, hMetamaterial-based dual-band six-port front-end for direct digital QPSK transceiver,h*Mediterranean Electrotechnical Conference (MELECON)*, May 2006].

The couplers are based on a novel CRLH cutoff even/odd-mode principle, allowing an UWB arbitrary level of coupling in planar form. The filters can achieve a bandwidth up to the theoretical limit of 200% using a tapered coupled-resonator CRLH structure. The UWB six-port front-end (receiver and transmitter) is a passive system integrating three CRLH hybrids and one CRLH power splitter. An additional interest of CRLH MTM structures for UWB, is their intrinsic dual-band property, which can be exploited to generate systems operating in the two separate UWB bands specified by some IEEE standards.

We shall present in this paper an overview of these novel MTM devices.

Microwave Circuit Applications of Resonant Type Left Handed Lines Based on Complementary Split Rings Resonators

M. Gil, I. Gil, J. Bonache, J. Garcia, and **F. Martin**

Universitat Autonoma de Barcelona, Spain

In this work, one-dimensional metamaterials based on complementary split rings resonators (CSRRs) are applied to the synthesis of artificial transmission lines with left handed transmission characteristics. The basic cell consists on a microstrip line loaded with CSRRs (which are etched on the ground plane) and series capacitive gaps. They are combined to achieve the required negative effective values of dielectric permittivity and magnetic permeability in a certain frequency band. The analysis of the electromagnetic behaviour and the equivalent circuit model of these structures reveals that the main electrical parameters of the lines (characteristic impedance and electrical length) can be controlled to some extent by using small unit cell structures. This represents an important advantage for the design of microwave devices, where miniaturization is a key issue. Moreover, by means of these structures it is possible to fabricate artificial lines with extreme values of characteristic impedance, not easily implementable in microstrip technology. We have applied these ideas to different microwave circuits and devices. For instance, we have designed power dividers (see Fig. 1), where area savings of 50% or more as compared to conventional realizations is possible. Other microwave circuits based on these artificial lines are also under investigation. It is believed that left handed lines based on CSRRs can find practical application in narrow band microwave circuits and systems.

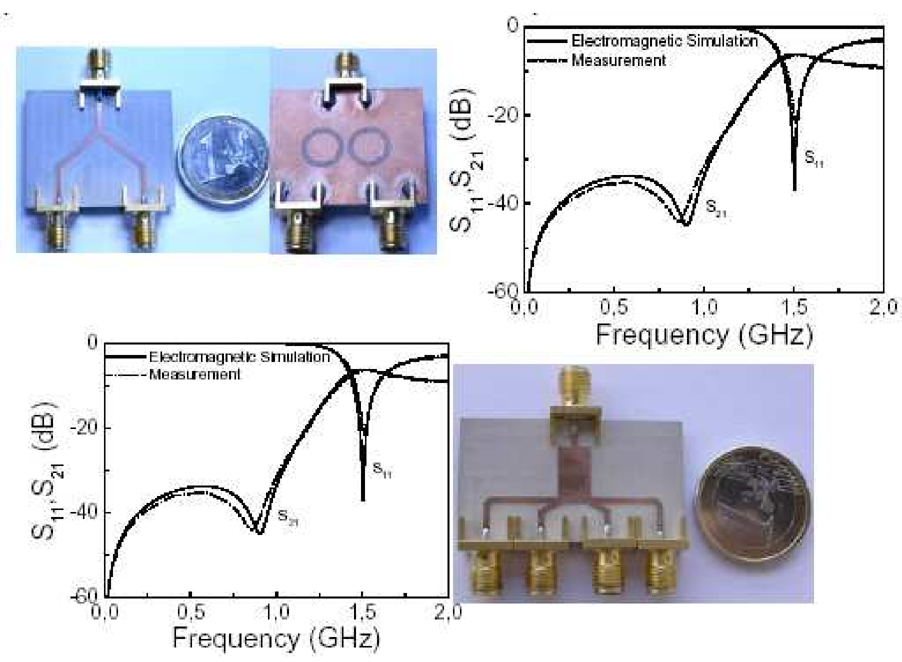

Figure 1: Some practical implementations of power dividers and frequency responses (simulated and measured).

Session 1A3
Computation in Electromagnetics for Ultra Wide Band Applications

The Application of Domain Decomposition Method in Parallel Computing Electromagnetic Field

T. Li
Wuhan University, China

With the development of high performance parallel computing technology, good arallel algorithom is as important as node-node communication velosity and load ba- lancing to improve parall effeciency. Domain decomposition method(DDM) is an algorithm fitting well for parallelism. DDM decomposes the whole domain of question into several coupled subdomains, and solve subdomains on parallel computers and reduce mem- ory storage requirements and CPU time. For the model: $\begin{cases} -\delta u + u = r, & \Omega \\ u = 0, & \partial\Omega \end{cases}$ First,divide the domain Ω into some subdomains Ω_i, then divide each sub-domain into finite element mesh, let $\Omega = \cup\Omega_i, \Gamma = \partial\Omega_i$. The functional with Lagrange multipiler λ is as follow:

$$J(u, \lambda) = \sum_i \{\frac{1}{2}a_i(u, u) - \int_{\partial\Omega_i} u\lambda dS - (f, u)_{\Omega_i}$$

matrix equation is

$$J_i(u.\lambda) = \frac{1}{2}U_i^\tau A_i U_i - U_i^\tau B_i \lambda_i - U_i^\tau f_i$$

The minimal energy expression is

$$J_i(u.\lambda) = -\frac{1}{2}\lambda_i^\tau B_i^\tau A_i^{-1} B_i \lambda_i - \lambda_i^\tau B_i^\tau A_i^{-1} f_i - \frac{1}{2} f_i A_i^{-1} f_i. \tag{1}$$

We can calculate U_i by calculating boundary stiff matrix $-B_i^\tau A_i^{-1} B_i$ and equivalence force $B_i^\tau A_i^{-1} f_i$ through above equation.

One examples followed as the finite elements and the edges of an area are divided into five groups by DDM. Each group of the matrix coefficients is stored into each co- mputer (node), and the six nodes are connected with a fast Ethernet. The FEM calcul- ations are parallelized with the node.node communication by a message passing inter- face (MPI).

REFERENCES

1. Guoping Liang, Ping Liang. The langrage multiplier domain decomposition method of hybrid finite element, *J. Computation Math.*, Vol. 3 1998.
2. Kenichi Takano, El-Amine Salhi, Sakai, and Moris Dovek, gWrite Head Analysis by Using a Parallel Micromagnetic FEM,h *IEEE Trans. Magn.*, vol. 41, no. 10, Oct. 2005.

EME Analysis of Ultra-Wide Band, Quasi-Adiabatic Dielectric Tapered Waveguides

T. G. Li and **H. W. Chang**
National Sun Yat-sen University, Taiwan

In optoelectronics integrated planer lightwave circuit (PLC), the dielectric tapered waveguides are used as spot-size converters to improve the two-way coupling coefficients between two waveguides with very different mode field profiles. To minimize the radiation loss, the change in the cross section of the tapered waveguide must be kept small. An ideal adiabatic waveguide suffers neither radiation loss nor mode conversion loss and have ultra wide optical bandwidth. In the reality the tapered waveguide is shaped quasi-adiabatically to keep the overall device length short. At present, no exact EM wave theory can handle such large (up to several thousand wavelengths) and complex devices. Approximation methods such as the beam propagation method (BPM), time-domain finite-difference (FD-TD) and frequency-domain finite-difference (FD-FD) methods are used to analyze and optimize the design. In this paper, we propose to study this structure using the complete eigen-mode expansion technique (CEMET). The device is first transversely sliced into many sections made of constant layered structures. The optical waveguide modes for each section are computed first using a semi-analytical layered code. The total EM fields are expanded in terms of these layered modes using orthogonal projection along each interface. The CEMET includes all guiding modes as well as higher-order modes that BPM normally ignores. Like BPM, CEMET assumes uni-directional wave propagation inside tapered waveguides, the computational costs are much less than methods (e.g. FD-FD) assuming bi-directional traffics. The performance of several quasi-adiabatic tapered waveguides will be demonstrated.

Filter Effect of FDTD for Broadband Signals

A. Thiry, F. Costen, and **A. Brown**

The University of Manchester, U.K.

UltraWide Band (UWB) signals has a variety of applications, from imaging to positioning, to communications. To design new applications and improve the existing ones, simulations are required because of the high cost involved in field testing and the difficulty to assess the results. The Finite-Difference Time-Domain (FDTD) method [1] is a simple time-domain Maxwell's equations solver, suitable for the analysis of the propagation of the transient signal. The wide frequency-range of interest is covered in only one numerical simulation. Thus FDTD is well suited for UWB systems. Typically, a point source is applied for the excitation. This point source produces a spherical wave in 3D FDTD, especially in the near-field.

The most obvious problem is the dispersion. This is related to the fact that as opposed to single frequency waveforms, UWB signals do not have a clear practical higher frequency to define the simulation parameters. In effect, there are some frequencies that are higher than the frequency of interest. This means that some high frequency components are close to the system cut-off frequency and thus are traveling at a lower speed than lower frequencies [2]. This makes the waveform get distorted as it travels, and also some frequency components cannot travel in the FDTD system. In short, the FDTD simulation acts as a filter for the UWB waveforms.

The work presented in this paper reveals a frequency-domain filter for UWB waveforms which arises when FDTD is used. These results are derived from the transfer function of the FDTD system which are independent of the UWB waveform used. The validity of the transfer function is then assessed on a set of UWB waveforms. The calculated transfer function is verified with numerical simulations.

REFERENCES

1. K.S. Yee. Numerical solution for initial boundary value problems involving maxwell's equations in isotropic media. *IEEE Trans. Antennas Propagat.*, AP-14:302E07, May 1966.
2. L.N. Trefethen. Group velocity in finite difference schemes. *SIAM Review*, 24:113-36, 1982.

Development of Dielectric Filled Tem-Horn Antenna

S. Norouzi, C. Ghobadi, and **J. Noriniya**

antennas for impulse Ground Penetrating Radar (GPR) should be designed specially to radiate pulses with given properties into the ground and receive pulses scattered from subsurface objects. Due to their usage in the impulse system, the antenna should be ultra wideband with a linear phase Characteristic and with a constant polarization. Despite of the fact that GPR antennas operate near the ground, the antenna performance should be independent from ground properties, which also is a very important demand. One of the best known antennas for radiation of short pulses is the TEM-horn. This antenna may radiate signals over an in ultra-wide frequency band and has a linear phase characteristic over this band. However attempts to use this antenna in GPR systems for radiating into the ground were not successful when the antenna were situated close to the ground. The reason for this failure is that the basic TEM-horn is not matched to the ground and the ground reflection causes strong late time ringing. Besides the basic TEM horn antenna has large physical dimensions. To overcome these disadvantages a dielectric filled TEM horn antenna has been developed and has been measured as a single antenna and as a part of a Tx-Rx GPR system.

Design of the Broadband Bandpass Filter Using Suspended Substrate

J. S. Kim and **S. G. Byeon**

Korea Electronics Technology Institute, Korea

The suspended substrate is useful for realizing broadband, highly-selective filters. Its main advantages are small size, high "Q" and good temperature stability. This paper presents the realization of the broadband bandpass filter(BPF) using suspended substrate. This BPF features broadside-coupled stripline with broadband characteristics. A BPF with the center frequency of 4.5GHz is designed and fabricated. In the measurement, the lower and higher cutoff frequencies of the passband are equal to 1.92 GHz and 6.33 GHz, respectively. The measured insertionloss of BPF is less than 1dB and return loss more than 10dB in the passband. The measured results agree very well with the EM simulation results.

REFERENCES

1. I.D. Rhodes, "Suspended Substrate Filters and Multiplexers," *Proceedings of 1986 European Microwave Conference,* 16th EuMc, pp. 8-8..
2. P. Bhartia and P. Pramanick, gComputeraided Design Models for Broadside-coupled Striplines and Millimeter-wave Suspended Substrate Microstrip Lines,h *IEEE Transactions on Microwave Theory and Techniques,* Vol. 36, No. 11, November 1988.

A Fully Integrated CMOS RFIC 3.1-10.6 GHz Ultra Wideband Low Noise Amplifier with Inter-Stage Inductor

M. L. Her, M. Y. Shen, C. Y. Fan, and **Y. Z. Wang**

Feng Chia University, Taiwan, R.O.C.

Recently, the ultra wide-band (UWB) technology has been allocated in the spectrum from 3.1 to 10.6 GHz by the US Federal Communication Commission (FCC). In this paper, we propose a new structure of UWB low noise amplifier (LNA) that can achieve good input/output matching, high linearity, and excellent wide operating bandwidth. Additionally, the gain flatness can be maintained within 1 dB in the whole operating bandwidth. The UWB LNA consists of RC shunt-feedback circuit, the modified band-pass Chebyshev filter circuit, and the inter-stage gain amplifier. The proposed UWB LNA is designed and simulated based on a standard 0.18 m RF CMOS process.

Fig. 1 shows the simplified configuration of the UWB LNA. In the gain amplifier, the principal function of the inter-stage inductor, Lb, which can reduce Q factor of the circuit, and improve gain flatness in all sub-bands. Consequently, the cascode amplifier with inter-stage inductor provides good isolation between input and output ports, as well as good gain bandwidth. In the input impedance matching circuit, we adopt the modified band-pass Chebyshev filter with the RC shunt-feedback circuit to achieve the optimized wideband input reflection coefficient.

The simulation results of a 3.1 GHz to 10.6 GHz UWB LNA are shown in Fig. 2. It is performed using Agilent ADS simulator. The results show that adjusting the values of R_f and C_f, the input/output return loss (S_{11}, S_{22}) less than -10 dB, and the maximum power gain 10 dB within the 3 dB bandwidth from 2.4 to 11 GHz can be obtained.

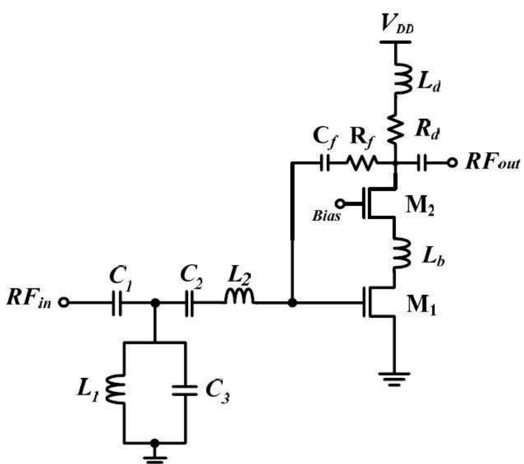

Figure 1: Proposed UWB CMOS LNA topology

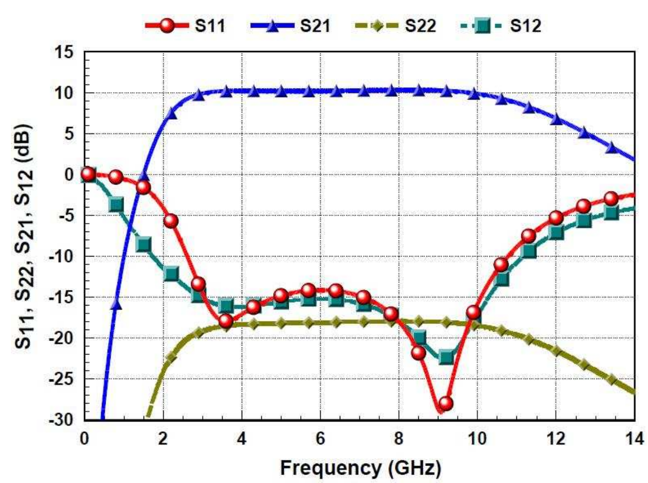

Figure 2: Simulation performance of UWB CMOS LNA

The authors would like to thank the National Science Council of the Republic of China, Taiwan, for financially supporting this research under contract no. NSC 94-2213-E-035-014, and the Chip Implementation Center, National Science Council of the R.O.C., for their assistance with chip fabrication.

Session 1A4
Microwave and Millimeter-Wave Circuits

An Oscillator with Reduced Phase Noise and Improved Harmonic Characteristics Based on a Corrugated CPW EBG Structure

C. G. Hwang
Korea Advanced Institute of Science and Technology (KAIST), Republic of Korea
N. H. Myung
Korea Advanced Institute of Science and Technology (KAIST), Republic of Korea

This paper presents a new microwave oscillator incorporating a corrugated coplanar waveguide (CCPW) electro-magnetic bandgap (EBG) structure as its terminating resonance component. The use of the compact CCPW EBG structure effectively reduced the phase noise and improved the harmonic characteristics of the microwave oscillator circuit without additional backside processing or drastic size increment. The higher quality factor of the structure relative to that of the conventional CPW resonator plays a role of phase noise reduction of the oscillator circuit. In addition, the unique harmonic characteristic of the CCPW plays a role of harmonic suppression of the oscillator circuit, which leads to enhancement in dc-ac power efficiency of the circuit. The fully planar CCPW oscillator oscillating at a frequency of 5.41 GHz showed a phase noise characteristic of -90.2 dBc/Hz at 100 kHz offset and a second harmonic suppression of -42.67 dB. The results constitute a greater than 10dB improvement in phase noise performance and more than 20 dB improvement in second harmonic suppression when compared to those of a conventional CPW oscillator without the CCPW structure. The total size of the CCPW EBG structure corresponds only to 0.57 $\lambda_g \times 0.45\lambda_g$, where λ_g is the wavelength of resonance frequency. The fabricated circuit can be easily applied to the MMIC due to its small size and uniplanar structure characteristic.

A Novel Compact CPW Bandpass Filter with Super-wide Stopband Suppression

S. S. Liao, C. Y. Tao, P. T. Sun
H. W. Liu and **C. Y. Chien**

Feng-Chia University

In the RF/MW front-end of the modern communication system, bandpass filters with wide stopband and high selectively are usually required to enhance the overall system performance. The parallel-coupled microstrip filter has been used due to its planar structure, ease of synthesis method, and low cost [1]. The disadvantages of this filter are the large size and suffer from the spurious responses at$2f_0$.Many methods have been proposed to overcome the latter problem [2]-[3]. However, they increase the cost or complicate the original filters. Also the circuited dimension is still too large. On the other hand, the coplanar waveguide (CPW) are ease in series and shunt connections, no via holes, insensitive to the substrate thickness, and low dispersion effect [4]. In this study, we propose a novel miniaturized CPW bandpass filter with super-wide stopband suppression, and reveal a good shape factor.

The design method used a concept of frequency combiner with high Q factor which reveals super wide harmonic suppression at least the two and half times passband frequency. The method was demonstrated on the realization of bandpass filter operating at 2.4 GHz by way of the full-wave simulation and measurement of the prototype. All the simulated S-parameters of this filter are obtained from the full-wave Sonnet em simulator, as shown in the below figure. The implemented circuit in this paper are fabricated on the FR4 substrate ($\epsilon_r = 4.7$, $\tan\delta = 0.022$, thickness = 0.8mm,and the metal thickness = 0.02mm). The proposed filter has the performances better than that of the conventional $\lambda/4$ bandpass filter. The dimension of this novel bandpass filter compared to the conventional designs is about 20%. The element size of the component can easily be patterned by using standard printed-circuit etching processes. It is quite useful in the MIC's and MMIC's application. The authors are grateful to support from the National Science Council of Taiwan in this project. (Project No NSC 94-2213-E-035-013)

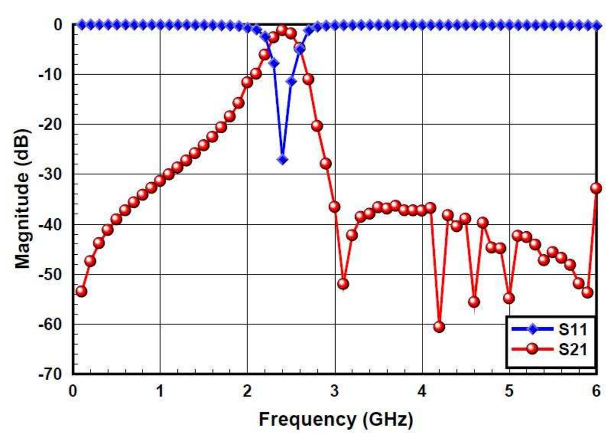

Figure 1: Simulated S-parameters.

REFERENCES

1. D.M. Polar, Microwave Engineering, 3rd, ed. *New York: Wiley*, 2005, Chap8.
2. C.Y. Chung and T. Itoh," A modified parallel-coupled filter structure that improve the upper stopband rejection and response symmetry" *IEEE Trans. Microwave Theory Tech.*., MTT-39, Feb. 1991, pp. 310-314.
3. I.J. Bahl." Capacitively compensated high performance parallel-coupled microstrip filters," in IEEE MTT-S Int. *Microwave Symp. Dig.* , 1989, pp.679-682.
4. S.S. Liao, H.K. Chen, Y.C. Chang, and K.T. Li," Novel reduced-size Coplnar-waveguide bandpsaa filter using the new folded open stub structure," *IEEE Microwave and wireless component Lett.*, vol.12, No.12, Dec. 2002, pp. 476-478.

A Novel Miniaturized Planar Microstrip Branch-Line Coupler

S. S. Liao, Y. F. Tseng, C. Y. Lai, and **S. H. Su**

Feng-Chia University, Taiwan R. O. C.

C. Y. Gun

Nan-Kai Institute of Technology, Taiwan R. O. C.

Branch-line coupler is one of the most popular passive circuits used for microwave and millimeter-wave applications. It is commonly used in balanced amplifiers and mixers for achieving good return loss, and spurious signal rejection. However, one of the major disadvantages for the branch-line couplers is the large circuit dimension. Many methods have been proposed to overcome this problem [1]-[2]. Lumped-elements achieve significant size reduction but are difficult to scale much beyond the microwave region [1]. Meandered microstrip lines are used to form compact-size, but these employ high-dielectric-constant substrates to reduce the physical length [2]. [3] used the artificial transmission line, which considers capacitive loading, and unoccupied internal region of the coupler to miniaturize size. Unfortunately, the overlap problem limited its size reduction. It only saves 37% circuit dimension. On the other hand, we had presented a non-symmetrical T-shape structure to avoid the overlap problem; it reduced circuit size up to 55% [4]. In this study, we solve the overlap problem by using a symmetrical T-shape structure and quasi-lumped elements approach to reduced circuit size up to 70%.

The design method uses explicit formulas and considers technology constrains and the area occupied by the circuit. The method was demonstrated on the realization of couplers operating at 2.4 GHz by way of the full-wave simulation and measurement of the prototype. All the simulated S-parameters of this coupler are obtained from the full-wave Sonnet em simulator. The implemented circuit in this paper are fabricated on the FR4 substrateei$\epsilon_r = 4.7$, $\tan\delta = 0.022$, thickness = 0.8mmj,and the metal thickness = 0.02mm. The simulated results at 2.4GHz are: $S_{11} = -31.2$dB, $S_{41} = -22.8$dB, $S_{21} = -3.66$dB, $S_{31} = -3.45$dB and the phase difference is 90.1^0. The dimension of this novel coupler compared to conventional designs is only 30%. The element size of the component can easily be patterned by using standard printed-circuit etching processes. It is quite useful in the MIC's and MMIC's application.

The authors are grateful to support from the National Science Council of Taiwan in this project (Project No NSC 93-2213-E-035-025), and the measured support from Universal Scientific Industrial Co., Ltd..

REFERENCES

1. W. S. Tung, H. H. Wu, and Y. C. Chian ”Design of microwave wide-band quadrature hybrid using planar transformer coupling method,” *IEEE Ttrans. Microve Theory Tech.*, vol.51, no.7, pp.1852-1856, Jul. 2003.
2. H. Tanaka, Y. Sasaki, T. Hashimoto, Y. Yagi, and Y. Ishikawa,” Miniaturized 90 degree hybrid coupler using high dielectric substrate for QPSK modulator,” *in IEEE MTT-S.Int.* Dig., Jun. 1996, pp. 793-796.
3. K. W. Eccleston, S. H. M. Ong.,” Compact planar microstripline branch-line and rat-race couplers,” *IEEE Ttrans. Microve Theory Tech.*, vol.51, no.10, pp.2119-2125, Oct. 2003.
4. S. S. Liao, P. T. Sun, N. C. Chin, and J. T. Peng,” A novel compact-size branch-line coupler,” *IEEE Microwave and wireless component Lett.*, vol.15, No.9, pp. 588-590, Sep. 2005.

Design and Tuning of Planar Filter Having Optimal Pass Band Response

R. C. Hsieh, Y. C. Chen, H. H. Chen, and **Y. H. Chou**
Huafan University, Taiwan, R.O.C.

An easy and efficient tuning method to design planar direct coupled band pass filter is introduced in this work. The Chebyshev filter, N=3 as shown in Fig. 1, is taken as an example to demonstrate the design and tuning procedure. The filter has center frequency $f_0 = 2.5GHz$ and fraction bandwidth $FBW = 0.05$. The miniaturized hairpin resonators serve as the resonators of the filter. Tap in positions, T_1 and T_2, of the two feed lines controlled the input and output coupling of this filter. By varying the lengths of the coupled lines, L_1, L_2 and L_3, the resonant frequency of resonators can be tuned. The coupling coefficient between the resonators can be adjusted by changing the separation distances, S_1 and S_2. The filter shall possess the same symmetric property as the coupling matrix of equivalent circuit dose. Only four dimensions need design, they are T_1, L_1, L_2 and S_1. The tuning method is used to design these four parameters such that the planar filter will has optimal pass band response. This means the filterfs reflection coefficient will close to that of equivalent circuit over the pass band.

The first step of the tuning procedure is to design the resonant frequency and tap in position of the first resonator. The 2^{nd} and 3^{rd} resonators are removed from the full wave simulation in this stage. It is very easy to design L1 and T1 such that the simulation result has the same group delay response as that of the equivalent circuit. In the next step, the reference plane in the full wave simulation is set up according to the phase of reflection coefficient. The resonant frequency of the 2^{nd} resonator and its coupling with the 1^{st} resonator is tuned in the next step. The zeros and poles of the reflection coefficient are taken as a reference in designing L_2 and S_1. The filterfs reflection coefficient, after the above three design stages, is compared with that of equivalent circuit in Fig. 2. In order to make the filterfs response close to that of equivalent circuit, the four dimensions are further fine tuned by computer optimization technique. Fig. 2 shows that the filterfs response is very close to the optimal response after the optimization process. The variations of the four parameters are less than 5% during the optimization process. This means the filter, designed after the tuning stages, is very close to the best design filter.

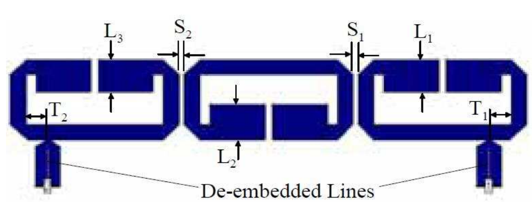

Figure 1: The planar direct coupled filter.

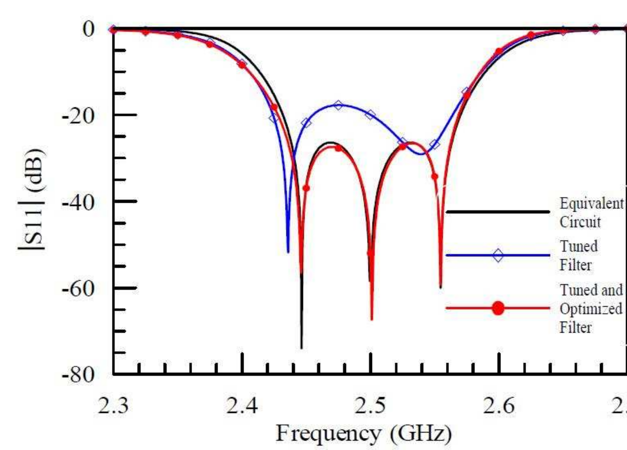

Figure 2: The reflection coefficient of the best design filter.

A Novel UWB Bandpass Filter

K. M. Shum, W. T. Luk, C. H. Chan, and **Q. Xue**
City University of Hong Kong, China

Filters with high performance and compact size are highly desirable in the emergent ultra-wideband (UWB) technology. Microstrip parallel coupled-line filters have been found one of the most commonly use designs. However, they have a disadvantage of slow roll-off beyond the passband. To improve the roll-off, an open-ended stub is tapped at a half-wavelength ($\lambda/2$) resonator to provide a transmission zero at the desired frequency. By adding one more stage of that resonator and stub, a three-pole bandpass filter with two transmission zeros at the lower and upper edges of the passband was achieved [1]. In [2] two open-ended stubs with different stub lengths were tapped to the $\lambda/2$ resonator to obtain two transmission zeros and simultaneously reduce the overall size of the filter. However, further reduction of the filter circuit area remains desirable.

In this paper, we propose a UWB bandpass filter using a single dual-band stub (DBS) to replace the two open-ended stubs with different stub lengths. DBS is a quarter-wavelength stub, at the higher frequency, terminated by a compact microstrip resonant cell (CMRC) [3]. The total length of the stub and the CMRC is quarter-wavelength long at the lower operating frequency of this DBS. Due to the slow-wave effect of the CMRC, the overall length of the DBS will be much shorter than the length of an equivalent quarter-wavelength stub at the lower frequency. The DBS is to be properly tuned to control the two transmission zero locations of the filter. In order to further reduce the size of the filter, the coupled lines of the proposed filter will be meandered, leading to a compact size of $0.26\lambda_g$ by $0.32\lambda_g$. Subsequently, the proposed filter design was fabricated and measured to validate the proposed methodology. There are good agreements between the experimental and simulation results.

REFERENCES

1. J. R. Lee, J. H. Cho and S. W. Yun, "New compact bandpass filter using microstrip $\lambda/4$ resonators with open stub inverter," *IEEE Microw. Guid. Wave Lett.*, vol. 10, no.12, pp. 526-527, Dec. 2000.
2. L. Zhu and W. Menzel, "Compact microstrip bandpass filter with two transmission zeros using a stub-tapped half-wavelength line resonator," *IEEE Microw. Wireless Comp. Lett.*, vol. 13, no.1, pp. 16-18, Jan. 2003.
3. T. Y. Yum, Q. Xue and C. H. Chan, "Novel subharmonically pumped mixer incorporating dual-band stub and in-Line SCMRC," *IEEE Trans. Microw. Theory Tech.*, vol. 51, no. 12, pp. 2538-2547, Dec. 2003.

PLL Assisted Injection Locking Phase Control

K. C. Wan
City University of Hong Kong, China
Q. Xue
City University of Hong Kong, China

Intelligent scanning antenna is essential to the grooming of user and data rate in wireless communication systems. Cost effective design are required for those modern communication technology. Phase control plays an important role in this intelligent scanning antenna technology. It is the core hardware control unit of the system. However, the most common design employing phase shifters are bulky, expensive, complicated and large insertion loss of microwave. So that, some phased source techniques are invented.

In this paper, the design of a PLL assisted injection locking phase control is presented, which can be used in the mobile base station, RFID, radar and wireless communications, etc. The slave oscillators are controlled by PLL at the same frequency as the master oscillator while it is injection locked by its master oscillator on the other hand. This structure makes the slave oscillators and the master oscillator operate at a frequency as close as possible making the slave oscillators injection locked by its adjacent element easily in the case of low injecting power and also the probability of mode jump is minimized, such that the structure in the RF section can be simplified. At the mean time, the problem of narrow locking range of injection locking can be totally solved as the oscillators are driven to its desired frequency by the PLL. Measurement results show the idea works in locking range improvement and RF section structure simplification.

Intelligent Use of the Non Uniform Transmission Lines to Design Active and Passive Microwave Circuits

M. Boussalem, H. Gaha, F. Choubani, J. David, and **R. Crampagne**
6'TEL - SUP'COM - TUNISIA, France

To improve the performance of microwave circuits and particularly the non linear active or passive circuits, we have suggested to introduce non uniform transmission lines due to their frequency behavior they can eliminate some undesirable frequencies.

The analysis of such structures is given by a numerical calculation program based on the work of Hill, which consists in determining the general solution of the propagation distribution equation of the electric and magnetic field and to deduce the accurate model of the line. Therefore, several non uniform transmission lines with various profile (linear, exponential, hyperbolic) were analyzed. Their contribution to control, reduce and eliminate the harmonic frequency, generated by the non linearity of some active and passive microwave circuits, were experimentally validated.

Actually, the non uniform transmission lines have a frequency behaviour which strictly depends upon their forms and their profiles of non homogeneity. While the transmission structures resonate in a regular multiple of fundamental frequencies, the non uniform lines resonate on frequencies which are different from integer multiples of fundamental.

In this paper, we have used the non uniform transmission lines (NUTL) to design the output matching network of a non linear power amplifier. The immediate result, we have notified, is that harmonics are sharply reduced by such use of NUTL. On the other hand, we have applied cascaded NUTL to design filters by microstrip technology ; in order to get rid of harmonics in attenuated bands. Hence, we have optimised the profiles of the different elements of non uniform filter whose each element has the impact of removing harmonics of its adjacent element.

Session 1A5
Extended/Unconventionl Electromagnetic Theory, EHD(Elecrohydrodynamics)/EMHD (Electromagnetohydrodynamics) and Electrobiology

Laboratory Evidence of Electric Reconnection Model by a Universal Electric-Cusp Type Plasma Reactor and Possible Applications to Diamond and New Material Production

H. Kikuchi
Institute for Environmental Eletromagnetics, Japan

It is now recognized that there are three kinds of merging-reconnection phenomena, fluid vortex, magnetic, and electric reconnection in the regime of hydrodynamics (HD), magnetohy- drodynamics (MHD), and electrohydrodynamics (EHD), respectively. While fluid vortex and magnetic reconnection are known, in particular the latter is so familiar to plasma physicists as well as geo-astro-physicists and has extensively been investigated for the past four decades on the basis of MHD [1], there have never appeared any ideas on an electric version of field line merging reconnection surprisingly, except the authorfs reports [2]. This does not mean no exist- ence or importance of Electric Reconnection, but simply means no attention of scientists to that so far. Analogously, electric reconnection concept should be evolved. on the basis of EHD for unconventional plasmas including dusty and dirty plasmas and/or aerosols that has been devel- oped recently. When an object and/or dust grain is placed in an electric cusp region formed by an electric quadrupole, electric field line merging towards the object or grain from the four poles and subsequent electric reconnection occur and, if the background gas pressure is beyond the breakdown threshold, are. followed by electric discharge. Such a laboratory experiment was per- formed by using a universal electric-cusp type plasma rector [3] for the first time. This paper reports successful results that a catastrophe from zero to very high electric field by placing an object in an electric cusp region and consequent object-related electric reconnection followed by electric discharge occurs, and indicates its possible applications to diamond and new material production. Specifically, when an object (semispherical lead) is placed at the electric cusp centre on a copper plane, electric discharge from both electrodes to an object only occurred as a result of object-related electric reconnection. When an object is shifted 1 cm left from the cusp centre on a copper plane, electric discharge from both electrodes to an object still occurred. like the above case as a result of object-related electric re- connection. This indicates that the object is still inside a cusp region. When an object is placed under the positive electrode on a copper plane, electric discharge turned between positive and negative electrodes only. Discharge from electrode(s) to the object never occurred, indicating that the object is no longer in a cusp region. These observations are just laboratory evidence of the electric cusp-reconnection model pro- posed more than a decade ago. In addition, it has been observed during electric discharge that dust grains are moving or EHD wind flows inside the device and dust collection by an object and the electrodes took place. This is thought to be due to electric forces exerted on induced or polarized charges of dust grains. In particular, dust collection by an object seems to be much stronger than the electrodes Sharp discharge to the object placed in an cusp region appeared to oxidize it. in contrast to conventional uniform RF discharge for thin diamond phragm formationDWhen some seed of diamond or new material is placed in an cusp region on a copper plane, one might expect riper one. Along this line, an attempt is in progress.

REFERENCES

1. Hones, E.W., Jr. (ed.): Magnetic Reconnection in Space and Laborato-ry Plasmas, Geophysical Monograph 30, American Geophysical Union, Washington, D.C., 1984,
2. Kikuchi, H., Elect ohydrodynamics in Dusty and Dirty Plasmas, Kluwer Academic Publishers, Dordrecht/The Netherlands, 2001.
3. .pp.93-94, in [2]

Generation of Solar Magnetic Fields: Contribution of Octupolar Seed Field

D. K. Callebaut [1], **A. H. Khater** [2]

[1]University of Antwerp, Belgium
[2]Beni-Suef University, Egypt

The exact solution for the cinematic dynamo problem in spherical coordinates (r, θ,ϕ)

$$\partial_t \mathbf{H} \quad = \quad curl(\nu \times \mathbf{H}) \tag{1}$$

$$\nabla \cdot \mathbf{H} \quad = \quad 0 \tag{2}$$

is given in [1]. Here **H** is the magnetic field and ν is the azimuthal velocity, which is supposed to be an arbitrary function of r and θ only. Using a bipolar seed field yielded a qualitative agreement with the sunspot butterfly diagram and the polar faculae butterfly diagram. Next we have investigated the case that a quadripolar seed field resides in the Sun (maybe in the whole convective zone or just only in the tachocline at the bottom of the convective zone) as some observations[2] reveal a quadripolar and even an octupolar contribution to some surface phenomena. A combination of a bipolar and a quadripolar field yields a fair agreement with observations, which may still be improved by the (weak) octupolar contribution. The ratio of the various components may be determined by previous observations or by a best fit. The separation between the sunspot region and the polar faculae, although both are generated by the same mechanism, is manifest: the region where the radial variation of the angular frequency of the rotation vanishes.

REFERENCES

1. Callebaut, D. K., ”Exact solution of simple cinematic dynamo”, *Solar Phys.*, submitted.
2. Makarov, V. I., Tlatov, A. G. & Callebaut, D. K.: ”Increase of the magnetic flux from polar zones of the Sun in the last 120 years”, *Solar Phys.* 206 (2), 383-399, 2002.

Periodic Magnetic Fields from MHD Evolution Equation

D. K. Callebaut
University of Antwerp, Belgium

The evolution equation for the magnetic field, **H**, in ideal (i.e. with perfect conductivity) magneto-hydrodynamics (MHD) reads

$$\partial_t \mathbf{H} = curl(\nu \times \mathbf{H}) \tag{1}$$

where $\nu$is the azimuthal velocity. Moreover, the field satisfies the equation of flux conservation div $\mathbf{H} = 0$. In reference 1 we gave the solution of this cinematic dynamo for the case thatν is supposed to be an arbitrary function of r and θ only (spherical coordinates):r,θ,ϕ). This solution consists of two parts. A first part is independent of the azimuth and for which the azimuthal component of **H** grows linearly with time: this is a real dynamo term and has been studied as such. The second part contains r and θ and is moreover periodic in a combined variable ωt -ϕ with the angular frequency. This part waxes and wanes so that it does not seem of direct interest to the dynamo problem. However, as it may interact with the small more or less regular motions which are superposed on the global differential rotation given by ν, it is studied here. Explicit expressions are obtained using a Fourier decomposition.

REFERENCES

1. Callebaut, D. K., "Exact solution of simple cinematic dynamo", Solar Phys., submitted.
2. Callebaut, D. K. and Makarov, V. I., "Generation of Sunspots and Polar Faculae from a Cinematic Dynamo ", Proc. IX Pulkovo Internat. Conf. on Solar Physics: '*Solar Activity as a Factor of Cosmic Weather*'. 4-9 July 2005, in press.

Powerful Non-linear Plasma Waves from Moderate First Order Perturbations in Cylindrical Coordinates

D. K. Callebaut [1]and **G. K. Karugila** [2]

[1]University of Antwerp, Belgium
[2]Faculty of Science, SUA, Tanzania

In the non-linear analysis of plasma oscillations using the Callebaut-Fourier method we obtained convergence limits in Cartesian coordinates. For a cold plasma the first order amplitude may not exceed e^{-1} or 37 % of the equilibrium density, n_0, otherwise the total series diverges. This applies to the sum of all first order perturbations; thus e.g. some 30 perturbations each of about 1% of n_0 yield together with their higher orders a wave which has a gigantic peak for certain phases. This is important for the triggering of instabilities of other phenomena in the near or far neighbourhood. E.g. several minor perturbations originating from the turbulent surface of the Sun may combine to trigger prominences, solar flares, coronal mass ejections, etc. in the solar atmosphere. The latter eruptions, when approaching the Earth, may similarly contain several minor waves which combine to block power generators or air planes, etc.

These powerful waves may be relevant too for the ball lightning phenomena. However the wave should run around in the lightning ball. As a first step to this we consider here waves in a cylindrical configuration. This may be useful for cylindrical and toroidal plasma configurations as well.

REFERENCES

1. Callebaut, D. K. and Karugila, G. K., "Non-linear Fourier Analysis for Un-magnetized Plasma Waves", *Physica Scripta*, Vol. 68, No. 1, 7-21, 2003.
2. Callebaut, D. K. and Karugila, G. K;, "Powerful Non-linear Plasma Waves from Moderate First Order Perturbations", Proc. PIERS 2005, Hangzhou, China, 724-728, 2005.
3. Callebaut, D. K. and Karugila, G. K., "Non-linear Fourier Analysis for Un-magnetized Multi-species Waves", Canadian Journal of Physics, Submitted.
4. 4) Callebaut, D. K., Karugila, G. K. and Kikuchi, H., "Non-linear Stability of a Gravitating Medium with Cosmological Constant", *Kuwait J. Sci. Eng.*, Vol. 31, No 2, 33-45, 2004.

Similarities and Differences Among Parametrically Amplifying Traveling-Wave Antennas, Traveling-Wave Tubes, and Esaki Diodes

H. Kikuchi
Institute for Environmental Eletromagnetics, Japan

Parametrically amplifying traveling-wave antennas invented by the present author are somewhat analogous to traveling-wave tubes and Esaki diodes in function and characteristics, though there are essential differences. It is shown in this paper that similarities and differences among param- etrically amplifying traveling-wave antennas, traveling-wave tubes, and Esaki diodes.are elucidated in detail. Parametrical amplification of the traveling-wave antenna corresponds to amplification of traveling wave tubes and the incident waves along the wire play a role of electron beams. There are, however, essential differences between them. The role of electron beams in traveling wave tubes is an amplification only when an external microwave is passing through a helical circuit. In contrast, there are twofold roles of an incident wave in the present traveling antenna. One is to induce a current wave along the wire. The other is to amplify its induced current wave at the same time. Further, there is a difference that the coupling to a helical circuit of electron beams is capacitive for traveling-wave tubes but the coupling to the wire of incident waves is inductive for the present antenna. While the present antennas are expressed by an equivalent active distributed parameter line whose shunt conductance G is negative in the transition region, the resistance in the equivalent lumped circuit of Esaki diodes is also negative. In this respect, there is some correspondence or analogy is seen between them, though those negative effects are different. The negative shunt conductance of the present antenna leads to new results that the attenuation constant of the induced current wave decreases with increasing frequency and the wave-mode becomes a fast wave, while the negative resistance of Esaki diodes is the result of quantum-mechanical tunnel effects.

Session 1A6
Dosimetry of Human-Body Exposure to High-Frequency Electromagnetic Fields I

Suitability and Limitations of Fast Scanning Systems for Demonstration of Compliance with SAR Standards

S. Kühn, T. Schmid, D. Schmid, and **N. Kuster**

IT'IS Foundation, Swiss Federal Institute of Technology

INTRODUCTION: Dosimetric compliance tests are extremely time-consuming, especially since all configurations with every accessory must be evaluated. Faster SAR measurement techniques are desirable, e.g., for evaluation of the worst-case configuration or precompliance testing. SAR information provides further valuable information such as: 1) output power under loaded conditions, as indicated by a different spatial peak SAR if the absorption pattern is not altered, and 2) changes of the internal RF path, e.g., by poor contacts, as indicated by a modified SAR pattern.

OBJECTIVES: To develop a fast dosimetric SAR scanner simulating the test requirements for body-mounted testing and satisfying the requirements for the testing of all devices at the production line, i.e., an extremely short measurement and evaluation time of less than 3s and great reliability independent of the device position. Also, the development of a novel design tool for RF engineers to reduce EMF exposure by implementing improved antenna design.

METHODS: The assessment system (iSAR) (Fig. 1) consists of a block of semi-solid absorbing material developed to approximate the specifications of IEEE 1528, IEC 62209 and other standards in the frequency range of 300MHz to 6GHz. A sensor array consisting of x,y-polarized diode-loaded dipoles is immersed in gel at 4mm below the surface. The cover is 2± 0.1mm thick as required by the standard. In the basic configuration, a sensor array of 256 dipoles covers an active measurement area of 240mm × 120mm. The density of the sensor array is suffcient to reliably assess the exposure, i.e., 15mm. The measured field values of all sensors are amplified, acquired and integrated in parallel, such that the total assessment time is less than 3 s. A novel compensation algorithm was implemented to accurately assess the SAR from devices applying modern communication systems, e.g., for TDMA signals with complex frame structures. New algorithms had been developed by several groups (e.g.,MOTOROLA-algorithm, SUPELEC-algorithm) to enable estimation of the spatial peak SAR values only based on the area scan for a large majority of products with high reliability; a similar algorithm is employed in iSAR.

RESULTS: iSAR scans are equivalent to the area scan tests required for body mounted devices by IEC 62209 Part II. This scanner reduces the total measurement time to $< 1\%$ of conventional scanners with a relative uncertainty of less than 1dB and high repeatability of better than 0.5 dB. The specifications of the system are summarized in Tab. 1.

DISCUSSION: We present a novel dosimetric assessment system satisfying the requirements of precompliance, production line testing and rapid prototyping. The system reduces the total assessment time to less than 1% of conventional scanners.

ACKNOWLEDGMENT: We would like to acknowledge the support of SPEAG, Switzerland during the development of the scanner.

On-Site SAR Distribution Estimation in Actual Electromagnetic Environment Based on Spatial Impulse Responses

J. Q. Wang and **T. Takahashi**

Nagoya Institute of Technology, Japan

During the compliance assessment of base station and broadcast antennas, an incident electric field intensity or power density is being used as a reference level, which should never yield a larger wholebody average specific absorption rate (SAR) than the basic safety limit. However, the relationship between the reference level and the whole-body average SAR was derived based on a free-space planewave exposure dozens of years ago. The exposure from the base station or broadcast antennas is quite different from a plane-wave exposure in actual environment so that the compliance assessment results based on the present reference level may be questioned. An on-site SAR measurement technique is therefore useful to cope with this problem.

The SAR is determined from the electric field inside a human body. According to the equivalence theorem, the electric field inside the human body can be expressed as

$$E(r) = \oint_s G(r, r^{'}) M_s(r^{'}) dS^{'} \simeq \sum_{n=1}^{N} G(r, r_n^{'}) M_s(r_n^{'}) \Delta S_n^{'} \tag{1}$$

where S is a closed surface surrounding the human body, $G(r, r^{'})$ is the tensor Green's function and $M_s(r^{'})$ is the equavilent surface magnetic current density which is related to the incident electric field $E_i(r^{'})$ by $M_s(r^{'}) = E_i(r^{'}) \times \hat{n}$. Let $M_s(r_n^{'}) = \delta(r_n^{'})$, we have the electric field component $E(r, r_{'}^{n}) = G(r, r^{'}) \Delta S_{'}^{n}$. Sn which can be considered as a spatial impulse response. If we know all the spatial impulse responses in advance, we can express the electric field inside the human body as

$$E(r) \simeq \sum_{n=1}^{N} E(r, r_n^{'})[E_i(r_n^{'}) \times \hat{n}] \tag{2}$$

This means that as long as we measure the incident electric field at N observation points, we can then estimate the electric field inside the human body as well as the SAR by simple summation and multiplication of N spatial impulse responses that are derived in advance and stored. This makes the on-site SAR measurement become possible.

To examine the validity of this method, we compared the SAR distributions estimated from the spatial impulse responses with that calculated from conventional finite difference time domain (FDTD) method. We employed an anatomically based whole body human model and calculated its spatial impulse responses in a plane in front of the human body in advance. At first, we investigated a situation of plane-wave incidence at 800 MHz. We used 152 spatial impulses (with a spatial spacing of 0.3 wavelength) for the SAR distribution estimation. The result showed good agreement with the conventional FDTD result. We then investigated a situation for a 2 GHz base station antenna in a corridor environment. We used 882 spatial impulses (with a spatial spacing of 0.25 wavelength) for the SAR estimation. Although some differences was found around the region where the incident electric field varied rapidly, fair agreement between the spatial impulse response estimation and the conventional FDTD calculation was stilled observed. Compared to a computation time of several hours for the conventional FDTD method in a personal computer, the SAR estimation based on the spatial impulse responses only required less than one second.

This method is therefore promising for on-site SAR measurement.

Analysis of the RF exposure of children using handsets

J. Wiart[1], **A. Hadjem**[1], **D. Lautru**[3], **I. Bloch**[2], **R. D. Seze**[3], **M. F. Wong**[1], and **V. F. Hanna**[3]

[1]France Telecom R & D, France
[2]Ecole Nationale Supérieure des Télécommunications, France
[3]Université Paris VI Jussieu, France

With the increase number of children using a handset there is a public concern about their specific Radio Frequency (RF) exposure and their possible sensitivity to RF. Previous studies based on numerical methods, have analyzed the energy absorption of RF, induced by handset, in the heads of children. But, since MRI based model of children are difficult to obtain, these studies have been often based on adult head modified using non-uniform down scaling of adult head. The main limit of this approach is linked to the specific growth of organs. For instance the neurocranium of a five year old child has a volume of 1200 cm^2 and the volume of an adult skull is about 1300-1450 cm^2. From 5 to 18 years the volume of a brain is quite stable but in the same time the thickness of the skull increases of about 75%.

Therefore, in the frame work of the French RNRT ADONIS project (www.tsi.enst.fr/adonis) we developed children heads model based on MRI. Images corresponding to children at different age have been selected. Tissue recognition (segmentation) has been performed in 3D. This approach provides the continuity of tissues in all direction (which is not the case with a segmentation slice per slice). Different model corresponding to 4, 5, 6, 8, 9 and 12 years old have been built. Using these models, model of handset and the Finite difference in Time Domain (FDTD) method the maximum Specific Absorption Rate (SAR) over ten grams in the head as well as the maximum SAR over 1 grams in tissues has been evaluated.

Comparison of SAR evaluated in these head has been carried out. The SAR assessed in children has been also compared to SAR assessed in different adult head. We analyzed also the influence of the variability of organ (such as pinna) that exists for the same class of age. This presentation presents the result of segmentation, SAR calculations and comparison.

Anatomical and physical characteristics for deformed whole-body child models based on Japanese body dimensions data and comparison with MRI-Base European child head models

T. Nagaoka and **S. Watanabe**
National Institute of Information and Communications Technology, Japan

J. Wiart
France Telecom R & G, France

Recently, there is growing interest in the safety of children exposed to radio-frequency electromagnetic fields. However, it is difficult to develop high-resolution whole-body child models for numerical dosimetry of children because there are ethical problems in obtaining anatomical data of a healthy child by fixing the child inside an magnetic resonance imaging (MRI) scanner for long time. Moreover, we must spend tremendous amounts of money and time to develop new high-resolution models even if the anatomical data is obtained. Therefore, we developed whole-body child models by deforming the adult model. Electromagnetic power absorption in the human body is dependent on the shape and size of the body. If an adult model is homogeneously scaled to match the height and weight of a child, the scaled model is not suitable for a child's figure because parts of a human body differ in patterns of growth. Therefore, we measured the dimensions of various body parts of 3-, 5- and 7 -year-old based on measurement regions described in Japanese body dimension data[1]. The averaged dimensions were determined based on the data of five children in each age group. The anatomical model of adult male [2] was transformed to fit the dimensions data of children using the free form deformation (FFD) algorithm which doesn't suffer from the limitation of shape to transform. As the results, the ratios of body-part dimensions of the developed child models were different from those of the adult model. These child models were smoothly transformed. The anatomical structures of these models were also maintained. To verify anatomical and physical characteristics of developed models, the masses of tissues and organs of these models were compared with the average values for Japanese. Moreover, the head parts of our child models were compared with child head models which were developed based on the MRI data of European children. The anatomical and physical details of developed child models and SAR characteristics are demonstrated in this presentation.

REFERENCES

1. NIBH, Human body dimensions data for ergonomic design, *Research Institute of Human Engineering for Quality Life*, Tokyo, Japan (1996).
2. T Nagaoka, et al., "Development of realistic high-resolution whole-body voxel models of Japanese adult males and females of average height and weight, and application of models to radio-frequency electromagnetic-field dosimetry," *Phys. Med. Biol.* , Vol.49, pp.1-15, 2004.

FDTD Calculation of Temperature-Rise in Human Body for Far Field Exposure at ICNIRP Reference Level

T. Asano A. Hirata, and **O. Fujiwara**

Nagoya Institute of Technology, Japan

There has been increasing public concern about adverse health effects of human exposure to electromagnetic (EM) waves. In the radio frequency (RF) region, the heat evolved by EM absorption is known as a dominant factor to induce physiological effects. According to the ICNIRP (International Commission on Non-Ionizing Radiation Protection) safety guidelines, whole-body average specific-absorption-rate (SAR) is being used as a measure of basic limit for radio frequency (RF) far-field exposure. The limit is 0.4 W/kg for occupational exposure or 0.08 W/kg for public exposure [1]. An incident electric /magnetic field or power density, which does not produce the EM absorption exceeding the above basic limit, is used as a reference level. EM absorption of the human body at the ICNIRP reference level shows the double-humped frequency characteristics: the first peak appears at several tens megahertz where whole-body resonance occurs and the second around 2 GHz caused by the increase of the reference level with the increase of the frequency.

In these circumstances, it is essential to investigate the temperature rise in the human body in the whole-body resonance and GHz regions. Firstly, the FDTD method is employed for calculating the SAR in the human body. Then, the temperature increase is calculated by solving a bio-heat equation, which governs the heat transportation in the human body. An algorithm is proposed for treating the blood flow temperature as variable. Note this constant blood temperature was used in most previous paper. For our computational results, it is found that temperature increases at the hypothalamus are comparable in the whole-body resonance and GHz frequency regions. The time evolutions of temperature increases, however, are different, which is caused by the difference of EM absorption mechanism in these frequency regions. The difference of temperature increases using proposed and conventional algorithms will also be presented at the conference.

Session 1P1
Young Scientists Research for Applied Electromagnetics

Design and Analysis of Dispersion Compensating Photonic Crystal Fiber Raman Amplifiers

S. K. Varshney, K. Saitoh, and **M. Koshiba**
Hokkaido University, Japan

An interest has been revived in silica based fiber Raman amplifiers (FRAs) after the successive fabrication and commercialized availability of high-powered laser diodes [1]. FRAs are one of the most key enabling technologies to upgrade the transmission bandwidth of the WDM networks. Because the spectral region where significant Raman gain occurs depends primarily on pump wavelength and power. On the other hand, photonic crystal fibers (PCFs), thin silica strands with running microscopic sized air-holes in cladding, have exaggerated interest to acts as a strong Raman gain media [2-5]. This is due to the fact that they offer a small modal effective area without doping the core of the fiber, giving high Raman gain efficiency. The precise control over the air-hole diameter d and lattice constant Λ can generate a suitable PCF structure with high negative dispersion characteristics, integrating the Raman amplification and dispersion compensation in a single module.

Here, we have investigated Raman amplification properties of a dispersion compensating photonic crystal fiber (DCPCF) over the C-band using a single pump. To accurately obtain the Raman gain efficiency of the DCPCF, highly efficient full-vectorial finite element method with curvilinear edge elements [6] is used. Further, set of Raman propagation equations are solved and thus the DCPCF is characterized in terms of its Raman performances such as gain, optical signal-to-noise ratio, double Rayleigh backscattering, and noise figure. The proposed DCPCF exhibits a high negative dispersion of -576 ps/nm/km at 1550 nm wavelength and shows peak Raman gain efficiency of 6.05 W^{-1}. km^{-1} at a frequency shift of 13.1 THz. Additionally, the fiber shows negative dispersion slope and thus causes coarse dispersion compensation over the range of operating wavelengths. The module comprised of 5.2-km long designed DCPCF, attains the high gain values (upto 21 dB) and noise figure of about 8.0 dB over the C-band. Figures 1 and 2 represent the Raman gain efficiency as a function of wavelengths for a pump of 1455 nm and net gain spectra for 5.2-km long DCPCF Raman amplifier.

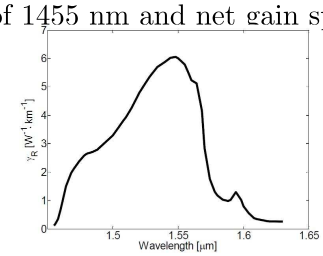

Figure 1: Raman gain efficiency as a function of wavelength for a pump of 1455 nm.

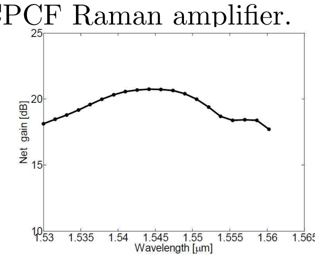

Figure 2: Net gain spectra for 5.2-km long DCPCF module.

REFERENCES

1. M. N. Islam, *Raman Amplification for Telecommunications 1* (Springer, 2003).
2. C.J.S. de Matos, K. P. Hansen, and J. R. Taylor, gExperimental characterization of Raman gain efficiency of holey fiber,h *Electron. Lett.*, 39, 424-425 (2003).
3. M. Bottacini, F. Poli, A. Cucinotta, and S. Selleri, gModeling of photonic crystal fiber Raman amplifiers,h *J. Lightwave Technol.*, 22, 1707-1713 (2004).
4. Shailendra K. Varshney, K. Saitoh, and M. Koshiba, gNumerical investigation of Raman properties of photonic crystal fibers,h Optical Amplifiers and Applications (OAA), August 7-10, 2005, Hungary.
5. Shailendra K. Varshney, K. Saitoh, and M. Koshiba, gRaman performances of ultralow loss photonic crystal fiber amplifiers,h CLEO/Pacific Rim, July 11-15, 2005, Tokyo, Japan
6. K. Saitoh and M. Koshiba, gFull-vectorial imaginary-distance beam propagation method based on a finite element scheme: application to photonic crystal fibers,h *IEEE J. Quantum Electron.*, 38, 927-933 (2002).

Cryogenic Tailoring of the Electrodynamic Properties in Superconducting Photonic Crystals: Realization of Tunable Metamaterial Platforms for THz Applications

N. J. Florous, K. Saitoh, and **M. Koshiba**
Hokkaido University, Japan

In the last decade, we have witnessed an ongoing interest in photonic crystals (PCs), which are artificially periodic structures exhibiting electromagnetic band-gaps [1]. Photonic crystals have evolved into a very promising approach for the ultimate control of the electromagnetic propagation into solid structures. Most of the unusual properties of PCs are based on the partial or complete existence of photonic band-gaps, a natural consequence of the structural underlying periodicity. Towards tunable PCs, it has already been proposed that PCs constructed with ferroelectric or ferromagnetic materials could be tuned by means of an external electric or magnetic field, respectively [2]. It was also proposed that PCs of the inverse opal type could be doped with a liquid crystal, where such a structure could be tuned by means of a localized electric field, as well as by a temporal modulation based on the Pockelfs effect [3]. The tunability of PCs with semiconducting constituents, have also been proposed recently.

It has been conjectured that devices along with unconventional switching mechanisms, such as the Josephson junctions associated with superconductors, will be necessary to achieve blistering speeds in supercomputing facilities. To this end the PC platforms with superconducting constituents is a very promising combination for the dynamic controllability of the electromagnetic power flow, since superconductors are known to be the most sensitive materials to external thermal fluctuations. However such a study has not been performed so far leaving the study of PCs with superconducting constituents an open problem in applied electromagnetics.

In this paper we use an extended analytical technique based on the Scattering Matrix Method (SMM) [4], to investigate the cryogenic properties of finite-sized superconducting PC circuits. Such tunable characteristics of a PC circuit are demonstrated in Fig. 1. As a superconducting material we assume high-Tc superconducting cylinders of the type: $Bi_{1.85}Pb_{0.35}Sr_2Ca_2Cu_{3.1}O_y$ with parameters: $\lambda_L(0) = 23.5\mu$m, and $T_c = 107K_o$ [5], arranged in such a way as to form a sharp waveguide bent. From Fig. 1 we can clearly observe the highly tunable characteristics of such a PC circuit based on a superconducting metamaterial platform, obtained by varying the external temperature.

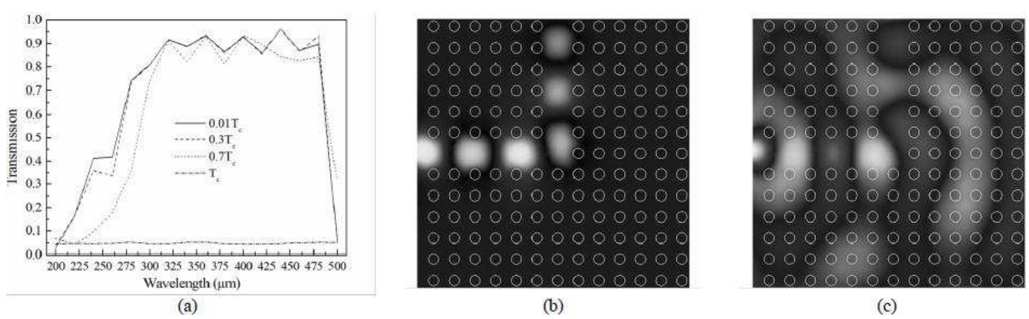

Figure 1: (a) Transmission characteristics as a function of the wavelength at various temperatures. Norm of the electromagnetic field (EM) distribution for $\Lambda = 385\mu$ m at (b) T=0.15Tc, and (c) $T = 0.85T_c$. Notice the strong delocalization of the EM field distribution as the temperature approaches the superconductor's critical temperature-Tc near which, the metamaterial platform is almost transparent to the EM field.

REFERENCES

1. J. D. Joannopoulos, R. D. Meade, and J. N. Winn, Photonic Crystals: Molding the Flow of Light. Princenton, NJ: Princeton Univ. Press, Sept. 1995.
2. A. Figotin, Yu. A. Godin, and I. Vitebsky, gTwo-dimensional tunable photonic crystals,h *Phys. Rev. B.*, vol. 57, pp. 2841-2848, Feb. 1998.
3. H. Takeda, and K.Yoshino gTunable photonic band gaps in two-dimensional photonic crystals by temporal modulation based on the Pockels effect,h *Phys. Rev. E.*, vol. 69, pp. 16605-16608, Jan. 2004.
4. N. Florous, and M. Koshiba, gRigorous scattering matrix method for the analysis of electromagnetic wave propagation in photonic crystal waveguides,h International Conference on Computational Electromagnetics and its Applications, ICCEA-2004, Beijing-China, Nov. 2004.
5. P. Poole, Superconductivity, Academic Press, San Diego, 1995.

Spectral Considerations About 2D Paraxial and Non-Paraxial Beam Solutions

R. M. Isla and **M. J. G. Morales**
ETSIT Universidad de Valladolid, Spain

Theoretical and applied research in beam fields has been focused onto the very well-known paraxial beam solutions named "Gaussian Beams". This has happened, in part, because of the fact that the Fourier Transforms of gaussian distributions are gaussian distributions as well. In this paper, it is showed that the plane wave spectra of beam solutions without any restriction is also a very simple distribution, the plane wave spectra of gaussian beams have, at least, the same problems as the full-space beam solutions.

We start from the beam field generated by the complex source method [3,4] as the beam field. The time dependence is with $e^{-i\omega t}$. Let the field be the electric field. This field is refered as Complex Beam (CB).

$$\vec{E}_{CB}(x,y) = \hat{z}\frac{i}{4}H_0^{(1)}(k_0 R) \tag{1}$$

where $R = \sqrt{x^2 + (y - ib)^2}$ and $b > 0$. It is shown [4] that the High Frequency Far Field condition and paraxial approximation lead to the Gaussian beam solution(GB):

$$\vec{E}_{GB}(x,y) = \hat{z}\frac{e^{i\frac{\pi}{4}}}{2\sqrt{2\pi}}\frac{e^{k_0 b}e^{-\frac{x^2}{w^2(y,b)}}e^{ik_0(y+\frac{x^2}{2\mathcal{R}(y,b)})}}{\sqrt{k_0(y-ib)}} \tag{2}$$

where $w(y,b) = \sqrt{(2b/k)(1 + y^2/b^2)}$ is the beam width and $\mathcal{R}(y,b) = (b^2/y)(1+y^2/b^2)$ is the curvature radius of the beam phase front. The 2D plane wave spectrum [2] can be easily calculated for the last expressions. For the complex beam, the plane wave spectrum is found to be through the integral representation of the zeroth-order Hankel function of the first kind [1,2]:

$$P_{CB}(\beta) \propto e^{k_0 b \sin(\beta)} \tag{3}$$

And for the gaussian beam, the plane wave spectrum is found via Fourier Transform of the field evaluated in $y = 0$ and its relationship among the plane wave representation of a generic 2D field (the 2D plane wave spectrum is not the Fourier Transform of the electric field).

$$P_{GB}(\beta) \propto \sin(\beta)e^{k_0 b - \frac{k_0}{2b}\cos^2(\beta)} \tag{4}$$

Interpretation of the results and a comparison between them will be done. We have previous knowledge about the validity of the gaussian beam at its minimum width [4]. In this way, it is possible to track the paraxial condition for several values of parameter b in the spectral domain. Other conclusions involving the currents that generate the beam fields will be also presented.

REFERENCES

1. M. Abramowitz and I. A. Stegun, editors. Handbook of Mathematical Functions. Dover Publications Inc, New York, 9 edition, 1970.
2. P. C. Clemmow. The Plane Wave Spectrum Representation of Electromagnetic Waves. Oxford University Press & IEEE Press, Oxford & New Jersey, 1 reissued edition, 1996.
3. L. B. Felsen. Complex source point solutions of the field equations and their relations to the propagation and scattering of gaussian beams. Symposia Mathematica, 18:39.56, 1976.
4. E. Gago-Ribas, M. J. González Morales, and C. Dehesa MartL.nez. Analytical parametrization of a 2d real propagation space in terms of complex electromagnetic beams. *IEICE Transactions on electronics*, E80-C(11):1434.1439, 1997.

Miniaturized LTCC Lumped-Element Transmission Line and Its Applications

Y. S. Lin
National Central University, Taiwan

K. M. Li
Chi-Mei Communication System Inc., Taiwan

Quarter-wavelength ($\lambda/4$) transmission lines are widely used as building blocks for RF/microwave passive component designs such as power dividers and hybrid couplers. At low frequencies, a $\lambda/4$ line is quite long. Therefore, the miniaturization of transmission line is crucial for size reduction of RF/microwave passive components. Conventionally, size reduction of the transmission line can be accomplished by using lumped inductors and capacitors to realize the T- or π-equivalent circuits of transmission line. However, these equivalent-circuit models may only be considered as equivalents to transmission lines in a very narrow bandwidth. To expand the applicable frequency range, the modified-T equivalent-circuit may be adopted. It is accomplished by introducing a small positive mutual inductance L_M between the two series inductors L_s in a conventional T-equivalent circuit of a transmission line, along with a coupling capacitor Cp between the input and output ports. The positive mutual inductance L_M will in effect increase the magnitude of shunt impedance to ground at higher frequencies. In addition, the series capacitor C_p will provide a proper signal path at higher frequencies between the input and output ports. Therefore, lower insertion loss at higher frequencies may be obtained compared to the conventional T-equivalent circuit, and the bandwidth of the transmission-line equivalent is much expanded. Given the required characteristic impedance and electrical delay, the element values in the modified-T equivalent-circuit can be obtained analytically.

In this study, by taking advantage of the multi-layered low temperature co-fired ceramic (LTCC) substrate, the modified-T equivalent-circuit may be conveniently realized in a very compact circuit area. Here, the two series inductors L_s are realized by spiral metal strips L_a and L_b. The spiral inductors L_a and L_b are stacked-up vertically and the orientations of them are designed in the same sense, such that a positive mutual inductance $L_M$is established between them. The coupling capacitor C_p is also conveniently formed between the two spiral inductors in this way. The shunt capacitor $C_s$is implemented by the sandwich-type metal plates and the bottom ground plane. Due to the vertical arrangement of circuit elements and the utilization of mutual coupling, the resulted circuit may achieve a very compact size while maintaining a frequency response close to that of a transmission line for a wide frequency range. Specifically, a LTCC lumped-element transmission-line is designed with a characteristic impedance of 50ohm and an electrical length of 90o at about 1.8 GHz. The measured insertion loss is less than 0.5dB up to 6GHz, and the measured return loss is better than 20dB up to 5.5GHz. The circuit area occupied by this LTCC lumped-element transmission-line is $1mm \times 1mm$, which is only about ($\lambda/65$) ($\lambda/65$). In addition, the proposed LTCC lumped-element transmission-line is also implemented in the design of a miniaturized Wilkinson power divider. By employing the proposed lumped-element transmission-line in LTCC circuit/module designs, the circuit/module size can be reduced significantly while maintaining good performance in a wide frequency band.

Application of LOD-FDTD Methods to Optical Waveguide Analyses

J. Shibayama, M. Muraki, R. Takahashi, J. Yamauchi, and **H. Nakano**

Hosei University, Japan

The performance of the implicit finite-difference time-domain methods (FDTDs) for the analyses of optical waveguides is compared with that of the traditional explicit FDTD. For the implicit methods, the alternating-direction implicit (ADI) FDTD [1], [2] and the envelope ADI-FDTD [3] are investigated. In addition, a recently developed LOD-FDTD [4] and its envelope version are presented and discussed.

Numerical dispersion analysis is performed for each method, demonstrating the improved dispersion properties of the envelope ADI- or LOD-FDTD. Numerical results of a waveguide grating [5] reveal that the wavelength responses obtained from the ADI- or LOD-FDTD gradually shift toward a longer wavelength, as the time step (Δt) is increased. For the envelope ADI- or LOD-FDTD with $\Delta t = 8\Delta t_{\mathrm{CFL}}$, in which Δt_{CFL} is determined by the stability criterion, the response is in good agreement with that of the FDTD, showing the comparable CPU time to that of the FDTD.

Furthermore, we calculate the wavelength response of a waveguide with high reflection coatings [6]. For this model, small spatial sampling widths are required to obtain desired accuracy. As a result, the CPU times of the envelope LOD-FDTD with $\Delta t = 16\Delta t_{\mathrm{CFL}}$ and $32\Delta t_{\mathrm{CFL}}$ are reduced to 50% and 25%, respectively, of the CPU time of the FDTD, while maintaining comparable accuracy.

REFERENCES

1. T. Namiki, "A new FDTD algorithm based on alternating-direction implicit method," *IEEE Trans. Microwave Theory Techniques*, vol. 47, no. 10, pp. 2003-2007, 1999.
2. F. H. Zheng, Z. Z. Chen, and J. Z. Zhang, "A finite-difference time-domain method without the Courant stability conditions," *IEEE Microwave Guided Wave Letters*, vol. 9, no. 11, pp. 441-443, 1999.
3. H. Rao, R. Scarmozzino, and R. M. Osgood, Jr., "An improved ADI-FDTD method and its application to photonic simulations," *IEEE Photon. Technol. Lett.,* vol. 14, no. 4, pp. 477-479, 2002.
4. J. Shibayama, M. Muraki, J. Yamauchi, and H. Nakano, "Efficient implicit FDTD algorithm based on the locally one-dimensional scheme," *Electron. Lett.*, vol. 41, no. 19, pp. 1046-1047, 2005.
5. J. Shibayama, M. Muraki, J. Yamauchi, and H. Nakano, "Comparative study of several time-domain methods for optical waveguide analyses," *IEEE/OSA J. Lightw. Technol.*, vol. 23, no. 7, pp. 2285-2293, 2005.
6. J. Yamauchi, S. Sasaki, and H. Nakano, "Pulse excitation scheme for the analysis of wide-band characteristics of optical waveguides," *IEEE Photon. Technol. Lett.*, vol. 17, no. 2, pp. 357-359, 2005.

Computation of Scattering from Randomly Distributed Dielectric Circular Cylinders

N. Nakashima and **M. Tateiba**
Kyushu University, Japan

Multiple scattering by many random particles has been theoretically studied. In order to deal with random media composed of several kinds of particles in shape, size and material, we consider computational analysis as a suitable method and use a Monte Carlo simulation. As the first step, this paper treats electromagnetic (EM) wave scattering from randomly distributed cylinders. Fast techniques are presented and applied to the computation of scattered near and far fields from a realization of random medium. Numerical results provide the normalized average power density for the coherent component and incoherent components of scattered fields.

Let us consider the two-dimensional problem of EM wave scattering by infinitely long dielectric cylinders. We formulate this problem in an integral equation form and discretize it into a linear system of equations by means of the boundary element method. The linear system is numerically solved by a Generalized Minimal Residual (GMRES) method with our acceleration techniques: a fast multipole algorithm (FMA) and two-step preconditioning (TSP). The FMA expedites matrix-vector product in iterative process. This algorithm is similar to the Multilevel Fast Multipole Algorithm (MLFMA) but differs in the computation stages. TSP is composed of two preconditionings: Half Reduction and block Jacobi. Half reduction preconditioning is based on the idea of the Schur complement of lower half of coefficient matrix and reduces the number of unknowns for the linear system in half. Block Jacobi preconditioning accelerates convergence of an iterative process.

As numerical examples, we consider scattering from 4225 cylinders in a square region whose fractional volume is 0.1. The radii, relative permittivities and relative permiabilities of cylinders are all the same and assumed as $k_a = 1.0$, $\epsilon_r = 2.0$ and $\mu_r = 1.0$, respectively. Here, k is the wavenumber of background medium. We first show the normalized power density for far and near scattered field from regularly placed cylinders. Next, we prepare 100 realizations of random medium and compute far and near scattered fields for them. Then we show the normalized average power density for the coherent and incoherent component of far and near scattered fields. Through these results, the characteristics of scattered fields by random medium are discussed. Moreover, we show the reduction of computation time and the amount of used memory by using two fast techniques.

Application of CIP Method to Electromagnetic Field Analysis for Numerical Dosimetry of Electromagnetic Field Expoure

K. Sasaki, Y. Suzuki, and **M. Taki**
Tokyo Metropolitan University, Japan

Finite-Difference Time Domain (FDTD) method has been widely used for dosimetry in electromagnetic field exposure because of its simple algorithm. However, ordinary FDTD method needs elaborate absorption boundary condition and numerical diffusion and dispersion do not avoid in case of treating wide band waveform. As one of technique to improve matters mentioned above, we propose application of Cubic-Interpolated Propagation (CIP) scheme [1] to electromagnetic field analysis for numerical dosimetry. CIP scheme has been developed in the field of computational fluid dynamics and has nature of good flux conservation as one of flux-corrected transport scheme. Recently, CIP scheme is applying to electromagnetic wave propagation in the heterogeneous lossy medium [2].

The purpose of this study is to apply CIP solver to analyses including biological tissue equivalent dielectric medium which has approximately 1 to 50 relative permittivity at few GHz [3]. We examine 1D problem to confirm availability of this method. The calculation condition is as follows. The analysis region is $0 \leq z \leq 2$ m. Mesh size Δz and time step Δt is 5.0×10^{-3} m and 2.0×10^{-12} s, respectively. Relative permittivity from 1 to 100 are given within the region $1 \leq z \leq 2$ m. A period of 1 GHz sinusoidal wave is given in the region of $0 \leq z < 1$ m as an initial condition of $t = 0$ s , and is advected to positive direction along z axis. Amplitude of reflection and transmission wave are observed with sweeping relative permittivity. It is found that ordinary CIP scheme do not deal with such a wide range of relative permittivity, because errors from exact solution is very large in case of $\varepsilon_r > 5$. To improve behavior of solution, velocity of wave is averaged in the vicinity of boundary of medium. When this process is adopted for CIP scheme, numerical solutions are significantly improved. We obtain prospect of application of CIP scheme to dosimetry as for electromagnetic field exposure.

REFERENCES

1. T. Yabe and T. Aoki: gA universal solver for hyperbolic equations by cubic-polynomial interpolation I. One-dimensional solverh, *Comp. Phys. Comm.* 66, pp.219-232 (1991).
2. S. Watanabe and O. Hashimoto: gAn examination about method for analyzing electromagnetic field using CIP method considering lossy dielectric and magnetic materialsh, *IEICE Trans. Elec.* (Japanese Edition), Vol.J88-C, pp568-569, (2005), in Japanese
3. S. Gabriel, R. W. Lau, and C. Gabriel: gThe dielectric properties of biological tissues: III. Parametric models for the dielectric spectrum of tissuesh, *Phys. Med. Biol.*, 41, pp. 2271—2293 (1996)

Performances of a RFID Antenna Using a Biological Tissue-Equivalent Solid Phantom

D. Ochi, M. Takahashi, and **K. Ito**
Chiba University, Japan
K. Uesaka
Hitachi, Ltd., Japan

In recent years, radio frequency identification (RFID) is becoming a widely used technology. For example, RFID tags are used for logistics, person authentication, electronic money, etc. In case a RFID tag is stuck to a human, the human body affects the characteristics of the antenna.

This time, the authors simulated a RFID antenna with a human body using the finite difference time domain method. Figure 1 shows the structure of the simulated antenna. The dimension of the antenna is 53 1.5 0.045 mm3. It is composed of an aluminum sheet and a polyethylene terephthalate sheet. We put the IC chip on the feeding point, in order to communicate with a RFID reader. The IC chip is a -chip fabricated by Hitachi, Ltd. The operating frequency of the antenna is fixed to 2.45 GHz which is one of the industrial, scientific and medical frequency. The antenna is stuck to the arm of a human. In this simulation, the model for the arm is a simplified structure, simulated by a biological tissue-equivalent solid phantom. The phantom has a rectangular shape measuring $450 \times 50 \times 50\ mm^3$. The antenna characteristics are obtained by numerical calculation. We investigated two calculation models, which are the antenna with and without the human body, respectively, and considered the differences in the numerical simulations. As a result, we confirm that the antenna can be use with the human body.

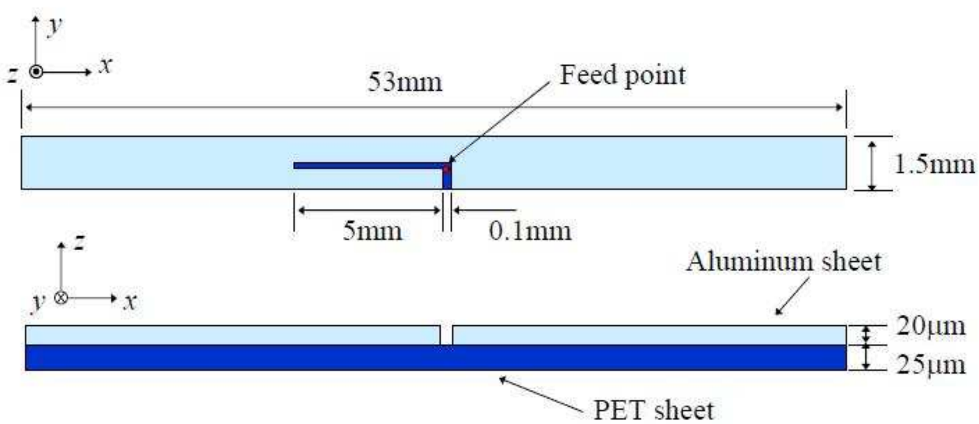

Figure 1: Structure of the antenna

Review of Thermal Elevation Due to Handset Antennas

A. Hirata [1], **O. Fujiwara** [1], and **T. Shiozawa** [2]

[1]Nagoya Institute of Technology,Japan
[2]Chubu University,Japan

In recent years, there has been an increasing public concern about the health implications of electromagnetic (EM) wave exposure with the use of mobile telephones. Therefore, public organizations have established safety guidelines/standards for EM wave absorption. For RF near field exposures, these standards are based on the spatial peak SAR (specific absorption rate) for any 1 or 10g of body tissue. However, one of the dominant factors which induces physiological effects and damage to humans due to EM wave exposures is the temperature increases. A temperature increase of 4.5^oC in the brain has been noted to be an allowable limit which does not lead to any physiological damage (for exposures of more than 30 minutes). Additionally, the threshold temperature of the pricking pain in skin is 45^oC, corresponding to the temperature increase of $10 - 15^oC$. Thus, several groups have investigated the temperature increase in the head due to handset antennas. Note that different averaging scheme and mass are used for each guideline/standard. In view of these circumstances, the relation between peak spatial-average SAR and temperature increase is of great interest. The authors have statistically investigated the correlation between peak SAR and maximum temperature increase in [1]. Then, they were found to be reasonably proportional to each other, while these distributions are different, which was attributed to heat diffusion. This result implies the effectiveness of peak spatial-average SAR as a measure for predicting maximum temperature increase in the human body. The effect of averaging mass and scheme on this correlation is explained in terms of Greenfs function for the bio-heat equation, which governs the heat transport in the human body.

REFERENCES

1. A. Hirata and T. Shiozawa, gCorrelation of maximum temperature increase and peak SAR in the human head due to handset antennas,h *IEEE Trans. Microwave Theory & Tech.*, vol.51, no.7, pp.1834-1841, Jul. 2003.

Static Stability and Plate Spacing for Diamagnetic Levitating Magnets

J. N. Ho
University of Washington, U.S.A.

W. C. Wang
University of Washington, U.S.A.

This paper analyzes the static stability of a diamagnetic levitating magnet. Balancing forces is necessary but does not guarantee stable levitation. Restoring forces (minimizing potential energy) of a levitating magnetic around the zero force point is also required. An equivalent statement is that any small displacement from the zero force point causes the magnet to return to the zero force point. A derivation using this concept gives a stability criterion for cylindrical levitating magnets. The criterion controls the spacing of the diamagnetic plates needed to stably levitate a magnet. This was verified by experiments using regular graphite and pyrolitic graphite plates. When adjustment for plate thickness is included, theoretical stability requirements and experimental results match well.

Session 1P2
Scattering by Canonical Objects

Effect of the Interface Separating a Homogeneous Medium and a Photonic Crystal

R. Pierre, B. Gralak, T. Decoopman, G. Tayeb
S. Enoch and **D. Maystre**
CNRS, Institut Fresnel, France

The concept of negative index materials has been introduced by V. G. Veselago [Sov. Phys. Usp. **10**, 509 (1968)]. J. B. Pendry remarked that such materials should permit to realize a new flat lens with, a priori, unlimited resolution [Phys. Rev. Lett. **86**, 3966 (2000)]. Although there is some controversial discussion about the negative index materials, it is clear that the amplification of the evanescent waves induced by this class of new materials will have very important applications for subwavelength imaging, as well as for light trapping [S. Guenneau *et al.*, Optics letters **30**, 1204 (2005)]. And now, the challenge is to design composite structures presenting properties as close as possible to the ones of negative index materials.

Periodic structures made of metallic wires or "double C resonators" possess some properties similar to the desired ones. However, the relevance of these metallic structures should decrease if the "visible domain" (when the wavelength is smaller than $1.5\mu m$) is considered. Indeed, at these wavelengths, absorption takes place in metals and fabrication becomes difficult since these structures are used in the "homogeneization domain" (when the dimensions of the unit cell of the periodic structure are much smaller than the wavelength). Purely dielectric periodic structures, the second kind of structures expected to mimic negative index materials, do not suffer from absorption and present interesting properties in the "resonance domain" (when the dimensions of the unit cell of the periodic structure are similar to the wavelength). Since very important applications are expected in the visible domain, this communication is devoted to dielectric periodic structures.

Determination of effective properties of dielectric structures working in the resonance domain is a difficult task. It is then convenient to separate the general concept of negative index materials in three phenomena: negative refraction, effect of the "cut interface" (*i. e.* the interface separating a periodic structure and an homogeneous medium), and amplification of evanescent waves. Negative refraction with photonic crystals is now a well-known phenomenon: it has been predicted [B. Gralak *et al.*, J. Opt. Soc. Am. A **17**, 1012 (2000)] and then demonstrated in experiments [E. Cubukcu *et al.*, Nature **423**, 604 (2003)]. From our knowledge, the effect of the "cut interface" has been slightly studied from an empiric way and is not clearly understood. Also from our knowledge, the amplification of the evanescent waves has not been studied.

In this communication, we consider one-dimensional periodic structures in order to take advantage of their simplicity which permits to use a new theoretical method. This method starts with the definition of the reflection coefficient on a one-dimensional crystal, denoted by r_c. As a second step, we consider a simple structure with properties as close as possible to the ones of the one-dimensional crystal: this equivalent structure is a homogeneous medium with permittivity ε_a and permeability μ_a chosen such that they provide the same dispersion law as the one inside the crystal. The equivalent homogeneous medium is then in general anisotropic, and the reflection coefficient on it is denoted by r_a. Finally, the identification $r_a = r_c$ of the two reflection coefficients provides an analytic expression of the equivalent permittivity and permeability of the crystal.

We first show that the equivalent permittivity and permeability take in general complex values: and we show that these quantities are purely real in the case where the unit cell of the one-dimensional periodic structure is symmetric with respect to a horizontal plane. We then have restricted the possibilities for the "cut interface" from the obtained analytical expressions. We also show that the equivalent permittivity and permeability present very small variations with the wave vector. We have shown that the effective properties for the evanescent waves are the same as the ones for propagating waves. Finally, numerical examples are shown in the case of two-dimensional structures.

Scattering by a Finite Grating on a Substrate

E. Marx
National Institute of Standards and Technology, U.S.A.

The integral equations that are used to determine the fields scattering of a strip on a substrate [1] can be applied to the problem of scattering by a number of similar or identical strips on a substrate, which amounts to a finite grating. Thus, the scattering patterns and microscope images of a finite number of lines, such as eight or 21, can be compared to those of an infinite grating. The latter can be obtained using similar integral equations [2] or the rigorous coupled-wave analysis method [3].

For a single plane wave incident on a finite grating, the far-field distribution of scattered field intensity as a function of angle can be determined by integration of the boundary functions that are computed using the integral equations. Essentially, this distribution consists of a series of lobes [4] centered about the directions given by the grating equation for scattering by an infinite grating. The energy flux in a lobe is proportional to that scattered in a particular direction for an infinite grating, and it depends on the shape of the strip or line. The exception is the zeroth-order lobe, which does not contain the energy reflected by the substrate, which in the finite grating is a plane wave that cannot be added directly to the cylindrical scattered waves.

Microscope images obtained using a set of incident waves that form an illumination cone of small aperture are similar to those obtained for infinite grating, especially for the central lines. These simulated images can be compared to those obtained for infinite gratings by assuming that the series of lines is infinite and that the central line can be used to obtained the coefficient for a Fourier series.

In computer codes developed to simulate the scattering of finite gratings, the number of lines is limited by the memory required in a point-matching calculation to represent correctly all the lines. If the behavior of the unknown divergent surface functions near edges of the lines, the number of points required to represent these functions could be reduced and the number of lines could be increased. The shape of each line is assumed to be an arbitrary rhomboid, although this is not an essential limitation of the codes.

Both the intensity distribution for the far fields and the microscope images will be shown for representative examples taken from work done for the semiconductor industry. Of special practical interest are the lines of dimensions that are significantly smaller that the wavelength of the light used to illuminate the grating.

REFERENCES

1. E. Marx, "Scattering by an Arbitrary Cylinder at a Plane Interface: Broadside Incidence," *IEEE Trans. Antennas Propagat.*, vol. 37, pp. 619-628, 1989.
2. D. Maystre, "Integral methods," in Electromagnetic Theory of Gratings, R. Petit, Ed. Berlin: Springer Verlag, ch. 3, 1980.
3. M. G. Moharam, E. B. Grann, D. A. Pommet, and T. K. Gaylord, "Formulation for stable and efficient implementation of the rigorous coupled-wave analysis of binary gratings," *J. Opt. Soc. Am. A*, vol. 12, pp. 1068-1076, 1995.
4. P. Beckmann and A. Spizzichino, The Scattering of Electromagnetic Waves from Rough Surfaces, New York: Pergamon, ch. 4, 1963.

Rigorous Study of Electromagnetic Transmission through a Rectangular Aperture in a Perfectly Conducting Screen

H. Serizawa
Numazu National College of Technology, Japan
K. Hongo
Toho University, Japan

Transmission of electromagnetic waves through a rectangular aperture has received considerable attention and has been studied by a variety of methods [1-4]. However, rigorous results of transmission coefficients have not yet been provided. In this paper, we rigorously study the transmission of electromagnetic plane wave through a rectangular aperture in a perfectly conducting infinite screen by using the method of the Kobayashi potential (KP) [5]. It is assumed that the screen has infinitesimal thickness and coincides with the plane z=0 in the Cartesian coordinates (x, y, z), and the incident plane wave exists in the half-space z¿0. The purpose of the study is to obtain reference data of the transmission coefficient and clarify its dependence on various parameters, such as an aperture size and incident angle of the plane wave.

The procedure of the present method is summarized as follows. We use the two-dimensional Fourier spectral representation of the vector potentials for the diffracted fields in both regions of half-spaces (the integrands are the elementary solutions to the three-dimensional wave equation in a Cartesian coordinate system). Enforcement of the required boundary conditions leads to the dual integral equations, which can be solved by applying the discontinuous properties of the Weber-Schafheitlin (WS) integrals and the concept of the projection (the basis functions of the functional space are the Jacobi's polynomials). In this process, the diffracted fields in each region are expressed by a linear combination of wave functions that satisfy the boundary condition on the conducting screen and the proper edge condition, that is, the fields have singularities at edges. Finally, the problem is reduced to the matrix equations whose matrix elements are infinite integrals that include four Bessel functions. These integrals can be computed with desired accuracy by applying the asymptotic expansion of the Bessel function. Once the expansion coefficients are determined by solving the matrix equations, physical quantities such as the radiation pattern and aperture fields can be readily obtained from their concise expressions. There may be two possibilities to obtain the transmission coefficient. One way is to integrate the radiated power over the hemi-sphere (z¡0), and the other is to use the simpler forward scattering theorem [6]. We use the latter idea, that is, we only use the forward-scattered field to calculate the transmission coefficient. Using a rigorous solution derived by the KP method, we show the dependence of the transmission coefficient on the dimension of the aperture, on the incidence angle of the plane wave, and on the polarization of the incident wave.

REFERENCES

1. C. Huang, R. D. Kodis, and H. Levine, "Diffraction by apertures," *J. Appl. Phys.*, vol. 26, pp. 151-165, 1955.
2. R. F. Harrington and J. R. Mautz, "Electromagnetic transmission through an aperture in a conducting plane," *AEU*, vol. 31, no. 2, pp. 81-87, 1977.
3. C. M. Butler and K. R. Umashankar, "Electromagnetic penetration through an aperture in an infinite planar screen separating two half-space of different media," *J. Appl. Phys.*, 1976.
4. R. Leubbers and C. Penney, "Scattering from apertures in infinite ground planes using FDTD," *IEEE Trans. Antennas Propagat.*, vol. 42, no. 5, pp. 731- 736, May 1994.
5. K. Hongo and H. Serizawa, "Diffraction of electromagnetic plane wave by a rectangular plate and a rectangular hole in the conducting plate," *IEEE Trans. Antennas Propagat.*, vol. 47, no. 6, pp. 1029-1041, Jun. 1999.
6. J. J. Bowman, T. B. A. Senior, and P. L. E. Uslenghi, *Electromagnetic and Acoustic Scattering by Simple Shapes,* Amsterdam: North-Holland, 1969.

Diffraction of Electromagnetic Plane Wave by an Impedance Strip and a Slit in an Impedance Plane

K. Hongo

Toho University, Japan

A. Imran and **Q. A. Naqvi**

Quaid-I-Azam University, Pakistan

Electromagnetic plane wave diffracted by a slit in an impedance plane and, its complementary problem, scattered by an impedance strip are formulated rigorously in the form of dual integral equations (DIE). The solution of a part of the DIE is constructed by applying the discontinuous properties of the Weber-Schafheitlinfs integrals. We assume that the electromagnetic field is finite at the edge. Using the projection solves the remaining equation of the problem reduces to matrix equation. The matrix elements are given in terms of infinite integrals that contain the poles for special values of surface impedance and these integrals can be numerically. For comparison we derive the physical optics (PO) approximate solutions for slit and strip problems by applying the equivalent current method. We find that a simple relation exists between the slit and strip solutions. We compute far diffracted patterns for various widths and angles of incidence and compared them with the corresponding the PO solution. The agreement is fairly good.

Nullification Theorem for the Sommerfeld Integral in the Theory of Electromagnetic Scattering by Impedance Wedges

A. Osipov
DLR Microwaves and Radar Institute, Germany

The Sommerfeld integral is a plane wave expansion of solutions of the Helmholtz equation in the cylindrical coordinate system. This expansion is, therefore, particularly suitable for representing fields in wedge-shaped domains. The spectra, which describe the amplitudes of the partial plane waves in the expansions, are found from boundary conditions on the faces of the wedge. Inserting the Sommerfeld integrals into the boundary conditions leads to homogeneous integral equations of the first kind, and to find their solution, one invokes the nullification theorem 1 which states that

$$\int_{\gamma_+} e^{-ik\rho\cos\alpha} f(\alpha) d\alpha = 0, \quad 0 \leq k\rho < +\infty$$

if $f(\alpha) = \sin\alpha \sum_{m=1}^{M} C_m \cos^m \alpha$ with arbitrary coefficients C_m, and γ_+ is the upper loop of the Sommerfeld integration contour.

The nullification theorem is, therefore, an integral part of any approach that uses the Sommerfeld integral to represent solutions of diffraction and scattering problems in wedge-shaped domains. The appearance of the arbitrary trigonometric polynomials in the functional equations for the spectra leads to undefined constants in the solution and, thus, jeopardizes uniqueness. The consequences of this fact have not been discussed in sufficient detail in the literature so far. This paper is intended to close this gap by looking at implications of the nullification theorem for the three types of problems involving impedance wedges: (a) normal incidence on an impedance wedge (the classical Maliuzhinets problem); (b) oblique incidence on impedance structures with the included wedge angle 0, $\pi/2$, π, and $3\pi/2$; (c) a wedge with higher-order impedance boundary conditions.

Even in the case of normal incidence on a wedge with the standard (first-order) impedance boundary conditions, a rigorous treatment of the problem should account for arbitrary polynomials with $M = 1$. The paper shows that these polynomials can be excluded from the analysis by considering solvability conditions for the functional equations satisfied by the spectrum and by exploiting the invariance of the Sommerfeld integral with respect to addition of an arbitrary constant to its integrand. All available solutions for the skew incidence case have used modified impedance boundary conditions of second order, and have apparently ignored the possibility that arbitrary polynomials with $M = 2$ may enter the functional equations for the spectra. The paper proves the correctness of these solutions by showing that they meet the standard form of the boundary conditions as well, for which the unknown constants can be set to zero. A further class of problems, in which the nullification theorem plays a key role, is the case of impedance boundary conditions of the order higher than 1. Solutions of such problems necessarily include undefined constants, and to obtain a unique solution, one has to impose additional conditions which, for example, may have the form of certain relations between field components at the edge of the wedge (contact conditions). In contrast to mathematically related problems of diffraction of sound waves by angular junctions of thin elastic plates, where the contact conditions have a clear physical meaning, formulation of contact conditions in electromagnetics is a complicated and still unsolved problem.

REFERENCES

1. G.D. Maliuzhinets, "Inversion formula for the Sommerfeld integral," *Sov. Phys. Doklady*, **3**, pp. 52–56, 1958.

New Numerical Experiments in Scattering by Dielectric Wedges

E. Marx
National Institute of Standards and Technology, U.S.A.

When a plane wave is incident on a dielectric wedge of infinite cross section, some of the components of the fields near the edge of the wedge diverge, following a negative fractional power law of the distance from the edge. The same behavior is expected of fields near the edge of a wedge of finite cross section or of sharp edges in other scatterers. One can use singular integral equations (SIEs) [ ] or hypersingular integral equations (HIEs) [ ] to investigate the behavior of the field components near the edge of a dielectric wedge. The unknown boundary functions in the single-integral-equation method also diverge near the edge. If the rate of the divergence could be firmly established, this behavior could be built into the form of the function and there would be no need to concentrate patches near an edge in the numerical solution of a problem. For a dielectric wedge, power series solutions [,] indicate that the behavior remains essentially that of static fields, determined by the permittivity and permeability of the wedge material, that of the surrounding medium, usually assumed to be free space, and the angle of the wedge. For oblique incidence, this means that the behavior of the fields should be that of the TE and TM modes [,]. Numerical experiments with a finite dielectric wedge show disagreements between the computed and the expected behavior. For the HIE, the unknown boundary functions remains constant near the edge and the numerical difficulties come from the highly singular behavior of the kernel.

Agreement with the expected behavior occurs only for particular directions from the edge for TE and TM modes. The theory fails to indicate where the expected asymptotic behavior sets in, if at all; this usually occurs at a small fraction of the wavelength. For oblique incidence, the behavior of the fields near the edge depends on the direction of incidence, polarization, and the direction of approach to the wedge, which is not the case for the static fields. Some of the results depend on the approximations used in the numerical solution of the problem, especially for the SIE. There is also a dependence of the amplitude of the fields on the size of the finite wedge, which may be due to the overall scattering cross section of the wedge. The difficulty of matching two waves propagating at different speeds in different media on the two sides of a dielectric wedge as well as in the outside medium on the continuation of the sides suggests that there may be no general rigorous solution for this scattering problem. For perfectly conducting wedge, where the fields on one side of the boundary vanish, there is good agreement between the predicted and computed behavior of the field components.

REFERENCES

1. E. Marx, "Computed Fields Near the Edge of a Dielectric Wedge," *IEEE Trans. Antennas Propagat.*, vol. 38, pp. 1438-1442, 1990.
2. E. Marx, "Electromagnetic Scattering from a Dielectric Wedge and the Single Hypersingular Integral Equation," *IEEE Trans. Antennas Propagat.*, vol. 41, pp. 1001-1008, 1993.
3. J. Meixner, "The Behavior of Electromagnetic Fields at Edges," *IEEE Trans. Antennas Propagat.*, vol. 20, pp. 442-446, 1972.
4. G. I. Makarov and A. V. Osipov, "Structure of Meixner's Series," *Radio Phys. Quantum Electron.*, vol. 29, pp. 544-549, 1986.
5. C. Bergljung and S. Berntsen, "Diffraction by a Dielectric Wedge at Skew Incidence," Q. Jl. *Mech. appl. Math.*, vol. 54, pp. 549-583, 2001.
6. A. V. Osipov, "Analysis of Electromagnetic Diffraction by Wedges with the Method of Edge Functions," Proceedings of the General Assembly of URSI, Maastricht, The Netherlands, paper #1235, 2002.

Canonical Solutions for Scattering by Penetrable Wedge Structures

P. L. E. Uslenghi
University of Illinois at Chicago, U.S.A.

The scattering of electromagnetic waves by wedges made of penetrable materials is a difficult boundary-value problem that cannot presently be solved exactly, except in very special cases. This work considers several special cases in which the solution is not only exact, but also in closed-form and coincident with the geometrical optics solution. If the structure contains more than one edge, then all edges are parallel to one another. The primary field is a plane wave (or waves) propagating in a direction perpendicular to all the edges of the wedge structure, that is, a two-dimensional problem is analyzed. In some cases involving isorefractive materials and/or specific metamaterials, it is possible to derive the exact solution at oblique incidence with respect to the edges from the solution at normal incidence. Some general rules are given that are satisfied in all cases considered and may be useful in discovering additional exact and closed-form solutions. In all cases when geometrical optics provides the exact solution, all edges of the structure do not scatter and all field components remain finite when the observation point approaches any one of the edges.

All the exact solutions that were found made use of one or more of the following properties: behavior of the fields at the surface of a perfect electric or perfect magnetic conductor; total transmission at Brewster's angle; isorefractive or isoimpedance properties of the materials filling the wedge regions. These properties may limit the validity of the solutions found to specific polarization and/or direction of incidence of the primary wave, and may require more than one penetrable wedge region and/or more than one primary wave to satisfy the boundary conditions. A notable exception is the case of a right-angle wedge made of a lossless double-negative material whose refractive index is the opposite of that of the space surrounding the wedge, whereas the intrinsic impedances of the two media are the same. Geometrical optics provides the exact solution for a plane incident wave of arbitrary polarization, for any angle of incidence within a ninety degrees sector that guarantees that both faces of the wedge are illuminated. This is the only exact and closed-form solution presently available for the scattering of a single plane wave by a single penetrable wedge.

Exact Scattering by Penetrable Paraboloidal Structures

P. L. E. Uslenghi
University of Illinois at Chicago, U.S.A.

The paraboloid of revolution is a unique three-dimensional shape that, in certain cases, permits an exact geometrical optics solution to the boundary-value problem when the primary field is a plane electromagnetic wave at axial incidence. The first of these solutions was obtained by C. E. Schensted in 1955 for a convex perfectly conducting paraboloid, and a second solution was obtained by Roy and Uslenghi in 1997 for a convex isorefractive paraboloid.

Recently, Liang and Uslenghi (IEEE-APS Intl. Symposium and URSI Meeting, Washington, DC, July 2005; URSI National Radio Science Meeting, Boulder, CO, January 2006) have obtained an exact geometrical optics solution for a convex paraboloidal structure made of any number of layers of isorefractive materials separated by confocal and coaxial paraboloids of revolution.

In this work, novel solutions are presented for paraboloidal structures made of a double-negative (DNG) and lossless metamaterial with a refractive index that is the opposite of the refractive index of the surrounding medium and an intrinsic impedance that is the same as that of the surrounding medium. In the first configuration, the two regions of space are separated by a paraboloidal surface of revolution and the primary plane wave is axially incident on the concave side of the paraboloid. In the second configuration, a paraboloidal DNG radome bounded by two confocal and coaxial paraboloidal surfaces of revolution is subjected to a primary plane wave axially incident from either the concave or the convex side of the radome. In all these cases, we prove that the geometrical optics solution is the exact solution to the problem.

Possible extensions of these exact solutions to other structures are discussed. In some cases, such as for a circular cone of DNG material under axial incidence, the geometrical optics solution is easily obtained but does not coincide with the exact solution

Open Shells of Revolution: Method of Analytical Regularization

S. B. Panin, P. D. Smith, and **E. D. Vinogradova**
Macquarie University, Australia
S. S. Vinogradov
University of Sydney, Australia

At present scattering from bodies of revolution is studied mostly by direct numerical techniques. Frequently, codes based on these techniques require powerful computer resources, but usually no guarantee on the accuracy of computations is available. This arises because the customary approach is based on numerical solution of the first kind Fredholm equation which is deducible from the single-layer potential representation. It is well-known that this equation is ill-posed, and as a consequence, the computational scheme is neither stable nor convergent. Thus it is highly desirable to transform this equation into a second kind Fredholm equation which provides a stable and fast converging computational algorithm that enables us to reach any required accuracy of computation. A transformation technique for canonically shaped open shells (spheres, spheroids, cylinders, etc.) was developed in [1] by applying a method of analytical regularization.

The first step in the generalization of this method [1] to diffraction from arbitrarily shaped open shells of revolution is to solve the corresponding electrostatic potential problem for ideal conductors in the form of open arbitrarily profiled shells with a circular hole. It should be noted that the idea of such a generalization was first considered in [2]. Technically, the problem is solved as follows. Starting with the integral equation formulation, we decompose a scaled version of the Greenfs function for the body of revolution into a singular part, which corresponds to the spherical geometry, and a remainder that is regular. The latter part is regular because of the specially chosen scaling of the Greenfs function. An efficient calculational technique for the coefficients of the Fourier expansion of the remaining part of Greenfs function was obtained. The inverse operator corresponding to the singular part may be explicitly and analytically constructed. When the inverse operator is applied to the decomposed integral equation, it is transformed to the desired second kind Fredholm equation, in the form of an infinite system of linear algebraic equations. This system is very effectively solved by a truncation method; the fast convergence of this technique is proved theoretically. A technique based on well-known discontinuous series was used to improve the convergence of the series for the surface charge density; this allows us to evaluate the charge density efficiently and accurately, especially at the screen edge where the density has a singularity.

This general approach effectively parallels that developed previously for canonical shells. The calculation of the surface charge density for various shapes of open conductors is presented. Although important in itself, this method and the obtained solution provide the first, and perhaps the major, step in the comparable analysis of full wave scattering problems for open shells of revolution.

REFERENCES

1. S.S. Vinogradov, P.D. Smith, and E.D. Vinogradova. Canonical problems in scattering and potential theory. Part I: Canonical structures in potential theory; Part II: Acoustic and Electromagnetic Diffraction by Canonical Structures. Chapman & Hall/CRC, 2001, 2002.
2. Yu.A. Tuchkin. gAnalytical regularization method for wave diffraction by bowl-shaped screen of revolutionh Ultra- Wideband, Short-Pulse Electromagnetics 5 Edited by P.D. Smith and S.R. Cloude, Kluwer Academic/Plenum Publishers, pp.153-157, 2002.

Diffraction of Electromagnetic Plane Wave by a Perfectly Conducting Disk

K. Hongo
Toho University, Japan

Q. A. Naqvi
Quaid-I-Azam University, Pakistan

Electromagnetic field scattered by a perfectly conducting disk is formulated rigorously and its solution is derived by applying the method of the Kobayashi potential which uses the discontinuous properties of Weber-Schafheitlin's integrals. We introduce two components of vector potentials of magnetic and electric types and derive the dual integral equations (DIE) for the tangential components of electric and magnetic (or equivalently induced surface current densities) fields. The cylindrical components of the magnetic field are expanded by a set of functions which satisfy a part of the DIE, the Maxwell's equations on the surface of the disk, and the required edge condition. We derive the spectral functions for the current densities by applying the vector Hankel transform proposed by Chew and Kong. The remaining equations of the DIE is solved by applying the projection and the problem reduces to the matrix equation. Thus two scalar wave functions satisfy the boundary condition, radiation condition and edge condition. This is quite different from the works of Meixner, Katsura and Nomura which introduced an extra scalar wave functions to make the total field satisfy the edge condition. The matrix elements are given by infinite integrals of single variable and they are expressed in terms of infinite series with respect to the normalized radius of the disk. Thus we can derive the low frequency approximate analytical expressions for this problem, though we have not completed yet.

Some numerical results for far scattered field pattern are obtained and some of them are compared to the corresponding physical optics solution. The agreement is fairly good.

Session 1P3
EMC Problems on Printed Circuit Boards and Common Mode

Analysis of Common Mode Propagation Based on Single Conductor Line

T. Hisakado and **K. Yoshimura**
Kyoto University, Japan
K. Okumura
Hiroshima Institute of Technology, Japan

The common mode radiation is an important problem for reducing EMI. In the case of two conductor transmission lines, the common mode has no explicit return path whereas the differential mode has the return path. The purpose of this paper is to clarify the mechanism of common mode propagation which has no explicit return path. In order to simplify the problem, we consider a single conductor line which also has no explicit return path. A. Sommerfeld originally studied the modes on single conductor lines using Hankel function [1] and G. Goubau analyzed the surface waves in detail [2]. However, it is not clear how the modes are generated and propagate on the semi-infinite single conductor line. We reveal the mechanism using semi-infinite single conductor line.

First, by a real experiment we observe the generation of a common mode on two conductor line with dielectric coat. We confirm that the common mode propagates close to the light speed whereas the differential mode propagates at about two thirds of the light speed.

Next, we consider a semi-infinite cylindrical perfect conductor line and supply current at the origin. Using electric field generated by the current and charge on the central axis of the single conductor line, we derive an integral equation based on the boundary condition on the surface of cylindrical perfect conductor. We solve the integral equation numerically in the complex frequency domain and obtain the waveforms in time domain using numerical inversion of Laplace transform. Figure 1 and 2 represents respectively the current waveforms and the charge when a step current is supplied at the origin. We can confirm that the step current propagates with distortion. The results are also confirmed by FDTD method.

Finally, we give the mechanism of current propagation by using current induction. The proposed method is based on the model that the source current causes the electric field and then the electric field generates induced current. The repeated action of current induction generates the current propagation and the key factor is the electric field by the stored charge. The proposed method reveals the cause-and-effect relationship of current propagation. On the other hand, the FDTD method is based on only the action through medium and cannot simulate the cause-and-effect relationship.

REFERENCES

1. A. Sommerfeld, Electrodynamics, Academic Press, New York, 1964.
2. G. Goubau "Surface Wave and Their Application to Transmission Lines" Journal of Applied Physics, Vol.21, pp119-1128, 1950.

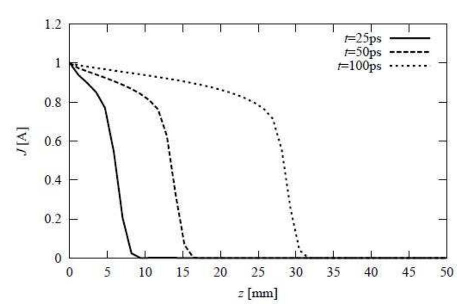

Figure 1: Current waveform

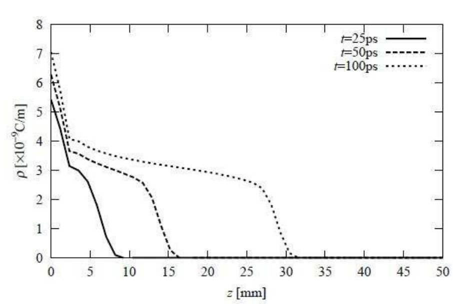

Figure 2: Charge waveform

Analysis on 20H Rule Applied Printed Circuit Board

S. Ikami and **A. Sakurai**
IBM Japan, Japan

The effect of so-called "20H rule" was studied with EM solver using MoM method. The rule recommends that the power plane should be shrunk against the ground plane by 20 times of the distance between the planes to realize lower EMI radiation.

The radiated electric field was calculated for the frequency range of 10MHz to 2GHz. The contributions of each three directional common and differential modes current were calculated using the electric and magnetic dipole moment calculation. It was found that there arises common mode radiation when the 20H rule was applied. At the resonance frequencies, the common and differential mode radiations are observed in relation to its resonance mode, the common mode radiation due to y- or x-directional electric dipole moment for TM01 or TM10 respectively.

Considering the common mode current occurrence is a fundamental nature of the electromagnetic radiation, it is concluded that the application of the rule increases the radiation.

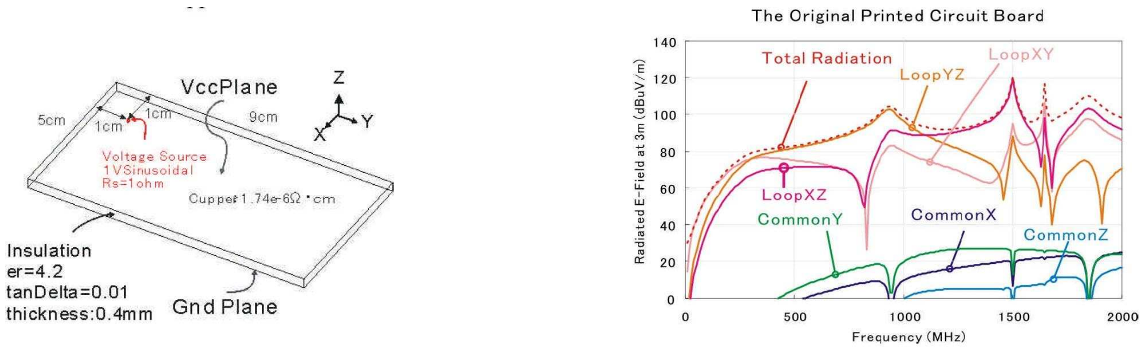

"Total Radiation" is calculated by EM solver. "CommonX, Y and Z" are the radiated E-field calculated from x, y or z component of electric dipole moment of the current distribution. . "LoopYZ, XZ and XY" are the radiated E-Field calculated from x, y or z component of magnetic dipole moment.

Figure 1: Printed Circuit Board model without 20H Rule and Radiated E-field at 3m. bv

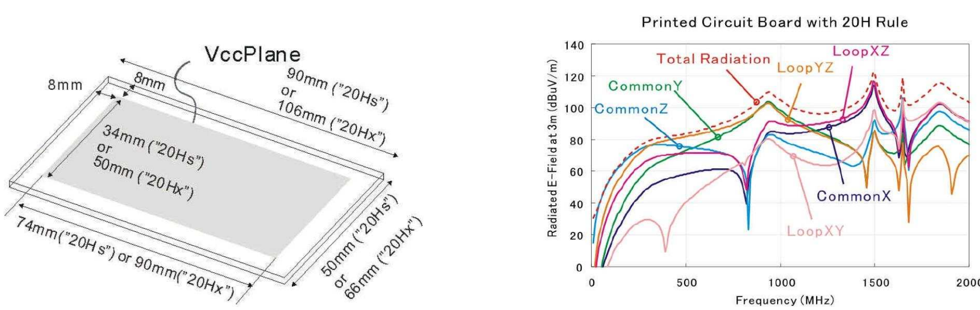

Figure 2: Printed Circuit Board model with 20H Rule

Common- and Differential-Mode Components at Asymmetric Pattern-Layout Lines on PCB

Y. Kami and **F. Xiao**
University of Electro-Communications, Japan

Recent demand in the technology of electronics equipment, at operation in high speed /high frequency, high performance, and low power, is calling for high-density trace pattern layout of in a printed circuit board. In multiconductor transmission line systems, a two-conductor transmission line above a ground plane is fundamental. The two-conductor-line system is effectively used as an important part in microwave circuits such as coupled line and filter element. In a field of electromagnetic compatibility (EMC), nearby conductors induce interference currents in each other line. This phenomenon is known as a term of crosstalk in the EMC field. To establish the high performance of electronics equipment, the interference should be reduced as possible to maintain signal integrity over some specification.

For a two-conductor-line system above a ground plane such as two trace lines on a printed board backed with a ground plane, there are two independent or orthogonal modes. Typically, one is named differential mode and another common mode in the EMC field. The differential-mode current is defined as a component flowing of the same magnitude and out-of-phase in both conductor lines, and the common-mode current as one of the same and in-phase. That is, the common-mode current flows in the same direction in two lines, so that the current corresponds to an antenna current. This is the reason why the common-mode current should be suppressed as possible. When a two trace lines are in parallel and in single-end-type excitation, both mode currents inevitably exist in the lines. If a trace layout is asymmetric in a two-conductor line system, the common-mode component may increase even for a perfect ground plane.

Here we study the common-mode and differential-mode components generated in a set of two parallel trace lines on a printed circuit board backed with a ground plane. The telegrapher's equations are here adopted to analyze the transmission characteristics. For applying a modal analysis technique, mode conversion matrices regarding the relationship between the line voltage/current and the mode voltage/current are discussed. From a set of solutions, the network function in a form of scattering matrix is considered to compare the measured results.

Finally, the technique is verified by comparing the measured and computed results for some models.

Extraction of Parasitic and Stray Capacitances from 1-Port Measurements

U. Paoletti and **O. Wada**

Kyoto University, Japan

Due to the increase in the density of interconnects in IC packages and boards, parasitic capacitive coupling increases. With the increase of clock frequency of digital circuits, the effect of small parasitic capacitances becomes significant. It is therefore important being able to calculate and measure even small capacitances. In order to verify numerical methods for capacitance calculations, it is also important to measure very small capacitances. The major problem in this type of measurements, is that the capacitive coupling between probe and DUT can affect the results. This effect is larger when the probe presents large metallic parts near the probe tips, typically the ground tip. On the other hand, these measurements can present very high repeatability. For this reason, de-embedding techniques are needed, which allow to eliminate the effect of the probe.

Even if a network analyzer open-short-load (OSL) calibration is conducted, the capacitance can still be affected by the stray capacitances of the probe. For example, the measured capacitance may change by inverting the polarity of the probe tips. Special and very expensive probes are often used, which are designed for reducing the capacitances between probe tips, and between probe tips and DUT. In the present work, a probe with a bulky ground has been used, whose effect cannot be neglected. The proposed de-embedding procedure can be applied also for estimating the effect on the results of the former type of probes.

n a zeroth order approximation the capacitance between probe tips, or more precisely, the residual capacitance between probe tips after an OSL calibration has been conducted, is subtracted from the measurement results.

In a first order approximation, the capacitances between each probe tip and the terminals of the port under consideration are taken into account. In order to calculate these capacitances, four additional measurements are required, with one probe tip on one terminal and the second probe tip touching only the substrate. A necessary condition, which must be verified before any calculation, is that the measurement results with one open probe tip do not depend on the position of the probe tip on the substrate. With the first order approximation, only total capacitance at each port can be calculated.

The second order approximation is aimed at the measurement of node-pair capacitances [1], and it takes into account the series connection with nodes not connected to the probe tips, with a maximum of two node-pair capacitances in series. It is usually not necessary to consider all possible combinations. In fact, depending on the measurement results, some of the series connections can be neglected.

Higher order approximations could be defined in the same way. For example, in a third order approximation, the series connections of three node-pair capacitances are also considered. However, the complexity of calculations increases very quickly, and the solution is practicable probably only under particular assumptions depending on the DUT. In the considered example a second order approximation was sufficient for obtaining an error smaller than 0.1 pF. The accuracy has been verified with additional measurements, and with simulation results based on a combination of pseudo-analytical techniques, a two-dimensional finite element method tool (ANSOFT MAXWELL SV) and a threedimensional boundary element method tool [2].

REFERENCES

1. A.E. Ruheli: *Circuit Analysis, Simulation and Design,* section 11.1, North-Holland, 1987.
2. K. Nabors and J.White: "Multipole-Accelerated Capacitance Extraction Algorithms for 3-D Structures with Multipole Dielectrics," *IEEE Transactions on Circuits and Systems-1*, vol. 39, no. 11, pp. 946-954, Nov. 1992.

Excitation of Electromagnetic Modes by a Signal Transmission Line Overpassing a Slit of Return Plane

T. Matsushima, Y. Sakai, K. Iokibe, Y. Toyota, and **R. Koga**
Okayama University, Japan
T. Watanabe
Industrial Technology Center of Okayama Prefecture, Japan
O. Wada
Kyoto University, Japan

Printed circuit boards (PCBs) have a separated power or ground plane when multiple power supply on the same layer or lateral noise isolation are needed. In general, a transmission line with such a separated plane as a return path degrades signal integrity and increases electromagnetic interference (EMI)[1]. In order to solve these problems, it is necessary to understand the electromagnetic field near the slit which intersects the transmission line. First, unintentional modes excited at the slit are investigated in detail by using FDTD. Then, a signal transmission model that relates between the differential mode and unintentional modes excited due to the slit is proposed. This model has the advantage that it requires no numerical calculation over the entire PCB as far as the structure near the slit is kept unchanged.

To investigate the unintentional modes, this paper deals with a 3-layer PCB with a slit on the middle layer as shown in Fig. 1. In addition to, the bottom layer is large enough to cover the slit in the middle layer. According to FDTD calculation, differential mode having been propagated along the microstrip line, when it arrives at the slit, is separated into multiple modes: differential mode that reflects backward and runs through, slot line mode that propagates along the slit and parallel plane mode that spreads cylindrically between the return and GND planes when the differential mode arrives at the slit. The slot line mode and the parallel plane mode are distinguished by taking into account that the power density of parallel plane mode is inversely proportional to the distance from the excitation point and slot line mode propagates without attenuation.

In the 3-layer PCB with a slit, the proposed signal transmission model consists of four kinds of block diagrams such as microstrip line, slot line, parallel plane and transfer factor as shown in Fig. 2. The transfer factor is defined as power conversion factor, which is a power ratio of common mode to differential mode and expressed in a matrix form like S matrix. The transfer factor is obtained by the electromagnetic calculation near the slit, since it is determined only by the structure of the intersection between signal line and slit.

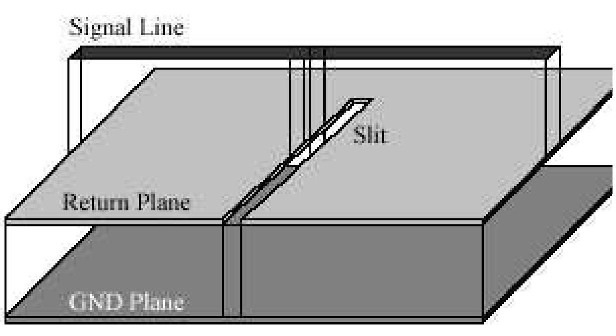

Figure 1: a 3-layer PCB having a slit on the middle layer

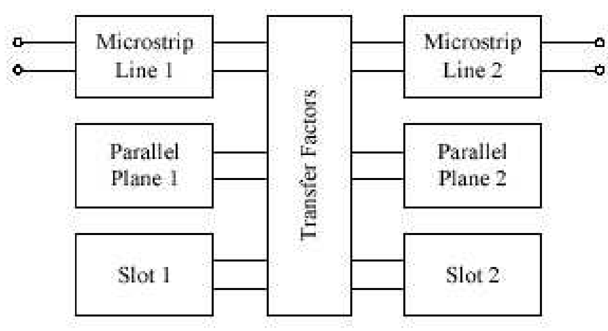

Figure 2: a signal transmission model

REFERENCES

1. F.B.J. Leferink, "Reduction of printed circuit board radiated emission," *Proc. IEEE Int. Symp. Electromagnetic Compatibility*, pp.431-438, Aug. 1997.

Crosstalk Analysis of Two Bent Lines Above a Ground Plane

S. W. Park [1], **F. Xiao** [1], **D. C. Park** [2], and **Y. Kami** [1]

[1]The University of Electro-Communications, Japan
[2]Chungnam National University, Japan

In a printed circuit board (PCB), there are various layouts of trace line on a standpoint of transmission line theory. Even if one trace line is designed independent, nearby trace lines affect it, that is, there interference occurs. The phenomenon is called as coupling or crosstalk. In a field of electromagnetic compatibility (EMC), the crosstalk becomes one of serious topics according as a high-density layout of trace line is demanded in a small sized package and for high-speed operation.

The crosstalk between parallel trace lines can be analyzed using the telegrapher's equations regarding line-voltage and line-current vectors under an assumption of transverse electromagnetic (TEM) mode propagation or at least quasi-TEM mode. In a PCB, there exist not only for straight lines but also for bent lines. Applying the telegrapher's equations to such complex layout containing bent lines is almost incompetent. But the telegrapher's equations are so concise and simple that we are familiar to them.

The telegrapher's equations for multiconductor line fundamentally consist of capacitive and inductive couplings in the concept of circuit theory, which correspond to electric- and magnetic-field couplings, respectively. When a transmission line is excited by external electromagnetic fields, a current is induced in the line, that is, the coupling phenomenon occurs there. By applying Maxwell's equations to this phenomenon, the modified telegrapher's equations can been resultantly obtained in a form that the external fields play as roles of distributed voltage and current sources along the line, which correspond to magnetic- and electric-field couplings.

To analyze the crosstalk between lines in a form of straight and bent lines, and two parallel-but-bent lines, and so on, we apply the concept mentioned above. Taking account of electromagnetic fields caused by currents flowing in various line sections, the network functions in a form of ABCD matrix are derived. The proposed network functions are verified by comparing the computed and the measured results for various types of line systems.

Determination of Absorbing Materials' Complex EM-Parameters via Scalar Reflectometer

C. P. Chen[1], **Z. W. Ma**[2], **T. Anada**[1], and **J. P. Hsu**[1]

[1]Kanagawa University, Japan
[2]Saitama University, Japan

1. Introduction

So far, some open-ended coaxial reflection probe(OECRP)-based techniques have been proposed to nondestructively and simultaneously determine the complex-EM-parameters, e.g. gtwo-thickness methodh(TTM) [1][2], gfrequency-variation Methodh (FVM)[1][2], gcombination methodh[1], etc.. All the above-mentioned methods are based on measuring the complex reflection coefficients of the sample loaded OECRP by the vector reflectometer. Obviously, for vector reflection, accurate phase detection, which relies strongly on the test samplefs surface condition, requires more carefulness in sample preparation [1][3]. In addition, especially, the price of vector reflectometer is generally over two times higher than scalar one. Accordingly, to cater for the always-requirement of cost-down, in this paper, an improved, lower cost(scalar reflectometer based) method—-gmulti-thickness methodh (MTM) for complex EM parameters will be studied.

2. Theory for MTM

The measurement configuration of a short-circuited microwave absorbing coating with a flanged open-ended coaxial probe has been shown in [2]. As well known, in reflection method, EM parameters are indirectly determined from the information of reflection coefficients. To simultaneously extract both complex EM-parameters($\dot{\epsilon}, \dot{\mu}$), which embody 4 scalars, the key point is to find at least 4 scalar reflections under different test conditions. In MTM, 4 scalar reflections are obtained by measuring the sample with 4 different thicknesses as:

$$\begin{cases} |\dot{\Gamma}_{m1}| = |\dot{\Gamma}_{c1}(\epsilon_r^{'}, \epsilon_r^{''}, \mu_r^{'}, \epsilon_r^{''}, f, d_1 \cdots)| \\ |\dot{\Gamma}_{m2}| = |\dot{\Gamma}_{c2}(\epsilon_r^{'}, \epsilon_r^{''}, \mu_r^{'}, \epsilon_r^{''}, f, d_2 \cdots)| \\ |\dot{\Gamma}_{m3}| = |\dot{\Gamma}_{c3}(\epsilon_r^{'}, \epsilon_r^{''}, \mu_r^{'}, \epsilon_r^{''}, f, d_3 \cdots)| \\ |\dot{\Gamma}_{m4}| = |\dot{\Gamma}_{c4}(\epsilon_r^{'}, \epsilon_r^{''}, \mu_r^{'}, \epsilon_r^{''}, f, d_4 \cdots)| \end{cases} \tag{1}$$

where subscripts m/c denote measured/calculated, respectively.

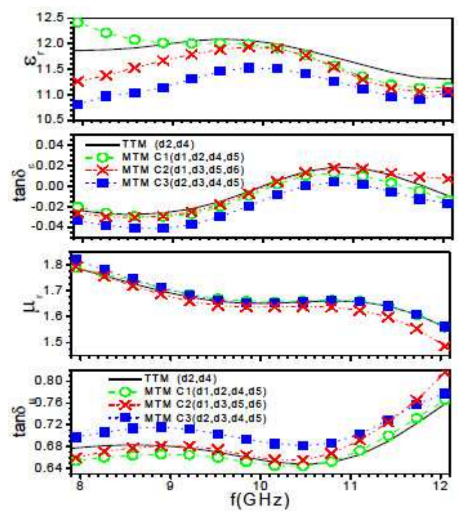

Figure 2: Broadband frequency-swept measurements for sample Sj1(d1−d6 = 0.56, 1.21, 1.77, 2.39, 3.05, 5.51(mm))

3. Experimental Verification

An X-band frequency-swept measurement was carried out on a typical absorbing material Sj1. The fitted measurement results by both MTM under different thicknesses combinations and TTM are shown in Fig.2. The results measured by MTM under all 3 selections of thicknesses combinations have good agreements with the reference data by TTM, which verified the effectiveness of MTM.

4. Conclusion

Scalar reflectometer based gmulti-thickness methodh(MTM) has been studied while its feasibility has been validated by the good comparison between MTM results with reference data.

REFERENCES

1. Xu Deming, et al, gRecent Advance on Open-Ended Coaxial probe measurement Techniques,h*2002 APMC Proceedings*, vol.2, Japan, 2002, pp.999-1006.
2. Chen ChunPing, et al, gFurther Study on Two-Thickness-Method for Simultaneous Measurement of Complex EM Parameters Based on Openended Coaxial Probe,h *EuMC2005*, Paris, Oct.,2005
3. James Baker-Jarvis et al., gAnalysis of an Open-Ended Coaxial Probe with Lift-Off for Nondestructive Testing,h *IEEE Transactions* on IM-43, no.5, pp.711-717, Oct. 1994.

An Estimating Technique for the Complex Reflection Coefficients of the EM-Wave Absorbers in the Millimeter-Wave Region

Y. Kogami and **A. Yanagisawa**
Utsunomiya University, Japan

An estimating method for the millimeter wave absorber is investigated. The rotating electric field vector method[1] is well known for a measurement technique in the free space method. As this technique is applying with the vector measurements, the measurement system may be very expensive, especially for millimeter-wave region. In this study, a modified technique[2] is applied for the complex reflectivity evaluation with scalar measurements. The measurement system is shown in Fig. 1. The situation of the interference between the reflected wave and direct wave changes when the distance between the horn antenna and the metal plate which the sample is located on is changed. By measuring the interference situation, we can extract the reflected wave only, and estimate the complex reflection coefficients. Fig. 2 is an example of measured results at millimeter-wave frequencies.

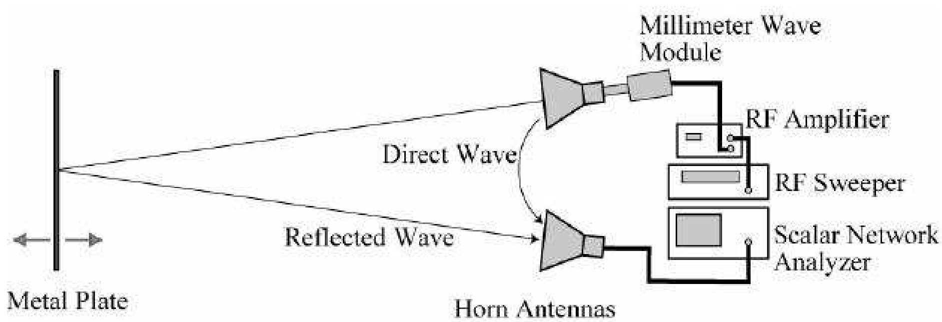

Fig.1. Measuring system

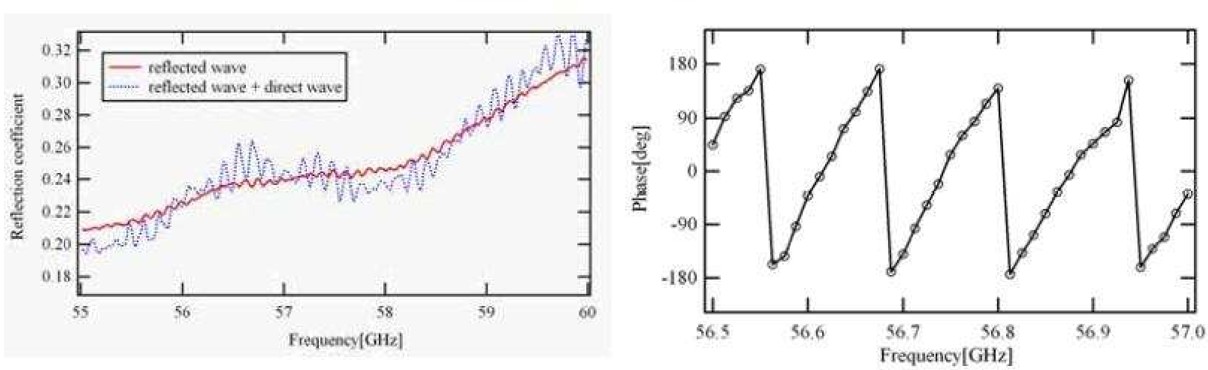

(a) Reflectivity (b) Phase

Fig.2. Measured results of the complex reflection coefficient of an absorber.

Design of Cylindrical Microwave Absorber Using Epoxy Resin Mixed with Micro Balloons and Carbon Short Fibers

T. Doi [1], **Y. Suzuki** [1], **T. Soh** [2], and **O. Hashimoto** [1]

[1]Aoyama Gakuin University, Japan
[2]The Yokohama Rubber Co.,Ltd, Japan

In this paper, the design of a cylindrical microwave absorber to prevent false images from appearing when using the antenna or the radar, are examined. This absorber is a metallic bar covered with an absorption layer, and also the matrix material of the absorption layer is epoxy resin mixed with micro balloons, loss materials of that are carbon short fibers. The complex relative permittivity ($\dot{\varepsilon}_r$) of the material in various content of carbon short fiber (0, 1, 3phr), is measured in the frequency range from 2.0 to 12.0GHz by transmission line method using coaxial line. Figure 1 shows an example of the results of measurement (1phr). Figure 2 shows a top view model of the cylindrical absorber, where the radius of the metallic bar is a[mm], the radius of the absorber is b[mm], the thickness of the absorption layer is d[mm] and incident angle of electromagnetic wave is ϕ[$^\circ$]. In this model, scattered wave is calculated by Maxwell's equations, the absorption is defined by the ratio of two electric field intensities of scattered wave at observation point ρ[m]. One is from the cylindrical absorber, the other is from the metallic bar without the absorption layer. Figure 3 shows a design chart of the cylindrical absorber for TE and TM wave at 9.4GHz (a is 101.6mm and ϕ is 0 $^\circ$). In this figure, three circular marks are measured $\dot{\varepsilon}_r$ with respect to each content of short carbon fiber, a broken line shows approximate curve of them and continuous lines shows the combination of optimal $\dot{\varepsilon}_r$ and d for designing the cylindrical absorber. The absorber can be designed at intersection point of these lines, where its $\dot{\varepsilon}_r$ and d are 9.24-j3.71 and 2.68mm, respectively. Figure 4 shows the calculated absorption characteristics based on designed values. As a consequence, it is confirmed that the absorptions for both waves are more than 35dB at 9.4GHz and also more than 20dB in the frequency band from 9.09 to 9.76GHz. The measurement of the absorption for the cylindrical absorber shown in this paper will be presented in

Acknowledgement

This work was financially partly supported by the Grant-in-Aid for 21st COE Program fraom the Ministry of Education, Culture, Sports, Science and Technology (MEXT) of the Japanese Government.

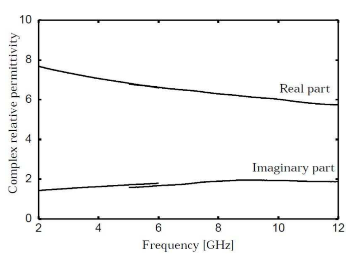

Figure 1: Complex relative permittivity

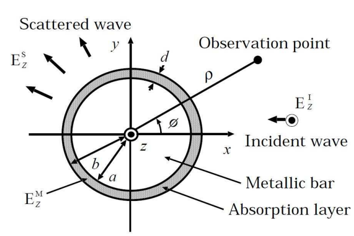

Figure 2: Model of a cylindrical absorber

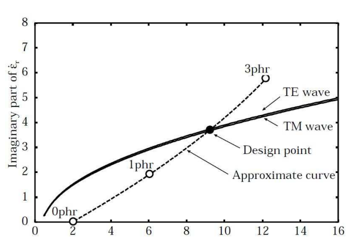

Figure 3: Design chart of a cylindrical absorber

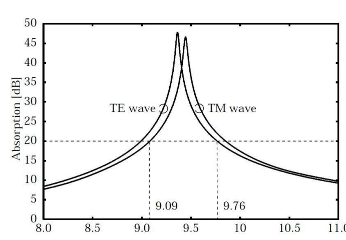

Figure 4: Calculate absorption characteristics

Session 1P4
Advances in Detection and Imaging: from Algorithms to Systems and Applications

Synergistic Exploitation of Divide and Conquer Strategies for Inverse Scattering Problems

M. Benedetti [1], **D. Franceschini** [1], **M. Lambert** [2], **D. Lesselier** [2], and **A. Massa** [1]

[1]University of Trento, Italy

[2]Signaux Systmes, France

Generally speaking, inverse scattering problems are characterized by a high complexity in terms of both the mathematical model and computational costs. As a matter of fact, ill-posedness and nonlinearity are very difficult issues to be carefully addressed in order to allow faithful reconstructions. Moreover, in order to obtain a suitable representation of the scenario under test, customized strategies [1][2] and efficient optimization methodologies [3][4] are needed. In such a framework, recent developments reported in literature suggest splitting the original problem in a series of successive sub-problems according to the general strategy of 'divide and conquer'. Then, each partial solution is profitably used as initialization for solving the successive problem, which turns out to be more and more close to the original one even though characterized by a reduced complexity because of the information on its solution acquired at the previous steps. In such a framework, two different guidelines have been taken into account. The former improves at each step the resolution accuracy in a subset of the whole investigation domain by considering a more detailed multiresolution description of the unknown scatterer profile [5][6]. On the other hand, an alternative strategy is that of acquiring at each step of an iterative process some information on the problem solution thus composing a sort of puzzle whose finnal "shape" fits the description of the scatterer under test [7].

As far as the so-called multiresolution strategies are concerned, a non-negligible problem is that of defining a criterion for identifying the number of regions-of-interest (RoIs) where the synthetic zooming takes place. Towards this end, various solutions have been proposed based on image processing techniques [8]. In such a contribution, such an issue is addressed by considering a shape-based representation of the scatterer. At each step of the multistep process, the RoIs defined at the previous step are processed through a level set method [1] in order to better estimate the support of the RoIs at the successive steps. Then, according to the standard IMSA, different levels of resolution are allocated in the investigation domain (i.e., higher in the RoIs de

ned at the current step and with a decreasing order in those estimated at previous steps) and a pixel-based reconstruction is carried out through a suitable optimization strategy [4].

A selected set of preliminary numerical results carried out in noiseless as well as noisy scenarios gives some indications on current limitations and potentialities of the proposed approach.

REFERENCES

1. A. Litman et al., "Reconstruction of a two-dimensional binary obstacle by controlled evolution of a level-set," *Inverse Problems*, vol. 14, pp. 685706, 1998.
2. R. Ferraye et al., "Reconstruction of complex and m ultiple shape object contours using a level set method," *J. Electromagn. Waves Applic.*, vol. 17, pp. 153-181, 2003.
3. A. Massa et al., "Parallel GA-based approach for microwave imaging applications," *IEEE Trans. Antennas Propagat.*, vol. 53, pp. 3118-3127, 2005.
4. M. Donelli al., "Computational approach based on a particle swarm optimizer for microwave imaging of two-dimensional dielectric scatterers," *IEEE Trans. Microwave Theory Techn.*, vol. 53, pp. 1761-1776, 2005.
5. S. Caorsi et al., "A new methodology based on an iterative multiscaling for microwave imaging," *IEEE Trans. Microwave Theory Techn.*, vol. 51, pp. 1162-1173, 2003.
6. A. Baussard et al., "Adaptive multiscale reconstruction of buried objects," *Inverse Problems*, vol. 20, pp. S1-S15, 2004.
7. O. Bucci et al., "Intelligence and strategy in the solution of nonlinear inverse scattering problems," Proc. URSI EMTS 2004, pp. 694-696, 2004.
8. S. Caorsi et al., "Detection, location, and imaging of multiple scatterers by means of the iterative multiscaling method," *IEEE Trans. Microwave Theory Techn.*, vol. 52, pp. 1217-1228, 2004.

Integration of a Fuzzy Logic System with the Contrast Source Inversion Method-A Numerical Validation

A. Casagranda [1], **D. Franceschini** [1], **A. Massa** [1], **P. M. van den Berg** [2], and **A. Abubakar** [3]

[1]University of Trento, Italy
[2]Delft University of Technology, The Netherlands
[3]Schlumberger-Doll Research, U.S.A.

The electric properties of an unknown region cannot be determined with arbitrary accuracy when the scenario is probed by means of electromagnetic waves. In fact, different corrupting factors (i.e., the measurement errors and the environmental noise) and the intrinsic ill-posedness of the problem highly a affect the performances of whatever reconstruction technique. Moreover, the limited amount of information on the scenario under test collectable from scattering experiments is an additional limiting factor to be carefully taken into account addressing practical applications like sub-surface inspection, medical imaging or non-destructive testing. In order to overcome such intrinsic drawbacks, the use of suitable strategies is mandatory. As far as the presence of noise in the data and the measurement errors are concerned, a possible countermeasure has been proposed and validated in [1], where an innovative fuzzy-logic-based [2] strategy has been presented. The fuzzy system (FLS) is able to provide two series of coefficients used as weighting parameters in the cost function, defined when recasting the inverse scattering problem in term of an optimization one. Thanks to the FLS, a direct (and expensive) estimation of the noise or a priori assumptions on the level of noise are avoided, but the corruptions and the errors in the scattering data are taken into account in an unsupervised fashion.

Concerning the mathematical formulation, in [1] the problem has been stated in terms of contrast and field unknowns. In this contribution, maintaining the same FL approach for estimating the noise impact, the data and state equations have been redefined in terms of contrast function and contrast sources. Such a formulation has been proposed in [3] (*Contrast Source Inversion method*, CSI) and it is based on the modified gradient method and on the source-type integral equation method. It has been proved to be a very powerful algorithm, showing robustness to noise and computational efficiency. Moreover, in [4], a regularization term based on the minimization of the total variation (TV) of the scenario has been proposed to further enhance the quality of the reconstructions. Successively, to avoid the calibration of any artificial parameter, the regularization has also been proposed as a multiplicative factor of the original cost functional.

In this work, selected results from extensive numerical simulations will be presented to assess the performances of an integrated inversion scheme based on the CSI method and the Fuzzy Logic Systems. The results will also highlight the interaction effects between the fuzzy regularization coefficients and the regularization approach based on the total variation for both single and multiple-frequency data sets.

REFERENCES

1. R. Azaro, A. Casagranda, D. Franceschini, and A. Massa, "An innovative fuzzy-logic-based strategy for an effiective exploitation of noisy inverse scattering data," Progress in Electromagnetics Research, PIERS 54, pp. 283-302, 2005.
2. L. A. Zadeh, "Fuzzy sets," *Inf. Contr.*, vol. 8, pp. 338-341, 1965.
3. P.M. van den Berg and R.E. Kleinman, "A contrast source inversion method," *Inverse Problems*, vol. 13, pp. 211-277, 1997.
4. P.M. van den Berg and A. Abubakar, "Contrast source inversion method: state of the art," Progress in Electromagnetics Research, PIER 34, pp. 189-218, 2001.

A Stable and Fast 3-D Imaging Algorithm for UWB Pulse Radars with Fractional Boundary Scattering Transform

T. Sakamoto and **T. Sato**
Kyoto University, Japan

The UWB (ultra-wideband) pulse radar is a promising candidate as an environment measurement method for robots. Radar imaging for a nearby target is known as an ill-posed inverse problem, on which various studies have been done. However, conventional algorithms require long computational time, which makes it difficult to apply them to real-time operations of robots. We have proposed a fast radar imaging algorithm, the SEABED algorithm, for UWB pulse radars [1, 2]. This algorithm is based on a reversible transform, IBST (Inverse Boundary Scattering Transform), between the target shape and the observed data. This transform enables us to estimate target shapes quickly and accurately in a noiseless environment. However, in a noisy environment the image estimated by the SEABED algorithm is degraded because IBST utilizes differential operations. In this paper, we newly introduce a FIBST (Fractional IBST), which is obtained by expanding the conventional IBST, which enables us to deal with the intermediate space between a real and data spaces, and propose a stable 3-D imaging algorithm by using the FIBST.

In our system model, UWB mono-cycle pulses are transmitted at a fixed interval and received by the same omni-directional antenna. We express a real space with the parameters (x, y, z). The antenna is scanned on the x-y plane in the real space. We define s(X, Y, Z) as the electric field received at the antenna location $(x, y, z) = (X, Y, 0)$, where we define Z with time t and the speed of the radiowave c as $Z = ct/(2\lambda)$. The transform from the data space (X, Y, Z) to the real space (x, y, z) corresponds to the imaging we deal with in this paper. We normalize x, y, z, X, Y and Z by λ, the center wavelength. In the SEABED algorithm, quasi-wavefronts (X, Y, Z) are extracted from the received data s(X, Y, Z). Next, we apply smoothing to the quasi-wavefront to suppress noises. Finally, we apply IBST to the smoothed quasi-wavefront to obtain the final image as

$$\begin{aligned} x &= X - Z\partial Z/\partial X, \\ y &= Y - Z\partial Z/\partial Y, \\ z &= Z\sqrt{1 - (\partial Z/\partial X)^2 - (Z\partial Z/\partial Y)^2}. \end{aligned} \tag{1}$$

The smoothing effectively works for concave targets because the quasi-wavefront is smooth for a concave shape. However, for general cases the quasi-wavefront is not necessarily smooth, so the image resolution can be degraded by unsuitable smoothing. To resolve this problem, we introduce FIBST by expanding the conventional IBST, and transform the data to an intermediate space between the real and data spaces, where the smoothing process hardly degrades the resolution. FIBST is expressed as

$$\begin{bmatrix} x_\theta & \alpha & \beta \\ y_\theta & \alpha & \beta \end{bmatrix} = \begin{bmatrix} X \\ Y \end{bmatrix} - ZR(-\theta)\begin{bmatrix} \alpha & 0 \\ 0 & \beta \end{bmatrix} R(\theta) \begin{bmatrix} \partial Z/\partial X \\ \partial Z/\partial Y \end{bmatrix},$$

$$z_\theta, \alpha, \beta = Z\sqrt{1 - [\partial Z/\partial X\ \partial Z/\partial Y]R(-\theta)\begin{bmatrix} \alpha & 0 \\ 0 & \beta \end{bmatrix} R(\theta)\begin{bmatrix} \partial Z/\partial X \\ \partial Z/\partial Y \end{bmatrix}}. \tag{2}$$

In our propsed stable imaging algorithm, we select suitable parameters (θ, α, β)depending on the roughly estimated target shape, and apply the smoothing process to $x_{\theta,\alpha,\beta}, y_{\theta,\alpha,\beta}, z_{\theta,\alpha,\beta}$ and finally apply FIBST again to obtain the final image.

REFERENCES

1. T. Sakamoto and T. Sato, gA Target Shape Estimation Algorithm for Pulse Radar Systems Based on Boundary Scattering Transform,h *IEICE Trans. on Commun.* vol. E87.B, no. 5, pp. 1357.1365, May, 2004.
2. Takuya Sakamoto and Toru Sato, gA fast algorithm of 3-dimensional imaging for pulse radar systems,h Proc. 2004 IEEE AP-S International Symposium and USNC/URSI National Radio Science Meeting, vol. 2, pp. 2099.2102, June, 2004.

Full Newton Method for Electromagnetic Inverse Scattering, Utilizing Explicit Second Order Derivatives

M. Norgren
Royal Institute of Technology, Sweden

T. Takenaka
Nagasaki University, Japan

In several areas of applied sciences such as geophysical exploration, medical imaging and non-destructive testing, one often encounters nonlinear inverse scattering problems. Substantial effort has been spent to reconstruct the shape, location, internal structure and material parameters of an unknown object from measurements of the fields scattered by the object.

Many reconstruction algorithms are based on local optimization methods, in which the solution is determined by minimizing a suitably defined cost-functional. The most common among the local methods are first order (gradient) methods, like the steepest descent and the conjugate gradient method, or semi-second order (so called quasi-Newton) methods, like the Gauss-Newton method and the Levenberg-Marquardt method. The full Newton method, which utilizes the complete second order information, usually has a superior convergence rate when approaching the minima, but is in most cases rejected (in favor of lower order methods) due to the computational burden to calculate the second order derivatives. When considering inversion of continuously varying heterogeneous electromagnetic material parameters, the computation time for the derivatives of the cost-functional becomes a bottle-neck. For gradient methods, this problem can be alleviated by utilizing the (first order) Frechét differential and the solution of the adjoint scattering problem, whereby the gradient can be calculated explicitly and with a minimal computational cost. This approach has been used widely for solving various inverse scattering problems in one, two or three dimensions, both in the frequency domain and in the time-domain; see e.g. [1,2]. However, less interest and effort has been spent on extending this technique to the treatment of second order derivatives.

In this presentation, we consider the full Newton metod for solving the frequency-domain inverse scattering problem for a nonuniform transmission line. In addition to the gradient, the complete hessian function for an arbitrary set of continuous parameters is derived utilizing the second order Frechét differential. The adjoint transmission line problem is formulated and the explicit expressions for the gradient and the hessian are presented. It is straight forward to extend the framework to the three-dimensional case with a scatterer of a general bianisotropic medium, and the corresponding expressions are presented as well. For the transmission line, reconstruction results are presented where the reconstructions have been made both from synthetic as well as measured reflection data

REFERENCES

1. H. Zhou, T. Takenaka and T. Tanaka, *Time-Domain Reconstruction of Lossy Objects using Dipole Antennas*, Microwave Opt Tech Lett 44(3), 238-243, 2004.
2. M. Norgren, *On the problem with intermodal dispersion when using multiconductor transmission lines as distributed sensors*, PIER 56 Progress In Electromagnetic Research, J. A. Kong ed., EMW Publishing, Cambridge, MA, USA, 129-150, 2006.

Two Dimensional Reconstruction from Multifrequency Scattering Data by Means of Construction of the Equivalent Current Distribution

K. Ishida
Kyushu Sangyo University, Japan

M. Tateiba
Kyushu University, Japan

The inverse scattering problem of reconstructing a complex object in structure from the measured scattered waves has difficulties due to nonlinearity and ill-posedness. With the aim of decreasing the difficulties, some researchers deal with the source type integral equation and investigate the nonradiating(unmeasured) equivalent current which contributes nothing to the scattered waves outside the object[1]. The authors have studied the scattering problem using T-operator which transforms incident waves into the equivalent currents[2]. The T-operator is identified with the equivalent current for any incident waves. It is shown that the scattered wave is linearly related to the equivalent current and that the object is reconstructed from the equivalent current through a linear relation.

In this paper, an approach is presented for reconstructing an inhomogeneous object in a circular region[3]. We can relate the scattered waves directly to the incident waves by so-called T-matrix. Supposing that the incident waves are plane waves propagating in all directions and the scattered waves in far region are measured around the object, we can obtain the T-matrix elements. An orthonormal set of functions is introduced to express the equivalent current such that the subset of the orthonormal set is a set of functions which forms the incident waves. If the incident wave is expressed in terms of the subset, a specific subsequence of expansion coefficients of the equivalent current becomes a measured quantity which corresponds to the T-matrix elements, and the others are unmeasured quantities which cannot be observed from the scattered waves; that is, measured and unmeasured equivalent currents are separated explicitly.

The region is divided into small cells to express the inhomogeneous object. The cost functional of the object and the unmeasured equivalent current is defined as a discrepancy of the equivalent currents over the region. We can reduce the inverse scattering problem to minimization of the cost function to find the optimal unmeasured current and object. Assuming that the object and the measured equivalent current are given, we get a linear equation for the unmeasured equivalent current. Assuming that the measured and unmeasured equivalent currents are given, we get a linear equation for the object. The two linear equations are solved, by turns, as the linear least-squares problem.

The algorithm avoids employing a nonlinear optimization algorithm, solving the direct scattering problem, and using a special additional regularization.

Numerical examples show that the algorithm works well under noisy conditions. We can adapt the algorithm for use of multifrequency scattering data. Numerical examples also show that the object with high contrast is reconstructed by use of multifrequency scattering data.

REFERENCES

1. T. M. Habashy, M. L. Oristaglio, and A. T. de Hoop, *Radio Sci.*, 29(4), 1101-118, 1994
2. K. Ishida and M. Tateiba, *Progress in Electromagnetics Research Sympo. Proc.*, 25, 1998.
3. K. Ishida and M. Tateiba, *Proc. 2005 Int. Sympo. on Antennas and Propagation*, 1073-076, 2005.

A Robust and Fast Imaging Algorithm with an Envelope of Circles for UWB Pulse Radars

S. Kidera, T. Sakamoto, and **T. Sato**
Kyoto University, Japan

Introduction UWB pulse radar systems have a high potential for a high-resolution imaging in indoor environments. We have already proposed a fast imaging algorithm called SEABED based on a reversible transform BST(Boundary Scattering Transform) between the received signals and the target shape. However, the image obtained by SEABED deteriorates in a noisy environment because it utilizes a derivative of received data. In this paper, we propose a robust imaging method with an envelope of circles.

Proposed Algorithm We utilize a mono-static radar system. We assume a convex target which has a clear boundary. We define (x; y) as a point in the real space. An omni-directional antenna is scanned along x axis. X is the x coordinates of the antenna location, and Y is the range, which can be measured by UWB radars, as shown in Fig. 1. The curve (X; Y) is called a quasi wavefront. SEABED estimates the target image with a reversible transform BST between the target boundary and the quasi wavefront. However, the image of the SEABED deteriorates in a noisy environment because it utilizes dY=dX in the BST. To solve this problem, we propose a robust imaging method with an envelop of circles. In this method, we plot a circle $(x - X)^2 + y^2 = Y^2$ for each (X; Y) as shown in Fig. 2. We have proven that an envelope of these circles corresponds to the target boundary. By utilizing this relationship, we estimate the target boundary as an envelope of circles. This method transforms the group of points (X; Y) to the group of points (x; y) without the derivative dY=dX. Therefore it can achieve a stable imaging even in a noisy environment.

Performance Evaluation Fig. 1 and 2 show the estimated points with SEABED and the proposed method, respectively. Here we set the sampling number to 101, and S/N to 6:0 dB. We confirm that the estimated image of SEABED deteriorates, and cannot reconstruct the outline of the target boundary due to the noise. On the contrary, the image obtained by the proposed method is stable and precise. This is because the proposed method does not spoil the information of the inclination of image. The calculation time of this method is within 0.2 sec for Xeon 3.2 GHz processor, which is short enough for realtime operations.

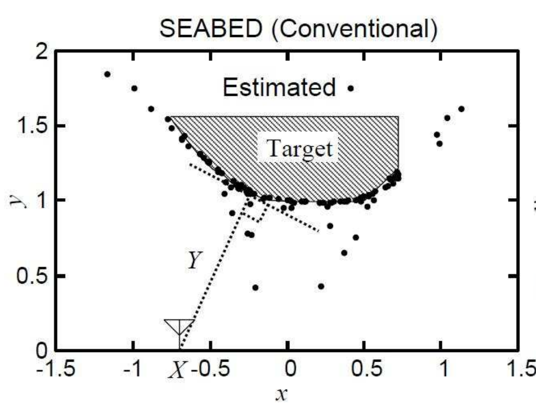

Figure 1: Estimated image with SEABED.

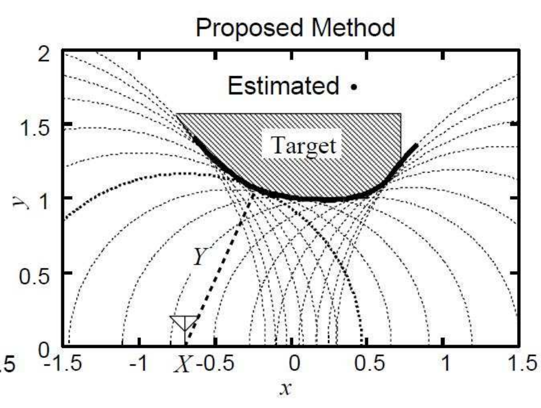

Figure 2: Estimated image with the proposed method.

Electromagnetic Inverse Scattering of Cylindrical Objects Using a Multigrid Optimization Method

M. Tanaka
Oita University, Japan

Electromagnetic imaging of internal properties of unknown scattering objects is very useful in a variety of applications such as biomedical imaging, nondestructive testing of materials, and detection of underground objects. It is desirable to reduce the computational cost to obtain a convergent solution to the electromagnetic inverse scattering problem. It is the purpose of this paper to investigate the convergence acceleration of an iterative inversion algorithm of reconstructing the relative permittivity of a cylindrical object based on a multigrid optimization method. The object situated in a homogeneous background medium is assumed to be illuminated with multifrequency TM cylindrical electromagnetic waves. As is well known, the electromagnetic inverse scattering problem can be formulated as the solution to a nonlinear integral equation for a contrast function, which is related to the relative permittivity of the object. The method of moments with pulse-basis functions and point matching is employed to discretize the equations for the total electric field inside the object and the scattered electric field. The contrast function can be determined by minimizing a cost functional, which is defined as the norm of a discrepancy between the scattered electric fields measured and calculated for an estimated contrast function. Note that the scattered electric field is simulated by using the FFT-CG method. The multigrid optimization method, which is composed of the conjugate gradient method, the frequency-hopping technique, and the multigrid method, is applied to the minimization of the cost functional. The multigrid method is eRective in accelerating the rate of convergence.

Simulated results are obtained for some dielectric circular cylinders using the multifrequency scattering data in microwave region. We employ the six frequencies of 1, 2, 3, 4, 5, and 6GHz. The object located in free space is successively illuminated by incident waves from 36 diRerent directions for one frequency. For each illumination, measurements of the scattered electric field are made at 36 discrete observation points equally spaced along a circle of radius 2λ, where λ is the free-space wavelength for the frequency of 6GHz. The $2\lambda \times \lambda$C square region containing the object and the background medium is uniformly subdivided into 32×32 or 16×16 elementary square cells corresponding to the fine grid or the coarse one. The initial guess of the contrast function is now assumed to be zero. Figure 1 illustrates the reconstructed results of the relative permittivity ϵ_s of a stratified circular cylinder.The radii and the relative permittivities of the two concentric layers are, respectively, 0.4λC0.8λ and 4.0, 7.0. The current frequency is changed to the next higher-frequency when the relative residual error δ in the scattered electric field is $\delta < 10^{-2}$. The final convergent solution for $\delta < 5 \times 10^{-4}$ is obtained after 72 iterations. For reference, the true profile of the relative permittivity is also shown by the thin solid line in Fig. 1. The numerical results demonstrate the eRectiveness of the reconstruction scheme proposed.

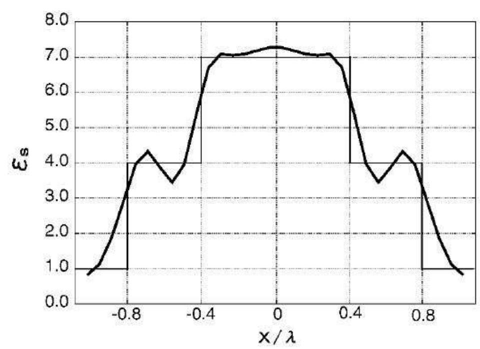

Figure 1: Reconstructed results of the relative permittivity.

Real Data Microwave Imaging Using Time Reversal Techniques

V. Chatelee, A. Dubois, I. Aliferis, J. Y. Dauvignac and **C. Pichot**
Université de Nice, France

We examine an electromagnetic inverse scattering problem, namely the detection and localization of unknown targets using only the scattered field measured on a few receivers. Here, we consider the case of free-space experiments where a set of ultra-wideband antennas, located along a horizontal line, successively illuminate a cylindrical object whose length is large compared to the wavelength. The scattered field is measured along the same line. This is generally referred to as a multi-static limited-aspect configuration.

Real data are collected in an anechoic chamber from the so-called SIMIS (Synthetic Impulse Microwave Imaging System) that uses an array of eight ultra-wideband Vivaldi-type ETSA antennas [1] associated with a vector network analyzer [2]. The total field, which corresponds to the sum of the incident field (in the absence of target) and the scattered field (contributed by the target), is measured over a large frequency band (typically 2–8 GHz); time-domain data are obtained via an inverse Fourier transform. An appropriate time gating, excluding the early response, yields the scattered field. Frequency-domain scattered field data can then be obtained by another Fourier transform, if necessary. Following this procedure, we can perform a single measurement instead of a differential one (with/without object).

Two qualitative inversion algorithms exploit the experimental data. Both algorithms use time reversal techniques, based on the invariance of the wave equation under replacement of t by $-t$. The first one is the Time Reversal method (TR) [3], applying to time-domain data, and the second one is the DORT method [4] (French acronym for Time Reversal Operator Decomposition) which operates in the frequency domain.

In both cases, the obtained result is a numerically synthesized (transient/harmonic, respectively, for the TR/DORT method) electromagnetic wave that focuses selectively on the targets present in the investigated area, thus detecting and localizing them.

REFERENCES

1. E. Guillanton, J.-Y. Dauvignac, C. Pichot, and J. Cashman. A new design tapered slot antenna for ultra-wideband applications. *Microwave and Optical Technology Letters*, 19(4):286–289, November 1998.
2. C. Pichot, J.-Y. Dauvignac, C. Dourthe, I. Aliferis, and E. Guillanton. Inversion algorithms and measurement systems for microwave tomography of buried objects. In *Proceedings of the 16th IEEE Instrumentation and Measurement Technology Conference, IMTC/99*, volume 3, pages 1570–1575, May 24–26, 1999. Venice, Italy.
3. C. Tsogka and G. C. Papanikolaou. Time reversal through a solid-liquid interface and super-resolution. *Inverse Problems*, 18(6):1639–1657, December 1999.
4. C. Prada and M. Fink. Eigenmodes of the time reversal operator: A solution to selective focusing in multiple-target media. *Wave Motion*, 20(2):151–163, September 1994.

On Flight Tests of a Millimeter-Wave Radar for Obstacle Detection

B. D. Nguyen [1], **C. Migliaccio** [1], **C. Pichot** [1], **K. Yamamoto** [2]
N. Yonemoto [2], **K. Yamada** [2], and **H. Yasui** [3]

[1]Université de Nice, France
[2]Electronic Navigation Research Institute, Japan
[3]Fundamental Engineering Division IHI Aerospace, Japan

Helicopters and small aircraft, flying at low altitude in the visual flight rules often face hazardous conditions by long and thin objects as power lines [1] due to their invisibility or poor visibility under bad weather conditions.

The objective of this paper is to present hardware and software techniques and experimental results for an obstacle detection and warning system for civil helicopters [2]. A primary target for our system concerns power line detection. The complete system includes an infrared (IR) camera, a color camera and a MMW radar as its sensors. Software techniques to fuse color and IR images and to enhance targets have also been studied. In this paper, we put emphasis on the development of on board radar. An experimental MMW radar has been constructed to investigate the detection range.

In a first set-up, a 94 GHz FMCW radar has been developed using a classical Cassegrain antenna. On flight measurements show that the radar detects a power line 800 m away and its range error is less than 2%. Nevertheless, radar size and cost can be drastically reduced using printed reflector antenna.

The printed antenna is a Fresnel reflector combining /8 and /4 phase zone compensation by means of circular shaped patches [3]. Measured gain and radiation pattern are close to those of the initial antenna. The primary source consists of a small frequency selective surface (FSS) pasted on the aperture of a standard open WR-10 waveguide. It provides a return loss less -25dB over the operating frequency bandwidth of the radar.

Helicopter flight tests have demonstrated the validity of the system detection ability and real time display.

REFERENCES

1. K. Sarabandi, M. Park, "A radar cross-section model for power lines at millimeter-wave frequencies", *IEEE Trans. Antennas Propagat.*, vol. 51, No. 9, pp. 2353-2360, Sept. 2003.
2. K.Yamamoto, K.Yamada, N.Yonemoto, H.Yasui, S.Nasu, H. Nebiya, C. Migliaccio, B.D. Nguyen, Ch. Pichot, "94 GHz FMCW radar for obstacle detection". Proceed. International Radar Symposium IRS2003 (Dresden, Germany), pp. 481-486.
3. B.D. Nguyen, C. Migliaccio, Ch. Pichot, "94 GHz zonal ring reflector for helicopter collision avoidance". *Electron. Lett.*, Vol. 40, No. 20, pp. 1241-1242, Sept. 2004.

Cramér-Rao Lower Bounds of Time Domain Inverse Scattering Problems of Multilayer Structures

M. Gustafsson
Lund University, Sweden
S. Nordebo
Växjö University, Sweden

Inverse scattering problems are in general ill-posed, i.e., they are not well-posed in the sense of existence, uniqueness, and continuously dependence of the solution on the data. The uniqueness theorems typically show that the solution is unique if data is available from all possible measurements. This is very important but not sufficient from a practical point of view. Further, since the solution of ill-posed problems does not depend continuously on the data, the eRect of noise on the solution is amplified in a way that calls for proper control. For this purpose, a sensitivity analysis based on regularization theory is often used to control the imaging error. However, these approaches do not give a qualitative measure on the information content of the inversion data.

Estimation theory is a classical and well developed area within signal processing research and mathematical statistics. Over several decades the Cramér-Rao lower bound has been subjected to many revivals and has become the dominating tool in areas such as statistical signal processing, array signal processing and systems and control theory. There is obviously many connections between inverse scattering and estimation. The Cramér-Rao lower bound is a quantitative measure that give us the best possible measurement performance associated with any unbiased estimation, a performance which is achievable with linear models, and asymptotically achievable under very general conditions.

In inverse scattering problems of a multilayer slab the fields are observed at one side of the object or at both sides, i.e., one uses reflection and (or) transmission data. The one-dimensional case have been thoroughly studied in both the time- and frequency-domains. The one-dimensional inverse scattering problem of an inhomogeneous slab is preferably solved in the time-domain with wave splitting and least-squares optimization. The wave splitting algorithms are restricted to identification of the permittivity or simultaneous identification of the permittivity and conductivity.

In this paper, the inverse scattering problem of a multilayer structure is analyzed with the Fisher information matrix and the Cramér-Rao lower bound. The Cramér-Rao lower bound quantifies the illposedness of the inverse problem in terms of resolution contra increase in noise from the observed data to the estimated parameters. It is shown that the resolution is inversely proportional to the bandwidth of the reflection data and that the Cramér-Rao lower bound increases linearly with the number of slabs. The transmission data gives a rank one Fisher information matrix with which can reduce the Cramér-Rao lower bound approximately a factor of four. Moreover, the eRect of dispersive material parameters and simultaneous estimation of two material parameters are analyzed. The results are illustrated with numerical examples.

Theory, Method, Experiments and Conclutions About the Strong and Weak Nuclear Forces in Einstein Theory of Relativity

E. Camps
Central University of Venezuela, Venezuela

My research on the field of atomic structures and electromagnetic forces on diamagnetic/dielectric materials lead to the positive detection of the weak and strong nuclear forces predicted by Dr. Einstein and its relations with protons, neutrons and electrons. Quantic levels in a new perspective. The historic background of the atomic theory that inspired the research.Understanding electromagnetic charges under dynamic conditions.Positive-negative, North-South integration in nuclear arquitecture. Instruments and experiments designed to detect the weak nuclear force.Hydrolics mechanics and calculus in the study of the weak force do work.Vortex and venturi effects. Electromagnetics and the strong force.Maxwell integration of electricity and magnetism revised.Experiments and probes developed to detect the strong force. Practical explanation and demostration of the existence of both forces, its effects,modes,strenght,properties and dimentions.Methods and techniques to detect and study the forces under controled lab enviroment and outdoors.Data collected and analysis.

Session 1P5
Metamaterials, Nano-Optics, and Nano-Electromagnetism

Subwavelength Imaging in Stratified Photonic Crystal Slab

H. F. Zhang[1,2], **L. F. Shen**[1,2], **J. T. Huangfu**[1,2], **Y. Yuan**[1,2], **L. X. Ran**[1,2], and **J. A. Kong**[1,3]

[1]Electromagnetics Academy at Zhejiang University, China
[2]Zhejiang University, China
[3]Massachusetts Institute of Technology, U.S.A.

We demonstrate for the first time subwavelength imaging in stratified photonic crystal slab structured by both square and triangular lattices. In virtue of equifrequency contour analysis and FDTD calculation, both near field and far field images are displayed. Subwavelength imaging in stratified photonic crystal slab consisting of only triangular lattice photonic crystal is also studied and it exhibits more flexibility than the single layer counterpart. That is, we could change the objective distance freely while keeping the image distance constant and vice versa.

As we know, the square lattice PC slab could act as a superlens in the ΓM direction only in the near field since its frequency contour is hyperbola like rather than rounded. However, the square-triangular stratified PC slab proposed here could well form a far field image whose full width at half maximum (FWHM) is about 0.46λ in the transversal direction by plotting electric field intensity distribution across the image. The field propagation map are shown in Fig. 1(a) and Fig. 1(b). Similarly, the triangular-square lattice PC is also studied and the field propagation maps are displayed in Fig. 1(c) and Fig. 1(d).

In addition, distance between object and image in single layer PC slab could not be too long since with the increase of the slab thickness resolution dropped. However, the triangular-air-triangular stratified PC slab is unrestricted and hence farther field imaging. Moreover, stratified PC slab provide more flexibility than the single layer counterpart in changing the objective and image distances which is rather useful in optical imaging system and particularly optical lithography.

Acknowledgement

This work is supported by the Key Project of National Science Foundation of China (NSFC) under Contract No. 60531020.

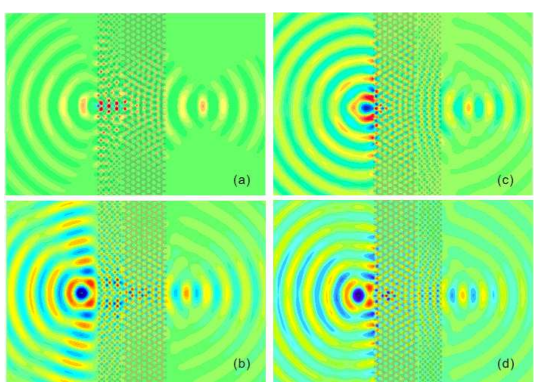

Figure 1: Electric field distribution of (a) square-triangular lattice stratified PC slab with near field source, (b) square-triangular lattice stratified PC slab with far field source, (c) triangular-square lattice stratified PC slab with near field source, and (d) triangular-square lattice stratified PC slab with far field source.

Theoretical Studies on Meta-materials: Modulations of Super Imaging Oscillations and the Eigenmodes of Metallic Ring Systems

L. Zhou [1], **X. Huang** [1], **C. T. Chan** [2], and **S. T. Chui** [3]

[1]Fudan University, China
[2]Hong Kong University of Science and Technology, China
[3]University of Delaware, USA

In this talk, we present some of our recent theoretical studies on meta-materials. In the first part, we discuss how to handle the intrinsic image instabilities found previously in the focusing process with a meta-material "super" lens. In the second part, we introduce a rigorous (in the sense to consider the inductive/capacitive effects completely) approach to study the eigen resonance modes of any metallic ring like systems, and illustrate some of its applications.

It was demonstrated previously that the image focused with a $\epsilon = \mu = 1$ meta-material lens is intrinsically unstable, and adding absorption stabilizes the image at the price of degrading the image resolution. Here we study the relationship between "switching-on" time and the intrinsic response of the meta-material lens, and find that a stable image with the highest possible resolution can be obtained in the shortest duration, if the switching time matches the intrinsic focusing speed of the lens. We demonstrate that the image oscillations, although appearing different and complicated in different situations, are all dictated by the interactions between the source spectra and the lens surface modes, and can be efficiently modulated by the lens thickness and the material parameters.

To study the eigenmodes of a metallic system in ring geometry, we develop an approach which rigorously considers all inductive/capacitive effects. Application to a single-ring split ring resonator (SRR) reveals that the odd-numbered modes exhibit both magnetic and electric responses while the even ones only electric responses; the SRR shows a bi-anisotropy for the odd-numbered resonances. Symmetry restriction allows a plane wave to excite only certain resonance modes of a SRR. Simulations on realistic structures verify all theoretical predictions. Calculations for a double-ring case suggest "optic (acoustic) modes" of asymmetric bi-anisotropy that are much more electric (magnetic) in character.

Clustered Dielectric Particle Metamaterials (CDP-MTMs)

C. Caloz and **M. Coulombe**
École Polytechnique de Montréal, Canada

Y. Horii
Kansai University, Japan

A. Rennings
Duisburg-Essen University, Germany

Most metamaterials (MTMs) reported to date, either of resonant or transmission line type, include metallic particles. This fact severely restricts their potential for millimeter-wave devices, where ohmic losses often tend to be prohibitive, and even more for optical applications, where most metals exhibit a plasmonic behavior with extremely low conductivity. For this reason, various solutions optical MTMs are currently being explored by several groups around the world. While some groups are following the avenue of plasmonic structures still based on metal but used as negative permittivity hdielectricsh, we have elected the avenue of real dielectrics. We report here our efforts toward designing an efficient all-dielectric negative refractive index (NRI) MTM.

Conventional photonic crystals can produce NRI effects, but they do not provide true refraction because of their dominantly diffractive nature; as a consequence, for instance, no NRI focusing may exist inside a conventional photonic crystal. In contrast, we report here novel clustered dielectric particle (CDP) MTMs, which can exhibit *homogeneous,* i.e. *true,* NRI, with clearly identifiable guided wavelength and macroscopic parameters. CDP-MTMs are constituted by the periodic repetition of molecule-like clusters of dielectric atom-like particles. The clusters support coupled dielectric modes generating, which are responsible for the isotropic and homogeneous nature of the MTM.

Several configurations of 1D, 2D and 3D CDP-MTM structures are analyzed by full-wave electromagnetic simulations. Preliminary experiments are presented.

Directed Subwavelength Imaging Using a Layered Metal-Dielectric System

B. Wood and **J. B. Pendry**
Imperial College London, U.K.

D. P. Tsai
National Taiwan University, Taiwan R.O.C.

A system consisting of thin layers of alternating metal and dielectric has recently been the subject of considerable interest. It has been proposed as a superlens, capable of subwavelength resolution, obtained by the transmission of the near field via coupled surface plasmons. We have investigated a different regime of operation, in which the permittivity of the metal and dielectric layers are no longer matched.

We can model the system as an effective medium with homogeneous anisotropic permittivity; at frequencies of interest, the components of the permittivity take different signs. Propagation of P-polarized waves is then supported for an unlimited range of real wavevectors: taking a slice through the dispersion relation at constant frequency gives a hyperbola rather than a circle or ellipse. In addition, there is now a preferred direction of propagation, at some fixed angle to the symmetry axis of the medium.

We have shown that a slab of such a material can form an image with subwavelength details. The position of the image depends on the ratio of the two different components of the permittivity. Since these components do not have the same frequency dependence, the image can be moved by changing the frequency.

We have shown that a slab of such a material can form an image with subwavelength details. The position of the image depends on the ratio of the two different components of the permittivity. Since these components do not have the same frequency dependence, the image can be moved by changing the frequency.

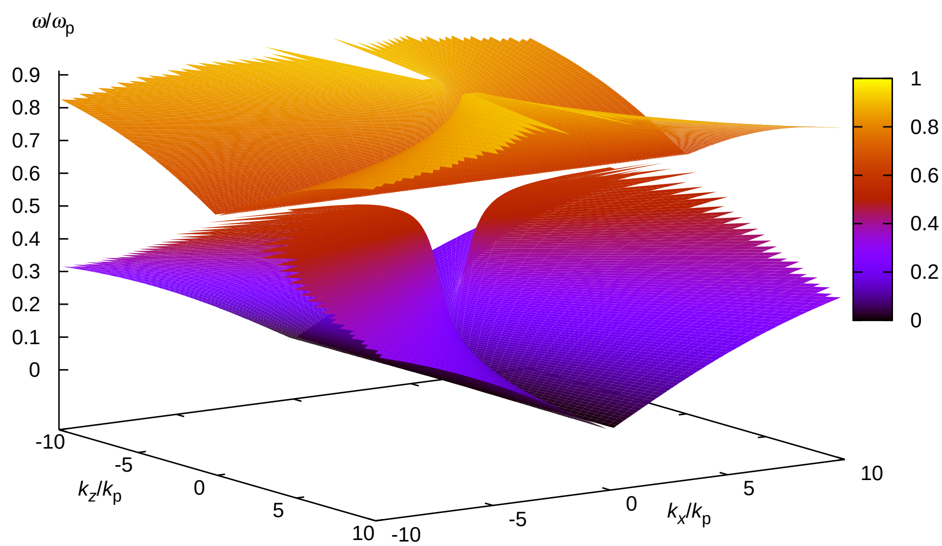

Figure 1: The first two bands of the dispersion relation for a metal-dielectric layered system, treated in the effective medium approximation.

Optical Imaging Below the Diffraction Limit with a Far-Field Superlens: Theory and Experiment

S. Durant, Z. Liu, H. Lee, Y. Pikus
Y. Xiong, N. Fang, C. Sun, and **X. Zhang**
University of California, U.S.A.

Optical imaging with resolution well beyond the diffraction limit with so-called superlenses [1] has been recently experimentally demonstrated [2]. Images formed by such superlenses are, however, in the near-field only, or a fraction of wavelength away from the lens [3]. In this paper, we propose a far-field superlens (FSL) device and we show theoretically that when an object is placed in close proximity of such a FSL, a unique image can be formed in far-field. As an example, we design numerically an optical FSL made of silver/glass working at 376nm, and we demonstrate imaging of 40 nm lines with a 30 nm gap from far-field data. The essential role of surface plasmon polariton is emphasized along a numerical study of the transmission properties of a metal/dielectric optical FSL [4]. Experimental realization and imaging [5] of a nano wire pair will be shown demonstrating the FSLfs ability to resolve 50 nm feature sizes.

REFERENCES

1. J. B. Pendry, gNegative refraction makes a perfect lensh, *Phys. Rev. Lett.* 85, 183966 (2000).
2. N. Fang, H. Lee, C. Sun, and X. Zhang, gSub-diffraction-limited optical imaging with a silver superlensh, Science 308, 534 (2005).
3. V. Podolskiy and E. Narimanov, gNear-sighted superlensh, *Opt. Lett.* 30, 76 (2005).
4. S. Durant, Z. Liu, J. Steele, and X. Zhang, gTheory of the transmission properties of an optical far-field superlens for imaging beyond the diffraction limith, accepted for publication, JOSA B (2006).
5. Z. Liu, S. Durant, H. Lee, Y. Pikus, N, Fang, Y. Xiong, C. Sun and X. Zhang, gA farfield optical superlensh, submitted (2006).

Study of Negative Refraction in Photonic Crystals Including Infinitely Conducting Metal

R. Pierre, Boris Gralak, and **G. Tayeb**
CNRS, Institut Fresnel, France

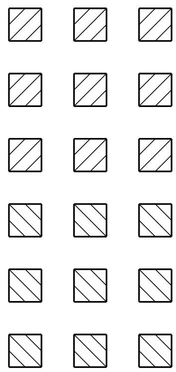

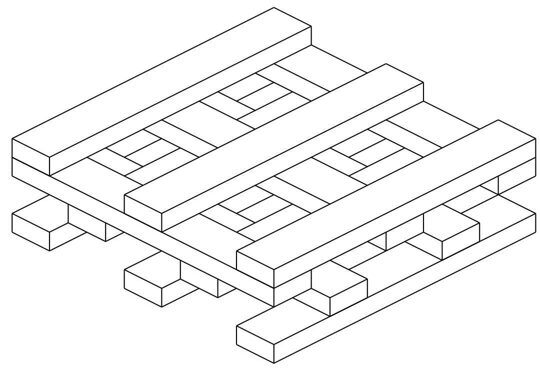

The concept of negative index materials has been introduced by V. G. Veselago [Sov. Phys. Usp. 10, 509 (1968)]. The most spectacular phenomenon produced by these materials is certainly the amplification of evanescent waves which would have very important applications for subwavelength imaging [Phys. Rev. Lett. 86, 3966 (2000)], as well as for light trapping [S. Guenneau et al., Optics letters 30, 1204 (2005)]. This is why the community is focusing on the design of composite structures presenting properties as close as possible to the ones of negative index materials.

Periodic structures made of metallic wires or gdouble C resonatorsh [D. R. Smith et al., Phys. Rev. Lett. 84, 4184 (2000)] were the first composite structures proposed to mimic negative index materials. Indeed, these structures possess a huge advantage since physical arguments permitted to predict that they will have the prerequisite properties. Nevertheless, from our knowledge, these structures did not find a good three-dimensional candidate with negative index property. This is why we propose in this communication to study the properties of other kinds of metallic periodic structures: two-dimensional crystals (on the left of the figure) and three-dimensional woodpile crystals (on the right of the figure) made of infinitely conducting rectangular rods.

From a numerical point of view, this problem can be reduced to the study of Maxwellfs equations in presence of infinitely conducting lamellar gratings. This subject has been widely studied at the beginning of the eighties [L. C. Botten et al., Optica acta 28, 1103 (1981)]. However, a rigorous and detailed use of these previous results leads to numerical instabilities, especially when the S or R algorithms are used. From our knowledge, the only one numerically stable formulation has been presented in a particular case [Z.-Y. Li et al., Phys. Rev. B 67, 165104 (2003)]. In the present communication, we show that the source of numerical instabilities is the inversion of a non-invertible matrix resulting from the product of an invertible change basis with a non-invertible projection. From our analysis, we determine all the structures where the S or R algorithms can be used without numerical instabilities.

Finally, we show the numerical results of our investigation of negative refraction in two-dimensional crystals and three-dimensional woodpile crystals including infinitely conducting metal. Our numerical investigation is based on dispersion diagrams, and on maps of the field in presence of finite-thickness structures.

Topological Considerations in the Frequency Response of SRR Loaded Microstrip Line

F. Falcone, M. Navarro, M. Beruete, T. Lopetegi, M. A. G. Laso, and **M. Sorolla**
Universidad Publica de Navarra, Spain

Great advances have been achieved in the study and experimental demonstration of Metamaterial structures in a very wide frequency range. In the microwave and millimetre wave range, transmission line approaches (reversing the conventional L series, C parallel behaviour by predominant C series, L parallel one) as well as Split Ring Resonators combined with thin metallic wire media have experimentally proven Left-Handed behaviour. SRR particles have been successfully introduced in planar circuit technology, such as microstrip and coplanar waveguide, leading to compact devices such as couplers and filters. In this work, the effect of varying the topological disposition of SRR particles loading a microstrip line will be analyzed. By means of full wave simulation results as well as by measured prototypes, the optimal configuration in rejection terms will be foreseen. These results aid in the implementation of practical devices in low cost planar circuit technology

All-Dimensional Subwavelength Metamaterial Cavity

H. Li
Tongji University, China

We propose the all-dimensional subwavelength metamaterial cavity and realize it in microwave region, which is from the conventional hollow cuboidal cavity but with one or more surfaces replaced by magnetic planar metamaterials. The boundary conditions of the cavity modes is governed by the arbitrary reflection phase from the magnetic surface at oblique angle incidence which can support modes with hence lift away the limit on the cut-off frequency of a conventional hollow cavity with same dimensions. In principle, the size of the metamaterial cavity can be infinitesimal compared to the working wavelength. Several metamaterial cavities are fabricated each with two metallic mesh surface to leak out the wave, which enables us to detect the return loss and radiation patterns of a small monopole inside the cavity. Measurements are in good agreement with the numerical simulations. In our experiment each dimension of the smallest cavity is smaller than a quarter of wavelength.

On the Modeling of Structured Bianisotropic Materials

O. Ouchetto[1], **S. Zouhdi**[1], and **B. Miara**[2]

[1]Laboratoire de Génie Electrique de Paris LGEP-Supélec, France
[2]Laboratoire de Modélisation et Simulation Numérique, France

A novel homogenization technique, combining an asymptotic multiscale method with wavefield conception, is proposed for computing the quasi-static effective parameters of a three-dimensional (3D) lattices of general bianisotropic composite materials. This technique is based on the decomposition of the fields into an averaged non-oscillating part and a corrected term with micro-oscillation. This paper provides an original and accurate way to model the electromagnetic fields in fine microstructures of bianisotropic particles with complex inclusion shapes when the wavelength is larger than the periodicity of microstructure. The effects of the interaction between edges and corners of adjacent inclusions on the macroscopic effective parameters have been studied, and numerical results and verifications have been presented.

Acknowledgments: This study was supported by the European Network of Excellence Metamorphose and the European project "Smart Systems" HPRN-CT-2002-00284.

Highly Directive Antenna Based on Anisotropic Metamaterials

Y. Yuan[1,2], **J. T. Huangfu**[1,2], **L. F. Shen**[1,2], **L. X. Ran**[1,2], and **J. A. Kong**[1,3]

[1]Electromagnetics Academy at Zhejiang University, China
[2]Zhejiang University, China
[3]Massachusetts Institute of Technology, USA

In this paper, a highly directive antenna based on anisotropic metamaterials is presented theoretically and experimentally. The condition for highly directive radiation based on anisotropic medium is presented, and is confirmed by FDTD simulation results. Ideal half-power beamwidth of the antenna is obtained, and effects of various factors on the performance of the antenna are further discussed. The theoretical predictions are confirmed by experiments.

Figure 1 and figure 2 show the near field and far field radiation pattern of the antenna, respectively. As is shown in figure 1, the EM wave is radiated from the slab, in the center of which a line current is situated. The wavefronts are nearly parallel with the interface of the slab, which implies that the radiated wave is in the direction of the normal of the interface between the slab and the freespace. In the figure 2, far-field radiation pattern of the antenna show that a sharp beam is obtained. Sidelobes are also suppressed after optimization of parameters.

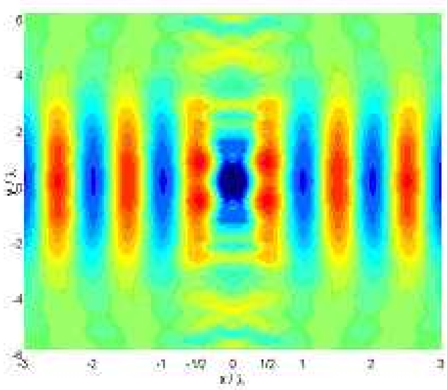

Figure 1: Near field of the antenna

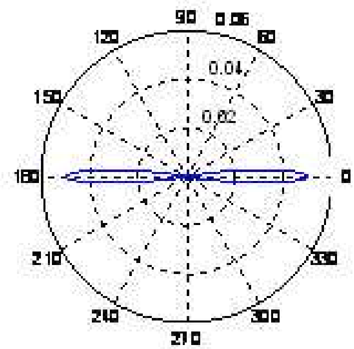

Figure 2: Radiation pattern of the antenna

Negative Refraction of Evanescent Waves Using 5-Fold-Symmetry Structure

Y. Feng
Xi'an Jiaotong University, China

J. Wu
China Research Institute of Radiowave Propagation, China

J. P. Song
Xi'an Jiaotong University, China

In this paper, We construct a metamaterial with 5-fold-Symmetry geometry of a 3-D array, calculate permeability and magnetic permeability ,and simulate of the LHM using FDTD. We get some interesting conclusion.

Session 1P6
Dosimetry of Human-Body Exposure to High-Frequency Electromagnetic Fields II

Studies on the Mechanisms of Possible Biological Effects of Radiofrequency Fields

K. R. Foster
University of Pennsylvania, U.S.A.

Biological effects of radiofrequency (RF) fields, particularly those that might be relevant for human health, have been much debated for many years. In the past several years, several groups of investigators in the United States, under support of MMF (an industry group), have undertaken a new examination of possible mechanisms of interaction between RF fields and biological systems, in search of potential mechanisms for nonthermal effects under exposure conditions that might be allowed by present-day (IEEE and ICNIRP) exposure guidelines. Mechanisms considered include coherent excitation of vibrational modes of macromolecules, "microthermal" heating, disturbance of the counterion layer surrounding macromolecules, and quantum interactions. This talk will review the major findings of this research. The general conclusion from these studies is that a wide variety of interaction mechanisms is conceivable, but that quantitative analysis of the proposed mechanisms, taking into account dissipative effects, generally leads to thresholds for causing observable changes in biological systems by RF fields that are far above levels needed to produce thermally significant changes.

Rf Exposure And Compliance Standards

C. K. Chou [1], and **R. Petersen** [2]
[1]Fort Lauderdale, U.S.A.
[2]Associates LLC, U.S.A.

As early as the mid-50's, limits for exposure to RF energy were recommended by various agencies and organizations throughout the world. The first RF exposure standard published in the USA (USAS C95.1-1966) was based on a simple thermal model and limited exposure to 10 mW/cm^2 averaged over any 0.1 h interval over the frequency range of 10 MHz to100 GHz. In the 70's, dosimetry studies revealed that the interaction of RF energy with biological bodies is extremely complex, and a frequency-independent limit over a broad frequency range is unrealistic. The 2$^{\text{nd}}$ revision of the 1966 standard (ANSI C95.1-1982) incorporated dosimetry, which resulted in frequency-dependent limits based on whole-body-averaged SAR. Limits on peak spatial-average SAR were included for localized exposure. In 1986, the National Council on Radiation Protection and Measurements (USA) recommended an upper tier (the same as that of the 1982 ANSI standard) for occupational exposure, and added a lower tier for exposure of the public. The IEEE C95.1-1991 and C95.1-2005 standards also contain two tiers. The upper tier includes a 10 fold safety factor; the lower tier has an additional factor of 5, i.e., a total safety factor of 50 below the threshold for effects considered adverse. The International Commission on Non-Ionizing Radiation Protection (ICNIRP) adopted the same approach and published guidelines in 1998. Although the ICNIRP guidelines and the 1991 IEEE standard are based on limiting the whole-body-averaged SAR in the resonance region to 0.4 W/kg and 0.08 W/kg for the upper and lower tiers, respectively, the peak SAR limits differ, both in magnitude and averaging volume. This discrepancy caused confusion for the general public, extra burdens for manufacturers, and discordance among the regulators. During the revision process that led to IEEE C95.1-2005, consideration was given to harmonizing with the ICNIRP guidelines where scientifically justifiable. Although there are minor differences between the two documents, the peak SAR limits in IEEE C95.1-2005 and the ICNIRP guidelines are now identical.

There are a number of standards that can be used to ensure compliance with the safety standards. For whole body exposures, compliance with the MPEs or reference levels can be determined by measurement of the incident fields using survey meters or similar devices and a number of standards that describe such techniques are available, e.g., IEEE C95.3-2002. For near field exposures from specific devices, determination of the SAR is usually required. In 1996, an IEEE committee began drafting a standard that specifies measurement protocols for certifying that mobile phones meet peak spatial-average SAR requirements. The result of this effort is IEEE 1528-2003. The European Committee for Electrotechnical Standardization (CENELEC) published a similar standard (EN50361) in July 2001. There were some differences between the two standards, e.g., in some tissue stimulant parameters for certain frequencies, and therefore some products are required to be tested twice, once for the European market and once for other parts of the world. This unnecessary duplication emphasized the need for a globally harmonized test method. The International Electrotechnical Commission (IEC) Technical Committee 106 (TC-106) published its standard (IEC 62209-1) in Feb 2005, which is in complete harmony with IEEE 1528-2003, and will replace the CENELEC standard. Currently, IEC TC-106 is working on a standard (P62209-2) for certifying compliance of other portable wireless devices, e.g., body-mounted devices. Another project team is working on a base station compliance standard (P62232).

The authors have participated in the development of both exposure and measurement standards. During committee deliberations on the compliance standards, the focus was on precision; during development of the exposure standard the focus was on conservatism. Worst case assumptions were considered in both. While it is always good practice to make precise and accurate measurements, there is a trade-off when assessing compliance of a device with limits that have large safety margins built in. In this case, whether or not a product meets a specified limit is a compliance issue - not a safety issue. The goal should be agreement on a realistic compliance method. We should not be in a position where we can't see the forest for the trees. Harmonization is the key issue for exposure and measurement standards.

Novel SAR Measurement Method Using Surface Scanned Electric Field

T. Onishi, K. Kiminami, and **S. Uebayashi**
NTT DoCoMo Inc., Japan

INTRODUCTION: The compliance test procedures for Specific Absorption Rate (SAR) measurement with respect to mobile phones were standardized by the IEC and other standardization bodies. The procedure described in the standards enables precise measurement. However, a method for rapidly performing the SAR measurement has been desired because three-dimensional (3-D) scanning is time consuming. Presently, another SAR measurement procedure that covers various conditions, e.g. body-mounted devices, is being developed by the IEC [1]. We have proposed a SAR estimation method, which theoretically estimates the 3-D SAR distribution from surface scanned (2- D) electric field measurement data [2]. The method can shorten the SAR measurement time while maintaining the same level of SAR estimation accuracy. This paper discusses the actualization of the faster SAR measurement using the proposed estimation method.

METHODS: The SAR estimation method theoretically estimates the 3-D SAR distribution from surface scanned (2-D) electric field measurement data, which basically applies the Equivalent theorem and the Maxwellfs equations [2]. First, the magnetic field is estimated using the measured electric field based on the integral form of the Maxwel's equation. Then, 3-D SAR distribution can be estimated using the measured electric and estimated magnetic fields employing the Equivalent theorem. Since the estimation method requires the phase of the electric field, an Electro-Optic (EO) probe is employed because it can measure simultaneously the amplitude and phase of the electric field [3]. The EO probe comprises EO crystals, some optical components, and an optical fiber, i.e. no metal. One idea to decrease the measuring time is to use multiple probes [4]. When this estimation method is used, a 2-D probe array provides sufficient data to estimate the 3-D SAR. An additional feature when using the EO probe is that it can measure the SAR at multiple frequencies at the same time. Therefore, it is expected that the SAR measurement of wireless devices with simultaneous multi-band transmissions can be performed. It is noted that broad-band characteristics of the phantom, which can covers desired frequency range, is necessary.

DISCUSSION: Numerical and experimental validations with respect to the proposed estimation method were performed. The model used in this study comprises a half-wave dipole and a cubic acrylic container (200 mm x 200 mm x 200 mm), which was filled with a tissue-equivalent liquid. The frequency was 1950 MHz. The liquid has the relative permittivity of 40.0 and the conductivity of 1.40 S/m at this frequency. Since in this validation we used only one probe, the 2-D electric fields were measured by scanning the EO probe. The minimum sensitivity and linearity of the probe is less than 1.4 mW/kg and ± 0.4 dB, respectively. These values satisfy the requirements for the IEC standard [5]. It was also confirmed that the EO probe can discriminate between two frequencies [3]. The estimated SAR distributions agree with the measured one very well. The results showed that the 10g-average SAR can be estimated from the two-dimensional measured electric field data within 1% compared to the original 10g-average SAR.

CONCLUSION: The SAR measurement method, which is mainly based on the proposed estimation method and multiple EO probes, was discussed. Numerical and experimental validations of the estimation method were performed. The results confirmed that the proposed estimation method estimates the 3-D SAR distribution using the 2-D electric field data to within 1%. The method enables not only faster measurement, but also measurement of multi-band transmissions.

REFERENCES

1. IEC TC106 PT62209 Part2 (draft).
2. T. Onishi, et al., 28th URSI GA, KP-44, New Dehli, India, Oct. 2005.
3. T. Onishi, et al., 27th BEMS Meeting Dublin, P-C-21, Ireland, June 2005.
4. T. Iyama, et al., IEEE AP-S, pp. 3597 . 3600, Monterey, USA, June 2004.
5. IEC 62209-1, Feb. 2005.

Variation of Measured Maximum Local SARs between Standard-Compatible Measurement Systems (Part 3)

L. Hamada and **S. Watanabe**
National Institute of Information and Communications Technology, Japan
Y. Miyota and **K. Sato**
NTT Advanced Technology Corporation, Japan
T. Iwasaki
The University of Electro-Communications, Japan

In most countries, measurement of the specific absorption rate (SAR) has been required for cellular phones. The procedure of the SAR measurement and the specification of the measurement system are described in international standards such as IEC 62209-1[1]. The standard procedure recommends that SAR measurement systems for the compliance test should consist of a human head phantom, a SAR-probe, a scanning system, and a post-processing PC [1] - [3].

We have previously presented the comparison of the measured maximum local SARs of cellular phones between three commercially-available SAR measurement systems: SPEAG DASY3, DASY4, and IndexSAR SARA2 [4] [5]. In those studies, the angles of the SAR probe to the inner surface of the head phantom shell were significantly different between the systems. In addition, the SAR value was dependent on the position of the peak SAR for each handset under test. It was because the insertion angle of the probe to the phantom shell differed by the measurement position. In this study, we performed some additional measurements using that three measurement systems and a new system developed by ourselves. As a result of the comparisons of the SAR measurement between these measurement systems, the difference of the SAR value was also dependent to the insertion angle of the probe, but the maximum variation was less than 30% which is the maximum expanded uncertainty required in IEC 62209-1 [1]. At the conference, we will present detailed measurement data to identify the factors which have large effect to the measurement result.

REFERENCES

1. IEC international standard 62209-1, (2004. 2).
2. IEEE, Std 1528-2003, (2003. 12).
3. Association of Radio Industries and Businesses (ARIB) in Japan, STD-T56 Ver2.0, (2002. 2).
4. S. Watanabe, et al. Bioelectromagnetics 2005, Dublin, Ireland, pp. 489-492 (2005.6).
5. S. Watanabe, et al., 26th Annual Meeting of the Bioelectromagnetics Society, Washington DC, USA, pp. 160-161 (2004. 6).

Study on Dielectric Properties of Phantom Material for SAR Test in a Human Body

A. K. Lee, J. I. Choi, D. U. Sim, and **H. D. Choi**
Electronics and Telecommunications Research Institute, Korea

The present standards such as IEEE Std 1528 and IEC 62209-1 for compliance test with radiation safety limits generally deal with hand held devices to be used close to the human head. Dielectric parameters of tissue simulating liquids for the compliance test in these standards are defined based on the worst-case tissue layer composition and thickness for the user group including adults and children in the region of the ear and the temporal bone with respect to absorption at each frequency.

Meanwhile the wireless communication devices mounted on the human body such as PDA (personal digital assistant) have been rapidly appeared. The SAR (specific absorption rate) determining procedure for local exposure from body-mounted devices is under consideration in IEC TC106. The body-mounted devices radiate RF field to waist, abdomen, chest etc of the human body. The compositions and thicknesses of the trunk are significantly different from those of the head.

In this paper, the maximum SAR values have been analyzed in three hundred one-dimensional multilayered models. The multi-layered models are extremely various in composition and thickness of tissues, which were obtained from the Korean adult human body model. At discrete frequencies in the range of 300 . 6000 MHz, peak 1-g and 10-g SARs for incidence of a plane wave were calculated in each layered model. The SAR values were analyzed statistically and the 90_{th} and 100_{th} percentile SARs at each frequency were compared with those in the head-equivalent tissue.

The SAR values in the layered models using the human trunk were higher than those for the head tissue at most of the frequencies. Therefore, new dielectric parameters of tissue-simulating liquids need to be derived for SAR compliance test of the body-mounted devices. New permittivity and conductivity at each frequency should not underestimate SAR value but it is also not desirable to overestimate it excessively. In this paper, we regarded the 90_{th} percentile value of 1-g and 10-g SARs as the proper SAR levels evaluated in the flat phantom. However, more discussion on this SAR level is required. The permittivity and conductivity were investigated which produce the 90_{th} percentile 1-g and 10-g SAR values in an infinite flat phantom at each frequency.

Below about 600 MHz, dielectric properties available for the 90_{th} percentile SAR did not exist. At a few upper frequencies, the derived dielectric properties (ϵ and σ) were validated by comparing SAR distributions on the surface of the Korean anatomical voxel model. (a) 1 g SAR at 835 MHz (b) 1 g SAR at 2000 MHz Figure 1. Comparison of SAR values in the anatomical human body and the flat phantom.

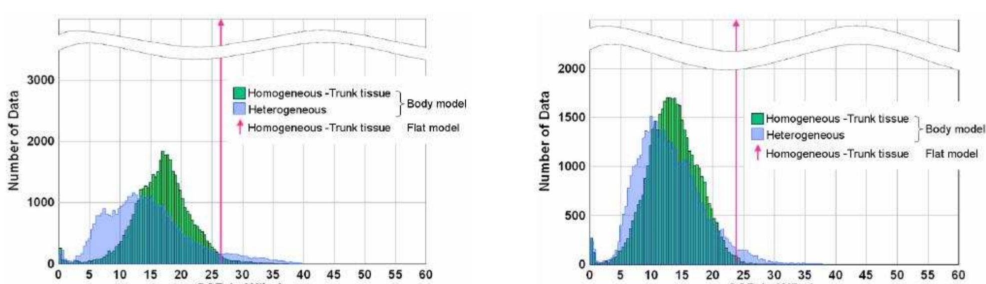

(a) 1 g SAR at 835 MHz (b) 1 g SAR at 2000 MHz

Figure 1: Comparison of SAR values in the anatomical human body and the flat phantom.

SAR Measurement within the Phantom by Thermo-Chromic Liquid Crystal

Y. Suzuki, M. Baba, and **M. Taki**
Tokyo Metropolitan University, Japan
K. Fukunaga and **S. Watanabe**
National Institute of Information and Communications Technology, Japan

We have developed a new technique to measure three-dimensional (3D) specific absorption ratio (SAR) distributions in transparency gel phantom. This technique is based on 3D temperature distribution imaging by means of micro-capsulated thermo-chromic liquid crystal (MTLC).

In this study, MTLC is used as temperature sensor. The diameter of the micro capsule is about 20 to 30 micrometer. Liquid crystal with cholesteric phase is encapsulated by urea resin. When the visible light is projected on transparency substrate including MTLC, the color image corresponding with each temperature value is observed. The wavelength of scattered light by MTLC becomes shorter with the increase of temperature. In other words, the scattered light changes in its color from red to purple with the increase of temperature. MTLC are used to suspend uniformly in the transparency substances such as liquid, gel or solid.

To realize temperature-imaging technique, high-molecular gel constructed from gcarrageenanh, which is extracted from seaweed and has high transparency, is employed as the substrate of the tissue equivalent phantom. The dielectric properties of the phantom are adjusted by mixing sucrose, propylene glycol (PG) and potassium chloride (KCl). We can adjust a value of complex permittivity of phantom to that of muscle at 900MHz and 1.5GHz.

We expose the electrical tissue equivalent phantom to 1.5GHz electromagnetic field. A dipole antenna is used to irradiate the phantom containing MTLC. The temperature distribution, which is visualized by scattering light from red to purple, on the plane lit up by the slit light is obtained clearly. Time evolutional images of two-dimensional (2D) temperature distribution inside of phantom are captured by CCD digital camera. Digitized captured images are transformed into temperature value by using Hue-Saturation-Luminance (HSL) color scheme. Internal 2D SAR distribution on the cross section visualized by slit light is estimated from temperature elevation over a short period of time. This technique enables non-destructive and non-invasive SAR measurement within the phantom. Moreover, it is possible to reconstruct 3D SAR distribution by sweeping imaging cross section.

A Precise Electromagnetic Field Estimation in Elevator Considering of Implantable Cardiac Pacemaker EMI From Cellular Radios

L. Harris [1], **A. Simba** [1], **T. Hikage** [1], **T. Nojima** [1]
M. Omiya [1], **S. Watanabe** [2], and **T. Shinoduka** [2]
[1]Hokkaido University, Japan
[2]National Institute of Information and Communications Technology, Japan

The purpose of this study was to estimate the Electromagnetic field (EMF) distributions in environments surrounded by conductive surfaces, e.g., train carriages or elevators. Here, we refer to this kind of environment as a semi-echoic environment (SEE). However, precise measurements in the actual environment are difficult because of disturbing of fields due to the presence of measuring equipments or human body. In this paper, we carried out precise numerical simulations to examine the EMF in actual elevators. Additionally, a simplified histogram estimation method for electric field strength was developed to deal with the complicated EMF distributions. Here, the relative field strength normalized to a certain reference level determined from the experimentally obtained maximum interference distance of implantable cardiac pacemakers was used. This allows the EMI risk to pacemakers by cellular radio transmission to be quantitatively evaluated. The numerical model of the elevator is shown in Fig. 1. By way of example, this is a case in which one user is present in the elevator. In this paper, we used 1-cm cubic cells for FDTD modeling. In the actual environment, the effects of losses due to the human body cannot be disregarded. Then, in order to examine the realistic and complicated situations where humans are present in the elevator, we apply the homogeneous human phantom model in the FDTD analysis. They have realistic shapes and homogeneous electric parameters. Here we use a half-wavelength dipole antenna to represent a cellular radio operating in the 2 GHz band. The antenna is set 20 mm from the human phantomfs head and 158 m from the floor.

Following this, we used field histograms to estimate the percentage of areas having the same field strength in the inside plane of elevator. The histogram was useful in carrying out a complete estimation of the whole area. As the reference value, we took the EMF strength at the maximum interference distance mentioned in the objective above. Also, we chose to use the plane 1.3 m from the floor to estimate histograms. The percentage of the area whose electric field strength exceeds this reference value gives an indication of the possibility of EMI negatively impacting the pacemaker. We can identify whether or not a pacemaker malfunction will occur by identifying those areas where EMF exceeds the reference value.

The histogram is shown in Fig. 2. The EMF strength inside the elevator did not exceed the reference value. This result suggested that the EMF strength inside the elevator did not exceed the safety levels with regard to pacemaker operation. Further investigations for specific absorbing rate (SAR) of passengers in elevators by using inhomogeneous human phantom model are being conducted.

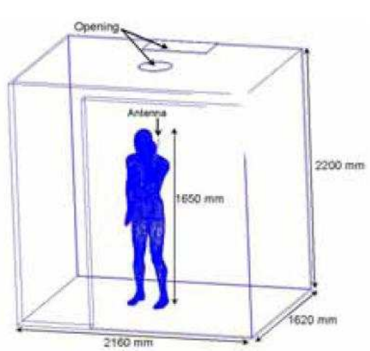

Figure 1: FDTD model for elevator.

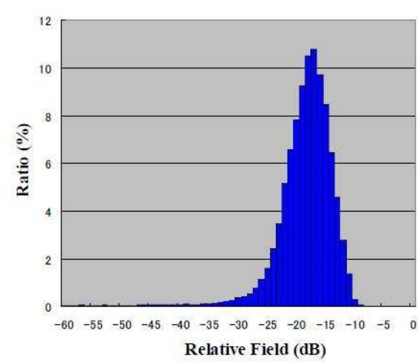

Figure 2: Histogram in the case of one mobile phone user.

A Gain Calibration of Antennas in Conducting Medium Using Friis Formula in Fresnel Region

N. Ishii [1,2], **T. Akagawa** [1], **K. Sato** [3]
L. Hamada [2] and **S. Watanabe** [2]

[1]Niigata University, Japan
[2]National Institute of Information and Communications Technology, Japan
[3]NTT Advanced Technology Corporation, Japan

A new method of calibrating a SAR (Specific Absorption Rate) probe is required to estimate SAR values of various mobile communication devices above 3GHz. A conventional calibration with the waveguide is widely used from 300MHz to 3GHz; however, it may clear the effect of the radius of the SAR probe above 3GHz. This is because the radius is comparable with the dimension of the cross section of the waveguide. Therefore, alternative method should be developed.

In our method[1], gain of a reference antenna is calibrated on the basis of the Friis formula in the conducting medium using the vector network analyzer. Then, the magnitude of the field radiated by the antenna is correspondent to the value of the output voltage of the SAR probe. In practice, two identical antennas are connected to the port 1 and 2 of the network analyzer, and then the magnitude and phase of S_{21} between two ports can be measured as a function of the distance between two antennas. These data can be fit into the curve of the Friis formula and then gain and attenuation/phase constants of the medium can be estimated. However, the attenuation in the tissue equivalent liquid is so high that it can be difficult to measure the S_{21} in the far field region. For example, the attenuation in that liquid is $\alpha = 464$dB/m at 2.45GHz, so the measurable range in the far-field is limited. Above 3GHz, the attenuation is much larger, so the measurable range is more limited.

To overcome this difficulty, we can introduce the Friis formula in the Fresnel region, which includes $1/r^3$ term[2] and $e^{-c_1/r}$ contribution, where r is the distance between two antennas and c_1 is a constant. That is,

$$\begin{aligned} |S_{21}|^2 &= |S_{21}|^2_{\text{far field region}} \cdot e^{-c_1/r}\left(1+\frac{c_2}{r}\right) \\ &= (1-|S_{11}|^2)(1-|S_{22}|^2)\frac{G_1 G_2 e^{-2\alpha r}}{(2\beta r)^2} \cdot e^{-c_1/r}\left(1+\frac{c_2}{r}\right) \end{aligned} \tag{1}$$

where S_{11} and S_{22} are reflection coefficients at port 1 and 2, G_1 and G_2 are gains of the antennas connected to port 1 and 2, α and β are attenuation and phase constants of the liquid and c_2 is a constant. Although we cannot avoid using a nonlinear regression, we can estimate gains and attenuation/phase constants if their initial values are appropriately selected. The proposed method can be checked by comparing the results fit in the Fresnel region with those in the far-field region. Thus, the gain of the reference antenna can be calibrated by using the Friis formula in the Fresnel region for the highly conducting medium.

REFERENCES

1. N. Ishii et al.:"Proposal of Accurate SAR-probe Calibration Using Reference Antennas in the Liquid at Higher Frequency," Proc. 28th URSI-GA, A11.7(01767), (2005-10).
2. J. R. Pace: "Asymptotic Formulas for Coupling Between Two Antennas in the Fresnel Region," IEEE Trans. Antennas & Propagat., vol. AP-17, no. 3, pp.285–291, May 1969.

Numerical Simulation of Helical Dipole Antenna Using the MoM/FDTD-Hybrid Method

P. Pongpaibool and **S. Watanabe**
National Institute of Information and Communications Technology, Japan
S. Mochizuki and **H. Shirai**
Chuo University, Japan
T. Uno
Tokyo University of Agriculture and Technology, Japan

In recent years, the Finite Difference Time Domain (FDTD) method [1] is one of the most popular numerical techniques for the solution of electromagnetic problems and the dosimetric evaluation of specific absorption rate (SAR) in the human body. However, this method encounters difficulty in modeling the electromagnetic sources of wire or curved structure antennas that do not conform to the FDTD lattice. On the other hand, the Method of Moment (MoM) [2] works well for these complex antennas, but not for a human body.

The MoM/FDTD-hybrid method has been proposed to overcome these difficulties [3,4]. There are few reports of the application to practical problems becuase these methods require difficult and complex techniques, especially in the iteration procedure between the MoM and the FDTD. To avoid these troublesome, a new iteration scheme for the MoM/FDTD-hybrid method has been developed [5]. In this technique, relatively simple iteration procedures are used. In the first step, the calculated near-fields of the antenna in the MoM are used as the incident fields in the scattering field formulations of the FDTD method. Next, the induced voltage at each segment of wire antenna models in the MoM is evaluated from the scattering fields calculated in the FDTD and then added in the MoM matrix equations, like as the feed voltage at the feeding gap segment. The steady-state solution is evaluated from the convergent value after several iterations between the MoM and the FDTD steps.

In this paper, we applied this MoM/FDTD-hybrid method to a scattering problem including a helical dipole antenna according to its frequently used for the cellular phones. The calculated near-fields of the helical dipole antenna that agree well with the measured near-fields are used as incident fields in the FDTD method. In the preliminary investigation of the electromagnetic coupling between half-wavelength helical dipole antenna and half-wavelength thin wire, the simulation results such as the input impedance and the current distribution on both helical dipole antenna and thin wire have confirmed the good agreement of the MoM/FDTD-hybrid method comparing with the MoM. Moreover, both input impedance and current distribution converge to the MoM after about 2 iterations.

REFERENCES

1. A. Taflove, Computational Electrodynamics: The Finite-Difference Time-Domain Method, Artech House, 1996.
2. R. F. Harrington, Field Computation by Moment Method, The Macmillan Co., 1968.
3. G. Cerri, S. Chiarandini, P. Russo, and A. Schiavoni, "Electromagnetic coupling between arbitrarily bent wires and scatterers analysed by a hybrid MoMtd/FDTD approach," IEE Proc. Microw., Antennas and Propag., vol.147, no.4, pp.261–266, Aug. 2000.
4. M. A. Mangoud, R. A. Abd-Alhameed, and P. S. Excell, "Simulation of human interaction with mobile telephones using hybrid techniques over coupled domains," IEEE Trans. Microwave Theory Tech., vol.48, pp.2014–2021, Nov. 2000.
5. S. Mochizuki, S. Watanabe, M. Taki, Y. Yamanaka, and H. Shirai, "A new iterative MoM/FDTD formulation for simulating human exposure to electromagnetic waves," IEICE Trans. Electron., vol.E87-C, no.9, pp.1540–1547, Sept. 2004.

SAR Characteristics of a Human Standing on Low-Loss Ground Plane Exposed to VHF Electromagnetic Plane Wave

S. Watanabe[1], **K. Arai**[1,2], **T. Nagaoka**[1], **M. Taki**[3], **A. Hirata**[4]
J. Wang[4], **O. Fujiwara**[4], and **T. Uno**[2]

[1]National Institute of Information and Communications Technology, Japan
[2]Tokyo University of Agriculture and Technology
[3]Tokyo Metropolitan University
[4]Nagoya Institute of Technology

The whole-body resonance of a human body standing on the ground plane is one of the most important phenomena for radiofrequency (RF) safety guidelines. This phenomenon appears in VHF band where the wavelength is comparable with the tall length of human bodies. It is also known that the resonant frequency of the human body standing on the ground plane is about half of that of the human body in free space. In most previous studies, however, the ground plane has been assumed as a perfect electrical-conductor wall while actual ground plane is low-loss dielectric in VHF band.

The objective of this study is therefore to clarify details of SAR characteristics of human bodies standing on realistic low-loss ground plane.

Recently millimeter-resolution voxel human models have been used for human-body SAR calculations of finite-difference time-domain (FDTD) method, which is known as the most powerful numerical simulation methods for voxel human models. It is however difficult to use those voxel human models in FDTD calculations including the low-loss ground plane because significat volume under the groung plane, i.e., several-meter ground material region, must be considered in the calculation region in order to simulate accurate reflection and diffraction on the ground plane, which results in significant increase of required computer memory and calculation time. In order to overcome this problem, we have applied perfect-matched-layer (PML) absorbing boundary conditions (ABCs), which matched to electrical properties of the low-loss ground plane, just several-cells below the ground plane.

In this presentation, we first demonstrate the validity of the application of the PML-ABC just below several-cells below the ground plane. Then, we show the frequency characteristics of the human bodies (Japanese adult male and female and children) standing on the realistics low-loss ground plane. Finally we discuss a possibility of relaxation of the RF safety guidelines for human bodies standing on the realistic ground plane.

Complex Permittivity Measurement of Blood in Millimeter Wave Band

H. Wakatsuchi[1], **M. Hanazawa**[2], **S. Watanabe**[2], **M. Kouzai**[3]
A. Nishikata[3] and **O. Hashimoto**[1]

[1]Aoyama Gakuin University, Japan
[2]National Institute of Information and Communications Technology
[3]Tokyo Institute of Technology

Recently, utilized frequency band is shifted to high frequency region and electromagnetic dosimetry is required in order to evaluate health hazard of such high-frequency electromagnetic fields. This area of science deals with a simulation of exposure and calculation of internal field in an exposed biological structure. Permittivities of each tissue are required to calculated electromagnetic dosimetry. It is well known that the permittivities of biological tissues have frequency dispersion. So great number of measurement methods of a dielectric constant have been studied at various frequency bands. However, to our knowledge, permittivities of tissues have not been established in millimeter wave bands. Accurate permittivities of biological tissues and organs in millimeter wave bands have been strongly required for evaluation of health effects of millimeter-wave exposure. So we measured a permittivity of blood and plasma up to 50 GHz using a commercial probe (Dielectric Probe 85070E (Agilent Technology)) and a VNA (Vector Network Analyzer E8316A (Agilent Technology)). The probe was calibrated using a short block, deionized water and air. A permittivity of ethanol was measured after each calibration in order to check reproducibility of measurement. And temperature of blood was set to about 38 degree C. As results, these measurement values show good repeatability. Next we compared with measurement values of a dielectric tube method. These results are in good agreement with them too. From the result, it was confirmed that the probe could be used for measurement of the other tissue. Using the measured permittivities we calculate SAR distribution and thermal elevation of an exposed rabbit eye. Near future, we plan to measurement of permittivity of variation biomedical tissues at more high frequency region.

Session 2A1
Electromagnetic Precursors of Earthquakes

Electomagnetic Phenomena Associated with Earthquakes: Review

M. Hayakawa
The University of Electro-Communications, Japan

After the disastrous Kobe earthquake, the former Science and Technology Agency (STA) of the Japanese Government proposed the Intergrated Earthquake Frontier Project. Within the framework of the project, two institutions (RIKEN (Physical and Chemical Institute) and NASDA (National Space Development Agency of Japan)) were asked to carry out over five years a feasibility study of the use of electromagnetic phenomena in short-term earthquake prediction. Since 1996 the RIKEN group has been engaged in the study of earth current and related phenomena. Meanwhile, under the NASDA project named gEarthquake Remote sensing Frontier Projecth (for which I was responsible), we performed an overall study of seismo-electromagnetic phenomena occurring not only in the lithosphere, but also in the atmosphere and ionosphere. Our five-year study has indicated a new finding that the seismic effect expresses itself not only in the lithosphere (such as by ultra low frequency (ULF) electromagnetic emissions, acoustic emissions etc.), but also in the atmosphere and ionosphere (by means of pre-existing transmitter signals). Most importantly, we find convincing evidence for seismo-ionospheric perturbations on the basis of subionospheric very low frequency (VLF)/ low frequency (LF) signals. We have established a new challenging scientific field, gLithosphere-atmosphere-ionosphere couplingh or gElectromagnetics in the coupled lithosphere-atmosphere-ionosphere systemh. The study of this coupling would contribute to scientific short-term earthquake prediction. This paper reviews first a lot of scientific output from our NASDAfs Frontier Project including the most important seismo-ionospheric perturbations, in-situ observation of plasma density, GPS monitoring of total electron contents, seismo-atmospheric perturbation and finally lithospheric emissions. Then, we present our further latest results on recent large earthquakes in Japan and abroad and also indicate what we have to do in future.

The Observation of DC/ULF Emissions at Nakatsugawa, Japan in Possible Association with the Niigata-Chuetsu Earthquake

K. Ohta [1], **N. Watanabe** [1], and **M. Hayakawa** [2]

[1]Chubu University,Japan
[2]University of Electro-Communications,Japan

We have three orthogonal induction coils (1.2m permalloy) as magnetic sensors and we observe three magnetic field components (B_x, B_y and B_z ; x, y are the horizontal axes, and z, the vertical axis) at Nakatsugawa (Geographic lat. 35.4^o N, long. 137.5^o E) in Japan. The signals from magnetic field components are amplified by means of pre-amplifiers (gain=66dB) with the low pass filter (with cutoff of 30Hz). Then the signals are converted by means of an A/D converter with sampling frequency of 100Hz, and they are stored on a hard disc every six hours. Signal analysis is based on the FFT with the data length of 1024, so that the temporal resolution is about 10 seconds and the corresponding frequency resolution is about 0.1Hz. We can measure the amplitude ratio and phase difference among the three components in the frequency range from 0Hz to 50Hz. The temporal evolution of the magnetic field intensity (horizontal B_y component: sensitive to the waves propagating in the NS meridian plane) at a particular frequency of 0.1Hz (to be exact, this frequency means the frequency below 0.1Hz) is given by FFT method. The intensity of background noise averaged over one file with duration of six hours. We noticed the significant difference between below 0.1Hz and another higher frequency. Only background nose of 0.1Hz does not show a regular diurnal pattern, and the intensity of 0.1Hz rises up for long hours before the big earthquakes.

The intensity of +3dB above the average level during one month of October in 2004 rises on 2 and stops on 6. This term is just 21-17 days before the Niigata-Chuetsu earthquake. The direction finding is the conventional goniometer by using only the two horizontal magnetic components. The measuring accuracy of the goniometric direction finding depends on the antenna length and antenna alignment accuracy. The length of one induction magnetometer is only 1.2m, so that the overall estimate of the measuring accuracy is on the order of $\pm 10^o$. The azimuth is indicated northward from the geographic East direction (as estimated from $\tan^{-1}(B_y/B_x)$). The average azimuth of DC/ULF emissions at the frequency below 0.1 Hz during October 2-6, is found to be extremely stable and about 55^o northward from the east, which means the noises during this period are arriving from 55^o north of the east. The angle from Nakatsugawa to the epicenter of the Niigata-Chuetsu earthquake is 60^o.

Progress in Three-Dimensional FDTD Maxwell's Equations Modeling of Global Impulsive ULF/ELF Propagation

J. J. Simpson and **A. Taflove**

Northwestern University, U.S.A.

Propagation of ultra low-frequency (ULF: 0-3 Hz) and extremely low-frequency (ELF: 3-300 Hz) electromagnetic waves in the Earth-ionosphere waveguide is an important area of investigation. Currently, ULF/ELF phenomena form the physics basis of remote-sensing investigations of lightning and sprites, global temperature change, subsurface structures, submarine communications, and potential earthquake precursors.

This paper succinctly reviews computational modeling research by our group in this area. Specifically, we are pursuing finite-difference time-domain (FDTD) Maxwell's equations simulations of global impulsive ULF/ELF propagation. Our goal is to construct and apply numerical algorithms which can include intricate details of the Earth's curvature and topography, as well as the inhomogeneous and anisotropic electrical properties of the lithosphere, oceans, and ionosphere.

Our initial work was based upon a three-dimensional (3-D) spherical-coordinate, latitudelongitude grid. This employed an adaptive East-West cell-combination technique to reduce the eccentricity of the grid cells in the polar regions, thereby yielding a greatly improved computational efficiency relative to conventional spherical-coordinate formulations. Furthermore, the grid allowed for variable cell size in the radial (vertical) direction. Overall, the latitude-longitude grid provided propagation modeling results accurate to $\pm$1dB over the ELF range 50-500 Hz. This accuracy was obtained using only a laboratory computer to process a high-resolution ($\sim 40 \times 40 \times 5$ km) model of the complete Earth-ionosphere cavity within $\pm$100km of sea level. We first reported the usage of this model to simulate hypothesized electrokinetic currents in the lithosphere prior to the Loma Prieta earthquake for comparison with measured data obtained by Fraser-Smith of Stanford University. Later, we applied this model to explore a novel potential ELF radar for major oil deposits.

Subsequently, we developed an alternative 3-D geodesic grid of the global Earth-ionosphere waveguide. This model employs hexagonal and pentagonal grid cells to span the spherical surface at each radial coordinate, and also allows for variable cell size in the radial direction. The geodesic grid is superior to our previously reported latitude-longitude grid in a number of respects. First, the geodesic grid completely avoids grid-cell convergences at the North and South Poles. Therefore, it provides much more isotropic wave propagation and is simpler to construct. Second, the geodesic grid ports efficiently to a massively parallel supercomputer. Third, it permits an easier interchange of data with state-of-the-art Earth-simulation codes used by the geophysics community. To date, we have applied this new geodesic grid model to explore a novel potential ELF radar for ionospheric depressions hypothesized to exist prior to earthquakes. We hope in future work to incorporate details of the plasma physics in the ionosphere as well as to further improve the spatial resolution and maximum depth and height of the grid.

Wave Propagation Mode of Earth-Origin EM Pulses as a Precursor of Earthquake

M. Tsutsui
Kyoto Sangyo University, Japan

We developed a method of finding arrival directions of earth-origin electromagnetic (EM) pulses from detected electric E and magnetic H components of the pulses. The sensor system is composed of a vertical electric dipole antenna and horizontally- and orthogonally-arranged two search coils, which is inserted into a bore-hole of 10 cm in diameter and 100 m in depth. We detected electric and magnetic pulsed waveforms just when an earthquake occurred in Jan 6, 2004. From these waveforms, we first derive frequency dispersion characteristic curves of each field component. Next using amplitudes and phases of three EM components in all frequencies obtained in deriving their dispersion curves, we could provide frequency-dependent arrival directions by Poynting vector E x H, and could determine a true arrival direction of the pulse. Third, we could determine propagation distance of the EM pulse, by comparing the dispersion curve with theoretical curves of tweek atmospherics, and we picked up one of the theoretical curves which matched with the measured one. As the result, the source location of the EM pulse was just in the epicenter of the earthquake. Therefore, we could find that the earth-origin EM pulses could have a possibility of a precursor of the earthquake [1].

In the analysis, however, we used theoretical dispersion curves for determining the propagation distances of the measured pulses. Hereafter, we need to determine source locations of EM pulses by direct measurement. For this purpose, we are preparing to establish a network observation system which is composed of plural observation sites equipped by the same detection and analysis system developed here. In the network system, we could determine source locations of earth-origin EM pulses directly and on real time basis by means of triangular measuring method in which each detection site measures arrival directions.

Furthermore, we need to know wave propagation mode of the detected EM pulses, and need to explain the necessity of using bore hole for detecting earthquake related EM pulses. For this purpose, we are thinking of a specific wave mode and also preparing to make another sensor system to prove the existence of the wave mode.

REFERENCES

1. Minoru Tsutsui, Identification of earthquake epicenter from measurements of electromagnetic pulses in the Earth. GRL, V0l. 32, L20303 , 2005.

Propagation Anomaly of Oversea VHF Waves and Possibility of Relations to Earthquakes

T. Takano, K. Sakai, I. Nagashima, H. Nakata, H. Akaike
S. Ujigawa, A. Hirai, Y. Kawamura, and **S. Shimakura**
Chiba University, Japan

Various electromagnetic phenomena have been reported in recent years, which are possibly associated with earthquakes. The characteristics of these phenomena still have not been fully revealed yet because of the insufficient number of well-observed earthquakes.

We have observed electromagnetic waves in VHF band in Chiba prefecture, Japan. Broadband spectra from 47 to 76 MHz are observed with wide-band LPDA (Log- Periodic Dipole Array) antennas. In this frequency band, no commercial broadcasting stations are allocated in Japan. However, many strong broadcasting waves are sometimes observed and those are identified in frequencies to oversea TV broadcasting waves from Asian countries. Computer simulations of propagation of electromagnetic waves from oversea broadcasting stations are confirm seasonal and diurnal variations of these waves. We, therefore, concluded that TV waves at lower frequencies from Malaysia, Thailand, and/or Philippines are sometimes refracted by the F2 layer in the daytime ionosphere in spring and fall.

We found that TV waves from Malaysia at 48.25 MHz were sometimes heavily attenuated for a few hours when earthquakes occur in the Okinawa area, which is southern islands area of Japan. We propose a hypothesis that the attenuation is caused by some disturbance in the ionospheric E layer above the epicenters in Okinawa. Results of computer simulations suggest that a 10% enhancement or depletion of electron densities can explain the observed attenuation.

Other types of propagation observed in the frequency range are also investigated and compared to results of computer simulations. These results present good knowledge in propagation in the frequency range under the normal condision. This would be essentialy important to distinguish signals which could be related to earthquakes.

On Non-Linear Plasma Irregularities in the Ionosphere Due to Electromagnetic Precursory Signals from Earthquake

S. S. De, B. K. Sarkar, B. Bandyopadhyay, and **A. Guha**
University of Calcutta, India
B. K. De
Tripura University, India

Both experimental and theoretical studies of pre-earthquake processes establish the existence of various classes of electromagnetic signals which are generated at different stages of earthquake development. It has been established that there exists electromagnetic coupling between the processes within the Earth's curst and troposphere over the region of seismic and volcanic activity and anomalous variations within the ionosphere prior to strong earthquakes. The most probable physical model explaining the phenomena is based on the chemical influence of the emanations from the Earth's crust on the surface layers of the atmosphere which change the conductivity of the surface layer and thus modify the atmospheric electric field value within the active area.

The anomalous electric field penetrates into the ionosphere and creates variations in ion-composition, electron concentration, electron temperature, DC electric field etc. in the atmosphere.

In this presentation, the effects on the ionosphere of the electromagnetic waves from earthquake will be studied theoretically through some model calculations. The expressions of the variation of electron concentration and electron temperature as the ionospheric precursors of earthquake are deduced. The production of periodic inhomogeneities and their decay at different heights due to precursors at the active regions of the ionosphere as a whole have been considered through quasi-hydrodynamic equations. The systems of equations are solved for temperature and density fluctuations for the stated situation. Ion-collision energy losses are more than those of electrons and the ion conductivity is less than those of electrons. For this, ion heating is relatively small. The electron-neutral molecule collision frequency and the electron energy loss per collision with molecule depend on electron temperature. As a result, the equation for electron temperature variation becomes non-linear. The non-linear equation for electron density fluctuation has been obtained from the appropriate quasi-hydrodynamic equations. These are solved analytically, and partly numerically. The magnitude of variation of electron concentration and electron temperature as the precursory effects can be estimated by numerical analyses of the deduced results.

Anomalous Effect in Schumann Resonance Phenomena Observed in Japan, Possibly Associated with the Earthquakes in Taiwan

M. Hayakawa
The University of Electro-Communications, Japan

K.Ohta
Chubu University, Japan

The Schumann resonance phenomenon has been monitored at Nakatsugawa (near Nagoya) in Japan since the beginning of 1999, and due to the occurance of a severe earthquake (so-called Chi-chi earthquake) on 21 September 1999 in Taiwan we have examined our Schumann resonance data at Nakatsugawa during the entire year of 1999. We have found a very anomalous effect in the Schumann resonance, possibly associated with two large land earthquakes (one is the Chi-chi earthquake and another one' on 2 November 1999 (Chia-yi earthquake) with a magnitude again greater than 6.0). Conspicuous effects are observed for the larger Chi-chi earthquake, so that we summarize the characteristics for this event. The anomaly is characterized mainly by the unusual increase in amplitude of the fourth Schumann resonance mode and a significant frequency shift of its peak frequency ($\sim$ 1.0 Hz) from the conventional value on the. B,Y magnetic field component which is sensitive to the waves propagating in the NS meridian plane. Anomalous Schumann resonance signals appeared from about one week to a few days before the main shock. Secondly, the goniometric estimation of the arrival angle of the anomalous signal is found to coincide with the Taiwan azimuth (the unresolved dual direction indicates toward South America). Also, the pulsed signals, such as the Q-bursts, were 'simultaneously observed with the "carrier" frequency around the peak frequency of the fourth Schumann resonance mode. The anomaly for the second event for the Chia-yi earthquake on 2 November had much in common But, most likely due to a small magnitude, the anomaly appears one day before and lasts until one day after the main shock, with the enhancement at the fourth Schumann resonance mode being smaller in amplitude than the case of the Chi-chi earthquake. Yet, the other characteristics, including the goniometric direction finding result, frequency shift, etc., are nearly the same. Although the emphasis of the present study is made on experimental aspects, a possible generation mechanism for this anomaly is discussed in terms of the ELF radio wave scattered by a conducting disturbance, which is likely to take place in the middle atmosphere over Taiwan. Model computations show that the South American thunderstorms (Amazon basin) play the leading role in maintaining radio signals, leading to the anomaly in the Schumann resonance. Then, we have performed further analysis for five years, and we have come to the conclusion that the ionosphere above Taiwan is disturbed for all the land earthquakes ($M > 5.5$) in Taiwan.

Session 2A2
High-Frequency Techniques

A Ray-launching Estimation For Simple Indoor Wave Propagation Through High Lossy Walls

R. Sato [1], **H. Sato** [1], and **H. Shirai** [2]

[1]Niigata University, Japan
[2]Chuo University, Japan

In the field of the development of next generation wireless broadband communications including multihop network and MIMO technologies, it has been more significant to understand the complex indoor wave propagation mechanisms. For such complex propagation environments, Shooting and Bouncing Ray (SBR) or ray-launching method is one of the most powerful propagation estimation tools. The method is based on ray theory, i.e. high frequency asymptotic approximation. In general, the ray components utilized in such method are three GO rays (direct, reflected, and refracted or transmitted rays), and the contribution of diffracted rays. However, in indoor environment, lots of walls, which divide a indoor space into some parts of rooms, may be regarded as dominant scatterers. So simplified indoor propagation estimation by using only three GO rays except diffraction contribution may be useful.

In this paper, we focus on the transmitted component through an indoor wall, which is made up of high lossy dielectric material. According to the Snell's law, for lossy dielectric material, a refracted propagation (real) angle θ_t may be extended to a complex angle $\hat{\theta}_t$. In particular, when the lossy effect of the material is large, $\zeta m\{\hat{\theta}_t\}$ may not be negligible. In the ray-launching procedure, the complex angle θ_t must be replaced real shooting angle θ_t , when one needs to calculate the transmitted ray through such high lossy wall. However, it is not clear how one determines the appropriate real shooting direction θ_t inside the wall when the refracted angle becomes complex. In order to make this question clear, we will consider how to determine the appropriate real refracted angle θ_t , by comparing the numerical ray-launching solution with an analytical reference one. Here, as the reference field representation, the asymptotic solution for the Greens function problem in the presence of lossy dielectric slab is utilized, where the contribution of the complex transmission coefficient for the high lossy slab is also taken into account in the reference one. Discussion on the accuracy of the transmitted ray through the lossy wall (slab) will be done not only for two dimensional problem but also for simplified three dimensional one.

Diffraction Coefficients of Composite Wedge Using the Virtual Ray of Diffraction

S. Y. Kim
Korea Institute of Science and Technology, Korea

After Maxwell established the connection between electromagnetism and optics, the ray-tracing technique has been a ubiquitous force in high-frequency electromagnetic problems. Ordinary ray-tracing provides the geometrical optics(GO) field. Keller suggested a generalization of the Fermat's principle on diffracted rays produced by an incident ray which hits edges, corners, or vertics of boundary surfaces. But the geometrical theory of diffraction(GTD) could not be implemented by employing only the ray-tracing data because the initial value of diffracted rays should be determined from the exact diffraction coefficients of some canonical structures, e.g., perfectly conducting half-plane, wedge, and cone. Hence the applicability of the GTD scheme has restricted due to the lack of rigorous diffraction coefficients of such canonical structures as penetrable wedges and cones.

Recently we have developed the virtual ray of diffraction(VRD) method to provide diffraction coefficients of penetrable wedges in analytical form. The basic principle of the VRD method is deduced from the exact diffraction coefficients of a perfectly conducting wedge as follows; 1) the extended ray-tracing of actual rays in the physical region and virtual rays in its complementary region, 2) the one-to-one correspondence between the geometrical rays and cotangent functions of the diffraction coefficients, 3) adjustment of angular period of cotangent functions to satisfy the edge condition at the wedge tip, and 4) the null-field condition in the complementary region, which may be considered an extension of the complementary screen introduced by Sommerfeld.

The above VRD method is applied to the E-polarized diffraction by a composite wedge composed of perfect conductor and lossless dielectric. The ordinary ray-tracing provides the complete expression on the GO field including multiple reflections inside dielectric region. The corresponding PO solution consists of the GO field and the edge-diffracted field, of which diffraction coefficients are given by finite series of cotangent functions. The starting point of the virtual ray-tracing is the last actually-reflected ray in the physical dielectric region, which extends to the first virtual ray in the complementary dielectric region. And virtually multiple reflections occur inside the complementary dielectric region. Applying the one-to-one correspondence to the ray-tracing results, one may express the VRD diffraction coefficients as the same number series of the cotangent functions, of which angular period is adjusted to satisfy the edge condition at the wedge tip. It is assured that the VRD diffraction coefficients converge to zero in the complementary regions more closely than the PO solution.

High-Frequency Solution for Whispering Gallery Mode Radiation from a Cylindrically Curved Concave Conducting Surface

T. Ajiki, K. Goto, and **T. Ishihara**
National Defense Academy, Japan

Within a cylindrically curved concave conducting surface with its radius of curvature sufficiently larger than the wavelength, many whispering-gallery (WG) modes are excited which propagate along the concave surface without any loss. The lower the order of the WG mode, the more closely trapped near the concave surface. The lower-order WG modes propagate along the surface without the mode coupling in the form of adiabatic WG modes even along the variable radius of concave surface. Due to the characteristics of the WG modes described above, the WG modes have been utilized in the research and development of high-power WG mode type gyrotrons and laser resonators. In developing such devices, it is necessary to analyze the radiation of the WG mode from the aperture plane of the cylindrically curved concave surface into the free space.

In this paper, we shall examine a uniform asymptotic solution for a WG mode radiation from a cylindrically curved concave conducting surface.

In a breakthrough paper by Idemen and Felsen [IEEE Trans. Antennas Propagat., vol.AP-29, no.4, pp.571-579, July. 1981], the asymptotic solutions for a canonical problem have been given for the diffracted fields in the case when the WG mode is incident on the edge of a cylindrically curved concave conducting surface. They have applied the isolated saddle point technique for the asymptotic evaluation of the integral representing the scattered field of the WG mode and derived the nonuniform asymptotic solutions for the scattered fields by the edge of the cylindrically curved surface.

In this paper, by applying the new analysis method, we shall derive a uniform asymptotic solution for the WG mode radiation applicable in the transition region near the geometrical boundaries (reflection boundary and shadow boundary) produced by the incident modal ray, comprising the WG mode, on the edge of the curved surface [K. Goto and T. Ishihara, IEICE Trans, vol. J77-B-U, no.10, pp.539-547, Oct. 1994]. The uniform solution is represented by the summation of the geometrical ray solution converted from the modal ray of the WG mode and the uniform edge diffracted ray solution scattered at the edge. By comparing with the reference solution obtained numerically from the integral representation of the radiation field, we will confirm the validity and the utility of the uniform asymptotic solution proposed in this paper. We will show that the solution obtained from the conventional Fresnel-Kirchhoff diffraction formula deviates substantially from the reference solution as the observation point moves away from the beam axis.

Frequency-Domain and Time-Domain Asymptotic Analyses for Scattered Fields by a Cylindrically Curved Conducting Open Surface with a Varying Radius of Curvature

K. Goto, T. Ajiki, and **T. Ishihara**
National Defense Academy, Japan

The study on the scattering of electromagnetic field by the curved smooth conducting surface has been an important research subject for a variety of applications in the area of antennas and propagation. In the high-frequency analysis of the scattered field by an object with a complex shape, it is necessary to study the analysis method for the scattered field by the object with a simple shape. In the present study, high-frequency solutions for the diffraction of an electromagnetic wave incident on the conducting open curved surface with a varying radius of curvature are examined both in the frequency-domain and in the time-domain.

When the high-frequency electromagnetic wave is incident on the cylindrically curved conducting open surface with the constant radius of curvature, the scattered field can be obtained by summing all the scattered field constituents received at the observation point. The frequency-domain asymptotic solution for the scattered field consists of the edge diffracted ray, the surface diffracted ray, the geometrical ray, the whispering gallery mode (WG) radiation field, and the combination of these waves. High-frequency solution described above is expressed as the product of the coefficients or the field solutions for the local scattering phenomena [K. Goto, T. Ishihara, and C. Irimia, 2004 Korea-Japan Joint Conference on AP/EMC/EMT, pp.89-92, Seoul, Korea, Nov. 2004].

In this study, we shall extend the frequency-domain asymptotic solution for the scattered field by the constant radius of curvature to the one by the variable radius of curvature by applying the idea of the Keller's GTD. The WG mode for the constant radius of curvature is replaced by the adiabatic WG mode when the curvature changes slowly. The edge diffraction coefficient, the surface diffraction coefficient, and the launching (or attachment) coefficient, etc., for the constant radius curvature are extended by using the local radius of curvature. Furthermore, we shall derive the time-domain asymptotic solution by applying the saddle point technique or the Fourier transform method in evaluating the inverse Fourier transform. The accuracy and the validity of the asymptotic solutions both in the frequency-domain and in the time-domain are confirmed by comparing the asymptotic solutions with the reference solutions calculated numerically from the method of moment (frequency-domain) and from the hybrid method of moment and fast Fourier transform (FFT) method (time-domain).

A Study of Scattering Characteristics using Polygon Meshed PO

N. Lertsirisopon, M. Ghoraishi, G. S. Ching, and **J. Takada**

Tokyo Institute of Technology, Japan

Propagation mechanisms which degrade the performance of mobile communication system in urban areas are basically wall reflections, building edges and roof diffractions. From the experiment results [1], the scattering from some objects in the environment can have strong impact on the urban propagation channel. Careful analysis of these results reveals that these scattered objects, which can be any surroundingmetallic object, such as signboards, street lights, traffic lights and traffic signs, are involved in scatterering transmitted signals to the receiver [2].

Physical optics (PO), the approximation method for determining surface currents, is utilized to simulate the induced surface current to handle non-specular scattering in [3]. The simulation results showed good agreement with the experimental results and in the same manner, the PO approximation method can be applied to study the scattering of surrounding objects in the wireless communication environment.

In this study, to represent the data structures of scatterers, polygon meshes are used to model scatterer constructions including 2 dimensional (2D) and 3 dimensional (3D) geometrical objects. Polygon meshes represented by regular triangles can be easily generated by using intrinsic functions in MATLAB for 2D cases. For 3D cases, a mapping first of the 3D object to a 2D object is necessary to be able to use the MATLAB intrinsic functions. Then, the corresponding height is put back to the meshed 2D object to obtain the meshed 3D object. Using this "Polygon Meshed PO" method, the complex calculation of the induced current to examine the scattered field can also be simplified by summing the contribution on each triangle mesh. By defining the polygon mesh ratio as the ratio of the average triangle area to the square of the wavelength, the convergence of the simulated scattered field can be found.

This simulation program will then be used to evaluate scattering objects that cause significant amount of scattering in the wireless communication environment especifically from previously mentioned objects in an urban propagation channel. By utilizing the size and shape of these surrounding metallic objects, and parameters used in the experiments, the scattered fields can be calculated and compared with experimental results to help verify observations in the experiments. In addition, this simulation tool can give us an idea on the amount of scattered fields caused by both regular and irregular shaped objects in certain scenarios. Knowing these scattering characteristics can help better explain the effects of surrounding objects on the propagation channel.

REFERENCES

1. Mir Ghoraishi, Jun-ichi Takada, and Tetsuro Imai, "Identification of the Scatterers in the Urban Microcell Environments," *Technical report of IEICE*, WBS2004-164, AP2004-345, RCS2004-432, MoMuC2004-215, MW2004-342 (2005-03).
2. Mir Ghoraishi, Junichi Takada and Tetsuro Imai, "Investigating Dominant Scatterers in Urban Mobile Propagation Channel," *IEEE International Symposium on Communications and Information Technologies 2004 (ISCIT 2004)*, Oct., 2004 (Sapporo, Japan).
3. Hary Budiarto, Kenshi Horihata, Katsuyuki Haneda, and Jun-ichi Takada, "Experimental Study of Non-specular Wave Scattering from Building Surface Roughness for the Mobile Propagation Modeling," *IEICE Transactions on Communications,* vol. E87-B, no.4, pp. 958-966, Apr. 2004.

Symmetric High-Q Inductors Fabricated Using Wafer Level CSP and Novel Q-Factor Definition

Y. Aoki
Casio Computer Co.,Ltd., Japan

Recent advances in RFIC (radio frequency integrated circuits) require low-loss high-Q passive circuit components such as inductors, capacitors and transmission lines on silicon substrates. The WLP (wafer level chip size package) technology is considered to be one of the most promising technologies for the requirements. In the WLP, the isolation layer thickness can reduce the losses caused by low-resistivity silicon substrates, which are suitable for very large scale integration (LSI) of active devices, are avoidable. The conductor losses can also be minimized by using an appropriate wiring metal such as copper.

Low-loss high-Q spiral inductors, which can be applicable to the WLP, have been successfully fabricated on silicon substrates using the copper interconnect technology with polyimide isolation layers. In this dissertation, microwave characteristics for the spiral inductors, related with the size, the number of spiral turns, the isolation layer thickness, the silicon substrate resistivity have been investigated theoretically and experimentally, where the optimized polyimide thickness and the affordable copper inter-connect technology have been developed. A Q factor of 20 has been achieved at 3.9GHz with inductance values from 2-5 nH.

In conventional Q-factor evaluation for inductors, a short-circuited load condition is used, where Q-factor is represented by using Y-parameters as Q=Im1/Y11/Re1/Y11. However since structures for the spiral inductors are asymmetrical, the short-circuited load condition and the short-circuited source condition give different Q values, respectively. The Q value differences of about 100% have been often observed in the WLP. This result enabled a development of real symmetric inductor. The differences mainly come from differences in loss estimation.

Usually clip pattern inductors are thought symmetric inductors. However they also@give different Q values. The cause of different Q values is underpass of clip inductors. The Q value difference is able to reduce by underpass position.

A novel Q-factor definition and evaluation method are proposed for inductors. In a novel method, a complex conjugate impedance matching condition is retained both at an input port and an output port of the inductor. The maximum available power gain (GAMAX) is introduced to evaluate the energy loss in one cycle. This condition provides a unique insertion loss of passive devices. Thus the difference of the Q-factor depends only on the difference of magnetic and electric energy. The difference of the Q value is reduced. This proposed method can be applied not only to WLP spiral inductors, but also to the other passive components such as chip inductors, capacitors.

Study of High Fundamental Frequency Crystal-based Voltage Control Oscillator for 10 Gbit Ethernet Application

Y. C. Chen
Lunghwa University of Science and Technology, Taiwan

Nowadays, the operations of clock and data recovery (CDR), clock smoothing or frequency translation of optical fiber communication systems such as the SONET/SDH (Synchronous Optical Network / Synchronous Digital Hierarchy), are provided by voltage-tunable high frequency clock sources with, absolute pulling range exceeding $\pm$ 50 ppm in an operating temperature range of -40 to 85^{o}C, frequency-voltage linearity smaller than 10%, and phase jitter less than 1 pSec integrated from 12 KHz to 20 MHz of the offset frequency from the carrier. A voltage-controlled crystal oscillator (VCXO) is good for clocking up to about 100 MHz. For crystal to meet the requirements at high frequencies, high fundamental frequency (HFF) crystal blanks are required. In this paper, the developing procedures and test results for a 622.08 MHz HFF crystal-based voltage control oscillator are recorded. The VCXO is composed of a 155.52 MHz HFF crystal and a multiplier circuit to generate a 622.08 MHz clock. The test results include the variation of frequency over operating temperature range and control voltage range, and phase jitter. The pulling range, frequency-voltage linearity and phase jitter measured for the first prototypes are + 155ppm/-133 ppm, 9.6 % and 0.21 pSec, respectively.

Session 2A3a
Highly Miniaturized on Chip Passive Components for MMIC/RFIC Applications

A Highly Miniaturized Broadband On-Chip Impedance Transformer Employing PPGM on GaAs MMIC

Y. Yun, K. S. Lee, and **C. R. Kim**
Korea Maritime University, Korea

In this work, using a microstrip line employing Periodically Perforated Ground Metal (PPGM) on GaAs MMIC, a highly miniaturized and broadband on-chip impedance transformer was developed for application to low impedance matching in broadband. Its size was 0.132 mm_2 on GaAs substrate, which was 2.3 % of the one fabricated by conventional microstrip line. The transformer showed a good RF performance over a broadband including Ultra Wide Band (UWB).

Figure 1 (a) shows a top view of the microstrip line employing PPGM, and Figure 1 (b) corresponds to a cross-sectional view according to Y-Y direction of Fig. 1 (a). As is well known, conventional microstrip line without PPGM has only a periodical capacitance C_a (C_a is shown in Fig. 1 (b)) per a unit length, while the microstrip line employing PPGM has additional capacitance C_b as well as C_a due to PPGM. From this figure, we can see that the microstrip line with PPGM exhibits much lower characteristic impedance (Z_0) and shorter guided-wavelength (λ_g) than conventional one, because Z_0 and λ_g are inversely proportional to the periodical capacitance, in other words, $Z_0 = (L/C)^{0.5}$ and $\lambda_g = 1/[f.(LC)^{0.5}$

Using the PPGM structure, a highly miniaturized and low impedance on-chip transformer employing multisection lines was developed for broadband applications. Figure 2 shows a photography of the impedance transformer. Measured return loss S_{11} and insertion loss S_{21} are shown in Fig. 3. The three-section transformer exhibits return loss values lower than -9 dB from 2 GHz to 13 GHz, and insertion loss values lower than 1.2 dB in the above frequency range, which reveals that the three-section transformer can be applied for on-chip matching component between low impedance devices in a broadband including UWB.

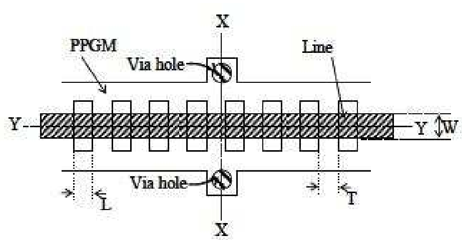

Fig. 1 (a) A top view of the microstrip line employing PPGM

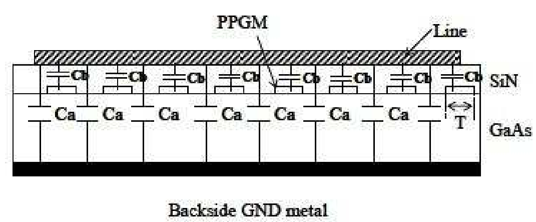

Fig. 1 (b) corresponds to a cross-sectional view according to Y-Y direction of Fig. 1 (a)

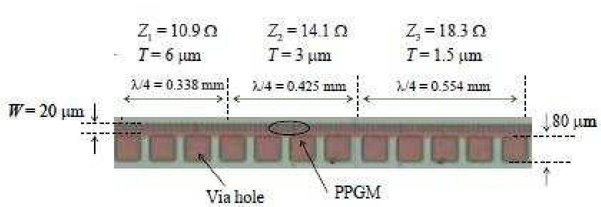

Fig.2 A photography of the impedance transformer

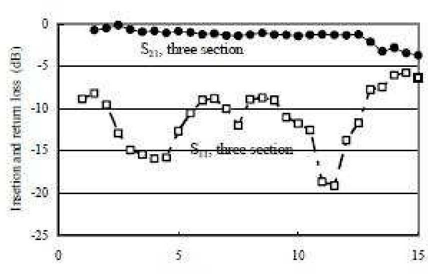

Fig. 3 Measured return and insertion loss

Highly Miniaturized and Low impedance On Chip Wilkinson Power Divider Employing Periodically Perforated Ground Metal on MMIC

C. R. Kim and **Y. Yun**
Korea Maritime University, Korea

In this paper we propose a low-impedance and highly miniaturized on-chip Wilkinson power divider on MMIC, which was fabricated by a microstrip line structure employing periodically perforated ground metal (PPGM). Using the microstrip line with PPGM, a miniaturized 13 power divider was fabricated. The size of the power divider was 0.110 mm2, which is 6 % of conventional one.

Figure 1 shows, the PPGM bend structure with single-sided via holes, and figure 2 corresponds to a cross-sectional view according to Y-Y direction of Fig. 1. As shown in Fig. 1, PPGM was inserted at the interface between SiN film and GaAs substrate, and it was electrically connected to backside ground metal through the via-holes. As is well known, conventional microstrip line without PPGM has only a periodical capacitance C_a (C_a is shown in Fig. 2) per a unit length, while the microstrip line employing PPGM has additional capacitance C_b as well as C_a due to PPGM. From this figure, we can see that the microstrip line with PPGM exhibits much lower characteristic impedance (Z_0) and shorter guided-wavelength (λ_g) than conventional one, because Z_0 and λ_g are inversely proportional to the periodical capacitance, in other words, Z_0 =(L/C)0.5 and $\lambda_g = 1/[f.(LC)^{0.5}]$.

In this work, highly miniaturized and low impedance on-chip Wilkinson power divider employing PPGM structure was fabricated on GaAs MMIC. Figure. 3 shows a photograph of the Wilkinson power divider. Its size was 0.117 mm2, which was 6% of the conventional one. Measured power division characteristics for the power divider are shown in Fig. 4. The equal power division characteristics were observed from 1 to 5 GHz.

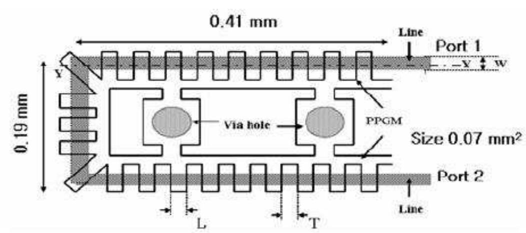

Fig. 1 PPGM bend structure with single-sided via holes

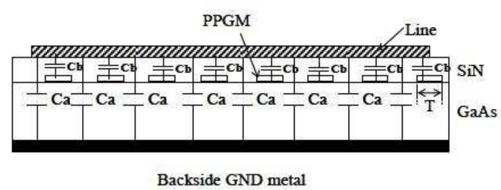

Fig. 2 A cross-sectional view according to Y-Y direction of Fig. 1

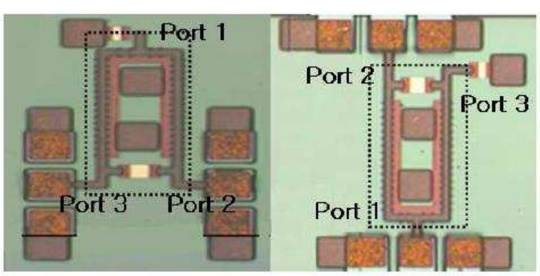

Fig. 3 Photomicrograph of the power divider

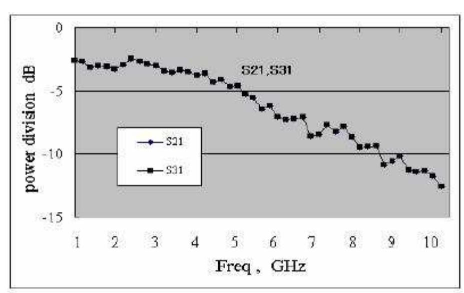

Fig. 4 Measured power division characterstic of the power divider

3-D 94 GHz Single Balanced Active Mixer using DAML-based Hybrid Ring Coupler

J. K. Rhee, S. C. Kim, D. An and **D. H. Shin**
Dongguk University, Korea

We reported 94 GHz, low conversion loss, and high isolation single balanced active-gate mixer based on 70 nm gate length InGaAs/InAlAs metamorphic high electron mobility transistors (MHEMTs). This mixer showed that the conversion loss and isolation characteristics were 2.5 $\sim$ 2.8 dB and under -30 dB, respectively, in the range of 93.65 $\sim$ 94.25 GHz. The low conversion loss of the mixer is mainly attributed to the high-performance of the MHEMTs exhibiting a maximum drain current density of 607 mA/mm, a extrinsic transconductance of 1015 mS/mm, a current gain cutoff frequency (f_T) of 330 GHz, and a maximum oscillation frequency (f_{max}) of 425 GHz. High isolation characteristics are due to hybrid ring coupler which adopted dielectric-supported air-gapped microstrip line (DAML) structure using surface micromachined technology. To our knowledge, these results are the best performance demonstrated from 94 GHz single balanced mixer utilizing GaAs-based HEMTs in terms of conversion loss as well as isolation characteristics.

Index Terms - MHEMT, 70 nm, single balanced mixer, hybrid ring coupler, DAML

Miniaturized Bandpass Filter Design with Periodic Stepped-Impedance Ring Resonators (PSIRRs)

J. T. Kuo and **Y. C. Chiou**

National Chiao Tung University, Taiwan

High-performance microwave/RF bandpass filters are highly required in modern wireless communication systems such as satellite and mobile applications. The microstrip ring resonator filters are attractive due to its versatile characteristics such as simple design, low radiation loss, and high selectivity [1]. In this study, a periodic stepped-impedance ring resonator (PSIRR) structure [2] is proposed to achieve circuit miniaturization and wide upper stopband. Fig. 1 shows layout of the proposed PSIRR with four cascaded periods; each consists of a hi-Z and a low-Z section. The characteristic impedance Z_3 is made slightly less than Z_3 to produce proper coupling between degenerate modes, and the coupling coefficient can be evaluated. The line-to-ring coupling configuration is exploited as the I/O feeders, and the input and output ports are spatially separated at 90° in electrical length. The dual-mode PSIRR bandpass filter is fabricated on a substrate with $\epsilon_r = 2.2$ and thickness = 0.508 mm. Fig. 2 demonstrates the simulated and measured results in a broad band. At the center frequency 2 GHz, the insertion loss and the return loss are better than 2.5 dB and 25 dB, respectively. The first unwanted resonance has a peak at 9.05 GHz or $4.5f_0$, demonstrating that the filter has a much wider upper stopband than the traditional ring resonator filters. Furthermore, the PSIRR occupies only $(0.55)^2 = 30\%$ of the area of a conventional ring resonator filter, thus a size reduction of 70% is achieved. The measured results agree well with the simulation.

Acknowledgements

This work was supported by the National Science Council, Taiwan, under Grants NSC 94-2213-E-009-073 and NSC 94-2752-E-009-003-PAE.

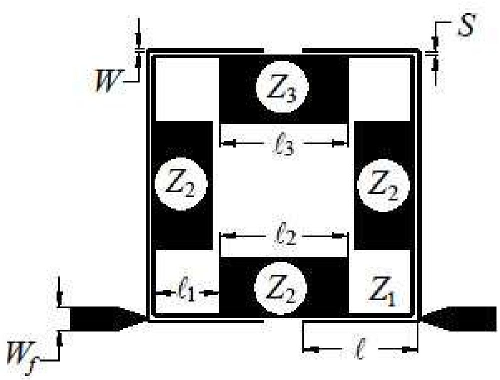

Figure 1: Layout for the proposed PSIRR filter with N = 4.

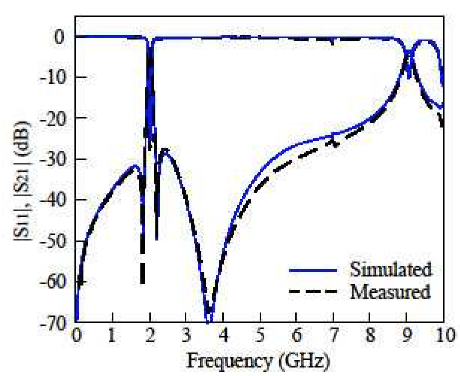

Figure 2: Simulated and measured results of the PSIRR filter.

REFERENCES

1. K. Chang, *Microwave Ring Circuits and Antennas*. New York: Wiley, 1996.
2. J.-T. Kuo and C.-Y. Tsai, "Periodic stepped-impedance ring resonator (PSIRR) bandpass filter with a miniaturized area and desirable upper stopband characteristics," to appear on the *IEEE Trans. Microwave Theory Tech.*, vol. 54, no. 3, Mar. 2006.

Session 2A3b
Innovation in Interconnects Modeling

Application of Wavelets in Circuit Modeling and Simulation

X. Zeng[1] and **D. Zhou**[1,2]
[1]Fudan University, China
[2]University of Texas at Dallas, U.S.A.

W. Cai
University of North Carolina, U.S.A.

As SOC chips develop to higher and higher speed, the singularity problem in high speed circuits has remarkably challenged the accuracy and speed of the state-of-the-art circuit simulators. For instance, in analog behavioral modeling, model order reduction of interconnects, steady state analysis of nonlinear circuits and noise analysis, the global functions, such as polynomial function, Chebyshev function, harmonic function and sampling function, are employed by the traditional simulation approaches. These global functions require much more number of basis functions to achieve higher accuracy when dealing with singular waveforms. However, the augment of the number of global functions will drastically increase the computation cost. Nevertheless, the approximation errors cannot be evenly reduced no matter how many higher order basis functions are used in circuit simulation. It is therefore desperately demanded to exploit new methodologies for high speed and high accuracy simulation.

In this invited survey, we present the research results for applying wavelets to catch the singularities existed in high speed systems. We have proposed to employ the local support wavelet basis functions to replace the global functions and make use of the wavelet adaptivity to enhance speed and accuracy. For instance, we have proposed the wavelet method and fast Sylvester equation solver for time domain model order reduction, which can drastically improve the reduction accuracy and speed up simulation time by one or two orders than the existing model order reduction methods like those based on Chebyshev expansions. In application of behavioral modeling of analog circuits, we have proposed a wavelet collocation method with nonlinear companding technique to reduce model errors and control the error distribution continuously according to the system simulation requirement. For steady state analysis of nonlinear circuits, we have proposed wavelet balance approach which is a promising counterpart to further improve the simulation accuracy and efficiency compared to the harmonic balance approach. The wavelet theory has also been successfully applied to noise analysis and clock network analysis, frequency domain analysis etc.. Compared with the traditional approaches, the wavelet methods can significantly improve the simulation speed and accuracy, and consequently open a new direction for high speed circuit simulation.

A Time-domain Approach for Transforming Broadband SPICE-Compatible Models of Power Delivery Networks with Resonance Effect

C. C. Wang, C. W. Kuo, C. C. Kuo, and **J. S. Hsieh**
National Sun Yat-Sen University, Taiwan R. O. C.

T. L. Wu
National Taiwan University, Taiwan R.O.C.

Resonance noise, or power/ground bounce noise, on the power and ground planes of high-speed circuit packages is one of main concerns of the signal integrity (SI) or power integrity (PI) issues. This paper proposes a time-domain approach to extract the equivalent models of power/ground planes with the resonant effect being considered. Employing the general pencil of matrix method (GPOM), the pole-residue representation of the time-domain responses of the planes structure is obtained. The broadband SPICE-compatible model then can be transformed based on the simple network transformation method. It is found that the extracted models accurately predict the power/ground bouncing or resonance behavior in wide-band range. The developed models can be efficiently incorporated to the HSPICE simulator with considering the power/ground bouncing noise in high-speed circuits.

New Models for Controlling Signal Dispersion, Attenuation and Total Delay in the Design of Long High Performance Lossy Interconnects

R. H. Flake
The University of Texas at Austin, U.S.A.

A primary challenge faced in the design of high performance lossy interconnect (HPLI) data circuits in digital systems is to obtain and maintain signal integrity (SI) requirements on these lines while operating under severe signal dispersion and attenuation. As an example, designing 6 GHz half-meter serialized high-speed back plane digital interconnects currently demand overcoming high signal dispersive behavior and 30db attenuation while maintaining adequate SI specifications. Further improving the data rate in these interconnects presents a challenge.

The design and fabrication of HPLI with tight total interconnect signal delay requirements is perceived to be so difficult that special system design measures are usually employed or must be developed to remove the need for strict total interconnect delay specifications.

The recent discovery of a special waveform, called Speedy Delivery (SD), with controllable signal dispersion, attenuation and delay may significantly reduce the design challenge of improving the data rate of current state-of-the-art HPLI data lines. The precise models for the SD signal delay and this signalfs non-dispersive propagation behavior also make it possible to fabricate long interconnects meeting total delay specifications within limits that are the order of a high GHz clock period. Closed form non-dispersive time domain SD solutions of the lossy, frequency dependent parameter transmission line equation for HPLI have been obtained. The expressions for attenuation and signal delay computed from these SD solutions provide simple analytical design tools for HPLI with tight limitations on total interconnect signal attenuation as well as requirements on total delay.

A simple HPLI design improvement process utilizing the SD signal is proposed whose goal is to obtain a higher data rate from an existing interconnect designed with conventional digital signals. The process illustrates how coding additional bits by varying the SD signal shape parameter (gfrequencyh) could yield significantly higher HPLI data rate without requiring any tangible increase in the interconnect bandwidth.

A Quick Parasitics Extraction Tool for IC Interconnections

Y. Yang and **G. Wang**
Wuhan University, China

J. Xue
Fudan University, China

A tool capable of automatic interconnect parasitic resistance, inductance and capacitanceiRLCj extraction is described. With a GDSII layout format file and an interconnect technology description file as input, the tool displays the layout in 2-D/3-D modes, and extracts interconnect parasitics automatically for the selected critical nets or entire layout. Employing a multipole accelerated GMRES based fast three-dimensional (3-D) field solver, the tool extracts parasitic resistance, inductance and capacitance very quickly and accurately for arbitrary interconnects embedded in piece-wise constant dielectrics. The tool represents significant performances leap in 3-D interconnect inductance and capacitance extraction, making it well suited for high-accuracy interconnect characterization of critical nets, block IP, standard and custom cell designs. A grid-type parallel capacitance extraction solver is also integrated into this system, and the architecture of the parallel program can be extended to inductance extraction with careful interconnect partitions. The interconnect extraction tool also assembles a quick 2-D RLC extraction tool which is useful for some special applications. Architecture of the tool and numerical techniques of parasitics extraction solvers are discussed in this paper. Some examples to demonstrate the modeling capability, the efficiency and validity of the parasitics extraction solvers integrated into the tool are presented.

Extraction of Distributed Parameters of Multiple Coupled Transmission Lines from Electromagnetic Simulation Data and Its Application to Evaluation of Inductance Values of RFIC Inductors

J. T. Kuo [1], **T. Y. Liu** [1], , **H. H. Chen** [2] and **S. J. Chung** [1]

[1]National Chiao Tung University, Taiwan
[2]Huafan University, Taiwan

Multiple coupled microstrip lines are one of the basic structures in high-speed digital and radiofrequency (RF) integrated circuits (ICs). Field-theoretic analysis and circuit parameter extraction of such structures have attracted much attention from several research areas, such as microstrip filter design [1], RFIC inductors [2], and electromagnetic compatibility (EMC). Based on simulated 2N-port Z- or Y-parameters of an N-line system obtained by an electromagnetic software package, e.g., the IE3D [3], this paper aims at extracting the distributed parameters of the [R], [L], [C] and [G] matrices of multiple coupled microstrip lines for use in evaluating the inductance and loss of an RFIC inductor, as shown in Fig. 1. In the derivation, parameters also involved are the modal characteristic impedances, the attenuation constants, and the phase constants for the N eigenmodes of a set of N-coupled transmission lines embedded in a multilayer dielectric structure. In our study, the conductor lines can be of finite conductivity and finite metallization thickness, and the dielectric media can be lossy. Inductances and quality (Q) factors for several RFIC inductors are presented and compared with measured data.

This work was supported in part by the National Science Council, Taiwan, under Grants NSC 94-2213-E-009-073 and NSC 94-2752-E-009-003-PAE, and in part by the SRC program under contract 2003-TJ-1090.

REFERENCES

1. J.-T. Kuo and E. Shih, gWideband bandpass filter design with three line microstrip structures,h *IEE Proceedings - Microwaves, Antennas and Propagation*, vol.149, No.5, pp. 243-247, Oct. 2002.
2. J.-T. Kuo, K.-Y. Su, T.-Y. Liu, H.-H. Chen, and S.-J. Chung, gAnalytical calculation for DC inductances of rectangular spiral inductors with finite metal thickness in the PEEC formulation,h *IEEE Microwave Wireless Compon. Lett.* Vol. 16, No. 2, pp. 69-71, Feb. 2006.
3. Zeland Software, Inc., IE3D Simulator, Jan. 1997.

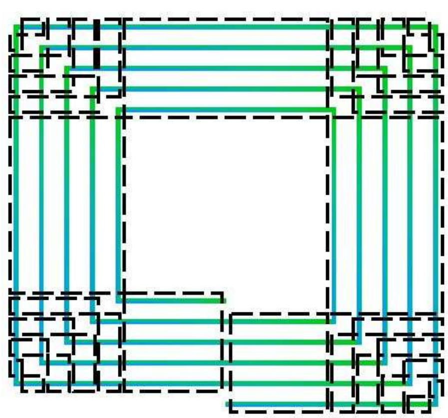

Figure 1: Layout of an RFIC inductor.

Session 2A4
Terahertz Technology

Oscillation of Resonant Tunneling Diodes Integrated with Slot Antennas in the Terahertz Range

M. Asada
Tokyo Institute of Technology, Japan

The terahertz (THz) frequency range between about 0.1-10THz is receiving considerable attention recently because of its many possible applications, such as in imaging, spectroscopy in chemistry and biotechnology, and high-capacity communications. For these applications, compact and coherent solid-state light sources are important key components. Quantum cascade lasers oscillating in the THz range have recently been reported from the optical device side. The development of various types of electron devices is also being progressed toward the THz range from the millimeter wave side. Resonant tunneling diodes (RTDs) have been considered as one of the candidates for THz oscillators at room temperature.

In this paper, we report on our recent results of RTD oscillators. Using GaInAs/AlAs double-barrier RTDs integrated with slot antennas on InP substrates, fundamental oscillation at 0.6 THz with output power of 8W and harmonic oscillation at 1.02THz with 0.6W were obtained at room temperature up to now. To our knowledge, the latter is the highest frequency to date from a room-temperature single semiconductor electronic oscillator, although it is a harmonic component. To investigate the possibility of fundamental oscillation over 1THz as well as high output power, a precise theoretical analysis was performed including all the parasitic circuit elements in RTDs and using three-dimensional electromagnetic simulation of slot antennas. Theoretical calculation agreed well with the measurements, and it was expected from this result that fundamental oscillation up to 2.4THz and output power of 70W at 1THz were feasible with optimized RTD and antenna structures.

Frequency tunability with bias voltage was also found, which is useful for frequency control and stabilization. The tuning range was 18GHz for the oscillator with the central frequency of 470GHz. The mechanism of the frequency change was attributed to the bias-voltage dependent transit time of electrons through the RTD layers resulting in the bias-voltage dependent capacitance. Theoretical analysis including this phenomenon agreed well with the measurement, and voltage-controlled oscillators around 1THz were also expected. The mutual injection locking between RTD oscillators was shown, in which RTD oscillators with different oscillation frequencies were locked into single frequency under simultaneous operation. This can be utilized in array configuration for high output power (1mW) with coherent power combining.

Terahertz Label-Free Biochip Sensors with Thin Metal Mesh

Y. Ogawa [1], **S. Hayashi** [1,2], **E. Kato** [3], **H. Yoshida** [1], **F. Miyamaru** [2], **C. Otani** [2] and **K. Kawase** [1,2,4]

[1]Tohoku University, Japan
[2]Institute of Physical and Chemical Research (RIKEN), Japan
[3]Advantest Laboratories Ltd., Japan
[4]Nagoya University, Japan

Many researchers have been investigating various methods for analyzing biomolecules using terahertz waves. This interest is explained by the fact that large molecules exhibiting complex structures have absorption peaks lying in the terahertz band; for example, the hybridization of DNA and the antigen-antibody reaction can be distinguished without labeling them with fluorescent agents. At present, the THz-TDS technique is used for most of the research on biomolecules in the terahertz region. Although THz-TDS is a sensitive detection method, it involves building complex and expensive systems. Consequently, a simpler and cheaper analysis method would be very beneficial. In parallel, research in the far-infrared using metallic meshes to build band-pass filters has started from around the 1960s. It became clear that the frequency characteristic is determined by geometrical parameters such as the grid step size and the aperture size, and the application in spectroscopic analysis was suggested. We have been developing a novel sensing method which uses the band-pass characteristic of a thin conductive metal mesh. This sensing method relies on the change in the transmittance of the terahertz radiation through a metal mesh when a sample substance is inserted in its openings; the transmittance changes not as much because of the absorption in the sample, but mostly because of the different refractive index of the medium in the openings. Our target is to develop a simple and cheap label-free biochip by using a monochromatic light source and a metal mesh.

In this study, we determined using a THz FTIR spectrometer that the transmittance through a conductive metal mesh approximately 5μm thick will change when the mesh apertures are filled with color ink or oil as test samples. For the biomaterial measurements, the ESD method was demonstrated in order to spray a metal mesh with a uniform quantity of protein. Additionally, to confirm the possibility of biochip sensors, we performed imaging experiments using a monochromatic source at 1 THz. In this presentation, a feasibility study for producing label-free biochip sensors using the technique of THz imaging will be reported.

Compact Terahertz Time Domain Spectroscopy System with 1.5-μm-Wavelength Femtosecond-Fiber-Laser

M. Suzuki and **M. Tonouchi**

Osaka University, Japan

Many researchers make progress toward developing pulsed terahertz (THz) systems based on Ti: sapphire lasers. The power dynamic range and bandwidth of broadband coherent THz radiation of the systems are achieved to be 1×10^6 and 4 THz, respectively. The systems are expected to be one of the powerful tools to open the new research fields in THz applications as time domain spectroscopy (TDS) and imaging. Downsizing the THz systems is an important issue for widening the THz applications. Development of compact THz systems requires compact femtosecond lasers as fiber lasers, which have a lot of advantages for the compact systems. The fiber lasers offer high performances in portability and stability. However, the wavelength of the output from the laser is 1.5 μm. Therefore, it is technological importance to develop efficient THz emitters and detectors for 1.5 μm laser operation.

Semiconductor surface radiation and photoconductive (PC) antennas are standard methods for generating THz pulsed fields. The antennas can be also used as detectors. Therefore, we have investigated THz emission properties of InSb, InAs and InGaAs excited by 1560, 1050, and 780 nm optical femtosecond pulses to explore an efficient infrared THz emitter. Additionally we have reported emission and detection properties of $In_{0.53}Ga_{0.47}As$-based PC antennas excited by 1560 nm pulses.

The amplitude of THz waves from our emitters has a strong dependence on the wavelength of excitation optical pulses. Bandwidths of the waves from all emitters are estimated to be similar values, which are around 4 THz. At high power 1560 nm excitation, InSb has the highest efficiency, whereas the efficiency of 780 nm-excited InSb becomes lower than that of the other emitters. In the case of 780 and 1050 nm excitation, p-InAs shows highest efficiencies compared to the others. p-InAs also shows the second highest THz amplitude in our emitters at 1560 nm excitation. From the results, we conclude that the decrease in 780-nm-exicted InSb originates from large effective mass of L valley carriers induced by intervalley scattering.

We have observed THz radiation from our InGaAs PC antennas excited by 1560 nm pulses. The bandwidth and power dynamic range of THz radiated field from the antenna are achieved to be 4 THz and 10000, respectively. Using our InGaAs PC antennas, we also have successfully detected THz field from a GaAs-based PC antenna.

Finally, we developed compact THz-TDS system with 1.5 μm femtosecond fiber laser operative up to 4THz.

A Newly Designed High-Performance Submillimeter-Wave Horn Antenna

M. Matsunaga
Ehime University, Japan

T. Matsunaga
Fukuoka Institute of Technology, Japan

This paper introduces a newly designed high-performance submillimeter-wave horn antenna - a submillimeter-wave horn antenna capable of maintaining higher levels of performance than either of the two types designed earlier by the authors as per the paper by M. Matsunaga et al. 2003 [1]. In particular, this new antenna will, within a very wide range of frequencies, radiate electromagnetic waves with higher gain, far lower loss and far lower cross-polarization than previously.

Corrugated horn antennae have long been used in designing low-loss horn antennae, for use in radio-astronomical telescopes [2], [3]. This is because of their well-known ability to radiate electromagnetic waves in symmetrical patterns. Note, however, that the corrugated horns used in conventional designs, with grooves provided at a uniform depth, width and period, have been found to be unsuited for the task for which they will ultimately be required.

The most difficult part in designing the new high- or higher-performance submillimeter-wave antenna has been the creation of a very low-loss feed horn - one that could be used in radio-astronomical telescopes. The new submillimeter-wave corrugated horn antenna introduced in this report has satisfied this design goal by using a mode-transform section inserted between the feed circular wave-guide and the flare of the antenna.

REFERENCES

1. Matsunaga, M., Matsunaga, T., and Sekimoto, Y., “An Experimental Study of Submillimeter-Wave Horn Antennae for a Submillimeter-Wave Array,” Publ. Astron. Soc. Japan, vol. 55, no. 5, pp. 1051 – 1075, 2003.
2. Clarricoats, P. J. B., and Olver, A. D., Corrugated Horns for Microwave Antennas (London: Peter Peregrinus Ltd.), 1984.
3. Goldsmith, P. F., Quasioptical Systems — Gaussian Beam Quasioptical Propagation and Applications(New York: IEEE Press), 1998.

Session 2A5
Numerical and Analytical Technologies of Photonic Devices I

Modelling of Er-Yb Codoped Glass Waveguide Amplifiers

E. Y. B. Pun and **K. Liu**
City University of Hong Kong, China

Erbium doped waveguide amplifier (EDWA) has attracted much attention due to its high gain, low noise, polarization insensitive, and possible integration with other integrated optical devices [1,2]. Numerical analysis of EDWAs based on the solutions of steady state rate equations and nonlinear propagation equations of a multilevel system have been reported [3-5], and the works focus on the amplifier gain characteristics. A widely used numerical approach is a combination of finite-element method with a Runge-Kutta algorithm [6], and this method has been shown to be very accurate. However, the computation time is long due to the evaluation of the transversal integrals, and the accuracy of the results depends not only on the accurate numerical calculations, but also on the accuracies in the characteristics parameters used in the models.

System applications require that a certain level of SNR be achieved at the receiver end, hence, the noise characteristics of EDWAs must be carefully evaluated if used in various system locations. However, there are few reports on the investigations of the amplifier noise.

In this work, Er-Yb codoped waveguide amplifiers were studied using an overlapping factors method [7]. Two overlapping factors, the integrations of the pump and the signal intensities with the Er ions distributions, were used, and the model overcomes some of the difficulties mentioned above. The waveguide parameters used were derived from a channel waveguide fabricated by ion-exchange process and field-assisted annealing (FAA) method [8]. Both the gain and the noise characteristics of the amplifiers were investigated, and there is good agreement between theoretical data and experimental results. It is shown that high pump power is useful in suppressing the amplified spontaneous emission power and thus decreasing the noise figure, and both the waveguide losses and the optical mode confinement factor have strong effects on the optical gain.

REFERENCES

1. O. Lumholt et al., *IEEE J. Lightwave Technol.*, vol.13, p.275-282, 1995.
2. J.M.P. Delavaux et al., *IEEE Photon. Technol. Lett.*, vol. 9, p.247-249, 1997.
3. M. Federighi et al., *IEEE Photon. Technol. Lett.*, vol. 5, p.227-229, 1993.
4. C. Lester et al., *IEEE J. Lightwave Technol.*, vol.13, p.740-743, 1996.
5. C. E. Chryssou et al., *IEEE J. Lightwave Technol.*, vol.19, p.345-349, 2001.
6. P. Torres and A.M. Guzman, *IEEE J. Lightwave Technol.*, vol.15, p.546-550, 1997.
7. J.A. Valles et al., *IEEE J. Quant. Electron.*, vol.32, p.1685-1694, 1996.
8. K. Liu and E.Y.B. Pun, *IEEE Photon. Technol. Lett.*, vol. 17, p.76-78, 2005.

Efficient Implementation of the Implicit FDTD Method Using the Locally One-Dimensional Scheme

J. Shibayama, R. Takahashi, J. Yamauchi, and **H. Nakano**
Hosei University, Japan

The finite-difference time-domain method (FDTD) has widely been used to obtain wide-band characteristics of optical waveguides. Note that a time increment (δ t) is limited by the Courant- Friedrich-Levy (CFL) condition. To overcome this problem, the alternating-direction implicit (ADI) FDTD has been proposed [1], [2]. We have alternatively introduced the locally one-dimensional (LOD) scheme [3] into the implicit FDTD [4]. The LOD-FDTD leads to simple implementation of the algorithm with a subsequent reduction in the CPU time, when compared with the ADI-FDTD.

In this article, the LOD-FDTD, developed for the TE waves [4], is extended to the one that handles the TM waves. To formulate the LOD-FDTD, we first apply the Crank-Nicolson scheme to Maxwellfs equations, resulting in implicit FDTD equations. After applying the LOD scheme to these equations, we obtain differential equations split into two steps. As a result, we derive two implicit and two explicit equations to be solved. This contrasts with the ADI-FDTD, in which two implicit and four explicit equations should be solved.

As an application, we analyze an optical waveguide with an endfacet [5] for both TE and TM waves. The results obtained from the LOD-FDTD perfectly follow those from the ADI-FDTD, since the basic equations are the same for both methods. In addition, the results are in a good agreement with those from the FDTD up to 10 $\delta\mathrm{t}_C FL$, where $\delta\mathrm{t}_C FL$ is determined by the stability criterion of the explicit FDTD. In this case, the CPU time of the LOD-FDTD is reduced to 80% and 50% of those of the ADI-FDTD and the FDTD, respectively.

REFERENCES

1. T. Namiki, gA new FDTD algorithm based on alternating-direction implicit method,h *IEEE Trans. Microwave Theory Techniques*, vol. 47, no. 10, pp. 2003-2007, 1999.
2. F. H. Zheng, Z. Z. Chen, and J. Z. Zhang, gA finite-difference time-domain method without the Courant stability conditions,h *IEEE Microwave Guided Wave Letters*, vol. 9, no. 11, pp. 441-443, 1999.
3. A. R. Mitchell and D. F. Griffiths, The finite-difference method in partial differential equations. John Wiley & Sons, 1980.
4. J. Shibayama, M. Muraki, J. Yamauchi, and H. Nakano, gEfficient implicit FDTD algorithm based on the locally one-dimensional scheme,h *Electron. Lett.*, vol. 41, no. 19, pp. 1046-1047, 2005.
5. J. Shibayama, A. Yamahira, T. Mugita, J. Yamauchi, and H. Nakano, gA finite-difference time-domain beam-propagation method for TE- and TM-wave analyses,h *IEEE/OSA J. Lightw. Technol.*, vol. 21, no. 7, pp. 1709-1715, 2003.

Numerical Study of the Dielectric Waveguide Termination With a Tilted Facet

C. M. Wang and **H. W. Chang**
National Sun Yat-sen University, Taiwan

In optical coupling between lasers and fibers, the fiber end is usually cleaved with a tilt angle in order to minimize the multiple reflections between the active and passive devices. This reduces the unwanted cavity effect so that the fiber grating external cavity laser will function as designed. However, the exact tilt angle must be carefully chosen because excessive tilting will cause spurious scattering. In order to analyze this problem we simply the problem by just examining a 1-D slab waveguide terminated with a tilted facet. We propose to use the T-matrix method, which is based on the analytical continuity principle of the exact analytic modal solutions satisfying the interface conditions on the tilt surface. The solutions are divided into two regions, region I for the incident and reflected fields and region II for the transmitted fields. To verify the T-matrix technique, we intend to apply the frequency-domain finite-difference (FD-FD) methods to study this problem. Under the T-matrix method the derived matrix equation for the unknown reflection/transmission coefficient is highly singular for large tilt angles, whereas the FD-FD calculation which is not very accurate can handle large tile angles. The FD-FD solutions are used to verify and compare the accuracy of T-matrix solutions. The advantages and disadvantages of the two methods will be addressed.

A Novel Formulation of the Fourier Series Expansion Method for Dielectric Waveguides Based on Periodic Fourier Transform

K. Watanabe
Fukuoka Institute of Technology, Japan

The Fourier-series expansion method (FSEM) [1.4] is a very effective approach to analyze many of waveguide problems, for example, junctions, tapers, and branches. FSEM introduces an artificial periodicity in the transverse direction and the electromagnetic fields are expanded in the Fourier series. The artificial period is chosen to be large when FSEM is applied to a waveguide transition in which the radiation occurs with a wide propagation angle. The radiated wave that achieves to the periodic boundary incidents from the opposite boundary, and causes unwanted interference to the guided wave field. However, from the view point of numerical computation, the artificial period has to keep small to reduce the truncation number for the Fourier series expansion because larger period makes the convergence slower. An idea to prevent such a difficulty has been proposed in which the perfectly matched layer is introduced to absorb the radiation [4].

This paper shows another approach for analyses of waveguide transition problems. Any function (x) that is absolutely integrable, uniformly bounded, and monotone for large jxj becomes periodic with the use of the periodic Fourier transform (PFT) [5]. The conditions for the function ensure the pointwise convergence of PFT but, generally, the electromagnetic fields propagating along dielectric waveguides do not satisfy them. However, PFT seems to be practically useful for wider class of function and, in this paper, PFT is formally applied to the waveguide transition problems. The transformed fields become periodic and then all field components can be expanded in the Fourier series without introducing the artificial periodic boundary. The Fourier coefficients, which are functions of the transform parameter, are approximated by introducing a discretization in terms of the transform parameter, and then the fields are fully described in matrix form. The wave propagation in each waveguide section uniform in the propagation direction can be solved as an eigenvalue analysis, and the boundary condition at the waveguide transitions are given by equating the Fourier coefficients in both sides of the transitions.

REFERENCES

1. C. H. Henry and Y. Shani, gAnalysis of Mode Propagation in OpticalWaveguide Devices by Fourier Expansion,h *IEEE J. Quantum Electron.*, Vol. QE-27, No. 3, pp. 523.530, 1991.
2. T. Hosono, T. Hinata, and A. Inoue, gNumerical Analysis of the Discontinuities in Slab Dielectric Waveguides,h Radio Sci., Vol. 17, pp. 75.83, 1982.
3. Y. Yamakita, K. Matsumoto, and K. Rokushima, gAnalysis of Discontinuities in Anisotropic Dielectric Waveguides, IEICE Tech. Rep., EMT-93-87, pp. 81.90, 1993.
4. K. Yasumoto, K. Watanabe, and J. Ishihara, gNumerical Analysis of Optical Waveguides with the Use of Fourier-Series Expansion Method Combined with Perfectly Matched Layer,h Microwave and *Opt. Technol. Lett.*, Vol. 34, No. 6, pp. 422.426, 2002.
5. J. Nakayama, gPeriodic Fourier Transform and Its Application to Wave Scattering from a Finite Periodic Surface,h *IEICE Trans. Electron.*, Vol. E83-C, No. 3, pp. 481.487, 2000.

Scattering of EM Wave by a Cylindrical Periodic Array Using Moment Method

I. Satou and **M. Yokota**
University of Miyazaki, Japan

Scattering of electromagnetic wave with periodic structure has been the important issues in electromagnetic theory. So far, many books and papers have been published[1,2].

Two-dimensional scattering problems which consist of circular cylinders have been analyzed, since the scattered fields are expressed in terms of cylindrical functions. In this paper, the moment methods are applied to the scattering of electromagnetic wave by periodic arrays of dielectric cylinders. The scattering fields are expressed in terms of volume integral form, and this equation is converted to the matrix equation by the moment methods and Bloch theorem. This method can be applied to more general cases such as that the objects are arbitrary shapes or inhomegeneous media or nonlinear media. The elements of the matrix equation include an infinite sum of Hankel functions multiplied by trigonometric angular dependencies. As is well known, the convergence of this infinite sum is so slowly. By using the Fourier integral representation of Hankel funcntions, the elements of the matrix equations are expressed by the integral of the elementary functions[3]. As numerical examples, the power reflection coefficient and scattering field are examined. Matrix calculation is derived from Generalized Minimum Residual (GMRES) method. Our results are compared with the previous ones and it is shown the good agreement.

REFERENCES

1. A.Ishimaru, Electromagnetic wave propagation, radiation, and scattering, Prentice Hall, 1991.
2. K. Yasumoto(Ed.) Electromagnetic Theory and Applications for Photonic Crystals, CRC Press, 2006.
3. K. Yasumoto and K. Yoshitomi, IEEE Trans. on Antennas and Propag., vol. 47, no.6, pp. 105.1055, June 1999.

Design of the DC Block with Defected Ground Structure

S. H. Choi and **K. H. Park**
Korea Electronics Technology Institute, Korea

Recently, researches on defected ground structure(DGS) and photonic bandgap(PBG) have been reported continuously. Each structure has its own properties. PBG which has periodic defect array on the ground plane provides wide and deep stopband properties. On the other side, DGS which has a specific pattern or non-periodic defect array on the ground plane provides a rejection band in some frequency range because it increases the effective inductance of a transmission line. These properties are used to improve performance of various circuits by means of removing harmonics. Sometimes DGS is used to reduce size of a circuit.

This paper suggests DC blocks that DGS applies to its ground plane. In the low frequency range, capacitors are used to block a DC component. DC blocks are more popular than capacitors in the high frequency range. In case of DC blocks, their line-width and line-gap should be tuned to obtain the wanted specification. But it suffers from size of line width and gap as frequency increases. By means of applying DGS in the DC block, it transforms a coupling method of circuit. Due to this phenomenon, the size of the DC block must be tuned unavoidably to obtain the initial performance. In this process, line width and gap are increased. Besides, harmonics of the DC block can be suppressed.

To verify performance of DC blocks with DGS, DC Blocks are fabricated on the Taconic TLX-9 substrate with the relative permittivity of 2.5 and the thickness of 20 mil. The center frequency of DC blocks is about 6.3 GHz. As a result of design and measurement, line width and gap of DC blocks with DGS are increased. Moreover, in case of DC blocks without DGS, a harmonic appears at 18.9 GHz. But this harmonic is suppressed in case of DC blocks with DGS.

Novel Wide-Angle Three-Dimensional BPM Based on the Alternating-Direction Implicit Method

J. Shibayama, T. Takahashi, J. Yamauchi, and **H. Nakano**
Hosei University, Japan

To efficiently analyze the field propagation in three-dimensional (3-D) optical waveguides, the beam-propagation method (BPM) based on the alternating-direction implicit (ADI) scheme has widely been employed [1] . However, the ADI scheme has not been extended to the Padé-based wide-angle equation [2], [3], since the straightforward extension gives rise to a zeroth-order splitting error term. This error dose not converge to zero, even when the longitudinal sampling width (Δ z) approaches zero. Chui and Lu [4] reformulated the wide-angle equation as in the ADI iteration scheme for elliptic problems. While this approach successfully solves the full-vectorial wide-angle equation, it requires several iterations resulting in a decrease of the efficiency of the ADI scheme.

Note that a circuit pattern in most planar wave-guiding structures is confined to the horizontal plane. This means that wide-angle beam propagation may occur only in the horizontal direction. Therefore, the application of the Padé approximant only to the horizontal direction is expected to be sufficient for most practical waveguide problems.

The purpose of this article is to present a 3-D semi-vectorial horizontally-wide-angle BPM based on the ADI scheme [5], in which the Padé approximant is applied only to the horizontal direction. The present formulation reduces the splitting error to the first order without resorting to an iteration procedure, in which the effect of the error can be suppressed with a reasonably small Δ z. The effectiveness of the present method is investigated through the analysis of tilted optical waveguides.

REFERENCES

1. J. Yamauchi, T. Ando, and H. Nakano, gBeam-propagation analysis of optical fibres by alternating direction implicit method,h *Electron. Lett. vol.* 27, no. 18, pp. 1663-1665, 1991.
2. D. Yevick and M. Glasner, gAnalysis of forward wide-angle light propagation in semiconductor rib waveguides and integrated-optic structures,h *Electron. Lett.*, vol. 25, no. 23, pp. 1611-1613, 1989.
3. G. R. Hadley, gWide-angle beam propagation using Padé approximant operators,h *Opt. Lett., vol.* 17, no. 20, pp. 1426-1428, 1992.
4. S. L. Chui and Y. Y. Lu, gWide-angle full-vector beam propagation method based on an alternating direction implicit preconditioner,h *J. Opt. Soc. Am. A*, vol. 21, no. 3, pp. 420-425, 2004.
5. J. Shibayama, T. Takahashi, J. Yamauchi, and H. Nakano, gA three-dimensional horizontally-wide-angle non-iterative beam-propagation method based on the alternating-direction implicit scheme,h *IEEE Photon. Technol. Lett.*, to be published.

Polarisation Issues in Photonic Wires for Biosensing Applications

S. T. Lim and **C. E. Png**
Institute of High Performance Computing, Singapore

Silicon Photonics is experiencing a dramatic increase in interest due to emerging applications areas and several high profile successes in device and technology development. Despite early work dating back to the mid 1980s, dramatic progress has been made in recent years. Whilst many approaches to research have been developed, the striking difference between the work of the early to mid 1990s, and more recent work, is that the latter has been associated with a trend to reduce the cross sectional dimensions of the waveguides that form the devices, which is vital for the realisation of a highly dense photonic integrated circuit. The fundamental question lies here: is it possible to fulfil simultaneously the single-mode and zero birefringence conditions for small cross-sectional structure? In this paper, a comprehensive study of small cross section channel waveguide, using the imaginary distance beam propagation method (IDBPM), will be presented. We will discuss the possibility of realising such waveguides for sensing applications based on photonic-bandgap microcavities with both tunability and sensitivity. We also provide a systematic study of the various physical parameters that can affect the Q factor and transmission properties in such waveguides. In order to make this technology viable, the waveguides must be tunable, have low attenuation, possess high Q factor, and can be switched. Can these be achieved simultaneously without changing the device width and height dimensions? Furthermore, can we meet these aims without placing unrealistic demands in fabrication? The electrical switching of this device is implemented using a /p-i-n /optical diode. The diode is predicted to require a ON state power of 81 nW with rise and fall times of 0.2 ns and 0.043 ns respectively. The length of the microcavity and the diameter of the air holes are finely tuned with reference to the Q factor and transmission. It will be shown that for certain desired resonant wavelength, the Q factor and transmission properties can be optimized by tuning the length of the cavity and the diameter of the two inner most air holes. This method allows ease of fabrication by not having to vary the waveguide width and height to obtain the tuning effects. Optical simulation was performed using 3-D finite difference time domain (FDTD) simulation method.

Vectorial Modal Analysis of 2-D Dielectric Waveguides with Simple Orthogonal Bases

R. G. Yang and **H. W. Chang**
National Sun Yat-sen University, Taiwan

We propose a vectorial basis-function expansion formulation for analyzing modal characteristics of the complex 2-D dielectric waveguides. To reduce costs and to shorten the product development cycle of integrated dielectric waveguides, it is crucial to be able to accurately compute the propagation constants () as well as the electromagnetic field profiles of these complex optical devices so that the devices will perform as intended. Although waveguide propagation constants can be very accurately computed, accurate 2-D vector field solutions are harder to compute especially when there are degenerate modes with similar β_s.

We first derive the coupled differential equations of the two transverse magnetic field components which satisfy the continuous boundary conditions across all material interfaces. Then we investigate and verify the accuracy of this method on 1-D rectangular waveguide so that we can apply the technique to those more complex 2-D waveguides. By means of linear combination of simple 2-D orthogonal bases, we expand the mode of rectangular dielectric waveguide. Through rigorous mathematical closed-form integration, we obtain the equivalent matrix whose eigenvalues and associated eigenvectors become the mode propagation constants and mode field distribution functions of the underlying 2-D dielectric waveguide. Whenever symmetry exists we can reduce the size of the problem by choosing appropriate boundary conditions in accordance to particular mode polarization desired.

We examined optical fiber modes both the step-index profile and the graded-index profile to confirm the accuracy and feasibility of our method. We get at least five significant digits of propagation constant and detailed field description of the rectangular dielectric waveguide. We believe that it is an effective method for modal analysis of 2-D complex dielectric-waveguides.

Session 2P1a
Polarimetric Radar Remote Sensing

A New FM-CW Pol-InSAR System for Laboratory Measurement

M. Ikarashi, K. Aoyama, J. Nakamura
Y. Yamaguchi and **H. Yamada**

Niigata University, Japan

A fully polarimetric and interferometric FM-CW radar system has been re-developed at Niigata University, Japan, for the purpose of laboratory measurement [1]. This paper presents the system design and its performance as a fully polarimetric POL-InSAR.

The system specification is as follows:
Sweep frequency : Any frequency and band within the Ku-band.
Default is from 14 GHz to 16 GHz.
Sweep time : 5 ms
Polarization : HH, HV, VH, VV.

Two sets of scattering matrix can be acquired simultaneously, one is for monostatic mode and the other is for bistatic mode, since the radar system has 4 independent receive channels. The separation distance (baseline) of transmitting and receiving antennas can be set in-between 20 cm to 100 cm.
Range resolution : 7.5 cm by default. Variable depending on the bandwidth of transmitting signal.
Polarization Isolation: less than -30 dB
Maximum Output Power : 20 dBm
Dynamic Range: 50 dB

Operating mode: monostatic, bistatic, and monostatic+bistatic=interferometric. Approximately 50 snapshots per second with each snapshot yielding the corresponding scattering matrices along the range bin.

A specific feature of the system is an addition of RF amplifier at the receiver antena. This serves to expand the dynamic range in sensitivity. A 16-bit A/D converter is equipped for IF signal sampling. The polarimetric mode is calibrated using a parallel plate waveguide oriented 45 degrees [2]. The system has been applied to various target imaging and detection. Preliminary measurement results will be shown in the presentation including SAR resolution, calibration, etc. The advantage of the system is quite fast data acquisition time compared to the conventinal network analyzer sytem.

REFERENCES

1. M. Nakamura, Y. Yamaguchi, H. Yamada, gReal-time and full polarimetric FM-CW radar and its applications to the classification of targets,h *IEEE Trans. Instrumentation and Measurement*, vol.47, no.2, pp.572-577, April 1999.
2. K. Kitayama, Y. Yamaguchi, Y. Takayanagi, H. Yamada, gPolarimetric calibration using a parallel plate waveguideh, *Trans. of IEICE*, vol.J-81-B, no.10, pp.914-921, 1998 (In Japanese)

Laboratory Measurements by a Fully Polarimetric FM-CW SAR in the Ku-Band

M. Ikarashi, J. Nakamura, K. Aoyama, Y. Yamaguchi, and **H. Yamada**

Niigata University, Japan

FM-CW radar is suitable for short range sensing. If equipped with fully polarimetric data take function, it can be a handy Polarimetric Synthetic Aperture Radar (POLSAR) as well as interferometric one (POL-InSAR) with additional receiving antenna pair of orthogonal polarization. The advantages of FM-CW radar system are cost-effective, handy, easy to change radar specifications, and quick data acquisition time compared to Network Analyzer in short range sensing. A Ku-band FM-CW POLSAR was designed for checking the results of airborne Pi-SAR and satellite ALOS-PALSAR as well as for other applications. Since the range and the range resolution of the developed radar can be adjusted easily, we have made several measurements in anechoic chamber.

Targets under test are concrete blocks imitating urban buildings, planted trees, metallic objects such as guard rails, etc. Various radar targets were imaged using the Ku-band FM-CW POLSAR in an anechoic chamber. Based on the polarimetric SAR image of specific targets, polarimetric analyses using four-component decomposition[1], entropy-alpha analysis[2], correlation data analysis were performed. The imaging results as well as polarimetric data analyses will be shown in the presentation.

REFERENCES

1. Y. Yamaguchi, M. Ishido, T. Moriyama, H. Yamada, "Four-Component Scattering Model for Polarimetric SAR Image Decomposition", *IEEE Trans. Geoscience Remote Sensing*, vol. 43, no.8, pp.1699-1706, Aug. 2005
2. S. R. Cloude and E. Pottier, "An entropy based classification scheme for land applications of polarimetric SAR", *IEEE Trans. Geosci. Remote Sensing*, vol. 35, no. 1, pp. 68-78, Jan. 1997.

Investigation on Seasonal Change of Water Area in Lake Sakata Based on POLSAR Image Analysis

R. Sato, Y. Yajima, Y. Yamaguchi, and **H. Yamada**
Niigata University, Japan

Lake Sakata, located in Niigata city, Japan, is one of the most important and rare wetlands. The lake is formed in the hollow region of a dune, and the freshwater of the lake is supplied only from spring water of the dune and rainwater. There is no inflow from rivers in the lake. So it is very significant to continuously investigate the seasonal changes of the water level and the vegetation area composed by the emerged and floating-leaved plants around the lake. So far, many investigations on the seasonal change have been done by using aerial photographs. However, such investigation method depends on the weather since aerial photographs can not be taken in bad weather condition. Also, by such aerial photographs, it is difficult to distinguish whether or not the invisible region under the emerged plants around the lake is water.

In this paper, we investigate seasonal change of the water area in Lake Sakata for few years by using Polarimetric Synthetic Aperture Radar (POLSAR) data. POLSAR is one of the most attracting microwave remote sensing technologies and independent of the weather condition. In order to classify the boundary between the water area and the fringe vegetation or ground area around the lake, statistical POLSAR image analysis is first carried out for both L- and X-band data (scattering matrix) obtained by airborne Pi-SAR system (provided by NICT and JAXA, Japan). Here, three-component scattering model of surface scattering, double-bounce scattering and volume scattering is applied for the image decomposition. Furthermore, to improve the accuracy of the classification, polarimetric scattering analysis for a simplified local model is also executed by using the FDTD method. The model simply simulates the local boundary region between the surrounding vegetation and the water areas, i.e. it is composed of lots of slender or thin dielectric pillars (as a vegetation area by emerged plants like reeds) on a PEC plate (as a water area). Finding out and taking into account the particular polarimetric scattering characteristics from the simplified model, it will be made clear what is the dominant source of each scattering component in the decomposed POLSAR image. Consequently, the seasonal change of the water area in the lake will be clarified.

Target Enhancement Oriented Fusion Method using Polarimetric SAR Data

Y. Chen and **J. Yang**
Tsinghua University, China

Polarimetric Synthetic Aperture Radar (SAR) can provide multi-dimensional radar images with different transmitting and receiving polarization states of antennas. For the application of target detection, an essential problem is to fuse multi-dimensional images into a single one to enhance the contrast between the targets and the clutters.

Previous target enhancement methods tends to combine polarimetric information to distinguish one kind of target from another kind of clutter. For instance, the Optimization of Polarimetric Contrast Enhancement (OPCE) is to choose optimal polarization states for enhancing a desired target versus an undesired clutter. By introducing more polarimetric parameters, Yang *et al.* proposed a Generalized Optimization of Polarimetric Contrast Enhancement (GOPCE) which could make the target/clutter contrast more distinguishable. However, in polarimetric SAR images, different targets and clutters show different polarimetric property, and it is difficult for previous methods to enhance multiple targets simultaneously. Therefore, in polarimetric SAR images, local target/clutter contrast enhancement is preferred.

In this paper, a novel fusion method is proposed for the enhancement of local contrast. The optimal local contrast of each pixel is first defined based on the Ratio Of Average (ROA) detector across multi-polarization images. Then the fused image with optimal local contrast is found in a least square minimization framework. It is proved that the solution can be obtained by solving a discrete Poisson equation via the Fast Fourier Transform (FFT) implementation. With polarimetric SAR data, we demonstrate the effectiveness of our method for target enhancement, where ship detection and road detection are used as examples.

Novel Target Decomposition Method based on Polarimetric Signatures

Y. Chen and **J. Yang**
Tsinghua University, China

Polarimetric signatures are an effective way to characterize the polarization properties of microwave backscatter. In the past years, these signatures have been used successfully to present the scattering characteristics of a wide rage of target types. However, most previous research work tend to provide a qualitative description rather than a quantitative analysis.

In this paper, we propose a mathematical framework for analysis of polarimetric signatures. The inner product between two polarimetric signatures is first defined, which is proved to have a simple representation of elements from the Kennaugh matrices. Distance measurement and similarity measurement are then defined to quantify the difference between two polarimetric signatures. All these parameters are shown to have a compact form which is convenient for calculation.

Based on the defined parameters of signatures, a novel target decomposition method is proposed which divide the target into several typical scattering mechanisms. The proposed decomposition method is based on the least square rule and can be carried out by the constrained quadratic programming. With polarimetric Synthetic Aperture Radar (SAR) data, we demonstrate that the signature based decomposition results are able to reflect the target's scattering mechanism, such as the component of single- or double- bounce, which can be helpful for weak target detection.

Optimization of Weather Data Quality and Radar Scan Rate Using Phased-Array Radar

T. Y. Yu and **M. B. Orescanin**
University of Oklahoma, U.S.A.

C. D. Curtis, D. S. Zrnić, and **D. E. Forsyth**
NOAA National Severe Storms Laboratory, U.S.A.

The Weather Surveillance Radar-1988 Doppler (WSR-88D) network in the United State has proven to be a vital instrument for meteorological and climatological applications. The current WSR-88D system completes a volume coverage pattern (VCP) within a minimum of approximate 4 min. However, faster scanning is often needed not only to increase the warning lead time but also to advance the understanding of fast-evolving weather systems. Although the data acquisition time to complete a sector scan or VCP can be reduced by increasing the antenna's rotational rate, the statistical error of radar estimates (reflectivity, mean Doppler velocity, and spectrum width) will increase due to a decrease in the number of samples used for processing. There are also mechanical limitations on the pedestal that restrict how fast the antenna can rotate. A novel approach to address these fundamental limitations is to use a phased array weather radar.

The recently installed S-band phased array radar (PAR) at the National Weather Radar Testbed (NWRT) in Norman, Oklahoma offers fast and flexible beam-steering through electronic beam forming. This capability allows implementation of a novel scanning strategy termed beam multiplexing (BMX) with the goal of providing fast updates of weather information with high accuracy. BMX has been developed to exploit the idea of collecting independent samples while maximizing the usage of radar resources. In other words, the radar will revisit the location of interest after the signals become uncorrelated. As a result, the statistical error of estimates can be minimized using fewer samples. During the revisit time, the radar will be tasked to scan other locations to optimize the usage of radar resources. As a result, the radar beam will be multiplexed over a designated region to provide measurements with lower statistical errors in a shorter period of time.

An improvement factor, which is defined by the reduction in data acquisition time using BMX to achieve the same data accuracy obtained with conventional sampling scheme, is used to quantify the performance of BMX. It is shown theoretically that fast updates without comprising data quality can be achieved using BMX, especially at small spectrum widths and high signal-to-noise ratios (SNR). Applications of BMX to weather observations are demonstrated on the NWRT. Statistical analysis is performed to verify the theoretical variance of signal power and mean velocity estimates using both BMX and conventional scanning strategies. Furthermore, the experimental results have demonstrated that the acquisition time can be improved using BMX by an average factor of two to four for SNR higher than 10 dB.

Session 2P1b
Subsurface/GPR

Measured Complex Permittivity of Borehole Cores Using Open-Ended Coaxial Probe

J. H. Jung and **S. Y. Kim**
Korea Institute of Science and Technology, Korea

Several kinds of cross-borehole radar systems have been used to detect deeply located man-made tunnels in the middle area of Korea. One of difficulties posed in analysis of the received radar signatures has been the significant variation of those attenuation and velocity profiles according to the depth. It leads us to postulate that the electrical properties of in-situ rock may be strongly inhomogeneous. In consequence, we need to prove the above postulate because the in-situ rock has been usually considered homogeneous granite during our past design of borehole antennas. We obtained a sufficient number of rock cores, which had been extracted in each 10 meter of depth from the boreholes located in 3 different sites.

In this paper, complex permittivity profiles of borehole cores are measured using open-ended coaxial probe in a wide range of frequency. In order to reduce the contact error between open-ended coaxial probe and borehole core, one-side surface of borehole core is polished flatly. And the processed cores are immersed in water for a while to adjust the humidity of dry cores similar to the underground rock in a real situation. Then reflection coefficients of borehole cores contacted to an open-ended coaxial probe are measured in a frequency range of 2.3 to 100 MHz using vector network analyzer. The measured reflection coefficients are inserted into our conversion program, which has been implemented by an improved virtual transmission-line model. A straightly numerical calculation provides the complex permittivity profile of the contacted core.

To verify the accuracy of our measurement procedure, we assume that the open-ended coaxial probe is contacted to the material with the same complex permittivity profile as the measured data. It is found that the reflection coefficients calculated numerically using the FDTD method approach to the originally measured reflection coefficients within the uncertainty of the vector network analyzer. For the borehole cores in a specific area, the loss tangent profile corresponding to the measured complex permittivity data approaches to the reference data only about 100MHz. In general, the real and imaginary parts of the measured complex permittivity profile vary from 6 to 14 and from 0 to 2.5, respectively, according to sampled depth and location of borehole cores. The above measured data are assured that the electrical properties of in-situ rock are strongly inhomogeneous.

GPR with an Electronically Steered Footprint

A. G. Yarovoy, P. Aubry, M. Tanigawa, A. J. Boonstra
W. V. Cappellen, H. J. Boer, and **L. P. Ligthart**

Delft University of Technology, The Netherlands

Ground Penetrating Radar (GPR) is a useful tool for detection of all kinds of electrical inhomogeneities in the ground, and is widely used in geological, geotechnical, archeological and forensic investigations. Exact localization of detected inhomogeneities and their characterization requires mechanical 2D scanning of the area under investigation with GPR and off-line processing of the acquired data. This state-of-the-art procedure can be improved by replacing mechanical scanning over the area by electrical scanning of the subsurface, similarl to far-field scanning in phased arrays. To investigate possibilities of the electronic steering of the antenna footprint in the near field, an arraybased GPR has been built. The antenna system consists of a single transmit antenna and 7 receive ones. For the transmit antenna a Vivaldi antenna has been used, while a shielded loop antenna has been used as a receive one. The antenna array has been optimized to provide high-resolution images of the shallow subsurface. Footprint steering has been implemented in the digital signal processing via true time delay of the received signals. Performance of the radar has been investigated experimentally. Electrical scanning along the array has been achieved, and 2D localization of buried objects without mechanical scanning has been demonstrated.

Design, Implementation and Calibration of Low Cost 1-2 GHz Step Frequency GPR for Metal Object Detection Under the Ground

J. Suryana, A. B. Suksmono, Sugihartono, and **A. Kurniawan**
STEI ITB, Indonesia

K. Tanaka and **K. Igarashi**
NICT, Japan

M. Iida
ARIB, Japan

Stepped Frequency Ground Penetrating Radar (SFGPR) is a promising alternative technique for realizing the GPR tranceiver which has more features than Pulse GPR technique. Moreover, with the decreasing of RF component costs in the market, the realization of GPR equipment would be cheaper than ten years ago.

In this paper, we describe the design and realization steps of low cost 1 - 2 GHz SFGPR transceiver for metal detection under the ground. Before using prototyped GPR for detecting the metal under the ground, several of calibration processes must be performed, namely phase calibration and monocycle pulse waveform calibration. After completing the calibrations, this low cost prototyped GPR would be ready for detecting the hidden object such as a metal plate 5 cm under the ground in our small test range size 25 cm $\times$ 75 cm $\times$ 10 cm. From the calibration and detection results, we concluded that the prototyped SFGPR passed the technical specifications of the design and could perform the metal detection under the ground with high SNR.

Keywords : Stepped Frequency, GPR, Metal Detector, Phase and Monocylce Calibrations

An Algorithm for 3-D Imaging of Subsurface Fractures in Directional Borehole Radar

T. Takayama and **M. Sato**
Tohoku University, Japan

Borehole radar is a kind of ground penetrating radars especially useful to explore deep subsurface structures. With a typical borehole radar system that uses a pair of dipole antennas for both transmission and reception, a radar image obtained in a single-hole reflection measurement is 2-dimensional image since it consists of reflection signals from all directions due to the omni-directional radiation pattern of antennas. Therefore, in order to interpret subsurface structure 3-dimensionally, reflection images obtained at several boreholes or 3-D cross-hole tomography are necessary, however, those are accompanied by high drilling cost. Under such circumstances, directional borehole radar is getting growing attention as it provides 3-D subsurface structures in a single-hole reflection measurement effectively and with low cost performance.

We developed an array type directional borehole radar system which consists of one dipole transmitting antenna and four receiving dipole antennas [1]. Four receiving antennas are evenly spaced on a circle having 6 cm diameter, forming uniform circular array. A magnetic compass is attached on the top of the array to measure the orientation angle of the array after being put in a borehole.

In this presentation, the array-type directional borehole radar system and a new direction of arrival estimation algorithm for three-dimensional imaging of subsurface structure are discussed. The algorithm originates from the idea to synthesize an arbitrary oriented loop antenna from 4 dipole antennas [2][3]. Advantage of this algorithm is that the radiation pattern synthesized by the signal processing is irrespective of the aperture size or the frequency, greatly appreciated when the aperture size is much shorter than the wavelength as in the directional borehole radar system. The procedure becomes computationally more efficient than conventional ones by using analytic signal, and also can be implemented in conjunction with F-K filtering and migration technique to obtain better results. The algorithm is applied to single-hole measurement dataset acquired in Korea to demonstrate the ability of detection and orientation of subsurface fractures.

REFERENCES

1. Takuya Takayama and Motoyuki Sato, "Evaluation of an Array Type Directional Borehole Radar System", IEEE IGARSS, International Geoscience and Remote Sensing Symposium, Korea, July 25-29 2005
2. Y.T.Chan, B.H.Lee, R.Inkol and Q.Yuan, "Direction Finding with a Four-Element Adcock-Bulter Matrix Antenna Array", *IEEE Transactions on Aerospace and Electronic Systems*, Vol.37, No.4, pp.1155-1162, October 2001
3. Jung-Ho Kim, Seong-Jun Cho and Seung-Hwan Chung, gThree-Dimensional Imaging of Fractures with Direction Finding Antenna in Borehole Radar Surveyh, Proceedings of the 4th SEGJ International Symposium, pp.291-296, Tokyo, December 1998

Simultaneous Estimation of the Position and Radius of a Reinforcing Bar and the Dielectric Constant of Concrete

Y. Mayumi, T. Tanaka, and **T. Takenaka**
Nagasaki University, Japan

Though concrete structures are made having a useful long life, they may soon start to be degraded because of being poorly designed and constructed and will be in deteriorated condition within twenty to thirty years. Therefore, it is necessary to make a close investigation of the condition of concrete structures with respect to cracks, cavities, and corrosion of reinforcing bars in order to prevent dangerous accidents such as drop of flakes or masses of concrete. The existence of the reinforcing bar near the surface of the concrete can be confirmed at the good accuracy with conventional concrete radars. However, it is very hard to estimate the accurate position of the reinforcing bar, if the electric constant of the concrete has not been known. We previously proposed the method for estimating the position of a reinforcing bar and the dielectric constant of the concrete at the same time. In this method, we assumed that the reflection point of the electromagnetic wave is fixed irrespective of the position of the radar. This is equivalent to having supposed the value of the radius of the reinforcing bar to be zero. As the value of radius of the reinforcing bar is finite size, the reflection point of the electromagnetic wave is change by the position of concrete radar. We must take the radius of the reinforcing bar into consideration to estimate the position of the reinforcing bar in the high precision. Furthermore in the strength diagnosis of the concrete structure the number and radius of the reinforcing bars are important factors. However, few methods for determining accurately the radius of the reinforcing bar have been proposed, as far as we know.

In this paper, we propose a method for locating the position and determining the radius of a reinforcing bar and the dielectric constant of concrete simultaneously. The procedure of the processing is as follows.

1) Input the initial guess of the position and the radius of the reinforcing bar and the dielectric constant of concrete.
2) Calculate an error which is defined by the difference from the measurement value and the estimated value of the arrival time of the reflected wave from the reinforcing bar.
3) Judge the convergence.
4) Improve the estimate by using least-square method with Taylor expansion.
5) Go to (2)

The effectiveness of the presented method has been confirmed using real measured data.

A Simple Inversion Technique of Cross-Hole Data for Location of Buried Pipes

K. Takahashi and **M. Sato**
Tohoku University, Japan

A new inversion technique to locate buried pipes has been developed. The inversion algorithm estimates the location by searching the minimum prediction error for the first arrival time. Thus, the technique is a kind of parameter optimization techniques and does not image anything, but it can indicate the location obviously. The comparison of the predictions with measurements is performed focusing on the arrival curve shape unlike conventional ray tomography. Thus, the arrival time picking does not affect the estimation, and the arrival curve can easily be selected by maximum amplitudes or thresholding, for instance. The technique can explicitly and efficiently use a priori information on the target in the forward modeling. Therefore, the inversion calculation can be done very quickly and is stable. The inversion technique is verified with field data for a metallic pipe. The inversion result can estimate the location successfully, however the result by a straight-ray tomography calculated from the same data sets is not useful. Moreover, the tomography takes calculation time more than two hundreds times of that for the inversion. Therefore, the inversion technique is suitable for this purpose and to use on site rather than conventional tomographic techniques, and it can provide useful information also to non-specialists of radar and geological technologies who are involved with civil engineering.

Localization of the Investigation Domain in Electromagnetic Imaging of Buried 2-D Dielectric Pipelines with Circular Cross Section

V. Thomas, C. Gopakumar, J. Yohannan, A. Lonappan
G. Bindu and **K. T. Mathew**
Cochin University of Science and Technology, India

Electromagnetic inverse scattering problems are computation intensive, ill-posed and highly nonlinear. When the scatterer lies in an inaccessible domain, the ill-posedness is even more severe as only aspect limited data is available. Typical algorithms employed for solving this inverse scattering problem involve a large scale non-linear optimization that generates values for all pixels in the investigation domain including those that might not contain any useful information about the object. This communication is concerned with the localization in the investigation domain prior to inverse profiling of buried 2-D dielectric pipelines having circular cross section. A custom defined degree of symmetry is computed for each transmitter position, which is a measure of the symmetry of the measured (synthetic) scattered field vector. The degree of symmetry vector computed for a scatterer is found to exhibit unique features for the geometric and electric properties of the dielectric pipeline. A probabilistic neural network is trained with the degree of symmetry vectors computed for different object configurations. It classifies the test degree of symmetry vector of the unknown scatterer presented to it into one of the classes that indicate the localized region in the investigation domain in which the pipeline is located. The Distorted Born Iterative procedure is employed for imaging the pipeline that has been localized. The reduction in the investigation domain reduces the degrees of freedom of the inverse scattering problem and the results are found to be much superior to those when the entire investigation domain is employed.

Session 2P2
Earth-Space Propagation

Rain Attenuation Characteristics in Fixed Wireless Access at 32 GHz

H. Sawada, K.Hamaguchi, and **H. Ogawa**

National Institute of Information and Communications Technology,Japan

In this paper, we describe the measurements of rain attenuation at 32 GHz band. This frequency range has been opened for fixed wireless access (FWA) in World Radio Communication Conference (WRC-2000). Our purpose is a feasibility study of this frequency band for a broadband FWA. Considering the metropolitan area network (MAN), measurements were carried out in Tokyo area of Japan. It has been continued since April 2002. Adjacent three links were used for the rain attenuation measurement, and rain gauges installed to along to these links for the measurement of rain rate. Transmitters installed at Yotsuya, Azabu, Akasaka radiate vertical polarized wave, and receivers at Aoyama captured each wave. Length of link is 2 km, opening angle in adjacent link are 70.4 and 107.2 degrees. The parabolic type antenna whose beam width is 2.2 degree and gain is 33dBi are used, and transmission power is 200 mW.

The rain attenuation coefficient for basically rain attenuation characteristics was calculated, and differential rain attenuation and joint probability of attenuation are shown for route diversity in mesh network. Duration for rain rate in fade dynamics research is also investigated for the estimation of packet communications.

The results showed that the rain coefficient agree with the review standards of Japan. The maximum differential rain attenuation in adjacent links was 40 dB. Maximum diversity gain of 5 dB was observed from joint probability of attenuation.

Construction of Rain Attenuation Predictive Model at FWA and Ka Band Satellite Communications

R. Saotome, T. Miyazato, and **S. Tamaki**
University of the Ryukyus, Japan

Okinawa Prefecture is the island area of subtropical climate. The islands is scattered over a large area of North, south, east and west. Therefore, there are many areas where the high-speed Internet network is not provided with basic services. In order to remedy the area, It is necessary to use the easy sub-millimeter wave band radio communications of high bandwidth called Ka band satellite communication(WIDNS: Wideband InterNetworking engineering test and Demonstration Satellite) and FWA (Fixed Wireless Access) as remedy. However, this frequency band is weak in rain. An attenuation of radio wave by the rain is called 'Rain Attenuation' and it is very important problem for the communication using high frequency band.

The technology of compensating degradation of the communication quality by rain attenuation is studied for many years. However, in the field of satellite communication, the research has been actively at Ku band. So, there are still few research examples of the rain damping characteristic in terrestrial communication and satellite communication at Ka band. The actual proof experiment using the 18GHz band FWA was conducted by North-South Daito island of Okinawa Prefecture from September, 2003. As a result of this experiment, we could obtain precious data sets. Furthermore, the propagation experiment using a 18GHz and 26GHz band FWA is due to be started between Tsuken island and University of the Ryukyus (about 17km) in April, 2006.

In this research we examine about the rain attenuation model based on a time series analysis technique and we do the molding of the rain attenuation characteristic in a short time.

A Proposal of Modified Lavergnat-Gole Model for Global Conversion of Different Integration Time Rain Rates

C. Ito and **Y. Hosoya**
Kitami Institute of Technology, Japan

Introduction

One-minute rain rate distribution is necessary to design the radio links using frequencies above 10 GHz. On the world wide basis, however, the observations of rain rate are made mainly with longer integration times such as 60 minutes in Japan (e.g. 60-minute of AMeDAS: Automated Meteorological Data Acquisition System of Japan Meteorological Agency). Therefore, the conversion method of rain rate with longer integration time to that with one minute integration time must be derived. In this paper, a new global different integration time rain rate conversion method, in which Lavergnat-Gole model is extended by using regional climatic parameters, is proposed.

Lavergnat-Gole model [1]

Lavergnat-Gole model for different integration time rain rates conversion can be used for arbitrary integration times [1]. This model was developed as an application of stochastic process for the time intervals between raindrop arrivals, and has reliable theoretical background. This model is given by equations (1) and (2). P1 is the rain rate cumulative probability obtained with a rain gauge of integration time t_1, and R_1 is rain rate for P_1. P_2 is the rain rate cumulative probability obtained with a rain gauge of integration time t_2, andR_2 is rain rate for P_2. It is recommended that the parameter a is equal to 0.115 for ITU-R rain climate zone E (Gometz-la-Ville, France), but it is pointed out that the parameter a has the regional dependence [1]. However, the specific prediction method of parameter α has not yet been derived.

$$P_2(R_2) = k^\alpha P_1(R_1), k \equiv t_2/t_1 \tag{1}$$

$$R_2 = R_1/k^\alpha \tag{2}$$

Proposed different integration time rain rates conversion model

Using KIT different integration time rain rates databank which contains 227 data sets from 54 locations in 23 countries [2], we analyzed effects of regional climatic parameters on parameter a in order to extend Lavergnat-Gole model to the world. As the result, a new model was obtained by using regional climatic parameters such as integration time T (min), absolute value of the latitude $\phi(^o)$, absolute value of the longitude $\lambda(^o)$, one-minute rain rates (mm/h) for 0.01% and 0.001%($R_{0.01}$ and $R_{0.001}$), the average number of thunderstorm days D_{th} (day), the average annual total rainfall M (mm) and the thunderstorm ratio β. Parameter a is given by equation (3) which is obtained by multiple regression analysis. Because measured $R_{0.01}$ and $R_{0.001}$ can not be used in this model, $R_{0.01C}$and $R_{0.001C}$ are used in equation (3). They are converged values in iterated calculation procedure, in which $R_{0.01}$ and $R_{0.001}$ from KIT-M β method are used as initial values. KIT-M β method is an estimation method for one minute rain rate, and uses only M and β as input parameters. This method is reported to have relatively good accuracy when only M and β are given[3].

$$a = 1.001 \times 10^{-3} T - 1.305 \times 10^{-3}\phi + 2.249 \times 10^{-6}\lambda - 1.932 \times 10^{-3} R_{0.01C} + 6.186 \times 10^{-4} R_{0.001C} \\ -1.209 \times 10^{-5} M + 6.012 \times 10^{-4} D_{th} - 0.1241\beta + 0.2881 \tag{3}$$

REFERENCES

1. J. Lavergnat and P. Gole, *J. Appl. Meteorol.*, vol. 37, no.8, pp.805-818, Aug. 1998.
2. C. Ito and Y. Hosoya, *Trans. Inst. Electron. Inf. Commun. Eng., B*, vol. J88-B, no.5, pp.948-955, 2005.
3. C. Ito, Y. Hosoya and T. Kashiwa, *Trans. Inst. Electron. Inf. Commun. Eng., B*, vol. J82-B, no.7, pp.1440-1445, 1999.

Propagation Characteristics of FM Broadcasting Waves at the Mid Niigata Prefecture Earthquake

S. Takahashi, M. Kobayashi, A. Kaneda, M. Nishi, and **T. Yoshida**

Hiroshima City University, Japan

Since the coming of the 1995 Hyogoken-Nanbu earthquake, eyes in some people have turned towards seismic electromagnetic (EM) phenomena. Some researchers insisted that they had received the 77.1 MHz FM broadcasting wave that had been reflected by the ionosphere during this earthquake, and such concerns about the relationship between earthquakes and EM phenomena have spawned a number of vigorous studies with diverse frequencies covering DC, ULF, ELF, VLF, LF, MF, HF and VHF bands. Despite these eRorts there is not always consensus on this issue because the phenomena would be quite subtle and only sensitive instruments installed under the EM-noiseless environments are required for detection.

We have been conducting 24 hours monitoring observations of FM broadcasting waves using PLL synthesized tuners at the Hitachi, Yokosuka and Nobeyama observational sites. All the three sites are monitoring FM Sendai (77.1 MHz) and the Nobeyama site is also monitoring FM Niigata (82.3 MHz). These systems were working at the Mid Niigata Prefecture Earthquake (MEQ) on Oct. 23, 2004, and we have obtained the observational data to discuss whether seismic propagation anomalies caused by the MEQ exist. Interestingly, the 82.3 MHz broadcasting wave passed above the epicenter of the MEQ.

In this meeting, we report the propagation characteristics of these broadcasting waves by comparison of the data on usual days and the MEQ day. We have confirmed that the ordinary propagation state of the frequency 77.1 MHz is subject to tropospheric propagation. In order to check the peculiarities of EM, we have verified all the data during Oct. 17-25, 2004. The results are that no anomalies could be seen at the three sites and the received level variations during this period were dominated by tropospheric propagation as usual. In addition, the results of 82.3 MHz observations were also the same as those of 77.1 MHz. Base on these results, we conclude that any EM phenomena related with the reflection or disturbance of the ionosphere were not detected before and after the MEQ.

Ground Wave Propagation over Mixed-Paths Including Tropospheric Ducting Effect

T. Kawano and **T. Ishihara**
National Defense Academy, Japan

The ground wave propagation over a homogeneous impedance surface has been investigated by many researchers, and it is known that the conventional Norton ground wave propagates in suburban and rural areas [L. Sevgi and L. B. Felsen, Int. Journal of Numer. Model. : Electronic Networks, Devices and Fields, vol. 11, pp. 87-103, Nov., 1998]. It is also known that, in addition to the conventional Norton ground wave, the slow-wave type surface wave propagates in urban areas along which the surface impedance of the earth is highly inductive [P. A. Hill and J. R. Wait, Radio Science, vol. 15, no. 3, pp. 673-643, May-June 1980]. The electromagnetic field over highly inductive impedance surfaces behaves in an unexpected manner because of interference between the Norton ground wave and the slow-wave type surface wave.

The ground wave propagation over an inhomogeneous impedance surface has also been investigated for many years. Typically the ground wave propagation over a land-to-sea mixed-path and an urban-to-suburban mixed-path are considered as some examples of the ground wave propagation over the inhomogeneous impedance surface. When the surface impedance along the propagation path changes abruptly, the ground wave is strongly affected by discontinuity of the surface impedances, as it occurs when the electromagnetic wave traverses a coastline from the land to the sea. In this case the recovery effect is observed in the sea portion over a land-to-sea mixed-path. The ground wave propagation will continue to be one of the most important means for wireless communication.

In this paper, through theoretical and experimental studies, we shall examine the ground wave propagation over homogeneous and inhomogeneous impedance surfaces. The limited number of the experimental confirmation for the mixed-path theory has been reported so far. Wait compared the mixed-path theory with the experimental data taken from Millington and shown the "recovery effect" occurring on the portion of the sea path [J. R. Wait, Proceedings of the IEEE, vol. 62, No. 8, pp.1061-1071, August, 1974]. Here, we will show both experimentally and theoretically the clear recovery effect occurring along the sea portion of the propagation path over a land-to-sea mixed-path. We will also show that unexpected propagation and attenuation phenomena of the electromagnetic field are observed in an urban area which is considered to be the area with a highly inductive impedance surface.

Study on the Propagation Environment Evaluation for the Land Mobile Satellite link Using GPS

W. Abidin, K. Fujisaki, and **M. Tateiba**

Kyushu University, Japan

Current mathematical models used to represent mobile satellite (MS) link especially the land mobile satellite have been developed based on propagation parameters obtained from measurements in countries such as in Europe, Northern America and Australia. For the proper planning of the Earth-space MS systems it is necessary to have appropriate propagation data to fit into these models. The availability of propagation data from different climatic zones especially in the less developed countries such as in the southern Asian region will enable mathematical models with sufficient accuracy to be developed. In the mobile satellite system, two main sources of signal degradation are shadowing effect and multipath fading. The shadowing is caused by the presence of obstacles that impedes the line-ofsight (LOS) signal such as building and trees. Multipath effect is due to the arrival of the reflected LOS signals of different amplitude and phase which can cause signal fluctuations. These reflections are due to the surrounding environment such as buildings, trees and electric poles. The fading statistical characterization requires data from large quantity of measurements to fit the parameters of the mathematical models used to represent the land mobile satellite link.

The common methods of studying the MS link by means of using the available satellite systems or airborne platforms such as helicopter or airplane are very costly and time consuming. This report investigates a cheaper, simpler but efficient measurement technique using the Global Positioning System (GPS) receiver to study the mobile satellite link. The commercially available GPS receivers are able to provide the related signal intensity data which have a big potential for the study of the MS link. This measurement technique allows a lot of data to be recorded simultaneously from different satellite at any instant of time for different number of propagation environments (urban, suburban, rural) with different elevations. The low cost, commercially available GPS receivers enables propagation data to be acquired even in the less developed countries.

In this report, the measurement method used to extract important statistical parameters for different propagation environments and elevation angles is explained and discussed. Furthermore, results obtained from the measured data are presented and comparison are made with those from other empirical models given in the Rec. ITU-R P.681-6 to show the feasibility of this technique in the study of MS link. The outcome of this report will enable MS link data to be acquired from any region of the world for any predefined environment of interest.

The Electromagnetic Fields of a Vertical Electric Dipole in the Presence of a Large Stratified Sphere

T. Fei, L. W. Li, and **T. S. Yeo**
National University of Singapore, Singapore
Q. Wu
Harbin Institute of Technology, China

The electromagnetic fields of a vertical dipole radiating in the presence of a stratified sphere is represented by infinite summation in spherical systems. It is known that the series usually has convergence problem when both the source and the observation point are on or close to the surface. For an electrically large sphere, the field is more difficult to calculate because the number of the series terms is about 10ka (a is the radius of the sphere, k is the wave number).

In this paper, a convergence acceleration method is used to compute the fields generated by a vertical electric dipole over a stratified large sphere. As a practical and interesting application, the simulation results are given for the fields near the surface of the earth. The convergence property is analyzed. The results are also compared with those by asymptotic methods based on Watson transformation.

Relationship Between Raindrop Size Distribution and Cross Polarization Discrimination of the Ka-Band Satellite Communications Link

H. Nishio and **Y. Maekawa**
Osaka Electro-Communication University, Japan

Recently, demand for higher capacity communications is increasing, as the satellite communications technology develops. To make the communication capacity higher, demand for the frequency band of more than 10GHz is still increasing. The dual polarization communications links are now widely adopted in C-band and Ku-band commercial satellite links from the viewpoint of frequency reuse. However, the deteriorations of the link quality due to rain attenuation and cross polarization discrimination (XPD) degradation on the earth-space propagation paths are caused by the precipitation particles in rain, such as rain drops and ice crystals.

In this study, the rain attenuation and XPD degradation on the earth-space propagation path with a higher frequency is measured at the earth station in our university, receiving the Ka-band beacon signal wave from Japanfs domestic communication satellite N-Star (19.45GHz, right hand circular polarization). At the same time, raindrop size distribution (DSD) is measured by an electric detector of raindrop diameters using an optical line image sensor. The relationship between the XPD characteristics including its cross-polar phase and the DSD is examined using these observational data, both of which have been accumulated for more than ten years since 1995. In addition, the frequency ratio of Ka-band to Ku-band radio waves has been precisely measured on the same earth-space path since 2004, receiving Ku-band radio wave from the N-Star by an IF checker for satellite broadcasting signals.

As a result, both cross-polar phase and frequency ratio observed at each rainfall event, on an average, agree well with their theoretical values based on the DSD that was detected at the same event. Thus, these two radio wave characteristics that are very important on the earth-space propagation-path conditions are closely related to rainfall types classified by three representative DSDs, such as Joss-drizzle, Marshall-Palmer (standard type), and Joss-thunderstorm. Also, the Joss-drizzle type that contains comparatively smaller DSD tends to be found in the stationary fronts of Baiu season, while the Joss-thunderstorm type with relatively larger DSD tends to be found in evening showers of summer season and the cold fronts of spring or autumn season. These effects on the cross-polar phase and frequency ratio should be taken into account to design more efficient satellite communications links using dual polarization systems or up-link power controls.

Rain Attenuation Characteristics in a 1-Hour-Rainfall Event

F. Minematsu, Y. Suzuki, K. Imai, and **K. Shogen**
Wireless Systems,NHK Science and Technical Research Laboratories, Japan

We have been conducting studies on a satellite broadcast system in the 21-GHz band. Effective rain attenuation compensation techniques should be needed for stable satellite broadcastings in the band. As one of the compensation techniques, a variable e.i.r.p. satellite system is proposed [1]. This satellite system can obtain high transmitting powers for only rainy areas to overcome the rain attenuation.

To determine the required transmitting powers for rainy areas, it is needed to estimate the rain attenuation in each rainy area for each period of rain. For this purpose, conventional rain attenuation estimation methods for yearly time percentages cannot be applied to the estimation.

Authors studied rain attenuation distributions and 1-minute-rain rate distributions in 1-hour rainfall events from 5 mm to 10 mm. It is found that each distribution can be approximated by a log-normal distribution as shown in Fig.1. Authors also studied the slant path adjustment factor needed to estimate the rain attenuation from 1-minute-rain rate at the same time percentage for each 1-hour-rainfall event. To calculate a rain height to obtain the adjustment factor for each 1-hour-rainfall, average ground temperature for each 1-hour rainfall event was used. Each estimated rain height of Tokyo for the 1-hour-rainfall of 5 mm to 10 mm is shown in Table 1. Relationship between the slant path adjustment factor and time percentage is shown in Fig.2. It is shown that each distribution of the factor differs by the 1-hour-rainfall and it is also found that difference among the factors becomes smaller at smaller time percentages.

REFERENCES

1. Y.Kawaguchi, H.Nakagawa, S.Tanaka and T.Yamada,hApplication of Phased-Array Antenna Technology to the 21-GHz Broadcasting Satellite for Rain-Attenuation Compensation,h Proc.ICC2002,pp2962-2966,2002

Table 1

1-Hour Rainfall	H0 [km] (Tokyo)
R=5mm	3.77
R=6mm	3.56
R=7mm	3.74
R=8mm	4.10
R=9mm	3.67
R=10mm	3.89
Average	3.79
ITU-R P.839-3	4.16

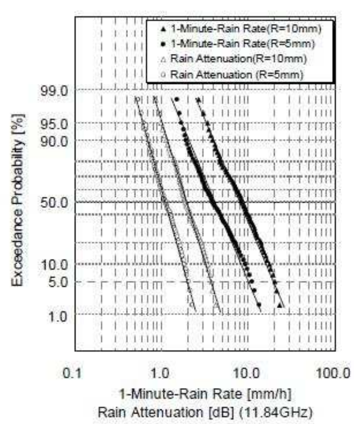

Figure 1

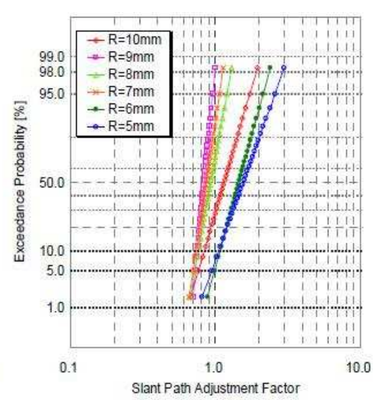

Figure 2

Table 1: Rain height H_0 for each 1-hour-rainfall and a predicted H_0 for Tokyo by ITU-R P.839-3
Figure 1: Rain attenuation of 11.84 GHz and 1-minute-rain rate distribution in a 1-hour-rainfall event
Figure 2: Slant path adjustment factor distribution for a 1-hour-rainfall event

Derivation of a Conditional Distribution of Fade-Slope by the Analysis of Absolute Slope

F. F. Fondjo, K. Fujisaki, and **M. Tateiba**
Kyushu University, Japan
T. Matsuoka
Kyushu Sangyo University,Japan

With the congestion of lower frequency bands and the permanent demand by commercial satellite traffic for high data rate transfer capability, satellite designers tend to move to Ka (30/20 GHz) and above frequency bands which provide a prompt response to their need. Unfortunately, these frequencies are subject to severe climatic eRects, especially rainfall, which generally constrain available bandwidth, thereby making the satellite link inefficient. This happens because link models used for estimation and control of satellite systems during the fading period, combined or not, refer to long-term and yearly averaged statistics. Therefore, real-time estimation and statistics of fades through the fade slope could be an alternative to efficiently understand the time to time behavior of satellite channels.

Many programs have been achieved by the European Space Agency and the NASA in order to efficiently characterize the satellite link for reliable services[1]. The data and results from these experiments are now used for link fade dynamics modeling and validation. Recently, these results have been adopted by the ITU-R community under the reference ITU-R P.1623[2]. However, most of the measurements stored in databases during these campaigns had been made in temperate zones of the Northern Hemisphere[3][4] where rainfall outages seem to be minimal and reveal less fade dynamics than tropical and subtropical areas. Hence, the ITU-R results do not agree mostly with data from experiments carried out in latter areas. It therefore seems important to make worldwide measurements and build more reliable models that may agree with experiment from most rain regions.

Since the real-time estimation of fades turns out to be difficult due to the randomness of various physical phenomena aRecting the satellite link, it is essential to use an important database of receive signal level in order to guarantee that the derived fade slope model should be close to the reality of the link. Due to the lack of enough data and in order to reduce the error between the model and the data, we exploited the symmetric of the fade slope that has been observed and confirmed by other researchers. In the paper, instead of deriving the fade slope distribution from the complete data set, we used the absolute value of the slope to increase the data set and capture all variations of the distribution. Then, based on the obtained absolute fade-slope, we derived the conditional fade slope distribution.

REFERENCES

1. Julie F., Louis J. I. et al., "Fade Slope Analysis for Alaska, Florida, and New Mexico ACTS Propagation Data at 20 and 27.5 GHz," *Proc. of The IEEE*, Vol.85, No.6,pp926-035, June 1997.
2. Rec. ITU-R P.1632, Prediction method of fade dynamics on Earth-space paths, 2003.
3. Max M. J. L. van de Kamp, "Statistical Analysis of Rain Slope," *IEEE Trans. on Ant. and Prop.*, Vol. 51, No.8 August 2003.
4. Max M. J. L. van de Kamp, "Climatic Radiowave Propagation Models for satellite Communication systems," Ph.D dissertaion, Eindhoven Unv. Tech., 1999.

The Two-Sample Model: Short-Term Prediction of Rain Attenuation

M. V. D. Kamp
University of Bath, United Kingdom

Rain attenuation is one of the most fundamental limitations to the performance of satellite communication links in the microwave region, causing large variations in the received signal power, with little predictability and many sudden changes. In the Ka- and V-bands, the attenuation caused by rain is too severe to be accounted for by a fixed margin in the link budget. This is why Fade Mitigation Techniques (eFMTsf) are developed, which compensate for rain attenuation by adaptively improving the quality of the link only when the signals are degraded.

For the design of FMT systems, knowledge of not only the depth of fades to be expected is essential, but also of the rapidity at which these can change. In order to provide the necessary information for FMTs, a study of the dynamics of rain attenuation has led to the development of the eTwo-Sample Modelf.

The Two-Sample Model predicts the probability distribution of rain attenuation a short time after a measured value, dependent on the values of two previous samples of rain attenuation. This model can be used in the design of FMT systems, to determine the required tracking speed, and can be implemented in the FMTs themselves, to predict the probability of fades in the very near future. Furthermore, it can be used for data simulation models of rain attenuation, useful for channel modelling, to test FMTs.

Because the Two-Sample Model uses two previous samples, when used for short-term prediction of rain attenuation it predicts the attenuation distribution more accurately than similar models which use only one previous sample value. When used in simulation of timeseries data, the result of the Two-Sample Model represents better the dynamic behaviour of a rain attenuation event.

The Two-Sample Model has three parameters, which characterise the dynamic properties of the rain attenuation event, and depend on wind speed and the type of rain. The parameters valid for a particular link can be calculated from time series of attenuation measured on the same link, which allows their evaluation in different environments and climates, and during different wind and rain conditions. However, for many climatic configurations, propagation measurements are not available at all or not in sufficiently large quantities to represent the long-term characteristics of the link.

Because of this, theoretical expressions have been derived to calculate the Two-Sample- Model parameters from rain rate measurements. The expressions depend on wind speed, wind direction, vertical air velocity and rain height, and on the elevation and azimuth angles and the frequency of the link. The theoretical expressions have been compared to measurements of attenuation on a satellite link in the UK, and give good results on the long term. The verification of the dependence on meteorological parameters is limited by the resolution of the meteorological data used.

With these expressions, the Two-Sample-Model parameters for different configurations can be derived using only rain rate measurements and other meteorological data. This will provide a great opportunity for the assessment of the model parameters on many sites on earth where expensive satellite link measurements have not been performed, which will facilitate the design of FMTs for these sites. Furthermore, the results enable a wide study of the climatic dependence of the dynamic properties of rain attenuation, which can lead to the development of a global dynamic rain attenuation model.

Rain Attenuation Characteristics of Up and Down Link Radio Waves of Ku-Band Satellite Communications Observed in Japan and Indonesia

Y. Maekawa, S. Tsujuno, and **Y. Shibagaki**
Osaka Electro-Communication University, Japan
T. Sato, M. Yamamoto, H. Hashiguchi, and **S. Fukao**
Kyoto University, Japan

Rain attenuation of radio wave is significant in satellite communications using frequencies of higher than 10 GHz, and may become very severe even for Ku-band (14/12 GHz) radio waves in heavy rain regions like the tropics. This study presents rain attenuation characteristics of up- and down-link radio waves of Ku-band satellite communications obtained in both Japan and Indonesia for the past three years of 2003-2005. This satellite communications link connects Research Institute for Sustainable Humanosphere of Kyoto University (RISH) in Japan to Equatorial Atmosphere Radar Observatory (EAR; 0.3^{o}S, 100.3^o E) in Indonesia, using Japanfs domestic communication satellite Superbird C (144^o E in orbit). The up-link attenuation at each station which is usually difficult to detect at its own rainy station is successfully estimated from the down-link signal level measured at its opposite station. This uses the feature that SCPC (Single Channel Per Carrier) signals transmitted in the experiment are linearly amplified without saturation of the satellite transponders.

At EAR in Indonesia, a comparatively larger attenuation ratio between up and down links is, on an average, presented for the attenuation range of higher than 10 dB. This means the effects of rather smaller raindrop size distribution (DSD) than observed at RISH in Japan. The larger attenuation ratios are primarily found when the attenuation shows only one peak value in each rainfall event. Simultaneous X band radar observations also indicate that these larger ratios are caused by simple convective precipitating clouds with one single cell which may be typical to the equatorial region.

In this experiment, 1-min rainfall rates are measured by rain gauges located at each station. Using 0.01 % values of their cumulative time percentages, the yearly and worst month time percentages of the observed rain attenuation are in good agreement with the ITU-R (International Telecommunication Union . Radiocommunication Sector) predictions for both locations. At EAR in Indonesia, however, the time percentages of both up- and down-link attenuation become much smaller than the ITU-R predictions in the range of larger than 10 dB, indicating remarkable reduction of equivalent path length down to 2 km. The X-band radar observations reveal that this short path length is caused by a fairly localized structure of the simple convective precipitating clouds with one single cell frequently observed at EAR in Indonesia. Also, their intense echo cores of typical rain cells are limited to about 2 km along the propagation path with elevation angle of about 40which is comparatively lower for the tropical satellite communications link.

Diurnal and Seasonal Variations of Cloud and Water Vapor in the Troposphere

Q. W. Pan [1], **J. E. Allnutt** [2], and **C. Tsui** [1]

[1]Manukau Institute of Technology, New Zealand
[2]George Mason University, U.S.A.

Evidence of diurnal and annual periodicity in absorption levels through the atmosphere has been observed by meteorologists [1]. Long-term (four years) satellite beacon (12.75 GHz) measurement in Papua New Guinea proves that the cloud and water vapor contents vary due to the incident solar energy (i.e. thermal atmospheric tides). The level of the received clear-sky (absence of rain fade) beacon signal was the highest at 6:00am (coolest time of a day) and the lowest at 2:00pm (hottest time of a day) (Fig. 1). The co-located radiometer also showed similar pattern of the clear-sky noise temperature . 42 K at 6:00am and 46 K at 2:00pm. During the cooler season (April to September), the average received beacon level is about 0.5 dB higher than that in the hotter months (October to March). The result of analyzing over two years record shows that the major spectral component corresponds to a solar day (diurnal variation) and the other dominant component is a solar year (seasonal variation). These atmospheric tides have signification implications on low fade margin (e.g. 5 dB uplink and 3 dB downlink) VSAT system design. A change of 3 dB on just clear sky condition would eliminate the 3 dB downlink margin completely. It is believed that the results from this analysis (remote sensing using a satellite beacon) are the first to indicate the apparent annual and diurnal periodicity of atmospheric tidal effects due to solar heat on the mean clear-sky level of a satellite-to-earth transmission path through the atmosphere.

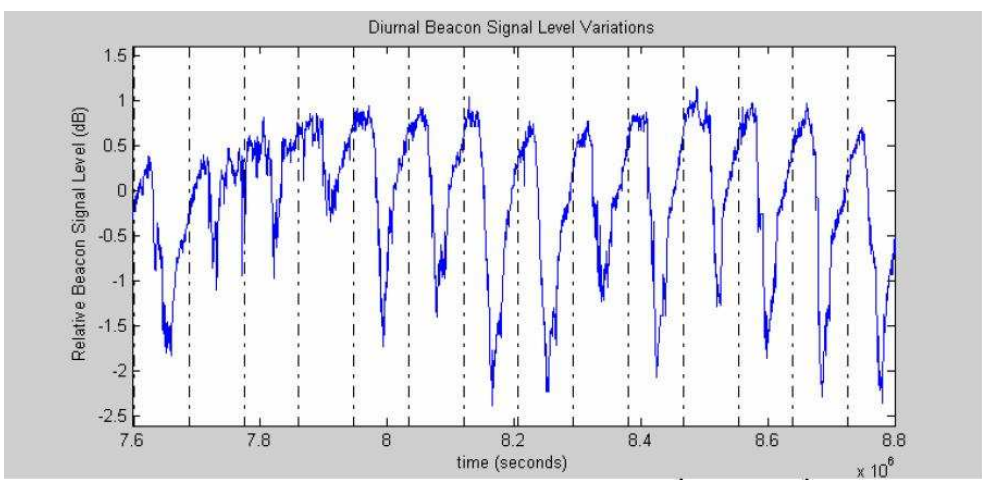

Figure 1: Diurnal beacon signal variations from April 30th to May 13th, 1994

REFERENCES

1. Pèrez-Muňuzuri, V: eForecasting of Chaotic Cloud Absorption Time series for Meteorological and Plume Dispersion Modelingf, *Journal of Applied Meteorology*, 1998, Vol. 37, pp. 1430-1443

Characterization of Rainfall Rate, Ku-Band Rain Attenuation and Tropospheric Scintillation at Indonesian Tropical Cities

J. Suryana and **U. Sastrokusumo**
Institute of Technology Bandung (ITB), Indonesia
K. Tanaka and **K. Igarashi**
National Institute of Information and Communications Technology (NICT), Japan
M. Iida
Association of Radio Industries and Businesses (ARIB), Japan

In this paper, we present our contribution of Rainfall rate and Ku-band rain attenuation measurements at Bandung. This measured data is an important complement to several of previous recorded data from other tropical cities in Indonesia for characterizing the Ku-band Satellite Propagation in Tropical area.

The two years of our experiment results indicate that the measured $R_{0.01}$ rainfall rate at Bandung is 120 mm/h and the measured $A_{0.01}$ rain attenuation is 17 dB. Therefore, the P region of ITU-R model is over estimated for Bandung, and we suggest that Q-region of ITU-R model is more suitable for Bandung. Another previous measurements which had performed in Indonesia confirmed with our conclusions that some cities in Indonesia have not only P-region of ITU-R model (such as Padang, Bengkulu an Makassar), but also N (Jayapura) and Q-region (Surabaya).

Based on 10 samples rainfall rate in Indonesian Archipelago, we have developed New Prediction Model of $R_{0.01}$ value for Indonesian cities. Relating to the rain attenuation statistics, we have found out, that the DAH Model is valid for Indonesia. We also have found out that if Bandung is modelled by Q-region of ITU-R, we should include the wetting antenna effects as the correction factor to the the ITU-R model for confirming with the measured $A_{0.01}$ rain attenuation.

Concerning to the tropospheric scintillation , we have noted that in a tropical region such as Indonesia, the magnitude of the Ku-band scintillation is seasonal dependence, reaching variance 0.4 dB (maximum) in rainy season and 0.2 dB (minimum) in dry season.

Session 2P3
Medical Applications

Complex Noninvasive Optical Scanning of Superficial Human Tissues in Examination of Patients with Vibration Disease

V. V. Tchernyi

Russian Academy of Science, Russia

D. A. Rogatkin, R. V. Gorenkov, V. N. Karpov, P. N. Lubchenko, and **V. I. Shumskiy**

Moscow Regional Research & Clinical Institute "MONIKI", Russia

Numerous industry workers all over the world have dealings with a strong mechanical vibration as with a daily technology process. Very often such long-time professional vibration causes the so-called professional gVibration diseaseh, in English literature gWhite fingers syndromeh, caused by a local vibration of hands. Among different clinical features of the vibration disease a leader's part of them consists of different cardiovascular and trophic disorders of tissues. So, the medical objects of the present study were the peripheral blood microcirculation, peripheral blood oxygenation and tissues hypoxia state in a superficial finger skin in patients' hands with vibration disease. For this purpose we have used a new noninvasive complex spectrophotometry diagnostic technique consisting of Laser-Doppler Flowmetry (**LDF**), Laser Fluorescent Diagnostics (**LFD**) and multi-wave Tissues Reflectance Oximetry (**TRO**). The noninvasive optical (laser) diagnostic methods are very promising in modern medicine and surpass many former ones for some indices and for significance of medical-and-biological information concerning tissue condition. They allow a doctor, in instance, to apply a real-time monitoring and different functional tests (tests with a load) to diagnose "in vivo" different vascular disorders, functional activity of endogenous fluorophores in tissues, blood microcirculation specialties, oxygen utilization in tissues, etc., that is very important for all patients suffering from the Vibration disease. The results show good possibilities of all mentioned diagnostic methods in estimation of different vascular disorders in patientsf hands. A good correlation between persistent microcirculation disorders and trophic disturbances revealed in tissues of distal ends of upper extremities of the patients with vibration disease was estimated. Additionally, in present study with the use of real and long-time TRO and LDF methods a good correlation between LDF and TRO data, including correlation in detected rhythms of blood microcirculation, was estimated as well.

Keywords: medicine, vibration disease, diagnostics, laser, fluorescence, oxygenation, blood flow, finger skin.

Clinical Trials of the Interstitial Microwave Hyperthermia by Coaxial-Slot Antennas

K. Saito [1], **S. Kikuchi** [1], **M. Takahashi** [1]
K. Ito [1], **Y. Aoyagi** [2], and **H. Horita** [2]

[1]Chiba University, Japan
[2]Tokyo Dental College, Japan

In recent years, various types of medical applications of microwave have been extensively investigated and developed. In particular, the minimally invasive microwave thermal therapies using thin applicators are of great interest. Until now, the authors have been studying the coaxial-slot antenna for interstitial microwave hyperthermia. This antenna is composed of a thin semirigid coaxial cable of 140 mm in length. Some ring slots are cut on the outer conductor of the cable and the tip of the cable is short-circuited. The operating frequency is 2.45 GHz, which is one of the ISM (Industry, Scientific, and Medical) frequencies. From our previous investigations, it is clear that the coaxial-slot antenna with two slots, whose distances of the upper slot and lower slot are 20 mm and 10 mm from the tip of the cable, respectively, keeps the heating region only around the tip of the antenna. We employed this antenna and experienced some actual treatments. Table 1 summarizes the results of the treatments which are performed by the coaxial-slot antennas. As shown in Table 1, we could observe the efficiency of the treatments whichever the heated site was. Moreover, any critical side effects including injury of skin etc. did not occur. Therefore, it is considered that we could effectively heat the tumor without any problems by use of the coaxial-slot antennas.

Table 1 Results of the treatments.

	Case 1	Case 2	Case 3	Case 4
Age	59	89	62	77
Sex	Female	Female	Male	Female
Primary	Gingiva	Soft palate	Esophagus	Lip
Pathology	Squamous cell carcinoma	Adenocarcinoma	Squamous cell carcinoma	Squamous cell carcinoma
Heated site	Supraclavicular node recurrence	Primary lesion	Supraclavicular node recurrence	Submandibuler node recurrence
Number of antennas	1	1	2 or 4	1
Follow up time	7.3 months	1 year 7 months	1 year 7 months	4 months
Result	- Dead of other metastasis - No evidence of tumor growth in heated site	- Alive without disease	- Alive without disease	- Alive - No evidence of tumor growth

Heating Characteristics of a Coaxial-Slot Antenna with Endoscope for Intracavitary Microwave Hyperthermia Aiming at the Bile Duct Carcinoma by Use of a Realistic Human Calculation Model

A. Hiroe, K. Saito, M. Takahashi, and **K. Ito**

Chiba University, Japan

In recent years, various types of medical applications of microwaves have widely been investigated and reported. Until now, the authors have been studying antennas for the microwave hyperthermia. Hyperthermia is one of the modalities for cancer treatment, utilizing the difference of thermal sensitivity between tumor and normal tissue. In this treatment, the tumor is heated up to the therapeutic temperature between 42 and 45°C without overheating the surrounding normal tissue.

There are a few methods for heating the cancer cells inside the body. Figure 1 shows the proposed scheme of a treatment aiming at the bile duct carcinoma using a coaxial-slot antenna with an endoscope for intracavitary hyperthermia. Figure 2 shows the structure of the proposed coaxial-slot antenna for this treatment. We investigated the heating characteristics of this antenna around the bile duct by conducting numerical calculations using a realistic human model. As a result of calculations, a region heated over 42°C is observed around the tip of the antenna. Therefore, the heating ability of the proposed antenna for intracavitary hyperthermia is confirmed.

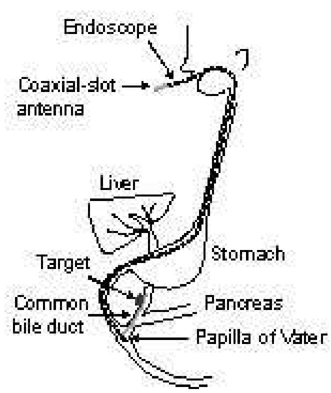

Figure 1: Scheme of the treatment.

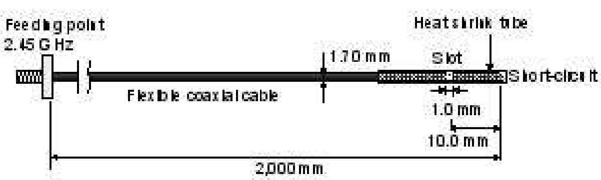

Figure 2: Structure of a coaxial-slot antenna with endoscope for intracavitary hyperthermia.

Preliminary Assessment of Electromagnetic Absorption in the Breast for Cylindrical Microwave Breast Cancer Detection Systems

J. E. Johnson and **T. Takenaka**
Nagasaki University, Japan

Microwave based systems for the detection of breast cancer have been under development for several years and are progressing towards a point where they can be practically utilized in a clinical environment. As these systems reach the clinical phase, it will be important to accurately assess potential safety hazards to patients. In particular, precautions should be taken to ensure that the amount of microwave radiation absorbed in patients during typical imaging sessions falls within prescribed guidelines for microwave exposure, such as those defined by the IEEE [1] and the ICNIRP [2]. Demonstrating that specific absorption rates (SARs) are within recommended safety limits is an important aspect in development of these systems, as they are being explored as a safer imaging modality than X-ray mammography, which utilizes ionizing radiation. In this paper, a preliminary assessment of expected SAR levels in microwave breast imaging systems of a cylindrical configuration is conducted. Although the study utilizes a simplified breast model, it provides significant insight into SAR levels that can be expected in a typical microwave breast cancer detection system.

For preliminary assessment of SAR levels in the breast, a simple breast model was formed using a 10cm diameter, hemispherically shaped section of normal breast tissue and a rectangular chest wall "block" covered with a 2mm thick skin layer. The breast model was illuminated with microwave signals radiated by both a simple half-wavelength dipole antenna and a broad-band, antipodal Vivaldi antenna. A commercial electromagnetic simulator (CST Microwave Studio) was utilized to calculate the electromagnetic fields in the breast model via FDTD simulation with grid sizes of 1.5mm or less. Specific absorption rate data were computed for various frequencies (1-6 GHz), antenna positions, and immersion liquids which would likely be utilized a typical cylindrical breast imaging system.

The results of the study provide insight into expected absorption levels in the breast during microwave imaging sessions. Most importantly, radiated power levels required to exceed exposure limits are shown to be well below those which might be utilized in a typical frequency-domain imaging system. Results also show that absorption occurs primarily in the skin, which has large conductivity compared to normal breast tissue. Tradeoffs when utilizing an omni-directional antenna (dipole) compared with a more directional antenna (Vivaldi) are also demonstrated. Overall, this study gives a preliminary indication that microwave-based imaging techniques for detection of breast cancer will remain well within standard safety guidelines.

REFERENCES

1. "IEEE standard for safety with respect to human exposure to radiofrequency electromagnetic fields, 3khz to 300ghz," *IEEE Standard* C95.1-1999, 1999.
2. "Guidelines for limiting exposure to time-varying electric, magnetic, and electromagnetic fields (up to 300 ghz)," *Health Phys.*, vol. 74, no. 4, pp. 494–522, 1998.

Experimental Test System to Assess the EMI from RFID Reader/Writer on Implantable Cardiac Pacemaker

S. Futatsumori, T. Kono, T. Hikage, and **T. Nojima**
Hokkaido University

B. Koike
Japan Automatic Identification Systems Association

RFID (Radio Frequency Identification) systems have been attracting wide interest as essential devices of ubiquitous network. In addition, newly UHF band RFID systems for long-range communication have been available in Japan since Jan. 2006. RFID are expected to be used in more various regions. Electromagnetic interference (EMI) by RFID reader/writer on medical devices is investigated and preventions of the EMI are currently discussed [1]. Furthermore, more detailed investigations such as effects of human body near the instruments and errors of experiment systems are required.

In order to estimate the EMI from RFID reader/writer precisely, experimental test systems which consist of antennas, a human torso phantom [2], implantable cardiac pacemakers and implantable cardioverter-defibrillators (ICD) are discussed in this paper. RFID systems are operating at different frequency bands employing various antenna types. Furthermore, these antennas are usually located at different positions. In order to measure the EMI from various RFID antennas with accuracy and repeatability, we develop a new test system. As shown in Fig.1, the system consists of a human torso phantom, a function generator, a chart recorder and a measurement platform. The two-axis sliding measurement platform that can measure RFID antennas moving parallel to the torso phantom (y-axis direction), while maintaining distance between the phantom and antennas (x-axis direction) is shown in Fig.2. All parts of this platform are made of dry wood. This system has advantages of high efficiency and reliable estimation.

We have carried out measurement of the EMI with this test system for 11 types of implantable pacemakers and ICDs so far. The obtained data will be used in assessment of the EMI using FDTD analysis in the future.

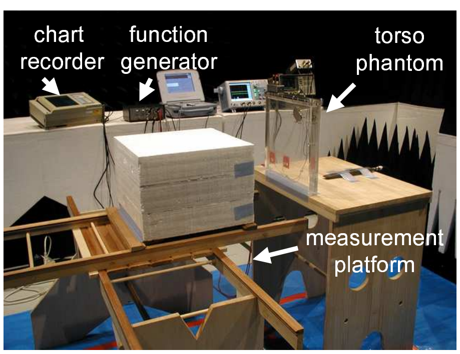

Fig. 1: Overall view of the experimental test system

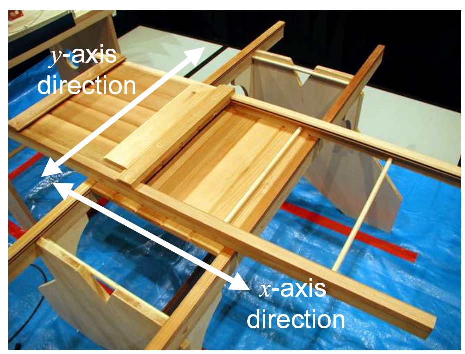

Fig. 2: The two-axis sliding measurement platform

REFERENCES

1. Ministry of Internal Affairs and Communications (MIC) of Japan, 'Investigation and research report of electromagnetic interference on medical devices (in Japanese)', MIC, Mar. 2005.
2. T. Toyoshima, et al., 'Electromagnetic interference of implantable cardiac pacemakers by portable telephones (in Japanese)', Japanese journal of cardiac pacing and electrophysiology, Vol. 12, No. 5, pp. 488-497, 1996.

Microwave Applicator for Local Thermotherapy

J. Vrba, T. Drizdal, R. Zajicek, L. Oppl, and **J. Vrba (jr.)**
Czech Technical University, Czech Republic
J. Kubes
Institute of Radiation Oncology, Czech Republic
J. Kvech
Radiation Oncology Dept., Czech Republic

We investigate and evaluate various types of microwave applicators suitable for local or deep local hyperthermia treatment, like e.g. waveguide applicators, lucite (horn) applicators, microstrip applicators and T-monopole applicators. These applicators are designed to work at 434 or at 70 MHz. In the conference contribution we would like to discuss its effective heating depth, based on the comparison of the theoretical and experimental results. Basic mechanisms and parameters influencing (limiting) heating effective depth are to be described and explained.

The basic type of applicator for local treatment is a waveguide applicator. The construction of such applicator is very simple and numerically modeled (i.e. by software SEMCAD calculated) and measured gSpecific Absorption Rateh (gSARh) distribution in front of the applicator aperture is well homogeneous and also the effective heating depth is approaching the theoretical limit of a plane wave. Modified results in SAR and temperature 3D distribution we can obtain e.g. by aid of Lucite cone applicator or by Tmonopole applicators.

Intracavitary Applicator for Thermotherapy and Imaging

J. Vrba [1], **M. Bolmsjö** [2], **R. Hlavac** [1]
J. Vrba (jr.) [1], and **L. Oppl** [2]

[1]Czech Technical University, Czech Republic
[2]University of Lund, Sweden

Paper deals with new results in the field of intracavitary microwave applicators used for Benign Prostatic Hyperplasia (BPH) treatment.

Costs and risks associated with clasical BPH treatment (TURP and open surgery) have promoted the development of minimally invasive methods. Microwave thermotherapy, varying forms of laser treatment, transurethral needle ablation, etc. have all been developed in the 1990s. The underlying principle behind these methods is to coagulate prostatic adenomatous tissue by means of heat. Of all the available minimal invasive treatment modalities, transurethral microwave is one of the most wide spread at present [1]. We have investigated basic types of microwave intracavitary applicators suitable for BPH treatment, i.e. monopole, dipole and a helical coil structures. These applicators are designed to work at 915 MHz. In the conference contribution we would like to discuss itfs effective heating depth, based on the comparison of the theoretical and experimental results. Basic mechanisms and parameters influencing (limiting) heating effective depth are described and explained in ref. [2, 3, 4].

The basic type of intracavitary applicator is a monopole applicator. The construction of this applicator is very simple, but numerically modelled (calculated by software product SEMCAD) and measured .Specific Absorption Rateg (.SARg) distribution along the applicator is more complicated. During measurements of SAR along the applicator we have found, that typically there is not only a one main .SARg maximum (first from the right side), but also a second and/or higher order maximas can be created, being produced by outside back wave propagating along the coaxial cable. To eliminate this second maximum and optimise the focusing of .SARg in predetermined area of biological tissue needs to use the helical coil antenna structure. After coil radius and length optimisation we have obtained very good results of .SARg distribution.

As a novel results of our work we could mention that various microwave applicators for prostate cancer or BPH treatment have been developed and evaluated. Theoretical analysis of effective heating depth of these applicators and its experimental evaluation will be given.

REFERENCES

1. De la Rosette J, DfAncona F, Debruyne F.: .Current status of thermotherapy of the prostateg, J Urol, 1997, 157: 430-438.
2. Vrba, J., Franconi, C., Lapes, M.: "Theoretical Limits for the Penetration Depth of the Intracavitary Applicatorsg. International Journal of Hyperthermia, 1996, Vol. 12., No. 6., pp. 737 . 742
3. Vrba, J., Lapes, M., Oppl, L.: gTechnical aspects of microwave thermotherapyh. Bioelectrochemistry and Bioenergetics, Vol. 48 (1999), pp. 305 . 309
4. Bolmsjo M, Wagrell L, Hallin A, Eliasson T, Erlandsson BE, Mattiasson A.: .The heat is on - but how? A comparison of TUMT devicesg. Br J Urol 1996: 78: 564-572

Acknowledgement: This research is supported by Czech Research Programme: .Transdisciplinary Research in the Area of Biomedical Engineeringg (J04/98: 210000012)and by Grant Agency of the Czech Republic, project: .Microwave Thermotherapy in Cancer Treatmentg (102/02/0128).

Application of the Wavelets to the Study of the Human Sleep Slow Oscillation

S. Barmada, A. Gemignani, A. Landi, and **D. Menicucci**
University of Pisa, Italy

During slow wave sleep, the electroencephalographic pattern is characterized by a succession of K-complexes, sleep spindles, and delta waves [1]. Despite this hypersynchronization of the electrical cortical activity, which is negatively correlated to the cerebral metabolism, the electrophysiological and molecular mechanisms of the brain remain intensely active ([2], [3]). In fact, intracellular recordings in animals have revealed that during K-complexes and delta waves, the membrane potentials of cortical neurons oscillates between state of deep hyperpolarization (down state) and state of wake-like depolarization (up state) [4]. Each down-and-up-state last a fraction of second (about 700 ms). During the down state, the electrical cortical activity is silent, whereas during the up state, an intense neural discharge is present. This cellular behavior was called "slow oscillation" and it represents the fundamental cellular phenomenon underlying neural activity in slow wave sleep (NREM sleep stage 3 and 4, or delta sleep). This cellular phenomenon is detectable also in sleep EEG pattern of humans and recently Massimini et al. [5] described that "sleep slow oscillations are traveling waves that sweep the human cerebral cortex up to once per second". Further, the authors pointed out that each slow oscillation has a definite site of origin, originating more frequently at anterior cortical regions and propagating to posterior cortical areas with a higher reproducibility across nights and across subject.

A primary goal of our research is the detection of instantaneous frequencies typical of the sleep slow oscillation in human EEG data. Slow oscillations have characteristic frequencies less than 1 Hz. Conventional methods, such as the ones based on the Fourier analysis, are based on the assumption of stationarity and linearity of the signal to be analysed. To deal with non-stationary signals, as the EEG waveforms, new techniques such as time-frequency analysis methods have received attention and gained acceptance. Among all available time-frequency analysis methods, the wavelet transform is by far the most popular technique, for its high-quality time and frequency localization properties [6].

Sleep EEG recordings were analysed during the first sleep episode of the night. All signals were band-pass filtered (0.1 - 4 Hz) and digitized at 250 Hz. Coifman and Daubechies Wavelets were considered. The results of the study indicate the effectiveness of the wavelet transform to detect the sleep slow oscillation in the human EEG. Our data are in a good agreement with the criteria applied in [5] for recognizing slow oscillation. Our approach differs from the usual study of the slow oscillation mainly based on the shape of the waveform, providing a method for an automatic detection of this bioelectrical phenomenon.

Due to the limitation of Heisenberg-Gabor inequality, the time and frequency resolution, however, cannot be accurate in both time and frequency domain: it is a compromise, such that a large scale wavelet must be chosen for determining general signal features and a small scale wavelet is a mandatory choice for extracting the signal details. Consequently, time localization is poor for low frequency signals and frequency resolution is poor for high frequency signals. Since the occurrence of slow oscillations during sleep is often relatively frequent and the interval between two slow oscillations is quite small during delta sleep the desired time-frequency methods should have fine resolutions both in time and in frequency domain. Therefore, after a first signal processing phase, based on the wavelet decomposition, different methods could be more easily applied for a sharp detection of the typical frequencies of slow oscillations (e.g. Hilbert-Huang method [7] could be properly considered).

REFERENCES

1. Steriade, M (2000). Neuroscience 101, 243-276.
2. Frank M.G., Issa N.P., Stryker M. P. (2001), 30, 275-287.
3. Tononi G, Cirelli C. (2003). Brain Res Bull, 62, 143-50.
4. Steriade M, Timofeev I. (2003). Neuronal plasticity in thalamocortical networks during sleep and waking oscillations. Neuron, 37, 563-76.
5. Massimini M, Huber R, Ferrarelli F, Hill S, Tononi G. (2004). The sleep slow oscillation as a traveling wave. J Neurosi, 24, 6862-6870.
6. Chui, C. K. (1991). An Introduction to Wavelets, Academic Press, New York.
7. Huang N. E., Shen Z, Long SR, et al. (1998). The empirical mode decomposition and the Hilbert spectrum for nonlinear and non-stationary time series analysis. Proc R. Soc, London A454, 903-995.
8. Tononi G, Cirelli C. (in press). Sleep function and synaptic homeostasis. Sleep Medicine Reviews.

Investigations on the Characteristics of Eddy Current Absorber in Inductive Implant Heating

C. Kawamurra and **Y. Kotsuka**
Tokai University, Japan

The authors have so far proposed and investigated experimentally the eddy current absorber to avoid unexpected eddy currents occurring in the inductive heating object. Theses stray eddy currents cause the problem that real local implant heating can not be achieved completely. This paper investigates theoretically the absorbing characteristics of eddy current absorber and clarifies its optimum material constant based on Finite Element Method (FEM) to eliminate unexpected hotspot regions. To investigate the absorbing characteristics of eddy current, the 3D Finite Element Method based on current vector potential is introduced. The eddy current density distribution and average loss distribution are analyzed. Fig.1 shows a model for analysis and Fig.2 shows normalized eddy current loss with eddy current absorber, which is normalized by the value of the average eddy current loss without absorber at the position 0.5 mm above the bottom side of a cubic phantom in the x-axis direction. From this figure, it is found that eddy current can be well suppressed using eddy current absorber. Further, we can find an optimum conductivity to compose eddy current absorber with the mutual relations between the conductivity of heating body surface and the surface conductivity of eddy current absorber. These characteristics are also investigated in an elliptical cylinder heating body.

Consequently, by introducing these techniques, ideal local heating in inductive thermal therapy can be established utilizing both the present eddy current absorber and a small implant with a high efficiency temperature rise.

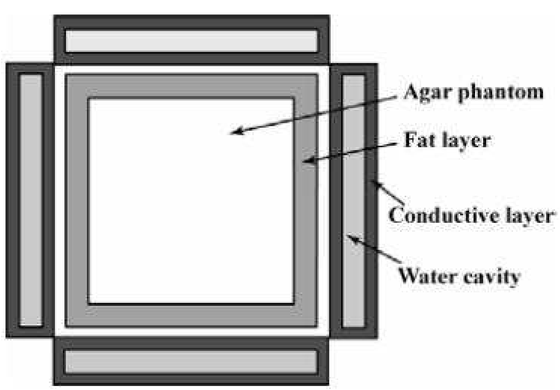

Fig. 1 Model for analysis.

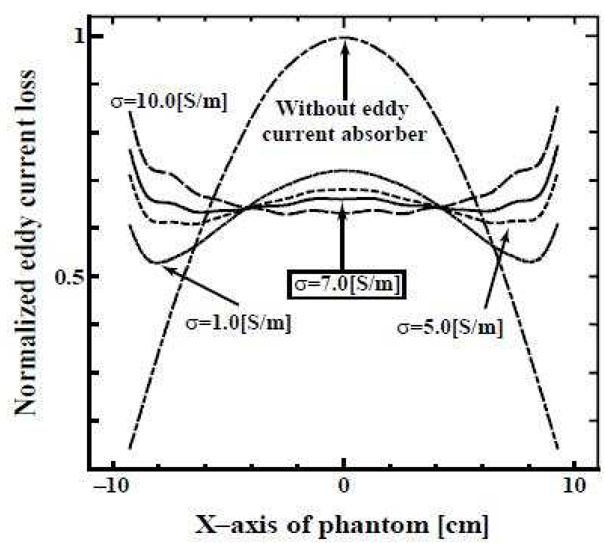

Fig. 2 Distributions of eddy current loss

Bounds for Power Deposition in Phantoms

B. Derat
SAGEM, France

J. C. Bolomey
Paris XI University, France

In many situations of practical relevance, electromagnetic power deposition in biological structures must be controlled, either to obtain compliance with exposure standards (wireless communications) or to reach therapeutic efficiency (hyperthermia treatments). Often in-lab measurements are conducted on simplified phantoms to investigate or check power deposition as well as resulting temperature increase. How such phantoms can constitute a representative test case constitutes a key issue, which impacts the adjustment of the dielectric constant of the materials used to build the phantom. In this paper, the equivalent junction model is used to assess the effect of the dielectric properties and to demonstrate that, for given radiating source and phantom shape, the deposited power can be bounded. In such a model the deposited power is calculated from the power budget between incoming and outgoing waves through a cylinder or a sphere surrounding the entire phantom (total deposited power) or a subdomain of the phantom (Specific Absorption Rate). According to the selected surface, the waves can be expanded in cylindrical or spherical modes. For separable phantoms, such as homogeneous or stratified cylinders or sphere, the scattering matrix, from which outgoing modes can be calculated, is diagonal and each mode can be considered separately. The coupling problem is then greatly simplified and can be reduced to the power transfer between a finite set of generators and complex loads, the characteristics of which depend on the phantom dimensions and dielectric properties. The equivalent junction model is still applicable if the phantom is located in the near-field region, or even in the reactive domain, provided interactions with the source can be assumed negligible. Examples will be provided for cylinders, either homogeneous or stratified.

Session 2P4
Advanced Computational Techniques and the Application for Microwave Devices

Three-Dimensional Numerical Analysis of Light-Beam Scattering from DWDD Disk Model

Y. Irifune, M. Miyake, and **T. Kojima**
Kansai University, Japan

We have developed numerical simulation techniques for the light-beam scattering and the detected signal characteristics from various types of optical disks as the digital versatile disk (DVD) and magneto optical (MO) disk so far. In our previous paper, we have demonstrated that the finite difference time domain (FDTD) method can be a powerful tool for the numerical simulation of light-beam diffraction from conventional MO disk structures [1], [2].

Recently, various technologies of higher density version for MO disk have been proposed. In those technologies, the domain wall displacement detection (DWDD) is one of excellent readout methods, which utilizes the characteristic of magnetic film called wall-displacement phenomenon by temperature gradient. This method has no limit of resolution in principle.

In the present paper, we try to apply the three-dimensional FDTD method to the analysis of the light-beam scattering and the characteristic of detected signal from DWDD disk model [3].

REFERENCES

1. Isao Kobayashi, Toshitaka Kojima, Shin-ichiro Fukai and Yiwei He, gNumerical Analysis of Light-Beam Diffraction from Magneto-Optical Disk Medium by FDTD Method,h *IEICE Trans. Electron*, vol.E84-C, no.9, pp.1189-1195, Sep. 2001D
2. Toshitaka Kojima, Toru Sasai, Isao Kobayashi and Yewei He, g(FD)2TD Analysis of Light-Beam Scattering from MO Disks with Land/Groove Recording Structures,h *IEICE Trans. Electron*, vol.85-C, no.10, pp.1776-1783, Oct.2002D
3. Shinichi Kai, Atsushi Fukumoto, Katsuhisa Aratani, Shunji Yoshimura, Keiichi Tsutsumi, Masayuki Arai, gOver 15-GB Capacity Domain Wall Displacement Detection Magneto Optical Recording Using a Digital Versatile Disc Dimensional Optical Head,h *Jpn. Appl. Phys.*, Vol.39, no.4A, pp.1757-1761, April 2000.

Dual-Pol Dual-Band Antenna Arrays In "Flexible" Liquid Crystal Polymer (LCP) Technology Using RF MEMS

A. N. Traille [1] and **M. M. Tentzeris** [2]
[1]Cobb County Research Facility, U.S.A.
[2]Georgia Electronic Design Center, U.S.A.

Miniaturization, portability, cost and performance have been the driving force for the evolution of packaging and system-on-package (SOP) approach in RF, microwave and millimeter wave applications. Recent research shows SOP to be a more feasible and low cost solution than system-on-chip (SOC) approach. Cost, electrical performance, integration density, and packaging compatibility are variables that are often at odds with each other in RF designs. Few material technologies are able address these considerations simultaneously. LTCC is a technology that has excellent electrical performance, dense multilayer integration, and good barrier properties, but it is relatively expensive compared to standard FR4. Most other substrate and packaging materials do not have low enough water absorption properties in tandem with multilayer construction capabilities to be considered for vertically integrated designs. Liquid crystal polymer (LCP) provides the all-in-one solution for such integration approach in terms of high quality dielectric for high performance multiband passive design, excellent substrate for heterogeneous SOP integration as well as for MEMS structures, enabling the implementation of multiband and reconfigurable modules. Liquid Crystal Polymer (LCP) is proving to be a valid alternative for high frequency designs due to its ability to act as both the substrate and package for multilayer constructions. It is a fairly new, low cost thermoplastic material and its unique performance for an organic material is comparable to ceramic-based substrates that are widely used in RF and microwave applications. Its dielectric constant is 3.19 at 20 GHz and increases very slightly with frequency up to 110GHz, while the loss tangent is very small (ˆ0.002). The low coefficient of thermal expansion (CTE) (8-17*10 -6) leads to better matching to silicon or chip package and provides better reliability. The low moisture absorption (˜0.04%) enables a better stability of performances. LCP offers large area processing capability that leads to tremendous cost reduction compared to commonly used LTCC substrate. Using vertical space allows the passive elements in RF front-ends to be efficiently integrated.

In this paper, we will present the potential of LCP as the substrate as well as the packaging material for wireless applications. In the following sections, the LCP fabrication process, its main characteristics and design examples will be described. A dual polarization, dual frequency 2×1 antenna array on LCP will also be presented. The frequencies of operation are 14 and 35 GHz. The 14 GHz antenna array is placed on the top layer of the LCP substrate, while the 35 GHz antennas are "sandwiched" in between the 14 GHz array and the ground plane on an embedded layer. Both arrays are fed by microstrip lines printed on the same layer as the corresponding array. The control of polarizations can be realized by the use of two small gaps in the feed lines, which introduces a small capacitance in each gap. Each array has been simulated and measured, separately, showing good agrrement. This design exhibits a high efficiency and a low cross-polarization level. Simulations of both arrays have been performed, separately, using the 3D full-wave simulation programs, EmPicasso and Micro-Stripes. The simulated results show a return loss of approximately -26 dB at a center frequency (f_c) of 13.99 GHz for polarizations X (x-directed feed) and -27 dB at f_c = 13.97 GHz for polarization Y (y-directed feed) for the 14 GHz structure. Additionally, the 35 GHz structure exhibits at return loss of approximately -25 dB at fc=35.15 GHz for polarization X and -32 dB at fc=35 GHz for polarization Y. The measured results for the return loss are as follows: the 14 GHz array has a return loss of approximately -23 dB at f_c = 13.72 GHz and -51 dB at f_c = 13.79 GHz for polarizations X and Y, respectively, while the 35 GHz array has a return loss of approximately -44 dB at fc=35 GHz and -30 dB at f_c = 34.81 GHz for polarizations X and Y, respectively. It can be seen that a good agreement is observed between the simulated and measured results for the return loss versus frequency plots for the 2×1sub-array. The -10 dB return loss percent bandwidths for the measured results are approximately as follows: 2.41% and 2.47% for polarizations X and Y, respectively, for the 14 GHz array and 1.57% and 1.72% for polarizations X and Y, respectively, for the 35 GHz array. The simulated results produced an efficiency of better than 85% for all array antenna designs. The switch of polarization is achieved through the use of embedded RF MEMS switches. We will present at the conference extensive results from the system-level design and optimization of these antenna arrays including electromagnetic (FDTD/Microstripes) and mechanical (FEM) effects, as well as modelling the full-wave performance of the utilized RF MEMS devices.

Finally an example of WLAN IEEE 802.11a compliant module on LCP will be also shown to demonstrate the power of this technology. A wireless transceiver system has been implemented, exploiting the capability of LCP to enable for low loss interconnections as well as for integration of embedded passives. It includes up-converting and down-converting stages, image canceling BPFs, PA module and variable gain LNA on the receiver side. The system has been measured and experimental results will be reported to show the great potential of the LCP as a valid alternative for MCM and SOP approaches.

The Modeling Technique of RF MEMS Structures with Transient Behavior

H. Iwamatsu and **M. Kuroda**
Tokyo University of Technology, Japan

Recently, MEMS technology that can operate at RF to millimeter frequencies is progressing rapidly [1]. MEMS are minimized electromechanical devices and systems that are realized using integrated micro fabrication method. The accurate performance of RF MEMS structures requires the computationally effective modeling of their transient and steady-state behavior including the accurate analysis of their time-dependent moving parts.

A novel numerical method for the analysis of the EM field variation in geometries involving moving boundaries is proposed and applied to solve the MEMS devices [2]. The dynamic behavior of the variable capacitor can be modeled by the combined effect of the spring and electrostatic forces. MEMS capacitor is assumed to consist of two parallel plates and the top plate is suspended by a spring with spring constant k and damping coefficient b. When a bias voltage is applied across the plates, the top plate is attracted toward the bottom plate and moves toward the bottom one until an equilibrium between the electric and the mechanical force is reached. From the dynamics of an electro-mechanical system, by using the coupling of the electrical and mechanical forces, the acceleration of the plates is derived.

In this paper, the numerical results that express the relationship between the acceleration , the velocity and the displacement of the plates and the damping coefficient are shown and the transient effect is accurately modeled. And also, the relationship between the bias voltage and the displacement is derived and it can be shown that the bias voltage can control the motion of the plates.

REFERENCES

1. Gabriel M. Rebeiz, gRF MEMS Theory, Design, and Technologyh, John. Wiley & Sons Publication, 2003.
2. Kohei Kawano, Shafrida Shahrani, Takashi Mori, Michiko Kuroda, Manos M. Tentzeris,h Dynamic and Electrical Analysis of MEMS Capacitor with Accelerated Motion Effectsh, Proc. of the 2005 IEEE ACES International Conference, April, 2005

Numerical Technique for the Analysis of 2D MEMS Structure by Using Overset Grid Generation

N. Hanim [1], **B. Piao** [2], **M. Kuroda** [1], and **S. Kuroda** [2]

[1]Tokyo University of Technology, Japan
[2]The University of Electro-Communications, Japan

For the effective modeling of new microwave devices or optical devices such as RF MEMS structures, it is important to derive the accurate analysis of the electromagnetic field evolution around the moving body. But it is difficult to solve these moving boundary problems numerically. In the preceding papers, our group has presented the body fitted grid generation method with moving boundaries and the applications for the analysis of the MEMS capacitor with moving parts [1].

In this paper, a new numerical technique called overset grid generation with moving boundaries [2],[3] is applied for the analysis of the electromagnetic filed. Here, this technique is implemented by the calculations of the moving objects that had been done by overlapping sub-lattice which moves on a stagnant main lattice and calculating each lattice alternately. Through interpolating the solution by other overlapped block, the solution on the moving point can be obtained. The interpolation equation will be an interface between the subs mesh and the main mesh.

MEMS technology is developing rapidly in RF field and the accurate design of RF MEMS structures requires the computationally effective modeling of their transient and steady-state behavior. This technique is applied for the analysis of 2D MEMS structures with non-uniform motion. Some complex motions are shown to simulate the MEMS devices, such as switches or capacitors. Through implementation of the overset grid generation, the relation between the motion and the displacement of the capacitors are shown. It is shown that this novel numerical technique can demonstrate the unique advantage to model 2D MEMS structures.

REFERENCES

1. M. Kuroda, N. Miura, M. M. Tentzeris, gA Novel Numerical Approach for the Analysis of 2D MEMS Based Variable Capacitors Including the Effect of Arbitrary Motions h *ACES Journal*, vol.19, no. 1b, pp. 133-138, (2004-3)
2. J. H. Ferziger, M. Peric, Computational Methods for Fluid Dynamics, Springer Verlag, (2001-12).
3. K. Imai, B. Piao, S. Kuroda, gNumerical Analysis of Flow around a Circular Cylinder Using Overset Gridh, 16th Computational Fluid Dynamics Symposium, pp. 26 (A26-4), Tokyo (2001-12).

Efficient Time Domain Calculation of Coupling Coefficient Between Two Resonators

I. Awai, T. Ishida, and **Y. Zhang**
Ryukoku University, Japan

Coupling coefficient is usually calculated from the split frequencies of two coupled resonators. One of the present authors clarified that the coupling coefficient is more properly defined in time domain [1] as,

$$k = \frac{T_0}{T_M} \tag{1}$$

where T_0 is the resonant period and T_m is the period of energy exchange between two resonators. The field amplitude in the coupled resonators #1 and 2 is schematically illustrated in Fig.1 as functions of time.

The finite difference time domain (FDTD) method is one of the most versatile numerical calculation procedures for the electromagnetic response of RF circuits in time domain. Hence, the combination of FDTD method with Eq.(1) should give a very efficient and reasonable measure to calculate the coupling coefficient. The time dependence of excitation signal is assumed to be

$$E = \cos \omega_c t \cdot \exp[-(t-3T)^2/T^2] \tag{2}$$

which is a Gaussian-modulated continuous wave. The angular frequency c is chosen hopefully equal to the resonant value of the uncoupled resonator. But it could be shifted considerably, since the resonator extracts a narrow spectrum around the resonant frequency f_r from the broad input spectrum. Thus we do not have to know fr in advance, resulting in reduction of the computation time. The calculation circuit is shown in Fig.2. A numerical example is depicted in Fig.3 with the calculated structure. The

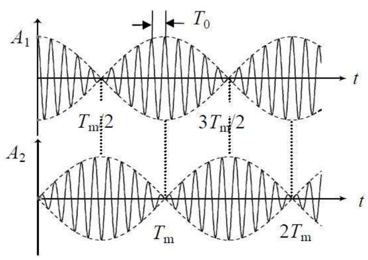

Figure 1: Energy exchange between two coupled resonators

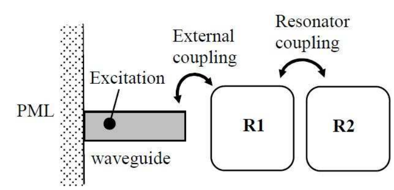

Figure 2: Excitation of coupled resonators from outside

periods T_o and T_m are calculated from the time response in Fig.3. The obtained coupling coefficient is 0.0344, which is the same as 0.0344 by the conventional frequency method. The number of computing steps is 7900, quite less than 65536 of the frequency method.

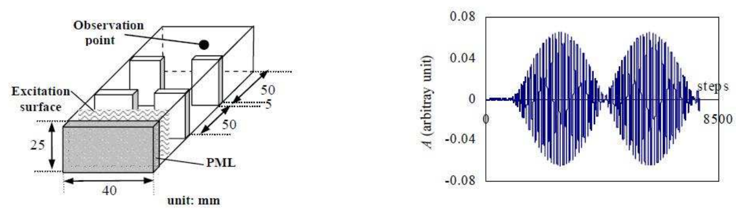

(a) two rectangular cavity resonators (b) time response of electric field

Figure 3: Calculation of coupling coefficient between two rectangular cavity resonators

REFERENCES

1. I. Awai, gNew Expressions for Coupling Coefficient between Resonatorsh, *IEICE Trans. Electron.*, E88-C, No.12, pp.2295-2301, Dec.2005.

A Rigorous Stability Analysis of Instability in ADI-FDTD Method with PML Absorber

J. N. Hwang and **F. C. Chen**
National Chiao Tung University, Taiwan

The alternating direction implicit finite-difference time-domain (ADI-FDTD) method is an attractive method due to its unconditional stable with large Courant numbers [1-3]. When the ADI-FDTD method is used to simulate unbounded region problems, an efficient absorbing boundary condition must be developed. A split field PML was employed with the ADI-FDTD method [4-5]. It was stated in [4] that this scheme is unconditionally stable with a homogenous PML medium. However, the conductivity is usually scaled for small reflection in general situation. This means the conductivity within the PML is inhomogeneous. The stability analysis for this scheme has not been studied thoroughly yet.

In this work, a rigorous stability analysis for the ADI-FDTD method with PML will be demonstrated. For simplicity, a 2-D TM wave will be studied to show the instability. In the conventional stability analysis matrixes, the magnetic conductivity $\sigma^*_{x\ i+1/2,j}$,$\sigma^*_{y\ i+1/2,j}$ are within the matrixes. However, by considering practical algorithms in the ADIFDTD method, both$\sigma^*_{x\ i+1/2,j}$, $\sigma^*_{x\ i+1/2,j}$ and $\sigma^*_{y\ i+1/2,j}$, $\sigma^*_{x\ i+1/2,j}$ will be within the proposed stability matrixes. The procedures to derive the stability matrixes will be presented. The inhomogeneous conductivities will cause instability in this scheme. To validate our stability analysis, a 3-D computation domain with PML absorber will be studied. When the inhomogeneous conductivity within the PML is considered, we will show that this scheme will be unstable in the PML interface and inside the PML regions. Both theoretical and numerical results are demonstrated to validate the instability of this scheme.

REFERENCES

1. T. Namiki, " new FDTD algorithm based on alternating-direction implicit method," *IEEE Trans. Microwave Theory Tech.*, vol. 47, pp. 2003-2007, Oct. 1999.
2. F. Zheng, Z. Chen, and J. Zhang, " finite-difference time-domain method without Courant stability conditions," *IEEE Microwave Guided Wave Lett.*, vol. 9, pp. 441-443, Nov. 1999.
3. F. Zheng, Z. Chen, and J. Zhang, "oward the development of a three-dimensional unconditionally stable finite-difference time-domain method," *IEEE Trans. Microwave Theory Tech.*, vol. 48, pp. 1550-1558, Sep. 2000.
4. G. Liu and S. D Gedney, "Perfectly matched layer media for an unconditionally stable threedimensional ADI-FDTD method," *IEEE Microwave Guided Wave Lett.*, vol. 10, pp. 261-263, July 2000.
5. C. C.-P. Chen, T.-W. Lee, N. Murugensan, and S. C. Hagness, "Generalized FDTD-ADI: an unconditionally stable full-wave Maxwells equations solver for VLSI interconnect modeling," in Proc. Int. Conf. Computer-Aided Design, San Jose, CA, Nov. 2000, pp. 156- 163.

Modelling Microwave Fixtures with the Genetic Algorithm

A. Adalev[1], **M. Hayakawa**[1], **N. V. Korovkin**[2], and **J. B. Nitsch**[3]

[1]The University of Electro-Communications, Japan
[2]Saint-Petersburg State Polytechnical University, Russia
[3]Otto-von-Guericke University, Germany

Measurements are performed at the reference plane of a measuring device (e.g. Network Analyzer), which is often separated from the Device-Under-Test (DUT) by an intervening fixture. This fixture can be represented as a couple of two-ports, between which the DUT is embedded (Fig. 1a). Therefore the de-embedding problem arises [1], which may be solved only if the parameters (S, T or so) of the two-port networks describing the fixture are known. The problem of fixture parameters determination (called unterminating or calibration) also cannot be solved directly. These parameters are obtained from the measurements made at the NA reference plane when known devices (standards) are embedded in the fixture. A weak universality of calibration and self-calibration techniques is caused by a limited assortment of standards and by problems related to accuracy of their characterization.

Here we propose a new method of fixture modelling based on the "Thru" experiment performed for an adapter and its flipped copy (Fig. 1b). Only one "Thru" experiment is performed for a symmetrical fixture, which is used very often in practice. Since the experimental data are not enough for the determination of adapter parameters at each test frequency, we propose to find them by solving an optimization problem of fitting the experimental characteristics in a certain frequency range $[f_1, f_2]$.

For this purpose we consider the adapter as N uniform lossless transmission lines connected in cascade (Fig. 1c). Each line is characterized by a couple of parameters: characteristic impedance Z_i and delay τ_i. When energy dissipation in the adapter becomes significant, fitting the experimental characteristics by using the lossless adapter model cannot be performed properly. In this case we consider the loss to be dissipated in a frequency dependent conductance $G(f)$ preceding the cascaded lines. Thus before solving the optimization problem we "clean" the data by de-embedding loss and embed it afterwards.

Due to a great number of optimization parameters and local extremes we use the genetic algorithm (GA) for solving the optimization problem. The investigations performed have revealed optimal GA parameters which enabled us to find the solution of the problem in relatively short time. Physically correct constraints for optimization parameters are proposed. Two experimental examples are discussed. The results of the experiments performed have validated a high efficiency of the method proposed and confirm that the accuracy of the de-embedding problem solution is close to the goodness of fitting the data of the "Thru" experiment.

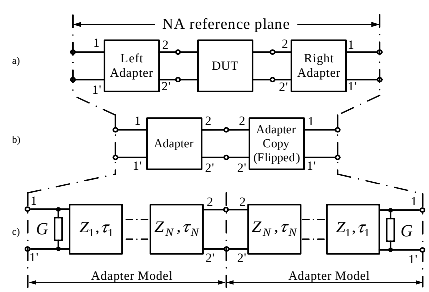

Figure 1: De-embedding stages: complete experiment (a), "Thru" experiment (b), and adapter model used(c).

REFERENCES

1. R. F. Bauer and P. Penfield, "De-embedding and unterminating," *IEEE Trans. Microwave Theory Tech.*, vol. 22, no. 3, pp. 282–288, 1974.

Expression of Radiating Wave from 2D Objects by Using a Series of Cylindrical Functions

K. Motojima
Gunma University, Japan

In this paper, a new expression for radiating wave by using the cylindrical function is proposed. In this method, radiating electromagnetic wave from 2D emitting objects, that is a array of line sources, is expressed by using the Hankel functions with unknown coefficients.

Virtual boundary which encloses the radiating 2D objects is applied to free space. Then, sampling points are placed on the virtual boundary at even intervals. The total number of sampling points is 2N+1. The virtual boundary is a circle which encompasses the radiating 2D objects. The boundary condition is applied to all sampling points on the virtual boundary. Applying the boundary condition, a complex (2N+1) by (2N+1) square matrix equation is formulated. Calculating the square matrix, the unknown coefficients within a series of Hankel functions can be determined. Once the unknown coefficients are obtained, the radiating electromagnetic wave can be easily calculated by using a series of Hankel functions. Moreover, far field data, such as radiating patterns, can be easily obtained by using an asymptotic expansion of the Hankel function.

In order to verify this expression, numerical experiments are performed. Line sources are adopted as radiating 2D objects. Radiating patterns from a linear array of line sources can be readily calculated by simple algebraic function. Comparison between the results by this method and the results by basic algebra shows the good agreement. It give the verification of this presented method. This method can be used for the accurate expression of radiating wave from 2D objects.

Preconditioned Parallel MLFMA Solution of Metamaterial Structures

L. Gürel, Ö. Ergül, T. Malas, and **A. Ünal**
Bilkent University, Turkey

Since metamaterials display unusual electromagnetic properties, their accurate electromagnetic modeling via integral-equation formulations becomes an important issue. The metamaterial structures considered in this study consist of split-ring resonators (SRRs) and thin wires arrays (TWAs), which exhibit double-negative properties. These structures have open surface geometries that require the use of electric-field integral equation (EFIE) for their electromagnetic modeling. In order to have a better understanding of the scattering and transmission properties of these metamaterial structures, we model and solve large numbers of SRR inclusions. Consequently, we need to solve large computational problems, and the acceleration power of the multilevel fast multipole algorithm (MLFMA) becomes essential. Since MLFMA employs an iterative solver, solution of large problems requires the reduction of number of iterations. Unfortunately, EFIE formulation tends to increase the number of iterations. Other integral-equation formulations producing better conditioned matrix equations, such as the combined-field integral equation (CFIE), are not applicable to open geometries. Therefore, effective strategies for the preconditioning of the iterative MLFMA solution should be developed.

In this talk, we consider the use of both exact and approximate inverses of sparse matrices containing electromagnetic near-field interactions of various strengths as preconditioners. For this purpose, incomplete LU (ILU) preconditioners and sparse approximate inverse (SAI) preconditioners are employed. By accelerating the convergence of the iterations in MLFMA, solutions of large metamaterial structures are targeted without resorting to simplifications involving homogenization, periodicity, and symmetry. Hence, the interactions of electromagnetic fields with large, albeit finite, SRR and TWA structures are modeled.

Multiport Network Method and Using It for Accurate Design of Spiral Antennas and Comparing Simulated Results with Experimental Results

S. Rajebi, C. Ghobadi, and **J. Nourinia**
Urmia University, Iran

Since the ultra wideband antennas development in the late 1950's, Archimedean spiral antennas have been widely applied in both airborne and ground based systems. The wide bandwidth and multimode characteristics of these antennas, along with their broad circular polarization (CP) beamwidths, are particularly well suited for direction finding (monopulse) systems. Unfortunately, until only recently, most of the driving point and radiation characteristics of Archimedean spirals have been determined empirically, gained through three decades of experimentation. A rigorous analytically based analysis of these antennas has been intractable. In this paper, Multiport Network Method as a powerfull method is presented for spiral

Leakage Fields in Patch Antennas and Modeling It with Multiport Network Model

S. Rajebi, C. Ghobadi, and **J. Nourinia**

Urmia University, Iran

Square spiral antennas have the merits of not only wide bandwidth and circular polarization but also compact size which makes them good candidate for mobile receiver applications. On the other hand, multiport network method is one of best CAD[1] techniques to design and analyze antennas and microstrip patch arrays.

First step in analyzing microstrip planar circuits is inspecting edge leakage fields. Several methods have been suggested for considering effect of these fields. In this paper, these methods are reviewed and then best and more accurate method is selected and applied to multiport network model of a square spiral antenna and in the end results of this applying are compared with results from no considering leakage fields case.

New Approach Using Universal Autonamous Blocks with Floket Channels for Rigourous Mathematical Modeling of Microwave Devices

G. S. Makeeva [1], **O. A. Golovanov** [2], and **M. P. Horvath** [3]
[1]Penza Military Institute of Artillery, Russia
[2]M. P. Horvath, Russia
[3]The George Washington University,U.S.A.

A new numerical method using universal autonomous blocks in the form of a rectangular uni-form parallelepiped with Floket channels (UBF) was developed for accurate electromagnetic modeling of microwave integrated devices (MID) and microwave engineering systems. The Floket channel is a rectangular multimode waveguide (WG), the fields satisfy the periodic boundary conditions on walls of WG.

The UBF method using the full-wave basis of eigenwaves, including TEM-wave propagating in virtual Floket channels, differs from the numerical methods of multimode autonomous blocks (AB) [1] or minimal AB [2] using the basis of TE-, TM- eigenwaves in virtual WG. Us-ing method of multimode AB it is necessary to extract a eature on edges (the tangential elec-tric fields are equal to zero in edges [1]) in the goal to change the slow convergence of computa-tional process. The limitation of basis of two orthogonal polarized TEM-waves in virtual WG of minimal AB [2] results in low effective computional algorithm.

The UBF method is different from the FTDM method that the fields of UBF are determined from solutions of 3D diffraction boundary problems (without simplification of Maxwell′s equa-tions and boundary conditions) and they satisfy the non-asymptotic radiation boundary condi-tions [3], that why it permits to join of UBF independently autonomously) .

The computational algorithm using UBF are performed in the following way. The 3D diffrac-tion problems for MID are formulated for aveguide transformer (WGT). WGT is the shielded domain containing metal or dielectric electrodynamical objects and having input sec-tions in connate multimode WG or strip-slot lines (SSL). This approach permits to solve the ex-terior or interior electromagnetic boundary problems equally. The 3D diffraction boundary problem at rigorous ectrodynamical statement for linear UBF was solved. H(TE)-, E(TM)- and TEM-eigenwaves of the rectangular Floket channel were in-vestigated. The longitudinal components of eigenwaves were determined by solving of 2D Helmholz‘s equations. The method of a recomposition of the linear UBF is developed.

Using the decomposition approach WGT are divided on subdomains in the form of the rectangular AB with Floket channels on bounds. The descriptor of linear UBF as a multimode multi-channel scattering matrix results by solving of key boundary problems for the rectangular parallelepiped. The multimode conductance matrix using the basis of eigenwaves of Floket channel at input sections of WGT was determined as a result of recomposition of UBF by Floket channels. After then this matrix is mapped to multimode conductance matrix using the basis of eigenwaves of WG or SSL, connected with input sections of WGT.

Using linear UBF the methodology of accurate electromagnetic modeling of MID was developed and results of mathematical simulation of MID on SSL were obtained. As a test pro-gram the relative propagation constant of fundamental mode in regular SSL, the modulus of scat-tering parameter of the transverse joint by the section of coupled SSL and the T-(tee) connector on SSL depending on the number of basic functions on UBF bounds were calculated. The com-parison of the results of numerical calculations to the test results, obtained by multimode AB method [2], shows that the developed UBF method is effective concerning a computing time for solving of 3D electromagnetic diffraction problems for MID and microwave engineering sys-tems with TEM-wave propagating.

REFERENCES

1. V.V. Nikolskiy, O.A. Golovanov. Radiotekhnika i elektronika, 24 (1979), 1070.
2. V.V. Nikolskiy, T.I. Lavrova., Radiotekhnika i elektronika, 23 (1978), 241.
3. O.A. Golovanov. Radiotekhnika i elektronika, 35 (1990), 1853.

Mesh of Various Propagation Models to Use in the Conception of a Proposed Wireless System: Application in the City of Curritiba - Brazil

H. Tertuliano, M. A. Betinipereira, and **C. A. Dartora**
Federal University of Parana, Brazil

This paper presents an original proposal for a conception of a wireless prediction technique system in order to customize the noise and interference parameters that degrade the capability of a real wireless system using a mesh of propagation models. The main goal is to select a few specified statistic propagation models like Lee-Picknard Optimized, Korowajczuk and Modified Micro cells and use then to observe the behavior of the BTS over co-channel and adjacent interference. For that, the city of Curitiba in the south of Brazil with more than two millions of inhabitants was chosen. The wireless specified system was constituted of ten base transceiver station BTS. It is important to observe that the radio-base station was located in the downtown and the predictions were made by the software CelpPlanWireless Global Technologies. The morphology and the topography aspects of the city was been take into consideration. Indeed, the building environment was described in the software in terms of statistical parameters, such as the average row spacing and the building height distribution, as a basis for making propagation predictions for the three used models. In each simulation one specific propagation model was considered and the relevant aspects of interference were inferred. After the simulation of each considered model, it was possible to observe the best behavior model and make adjustments.

In order to certify if the obtained results could be used in the real wireless world system, one local mobile telephone company has been made a practical simulation in the same downtown area. The used omni-directional antennas, frequency hope and technology was conserved by the company. Nevertheless they had used a database for the actual shapes of buildings in the region under study. The comparative analysis of the simulated results obtained through software and practical results obtained by measure, proven that the proposed technique that mesh different propagation models appears like viable because it can give adequate solution and offers many advantages over existing techniques like for instance:

REFERENCES

1. It is possible to detect points of interference in a system and use this technique to avoid critical points, because in greatest cities, a physical free space to put antennas is not so easy to find out.
2. 2. It is possible to cover a wide range of frequencies and technologies (FDMA, GSM, CDMA ONE c).
3. It provides an average value of adjacent and co-channel interference over the most single prediction mode used.

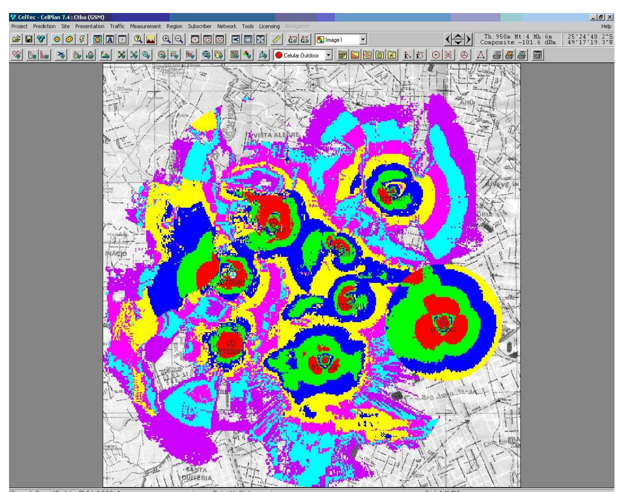

Figure 1: Obtained Results from Prediction in Curitiba downtown using the CelpPlanWireless Global Technologies using three different models.

Numerical Analysis of an Optical Near Field From an Aperture In a Metallic Layer -Application of the FDTD Method Combined with the Motion Equation of Ectron-

S. Kagawa [1], **Y. He** [2], and **T. Kojima** [1]

[1]Kansai University, Japan
[2]Osaka Electro-Communication University, Japan

Recently, a density growth is demanded in optical storage technologies. However, it is said that the upper limit of recording density by the current optical recording system is several tens of gigabits per inch square due to the optical diffraction limit even in the case of using a short wavelength. Then, as a technology that enables us to break down the optical diffraction limit, the optical near field technology has gotten a lot of attention.

In this paper, we try to perform two-dimensional numerical analysis of electric field distributions near a metallic nanoaperture that generates an optical near field by using the Finite Difference Time Domain (FDTD) method. We also carry out numerical analysis of readout characteristics of a recording mark of the disk model that consists of the nanoaperture and the phase change disk structure. In the present analysis, the FDTD method combined with the motion equation of electron [1], [2] is applied to a metallic medium whose permittivity can become negative at the optical wavelength range.

REFERENCES

1. Y. He, S. Kiyama and S. Adachi, "FDTD analysis of the near field of a dipole antenna immersed in a magneto-plasma" , IEICE technical report, AP2000-10, May 2000
2. S. Kagawa, Y. He and T. Kojima, "Light reflection characteristics from the semi-infinite metallic medium by the FDTD method combined with the motion equation of electron", Extended Abstracts of the Optics Japan 2005, 25aP1, pp.588-589, Nov. 2005.

Session 2P5
Numerical and Analytical Technologies of Photonic Devices II

Large-Mode-Area Single-Mode Holey Fiber with Low Bending Losses

Y. Tsuchida, K. Saitoh, and **M. Koshiba**
Hokkaido University, Japan

The photonic crystal fibers (PCFs) have attracted attention owing to their many unique properties [1]. Their operation usually relies on light being guided by the physical mechanism known as index-guiding [2] or photonic band-gap effect [3]. Especially, index-guiding PCFs, also called holey fibers (HFs) possess numerous unusual properties such as endlessly single-mode operation, extremely large or small effective area, and bend-loss edge at short wavelength. To numerically characterize HFs with large refractive-index difference between the pure silica and air regions, a complete vector model is required to predict sensitive quantities such as effective area, cutoff wavelength, and bending loss.

For conventional fibers, the effective area is limited by the fact that an increasing core size requires a correspondingly decreasing the index step between the core and the cladding in order to maintain singlemode operation. This imposes requirements on the control of the index profile, which is difficult to realize with index-raising doping of the glass. HF has a large potential in this area because of their endlessly singlemode properties combined with, in principle, unlimited large effective areas [4]. However, as with any fiber, the largest mode areas are ultimately determined by bending losses. It is therefore essential to gain an understanding of the factors that influence bending loss in HFs in order to form accurate predictions that can facilitate the improved bending loss design.

Large-mode-area (LMA) single-mode optical fibers offer low nonlinearity, and high damage thresholds, which are essential in high power and transmission applications. HFs are an attractive route towards such fibers and single-mode HFs with effective areas as large as 1000 μm_2 have been reported [5]. However, as with any fiber, the fundamental limit on mode area for practical applications is set by the bending losses. Although the bending losses of conventional HFs with uniformly distributed air-holes in the cladding have been shown to be comparable to those of conventional fibers, HF fabrication techniques permit a high level of design flexibility to improve their bending loss properties.

In this work, we consider a newly proposed HF with five air-hole rings as shown in Fig.1 and numerically investigate the possibility of realizing a LMA single-mode HF with low bending losses. The HF is made of pure silica with two kinds of air-hole diameter. The air-holes are arrayed in a triangular lattice with a pitch Λ, the air-hole diameters of the first ring are d1, and the other air-hole diameters are d. We find that the confinement loss of the higher-order mode can be controlled by changing the value of d_1 / Λ. This phenomenon can be explained by the fact that the difference between the effective index of the higher-order mode and that of the cladding modes which have the same parity as the higher-order mode can be controlled by the value of d_1/ Λ. We have successfully designed a LMA single-mode HF with low bending losses and mode area larger than 500 μ m ^{2} in the telecommunication window.

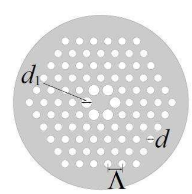

Figure 1: Schematic representation of a LMA holey fiber.

REFERENCES

1. J. C. Knight, T. A. Birks, P. St. J. Russell, and D. M. Atkin, *Opt. Lett.*, Vol. 21, 1547-1549, Oct. 1996.
2. T. A. Birks, J. C. Knight, and P. St. J. Russell, *Opt. Lett.*, Vol. 22, 961-963, July 1997.
3. J. C. Knight, J. Broeng, T. A. Birks, and P. St. J. Russell, Science, Vol. 282, 1476-1478, Nov. 1998.
4. J. C. Knight, T. A. Birks, R. F. Cregan. P. St. J. Russell, and J. -P. de Sandro, *Electron. Lett.*, Vol. 34, 1347-1348, June 1998.
5. J. Limpert, A. Liem, M. Reich, T. Schreiber, S. Nolte, H. Zellmer, A. Tunnermann, J. Broeng, A. Petersson, and C. Jakobsen, *Opt. Express*, Vol. 12, 1313-1319, April 2004.

Full-Vectorial Pseudospectral Frequency-Domain Method for Optical Waveguide Analysis

H. C. Chang
University of Miyazaki, Japan
P. J. Chiang
National Taiwan University, Taiwan R.O.C.

The pseudospectral method has long been applied to fluid dynamics problems [1] and has recently attracted more attention in computational electromagnetics due to its high-order accuracy and fast convergence characteristics. For time-varying problems, the so-called pseudospectral time-domain (PSTD) method offers an alternative technique for the problems usually solved by the finite-difference time-domain (FDTD) method. In this paper, we consider the application of the pseudospectral method to frequency-domain problems, in particular, the solution of optical waveguide modes, and develop a pseudospectral frequencydomain (PSFD) method. We show that the pseudospectral mode solver (PSMS) we establish based on the full-vectorial PSFD scheme with multidomain formulation possesses remarkably high accuracy. High-accuracy calculation of full-vectorial modes on optical waveguides is important in the design of some waveguide structures and related waveguide devices. In the PSMS, the computational domain in the waveguide cross-sectional plane is divided into several sub-domains of uniform material and with the dielectric interfaces falling on the domain boundaries, and the governing equation in each sub-domain is the Helmholtz equation. We apply the Chebyshev collocation method that can provide us with an exceptionally accurate means to calculating a function and its derivatives by the construction of global Chebyshev-Lagrange interpolating polynomials of different orders. The spatial derivatives of the field in the governing Helmholtz equation at the collocation points (the Chebyshev-Gauss- Lobatto points) can be obtained by a matrix operation. The Helmholtz equation is finally converted into a matrix eigenvalue equation. Not all sub-domains are of rectangular shape and proper curvilinear mapping technique is utilized for transformation between the rectangular coordinate and the curved one of a general sub-domain. Proper fulfillment of dielectric interface conditions is essential in achieving high numerical accuracy. In our formulation, the numerical stability and accuracy have been guaranteed by imposing alternative Dirichlet and Neumann types of boundary conditions between adjacent sub-domains. Analysis of the optical fiber and D-shaped fiber has demonstrated that numerical accuracy in the effective index up to the 10^{-8} order is easily achieved. We have further generalized the model by incorporating perfectly matched layer (PML) absorbing boundary conditions (ABCs) into the formulation so that complex propagation constants of leaky waveguide modes can be solved. We will present analysis results of different optical waveguide structures, including microstructured holey fibers. In the case of a six-hole microstructured fiber, we have compared our calculation with the well-known result of the multipole method [2] and found that our method can achieve numerical convergence with more digits in both the real and imaginary parts of the effective refractive index. The PSMS is thus a powerful mode solving scheme especially for the situation when very high accuracy in the waveguide-mode effective index is needed.

REFERENCES

1. C. Canuto, M. Y. Hussaini, A. Quarteroni, and T. A. Zang, Spectral Methods in Fluid Dynamics. New York: Springer-Verlag, 1988.
2. T. P. White, B. T. Kuhlmey, R. C. McPhedran, D. Maystre, G. Renversez, C. M. de Sterke, and L. C. Botten, gMultipole method for microstructured optical fibers. I. Formulation,h *J. Opt. Soc. Am. B*, vol. 19, pp. 2322. 2330, 2002.

A Domain Decomposition Method for Photonic Crystal Modeling

Y. Huang and **Y. Y. Lu**
City University of Hong Kong, China

The domain decomposition (DD) method has been extensively studied and applied to many different problems[1]. For wave propagation problems in photonic crystal devices, DD can be useful because there are many identical unit cells. In this paper, we present a variant of the DD method based on the Dirichlet-to-Neumann (DtN) map of the unit cells. The DtN of a unit cell maps of the wave field at the boundary of the unit cell to its normal derivative. Using this map, we can establish a sparse system of equations that solves only the wave field on interfaces between the unit cells. For a 2-D square lattice of circular cylinders of radius r and dielectric constant ϵ_1 embedded in a material with dielectric constant ϵ_2, the unit cell is the square given by $0 < x < a$ and $0 < y < a$ with a disk of radius r at the center. For the TE or TM polarizations, we have Helmholtz equations for a scalar function u, then the DtN map Λ is defined by

$$\begin{bmatrix} \partial_y u_0 \\ \partial_x v_0 \\ \partial_x v_1 \\ \partial_y u_1 \end{bmatrix} = \Lambda \begin{bmatrix} u_0 \\ v_0 \\ v_1 \\ u_1 \end{bmatrix} \tag{1}$$

where $u_0 = u(x, 0)$, $u_1 = u(x, a)$, $v_0 = u(0, y)$ and $v_1 = u(a, y)$. The operator Λ is approximated by a $4n \times 4n$ matrix, assuming that u_0, u_1, v_0 and v_1 are vectors of length n obtained from sampling at n points in the interval (0, a), such that $x_j = (j - 0.5)h$ for $h = a/n$. A partition of the matrix Λ gives 16 blocks of size $n \times n$. Meanwhile, Λ is actually obtained by assuming that the solution of the Helmholtz equation in the unit cell is given as a sum of 4n exact solutions based on Bessel functions. Once Λ is obtained, a system of equations can be obtained for $\{u_j, v_j\}$ (i.e. u on edges of the cells). These equations are obtained by imposing the continuity of the derivative of u on edges of the cells as computed from the DtN maps of the two opposite sides. Notice that such an equation is obtained from two neighboring cells and it involves seven unknown vectors (of length n). Therefore, we obtain a sparse system of equations. On the other hand, if we expand the solution near each cylinder as Bessel functions with suitable coefficients and solve the coefficients for all cylinders together [2], we obtain a linear system with a dense coefficient matrix. However, the method in [2] is more flexible as it allows arbitrary locations of the cylinders.

As an application of the DD method based on the DtN map, we study the transmission problem of a 2-D photonic crystal of finite thickness. We have a square lattice of circular cylinders with radius r for$0 < y < ma$ and $-\infty < x < \infty$, where a is the lattice constant, m is an integer representing the number of layers in the y direction. For $y > ma$ and $y < 0$, we have a homogeneous medium of dielectric constant ϵ_0. For$m = 16$, $r = a\sqrt{\pi}/2$, $\epsilon_0 = \epsilon_1 = 1$, $\epsilon_2 = 2.1$ and a normal incident wave, we are able to confirm the results in [3] using a very small n (5 or 9). The results in [3] are obtained based on a Fourier series of 2700 terms.

REFERENCES

1. A. Toselli and O. Widlund, Domain Decomposition Methods . Algorithms and Theory, Springer, 2005.
2. R. C. McPhedran, L. C. Botten, et al, *Physical Review E*, 60, vol. pp. 7614-7617, Dec. 1999.
3. K. Sakoda, J. Opt. Soc. Am. B, vol. 14, pp. 1961-1966, 1997.

Supermodes of Coupled Photonic Crystal Waveguides: a Tight Binding Analysis

L. C. Botten
University of Technology, Australia

C. M. de Sterke and **R. A. Hansen**
University of Sydney, Australia

One of the most studied applications of photonic crystals (PCs) are photonic crystal waveguides (PCWs), formed by creating a line defect in a PC and operating at frequencies inside a bandgap. Consequently, the light cannot propagate in the PC and is forced to remain in the defect which acts as a waveguide. The key diRerence with conventional guides is that for a PC, confinement is provided by Bragg reflection, in contrast to total internal reflection for conventional guides.

Coupled waveguides, which are waveguides that run parallel to each other and are sufficiently close so that their evanescent tails overlap, have applications such as directional couplers. These are particularly interesting in a PC geometry since the beat length of the supermodes, the size of which determines the length of the device, can be made very short. Recently, we showed such structures have properties that diRer significantly from conventional waveguides. For example, the fundamental mode of two PCWs can be odd, whereas the fundamental mode of a coupled pair of conventional guides is always even—a situation that can never arise in conventional structures.

In this paper, we generalise our previous theory to handle an arbitrary number of identical coupled PCWs and consider this geometry at long wavelengths where the analogy with conventional waveguides is strongest. We focus on the limit in which the guides are spaced sufficiently far apart so that their mutual coupling is weak. In this limit, the tight-binding (TB) approximation is a convenient tool to analyse the properties of arrays of identical scatterers. Developed originally in condensed matter physics for band structure calculations, it has also been used extensively in optics to obtain approximate expressions for the modes of coupled waveguides and typically involves an overlap integral over a waveguide involving the modal field in this guide and its neighbour. In this paper, however, we present a novel derivation of the TB results that does not involve overlap integrals but instead relies on the straightforward application of reflection and transmission coefficients. We thus find the propagation constants of coupled waveguides without first having to calculate the modal field of an isolated guide. Using this treatment we find that for coupled PCWs, the supermode ordering is the reverse of that for conventional waveguides when the field changes sign after a single period in the bulk PC and there is an odd number of periods between adjacent waveguides. As a consequence of this, we find that the fundamental supermode is odd when the number of waveguides is even and barriers separating them comprise an odd number of layers.

Enhancement of Nonreciprocal Phase Shifts Through the Utilization of Large Group-Velocity Dispersion in Magneto-Photonic Crystal Waveguides

N. Kono and **M. Koshiba**
Hokkaido University, Japan

This study demonstrates that nonreciprocal phase shifts [1] can be enhanced by utilizing line-defect waveguides in magneto-photonic crystals (MPCs) [2] with large group-velocity dispersion [3]. The nonreciprocal phase shifts are highly effective for the realization of nonreciprocal optical waveguide devices, such as optical isolators and circulators. Device sizes can be reduced, if this nonreciprocal effect can be enhanced.

MPCs are photonic crystals constructed of magnetic materials. The first report was released at the end of the 1990s, and at the beginning of the new millennium activity in this area is growing rapidly, as MPCs offer clear advantages such as the enhancement of the Faraday rotation seen in the one-dimensional crystals with defects. Recently, research on two-dimensional (2-D) MPCs [4] has also been gaining attention. MPC waveguides [5], created by introducing line defects into the 2-D MPCs, are more suitable for the on-chip integration of nonreciprocal devices with other reciprocal photonic crystal devices.

This study considers the 2-D MPC waveguide shown in Fig. 1. The direction of magnetization is parallel to the x-direction. A compensation wall [6] divides the waveguide into two equal halves with opposing directions of magnetization. This is the basis of nonreciprocal phase shifts for TM modes. Features of our model include the following: The material of the MPC is a typical magnetic garnet, with refractive index n = 2.3 and the Faraday rotation $|\theta_F| = 2880^o$/cm. The waveguide is created with a row of defects (missing air holes) in the hexagonal MPC. There is no variation in the x-direction.

Figures 2, 3, and 4 show the dispersion curves of the forward propagating modes, the group-velocity dispersion, and the nonreciprocal phase shifts, respectively, for different air hole radii r. Figures 2 and 3 confirm that the dispersion relation with large group-velocity dispersion, an important future of photonic crystal waveguide geometries [3], occurs also in the MPC waveguide. Figure 4 demonstrates how the nonreciprocal phase shift can be enhanced, for each radius, in the frequency band where the group-velocity dispersion increases. As the size of the air holes increases, the maximum value of the group-velocity dispersion rises, and the increment of the nonreciprocal phase shift grows.

REFERENCES

1. Y. Okamura, T. Negami, and S. Yamamoto, Appl. Opt. 23, 1886-1889 (1984).
2. M. Inoue, K. Arai, T. Fujii, and M. Abe., J. Appl. Phys., 85, 5768-5770 (1999).
3. M. Notomi, K. Yamada, A. Shinya, J. Takahashi, C. Takahashi, and I. Yokohama, Phys. Rev. Lett., 87, 253902 (2001).
4. Y. Ikezawa, K. Nishimura, H. Uchida, and M. Inoue, J. Magn. Magn. Mat., 272-276, 1690-1691 (2004).
5. N. Kono and M. Koshiba, Opt. Express, 13, 9155-9166 (2005).
6. N. Bahlmann, M. Lohmeyer, H. Dotsch, and P. Hertel, IEEE J. Quantum Electron. 35, 250-253 (1999).

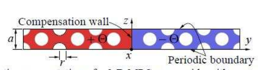

Fig. 1. Schematic representation of a 2-D MPC waveguide with a compensation wall.

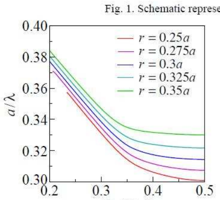

Fig. 2. Dispersion curves.

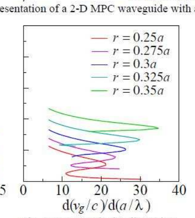

Fig. 3. Group-velocity dispersion.

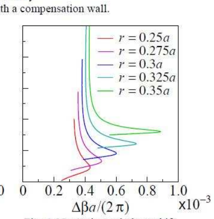

Fig. 4. Nonreciprocal phase shift.

All-Optical Logic Device by Photonic Crystal Directional Coupler with Kerr- Type Nonliner Material

X. Li, H. Maeda and **K. Uchida**
Fukuoka Institute of Technology, Japan

Photonic crystal (PC) structure is key component for the optical integrated circuit in next generation, because of its unique propagation characteristics based on the photonic band gap (PBG)[1]. The twodimensional pillar type PC waveguide is basically composed of periodic array of dielectric rods with a line of defect in free space, as illustrated in Fig.1. In two dimensional PC structure, the directional coupler is composed of two adjacent parallel lines of defect. By using nonlinear material in the vicinty of waveguides, the coupling length is affected by the input electric field amplitude of the light. If the coupler length and combination of two kind of optical signal with different amplitude were set suitably, it could be possible to switch the optical output port of the coupled waveguides. In this paper, finite difference time domain (FDTD)[2] simulation of all-optical logic device, which is composed of the line defect in hexagonal lattice is reported.

We consider composite space of lossless, isotropic, linear dielectric and Kerr-type nonlinear material. The electric field of TE mode, the displacement, and the polarization term due to Kerr effect hold the followings[3];

$$\epsilon_0 \epsilon_\infty E_y = D_y - P_K, \tag{1}$$

where ϵ_0 and ϵ_∞ are permittivity of free space and the saturated relative permittivity in the limit that frequency is infinitely high. The nonlinear Kerr effect is expressed by the term P_K. In Fig.1, A,B and S are input powers of logic gate and their summation. On the other hand, Q1 and Q2 are output powers with OR and AND characteristics, respectively. The truth table is inserted in the figure. The propagating electric field for S=1 ($E_S = 10$[mV/μ m]) and S=2 ($E_S = 10\sqrt{2}$[mV/μ m]) are depicted in Figs.2 and 3, respectively. The optical switching characteristics can be observed from these figures. Application of nonlinear dielectric material to PC structures will bring us more interesting optical devices in future.

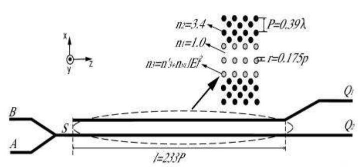

Input		SUM of A and B	Output	
			OR	AND
A	B	S	Q1	Q2
0	0	0	0	0
1	0	1	1	0
0	1	1	1	0
1	1	2	1	1

Fig.1 *OR/AND* Model and Truth Table of *OR/AND*.

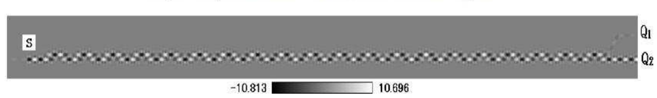

Fig.2 Electric Field Profile for Electric Field Amplitude $E_S = 10[mV/\mu m]$.

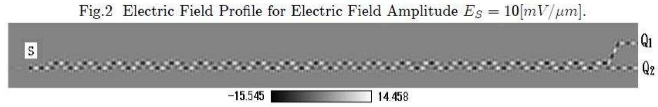

Fig.3 Electric Field Profile for Electric Field Amplitude $E_S = 10\sqrt{2}[mV/\mu m]$.

REFERENCES

1. S. Noda and T. Baba, Ed., Roadmap on Photonic Crystals, The Netherlands: Kluwer Academic Publishers, 2003.
2. K. S. Yee, gNumerical solution of initial boundary value problems involving Maxwellfs equation,h *IEEE Trans. on Antennas and Propagation*, vol.14, no.3, pp.302.307, March 1966.
3. D. M. Sullivan, gNonlinear FDTD Formulations Using Z Transform,h*IEEE Trans. on MTT*, Vol.43, No.3, pp.676.682, 1995.

Efficient, Low Reflection Coupling into Rod-Type Photonic Crystals

L. C. Botten
University of Technology, Australia

T. P. White, C. M. de Sterke, and **R. C. McPhedran**
University of Sydney, Australia

Many of the key applications of photonic crystals (PCs) depend on their ability to tailor the propagation of light at frequencies in a band. Examples are autocollimation, in which the light propagates with very small diRraction, and the superprism, in which the direction of light propagation depends strongly on the incident angle or on the wavelength of the light. However, in all applications of this type the light needs to be coupled into and out of the PC and it is important that this be accomplished effciently. Otherwise, not only does the optical power decrease, but also the stray light may aRect the operation of the device.

The coupling of light between free space and air-hole type photonic crystals has been studied previously by a number of research groups. In general, these groups found the coupling effciency to be inadequate and, accordingly, they were led to devise various interface modifications to improve the coupling. Typically, these involve changing the size or shape of the air holes, or adding an additional row of holes, which acts as an anti-reflection coating.

In contrast, in this paper we investigate the transmission into a rod-type photonic crystals and show, using a two-dimensional analysis, that for some wavelengths the transmittance can be close to perfect for a very wide range of incoming angles. Using a systematic analysis we demonstrate that the highly efficient coupling is associated with resonances of the individual inclusions, and we link these, via the properties of the cylinder diRraction gratings, to the properties of the bulk photonic crystal. Our analysis shows that high coupling efficiency can occur only in rod-type PCs, and not in PCs of the air hole-type, for wavelengths sufficiently long such that only the specular plane wave order can propagate (with all other orders evanescent) in the background medium.

Analysis of Electromagnetic Radiation from a Source Embedded in Photonic Crystals

K. Yasumoto, V. Jandieri, and **H. Toyama**
Kyushu University, Japan

In photonic crystals, the electromagnetic waves within a particular frequency band are prohibited or allowed to propagate in a particular direction. These features can be effectively used in the design of photonic crystal based antennas. Recently the electromagnetic radiation from a localized source coupled to photonic crystals has been extensively investigated using the array scanning method combined with the method of moments, the phased array method combined with the plane-wave expansion method, and the finite difference time domain method.

In this paper, we propose a novel approach to formulate the radiation from a localized source embedded in photonic crystals consisting of layered periodic arrays of parallel or crossed circular cylinders. The method employs the spectral domain approach. The source is transformed into an infinite periodic array of linearly phased sources in the spectral domain. For each of spectral components, the periodic sources excite the space harmonic fields. The spectral responses of the photonic crystal to the excitation of the arrayed sources can be calculated using the lattice sums, the T-matrix of a circular cylinder, and the generalized reflection and transmission matrices of the layered system. As a typical example of excitation, Fig. 1 illustrates a localized line source embedded in two-dimensional photonic crystals and its equivalent system in the spectral domain. The radiated field is obtained by a finite integral of the spectral responses with respect to the spectral parameter. For the source with a finite dimension, the spectral function of the current distribution is weighted on the integrand. The directivity and beam shaping of radiation related the far-zone fields can be easily calculated using the conventional asymptotic method without performing this integration.

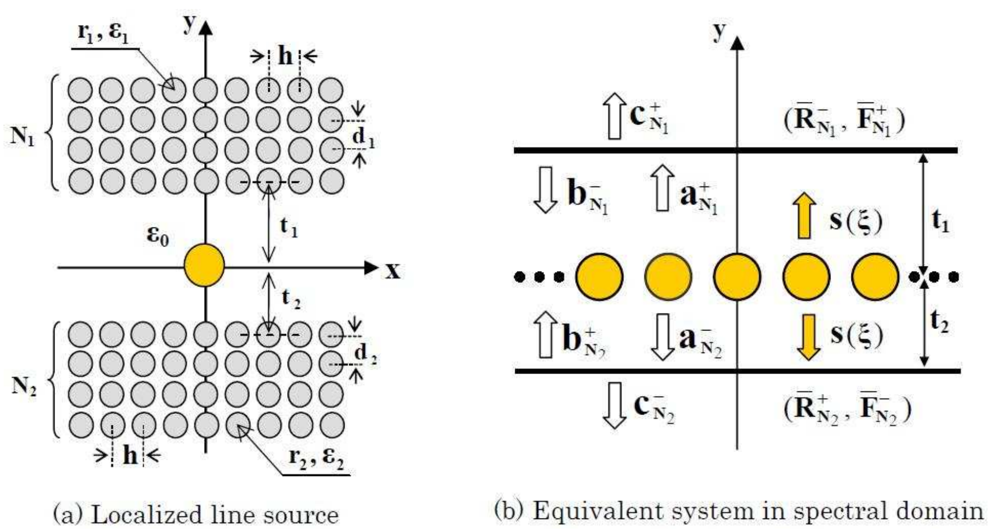

Figure 1: Schematics of (a) a localized line source embedded in two-dimensional photonic crystals and (b) an equivalent system in the spectral domain. The upper and lower photonic crystals are characterized by the generalized reflection and transmission matrices $(\bar{R}_{N_1}-,\bar{F}_{N_1}+)$ and $(\bar{R}_{N_2}+,\bar{F}_{N_2}-)$, respectively.

Analysis of Two-Dimensional Photonic Crystal Branching Waveguide with Microcavity

Y. Naka and **H. Ikuno**
Kumamoto University, Japan

Great interests have been given to the photonic crystal whose photonic band gap has attracted considerable possibility [1, 2]. By using the strong confinement of the light by the photonic band gap, it is expected that waveguide devices whose size is the order of the wavelength of light can be realized [2]. In fact, several microscale photonic crystal optical waveguide devices have been proposed [3.6]. It is important for designing high density integrated optical devices to clarify fundamental properties of basic photonic crystal waveguides such as straight waveguide, sharply bent waveguide, branching waveguide, directional coupler, and so on [5.8]. Particularly we need to develop a highly efficient transmission devices such as sharply bent and branching waveguides because a Fabry-PLerot resonance, which degrades the wavelength characteristics is caused by slight reflection from the bend/branch.

We propose a sharply branching waveguide with excellent transmission characteristics. The branching waveguide is composed of an input waveguide, two output waveguides and a microcavity making a resonant tunneling [7, 9]. Three waveguides are connected by microcavity and three additional air-holes are placed at the conjunction between the microcavity and waveguide. We analyze a characteristics of the sharply branching waveguide using the finite-difference time-domain (FD-TD) method based on the principles of multidimensional wave digital filters (MD-WDFs) [10, 11]; this method [7, 12] can easily be implemented and is more accurate than the conventional one, the Yee algorithm. The photonic crystals employed here is composed of circular air-hole in dielectric material on a triangular array. The optical waveguide can be created by removing one row of air-holes. The optical light is confined in the defect when incident frequency is inside of the photonic band gap, because electromagnetic field can not propagate in the photonic crystal which works as cladding layer. We calculate external quality factor Q of microcavity which connects a waveguide. We put an air-hole at the conjunction between the microcavity and waveguide and find that the external Q changes by radius of air-hole. From the results, we can match an impedance matching condition between an input waveguide and two output waveguides by adjusting radius of air-hole located at the conjunction. We show that reflected waves from the branch can be completely eliminated by adding additional airholes due to resonant tunneling. We also show that transmission bands can be controlled by adjusting radius of additional air-hole while keeping impedance matching condition.

REFERENCES

1. E. Yablonovitch, *Physical Review Lett.*, vol.58, pp. 2059.2062 (1987).
2. J.D.Joannopoulos, et al., Nature, vol.386, pp. 143.149 (1997).
3. S.Y.Lin, et al., Science, vol.282, pp. 274.276 (1998).
4. S.Fan, et al., *Physical Review Lett.*, vol.80, pp. 960.963 (1998).
5. Y.Naka, et al., Proceedings of 2001 URSI International Symposium on Electromagnetic Theory, Victoria, Canada, pp. 529.531 (2001).
6. Y.Naka, et al., Proceedings of International Union of Radio Science General Assemblies, Maastricht, Netherlands, p. D3.O.2 (2002).
7. H.Ikuno, et al., Radio Science, vol.35, pp. 595.605 (2000).
8. H.Ikuno, et al., Electromagnetic Theory and Application for Photonic Crystals (Ed. K.Yasumoto), Boca Raton, CRC Press (2005).
9. J. Wang, et al., *Appl. Phys. Lett.*, vol.60, pp. 654.656 (1992).
10. A.Fettweis, *Proc. IEEE*, vol.74, pp. 270.327 (1986).
11. A.Fettweis, Int. J. Numerical Modelling, vol.5, pp. 183.201 (1992).
12. Y.Naka, et al., *IEICE Trans. Electron.*, vol.E81-C, pp. 305.314 (1998).

Optical Characterization of Planar Photonic Crystal Resonant Cavities with Elliptically-Elongated Veins

N. J. Florous, K. Saitoh, and **M. Koshiba**
Hokkaido University, Japan

1. Introduction

Photonic crystals (PCs), are engineered materials in which, the refractive index modulation gives rise to stop bands for electromagnetic waves within certain frequency window. The accurate modeling of PC devices is an ongoing challenge. Despite the fact that numerical techniques based on the finite difference time domain method (FDTD) or the finite element computational scheme (FEM) have attracted the attention of many research groups all around the world, analytical techniques such as the scattering matrix method (SMM) [1], can provide a rigorous simulation tool for the optical characterization of PC devices with cylindrical inclusions. Since elliptical elongations may have some intriguing propagation characteristics, we devote the present paper to introduce an extended scattering-matrix theory using rigorous series expansion in Mathieu functions [2], for the optical characterization of finite-sized PC architectures with elliptical elongated veins, such as PC resonant cavities. This generalized scattering matrix approach which will be presented for the first time, allows the full characterization of PC circuits with ellipticallyelongated veins, using modest computational resources, thus making the proposed method a versatile analysis tool, which can be considered an attractive competitor against the wide simulators used so far, based on the FEM or the FDTD numerical techniques.

2. Numerical Results

We mainly focus our analysis on medium-sized PC resonant cavities formed by GaN dielectric cylinders with permittivities $\epsilon_c = 6$, in triangular configuration embedded in air as shown in Fig. 1(a), with pitch constant $\Lambda = 720$nm, minor semi-axis b = 272 nm while the major semi-axis is considered variable. The resonance spectra for three different choices of the variable ellipticitye=a b can be seen in Fig. 1(b). From these results we can conclude that for this particular configuration the quality factor takes its maximum value ($Q \simeq 1890$) when the ellipticity becomes e=1.2, with an up-shift in the resonance peak of about $\Delta\lambda_{res} \cong 70$ from the perfectly circular case. The elongated stretched action from the perfectly circular case can be therefore effectively used in designing compact resonant cavities with optimized quality factor, mainly for optimizing the performance of PC-based cavity lasers.

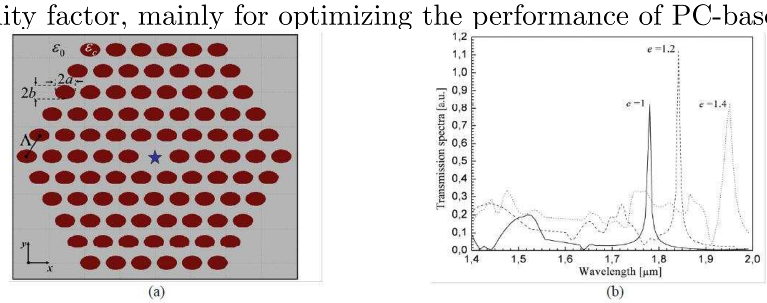

Figure 1: (a) Photonic crystal resonance cavity in triangular configuration, and (b) its resonance spectrum, for three different choices of the variable ellipticity e=1 (solid line), e=1.2 (dashed line), and e=1.4 (dotted line). The quality factor takes its maximum value when the stretched elongation factor of the ellipticity deviates from the circular case by e=1.2 (dashed line), with an estimated quality factor of about $Q \simeq 1890$.

REFERENCES

1. R. C. McPhedran, L. C. Botten, A. A. Asatryan, N. A. Nicorovici, P. A. Robinson, and C. M. Stekre,gCalculation of electromagnetic properties of regular and random arrays of metallic and dielectric cylinders,h *Phys. Rev. E.*, 60, 7614-7618, (1999).
2. P. M. Morse and H. Feshbach, Methods of Theoretical Physics. New York: Mc-Graw Hill, 1953.

Calculation of the Green's Function in Presence of Three-Dimensional Photonic Structures

B. Gralak
CNRS, Institut Fresnel, France

The Green's function in presence of three-dimensional woodpile structure is the solution E_ω of the equation

$$[\omega^2 \epsilon\mu - \mu\Delta \times \mu^{-1}\Delta\times]E_\omega = -\omega^2 \mu P\delta \tag{1}$$

where $\omega = lim_{\eta\downarrow 0}(\omega + i\eta)$ is the frequency (real number), ϵ is the permittivity, μ is the permeability, and the right side is the gpoint current sourceh: the latter is defined from a constant vector $\mathbf{p}$ in $\mathbf{R}^3$ and from δ, the three variables Diracfs distribution [$\delta(f) = f(0)$ for all gadmissibleh function $f : \mathbf{R}^3 \ni x \longmapsto f(x)$]. Let (e_1, e_2, e_3) be an orthonormal basis: every vector x in $\mathbf{R}_3$ is repaired by its

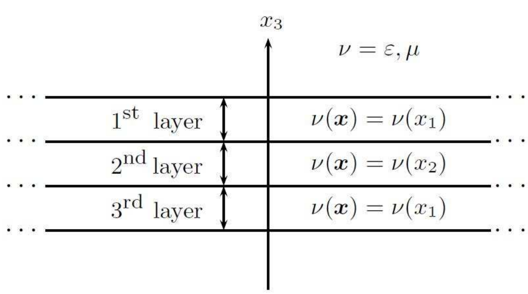

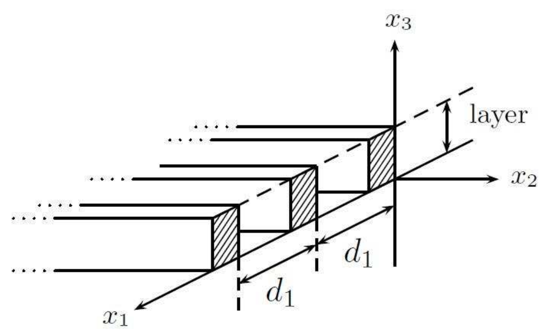

three components x_1, x_2 and x_3. Then a woodpile structure is defined as a stack in the direction x_3 of layers where " and μ are single variable periodic functions, this single variable being x_1 or x_2 (see the left figure, above): if this stack contains a finite number of layers, then the structure is a grating (for example, the structure is made of 3 layers on the left figure); if this stack is infinite, then the structure is a photonic crystal. In practice, each layer is made of periodically spaced and parallel infinite rods with rectangular cross section (on the right figure, " and μ are x_1-dependent functions with period d_1 and the unit cell of the layer is made of two rods): functions "and μ are piecewise constant.

The calculation of the Green's function requires a priori too huge computational time. However, this solution is very interesting since it provides the local density of states as well as the electromagnetic field radiated by a point light source.

I present shortly the method elaborated to solve this difficult problem. It is a combination of the gexact eigenvalues and eigenfunctionsh method together with the gtransfer matrixh method: both methods have been rigorously extended to woodpile structures. The first method is based on the use of a suitable basis leading to a fast convergence when compared to the use of Fourier basis. The second provides the possibility to integrate analytically in the gstacking directionh: the three-dimensional integration is reduced to a two-dimensional integration numerically.

Finally, I show numerical results obtained in the case of three-dimensional woodpile structures: the local density of states as a function of frequency ω or position x, and the map of electromagnetic field radiated by a point current source. In particular, I show the influence of a photonic bandgap on the local density of states, as well as the electromagnetic field radiated by a point current source in the presence of a slice of a woodpile crystal.

REFERENCES

1. B. Gralak, M. J. A. de Dood, G. Tayeb, S. Enoch and D. Maystre, gTheoretical study of photonic bandgaps in woodpile crystalsh, *Phys. Rev. E* 67, 066601 (2003).

Session 2P6
Electromagnetic and Optical Wave Technologies for Communications and Sensing

On Position and Attitude Determination in Bistatic SAR

S. Knedlik
University of Siegen, Germany

Starting with suggestions of passive micro-satellites that are simultaneously receiving signals transmitted from an existing spaceborne radar (e.g., Cartwheel [1], Pendulum [2]) for SAR Interferometry, bi- and multi-static SAR has become of rapidly increasing interest to the science community in recent years. Advantages of such configurations in comparison to usual monostatic SAR are the provision of additional information due to the bistatic reflectivity of targets, SAR imaging in along-track direction as well as the reduced vulnerability in military systems. Various combinations of carrier platforms for mounting transmitter and receiver antennas are possible, for instance satellites, airplanes and towers. Despite remarkable progress in the derivation of appropriate novel processing algorithms (e.g., [3], [4]) and in the development of the required technology, bistatic SAR imaging is far away from being operational, that is there are a lot of issues in research.

It is known that in case of SAR interferometry there are stringent requirements on base-line estimation and orbit determination, respectively (cf. [5]). Furthermore, in bistatic and multi-static configurations position and attitude determination is an important issue to guarantee an overlapping of transmitter and receiver antenna footprints (by appropriate antenna steering) during the mission. Moreover, for geo-referencing and for parameter estimation (for processing of the raw data) accurate knowledge of the position is needed.

In this paper we consider position and attitude determination with respect to future bistatic experiments which are under way.[1]Two possible constellations (airborne/airborne and satellite/airborne) are considered. In case of the planned hybrid (satellite/airborne) experiment, where the satellite has an orbit velocity of about 7.6 km/s compared with only 0.1 km/s of the airborne platform, there will be a difference in the velocities of both antenna footprints in the order of 70. Moreover, due to the high velocity of the satellite (TerraSAR-X), the overlap of the antenna footprints will be just a few seconds in maximum. We derive the requirements regarding position and attitude knowledge (e.g., with respect to accuracy, real-time capability, absolute vs. relative positioning). The focus of the proposed position and attitude determination strategy is to meet the requirements at low-cost. Therefore a sensor network . consisting of GNSS receivers and low-cost INS (gyroscopes, acceleration sensors) . is suggested. Several steps of a data fusion approach based on dynamic modeling and Kalman filtering, which allows optimal integration of redundant position and attitude information, are presented in detail.

REFERENCES

1. Massonnet: 'Capabilities and Limitations of the Interferometric Cartwheel,' *IEEE Transactions on Geoscience and Remote Sensing*, Vol. 39, No.3, pp. 506-520, 2001.
2. Moreira, Krieger, Mittermayer: 'Comparison of Several Bistatic SAR Configurations for Spaceborne SAR Interferometryf, IGARSS'01 (IEEE 2001 Geoscience and Remote Sensing Symposium), 2001, Sydney Australia
3. O. Loffeld, H. Nies, V. Peters, and S. Knedlik, 'Models and Useful Relations for Bistatic SAR Processing,' *IEEE Transactions on Geoscience and Remote Sensing*, vol. 42, no. 10, pp. 2031-2038, 2004.
4. K. Natroshvili, O. Loffeld, H. Nies, A. Medrano Ortiz, and S. Knedlik, 'Focusing of General Bistatic SAR configuration data with 2D Inverse Scaled FFT,' *IEEE Transactions on Geoscience and Remote Sensing*, in press
5. S. Knedlik, O. Loffeld, H. Nies: 'Sensitivity of DEMs generated from Interferometric Cartwheel Configurationsf, IGARSS'03 (IEEE 2003 Geoscience and Remote Sensing Symposium), 2003, Toulouse, France
6. J.H.G. Ender, O. Loffeld, et.al. 'Bistatic Exploration using spaceborne and airborne SAR sensors . A close collaboration between ZESS and FGANf, IGARSSf06 (IEEE 2006 Geoscience and Remote Sensing Symposium), 2006, Denver, USA, submitted

[1]Experiments based on FGANfs PAMIR (Phased Array Multifunctional Imaging Radar) system and TerraSAR-X (Germanyfs national remote sensing satellite which will be launched in June 2006; scientific utilization coordinated by German Aerospace Center (DLR)) are in preparation in a large coordinated joint package project between ZESS and FGAN, funded by the German Science Foundation (DFG) [6]. Position and Attitude Determination is a part of it.

Transmission Characteristics of UART-CSMA/CD Control Network with One-chip Microcontroller and RS485 Driver IC

C. Ninagawa, K. Yokohama, F. Aoi, and **H. Otake**
Mitsubishi Heavy Industries, Ltd., Japan
Y. Miyazaki
Aichi University of Technology, Japan

1. Introduction

In development of control networks for consumer products such as air-conditioning systems, the most important factor is hardware cost. Our goal is to realize a CSMA/CD (Carrier Sense Multiple Access with Collision Detection) network architecture without a network interface card, instead, with only a one-chip microcontroller and a signal driver IC.

2. UART-CSMA/CD Our proposed collision detection method requires only the UART (Universal Asynchronous Receiver Transmitter) built in the microcontroller as shown in Fig.1. Since an UART has a capability of receiving selftransmitting data simultaneously, our protocol software checks every self-transmitting byte data if the data has collided or not.

Taking an air-conditioner control network as an example, design specifications of our UART-CSMA/CD architecture have been set up as following. The electrical signal standard is RS485, the maximum length of the transmission line is 1000 m, and the maximum number of controllers (i.e. nodes) is 48. These specifications are quite reasonable for ordinary consumer products[1]. The RS485 signal standard was chosen because its differential voltage signal on the twisted pair of lines is robust for incoming electromagnetic noise.

3. Signal Transmission Since this network has to be installed in the most inexpensive way, any line termination impedance is without consideration. As the line length is very long (1000 m), influence of the signal reflection at the line terminal was investigated. The calculation of the step response for a distributed constant circuit model predicts existence of a "kink" in the rising part of the one-bit pulse waveform as shown in Fig.2. In the case of a typical twisted pair cable of 1000 m, the calculated width of the kink has been 17μ s. The experimental results confirmed this phenomenon. Since an UART receiver reads a bit signal at the 50 % point of the pulse, we decided the bit rate as 9.6 kbps.

4. Performance At this bit rate, communication performance has been evaluated by computer simulation as throughput and average delay in the case of 48 nodes each has Poisson distributed packet offered load. The reason to use Poisson distribution here is that it can be used as the approximation of many real processes[2]. The maximum throughput was 0.6, i.e. 60% of utilization of the transmission line. This performance is satisfactory for a random access protocol and for our challenge to the minimum hardware resource architecture. Experiments by actual printed circuit boards have confirmed the simulation results. In addition, conducted noise emission level was measured, and confirmed it was very lower than that of Ethernet.

5. Conclusion As overall, our proposed UART-CSMA/CD architecture is satisfactory for control networks whose cost is the most important factor.

REFERENCES

1. C.Ninagawa, F.Aoi, K.Yokohama, and T.Yoneda, "Distributed algorithm for signal polarity adjustment for air-conditioner control network," *Trans.IEE Japan*, Vol. 123-C, No.5, pp.919-927, 2003 (in Japanese).
2. S.Li and Y.Miyazaki, "A performance analysis of buffered DQDB network with request arrival process depending on its request counter value and its location on the buses," *IEICE Trans. Commun.*, Vol.E81-B, No.3, pp.493-502, 1998.

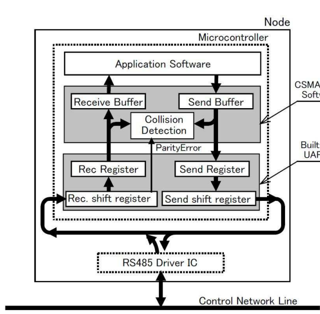

Figure 1: UART-CSMA/CD architecture

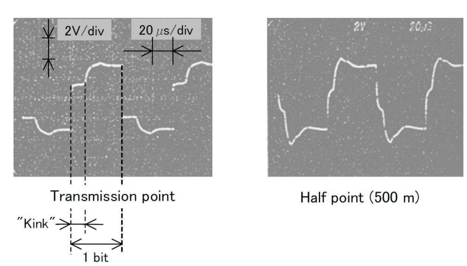

Figure 2: Differential voltage signal waveforms (No line termination impedance)

A Reconfigurable Quadri-Polarization Diversity Aperture Coupling Patch Antenna

Y. F. Wu, C. H. Wu, D. Y. Lai, and **F. C. Chen**
National Chiao Tung University, Taiwan

This paper presents a reconfigurable polarization diversity patch antenna, which can provide four polarization states either in a dual-linear polarization state or a dual-circular polarization state. This printed reconfigurable patch antenna was designed on two stacked low-priced FR-4 substrate of thickness 0.8 mm with a relative permittivity 4.4 to operate at 2.4GHz for the Wireless Local Area Network (WLAN) applications. Also, the substrate of the radiating patch and the substrate of the ground plane are separated by an air layer of thickness h=1 mm. The proposed antenna with two excitation ports consists of a square radiating patch on the top substrate, the two apertures on the ground plane and the feeding network under the ground plane were printed on the different side of the same dielectric substrate. The feeding network consists of the quadrature hybrid, five DC block capacitors with C=100pF, three RF choke inductors and eight pin-diodes to produce different excited paths. The quadrate hybrid can provide a 90 degrees phase difference with same magnitude to produce circular polarization states.

The proposed antenna is divided into two functional blocks: The inner functional block contains a quadrature hybrid which can produce dual-circular polarizations; while the outer functional block contains the dual parallel lines can result in dual-linear polarizations. By controlling the bias voltage of the inner pin-diodes properly, we can create a signal path from port 1 and port 2 that can generate a left-handed or a right-handed circular polarization. On the other hand, we control the outer pin-diodes properly to produce a pair of orthogonal linear polarizations state. Therefore, we can switch the polarization diversity state easily by controlling the DC bias voltage of the eight pin-diodes.

In conclusion, a reconfigurable patch antenna which can generate a pair of orthogonal linear polarizations or a pair of orthogonal circular polarizations would become a good candidate for future MIMO communication systems. Both the numerical and experimental results will be presented to validate our design. The detail design process and working principle will also be discussed in this presentation.

Bi-Directional Optical Transceiver Module Fabricated by 3-D Polymer Optical Waveguides for Visible-WDM Plastic Optical Fiber Communication

M. Kagami, M. Yonemura, A. Kawasaki, and **S. Kato**
Toyota Central R&D Labs., Inc., Japan
Y. Inui
Toyoda Gosei co., Ltd., Japan

Visible light sources are now being used in in-vehicle and in-house network applications, bringing advantages in both visibility and workability. In particular, current trends and subjects affecting the key devices used in these networks, such as visible light sources, optical fibers, optical circuits and transceiver modules, has been desired. We developed a polymer optical waveguide module [1]) that realizes bi-directional communication over a single plastic optical fiber (POF) with dual visible wavelength LED light sources, as shown in Fig. 1. The module is constructed using light-induced self-written (LISW) waveguides [2]), which enables a three-dimensional optical circuit for visible-WDM (wavelength division multiplexing) to be fabricated by an extremely simple process. We fabricated a module including a newly-designed WDM filter that was optimized for multimode waveguides, and we demonstrated 250Mbit/s communication using a pair of these modules that each contained one green ($\lambda = 495nm$) and one red ($\lambda = 650nm$) LED light sources by measuring the bit error rates (Fig.2). The results indicated that the system could transmit over more than 20m of POF in full-duplex mode.

REFERENCES

1. Yonemura, et al, *Opt. Letts.*,30, 2206 (2005).
2. M.Kagami et al., *Appl. Phys. Lett.*, 79, 1079 (2001).

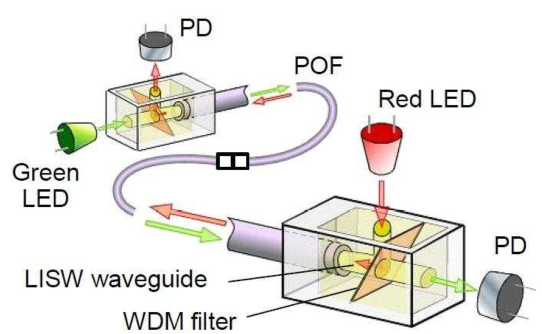

Figure 1: Diagram of bi-directional singlePOF communication using the polymerwaveguide modules.

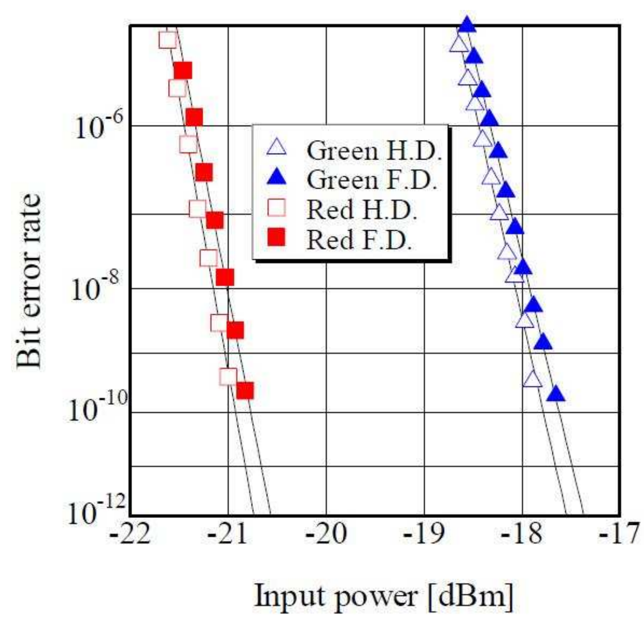

Figure 2: Results of the BERmeasurements. H.D.: Half Duplex,F.D.: Full Duplex.

Code Recognition Chracteristics in Optical Label Matching with Integrated-Optic Collinear Acoustooptic Devices

N. Goto
Toyohashi University of Technology, Japan

Y. Miyazaki
Aichi University of Technology, Japan

Collinear acoustooptic (AO) switch has a feature of wavelength-selective switching for WDM signals. [1,2] This feature can be used for photonic packet routing in WDM photonic networks. In this paper, application of the waveguide-type collinear AO switches to label recognition processor in photonic routing system is investigated. Optical label is supposed to be encoded in time and spectral domains. Collinear AO switches are considered to be used for label recognition by using multiple wavelength switching with rf control signals at multiple frequencies. By employing a combination of encoding in spectral and time domains, flexibility in routing control, and the number of represented labels can be increased. [3,4]

The code matching is a fundamental function to be required in label recognition. The processing of label recognition with collinear AO devices has the following advantages: (1) the processor can be formed as compact integrated optical circuits, (2) the label to be recognized can be easily changed within a relatively short time such as a few μs, (3) parallel processing for any combination of multiple wavelengths can be performed with a single AO module, and (4) although the output signal of the label recognition processing is obtained as an electric signal, the code matching processing is done optically and as quickly as in nano seconds. The output electric signals are electrically post-processed and then used to control optical matrix switches for packet forwarding.

It has been shown in our previous papers that orthogonal optical codes can be recognized. However, since only orthogonal codes were considered, the number of codes was as small as the number of the bits. In this paper, we investigate optical code matching characteristics in both spectral and time domains for optical binary codes using integrated-optic collinear AO devices. In particular, optical codes representing routing labels are investigated from a viewpoint of increasing the number of the codes. It is found that a half of binary BPSK codes in time domain can be recognized. Crosstalk in the code matching is also discussed.

REFERENCES

1. T. Kondo, Y. Miyazaki and Y. Akao: *Jpn. J. Appl. Phys.* **17** (1978) 1231.
2. N. Goto and Y. Miyazaki: *IEEE J. Selected Areas Commun.* **8** (1990) 1160.
3. N. Goto and Y. Miyazaki: *Jpn. J. Appl. Phys.* **44** (2005) 4449.
4. N. Goto and Y. Miyazaki: *IEEJ Trans.* EIS **125** (2005) 1784 [in Japanese].

Stub-Loaded Ridge Waveguides for Frequency-Scanning Antenna Application

M. Tsuji and **H. Deguchi**
Doshisha University, Japan

Stub-loaded ridge-rectangular waveguides of an open type are a candidate of millimeter-wave antennas[1]. These waveguides can easily produce a radiation in a single polarization along their length due to a leaky mode, possess flexibility in beamwidth, and scan the angle of maximum radiation by changing the frequency. Furthermore, their guide width can be reduced to less than a half wavelength by the ridging effect, so that for use of a scanning array antenna, extra main beam due to a grating lobe can be avoided. Figure 1 shows our recently developed stub-loaded ridge waveguide[2], which overcomes the drawback of the conventional one that the channel-guide leaky mode[3] propagates simultaneously together with the desired leaky mode and affects the radiation field. This guide has both a ridge and a stub guide on the same side, different from the conventional guide that they are set each other on the opposite side.

In this paper, we first investigate the guide structure to construct a leaky-wave antenna with low sidelobes that requires to keep the phase constant the fixed value and then to vary the leakage constant over the wide range along an antenna axis. The guide structure includes many conductor edges at which the fields diverge, so its leakage characteristics are accurately calculated by the modified mode-matching method incorporating the singular field behavior into the aperture-field expressions[1]. As a result, we find the effective structure, in which both the stub and the ridge are set symmetrically in the y direction and the lengths b2 and b3 are adjusted asymmetrically. Then we design an antenna with the beamwidth of 5 degrees and the Taylor distribution of -30dB sidelobes. The structure of the designed antenna and its radiation characteristics will be presented at the talk.

Furthermore, we investigate the excitation problem of this stub-loaded ridge guide. It is one way for the excitation to use the taper transition between this guide and the standard rectangular waveguide, but such transition becomes too long. Fortunately, if this guide is shorted at the aperture plane of the open end, its impedance value is almost same with that of the coaxial cable. As a result, we do not need a matching section for the coaxial feed, different from the case of the standard rectangular waveguide. The transmission and the radiation characteristics including the coaxial feed are calculated by the finite-element method, and their numerical results and experimental results for the fabricated antenna will be presented at the talk, too.

REFERENCES

1. M. Tsuji and H. Shigesawa, "Leakage properties of stub-loaded ridge-rectangular waveguides," IEICE Trans. Electron., vol. E88-C, no. 5, pp. 1853-1859, May 2005.
2. M. Tsuji, M. Tani, H. Deguichi, and H. Shigesawa, "Stub-loaded ridge waveguide of single-mode operation for use of leaky-wave antennas," Proc. Internfl Sypm. Antenna Propagat., vol. 1, pp. 197-200, Aug. 2004.
3. H. Shigesawa, M. Tsuji, P. Lampariello, F. Frezza, and A. A. Oliner, "Coupling between different leaky-mode types in stub-loaded leaky waveguides"h IEEE Trans. Microwave Theory Tech., vol. MTT-42, no. 8, pp. 1548-1560, Aug. 1994.

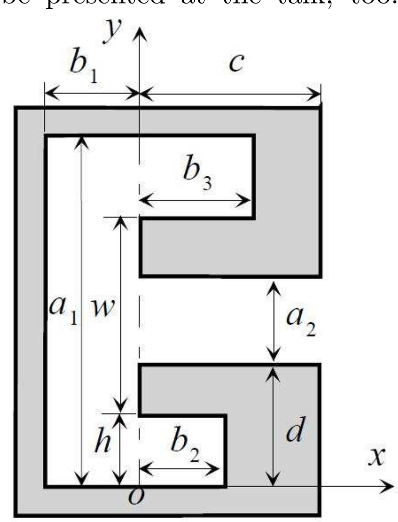

Figure 1: Cross-section view of a stub-loaded ridge waveguide.

Theoretical Analysis of Propagation characteristics in Medium Waves tTransmission from the Top of the Mountain

Y. Norimatsu
Nankai Broadcasting Ltd., Japan

K. Ono and **M. Matsunaga**
Ehime University, Japan

The transmitting station of the medium wave band is usually set up in the plains where the electric conductivity is essentially high. It causes electromagnetic environmental problems around the transmission place in the urban areas. The propagation characteristic of the medium wave band from transmitting station on the top of mountain has not been clarified though it is necessary to consider setting up the transmitting station in the mountain areas in which geographical features like Japan are complex. However, the researches on transmitting radio waves from the top of mountain are very few as far as the authors know. There are two main reasons. One is the propagation characteristics from transmitter to recievers as stated above. The another reasion is that the conductivity of mountain area is too low for efficient emission of radio wave.

Furutsu had presented the theory that handles an electric characteristic of earth and irregular terrain at the same time[1],[2]. In this report, the Furutsu's theory is applied to the analysis of propagation characteristic of the medium wave transmitted from the antenna on the top of a mountain. The mountains are modeled by the plateau of arbitrary hight with lower conductivity than those of plains. Numerical results thus obtained by our model verify that the field strengths at the propagation distance are nearly the same or even higher than those from transmitters setting up in the plains.

It is necessary to verify the radiation efficiency for lower electric conductivity at transmission place and the propagation characteristic in medium waves transmission from the top of mountain. An experimental verification is now being planned as a practical matter.

REFERENCES

1. K.Furutsu:On the theory of Radio Wave Propagation Over Inhomogeneous Earth., *J. Res. Nat. Bur. Stand.*, Vol.67D, No.1, pp.39-62(Jan-Feb, 1963).
2. K.Furutsu, R.E.Wilkerson, R.F.Hartmann: Some Numerical Results Based on the Theory of Radio Wave Propagation Over Inhomogeneous Earth., *Radio Science,* Vol.68D, No.7, pp.827-846(July, 1964).

Performance Limitations in CATV Networks Employing WDM System Due to Optical Fiber Nonlinearities

R. Balasubramanian[1], **Y. Miyazaki**[2], and **M. Kondo**[1]
[1]Synclayer, Inc., Japan
[2]Aichi University of Technology, Japan

Wavelength division multiplexing (WDM) technology has been given wide attention in the broadband optical networks in order to utilize the enormous bandwidth of the optical fiber. However, when optical waves of several signals having strong power over 5dBm, there arise many optical fiber nonlinear effects that lead to coupling crosstalk phenomena between several signals and limit the ultimate WDM network performance [1,2]. Typical wavelength band used in these networks is between 1310 nm and 1550nm. Subcarrier multiplexed optical systems have traditionally been used for cable television (CATV) distribution, and system operators have deployed narrow casting systems to serve different analog contents to different subscribers. More recently, in the access networks, systems are upgraded to handle two-way communication of voice, data and analog video overlay through WDM as in the case of Passive Optical Network (PON) system. When relatively strong optical signals of multiple wavelengths propagate along a single optical fiber, fiber nonlinearities lead to crosstalk between the signals of several wavelengths. The dominant fiber nonlinearities are stimulated Raman scattering (SRS) and cross phase modulation (XPM).

SRS in WDM systems is due to nonlinear coupling effect corresponding to optical pumping effect and thus the modulated optical signal causes modulation of all other co-propagating signals by pumping effect. XPM effect arises from the nonlinear refractive index of the fiber material, and thus the power of the modulated channel induces small change in the refractive index and in turn phase modulation of all other wavelength channels. We studied the SRS and XPM effects in the WDM system used in the CATV network.

We conducted experiments with dual wavelength WDM system with fiber lengths of 20km, where 1490nm and 1550nm are used for the downstream data and analog video transmission with the respective optical power of 10dBm and 15dBm.

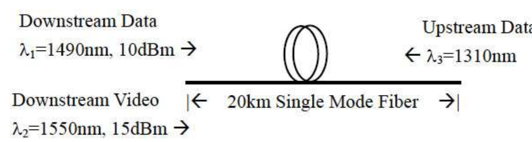

Figure 1: CATV network using WDM system

The data optical signal wave of wavelength at 1490nm will act as the pump wave, and when modulated, optical wave of this wavelength induces crosstalk on the video channel. We experimentally measured the crosstalk levels at the 1550nm video channel by modulating optical wave of the 1490nm data channel with the frequency range between 70 to 770MHz, which is typically used for CATV video distribution. We compared the measured data with the theoretical prediction and find good agreement between the results.

The SRS effects are predominant in the lower CATV carrier frequency range and the XPM effects are dominant in the higher frequency range. The overall measured crosstalk level is a combination of both of these nonlinear effects. We also studied the crosstalk levels with respect to the transmission system. A maximum of 20km transmission is typically used in the present FTTH systems. We analyzed how the crosstalk level varies with respect to the transmission distance. We discuss the major factors that affect the system performance and how these can be overcome in a practical system where a crosstalk level of less than -60dB is required.

REFERENCES

1. G. P. Agrawal, Nonlinear Fiber Optics, 3rd ed. (*Academic Press,* San Diego, 2001).
2. M.R.Phillips and D.M.Ott, "Crosstalk due to optical fiber nonlinearities in WDM CATV lightwave systems", *J.Lightwave Technol.*, vol.17, pp.1782-1791, 1999.

Electromagnetic Analysis of Circular Waveguides for Tera Hertz Transmission Using Conformal Mapping

Y. Miyazaki
Aichi University of Technology, Japan

Extremely high radio frequency technology of Tera Heltz frequency band is rapidly developed recently, particularly for electromagnetic wave generation of Tera Hertz frequency band[1]. These frequency bands are between Giga Hertz frequency band of millimeter waves and near optical band of infrared waves. However, transmission waveguides for Tera Hertz frequency bands have not been studied. Tera Hertz Signal Transmission of the TE_{01} mode in circular waveguide may be available for spectroscopic measurement and communication. The TE_{01} mode of circular waveguide has been enough investigated for low loss transmission of 50 G Hertz millimeter waves[2-4]. In this paper, the TE01 modes in circular waveguides with a few mm radius of over sizes are discussed for Tera Hertz electromagnetic waves of less than 300μm wavelength.

The TE01 modes have low loss characteristics for large radiuses of circular waveguides compared with wavelengths of Tera Hertz electromagnetic waves and are proportional to inverses of three powers of radiuses and roots of frequencies, when conductors of waveguide walls have non-dispersive conductivities. If conductivities of waveguide wall metals have dispersive characteristics in the Tera Hertz frequency bands and complex dielectric constants, attenuation characteristics are very different from those of millimeter wave cases.

When copper waveguide wall has conductivity of $\sigma = 5800 \times 10^7$ S/m, and radius of circular waveguide is 5 mm, attenuation constant of TE01 mode at 1 THz is 18 dB/km. Effects of dispersion characteristics of materials of waveguide wall should be studied for Tera Hertz frequency bands and less than 300μm wavelength.

In curved circular waveguides, the TM_{11} mode is generated from the TE01 mode as a spurious mode and the phase constants of these TE_{01} and TM_{11} modes are same propagation constants. Electromagnetic fields in curved circular waveguides are studied by conformal mapping method and integral equation with Green's functions. In order to avoid strong mode conversions at curved sections of circular waveguides, dielectric coated waveguide are available. However, dielectric losses at Tera Hertz frequency band should be considered for polymer plastics.

Mode conversions at waveguide imperfections at junctions such as offsets, tilts and deformations of circular cross sections are also discussed by using conformal mapping method. Miss matches of the order of μm yields large mode conversions.

Statistical characteristics of the TE_{01} mode propagation in circular waveguides are shown for irregular bends and random surfaces of waveguide walls. Randomness of the order of μm on the waveguide wall leads to large mode conversions and transmission losses. Mode filters of helical circular waveguides and mode transform converters are also discussed.

Based on this theory, electromagnetic technologies of the Tera Hertz frequency and wavelength of less than 300μm could be developed, particularly for transmission of communications and spectroscopic measurements.

REFERENCES

1. B. Ferguson and X.C. Zhang, Nature Materials, Vol. 1, pp.26-33 (2002).
2. K. Udagawa and Y. Miyazaki, Jour. of IECE, Japan, Vol.47, No. 8, pp.1186-1195 (1964).
3. K. Udagawa and Y. Miyazaki, Jour. of IECE, Japan, Vol.49, No.12, pp.2407-2417 (1966).
4. Akao and Y. Miyazaki, Trans. of IECE, Japan, Vol. 51-B, No. 11, pp.553-558 (1968).

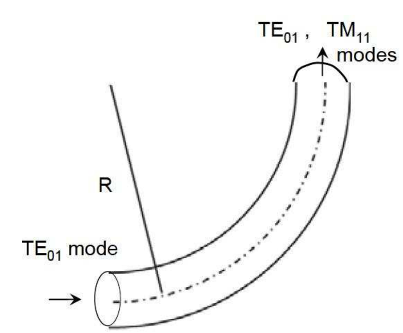

Figure 1: Mode conversions at curved circular waveguides

Long-Pulse Tunable Micro-Rod Yb:YAG Laser for Sensing Applications

R. Bhandari and **T. Kamiya**
SUNX Limited, Japan
T. Taira
Institute for Molecular Science, Japan

Long-pulse operation of solid state lasers is desirable for a number of applications. These include cases where a narrow transform-limited spectral width is desirable, such as in lidar and laser doppler velocimeter measurements. Other applications are efficient tunable laser radiation transmission through fibers for remote spectroscopy and medical uses, such as, laser diagnostics and phototherapy.

Long-pulse laser operation can be obtained by using very long cavities, or through careful electronic control of the loss of a continuously variable Q-switch [1]. However, there are limitations on the pulse width ($< 1\mu s$) and stability problems in these approaches. Here, we propose, a novel method for achieving long-pulse operation by operating the laser at a wavelength exhibiting low laser gain, and demonstrate its feasibility in a Q-switched, tunable Yb:YAG laser.

The schematic of a tunable Q-switched Yb:YAG laser structure proposed by us earlier is shown in Fig. 1 [2]. Using a double-plate birefringent quartz filter for wavelength tuning, we could obtain continuous tuning over the wavelength range 1029 1056 nm at a repetition rate of 10 kHz. Yb:YAG exhibits a varying gain over this wavelength range, which results in stretching of the Q-switched pulse. The pulse width varies from 0.12 s at 1029 nm to 3.6 s at 1056 nm. The results of wavelength tuning and pulse stretching are shown in Fig. 2.

Further, by inserting an etalon in the laser cavity, we could obtain single axial mode operation, having a spectral width of 720 MHz, at 1056 nm. The average power was 170 mW at 10 kHz.

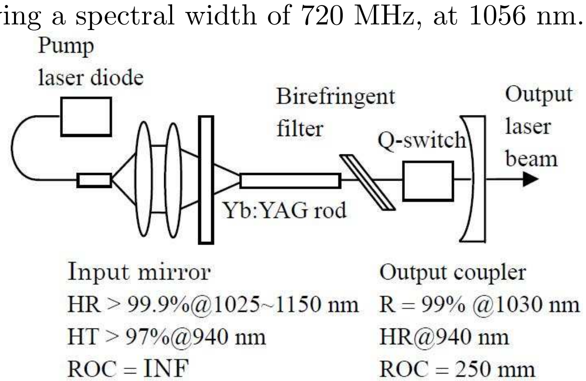

Figure 1: Schematic of the tunable Q-switched Yb:YAG laser

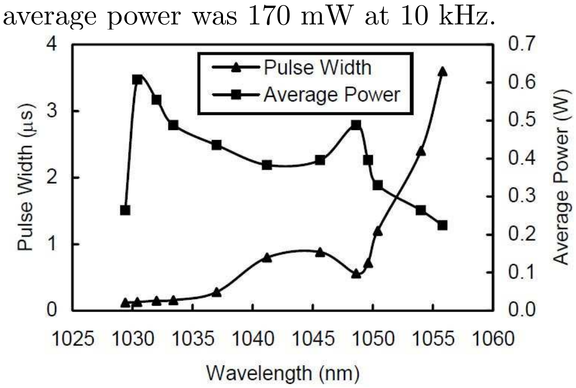

Figure 2: Laser tuning and pulse stretching characteristics

We have reported a new approach for the generation of long pulses. We have also demonstrated its feasibility in a tunable, micro-rod Yb:YAG laser structure, obtaining Q-switched pulses of 3.6 s width. This laser can be used as a seed in a MOPA configuration for obtaining a high power, long-pulse laser.

This laser will be extremely useful for a variety of applications, such as, lidar, laser doppler velocimeter and fiber-coupled laser diagnostic equipment for medical applications.

REFERENCES

1. 1. W. E. Schmid, "Pulse stretching in a Q-switched Nd:YAG laser," *IEEE J. Quantum Electron.* QE-16, 790-794 (1980).
2. 2. R. Bhandari, T. Kamiya, and T. Taira, "Widely tunable CW and Q-switched operation of thin-rod Yb:YAG laser," in Technical Digest of Conference on Lasers and Electro-Optics (CLEO 2005, Baltimore, USA, May 22-27, 2005), paper CMA6.

Radiation Characteristics of Meander Line Antennas with Planar Coupled Parasitic Meander Elements for RFID Tags

K. Taki [1] and **Y. Miyazaki** [2]

[1]Brother Industries, Ltd., Japan
[2]Aichi University of Technology, Japan

Radio frequency identification (RFID) technology using UHF bands is rapidly developing for automatic identification and small tag antennas are required for the purpose of reducing the tag sizes. An RFID tag consists of an antenna and an IC chip. Since passive RFID tags get all the energy needed to operate from the electromagnetic wave transmitted by readers, proper impedance match between the antenna and the IC is very important. The antenna should be directly matched to the IC without adding any external matching networks due to cost and fabrication issues. In the UHF band, especially below 1 GHz, meander line antennas are an attractive choice. However, the input resistance of small meander line antennas is too low and it is difficult to achieve direct impedance match.

In this report, meander line antennas with planar coupled parasitic meander elements have been proposed in order to increase the antenna input resistance and the radiation characteristics have been investigated by using the method of moment. A parasitic meander element is placed close to a driven meander element in the same plane and each convex section of the parasitic element is surrounded with that of the driven element as shown in Fig. 1 because this planar configuration is convenient to RFID tags and the total occupied area is small. The antenna input resistance and the resonant frequencies can be controlled with the convex section width of the parasitic element,w_2, and the spacing between the adjacent convex sections of the driven and parasitic elements, w_3.

The antenna length w0 was chosen to be about 0.2λ at 915MHz. When $w_1 = 5mm$ and $w_2 = w_3 = 0.5mm$, the input resistance was 55Ω which was five times larger than that without the parasitic element. The current distributions along each meander element and the radiation patterns are also investigated.

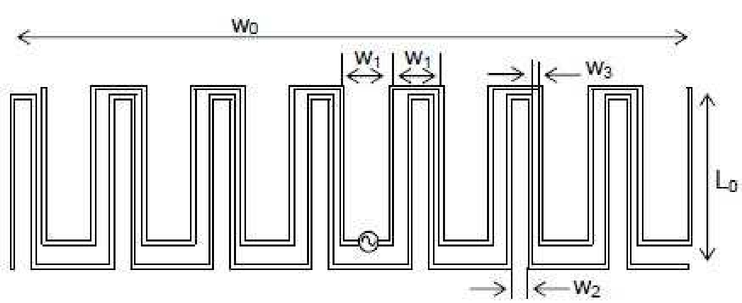

Figure 1: A meander line antenna with a parasitic meander element

Session 3A1
Microwave Phenomena on Superconductors I

Pulsed Tera-Hertz Radition from Femto-second Laser Excited Superconductive $YBa_2Cu_3O_7$ Antenna

S. S. Pai and **C. C. Chi**
National Tsing Hua University, Taiwan

We have observed the ultrashort electromagnetic pulse radiation from a current-biased bow-tie structure of $YBa_2Cu_3O_7$ thin film dipole antenna on MgO using 100 fs, 750 nm laser pulses. With the electro-optic detection, we obtained the THz pulses with 1.0 ps full width at half maximum, containing frequency components up to 1.0 THz. The THz peak amplitude dependence shows the saturation and a nonlinear behavior with a higher excitation pumping power and with the applied bias currents. The saturation on the dependence with the excitation powers exhibits the bolometric heating in nature. However, the nonlinear characterization of the THz radiation from the superconductive thin film antenna revealed that the inadequacy of pure supercarrier approximation on a two-fluid model. The ultrashort transient response and the deviation from the classical theory are discussed in relation to the quasiparticle dynamics of the nonequilibrium mechanism.

Theoretical Approach to Circular Polarization Dependence of Microwave-Induced Photoconductivity

T. K. Ng and **S. Wang**
Hong Kong University of Science and Technology, China

Recent measurements on the polarization dependence of the low field microwave photoconductivity and absorption of a two dimensional electron system revealed the notable immunity of the microwave induced resistance oscillations and the zero resistance regions to the sense of the circular polarization. Taking advantage of the general transport equation for the center of mass motion that provided an explanation to the radiation-induced Zero Resistance State, we further investigate the possibility of spontaneously generated motion in the system which we call slow mode. The result of a self-consistent calculation between the induced oscillation and the slow mode under low microwave field, is reported in this paper to explain the experimentally observed Polarization Insensitivity.

Critical Fluctuations in Superconducting $La_{2-x}Sr_xCuO_4$ Thin Films Studied by Frequency-Dependent Microwave Conductivity

T. Ohashi, H. Kitano, and **A. Maeda**
University of Tokyo, Japan

I. Tsukada
Central Research Institute of Electrical Power Industry, Japan

For high-T_c cuprate superconductors, large phase fluctuation effects in the underdoped region or the quantum fluctuation effects near the quantum critical point attracts much attention recently. Frequency dependence of microwave coductivity is a suitable probe to study these critical fluctuations, because the temperature and frequency dependences of the fluctuation-induced excess conductivity, $\sigma(T,\omega)$, provide the information of the correlation length and the characteristic time of the fluctuation. The critical exponents and universality class of the phase transition can be determined via a dynamic scaling analysis on $\sigma(T,\omega)$.

We measured $\sigma(T,\omega)$ of $La_{2-x}Sr_xCuO_4$ (LSCO) thin films with various Sr concentrations at the frequencies from 0.1 GHz up to 10 GHz using a microwave broadband technique.

All LSCO films showed a conductivity enhancement near T_c owing to the fluctuation effects. The temperature dependence of the superfluid density and the dynamic scaling analysis yielded the 2D-XY critical behavior for $x = 0.06$-0.14 and the 3D-XY critical behavior for $x = 0.15$-0.18. For the film with $x = 0.19$-0.24, a 2D-like behavior was observed again. The 2D behavior for the underdoped and overdoped region could be explained by the anisotropy and the size effect, respectively. However, the crossovers seem to be sharp though the interlayer coherence length is expected to change more gradually. Another interpretation is that the 3D behavior is attributed to the quantum fluctuation. The studis on the thickness dependence is now in progress to examine the size effect.

Precise Measurement of Frequency-Dependent Complex Conductivity of Superconducting Thin Film near Tc

T. Ohashi, H. Kitano, and **A. Maeda**
University of Tokyo, Japan

I. Tsukada
Central Research Institute of Electrical Power Industry, Japan

We present a non-resonant broadband technique to obtain the microwave complex conductivity of a metallic thin film as a function of the swept-frequency (from 50 MHz to 15 GHz) at any cryogenic temperature down to 10 K, by measuring both of the magnitude and the phase of the complex reflection coefficient, $S_{11}(\omega)$. The sample with the electric contacts which form a Corbino disk geometry is terminated by the end of a lossy coaxial transmission line through a modified 2.4 mm jack-to-jack coaxial adapter with a spring-loaded center conductor pin. For a precise measurement, it is quite important to calibrate the systematic errors included in the raw data of $S_{11}(\omega)$, which are mainly attributed to the change of the attenuation and phase-shift of the coaxial cable with increasing or decreasing temperature.

By applying this technique to several superconduting thin films, we measured the frequency dependence of the complex conductivity, $\sigma(\omega)(= \sigma_1(\omega) - i\sigma_2(\omega))$, of NbN and $La_{2-x}Sr_xCuO_4$ (LSCO) near T_c. We found that the usual calibration method using three known standards (open, short and load) was no longer useful in the vicinity of T_c, where $S_{11}(\omega)$ became very close to -1. This is because a very small error in the phase of $S_{11}(\omega)$ gives rise to an enormous error in the frequency dependence of both $\sigma_1(\omega)$ and $\sigma_2(\omega)$ when $S_{11}(\omega)$ is close to -1.

In this paper, we propose a new calibration method which is applicable in the vicinity of T_c. For both NbN and LSCO thin films, we succeeded in obtaining the excess conductivity due to the superconducting fluctuations, which showed a prominent divergent behavior in both $\sigma_1(\omega)$ and $\sigma_2(\omega)$ in the low frequency limit as the temperature approached T_c from above T_c. Details of the frequency dependence of the excess conductivity due to the superconducting fluctuations were analyzed by using a dynamic scaling theory of critical phenomena. We confirmed that the experimental results quantitatively agreed with the scaling theory very well, clearly indicating that our calibration method was quite useful in the vicinity of T_c.

We also discuss the influence of the dielectric substrate beneath the thin film sample, which is important for a thin film with less conductivity or thinner thickness, by using the 3D electromagnetic numerical simlations under the same boundary condition as for the above experimental probe.

Cu-Spin Dynamics in La2-xSrxCuO4 Probed by Zero-Field Muon Spin Relaxation

I. Watanabe[1], **T. Adachi**[2], and **Y. Koike**[2]

[1]RIKEN, Japan
[2]Tohoku University, Japan

A stripe model of spins and holes has been proposed to explain the mechanism of the high-Tc superconductivity[1)]. In order to understand the stripe model, we have been carrying out muon spin relaxation (μSR) experiments at the RIKEN-RAL Muon Facility and have been investigating the Cu-spin dynamics in $La_{2-x}Sr_xCuO_4$ within the μSR time window which is typically from 10^6 to 10^{11} Hz (Ref 2,3).

Figure shows zero-field SR time spectra of $La_{2-x}Sr_xCuO_4$ at x=0.115 where a statically stabilized stripes is expected below about 10 K. The time spectra were measured in high-temperature regions where stripes are dynamically fluctuating. The time spectrum in these temperature regions shows a typical Gaussian-shape as shown in the inset, meaning that the muon spin depolarizes by mainly nuclear dipole fields randomly distributed at the muon site. However, by means of precise measurements gathering higher statistics of muon events, we found a tiny change of the time spectrum started below about 100 K. After the analysis of time spectra, it was found that this tiny change was due to a change of the dynamical muon-spin depolarization behavior. This results in that the Cu-spin dynamics is expected to start to be suppressed below about 100 K at x=0.115. Taking into account that the carrier mobility in the normal state turned to be localized below the similar temperature region[4)], our present result could show a coupling of degree of freedoms between spins and holes which is an important scheme of the stripe model.

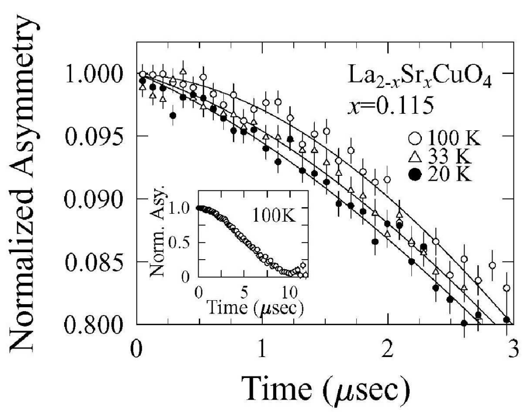

REFERENCES

1. J.M. Tranquada et al., *Nature (London)* 375 (1995) 561.
2. I. Watanabe et al., *J. Low Temp. Phys.* 131 (2003) 331.
3. I. Watanabe et al., *J. Mag. Mag. Matt.* 272-276 (2004) e1061.
4. G.S. Boebinger et al., *Phys. Rev. Lett.* 77 (1996) 5417.

Microwave Properties on $\mathrm{H_i - T_c}$ Superconductors

T. Endo, H. Zhu, A. K. Sarkar, and **A. Akiba**
A. Kamiya, H. Ooka, and **T. Morimoto**
Mie University, Japan

Soon after the discovery of High Temperature Superconductors (HTS), many researchers tried to measure magnetically modulated microwave absorption (MA) under magnetic field using conventional ESR apparatus. Then a lot of papers were published concerning MA on HTS. A mechanism of MA, however, was extremely complicated, so many people gave up to continue this research work. On the other hand, we have been keeping our efforts of MA research to utilize this technique widely to investigate variety of HTS materials such as granular bulks, single crystals and thin films. We have suggested nine individual mechanisms of MA such as viscous vortex motion, normal core microwave current and weak-link Josephson junction. These individual mechanisms were divided into two categories, vortex mechanism and screening current mechanism. The vortex mechanism is important in higher fields but MA always shows featureless spectrum in the high fields. On the contrary, it shows quite characteristic structures at very low fields. We are proposing the screening current mechanism, i.e., when a resultant current of screening current and microwave-induced current exceeds a critical current in a weak region or junction, then MA occurs. This is dominant in the low fields. We have tried to measure MAs on variety of HTS samples, and obtained one proposal that most of all the experimental results of MA in the low fields can be interpreted by this screening current mechanism. Therefore MA can give important views of the screening current and vortex state, solid or liquid. Because surface slope of flux distribution in a sample exactly depends on vortex state (solid or liquid), and MA is directly caused by the surface slope which is almost proportional to the screening current. On the base of this theory, we have obtained several important knowledge on HTS such as Reentrant Phase in Bi2212 single crystal. We will present such results and discussions in our Session.

Temperature Dependence of Microwave Absorption in Bi2212 Single Crystals

H. Ooka, A. K. Sarkar, A. Kamiya, K. Nakanishi, and **T. Endo**
Mie University, Japan

M. Shahabuddin
University of Jamia Millia Islamia, India

Introduction

High-temperature superconductors (HTS) are mostly expected for applications in high frequency devices, such as microwave filters used at base station of mobile phone system. It is important to elucidate characteristics of HTS at high microwave powers and temperature rise because they are use at high microwave powers in some case. In this work, we measured modulated Microwave Absorption (MA) spectrum on Bi2212 single crystals and studied microwave power dependence and temperature dependence of MA signal. We elucidated reentrant phase diagram by the results of temperature dependence of MA.

Experimental

We measured MA spectra of Bi2212 single crystals using cavity perturbation method under a magnetic field (Ha) sweep. We varied temperature (T) as a parameter, while measuring MA spectrum.

Results

From the temperature dependence of MA for the field configuration of Haab-plane, the spectrum contains first peak (P_1), Dip and broad peak (P_b). We obtained reentrant phase diagram by this results. The reentrant phase entrance is very narrow. It substantiates theoretically proposed reentrant phase diagram. For Ha//ab, the temperature dependences of the first peak signal intensity (S_{p1}) and field position (H_{p1}) give information about the Meissner phase. Those results suggest that the lower critical field line (H_{c1}) for Ha//ab is located at higher field side than for Ha⊥ab. This result and effectiveness of MA are examined now.

Microwave Power Dependence of Microwave Absorption in Bi2212 Single Crystals

T. Morimoto, A. K. Sarkar, A. Akiba
A. Nishio and **T. Endo**
Mie University, Japan

M. Shahabuddin
University of Jamia Millia Islamia, India

Introduction : High-temperature superconductors are mostly expected for the applications in high frequency devices such as microwave filters. It is important to elucidate the characteristic of high-temperature superconductor at high microwave power because of their uses for microwave antennas. We measured magnetically modulated microwave absorption (MA) on Bi2212 single crystals and studied a temperature dependence and a microwave power dependence of MA signal. In this paper, we report the microwave power dependence.

Experimental : We measured MA spectra of Bi2212 single crystals using cavity perturbation method under a magnetic field (Ha) sweep. We set sample temperature at about 77 K and varied microwave power (Pm) as a parameter, while measuring MA spectrum. We used different magnetic field configurations of Ha//c, Ha//ab and Ha//45^o in the measurements.

Results : MA spectra show big microwave power dependence. In Ha//c, a broad peak (Pb) and a dip shift to low magnetic field with increasing Pm. A first peak (P1) is very sharp, and shifted to high magnetic field with increasing Pm. For Ha//ab, the P1 peak is wider than for Ha//c and shifted to high magnetic field with increasing Pm too. In Ha//45^o, the dip is enhanced and Pb is shifted to high magnetic field with increasing Pm.

Session 3A2
Wave Scattering, Random Media and Wireless Communications I

An Antenna Array Approach for Propagation of Electromagnetic Waves in Different Media

A. E. M. S. Casimiro
University of Algarve, Portugal

The Huygen's Principle together with the Fourier Relation [1] can give a new insight to the reflection and refraction phenomena and the laws related with them. First we deal with the reflection and refraction of an electromagnetic wave when it crosses from one propagation media to a different one with a plane surface between the two media, and the result will be compared, for validation, with the Snells's Law.

In the classic framework it is usual to consider, the Fermat's Principle or the Malus Theorem [2] to deduce the Snell's Law. In the presented approach those principles are not necessary: the Snell's Law is a consequence of the "radiation and propagation proprieties" of the two media.

After, this procedure will be applied to atmospheric propagation where the "radiation and propagation proprieties" of the media are changed by the Space Weather conditions.

Let's consider the interface separating two transparent media and the line (virtual antenna) that an incident ray makes in that plane interface (fig.1). The ray comes from the media 2 to media 1. If we assume, using the Huygen's Principle, that the line is a virtual continuous radiating antenna array, the antenna elements will have different phases ϕ_d due to the delay that different part of the ray has because of the incidence angle. The array pattern can be seen as an window in the Inverse Fourier Transform of the Source distribution [1], and, in this case, is shifted with a value that depends of the delay. In the Polar representation this shift gives an angle that depends of the wavelength, as in the right side of fig. 2.

So in the same media of the incident ray, the angle is the same. On the other side the angle of refraction has the same sine function value as the angle of incidence, with multiplication by a constant related with the wavelength (fig 2), because the window is now different (beta 2 is different from beta 1).

The final result agrees with the Snell's Law, and with the reflection law, and it is therefore validated.. So the presented procedure, following a complete different way from the classic procedures, by using the concepts related with radiating array antenna [1][3], opens new possibilities of propagations studies using already developed

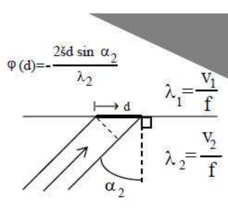

Fig. 1

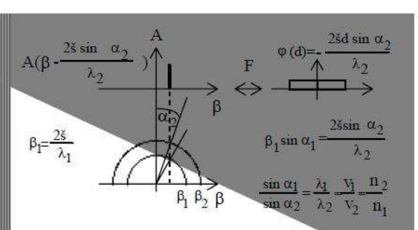

Fig. 2

REFERENCES

1. Grilo, Francisco. C.V., Casimiro, António. M. E. S.,"The Basic Relation Between Point Sources and the Produced Fields",PIERS, MIT, Cambridge, EUA, June 1991.
2. Pedrotti, Frank, S.J., Pedroti, Leno S., *Introduction to Optics*, Prentice-Hall International Editions, 1993.
3. Casimiro, António M.E.S., Azevedo, Joaquim A.R., Grilo, Alberto J.V."Dealing with the Useful Window Related with the Far Field Pattern",IEEE Pacific Rim 1995 Conference on Communications, Computers and Signal Processing, University of Victoria, Victoria, Canadá, May 1995.
4. Casimiro, António M.E.S., Azevedo, Joaquim A.R., "A Unification Procedure to the Analysis and Synthesis of Antenna Arrays",*JEMWA*, volume 19, number 14, page 1881-1896, 2005.

Propagation Characteristics on a Wet Road for a Inter-Vehicle Communication

A. Yamamoto[1], **K. Sato**[2], **H. Kida**[3], **K. Ogawa**[1]
M. Fujise[2], and **T. Horimatsu**[4]

[1]Matsushita Electric Industrial Co., Ltd., Japan
[2]National Institute of Information and Communications Technology, Japan
[3]JRC Ltd., Japan
[3]Fujitsu Ltd., Japan

The inter-vehicle communication (IVC) in the 60GHz band has received considerable attention. In IVC, a vehicle can communicate with vehicles both in front and behind interactively. Thus, the propagation path model for normal communication in IVC is obtained using the line-of-sight (LOS) condition. The 2-wave model, comprising a direct wave and a wave reflected from the surface of the road, has been shown to be effective in predicting the received power in the LOS case [1], [2]. However, there have been few efforts to investigate effects of water on the road surface on the propagation characteristics.

This paper presents the propagation characteristics on a wet road in the LOS case for IVC in the 60 GHz band. The received power as a function of a height of a receiving antenna between two communicating vehicles with fixed positions was examined. In comparison with the received power of the dry road, we show the effect of the water layer on the road on the received power. Furthermore, a 2-wave model, in which variations in the amplitude and phase shift of the road-reflected wave caused by road undulation are taken into consideration, was proposed for an accurate calculation of the received power on the road with dry and wet surfaces. The effectiveness of the proposed model was confirmed by both the propagation tests on the dry and wet road.

Wave Propagation Phenomena in Troposphere Over the Indian Subcontinent

S. K. Sarkar
National Physical Laboratory, India

A number of microwave (2 GHz-7 GHz) line of sight (LOS) communication links situated in the Indian northern, eastern, western and southern sectors were monitored. Considerable work has been carried out discussing the field strength variations and their relationship with the observed meteorological conditions. Studies were also made to show by using this LOS link data that the morning transition is characterized by an enhancement in the signal level for a short period of time and is associated with the rise of the ground based inversion due to solar heating of the ground. Simultaneous LOS microwave propagation studies showed that the link situated over coastal stations suffers heavy fading than the link located over plains. The LOS studies also included diagnosis of the fading problems, remedial measures to over come the fading from radio meteorological point of view, and the implementation of these remedial measures, frequency and space diversity, antenna tilting, path inclination etc. The performance deterioration of several links situated over Indian southern plains operating at 7 GHz was investigated. The effect of sea breeze on the performance of another line-of-sight (LOS) link operating at 6 GHz was studied. Correlation of meteorological parameters and LOS records showed that onset of sea breeze induced heavy fading on the link.

There is a shift in the focus of research studies as well as from the user point of view for satellite communications from C band to higher bands in India. The frequency more than 10 GHz is affected by rain. As far as Indian subcontinent is concerned, rain is the most important one. Systematic measurements of various precipitation parameters (rain rate, horizontal extension of rain, rain height, raindrops size distribution) have been carried out over different geographical regions of India. In addition to precipitation measurements, communication links operating in Ku and K bands are also monitored to investigate the effects of rain on the performance of communication systems.

The Bistatic Radar Cross-Section of a Large Size Body Embedded in a Random Medium

Z. Q. Meng
Fukuoka University, Japan

M. Tateiba
Kyushu University, Japan

When a body is embedded in a random medium, the radar cross-section (RCS) of the body may be remarkably different from that in free space. This special phenomenon is called backscattering enhancement, and has been one of important subjects for radar engineering, remote sensing, astronomy and bioengineering.

We have investigated the phenomenon by numerically analyzing the RCS of a body embedded in a continuous random medium, such as air turbulence, for more than ten years. Our approach is based on general results of both independent studies on the surface current on a conducting body in free space and on the wave propagation and scattering in a random medium. A non-random operator, called current generator, is introduced to get the surface current from any incident wave. The operator depends only on the body surface and can be constructed by Yasuura's method. On the other hand, the wave propagation in a random medium is expressed by use of Green's function in the medium. Here, a representative form of the Green's function is not required but the moments are done for the analysis of average quantities concerning observed waves. At first we made use of a simple approximation of the moments in the backward direction, and obtained many numerical results of monostatic RCS. We have found that the RCS in a random medium may be nearly twice as large as that in free space, under the condition that the body size is smaller than the spatial coherence length of incident wave. If the condition does not hold, we shows for a limited case that the RCS oscillates with the size of the body and becomes more than one hundred times as large as that in free space[1]. We also reveal that there is a depression of the RCS outside the backscattering enhancement peak. All the numerical results agree with the law of energy conservation. Moreover, we find that a second enhancement peak exists outside the depression in some cases[2], which peak is lower and wider than the peak in the backward direction. This paper shows the numerical results of bistatic RCS of a larger size circular cylinder embedded in a random medium. We can see the complicated oscillation of the RCS, i.e., enhancement and depression, in different directions, and discuss the new scattering characteristics with change in the size of the body in a fixed random medium.

REFERENCES

1. M. Tateiba, and Z. Q. Meng, "Wave scattering from conducting bodies embedded in random media", Progress In Electro-magnetics Research 14: Electromagnetic Scattering by Rough Surface and Random Media, PMW Publishing, Cambridge, MA, USA, pp. 317-361, 1996.
2. M. Tateiba, Z. Q. Meng and H. El-Ocla, "Scattering by Conducting Bodies in Random Media", *IEEJ Trans.* FM, Vol. 124, No. 12, pp. 1094-1100, 2004.

Effective Medium and Radiative Transfer Equation

G. Berginc
Thales Optronique, rue Guynemer, France

The description of the coherent propagation of an electromagnetic wave in random media in terms of the properties of the constituents has been studied extensively in the past decade. In most of these works, the basic idea is to calculate several statistical moments of the electromagnetic field to understand how the wave interacts with the random medium. In this paper, we are concerned by the first moment, which is the average electric field. Under some assumptions, it can be shown that the average electric field propagates as if the medium is homogeneous but with a renormalized permittivity, termed effective permittivity. The calculation of this parameter has a long history, which dates back from the works of Clausius-Mossotti and Maxwell-Garnett. Most of the studies are concerned with the quasi-static limit where retardation effects are neglected. In order to take into account scattering effects, quantum multiple scattering theory has been transposed in the electromagnetic case, but as a rigorous analytical answer is unreachable, several approximation schemes have been developed. One of the most advanced is the Quasi-Crystalline Coherent Potential Approximation (QC-CPA), which takes into account the correlation between the particles. Under the (QC-CPA) approximation, it is known that multiple scattering theory provides an expression for this effective permittivity. The numerical evaluation of this one is, however, a challenging problem.

The aim of this paper is to add some new approximations to the (QC-CPA) approach, which give us a tractable equation for the effective permittivity. The expression obtained contains the low frequency limit of the (QC-CPA) approach. At this limit, the (QC-CPA) equations can be written as a generalized Maxwell-Garnett formula and are proven to be in good agreement with the experimental results. Furthermore, the formula contains also the approximate formula due to Keller, which has been derived in using scalar theory, but seems to be in accord with the experimental data for particles larger than one wavelength.

Electromagnetic Wave Scattering From a 3-Dimensional Random Media Bounded With Rough Surfaces : Green Functions Formalism

G. Berginc
Thales Optronique, rue Guynemer, France

Volume and surface scattering is a topic, which has been studied in an extensive way in different domains such as radio-physics, geophysical remote sensing and surface optics. Nevertheless few works deal with the scattering of electromagnetic waves when volume and surface disorders are present. Most of these approaches are either numerical methods based on Monte Carlo simulations or radiative transfer theory where appropriate boundary conditions are specified. In this work we present a general formalism based on rigorous Dyson and Bethe-Salpeter equations, which take into account the scattering by the surface and the volume.

We then obtain an approximate expression for the coherent part of the scattered wave. We have formulated the solution of this problem using Green functions. As the equations we have obtained are similar to those used in scattering theory by an infinite random medium, we are able to introduce the coherent potential with the Quasi-Crystalline Approximation to calculate the effect of the random medium on the coherent field. With this approach, the random medium contribution is taken into account by an effective medium permittivity. The surface scattering contributions in the coherent field are included in the scattering operator of the system, which describes the scattering by the rough boundaries. This operator can be approximated using the usual scattering theories by random rough surfaces like the small-perturbation, the Kirchhoff approximation, or other more sophisticated theories (Small-Slope Approximation).

We give also an approximate expression for the diffusive part of the scattered electromagnetic intensity. A general approach for the calculation of the incoherent intensity scattered by a random medium with rough boundaries has been developed using a Green function formalism. The random medium consists of spherical particles whose physical repartition is described by a pair-distribution function. We derive the integral Bethe-Salpeter equation under the ladder approximation by using a standard procedure and, by differentiation, the vectorial radiative transfer equation. Furthermore, with the help of our formalism, the boundary conditions necessary to solve the radiative transfer equation are expressed in terms of the scattering operators of the rough surfaces. Finally, using the reciprocity properties of the Green functions, we are able to include the enhanced backscattering contributions to take into account every state of polarization of the incident and the scattered waves.

The Geometrically Based Single Bounce Multi-Ellipse Model for Indoor LOS Multi-Polarized Channel

H. Moon, S. Kwon, B. Lee [1], **J. Seok** [2], **C. Mun**[3],and **Y. J. Yoon** [1]

[1]Yonsei University, Korea
[2]Ministry of Information and Communication Radio Research Laboratory, Korea
[3]Chungju National University, Korea

In this paper, it is proposed the modified model from the established GBSBEM using multi-ellipse on vertical plane to be suitable at indoor LOS environments. This modified multi-ellipse model extends to quasi 3 dimension for closed indoor environments and uses multi-ellipse for considering the scatterers which are distributed randomly. Moreover patch scatterering model is introduced to this multi-ellipse model to take account of the scattering by scatterers. Through this paper, we find out the Co-pol field strength and the X-pol field strength from the multi-ellipse model and predicts Cross-polraization discrimination (XPD). And simulation results is compared with measurements. As a result, the more the number of scatterers, the smaller Co-pol field strength and the larger X-pol field strength and 45-pol field strength. Also the field strength is affected by the number and shape of scatterers because the ratio of scattering and reflection is changed. From the comparision, the predicted tendency is well agreed with the measurement tendency but the difference in power level is generated because of the diffraction.

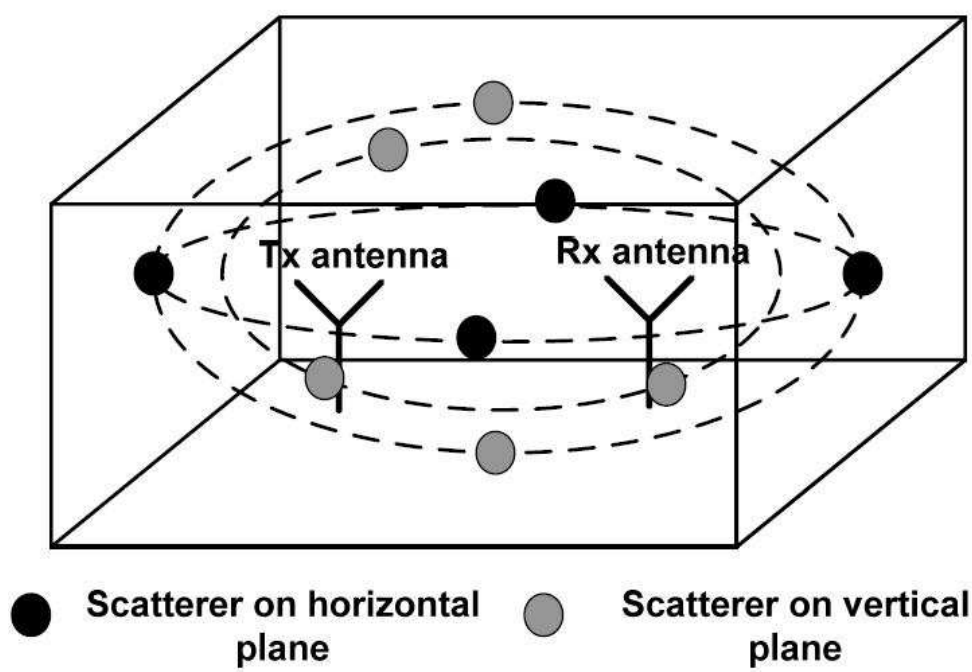

Figure 1: 3-D multi-ellipse modeling for indoor LOS channel

Properties of Metallic Photonic Band Gap Materials with Defects at Microwave Frequencies: Calculation, Experimental Verification and Application in Wireless Communications

S. Massaoudi [1,2], **A. de Lustrac** [1], **I. Huynen**[2], and **R. Talhi** [3]
[1]Université Paris-Sud, France
[2]Université Catholique de Louvain, Belgium.
[3]CNRS, France

We study the properties of a metallic photonic band gap material with defects at microwave frequencies. The material consists of a metallic prism made with 13 by 13 array of copper rods disposed in an isosceles right-angled triangle. Defects are created in this material by removing some rods. We show that this material behaves like homogenous and ultra-refractivity medium in its all authorized frequency bands. Also surface defects lead to the amplification of anomalous transmission and excitation of the new electromagnetic modes in forbidden frequency bands. These properties allow very interesting applications, such as controlable antennas with high directivity, or compact demultiplexer for WDM [1-2].

I. The results in authorised frequency band: The figure 1(a) shows the radiation pattern measured at 8 GHz of a prism without defect. The figure 1(b) gives the radiation pattern measured at 8 GHz of a prism with three defects on the surface of the material. The figure 1(c) shows the radiation pattern measured at the same frequency of a prism with three defects inside.

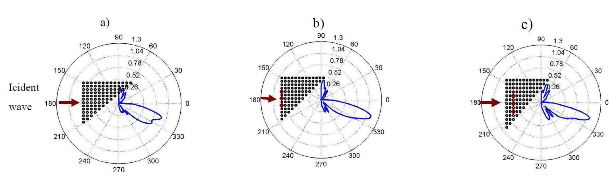

Figure 1: Measured near field radiation pattern at 8 GHz of a) the perfect PBG-prism b) the PBG-prism with three cavities (in red) placed on the surface c) the PBG-prism with three defects inside.

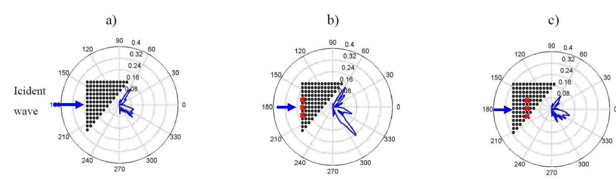

Figure 2: Measured near field radiation pattern at 12 GHz of a) the perfect PBG-prism b) the PBG-prism with three cavities (in red) placed on the surface c) the PBG-prism with three defects inside.

II. The results in forbidden frequency band: The figure 2(a) shows the radiation pattern measured at 12 GHz of the same prism without defect as in Fig. 1(a). This frequency being in the forbidden band for this structure, no significant radiation is observed. The figure 2(b) gives the radiation pattern measured when three defects are added on the surface: new electromagnetic modes are generated. The figure 2(c) shows that when the 3 defects are moved inside the material, the new modes disappear.

Experimental results in Fig. 1 and 2 are very well predicted by simulations using HFSS software [3].

REFERENCES

1. De-Lustrac A., Brillat T., Gadot F., Akmansoy E, The use of controllable photonic band gap (CPBG) materials: an antenna application, Optical-and-Quantum-Electronics. Jan.-March 2002; 34(1-3): 265
2. S. Massaoudi, A. Ourir, A. de Lustrac, efultrarefractive effect in a dielectric and metallic PBG-prism at microwave frequencies, PIERS, Hangzhou, China du 22-26 August 2005.
3. S. Massaoudi, PhD Thesis, Institut d ′Électronique Fondamentale, Université Paris-Sud, France, 2005.

Wave Reflection and Transmission from a Two-Dimensional Random Slab

Y. Tamura and **J. Nakayama**
Kyoto Institute of Technology, Japan

This paper deals with the reflection and transmission of a scalar plane wave from a two-dimensional random slab by the stochastic functional approach. The random slab is mathematically given by a homogeneous Gaussian random field in the transverse directions with infinite extent, and is uniform in the vertical direction with finite thickness(see figure 1). Using the shift invariant property of the homogeneous random field, the unknown random wavefield can be written by the stochastic Floquet form, which is given by a product of an exponential phase factor and a homogeneous random field. Such a homogeneous random field is represented in terms of a Wiener-Hermite expansion with unknown Wiener kernels. In a small fluctuation case, we employ the boundary condition, and use the multiply renormalizing approximation[1], to obtain explicitly an approximate representation of the Wiener kernels. Such Wiener kernels involves the multiple renormalized mass operator[1] given by a nonlinear integral equation, which represents multiple scattering effects in the two-dimensional random medium. We show how to evaluate practically such a nonlinear integral equation. By means of the first three order Wiener kernels, we shall calculate the first- and second-order incoherent scattering cross sections. It is then found that so-called scattering ring[2] and quasi-anomalous scattering[3] may appear in the first-order incoherent scattering. Moreover, in the second-order incoherent scattering, enhanced scattering appears as sharp peaks in the backscattering and anti-specular directions, for a small thickness case. For a large thickness case, however, gentle enhanced scattering[4] takes place as the scattering ring again.

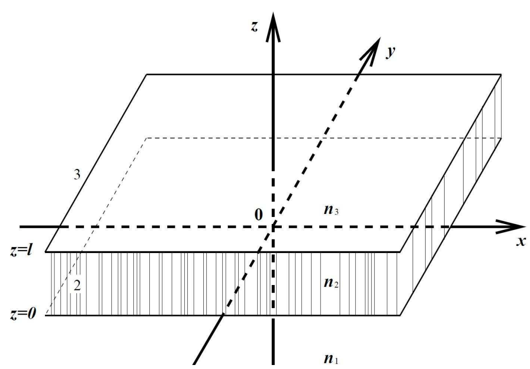

Figure 1: Geometry of the problem

REFERENCES

[1] Y.Tamura and J.Nakayama, "Wave reflection and transmission from a thin film with one-dimensional disorder", *Waves in Random Media* **14** 3 pp.435-465(2004)

[2] C.J.Oton, Z.Gaburro, M.Ghulinyan, L.Pancheri, P.Bettotti, L.Dan Negro and L.Pavesi, "Scattering rings in optically anisotropic porous silicon", Appl. Phys. Lett., **81** 26 pp.4919-4921(2002)

[3] T.Kawanishi, H.Ogura and Z.L.Wang, "Scattering of an electromagnetic wave from a slightly random dielectric surface: Yoneda peak and Brewster angle in incoherent scattering", *Waves in random media* **7** 3 pp.351-384(1997)

[4] Y.Tamura and J.Nakayama, "Enhanced scattering from a thin film with one-dimensional disorder", *Waves in Random and Complex Media* **15** 2 pp.269-295(2005)

Session 3A3
Periodic Structures I

Analysis of Thin Sinusoidal Metallic Gratings in Conical Diffraction

H. Wakabayashi and **J. Yamakita**
Okayama Prefectural University, Japan

Electromagnetic wave scattering by metallic gratings is one of fundamental problems in engineering of radio and optical waves. In most of the analyses of the metallic gratings, the grating is usually so thin electrically compared to a wavelength that thickness is neglected and calculations are carried out so that surface resistance and surface current distribution satisfy the boundary condition [1]. By neglecting the thickness, two-dimensional grating in addition to one-dimensional grating can be analyzed. Therefore, an investigation into the limits of the thickness of metallic gratings which can be neglected during analysis is very important in antennas engineering. In our previous work, thin metallic gratings with rectangular thickness profile placed in conical mounting were analyzed. By defining metallic grating as lossy dielectric gratings, the limit of thickness was investigated [2]. However, the analyses of the gratings whose thickness profile is not uniform along the boundary have not reported so far. In this paper, we demonstrate that a thin metallic grating with sinusoidal thickness profile placed in conical mounting can be approximated by a plane grating with surface resistance as a function of the position parameter. As for the method of analysis for thin metallic gratings, by partitioning the grating layer into multilayers having rectangular profiled gratings, the matrix eigenvalue calculations and the flux densities expansion approach are applied. As for the method of analysis for plane gratings with thickness of zero, the spectral Galerkin method is applied to the resistive boundary condition. From the comparison of the numerical results of thin metallic and plane gratings, the limit of the thickness is investigated.

Figure 1 shows a thin metallic grating with sinusoidal thickness profile placed in conical mounting. We consider the scattering problem by the grating with periodicity Λ and width W that is uniform in the y direction. Sinusoidal profile is defined as a function $f(z)$. The incident wave is given by a polar angle θ_i, an azimuthal angle ϕ_i and a polarization angle γ. Regions I and III, which have relative permittivity ε_1 and ε_3, are lossless materials. The grating layer in region II is described by relative permittivity $\varepsilon_2 = \varepsilon_2' - i\varepsilon_2'' = 1 - i\varepsilon_2''$ and thickness $d(z) = d\, f(z)$. As the thickness $d(z)$ is very small and the conductivity σ varies in such a way that the product σd stay finite, the materials of a thin metallic grating can be approximated by a plane grating with surface resistance $R_s(z)$:

$$R_s(z) = \frac{1}{\sigma\, d(z)} = \frac{1}{(1/Z_0)\, \varepsilon_2''\, k_0\, d\, f(z)} = R_{s0}\frac{1}{f(z)} \tag{1}$$

where R_{s0} is the resistance value in the maximum thickness on the thickness profile. Figure 2 shows the power transmission coefficients against thickness d/λ. Calculations are performed under $\varepsilon_1 = 1$, $\varepsilon_3 = 2.5$, $\Lambda/\lambda = 0.5$, $W/\Lambda = 0.5$, $\gamma = 90$ °and $\theta_i = \phi_i = 45$ °. In the analyses of metallic gratings, the number of the spatial harmonics is truncated to 201 and the number of partitioned layers is 42. In the analyses of plane gratings, the number of the spatial harmonics is truncated to 601, and a current expansion number of step function is 100. From this figure, the results for thin metallic gratings are close to those for plane gratings. We can find that thin metallic gratings with sinusoidal thickness profile can be treated as plane gratings with surface resistance as a function of the position parameter.

References

[1] K. Sumitani, H. Wakabayashi and H. Inai, "A study of uniform approximation of equivalent impedance sheet for parallel metallic gratings", IEEJ Trans. EIS., vol. 123, no. 11, pp. 1930–1935, 2003. (in Japanese)

[2] H. Wakabayashi, J. Yamakita, M. Asai and H. Inai, "Availability of resistive boundary condition for thin metallic gratings in conical mounting", IEICE Trans. Electron. vol. E87-C, no. 9, pp. 1560–1567, 2004.

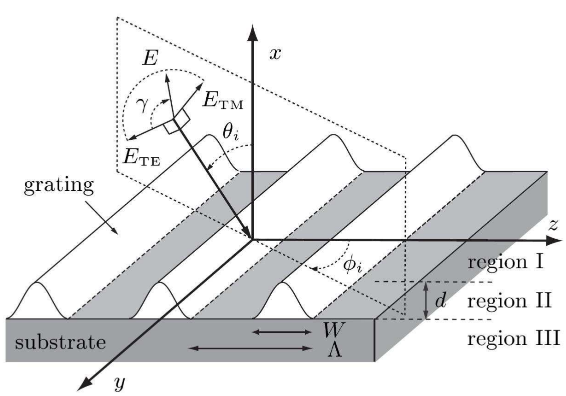

Fig. 1 A thin metallic grating in conical mounting.

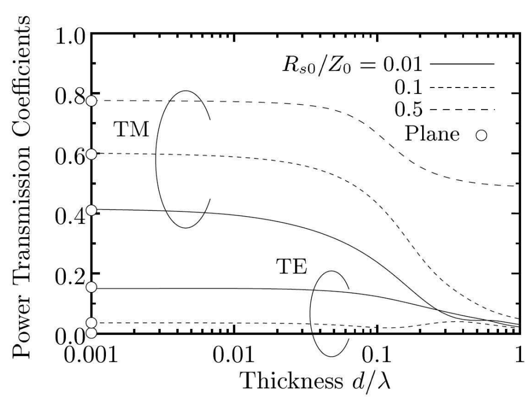

Fig. 2 Power transmission coefficients against thickness.

The Effect of Veins on the Complete Bandgaps in Two-Dimensional Photonic Crystals: Mie Scattering Meohanism

T. J. Yang and **W. L. Liu**

National Chiao-Tung University, Taiwan R. O. C.

B. Y. Gu

Chinese Acadamy of Sciences, China

The double-hybrid-rods structures of two-dimensional photonic crystals (PCs) of a square lattice is proposed to study the effect of viens on the complete photonic bandgaps. A double-hybrid rod consists of a square dielectric rod connected with dielectric veins on the middle of each side of dielectric square rod in air for a fixed filling factor The photonic band structures are calculated by plane wave method. The high frequencies complete band gap is found to be gradually decreased and then disappeared when the length of dielectric viens is gradually grown. The interesting result is the creating of low frequencies complete band gap when the length of viens extends to a certain length and beyond. In the structure of double-hybrid-rods, the symmetry and size of the square lattice does not change in the variation of length of the dielectric viens. But the size of dielectric rods does change, this will cause the different Mie scattering and shorten the distance among rods to increase the electromagnetic interaction each other between rods due to increase the length of viens. Thus the cause of creating of low frequencies complete band gap is due to Mie scattering of the double-hybrid-rods and strengthen the electromagnetic interaction among rods. Further results and discussion will be given in the presentation. (This work is supported by NSC of Rep. of China.)

The Diffraction Efficiencies by Multilayer-Coated Fouried Grationgs in Conical Mounting

[1]**M. Ohki,** [1]**K. Sato,** [2]**H. Sakurai**, and [3]**S. Kozaki**
[1]Shonan Institute of Technology, Japan
[2]Gunma College of Technology, Japan
[3]Faculty of Engineering, Gunma University, Japan

A multilayer-coated grating, which is alternately laminated by set of a low and a high refractive index on the relief metallic grating, is used as a beam-sampling mirror for the highpower lasers. The diffraction efficiency can be controlled by changing profile or the permittivity of a multilayer-coated dielectric media.

The resonance absorption anomaly occurs on grating surface composed of the metal in which the power of incident wave is absorbed at the specific incident angle. This also has large influence on the incident angle and intensity of the absorption so that the profile and the permittivity of a multilayer-coated dielectric on the grating rule the resonance anomaly. The diffraction problem of the plane wave which is illuminated arbitrary incident angle at the diffraction grating which has also periodic structure the problem of conical mounting in the one direction for the polarization conversion by T-matrix method[1]. Moreover, the diffraction problem by exposing the plane wave at the multilayer-coated dielectric diffraction grating is also analyzed by the differential method[2] with R-matrix expression.

In this paper, the plane electromagnetic wave diffraction problem was analyzed as a quasi-two-dimensional problem such as the multilayer-coated Fourier grating in conical mounting. The feature of the formulation by the concept of space harmonics was maintained at the incident medium and the substrate using the T-matrix method based on extinction theorem. And expression of R-matrix in the coating layer is presented by using recurrence matrix calculation. Numerical examples of - 1th diffraction efficiency (Rittrow mounting) are presented for the Fourier grating which is laminated by the dielectric of layers on the aluminum or silica substrate versus normalized layer thickness and the incident angle with azimuth angle.

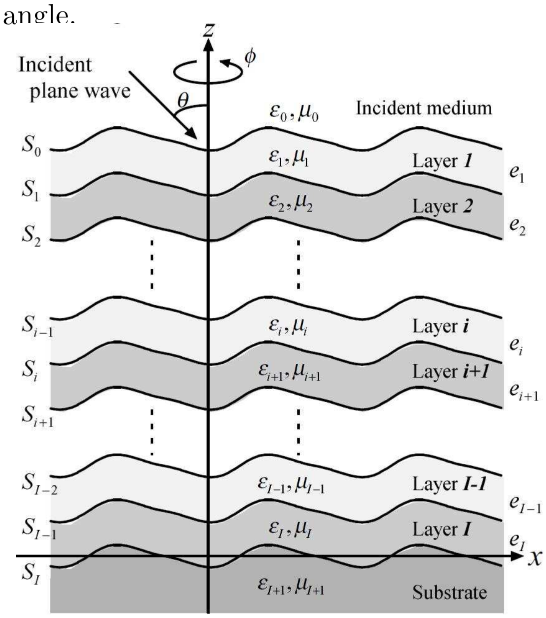

Figure 1: Geometry of the Problem

REFERENCES

1. S. L. Chuang, and J. A. Kong,"Wave scattering from a periodic dielectric surface for a general angle of incidence," *Radio Science,* vol.17, no.3, pp.545-557, May-June 1982.
2. L. Li, "Multilayer-coated diffraction gratings: differential method of Chandezon et al. revisited," *J. Opt. Soc. Am. A,* Vol.11, No.11, pp.2816-2828, Nov. 1994.

Precise Method for Analysis of Scattering Problem by an Imperfection of Finite Extent in a Plane Surface

M. Tomita, T. Sakashita, and **Y. Karasawa**

The University of Electro-Communications, Japan

In this paper, a new method based on the mode-matching method in the sense of least squares is presented for analyzing the two dimensional scattering problem of TE and TM plane wave incidence to the infinite plane surface with an arbitrary imperfection of finite extent. The semi-infinite upper and lower regions of that surface are a vacuum and a perfect conductor, respectively. Therefore the discussion of this paper is developed about the Dirichlet and Neumann boundary value problems. In this method, the approximate scattered wave is represented by the integral transform with band-limited spectrum of plane waves. The boundary values of those scattered waves are described by only abscissa z and Fourier spectra are obtained by applying the ordinary Fourier transform. Moreover, new approximate functions are made by inverse Fourier transform of band-limited those spectra. Consequently, the integral equations of Fredholm type of second kind for spectra of approximate scattered wave functions are derived by matching those new functions to exact boundary value in the sense of least squares. Then it is shown that the sequence of boundary values of approximate wave functions converges to the exact boundary value, namely, the boundary value of the exact scattered wave in the sense of least squares when the profile of imperfection part is described by continuous and piecewise smooth function at least. Moreover, it is shown that this sequence uniformly converges to exact boundary value in arbitrary finite interval of the boundary and the sequence of approximate wave functions uniformly converges to the exact scattered field in arbitrary subdomain in the upper vacuum domain of the boundary in wider sense when the uniqueness of the solution of the Helmholtz equation is satisfied with regard to the profile of the imperfection parts of the boundary.

Propagation Properties of Lightwave in Two-Dimensional Photonic Crystal Waveguide with Microcavity

K. Takamiya, N. Ohtsuka, and **M. Yokota**
University of Miyazaki, Japan

In the past few years, there has been tremendous activity in the fabrication and testing of photonic crystals from both the theoretical and the experimental points of view [1]. It is important for designing optical functional devices to clarify fundamental properties of basic photonic crystal waveguides, such as the straight waveguide, direction coupler, microcavity and so on [2].

In this article, two-dimensional photonic crystal (PC) waveguide with the microcavity is analyzed by FD-TD method [3] numerically. It has an absorbing boundary condition (ABC) at the edge of the window called Murfs ABC. We examine two kinds of the structures of the PC with microcavity. One is the triangular array and the microcavity is located along the waveguide. Another structure of the microcavity is by removing the several crystals in parallel with the PC waveguide. The effects of the number of removed pillars and location of the microcavity on the resonance are examined. From the numerical results, we show that resonance frequency can be determined by adjusting the number of removed pillars and location of the microcavity. It is shown that higherorder of the resonant modes appears when the number of removed pillars is adjusted. Also, the structure which takes out the light is examined from the practical point of view.

REFERENCES

1. J.D.Joannopoulos, R.D.Meade, J.N.Winn: hPhotonic Crystals.Molding the Flow of Light.h, Princeton University Press, 1995.
2. H.Ikuno, Y.Naka: hFinite-Difference Time-Domain Method Applied to Photonic Crystalsh, Electromagnetic Theory and Applications for Photonic Crystals, Ch.8, 2006.
3. A.Taflove, S.C.Hagness: hComputational Electrodynamics:The Finite-Difference Time-Domain Method (Second Edition)h, Artech House Publishers, 2000.

Band Structures of Phononic Crystals with Damping Effects

Y. H. Liu and **Chien C. Chang**
Academia Sinica, Taiwan R.O.C.

R. L. Chern
National Taiwan University, Taiwan R.O.C.

In this study, we develop a fast method for computing band structures of phononic band gap materials with particular emphasis on the effects of the density ratio and of the contrast of elastic constants. First of all, we explore an omnidirectional reflector in a wide range of frequencies by using one-dimensional layered structures. Next, we consider two-dimensional arrays of different media embedded in rubber. It is shown that the density ratio rather than the contrast of elastic constants is the dominant factor that determines the size of band gaps. If the density ratio is near 1, there would be no major gap bands no matter how large is the contrast of elastic constants. Third, we examine the modes of waveguide that propagate along the cylinder axis of two-dimensional phononic band gap materials. It is shown that by increasing the wavenumber along the axis, we have flat bands of frequencies; in other words, for the modes with wavelength shorter than the lattice constant, the energy transfers only along the cylinder axis.

In reality, materials have loss due to damping; the issue will also be addressed. Elastic constants with damping effects often depend on the frequency of acoustic waves so that the traditional algorithm of eigenvalue formulations is hard to apply to frequency-dependent phononic crystals problems. In our methodology, we use the waveguide formulation of elastic wave equations to overcome the difficulty arising from elastic constants with damping effects. Numerical results will be presented for one-dimensional layered structures and waveguide behaviors in two dimensions.

Exact Calculation of the Nonlinear Optical Response of One-Dimensional Photonic Bandgap Structures

K. Kim, D. K. Phung F. Rotermund, and **H. Lim**

Ajou University, Korea

We develop a generalized version of the invariant imbedding theory of wave propagation in nonlinear inhomogeneous media and apply it to the calculation of various optical characteristics including the amplitude and phase of the reflection and transmission coefficients, of one-dimensional nonlinear photonic bandgap structures. Our method allows us to obtain exact solutions of the problem of the self-action of electromagnetic waves in nonlinear media in a simple and efficient manner. We calculate the transmittance spectrum of 1D photonic crystals made of alternating linear and nonlinear dielectric layers as a function of the intensity of the incident wave. We observe a bistability in the spectrum when the intensity is sufficiently strong. We also calculate the transmittance spectrum and the electric field distribution associated with 1D nonlinear photonic crystals with a defect. We analyze the bistable defect spectrum in detail for both focusing and defocusing nonlinearities. We find that there is a strong enhancement of the electric field at the defect layer. Furthermore, we perform an extensive calculation of the nonlinear optical response of metal-dielectric 1D photonic bandgap structures and compare our theoretical results with recent experiments.

An Analysis of the Transfer Matrix Method on Band Structure of One Dimension Graded-Index Photonic

I. C. Tsai and **J. J. Wu**
Chung Hua University, Taiwan R.O.C
T. J. Yang
National Chiao-TUng University, Taiwan R.O.C

Abstract - The characteristics of guide wave scattered by graded-index photonic crystal are systematically investigated with the use of an equivalent network method. By carefully modulate the width of uniform layer, the higher order band gaps can be eliminated.

Stucture

A one dimension photonic crystal, a two-dimensional space (x z) with one dimension guiding (x), is considered by this letter. The unit cell is depicted in Fig. 1(a). The structure of unit cell which include two layers: one is the uniform layer with the width W_1 and the other is graded index layer with the width W_2.

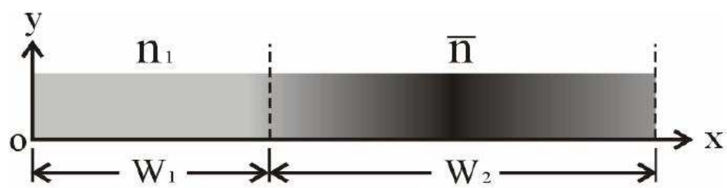

Fig.(1) a unit cell: a homogeneous layer in left side and a graded-index layer in right side

$$n_1 = 1.38,\ W_1 = 89nm,\ \overline{n} = 2.00,\ W_2 = 121nm$$

Numerical Analysis

Assume W_1 is 89nm. By using transfer matrix method, we illustrate the electromagnetic dispersion and reflection index diagrams. From Fig. 1(a)(b), the interest is that there is no bandgap in $2\omega_o$.

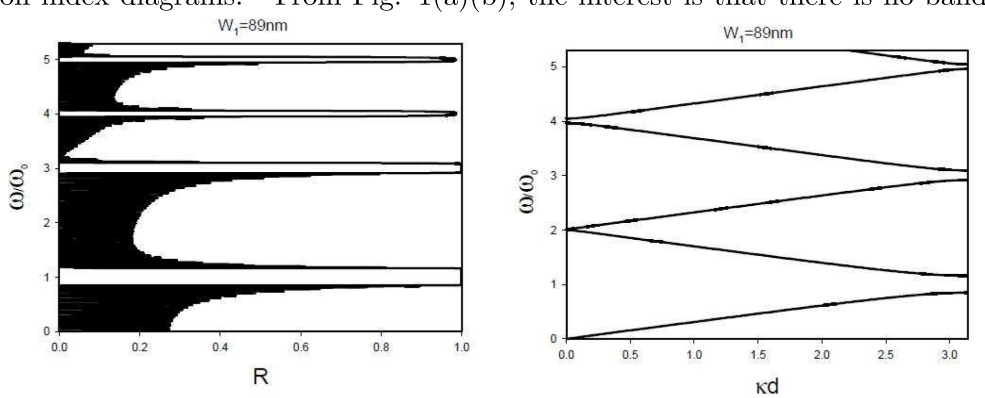

(a) (b)

Figure 2 (a) reflection index diagram (b) electromagnetic dispersion diagram: Second band gap is erased

First band Gap=0.3080, Second bandgap=0.0080, Third bandgap=0.1760, Forth bandgap=0.0840, Fifth bandgap=0.0840 , their reflection index are R1=1.0000, R2=0.0988, R3=0.1.0000, R4=0.9846, R5=0.9846. The fundamental frequency , ω_o , is 2583.7 (THz).

This phenomenon can be understood by harmonic suppression. We can calculate the input impedance to give the physical explains. If W_1 is 40nm, the third bandgap will be erased. If W_1 is 13nm, the forth bandgap will be erased. If W_1 is 22nm, the fifth bandgap will be erased. Therefore this type of periodic structures may provide another degree of freedom to design optical-frequency selector.
Notices: The refraction index of 1.38 is M_gF_2 . The refraction index of 2.35 is ZnS

Propagation Characteristics of Multilayered Circular Dielectric Gratings in Inhomogeneous Media with Loaded the Rectangular Dielectric Constants

R. Ozaki, T. Yamasaki, and **T. Hinata**
Nihon University, Japan

Dielectric gratings are widely used in integrated optics and acousto-optics, such as optical gratings, optical couplers, optical waveguide filters, and Photonic Crystal. Recently, the refractive index can easilybe controlled to make periodic structures by the development of manufacturing technology of opticaldevices. Accodingly, the numerical methods which are applicable to inhomogeneous gratings have been proposed. However, it is not treated the propagation characteristic in detail for Photonic Band Gap.

In this paper, the guiding problems of electromagnetic waves by Multilayered Circular Dielectric Gratings in Inhomogeneous media with loaded the rectangular Dielectric constants are analyzed using the combination of Fourier series expansion method and multilayer method. Our approach for the multilayer method differs from that of other method, so that the order of characteristic matrix equation depends on the modal truncation number, but does not depend on the number of layers. Therefore our method is effective to the guiding problems.

Numerical results are given for the propagation characteristics for multilayer circular dielectric gratings in inhomogeneous media with loaded the rectangular dielectric constants both for TE and TM modes. The differences in the propagation characteristics of the shape of rectangular dielectric gratings are discussed. We also discussed between the homogeneous medium and inhomogeneous medium for the circular dielectric gratings.

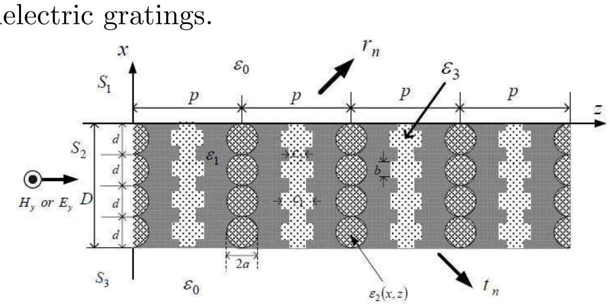

(a) Coordinate system

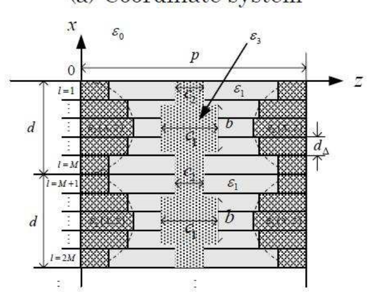

(b) Approximated inhomogeneous layers

Figure 1: Structure of multilayered circular dielectric gratings in Inhomogeneous media with loaded the rectangular dielectric constants.

Session 3A4
Plasmonic Nanophotonics I

Characteristics of Coupled Wedge Plasmonic Waveguides

M. Fukui, M. Haraguchi, D. F. P. Pile, and **T. Okamoto**
The University of Tokushima, Japan
D. K. Gramotnev
Queensland University of Technology, Australia

Recently, localized surface plasmons and propagating surface plasmons have attracted much attention as electromagnetic surface modes to enhance and confine electromagnetic fields in a nanometer-scale region [1,2,3]. Utilizing such a property, a variety of plasmonic waveguides have been proposed by various groups: strips [4], nanochains [1,2], wedges [5], grooves [6], gaps [7,8] and so forth. Among them, it has been confirmed that metal wedges can be fabricated with ease and can support propagating plasmon modes, the so-called wedge plasmon modes (WP modes) [5]. The propagation length of WP, L, propagating along a wedge is a few micrometers in the visible range and thus is not long enough.

In two coupled wedges with a nano gap, a coupled wedge plasmon (CWP) is expected to be excited [9]. L of such a mode should become longer than that of the WP of a single wedge, if most of electromagnetic energy associated with the CWP may exist in the gap and the surrounding of the metal wedge.

In this talk, we will mention characteristics of plasmon waveguides making use of properties of CWPs, compared with those of the WP, where metallic coupled wedges are placed in parallel each other, separated by a nano gap, on a glass substrate.

We employ the finite-difference time-domain method for simulating characteristics of the waveguide because of a complex structure of waveguides. For the angle of wedge θ ranging from 10° to 90°, the characteristics of silver waveguides have been investigated. The propagation constant of a CWP depends on θ and the gap distance d and it is larger than that of a WP in a single wedge with the same θ. For the incident light having a vacuum wavelength of 632.8 nm, L and the beam area size of CWPs are in the order of 10μm and in the range from $10^{-4}\mu\text{m}^2$ to $10^{-1}\mu\text{m}^2$, respectively. We have fabricated silver coupled wedge waveguides on a glass substrate by using the focused ion beam lithography. The attenuated total reflection method was employed for evaluating L of CWPs. The dependence of L on θ and d obtained experimentally agrees with those done by the simulation. It may be concluded that these coupled wedge plasmonic waveguide could be highly beneficial for nano-photonic circuit.

REFERENCES

1. J. R. Krenn, Nat. Mater., **2**, 210 (2003).
2. S. A. Maier, P. G. Kik, H. A. Atwater, S. Meltzer, E. Harel, B. E. Koel, and A. A. G. Requicha, Nat. Mater., **2**, 229 (2003).
3. T. C. Chu, W. C. Liu, D. P. Tsai, Opt. Comm., **246**, 561 (2005).
4. J. R. Krenn, B. Lamprecht, H. Ditlbacher, G. Schider, M. Salerno, A. Leitner, and F. R. Aussenegg, *Europhys. Lett.*, **60**, 663(2002).
5. D. F. Pile, et. al.: *Appl. Phys. Lett.*, **87**, 061106 (2005).
6. D. F. P. Pile and D. K. Gramotnev: *Opt. Lett.*, **29**, 1069 (2004).
7. K. Tananka and M. Tanaka, *Appl. Phys. Lett.*, **82**, 1158 (2003).
8. D. F. P. Pile and D. K. Gramotnev: *Opt. Lett.*, **29**, 1069 (2004).
9. M. Haraguchi, D. F. P. Pile1, T. Okamoto, M. Fukui and D. K. Gramotnev, *Opt. Rev.*, (accepted).

Plasmonic Crystals as Cathodes of Organic Light Emitting Devices

T. Okamoto and **J. Feng**
RIKEN, Japan
S. Kawata
Osaka University, Japan

Plasmonic crystals are the structures of two-dimensional surface relief gratings on metal surfaces, in which the dispersion relation and the radiation characteristics of the surface plasmons can be controlled by the grating pitch and the grating profile. In this paper we demonstrate two applications of the plasmonic crystals to the cathodes of organic light emitting devices (OLEDs).

In the first application we improved the photon extraction efficiency from OLEDs [1]. In general the efficiency is limited to ~20% because the emitted photon propagate along the emissive layer as guided modes due to the high refractive index of the layer. The obtained photon extraction efficiency of the OLED with a plasmonic crystal cathode, whose material is silver, was four times higher than the conventional one. The OLED with a plasmonic cathode also emits photons not only from the transparent substrate side but also the silver cathode side. The thickness of the plasmonic cathode we used is 50 nm, so that the emitted photons almost do not transmit the cathode without plasmonic crystal structures. In the OLED with a plasmonic cathode, however, the excited surface plasmons on the silver surface adjacent to the emissive layer resonantly transmit the silver cathode and excite the surface plasmons on the other side of the silver cathode with the assistance of the grating vector of the plasmonic crystals, and then radiate into free space.

The second application is OLEDs with highly directional emission with an organic dye with a narrow bandwidth of emission spectrum as an emitting material [2]. The OLEDs with a europium complex as an emissive layer show beam divergence of less than 4° and the beam direction is controlled by pitch of the grating.

REFERENCES

1. J. Feng, T. Okamoto, and S. Kawata, "Enhancement of electroluminescence through a two-dimension corrugated metal film via grating-induced surface-plasmon cross coupling," Opt. Lett. **30**, 2302 (2005).
2. J. Feng, T. Okamoto, and S. Kawata, "Highly directional emission via coupled surface-plasmon tunneling from electroluminescence in organic light-emitting devices," Appl. Phys. Lett. **87**, 241109 (2005).

Complex-Shaped Three-Dimensional Electromagnetic Micro-Nanostructures

H. B. Sun [1,2] and **S. Kawata** [2]

[1]Jilin University, China
[2]Osaka University, Japan

Laser micro-nanofabrication has been recently established as a powerful tool for fabrication of complicated-shaped three-dimensional (3D) micro-nanostructures using various media like liquid resins and transparent solids, due to its unique 3D prototyping capability and reasonably high spatial resolution [1-20]. Since the first use of this approach on photonic crystals (PhCs), PhCs of varied geometry and micro-nanomachines have been readily produced [1-24]. In this presentation we will show our latest research progress in artificially engineering advanced electromagnetic structures, including arbitrarylattice PhCs, hot-sites consisting of nano-dot dimers (Figure 1), and 3D metallic PhCs.

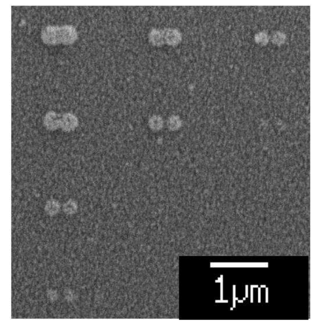

REFERENCES

1. H.-B. Sun, A. Nakamura, S. Shoji, K. Kaneko, and S. Kawata, *Opt. Lett.* 30, 881, 2005.
2. K. Takada, H.-B. Sun, and S. Kawata, *Appl. Phy. Lett.* 86, 071122, 2005.
3. J. Kato, N. Takeyasu, Y. Adachi, H.-B. Sun, and S. Kawata, *Appl. Phy. Lett.* 86, 044102, 2004.
4. H.-B. Sun, T. Suwa, K. Takada, R. P. Zaccaria, M. S. Kim, K.-S. Lee, and S. Kawata, *Appl. Phy. Lett.* 85, 3708, 2004.
5. H.-B. Sun and S. Kawata, Adv. Polymer Sci. 170, 169, 2004.
6. K. Shirota, H.-B. Sun, and S. Kawata, Appl. *Phy. Lett.* 84, 1632, 2004.
7. H.-B. Sun, A. Nakamura, S. Shoji, X.-M. Duan, and S. Kawata, Adv. Mater. 15, 2011, 2003.
8. K. Kaneko, H.-B. Sun, X. M. Duan, and S. Kawata, *Appl. Phy. Lett.* 83, 2091, 2003.
9. H. .B. Sun, K. Takada, M. S. Kim, K. S. Lee, and S. Kawata, *Appl. Phy. Lett.* 83, 1104, 2003.
10. K. Kaneko, H.-B. Sun X. M. Duan, and S. Kawata, *Appl. Phy. Lett.*, 83, 1426, 2003.
11. S. Shoji, H.-B. Sun, S. Kawata, *Appl. Phy. Lett.* 83, 608, 2003.
12. H.-B. Sun, M. Maeda, K. Takada, J. W. M. Chon, M. Gu, and S. Kawata, Appl. Phy. Lett. 83, 819, 2003.
13. H.-B. Sun and S. Kawata, J. Lightwave Technol. 21, 624, 2003.
14. H.-B. Sun, T. Tanaka, and S. Kawata, *Appl. Phy. Lett.* 80, 3673, 2002.
15. T. Tanaka, H.-B. Sun, and S. Kawata, *Appl. Phys. Lett.* 80, 312, 2002.
16. H.-B. Sun, K. Takada, and S. Kawata, *Appl. Phy. Lett.* 79, 3173, 2001.
17. H.-B. Sun, T. Tanaka, K. Takada, and S. Kawata, *Appl. Phy. Lett.* 79, 1411, 2001.
18. S. Kawata, H.-B. Sun, T. Tanaka, and K. Takada, Nature, 412, 697, 2001.
19. H.-B. Sun, V. Mizeikis, Y. Xu, S. Juodkazis, J.-Y. Ye, S. Matsuo and H. Misawa, *Appl. Phy. Lett.*, 79 (1), 1-3, 2001.
20. H.-B. Sun, Y. Xu, S. Juodkazis, K. Sun, M. Watanabe, S. Matsuo, H. Misawa, and J. Nishii, *Opt. Lett.* 26, 325, 2001.
21. H.-B. Sun, T. Kawakami, Y. Xu, J. Y. Ye, S. Matuso, H. Misawa, M. Miwa, and R. Kaneko, *Opt. Lett.* 25, 1110, 2000.
22. H.-B. Sun, S. Juodkazis, M. Watanabe, S. Matsuo, H. Misawa, and J. Nishii, *J. Phys. Chem. B*, 104, 3450, 2000.
23. H.-B. Sun, Y. Xu, S. Matsuo, and H. Misawa, *Opt. Rev.* 6, 396, 1999.
24. H.-B. Sun, S. Matsuo, and H. Misawa, *Appl. Phy. Lett.* 74, 786, 1999.

Experimental and Numerical Study of Plasma Resonant Light Scattering and Absorption from Nanospheres

H. Tamaru and **K. Miyano**
The University of Tokyo, Japan

In our recent studies, we have shown that numerical and semi-analytical analysis of scattering spectra from individual nanoparticles are possible using their actual morphologies and dimensions observed by SEM. It has revealed that subtle differences in their shape, size and environment all play important roles to their spectral responses. However, a parameter-free quantitative analysis of the magnitude of the fields are yet to be established at present. This is certainly a key element for the design of a strong local field enhancement, and in this talk, our current approaches in this aspect is presented.

Nanospheres provide powerful grounds for this study: Recent commercially available nanospheres of some 40 nm in diameters are quite regular in shape and uniform in size; Mie theory provides rigorous analytical solutions to compare with; and spheres can be numerically calculated using minimal computational resources.

Here, two-dimensional Au nanosphere films of various densities were fabricated using Langmuir-Blodgett technique, and their reflection and transmission spectra were acquired. Measurement of ensembles has a disadvantage in that it loses the individualities of the particles (which is somewhat less pronounced for the regular spheres in this case). Never-the-less, the use of a random two-dimensional array located at a dielectric interface have some pronounced advantages. One is that scattering and extinction will only appear in two distinct directions, and thus quantitative measurements of their absolute intensities are much easier. Another is that the coherent interference of the scattered light with the reflection from the dielectric interface can not only be used as a reference, but also be used to acquire the phase of the scattered light.

The experimental results will be discussed with respect to Mie theory and FDTD calculations.

Surface Plasmon Excitations due to Evanescent Waves of Molecular Luminescence and Emission Light from Plasmons

F. Kaneko, Y. Ohdaira, K. Shinbo, and **K. Kato**
Niigata University, Japan

It has been investigated that surface plasmons (SPs) on a metal surface are excited by evanescent waves of molecular luminescence in Kretschmann configuration of prism/metal thin film/ dye molecular ultrathin films when the dye molecules are irradiated by a laser beam from air to the films. Emission light through the prism is observed in the SP resonant conditions of the configuration as the SPs are excited in the system. Intensities and spectra of the emission light through the prism strongly depend upon emission angles, nano-structures of molecular films, nano-separations between metal and molecular film, luminescence properties of molecules and inter-molecular energy transfer. As the emission properties coincide with the resonant conditions of SP excitations in the configuration, it is thought that SPs on the metal surface are excited by evanescent waves of luminescence of dye molecules close to the metal surface, and the SPs propagating along the metal surface are converted to the emission light according to the resonant conditions of SPs in the configuration. Therefore, SP excitations due to molecular luminescence in the configuration can be conversely estimated from the emission light through the prism. Emission properties also depend upon the propagating directions of SPs excited by anisotropic evanescent waves of molecular luminescence as the molecules play as antenna. It is thought that the SP excitations and the emission light are very useful for device applications utilizing SPs, conversion between two- and three-dimensional optical waves and near field optics.

Coherent Near-Field Investigation of Plasmonic Structures

A. Nesci
Nanophotonics and Metrology Laboratory (NAM), Switzerland

O. J. F. Martin
Swiss Federal Institute of Technololgy (EPFL), Switzerland

The optics of plasmon-resonant metallic nanostructures has lately attracted a great deal of interest from a broad scientific community ranging from physicist to electrical engineers and biologists. This interest is articulated around two types of phenomena. On the one hand, nanoparticles where the strong field associated with localized surface plasmon resonances can enhance and confine chemical interaction at the nanoscale [1], thereby creating new functionalities for biophotonic circuits [2] or new approaches to optical data storage [3]. On the other hand, surface plasmon-polaritons (SPPs) propagating on metallic waveguides [4], which provide a new paradigm for the realization of optical circuits at the nanoscale [5, 6] fully compatible with silicon technology. Such surface modes can also be used to strongly localize light beyond the diffraction limit, with applications in imaging and nanolithography [7].

In this paper, some of the fundamental phenomena (propagation, absorption, reflection, radiation losses, etc.) that take place in plasmonic metallic systems such as metallic waveguides or nano-slits guiding structures, are investigated experimentally at the nanoscale. The plasmonic near-field is imaged with a heterodyne PSTM (Photon Scanning Tunneling Microscope) [8, 9], which is a particularly well suited tool to study the interaction of light with plasmon-resonant metallic nanostructures in the visible range [10]. Indeed, it allows the complete characterization of the optical near-field by giving full access to its amplitude and phase. Hence, it provides a full description of the wave character of SPPs and can strongly increase our understanding of SPP propagation and scattering at the nanoscale.

Application of this technique to the design and analysis of plasmonic devices with new functionalities for sub-wavelength optical signal processing will be described.

REFERENCES

1. J. P. Kottmann and O. J. F. Martin, Phys. Rev. B **64**, 235402 (2001).
2. R. P. van Duyne, Science **306**, 985 (2004).
3. J. Tominaga, T. Nakano, and N. Atoda, Appl. Phys. Lett. **73**, 2078 (1998).
4. J.-C. Weeber, J. R. Krenn, A. Dereux, *et al.*, Phys. Rev. B **64**, 045411 (2001).
5. S. I. Bozhevolnyi, V. S. Volkov, K. Leosson and A. Boltasseva, Appl. Phys. Lett. **79**, 1076 (2001).
6. S. Jetté-Charbonneau, R. Charbonneau, *et al.*, Opt. Expr. **13**, 4674 (2005).
7. O. J.F. Martin, Microelectronic Eng. **67-68**, 24, (2003).
8. A. Nesci, R. Dändliker and H. P. Herzig, Opt. Lett. **26**, 208 (2001).
9. M. L. M. Balistreri, J. P. Korterik, *et al.*, Appl. Phys. Lett. **77**, 4092 (2000).
10. A. Nesci and O.J.F. Martin, SPIE Proceedings, **5928**, p.59280U-1 to 9, San Diego, USA, (2005).

Plasmonic Enhanced Raman Spectroscopy for Nanoscale Characterizations of Molecular Vibrations

N. Hayazawa, Y. Saito, and **M. Motohashi**
RIKEN, Japan
S. Kawata
Osaka University, Japan

An optical microscope that is capable of showing images of molecules in nanometer scale has been a dream of scientists both in physicists, chemists, and biologists. However, it has been thought to be difficult due to the strict limitation of a spatial resolution because of the wave nature of light [1]. While there have been attempts to overcome the diffraction limit by using nonlinear response of materials [2], near-field optics could provide better detecting accuracy. Scanning near-field optical microscopy (NSOM) provides nanometer scale structural and chemical information. The development of apertureless NSOM, using a metallic probe [3], presents many advantages. For example, the potential for improved spatial resolution is tremendous because the metallic tip could locally interact with molecules at the very end of the tip apex. Moreover, in terms of Raman spectroscopy, the metallic tip can work as a surface enhancer as surface enhanced Raman Scattering (SERS) effect. This concept has been recently recognized as tip-enhanced Raman Spectroscopy (TERS) [4-9] in contrast to SERS. SERS and TERS are expected to be promising tools for nanoscale characterization of surface of materials. In this presentation, we developed TERS system both in transmission and reflection modes, and we characterized nanomaterials such as single walled carbon nanotubes and some crystals. For example, we observe localized strains in strained silicon by TERS in reflection-mode. TERS revealed that the Raman frequency and intensity of strained silicon were different within a crosshatch pattern induced by lattice-mismatch [10]. Micro Raman measurements, however, show only uniform features because of averaging effect due to the diffraction limit of light.

REFERENCES

1. M. Born and E. Wolf, Principles of Optics 7th edition. (Cambridge, 1999).
2. S. Kawata, H. -B. Sun, T. Tanaka, and K. Takada, Nature 412, 697 (2001).
3. S. Kawata, (Ed.) Near-Field Optics and Surface Plasmon Polaritons, (Springer, 2001).
4. N. Hayazawa, Y. Inouye, Z. Sekkat, and S. Kawata, Chem. Phys. Lett. 335, 369 (2001).
5. N. Hayazawa, Y. Inouye, Z. Sekkat, and S. Kawata, J. Chem. Phys. 117, 1296 (2002).
6. N. Hayazawa, T. Yano, H. Watanabe, Y. Inouye, and S. Kawata, Chem. Phys. Lett. 376, 174 (2003).
7. N. Hayazawa, Y. Saito, and S. Kawata, Appl. Phys. Lett. 85, 6239 (2004).
8. Y. Saito, N. Hayazawa, H. Kataura, T. Murakami, K. Tsukagoshi, Y. Inouye, and S. Kawata, Chem. Phys. Let9., 410, 136 (2005).
9. T. Ichimura, N. Hayazawa, M. Hashimoto, Y. Inouye, and S. Kawata, Phys. Rev. Lett. 92, 220801 (2004).
10. Y. Saito, M. Motohashi, N. Hayazawa, M. Iyoki, and S. Kawata, Appl. Phys. Lett. In press.

Plasmon Absorption Properties of Au/Polymer Nanocomposites: Dependence of Size and Shape

X. M. Duan [1], **M. Umemoto** [2], **W. Q. Chen,** [1], and **Y. Y. Cao** [1]

[1]Chinese Academy of Sciences, China
[2]Osaka University, Japan

It is well known that the interaction of light with free electrons in a metal nanostructure can give rise to surface plasmons. Plasmons provide a powerful means of confining light to metal/dielectric interfaces, which can generate intense local electromagnetic fields and significantly amplify the signal derived from analytical techniques that rely on light. With plasmons, photonic signals can be manipulated on the nanoscale. However, to benefit from their interesting plasmonic properties, metal structures with controlled size and shape must be fabricated on the nanoscale. Lots of researches on control of metal nanostructures by the colloid approach have been reported. On the other hand, controlling metal nanostructures in dielectric mediums is also interesting because the plasmonic properties of metal nanostructures will depend on the interface between metals and dielectrics. However, there are only a few reports discussed synthesis of metal nanoparticles in polymers without size and shape controlling for metal nanoparticles. In this paper, we report a facile synthesis approach of gold nanoparticles via photoreduction in polymer networks. With control of photoreduction condition, we successfully observed variety of plasmon absorption spectra depending on different size and shape of gold nanoparticles. The details will be reported in the conference.

Plasmonic Resonance Modes on Au Nanoparticles

H. J. Huang [1], **Y. H. Fu** [1], **H. P. Chiang** [1,2], and **D. P. Tsai** [1]

[1]National Taiwan University, Taiwan R.O.C.
[2]National Taiwan Ocean University, Taiwan R.O.C.

Studies of the light-material interactions based on the surface plasmon resonance of metallic nanoparticles attract lots of attention recently, and they have shown the importance for future applications. Previous studies might choose near-field scanning optical microscope (NSOM) to reveal the optical response of nanoscale samples. However, the coupling of optical probes to local sample structure, either an aperture or apertureless NSOM is a complex system for the measurement and analysis of plasmonic resonances. The true details may be distorted or altered significantly by the convolution of the interactions of sample and probe. In this paper, an inverted optical microscope with a full color, high resolution, and ultra low noise TE-cooled CCD camera is used to image the modes of plasmonic resonance on nanoparticles. Dissipation of near-field plasmonic resonances can be monitored in a far-field image under proper conditions. Images of different optical responses under various illumination conditions are investigated with a white light source. Different plasmonic resonance modes of the same Au nanoparticle under different illumination condition are imaged. An atomic force microscope (AFM) can be used for the manipulation and topographical imaging of different nanoparticles simultaneously. Information of size, shape and orientation of each metallic nanoparticle and its plasmonic resonance response can be acquired and studied. Results show interesting plasmonic resonance of single metallic nanoparticle and important coupling response of multiple nanoparticles. The control and manipulation of the collective plasmonic response reveal the potential of creating nanophotonic components for switching and amplification in near-field.

Keywords: nano-optics, surface plasmon resonance, Au nanoparticle, inverted system microscope, TE-cooled CCD

Session 3A5
Light Modulation Technology

High-Speed Optical Switching by PLZT Waveguides on Semiconductors

K. Nashimoto, N. Tanaka, M. LaBuda, D. Ritums, J. Dawley
M. Raj, D. Kudzuma, T. Vo, and **J. Fang**
Nozomi Photonics Co., Ltd., U.S.A.

High-speed optical switches are attracting increasing interest for variety of applications such as burst-switching and packet-switching for telecommunications and data communications including interconnection. For the high-speed optical switching, there are approaches based on materials such as $LiNbO_3$ and semiconductors. However, it is not easy to meet various requirements with those materials. As one of altanetive materials, (Pb,La)(Zr,Ti)O3 (PLZT) is very attractive in terms of dense integration, device miniaturization, high-speed control, and low power dissipation. Its efficient voltage-induced index change, that is, the electro-optic (EO) effect, can enable miniaturization of electrodes and low power dissipation. But, practically, PLZT requires epitaxial growth since single-crystal wafers are not yet available. It is also difficult to grow epitaxial EO waveguides with a propagation loss of less than 1 dB/cm. To grow low-loss and high-quality thin-film optical waveguides, solid-phase epitaxy (SPE) of EO materials including PLZT and LN has been developed. SPE is a simple, low-cost but reproducible process consisting of solution deposition and annealing. In addition to the motivation to grow EO waveguides, epitaxy is very interesting for constructing an electrode/waveguide/electrode sandwich structure as shown in Fig. 1. The structure can enhance low-voltage driving-device performance based on the narrow electrode gap geometry and the effective overlap integral of the optical field and the electric field. Using the SPE process, the structure of PLZT waveguides on Nb-doped semiconductive $SrTiO_3$ (NST) substrates has been developed. Directional coupler type optical switchs (Fig. 2) were fabricated using the PLZT waveguides. Efficient switching of light coupled in the waveguides was achieved by applying voltage between the top electrodes and the substrates to induce the excellent EO properties of PLZT waveguides including low-voltage and polarization independent index change. Switching time less than 3 ns and 20 dB extinction ratio at 10V were confirmed (Fig. 3).

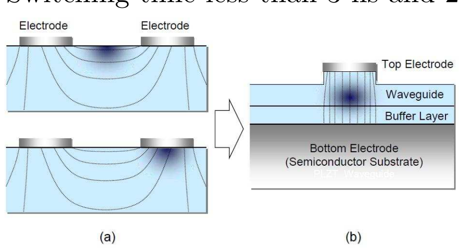

Figure 1: Coplanar electrode geometry (a) and sandwiched electrode geometry (b).

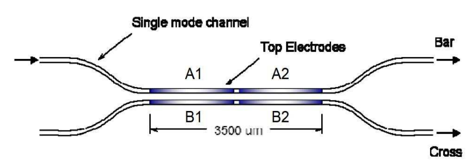

Figure 2: Top view of 1×2 dc switch in a PLZT waveguide.

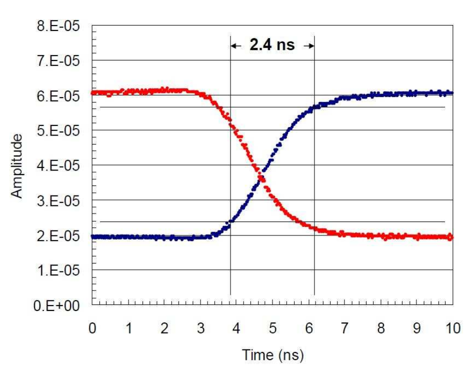

Figure 3: Active voltage response of 1×2 PLZT switch.

Property of Resonant Electrode of Coupled Microstrip Lines for Guided-Wave EO modulator

A. Enokihara and **H. Yajima**
Matsushita Electric Industrial Co., Ltd., Japan
H. Murata and **Y. Okamura**
Osaka University, Japan

Guided-wave electro-optic (EO) modulators with resonator electrodes can exhibit high modulation efficiency with band-operation for their short electrode length. This feature is promising for the ROF systems. Conventional EO modulators commonly use electrodes of the coplanar waveguide (CPW) structure. Here, we demonstrate a novel EO modulator using a resonator electrode of coupled microstrip lines (CMLs). The properties of the CML electrode were evaluated and the modulator operation at 60 GHz was experimentally confirmed.

Figure 1 shows the proposed modulator. The modulation electrode consists of two CMLs shorted at the both ends for the half-wavelength resonance. Coupled lines support odd and even propagation modes. The odd mode, where the voltage between the lines is twice of that of each line to ground, can particularly induce a high electric field around the optical waveguides. Moreover the cross sectional configuration is perfectly symmetric and ground electrode is separated in the bottom surface, so that some advantages, such as the zero frequency chirp in modulation and stability of the ground potential level, are expected.

The properties of the CML electrode on $LiNbO_3$ substrate were calculated using the conformal mapping method. Figures 2 show characteristics impedances Z_o and Z_e (a), and wavelength λ_o and λ_e of 60 GHz RF signals (b), for the odd and the even mode, respectively, as functions of gap spacing S, where the line width W is 48 μm. Since two modes have large difference in characteristic impedance, the odd mode resonance can be selectively excited with the feed line by adequately adjusting the feed point x. The wavelength λ_o of the odd mode decreases with S, which is caused by increasing the internal inductance.

The modulator was designed and fabricated for 60 GHz modulation with 1.3 m light, in order to confirm the millimeter-wave modulator operation. S and L were determined at 22 μm and 0.54 mm, respectively. The maximum of the modulation coefficient, m of 0.13 rad was obtained at around 61 GHz as seen from Fig.3, which corresponds to 2.4 rad by normalized at 1 cm resonator length.

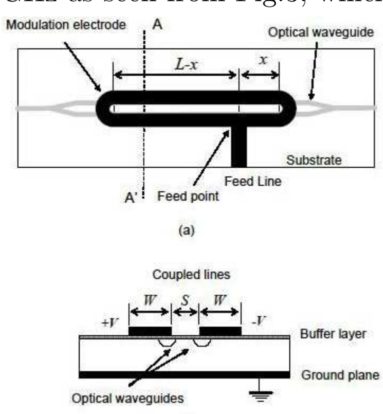

Figure 1: Structure of the modulator with a resonator electrode of coupled microstrip-lines; plane view (a) and cross section at the line A-A'(b).

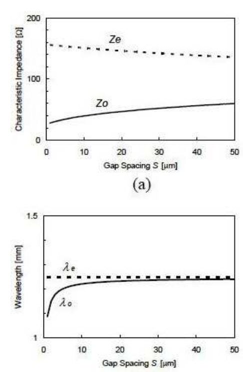

Figure 2: (a) Characteristics impedances and (b) wavelengths of 60 GHz RF signals, for the two modes

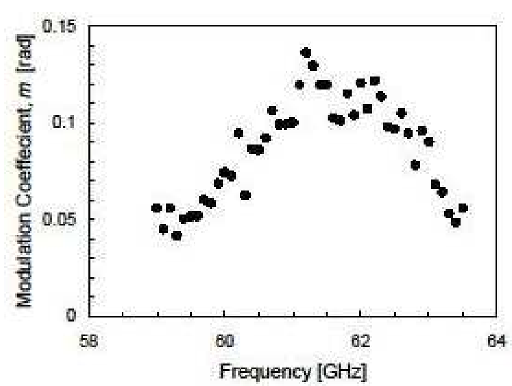

Figure 3: Frequency dependence of modulation coefficient, m, normalized at 100 mW signal input.

Ring Resonator-Based Electro-Optic Polymer Modulator and Its Linearity

H. Tazawa, Y. H. Kuo, and **W. H. Steier**
University of Southern California, U.S.A.

B. Bortnik, Y. C. Hung, I. Dunayevskiy, and H. R. Fetterman
University of California, U.S.A.

J. Luo and **A. K. Y. Jen**
University of Washington, U.S.A.

In microwave photonics applications, optical modulation technologies are essential to impose a microwave or a millimeter-wave signal on an optical carrier. Many of these applications require a sensitive modulator to reduce the driving power and a linear modulator to obtain high intermodulation-free dynamic range. Recently, resonant modulators have attracted great interest for microwave photonics applications. The enhancement of the modulation sensitivity by either a resonant electrode or an optical resonance reduces the driving power at the expense of a reduced operation bandwidth around the resonance frequency. Ring and disk micro-resonator based modulators are examples of optical resonator-based modulators. High Q optical resonances result in increased modulation efficiency but the RF bandwidth is limited by the resonator line-width. The modulators can therefore be operated at this bandwidth either at baseband or at an RF frequency equal to a multiple of the free spectral range (FSR) of the resonator. Electro-optic (EO) polymer and semiconductor ring resonator-based modulators have demonstrated baseband operation. Millimeter size $LiNbO_3$ disk resonator-based modulators have demonstrated efficient band-pass operation in the microwave and millimeter-wave region.

In this paper, we will present data on the band-pass operation in an EO polymer ring modulator. The modulator is made from highly nonlinear polymer AJL8/APC. The features of the modulator are as follows: (i) modest Q optical resonance and modulation at the FSR result in efficient modulation in a 7 GHz band around 28 GHz, (ii) the modulator is a waveguide device, whereas previous LiNbO3 disk resonator based modulators used prism coupling to input and output light, and (iii) the use of a traveling electrode rather than a capacitive electrode shows efficient modulation around the FSR frequency. Data on the operation at millimeter-wave frequencies which are the third and fourth multiples of the FSR is also included.

Then we will present experimental studies on linearity of an EO polymer ring modulator. The modulator shows a suppression of third-order distortion near a half transmission bias point. From the experimental transfer function and typical link parameters, the intermodulation-free dynamic range of the modulator is predicted to be 123 dB. A scheme to obtain ultra-high linearity using two ring modulators is also proposed.

Resonant Type $LiNbO_3$ Optical Modulator Array with Micro Strip Antennas

S. Shinada, T. Kawanishi, and **M. Izutsu**
National Institute of Information and Communications Technology (NICT), Japan

For the uplink of the radio on fiber (ROF) system [1], a high efficient conversion technique from millimeter wave to light wave is needed. We have proposed the optical modulator array with antennas as a novel converter [2]. The modulator array is driven by the received power of the connected antennas, therefore a low voltage driving is required for a modulator. The resonant type optical modulator has higher modulating efficiency than the conventional (traveling wave type) modulator [3], and its compactness can help the integration of the large number of array in a chip. In this paper, we demonstrated four aligned modulators on the Ti in-diffused optical waveguide in a $LiNbO_3$ substrate and connected antennas with each modulator. The characteristics of the modulator array in the experiment of the free space transmission of 10 GHz RF signal is presented.

We fabricated the resonant type optical modulators with stub electrode, which works for an impedance control. The proper impedance gives higher voltage signal to the modulating electrode and results in higher optical phase shift. We also fabricated 10 GHz resonant micro strip antennas (MSAs) which formed a square copper electrode (8.5 mm on a side) on a teflon substrate. Four MSAs were connected with each modulator and the modulators were aligned at 13 mm interval, which was corresponding to the light propagating length in Ti:$LiNbO_3$ for $(10\ \text{GHz})^{-1}$. Figure 1 shows the experimental setup of free space transmission of 10 GHz RF signal. We used a horn antenna as a transmitting antenna and the distance between the horn antenna and MSAs was an experimental parameter. An optical phase shift can be evaluated from the ratio between 0th and 1st peak intensities of modulating spectra [4]. Figure 2 shows the phase shift depended on the number of MSAs and the inset was optical spectra. The phase shift of 0.035 rad. was obtained at four antennas at the distance of antennas (Horn antenna - MSAs) of 1 m. The input power to the horn antenna was 31 dBm and the estimated received power of a MSA was -13.4 dBm. Larger phase shift will be obtained by the larger number of arrays.

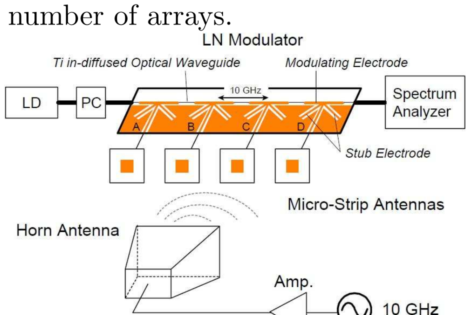

Figure 1: Experimental setup of the free space transmission of RF signal. A 10 GHz RF signal was generated by the horn antenna and received by MSAs. Four aligned modulators were driven by the received power.

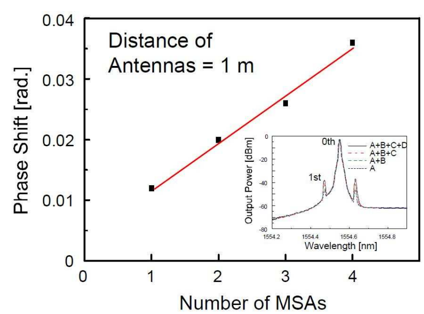

Figure 2: Optical phase shift dependence of the number of connected MSAs. The inset is spectra of optical signal modulated by received power of MSAs.

Acknowledgement

The authors would like to acknowledge M. Tsuchiya of NICT, S. Kurokawa of Advanced Industrial Science and Technology, K. Nishikawa of Kyosemi, and M. Andachi of Kyoto Prefectural Technology Center for Small and Medium Enterprises, for their useful discussions. This work was supported by the Japan Society for the Promotion of Science (JSPS) for Grants-in-Aid for Scientific Research (B) (♯16360183).

REFERENCES

1. W.D. Jemison, gFiber radio: from links to networks,h *microwave photonics 2001*, pp. 169-172, 2001.
2. M. Izutsu, *29th European Microwave Conference, Workshop M-FrW2*, Munich Germany, October 1999.
3. T. Kawanishi, S. Oikawa, K. Higuma, Y. Matsuo and M. Izutsu, *Electron. Lett.* vol. 37, pp. 1244-1246, 2001.
4. S. Oikawa, T. Kawanishi and M. Izutsu, *IEEE Photon. Tech. Lett.*, 15, pp. 682-684, 2003.

Broadband Antenna Measurement with Optical Fiber Link System

S. Kurokawa, M. Hirose, and **K. Komiyama**
National Institute of Advanced Industrial Science and Technology, Japan

We have proposed the optical fiber link antenna measurement system that can measure the calibrated S11 and S21 between two antennas under test (AUT) after OSLT calibration in one-pass two-port system[1][2]. Our measurement system is schematically shown in Figure 1. Our system consists of the transmitting and receiving optical-fiber link systems. The transmitting system consists of the Electro-Absorptive modulator, Erbium Doped Fiber Optical Amplifier (EDFA), optical fiber, zero biased Uni-Traveling-Carrier Photodiode (UTC-PD)[3], small type bi-directional coupler, and two optical reflection type Mach-Zehnder LiNbO3 optical intensity modulators (LN-modulators) with 50 ohm loads. The system can detect the reflection signal from the transmitting AUT and the reference signal toward the AUT. The receiving system consists of an optical reflection type LN-modulator and the optical field measurement system, to measure the transmission signal through the receiving AUT. Our system can measure the reference signal, the reflection signal, and the transmission signal in one-pass two-port model between the two AUTs. Then OSLT calibration can be adopted.

In this paper, in order to demonstrate the validity of our optical fiber link system, we compare the calibrated S11 and S21 results of two UHALP9108A1 Log-periodic antennas by our proposed optical-fiber link system with the ones by the conventional coaxial cable system in frequency-domain.

The measured $S_{11}(\omega)$ and $S_{21}(\omega)$ are shown in Fig. 2 and Fig. 3, respectively. The results of the S_{11} and S_{21} of the LPDAs by the optical fiber link system agree very well with those of the conventional coaxial system. It is shown by the comparison that the optical system has a good performance to measure S_{11} and S_{21} even in broad frequency range. In the case of frequency domain$S_{11}(\omega)$, the difference shows good agreement of the optical link system and the coaxial cable system in amplitude within about 0.5 dB, in phase within about 10 degrees over the range from 300 MHz to 2400 MHz except around sharp dips. In the case of frequency domain $S_{21}(\omega)$, the difference shows good agreement of them in amplitude of $S_{21}(\omega)$ within about 1dB and in phase within about 10 degrees over the range from 300 MHz to 1800 MHz without any resonance phenomena. Nevertheless, there still remains a small disagreement between the results by the two systems. It is caused by insufficient dynamic range of the optical system because the received signal is too small for the optical system. Further improvements on the dynamic range of the system are required for better performance to the degree of the conventional metal cable system. It will be realized, for example, by the improvement of the sensitivity of the LN -modulator.

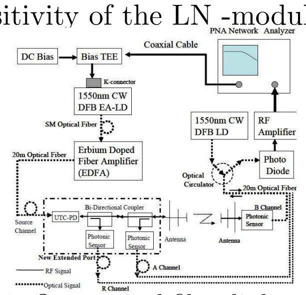

Fig. 1: Our optical fiber link antenna measurement system

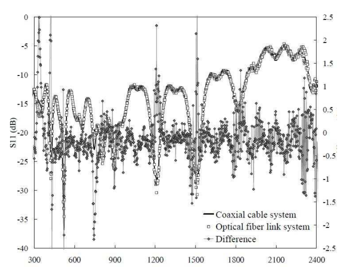

Fig. 2: Measured $S_{11}(\omega)s$ and the difference of $S_{11}(\omega)s$

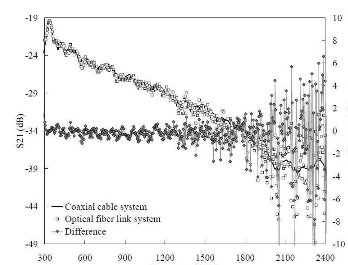

Fig. 3: Measured $S_{11}(\omega)s$ and the difference of $S_{11}(\omega)s$

REFERENCES

1. E8356A Users Manual, Agilent Technology.
2. M. Hirose, S. Kurokawa, and K. Komiyama, "Characteristics of a Novel Model of RF One-Path Vector Network Analyzer using Optical Transmission," *IEEJ Technical Report*, IM-05-33, pp.79-82, (2005-6). (In Japanese)
3. T. Ishibashi, N. Shimizu, S. Kodama, H. Ito, T. Nagatsuma, and T. Furuta, *Tech.. Dig. Ultrafast Electron. And Optoelectron*, pp.166-169 (1997).

Antenna Absolute Gain and Pattern Measurements Using Photonic Sensor and Compact Spherical Near-Field Scanner

M. Hirose, S. Kurokawa, and **K. Komiyama**
National Institute of Advanced Industrial Science and Technology, Japan

We have developed a new compact spherical near-field measurement system using a photonic sensor as a probe and successfully measured the 3D antenna patterns of a double-ridged horn antenna from 1 GHz to 10 GHz. This system consists of a compact spherical scanner and a photonic sensor that is used for the probe of the spherical near-field measurements. In our system, only one probe can be used for the wide frequency range measurements and the probe compensation is not needed in the measurements. For the system, we have proposed a simple calibration method using a double-ridged horn antenna for our system. We have calibrated the system by measuring the double-ridged horn antenna on the reasonable assumption that the antenna efficiency is 100 %. Comparing the absolute gain obtained by the proposed calibration method with the one decided by using three-antenna method at far-field range, we show that the agreement is good within 1 dB over the whole frequency range.

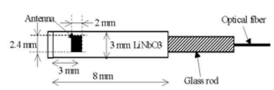

Fig. 1 Geometrical structure of the photonic sensor.

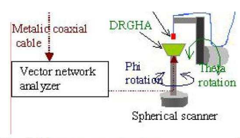

Fig. 2 Measurement setup

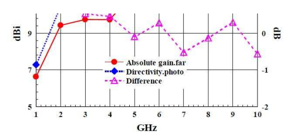

Fig. 3 Frequency characteristics of the absolute gain, the directivity, and their difference for EMCO 3115, which are measured by the three-antenna method (far) and the photonic sensor (photo).

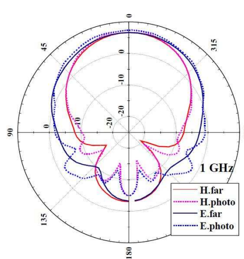

Fig. 4 Principal absolute gain patterns at 1 GHz (dBi in unit), on the E and H planes for EMCO 3115, measured by the three-antenna method (far) and the SNFMS using the photonic sensor (photo)..

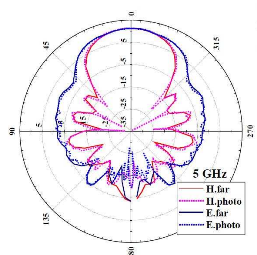

Fig. 5 Principal absolute gain patterns at 5 GHz on the E and H planes.

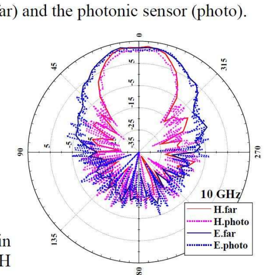

Fig. 6 Principal absolute gain patterns at 10 GHz on the E and H planes.

REFERENCES

1. M. Hirose, T. Ishizone, and K. Komiyama, gAntenna Pattern Measurements Using Photonic Sensor for Planar Near-Field Measurement at X Bandh, *IEICE Trans. Communications*, Vol.E87-B, No.3, pp.727-734, March 2004.
2. M. Hirose, S. Kurokawa, and K. Komiyama, hCompact Spherical Near-Field Measurement System for UWB Antennas,h 2005 IEEE APS Int. Sym, Vol.4, sp55p06a.pdf, Washington DC.
3. J. E. Hansen ed., Spherical Near-Field Antenna Measurements, IEE Electromagnetic waves series 26, 1988.

Resonant-Electrode-Type Optoelectronic Oscillator (RE-OEO) as a Single-Mode Oscillator

T. Sakamoto, T. Kawanishi, and **M. Izutsu**
National Institute of Information and Communications Technology (NICT), Japan

Optoelectronic oscillators (OEOs) [1-6] are very attractive devices for optical clock or subcarrier signal generation. One of the most important features of the OEO is that such signals can be generated without any external microwave sources. Clock recovery or other functions useful for optical signal processing are easily obtained by this technology. Especially, in microwave or millimeter-wave photonic technologies, OEOs can play significant roles as photonic local oscillators [2-6].

For these purposes, it is important to achieve single-mode oscillation using the OEO. Conventionally, RF or optical band-pass filter is necessary to avoid multi-mode oscillation since a wideband modulator is embedded in the OEO [1]. On the other hand, in our former report, we have proposed a much simpler OEO configuration, called resonant-electrode-type OEO (RE-OEO) [2], consisting of a resonant-electrode-type modulator. The modulator, employed in the RE-OEO, has a resonant structure in the modulation electrode [7][8][9], so that its modulation bandwidth is limited but the modulation efficiency is improved. Note that the RE-OEO can oscillate only at the frequency of the resonance without using any optical or RF filters, because the modulation efficiency out of the resonant frequency is suppressed. Therefore, single-mode operation is easily obtained. In addition, it is expected that the RE-OEO made of such modulators oscillate with lower threshold power. This scheme can greatly reduce complexity and cost of OEOs. First, in this paper, we describe principles of the RE-OEO that employs an optical modulator with a resonant electrode in double-stub structure. Second, basic oscillation characteristics of the RE-OEO are presented: Optical clock or subcarrier generation was achieved in a single-mode self-oscillating operation at a frequency of 6.9 GHz with an optical input threshold power of 0.01 mW. Finally, we report on properties of the RE-OEO injection locked to a microwave signal, which were evaluated with real-time time-frequency measurements.

REFERENCES

[1] X. S. Yao, and L. Maleki, "High frequency optical subcarrier generator," Electron. Lett., vol. 30, no. 18, pp. 1525-1526, 1994.

[2] T. Sakamoto, S. Shinada, T. Kawanishi, and M. Izutsu "Optoelectronic Oscillator Using Resonant-electrode-type LiNbO3 Modulator for FM Subcarrier Generation," 30th European Conference on Optical Communication (ECOC-IOOC 2004), WE4.P.49, 2004.

[3] T. Sakamoto, T. Kawanishi, and M. Izutsu, "Optical Frequency Comb Generation by Optoelectronic Oscillator Made of LiNbO3 Phase Modulator", Opt. Lett

[4] T. Sakamoto, T. Kawanishi, S. Shinada, and M. Izutsu, "Opoelectronic oscillator using LiNbO3 intensity modulator with resonant electrode," Electron. Lett. vol. 41, no. 12, pp. 2005.

[5] T. Sakamoto, T. Kawanishi, and M. Izutsu, "Optoelectronic Oscillator Using Push-Pull Mach-Zehnder Modulator Biased at Null Point for Optical Two-Tone Signal Generation", Conference on Laser and Electro Optics (CLEO/IQEC2005), CTuN5, May, 2005.

[6] T. Sakamoto, T. Kawanishi, S. Shinada and M. Izutsu, "Photo-electronic Oscillator for Frequency Comb Generation Fed Back with Asymmetric-filtered Deeply Phase-modulated Light", International Topical Meeting on Microwave Photonics (MWP 2004), MC16.

[7] M. Izutsu, T. Mizouchi, and T. Sueta, "Band operatioin of guided-wave light modulation with filter-type coplanar electrodes," IEICE. Trans., vol. E78-C, no. 20, pp. 55-60, 1995.

[8] T. Kawanishi, S. Oikawa, K. Higuma, Y. Matsuo, and M. Izutsu, "LiNbO3 resonant-type optical modulator with double structure," Electron. Lett., vol. 30, no. 20, pp. 1244-1246, 2001.

[9] A. Enokihara, H. Yajima, M. Kosaki, H. Murata, and Y. Okamura, "LiNbO3 resonant-type optical modulator with double structure," Electron. Lett., vol. 39, no. 23, pp. 1671-1672, 2003.

A Study on Dispersion Tolerance of 10Gbit/s $LiNbO_3$ Mach-Zehnder Modulator

T. Fujita and **S. Oikawa**
Sumitomo Osaka Cement Co., Ltd., Japan

Optical $LiNbO_3$ (LN) modulators integrated in the 300pin Multi Source Agreement (MSA) complied 10Gbit/s transponders for long-reach are key components in the metro-area networks, because of their high extinction ratio and low chirp characteristics. As the demand for higher bit-rate and longer transmission distance increases, optical LN modulators must preserve the quality of the modulated data and adapt to higher bit rate operation to carry additional error correction data. Several works in literature show the benefits of signal chirping on transmission performances [1]-[3]. In this paper, we focused on chirp factor and optical response of LN modulators and studied effect of those two parameters on the tolerance to dispersion, especially in 80km fiber transmission (=1600ps/nm).

Optical response of the transmitter is mostly equal to combined response of the LN modulator and the driver amplifier. Fig.1 shows transmitter optical response and output eye diagrams. Rise time and fall time (Tr/Tf) can be changed by reducing transmitter bandwidth. Thus, optical response of the transmitter is related to Tr/Tr of Eye diagram. Fig.2 shows received power at BER=10^{-12} as a function of Tr/Tf for BTB and after 95km(1620ps/nm) transmission. In this demonstration, the chirp parameter α of the LN modulator is -0.7 and operation bit-rate is 10.709Gbps. Fig 3 shows Q-MAP calculation at 10.7Gbit/s (SONET/SDH with FEC) and 11.1Gbit/s (10GbE with FEC). These results reveal that excess bandwidth deteriorates performance after transmission. We also confirmed that operation bit-rate rising from 10.7Gbit/s to 11.1Gbit/s causes more than 1dB deterioration of Q-factor.

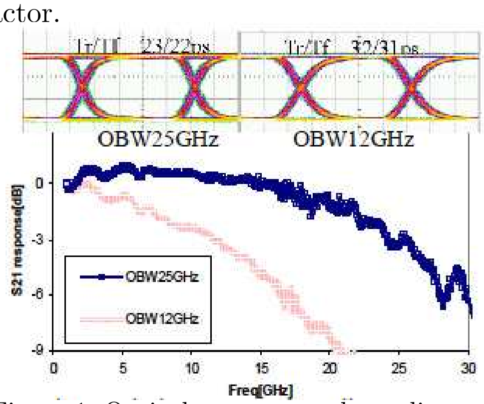

Figure 1: Optical response and eye diagrams

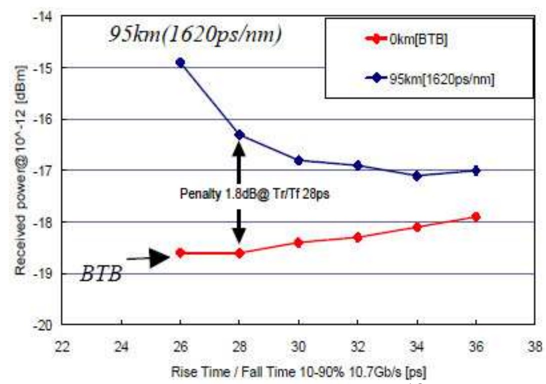

Figure 2: Recieved power at 10^{-12} vs Tr/Tf

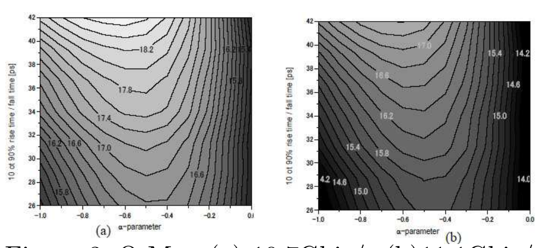

Figure 3: Q-Map (a) 10.7Gbit/s (b)11.1Gbit/s

REFERENCES

1. A.H.Gnauck, K.Korotky, et al, *IEEE Photonics Technology Letters*, Vol.3, No.10, Oct 1991
2. Jianjun Yu, Martin Fischer, *IEEE Photonics Technology Letters*, Vol.14, No.12, Dec 2002
3. P. Bravetti, G.Ghislotti, et al, *IEEE Journal of Lightwave Technology*, vol.22, No2, Feb 2004

Variable Frequency Shifting of a Continuous Light Wave Based on Multistage Phase Modulation

S. Hisatake and **T. Kobayashi**

Osaka University, Japan

Optical frequency shifters are expected to play an important role in various fields, including optical communication systems. A single-sideband frequency shifter (theoretical efficiency of 34%) [1] and Bragg diffraction type electro-optic frequency shifter (theoretical efficiency of 100%) [2] have been demonstrated. Although those techniques provide over 10-GHz frequency shifting, they are not suitable for a wide-range variable frequency shifter because the shifting amount can be manipulated only by change of the modulation frequency. In this paper, we propose and numerically demonstrate an efficient variable frequency shift technique for a continuous light wave.

The proposed frequency shifting process is shown schematically in Fig. 1(a). The shifting process consists of three stages: (i) phase modulation and chirp compression for generating a pulse train, (ii) center frequency shifting of the pulse train through a Doppler shift in a second phase modulation, and (iii) demodulation of the pulse train through a reverse process of (i). All EOMs are assumed to be driven at the same modulation frequency, f_m. The relative modulation phase between the EOM1 and the EOM2 is adjusted such that the chirp compressed pulses go through the medium of EOM2 at times when the refractive index increases or decreases at the fastest rate. Although the temporal intensity profile is not influenced by the second phase modulation, the optical pulse spectrum seems to have shifted as shown in Fig. 1(a). Filtering the $n^{"}_{max}$ component, we achieve continuous light wave whose frequency is shifted by $n^{"}_{max}$ from that of the input light wave.

Figure 1(b) shows the calculated characteristics of the destination sideband number $n^{"}_{max}$ and the shifting efficiency as a function of the modulation index of the EOM2. $n^{"}_{max}$ increases discretely with increasing $\Delta\theta_2$. The overall frequency shifting efficiency is approximately 40-50%. The shifting efficiency changes by 5% with a change in the modulation index of 1 rad. The destination frequency, which can be controlled by $\Delta\theta_2$, lies in the frequency grid spaced accurately by the modulation frequency f_m. This characteristic is useful for the frequency (wavelength) converters in wavelengthdivision multiplexing optical communication systems.

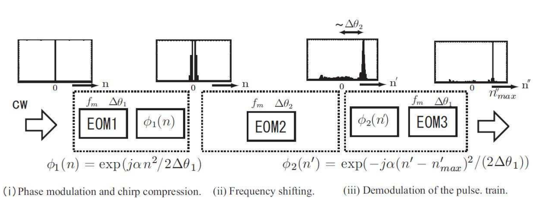

Figure 1: a) Schematic of the proposed frequency shifting process.

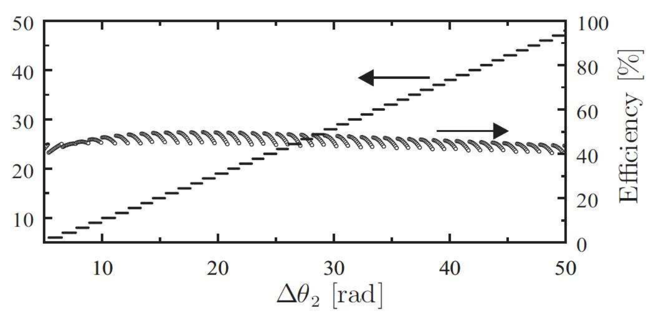

Figure 2: b) Shifting e.ciency and $n^{"}_{max}$ characteristics as a function of $\Delta\theta_2$

REFERENCES

1. M. Izutsu, S. Shikama and T. Sueta, *IEEE J. Quantum Electron.,* 17, 2225-2227(1981).
2. Shibuya, S. Hisatake, and T. Kobayashi, *IEEE Photon, Technol. lett.* 16, 1939-1941(2004).

Session 3A6
SAR/Polarimetry

ESPRIT-based Pol-InSAR Technique with Scattering Model Decomposition Preprocessing for Forest Analysis

H. Yamada, M. Yamazaki, and **Y. Yamaguchi**

Niigata University, Japan

Many decomposition techniques have been proposed in POL-SAR (Polarimetric SAR) image analysis. Among them, scattering model decomposition proposed by Freeman and Durden[1] will have a preferable feature for understanding POLSAR images because of the model based technique. They decomposed POL-SAR image into surface, double bounce, and volume scattering component. Decomposed result by the technique is always acceptable, however, it sometimes fails: power of decomposed component becomes negative. It would be caused by the assumption of the volume scattering as random oriented wires. In real forest, covariance matrix for the volume scattering component depends on probability distribution function (PDF) of tree trunks and branch. The extended technique has proposed by Yamaguchi, et al[2].

In this report, we employ the extended decomposition technique as the ESPRIT-based Pol-InSAR analysis. The ESPRIT-based POL-InSAR[3] is an alternative polarimetric SAR interferometry technique proposed by Cloude and Papathanassiou[4]. The technique discriminates interferometric phase of the ground and canopy top separately, then the forest height can be determined by the phase difference. In the proposed modified technique, the PDF for each patch in forest region is also one of unknown parameters to be estimated in addition to interferometric phases in the patch. We employ the decomposition technique as a volume scattering removal filter. As reported in [5], severe volume scattering components often causes phase errors in the ESPRIT analysis. Therefore, when the component can be correctly removed, the ESPRIT works properly. We propose a criterion for suitable PDF estimation in the ESPRIT processing. By this modification, estimation accuracy of interferometric phases in the dense forest region by the conventional ESPRIT-based technique is also improved. In the presentation, we will provide some experimental results of E-SAR and SIR-C/X-SAR data. These results show the potential not only the accuracy improvement of forest tree height estimation, but also the tree trunks and branch distribution in Pol-InSAR analysis.

REFERENCES

1. A.Freeman and S.L.Durden, "A three-component scattering model for polarimetric SAR data," *IEEE Trans. Geosci. Remote Sensing.*, vol.36, no.3, pp.963-973, May 1998.
2. Y.Yamaguchi, et al., "Four-component scattering model for polarimetric SAR image decomposition," *IEEE Trans. Geosci. Remote Sensing.*, vol.43, no.8, pp.1699-1706, Aug.2005.
3. S.R.Cloude and K.P.Papathanassiou, "Polarimetric SAR interferometry," *IEEE Trans. Geosci. Remote Sensing.*, vol.36, no.5, pp.1551-1565, Sept. 1998.
4. H.Yamada, et al., "Polarimetric SAR interferometry for forest analysis based on the ESPRIT algorithm," *IEICE Trans. Electron.*, vol.E84-C, No.12, pp.1917-1924, Dec.2001.
5. H.Yamada, et al., "Forest Height feature extraction in polarimetric SAR interferometry by using rotational invariance property", *Proc. of IGARSS 2003*, on CD-ROM, July, 2003.

Polarization Orientation Angle Analysis of Pol-SAR Using Multiple Flight Paths Dataset

K. Iribe and **M. Sato**
Tohoku University, Japan

It is well known that the polarimetric scattering property of the target changes with the radar illumination direction [1]. The change of the illumination direction corresponds to rotate the target on the horizontal plane, relatively. If the target rotates, the polarization state will change, and induce the polarization orientation angle shift in some cases [2]. There, we attempted the analysis of the orientation angle for target feature.

We used Pol-SAR dataset acquired by Pi-SAR. Several Pi-SAR datasets have been acquired over Sendai, Japan since 2001. During the data acquisition in February 2005, Pi-SAR flow above Sendai along a square loop flight paths within short period. Sendai area includes various kinds of land uses like downtown, forests, river and flat ground. By using Pol-SAR dataset of Sendai area acquired from multiple fight paths, the polarization orientation angle analysis on the basis of the effect of the azimuth incident angle is possible.

We calculated the orientation angle from Pol-SAR datasets of Sendai area. When we picked up the housing communities, a good agreement between the orientation angles and the azimuth angles of houses could be seen. Furthermore, it could be found that there are variations in the orientation angles induced by houses in certain cases, and the variation depends on the azimuth angle of the house. Some models about scattering components of the house were reported, they took up the wall and the roof of the house as scatterers. In addition to that, we consider the side wall as a scatterer which induces the orientation angle shift. And also, the different property of the orientation angle could be seen between X- and L-band dataset. It can be thought that the difference of the frequency band of the transmitted wave causes changes with the contributions of the Bragg scattering component. We will show the relationships between the property of the orientation angle and the Bragg scattering component.

REFERENCES

1. K. Iribe, M. Sato, gIncident Angle Dependence of Pi-SAR Polarimetric Scattering Characteristics,h Proc. of ISAP f04, Sendai, Japan, CD-R
2. H. Kimura, K. P. Papathanassiou, I. Hanjsek, gPolarization Orientation Effects in Urban Areas on SAR data,h Proc.IEEE Int. Symp Geoscience and Remote Sensing, IGARSS2005, Seoul, South Korea, July, 2005, CD-R

Modified Range Migration Algorithm for Airborne Squint Mode Spotlight SAR Data Procession

H. S. Shin and **J. T. Lim**
Korea Advanced Institute of Science and Technology, Korea

Synthetic aperture radar (SAR) is a powerful remote sensing technique that allows the generation of microwave images of the earth's surface, independently of weather condition and sun illumination. In particular, spotlight SAR is able to obtain a high azimuth resolution by steering the radar antenna beam during the raw data acquisition interval, to always illuminate the same area on the ground. Several algorithms have been developed for the reconstruction of SAR data [1]-[3]. Each has its own advantages and drawbacks. Conventional SAR methods like the polar format algorithm (PFA) typically employ the plane wave assumption. However, the range migration algorithm (RMA) method increases the resolution by modeling the actual spherical wave. Moreover, since the RMA technique has a computation effciency and produces acceptable results in a broadside situation, it is available for SAR data processing. However, if spotlight images are recorded in a squinted geometry, crucial problems arise in the RMA technique. That is, since the RMA technique requires phase compensation to a line unlike the PFA technique, the phase of scene center scatter is changed after motion compensation to a line [1]. Thus, the RMA technique cannot yield an acceptable performance in the squint mode. If this problem is not properly compensated during the SAR data processing, the quality of the final image in squint mode SAR is degraded. Also, since squinting could increase the flexibility with which a desired area on the surface is imaged within a flight path, it is necessary to process the squint mode SAR data. Though several methods have been studied in stripmap mode SAR with a squint angle, in the case of spotlight SAR with a squint angle, it is a still difficult task to obtain the high quality images [4]-[5]. Especially, in squint mode spotlight SAR, the PFA is accommodated [1]. However, this algorithm avails for a relatively small scene area. Thus, in this paper, we introduce an extension of the original RMA to enable a more effcient way of spotlight data processing with a squint angle. To solve the problem in the RMA with a squinted geometry, using an approximation and a coordinate transformation, we transform an original squinted raw data to a broadside-mode raw data. Then, we analyze the formulation using the principle of the stationary phase. Moreover, we test the proposed algorithm with some numerical simulations via a pulsed spotlight SAR simulator.

REFERENCES

1. CARRARA, W.G., GOODMAN, R.S., and MAJEWSKI, R.M.: 'Spotlight synthetic aperture radar signal processing algorithms' (Artech House, 1995)
2. SOUMEKH, M.: 'Synthetic aperture radar signal processing with MATLAB algorithms' (John Wiley & Sons, Inc., 1999)
3. CAFFORIO, C., PRATI, C., and ROCCA, E.: 'SAR data focusing using seismic migration techniques', *IEEE Trans. Aerosp. Electro. Syst.*, 1991, 27, (2), pp. 194-207
4. DAVIDSON, G.W., CUMMING, I.G., and ITO, M.R.: 'A chirp scaling approach for processing squint mode SAR data', *IEEE Trans. Aerosp. Electro. Syst.*, 1996, 32, (1), pp. 121-132
5. YEO, T.S., TAN, N.L., ZHANG, C.B., and LU, Y.H.: 'A new subaperture approach to high squint SAR processing', *IEEE Trans. Geosci. Remote Sens.*, 2001, 39, (5), pp. 954-968 1

Phase Unwrapping by Spreading Phase Singularity in Airbone Interferogram

R. Yamaki and **A. Hirose**
The Univirsity of Tokyo, Japan

Interferogram generated in InSAR systems and other radars, is used to yield digital elevation map (DEM) that expresses landscape. Since the obtained phase data is wrapped into $-\pi$ to π, we need to unwrap the phase value to construct a DEM. However, phase unwrapping is a diffcult problem to computers because the phase data contains many singular points (residues). For accurate estimation of the unwrapped phase, how to process the singular points is a cardinal problem. In 1998, Costantini (IEEE TRANSACTIONS ON GEOSCIENCE AND REMOTE SENSING,

Vol.36, No.3, pp.813 821, May 1998) proposed an efficient method based on network programming, which is now mainstream. This method solved the two main problems in conventional local phase unwrapping, i.e., where to place branch-cuts and how to search integration path. However, the network model is often yields hunnaturalh 2π cliffs just like the conventional branch-cut method does. There exist characteristic properties in the distribution of singular points. Based on the properties we consider that they originate from interference of electromagnetic wave where layover appears, or from unreliability of phase in shadowed area. Therefore, the phase singular points should be corrected in a continuous manner with its vincity, not in discrete way with 2π phase shifts.

In this paper, we propose a new phase unwrapping method with a preprocess to spread phase singularity (Singularity Spreading Phase Unwrapping : SSPU). Rotaion of the phase value means phase inconsistency. By compensating phase differences with continuous values to cancel the inconsistency, we spread the singularity around the singular point as shown in Fig.1. With iterations of this process, posivie and negative residue pairs combine each other and disappear without generating any unnatural cliffs. Isorated residues also become invisible since the singularity is broken into fractions around them or swept out of the image. With such above-mentioned effects, inconsistency in the whole image convergences to zero. After the spreading process, we can unwrap the phase data just by summing up the phase differences in any direction. In the network programming aproach, the more residue we have, the more calculation time is required. In the SSPU, contrarily, the calculation cost is very low and independ of residue density.

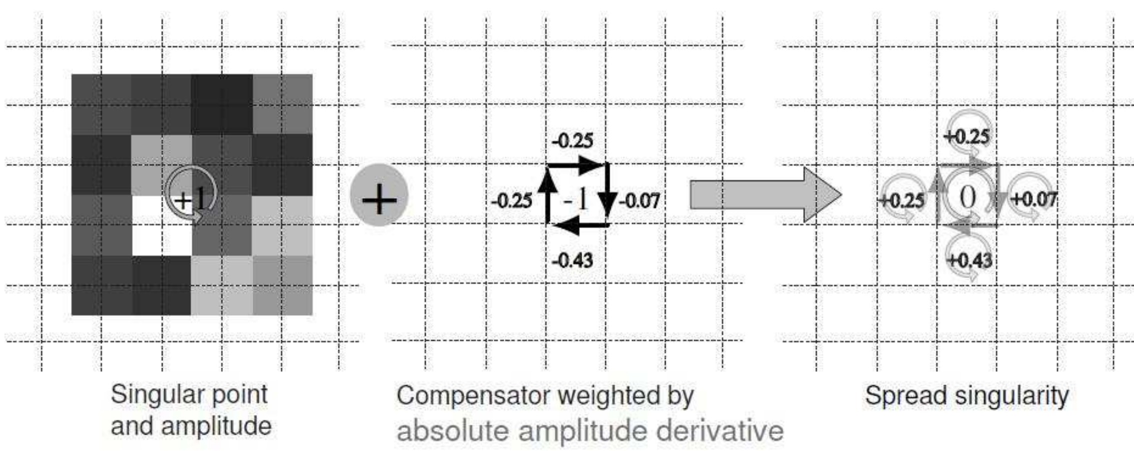

Figure 1: The "spreading" of the singularity

Evaluation of the Scattering Characteristics of Trihedral Corner Reflector for Polarimetric SAR Calibration

S. Kusano and **M. Sato**
Tohoku University, Japan

Polarimetric calibration is needed for exact observation of the polarimetric SAR data. Trihedral corner reflector is usually used for polarimetric calibration. Theoretical scattering characteristics of a trihedral corner reflector, i.e., HH component is equal to VV and cross-pol is neglible compared to co-pol, is well known in the following case: the size of the reflector is much larger than the transmission wavelength, and the incident direction is along symmetry axis of the reflector. However, if these conditions are not satisfied, theoretical scattering characteristics changes. The knowledge of the scattering characteristics of a trihedral corner reflector is needed for accurate polarimetric calibration. So, we investigated the scattering characteristics of a trihedral corner reflector with the simulation using the method of moment and the experiment in anechoic chamber for PALSAR polarimetric calibration.

From the result, it is found that cross-pol component of the scattered electric field strength is affected seriously by the azimuth angle. For example, when the azimuth incident angle is zero, the difference between co-pol and cross-pol of the scattered electric field strength is about 50dB. And, when the azimuth angle is 1 degree, the difference decrease to 20dB. In this case, cross-pol component is not negligible compared to co-pol component. However, the difference may increase with increasing the size of the reflector on the transmission EM wavelength. In the investigated area, the difference between HH and VV component is not stable, becase they are oscillating with converging. Larger size of the reflector or Larger incident angle is needed in order to conform HH to VV.

Now we are investigating the case of Larger incident angle.

Session 3A7
Novel Mathematical Methods in Electromagnetics I

Domain Decomposition Method for Conformal Modules Applied to the Design of On-Chip Passives in CMOS

J. X. Zhao
China Jiliang University, China

The domain decomposition method for conformal modules (DDM-CM), that was developed from the combination of conformal mapping theory and domain decomposition method, and its application in the design of passive devices on SOC, for exapmles, the resistance and inductance caculation of a longer thin film, the capacitance for arbitrary quadrilateral, and modeling the spiral inductors on SOI-CMOS substrates, are introduced in this paper. The advantage of DDM-CM is that the obtained result is simple and accurate, and that this method is free from solving the complex conformal mapping function and is valid for arbitrary contour of conductor as long as one can solve the conformal module.

Index Terms :DDM-CM, Applications, and Design of Passive Devices on SOC

Solving Stiff Inverse Problems Using Linear Relations Between Transient Characteristics

A. Adalev and **M. Hayakawa**
The University of Electro-Communications, Japan
N. V. Korovkin
Saint-Petersburg State Polytechnical University, Russia

The work is related to stiff inverse problems of electrical engineering. The inverse problem is considered as identification of mathematical model parameters by means of processing experimental data. Stiff problems have natural origins and appear more and more frequently in practice. To increase the model adequacy, we have to consider the processes and parameters of a device having essentially different scales (fast and slow, large and small). Being involved in the model simultaneously, they result in a high rate of model stiffness. The methods, developed recently for the analysis of stiff systems (direct problems), work with initially exact data and solve the problem of accuracy loss due to computational errors. However, these methods are useless for the inverse problems since computational errors are dominated by the experimental ones. Only direct measuring of model parameters, which is possible very rare, allows us to solve a stiff inverse problem accurate to the measurement precision. Otherwise the solution error may exceed the experimental one by several orders.

The first investigations were performed in relation with identification of linear electric circuits in the steady-state mode [1] considering ill-conditioned models. Here we present the latest results related to transient-mode identification. We discuss an electric circuit described by stiff ODE system with an ill-conditioned coefficient matrix being a very illustrative example. Actually the approach proposed is very general and may be used for any other objects.

A conventional approach of identifying model parameters in the transient mode is fitting the temporal variation of the measured responses, i.e. minimizing some residual functional. At least two drawbacks were found for the stiff system: (i) to obtain the functional value for a set of parameters one has to solve the stiff ODE system, which is a rather complicate and unstable process; (ii) for a stiff model, the functional is ravine-shaped, which makes difficulties for convergence of the minimization process. A new algorithm is proposed for the transient-mode identification in order to replace the conventional approach and overcome the drawbacks mentioned above.

It has been found that linear relations between transient characteristics measured for a stiff model are valid. The coefficients of the relations may be found by processing the experimental data according to the proposed technique. For the first time the linear relations were introduced in [2] and discussed in [3]. Here we present a new algorithm of their determination which is applicable for the identification problem and more convenient in practice. It has been shown that the linear relations may be obtained with accuracy close to the measurement precision level for a system with any arbitrary large rate of stiffness. Some technical details of experimental data processing are discussed. Being based on the linear relations determined, we propose a new formulation of the identification problem in the form of a nonlinear system of algebraic equations. The latter is proposed to be solved by a special iterative procedure involving a simplified sensitivity analysis.

REFERENCES

1. A. S. Adalev and N. V. Korovkin and M. Hayakawa, Identification of electric circuits described by ill-conditioned mathematical models," *IEEE Trans.Circuits Syst. I*, vol. 53, pp. 78–91, 2006.
2. Y. V. Rakitsky and S. M. Ustinov and I. G. Chernorutsky, *Numerical methods of solution of stiff systems*. Moscow: Nauka, 1979.
3. I. G. Chernorutsky, *Optimization methods in the control theory*. Saint-Petersburg: Piter, 2004.

Analysis of Coupling Between Two Rectangular Waveguides with a Common Flange

H. Serizawa [1] and **K. Hongo** [2]
[1]Numazu National College of Technology, Japan
[2]Toho University, Japan

A rectangular waveguide array has many practical applications in communication and radar systems, and mutual coupling between the waveguides has been studied by using an integral equation approach with a moment method or the related techniques [1-3]. In this paper, we propose an alternative analytical method based on the Kobayashi potential (KP) [4,5], which is expected to give more precise results, and we formulate the mutual coupling between two different-sized rectangular waveguides with a common flange. The flange and waveguides are assumed to be perfectly conducting, and the flange has the infinite extent and is located on the plane z=0 in the Cartesian coordinates (x, y, z). The purpose of our study is to investigate the effect of one guide (#2) on the radiation and modal characteristics of the other guide (#1) when only the waveguide #1 is excited by TE- and/or TM-modes that propagate in the positive z direction. To analyze this problem we introduce an equivalent magnetic current on the aperture #1. There may be two possibilities to specify this equivalent current. One way is to assume a single dipole current on the aperture such that the dipole field becomes the same as the radiation field from the waveguide. Another way is to assume the continuous equivalent current distribution that is given by the electric field distribution on the aperture. We use the latter idea, that is, we assume the continuous magnetic current on the aperture.

The procedure of the present method is summarized as follows. The z-component of the vector potentials is used to represent the fields in the waveguide. For the fields in the half-space (z¿0) we use the two-dimensional Fourier transforms of the x- and y-components of the vector potentials. By using the equivalent theorem the waveguide #1 is replaced by the equivalent magnetic current and we use a rigorous aperture field when the second guide #2 is absent (aperture #2 is covered by a perfect conductor). In the expressions of the vector potentials, we use the spectral representation for the Green function in free space, and then surface integrals on the aperture #1 are analytically performed. Enforcement of the required boundary conditions leads to the dual integral equations, which can be solved by applying the discontinuous properties of the Weber-Schafheitlin (WS) integrals and the concept of the projection (the basis functions of the functional space are the Jacobi's polynomials). In this process, the fields in the half space are expressed by a linear combination of wave functions that satisfy the boundary condition on the conducting flange. Finally, the problem is reduced to the matrix equations whose matrix elements consist of double infinite integrals and double infinite series. In contrast to the problem of a single waveguide, the equations include infinite integrals of four Bessel functions and two trigonometric functions. These integrals and series can be computed by applying the asymptotic expansion of the Bessel function with desired accuracy. Once the expansion coefficients are determined by solving the matrix equations, effects of the coupling on the radiation pattern and aperture fields can be readily obtained from their concise expressions.

REFERENCES

1. R. J. Mailloux, "Radiation and near-field coupling between two collinear open-ended waveguides," *IEEE Trans. Antennas Propag.*, vol. AP-17, no. 1, pp. 49-55, Jan. 1969.
2. T. S. Bird, "Analysis of mutual coupling in finite arrays of different-sized rectangular waveguides," *IEEE Trans. Antennas Propag.*, vol. 38, no. 2, pp. 166-172, Feb. 1990.
3. M. Mongiardo and T. Rozzi, "Singular integral equation analysis of flange-mounted rectangular waveguide radiators," *IEEE Trans. Antennas. Propag.*, vol. 41, no. 5, pp. 556-565, May 1993.
4. K. Hongo and H. Serizawa, "Diffraction of electromagnetic plane wave by a rectangular plate and a rectangular hole in the conducting plate," *IEEE Trans. Antennas Propagat.*, vol. 47, no. 6, pp. 1029-1041, Jun. 1999.
5. H. Serizawa and K. Hongo, "Radiation From a Flanged Rectangular Waveguide," *IEEE Trans. Antennas Propagat.*, vol. 53, no. 12, pp. 3953- 3962, Dec. 2005.

Singular Volume Integral Equations for Non-Stationary Problems of Electromagnetics in Three-Dimensional Material Media

A. B. Samokhin
Moscow Institute of Radio Engineering, Russia

In this report we consider the non-stationary electromagnetic problems. Assume that a medium filling bounded three-dimensional domain Q is characterized by the electric polarization vector $\vec{P} = \vec{P}(\vec{E}, x, t)$. Outside domain Q,the parameters of the medium are constant, i.e.ϵ_0,μ_0.It is necessary to determine the electromagnetic field excited in the medium by an external field with unstable time dependence. Using volume singular integral equations[1], that describe harmonic scattering problems from inhomogeneous dielectric bodies, and Fourier transformation techniques, we obtain the following singular integral equation for the above-mentioned problems

$$\vec{E}(x,t) = -\frac{1}{3\epsilon_0}\vec{P}(x,t) - \gamma_1 \int_Q \frac{1}{R}\frac{\partial^2 \vec{P}(y,\tau)}{\partial \gamma^2} dy + \gamma_1 \int_Q (\frac{1}{R}\frac{\partial^2 \vec{P}(y,\tau)}{\partial \gamma^2}, grad\ R) grad\ R dy -$$
$$-\gamma_2 \int_Q R(\frac{\partial^2 \vec{P}(y,\tau)}{\partial \tau}, grad) grad \frac{1}{R} dy + \gamma_3 \nu.p. \int_Q (\vec{P}(y,\tau), grad) grad \frac{1}{R} dy) + \vec{E_0}(x,t). \tag{1}$$

Here $\vec{E_0}$is the external electric field in free space; $R = |x - y|$is the distance between points $x = (x_1, x_2, x_3, x_4)$ and $y = (y_1, y_2, y_3, y_4)$; $\tau = t - R/c$; $(*, *)$ denote the inner product of vectors; $\nu.p.$ denote the singular integral, for which an infinitely small ball occupying the vicinity of the point $y = x$is extracted from the domain of integration; and .$\gamma_1 = 1/(4\pi\epsilon_0 c^2)$,$\gamma_1 = 1/(4\pi\epsilon_0 c)$,$\gamma_1 = 1/(4\pi\epsilon_0$Further, through use of time steps method, we show the effective way for numerical solution of integral equation.

REFERENCES

1. A.B. Samokhin, gIntegral equations and iteration methods in electromagnetic scatteringh, VSP, Utrecht, 2001.

Interfacial Operator for Computing Band Structures of Polaritonic Crystals

R. L. Chern
National Taiwan University, Taiwan R.O.C.

Chien C. Chang and **C. Chung Chang**
Academia Sinica, Taiwan ROC

It has been difficult to compute eigenmodes and band structures for frequency-dependent materials, in particular, for TE modes. The major difficulty comes from the nonlinear formulation of the eigenvalue problem. Several approaches have been proposed to study the present problem, including plane wave expansion method and vectorial eigenmode expansion method. Other approaches such as transfer matrix method, layer-Korringa-Kohn-Rostoker method, multiple multipole method, and finite-difference time-domain method can also be applied to frequency-dependent problems. Another difficulty comes from the special physical features of the solution. For example, resolving highly localized nature of surface plasmons in the dispersive metal, as well as surface phonons in the polar material, may require very fine resolution schemes. An even more critical situation is that the dielectric function changes sign across the dielectric-metal or dielectric-polar material interface over some frequency ranges. This will cause the change of type of the eigensystem and may induce numerical instability in solving the solutions.

In this study, we propose an interfacial operator approach to computing surface phonon modes for one- and two-dimensional periodic arrays of polar materials in a finite-difference formulation. The key aspect is to introduce an interfacial variable along the interface between the polar material and the surrounding dielectric. In particular, the interface variable represents the local strength of the surface phonon modes along the interface. In this approach, the apparently nonlinear eigenvalue problem can be reformulated as a quadratic eigensystem, and thus further reduced to a standard linear eigenvalue problem. Band structures can be computed directly without the need of examining transmission spectra like in the finite-difference time-domain method, or locating the mode frequency by testing an auxiliary function in other methods. The method has been applied to study four types of photonic crystals of polar materials. In particular, we have examined the effects of dimension, the size (filling ratio) effect, the effect of the intrinsic frequencies ω_T (the transverse optical phonon frequency) and ω_L (the longitudinal optical phonon frequency) as well as the geometric (shape) effect of the polar material. Physical details have been discussed regarding the crossing and anticrossing schemes of band dispersion, distribution of resonant cavity modes, localized nature of surface phonon modes, and lifting degeneracy by thinning polar materials, and the limiting behaviors of the band structures at the small limit of ω_T and large limit of ω_L.

Advances in Mathematical Methods for Electromagnetics: Nonlinear Problems and Nonselfadjoint Operator Theory (A Review)

Y. Shestopalov
Karlstad University, Sweden

Recent advances in mathematical methods for electromagnetics are connected with the development of specific branches of the theory of nonselfadjoint operator-valued functions (OVFs) and the respective parts of the spectral theory of open structures summarized in [1]. In fact, nonselfadjoint boundary-value problems (BVPs) for the Maxwell and Helmholtz equations under study occupy a specific place because the spectral parameter enters the boundary conditions in a nonlinear manner. This circumstance gives rise to different statements of singular linear and semilinear BVPs for Helmholtz and Schrdinger equations with complex-valued coefficients nonlinear both with respect to the solution and the spectral parameter [1, 2]. The solution methods for such problems are constructed in the series of papers (see [2]). It is shown that singular BVPs can be reduced to nonlinear Volterra and Fredholm integral equations and their characteristic numbers can be determined using contraction [2]. These results enable one to complete the theory of wave propagation in both linear and nonlinear layered structures on a single basis. An objective of mathematical modeling in electromagnetics is often to solve nonselfadjoint eigenvalue problems in unbounded domains. Here, investigation of the existence and distribution of eigenvalues (scattering frequencies) in the complex plane can be performed on the basis of the OVF spectral theory using explicit semi-inversion of scalar and matrix integral operator pencils defined on several intervals of integration [3].

Many important problems of the mathematical theory of wave diffraction and propagation in open structures were solved on the basis of these recently developed techniques and their generalisations; among them, the proof of existence and explicit determination of scattering frequencies of two-dimensional dielectric scattereres [4, 5]; the determination of soliton waves in layered waveguides filled with nonlinear media (see [3] and references therein); justification of interaction phenomena in slotted structures [1, 3]; and others.

REFERENCES

1. V. Shestopalov, Y. Shestopalov, Spectral Theory and Excitation of Open Structures, Peter Peregrinus Ltd., London (1996).
2. Y. Smirnov, H.W. SchEmann, Y. Shestopalov, Propagation of TE-Waves in Cylindrical Nonlinear Dielectric Waveguides, *Phys. Rev. E*, 71, pp. 0166141–10 (2005).
3. Y. Shestopalov, Y. Okuno, N. Kotik, Oscillations in Slotted Resonators with Several Slots: Application of Approximate Semi-Inversion, Progress in Electromagnetics Research, 39, pp.193–247 (2003).
4. Y. Shestopalov, V. Lozhechko, K. Kobayashi, Diffraction by a Rectangular Dielectric Cylinder, Proc. Progress in Electromagnetics Research Symposium, Osaka, Japan, July 18–22, 2001, p. 614.
5. Y. Shestopalov, Resonance Scattering by a Dielectric Cylinder, *J. Comm. Tech. Elec.*, 50 , 2, pp. 172–179 (2005).

Theoretical Analysis of Volume Integral Equation Method and Subhierarchal Parallel Algorithm for Solving Electromagnetic Diffraction Problem on a Dielectric Body in a Layer

Y. G. Smirnov
Penza State University, Russia

We consider a three-dimensional problem of the electromagnetic wave diffraction by a bounded dielectric body of arbitrary shape in the layer shielded by perfectly conducting planes. The problem is reduced to the volume singular integral equation (VSIE) and solved numerically by the Galerkin method. We have proved the convergence and obtained estimation of the rate of convergence for the method.

The main difficulties in the VSIE method are (a) very large time of calculations of the matrix elements when computations are performed with sufficiently high accuracy, and (b) occurrence of large and dense matrices in systems of linear algebraic equations obtained after discretization of the problem.

We demonstrate that when one uses VSIE method for the problem discretization, the matrix elements may be calculated independently. A natural way to calculate the matrix elements is utilization of parallel computations using supercomputers or clusters. Note in addition that in the diffraction problems, the structure of matrices is not arbitrary: we have the so-called structured matrices with O(n) different elements, where n denotes the matrix dimension.

We have created and elaborated efficient solvers for several types of diffraction problems on the basis of subhierarchal algorithms of parallel computations [1] that take into account the matrix structure. We solved 3D vector diffraction problems on bounded dielectric (or magnetic) bodies in a layer by this method.

REFERENCES

1. M.Yu. Medvedik and Yu.G. Smirnov. Subhierarchal Parallel Computational Algorithm and Convergence of Galerkin Method in Electromagnetic Diffraction Problem on Plane Screen. Izvestiya Vyzov. Povolzsky Region. Estestvennye Nauki, 5, pp. 3-19 (2004) (in Russian).

An Analysis of Characteristic Impedance of LPDA Feeder

F. Zhang, X. Y. Du, D. F. Zhou, and **Z. X. Niu**
Information Engineering University, China

Abstract - The formula of log-periodic dipole antenna(LPDA) input impedance given by Robert Carrel[1] is discussed and corrected in the paper. The new formula explains LPDA's feeder should be unparallel .The influence of angle variety on unparallel feeder lines is studied. According to the computed and measured results, it proves that the resistance of LPDA using unparallel transmission lines as the feeder performs better than that using parallel lines.

Summary - The log-periodic dipole antenna is one of the most useful of the frequency independent antennas.The characteristic impedance of transmission feeder makes great affection on LPDA performance[2].In practice, the performance such as the voltage standing wave ratio(VSWR) can't satisfy the request specially in low frequency when using the formula given by Carrel which required the feeder lines parallel to design LPDA. The way to improve performance for VSWR includes setting a short circuit or a matching load on the back of the feeder lines. They make structure complex. We find that the VSWR using unparallel feeder lines performances better than that using parallel lines. However, the formula given by Carrel requires feeder parallel so that the antenna's impedance can be matched to the feed-in resistance. In this paper, the formula is discussed and corrected. It explains LPDAfs feeder should be unparallel. The computed and measured results are shown to be in good agreement with the conclusion from the new formula.

Resonant Scattering by Layered Dielectric Structure with Weakly Kerr-Like Nonlinearity

V. V. Yatsyk
Nat. Acad. of Sci. of Ukraine, Ukraine

The transverse inhomogeneous, isotropic, nonmagnetic, linearly polarized, weakly nonlinear (a Kerr-like dielectric nonlinearity) dielectric layer is considered. The algorithms for the solution of nonlinear diffraction problems (with use of approaches developed in [1-3]) and the results of a numerical analysis of the diffraction problem of a plane wave on the weakly nonlinear object with positive and negative value of the susceptibility are shown. The effects: non-uniform shift of resonant frequency of the diffraction characteristics of a weakly nonlinear dielectric layer, i.e. its reduction when positive value of the susceptibility and increase at negative value of the susceptibility; itself the channeling of a field; increase of the angle of the transparency of the nonlinear layer when growth of intensity of the field (at positive value of the susceptibility); de-channeling of a field (at negative value of the susceptibility) are found out. These effects are connected to resonant properties of a nonlinear dielectric layer and caused by increase at positive value of the susceptibility or reduction at negative value of the susceptibility of a variation of dielectric permeability of a layer (its nonlinear components) when increase of intensity of a field of excitation of researched nonlinear object, see [4].

The principal fields where the results of our numerical analysis are applicable are as follows: the investigation of wave self-influence processes; the analysis of amplitude-phase dispersion of eigen oscillation-wave fields in the nonlinear objects, see [5]; extending the description of evolutionary processes near to critical points of the amplitude-phase dispersion of nonlinear structure; new tools for energy selecting, transmitting, and remembering devices; etc.

REFERENCES

1. Akhmediev N. N., Ankiewicz A., "Solitons," Moscow, Fizmatlit, 2003.
2. Schurmann H. W., Serov V. S., Shestopalov Yu. V., "TE-polarized waves guided by a lossless nonlinear three-layer structure", *Physical Review E,* vol. 58, no. 1, 1998, pp. 1040-1050.
3. Shestopalov V. P., Sirenko Yu. K., "Dynamic Theory of Gratings," Kiev, Naukova Dumka, 1989.
4. Yatsyk V. V., "The Numerical Simulations and Resonant Scattering of Intensive Electromagnetic Fields of Waves by Dielectric Layer with Kerr-Like Nonlinearity", *E-print: Computational Physics, http://arxiv.org/pdf/physics/0412109,* no. 12, 2004, pp. 1-11.
5. Yatsyk V. V., "Diffraction Problem and Amplitudes-Phases Dispersion of Eigen Fields of a Nonlinear Dielectric Layer", *E-print: Computational Physics, Optics, http://arxiv.org/pdf/physics/0503089,* no. 3, 2005, pp. 1-13.

Session 3P1
Microwave Phenomena on Superconductors II

High-Jc Processing for YBCO Thick Films by TFA-MOD Method

R. Teranishi, N. Mori, K. Yamada, M. Mukaida, and **Y. Shingai**
Kyushu University, Japan

J. Matsuda, K. Nakaoka, T. Izumi, and **Y. Shiohara**
Superconductivity Research Laboratory-ISTEC, Japan

The large-area and thick superconducting films with high crystallinity are required for most superconductivity applications. MOD process using trifluoroacetate precursors was applied to form thick YBCO films. The water vapor pressure during crystallization is a factor to control the supersaturation for the YBCO crystallization in this process. Then, the crystallization conditions such as P_{H2O} and heating rate were optimized to thicken the YBCO film maintaining high J_c performance. As a result, J_c depended strongly on both the water vapor pressure and the heating rate during the crystallization. Finally, a YBCO film with a high Ic value of 508A at 77K in self-field was fabricated with the YBCO film thickness of 2.7 μm under the optimized crystallization conditions.

Effect of 0-D Artificial Pinning Centers on Surface Resistance of Er123 Films

M. Mukaida [1,8], **A. Saito** [2], **R. Kita** [3,8], **T. Horide** [4,8], **K. Matsumoto** [4,8], **A. Ichinose** [5,8]
Y. Yoshida [6,8], **S. Horii** [7,8], **R. Teranishi** [1,8], **K. Yamada** [1], and **N. Mori** [1]

[1]Kyushu University, Japan
[2]Yamagata University, Japan
[3]Shizuoka University, Japan
[4]Kyoto University, Japan
[5]CRIEPI, Japan
[6]Nagoya University, Japan
[7]University of Tokyo, Japan
[8]CREST-JST, Japan

Surface resistances are evaluated for dilute Zn substituted high quality $ErBa_2Cu_3O_{7-\delta}$. Dilute Zn substituted high quality $ErBa_2Cu_3O_{7-\delta}$ films are grown on $SrTiO_3$substrates by a pulsed laser deposition technique. Targets used in the experiments are un-substituted, 0.3at.%, 0.5at.%, 1.0at.% and 10at.% Zn substituted $ErBa_2Cu_3O_{7-\delta}$ ceramics. Crystal structures and surface resistance are evaluated. Zn substitution into $YBa_2Cu_3O_{7-\delta}$ has been studied for understanding the origin of oxide superconductivity with substituting level of several ten %. In this study, dilute Zn below 1.0at.% is mainly adopted. Further substitution reduces its critical temperature. We intended to introduce zero-dimensional superconductivity killer atoms into CuO_2 plane as artificial pinning centers. The obtained Zn substituted $ErBa_2Cu_3O_{7-\delta}$ films are c-axis oriented without peaks from other phases. The sharp drop temperature of surface resistance decreases as the Zn substitution. However, the surface resistance at low temperature around 20K is almost the same among the $ErBa_2Cu_3O_{7-\delta}$ films with different Zn substituting.

Microwave Properties of Superconducting Magnesium Diboride Thin Films: Effects of Disorder

G. Ghigo [1,2], **D. Andreone** [3], **R. Gerbaldo** [1,2]
L. Gozzelino [1,2], **F. Laviano** [1,2], **B. Minetti** [1,2]
E. Monticone [3], **G. Ummarino,** [1], and **E. Mezzetti** [1,2]

[1]Politecnico di Torino, Italy
[2]Istituto Nazionale di Fisica Nucleare, Italy
[3]Istituto Nazionale di Ricerca Metrologica, Italy

The microwave properties of polycrystalline magnesium diboride (MgB2) thin films prepared by an in-situ method have been investigated [1]. Characterization of the films at microwave frequencies was obtained by a coplanar resonator technique, with measurements as a function of temperature, dc magnetic field and rf input power. The analysis of the experimental data results in the determination of penetration depth, surface impedance and complex conductivity. The first aim of this work is to set the experimental results in a consistent framework, involving the two-band model in the presence of impurity scattering. The energy gaps are calculated and the contribution of strong intraand inter-band scattering is considered. From the comparison between the calculated gap values and the experimental data it turns out that the temperature dependence of the penetration depth can be accounted for by an effective mean energy gap, while the temperature dependence of the surface resistance is accounted for by the single smaller gap. Since these findings rely on the same calculated gap structure, the required consistency is fulfilled.

A comprehensive understanding of the role of disorder in two-band superconducting MgB2 is an essential requirement for its use in potential applications. Therefore, the possibility to change the disorder level in the same sample, e.g. by means of irradiation, is an experimental tool of primary importance. Moreover, sample ageing has to be considered as a further source of disorder. Within this framework, we investigated the role of disorder in modifying the performance of the MgB2 resonators, characterized before and after successive uniform irradiations with 250MeV Au ions. We show the main features of the peculiar phenomenology concerning the effects of disorder on the electromagnetic response of the resonator, due to surface resistance reduction at low-temperatures and to non-monotonic residual resistance as a function of disorder level.

REFERENCES

1. G.Ghigo et al., *Phys. Rev.* B 71 (2005) 214522

Peculiarities of the Microwave Conductivity of High-Tc Single Crystals with Different Doping Levels

M. R. Trunin
Institute of Solid State Physics RAS, Russia

Results of recent investigations of the temperature dependences of the surface impedance $Z(T) = R(T) + iX(T)$ and conductivity $\sigma(T)$ in the ab-plane and along c-axis of high-Tc superconductors (HTSC) are discussed. The main attention is focused on the peculiarities of these dependences in single crystals of $\mathrm{YBa_2Cu_3O_{7-x}}$ with the oxygen deficiency varied in the range $0.07 \leq x \leq 0.47$ ($92 \geq T_c \geq 41K$) and of $\mathrm{Ba_{1-x}K_xBiO_3}$ with different potassium content $0.6 \geq x \geq 0.35$ ($5 \leq T_c \leq 31K$).

An analysis of the resistivity $\hat{\rho}(T) = 1/\hat{\sigma}(T)$ tensor in the normal state indicates that the optimally doped $\mathrm{YBa_2Cu_3O_{6.93}}$ is a three-dimensional anisotropic metal. As the oxygen content is decreased, the Drude c-axis conductivity changes to the hopping one, the crossover occurring at $\rho_c\rho_{ab} \approx 10^{-6}(\Omega \cdot cm)^2$In the superconducting state of $\mathrm{YBa_2Cu_3O_{7-x}}$ with $x > 0 : 35$ the behavior of the superfluid density $n_s(T, x) \propto \sigma^{''}_{ab}(T, x)$ can be treated in the framework of d-density wave (DDW) scenario of pseudogap in underdoped HTSC. The observed peculiarities of the imaginary part $\sigma^{''}_{ab}(T, x)$ of the c-axis conductivity at $T \ll Tc$ are determined by a strong decrease of the interlayer coupling integral with an increase of x.

Measurements of the surface impedance Z(T) in $\mathrm{Ba_{1-x}K_xBiO_3}$ crystals with $T_c = 11K (x \approx 0.5)$ and $T_c = 30K (x \approx 0.4)$ allow one to establish that the former is a BCS-superconductor (Z(T) saturates exponentially with lowering temperature at $T \ll T_c$) and the latter is not (Z(T) is linear at $T \ll Tc$). In addition, it is found that the temperature dependences of the upper critical field $H_{c2}(T)$ of the crystals with $T_c > 20K$ are similar to those in HTSCs, both exhibiting strong positive curvature. On the contrary, $H_{c2(T)}$ curves of the crystals with $T_c < 15K$ are in complete agreement with the BCS theory. The transition from BCS-type to HTSC-like superconductivity in $\mathrm{Ba_{1-x}K_xBiO_3}$is interpreted within Abrikosov's extended saddle-point model.

The report is based on recent review articles [1,2] of the author and latest experimental results.

REFERENCES

1. M.R. Trunin and A.A. Golubov. In-plane microwave response of high-Tc single crystals: Experiment and theory. in 'HTSC Spectroscopy', eds. N.M.Plakida, chapter 3, p.p.159-233 (Taylor and Francis, London and New York, 2003).
2. M.R. Trunin. Conductivity anisotropy and pseudogap in the microwave response of high-Tc superconductors. Physics-Uspekhi 48, 979 (2005).

Novel High-Precision Technique of the Microwave Spectroscopy of Solids in Strong Magnetic Fields

Y. A. Nefyodov, A. F. Shevchun, A. M. Shuvaev, and **M. R. Trunin**
Institute of Solid State Physics RAS, Russia

V. N. Egorov and **V. L. Masalov**
East-Siberian Research Institute of Physico-Technical and Radioengineering Measurements, Russia

Many problems of modern science and technology require absolute measurements (in Ohms) of the surface impedance along with its dependences on temperature, amplitude, frequency and dc magnetic field. To measure the impedance of small single crystals, one cannot use metallic cavity resonators whose quality factors are not high enough. Very high Q-factors are reached in superconducting cavities which have the disadvantage that application of dc magnetic fields is impossible. This problem is avoided in dielectric resonators (DR). DRs are usually dielectric discs with permeability ϵ_1 placed in a medium with dielectric permeability ϵ_2. In order to achieve high Q-factors of the open DR it is essential to minimize electromagnetic energy dissipation. To reduce dielectric losses one should use extremely low loss-tangent materials such as sapphire. To decrease radiative losses, the DR should operate on the so-called 'whispering gallery' modes with high-order azimuthal wave number.

On the base of sapphire DRs we have designed the test rig for measuring the microwave parameters of dielectric substrates. It operates at frequencies between 30 and 40 GHz and over a temperature range from -50 to $+70^o$C and allows the measurements of the following parameters of commonly used PCB materials: (i) dielectric constant of the dielectric substrate in the range from 2 to 10, (ii) loss tangent of the substrate in the range from 10_4 to 10_2, and (iii) ranging from 0.03 to 0.3- surface resistance of the laminating metal layer adjoining the dielectric material. An accuracy of 1% for permittivity measurements and a resolution of the order of 10_4 for their loss tangent has been shown at 40 GHz. Using the experience of working on this test rig we are developing a novel setup for precise surface impedance measurements of small solid samples (e.g. high-T_c superconducting single crystals) in dc magnetic Pelds up to 18 T. Electrodynamic calculations are made for the circular single-crystal sapphire DR mode structure with large azimuth index $n \gg 1$ The problem of the sample placing is discussed in detail. The major elements of a resonator cell and joints of the microwave setup are tested.

Field Sweep-Rate Dependence of Microwave Absorption in a-Oriented YBCO Superconductors

A. Akiba, H. Zhu, and **T. Endo**
Mie University, Japan

M. Mukaida
Kyushu University, Japan

Microwave filter devices consisting of high temperature superconductors should be widely distributed at the base stations for mobile communication system. Tunable microwave filters of the superconducting thin films are strongly expected for the next generation mobile system. So it is quite important to clarify the microwave loss properties of superconducting layer as a function of applied field and elucidate the mechanisms of microwave absorption under magnetic field. This is the report concerning field sweep-rate dependence of microwave absorption in a-Oriented YBCO Superconducting thin films.

Modulated microwave absorption was measured on a-oriented Y-Ba-Cu-O thin films by sweeping the field Ha applied along a-, b-, and c-axes with various sweep rates Rs. In low field, the signal S is the largest and shows the sharpest peak for $H_a//c$. S is medium and shows the broader peak for $H_a//c$ (perpendicular to the film plane). S is the smallest and shows the broadest peak for $H_b//c$. In the configuration of $H_a//c$, the highest density of surface screening current flows in CuO_2 plane. Whereas the lower density of currents flow out-of-plane in $H_a//c$, b. With increasing Ha (Abrikosov vortex density) in $H_a//c$, the screening current decreases fastest due to decoupling of weak superconducting regions and decoupling between the CuO_2 planes. Whereas with increasing Ha (Josephson vortex density) in Ha//a, b, the screening currents do not decrease so much. At a low field of $H_a = 40$ G, S increases with increasing Rs for the three configurations. Sc for $H_a//c$ increases fastest, Sa for $H_a//c$ moderately, and Sb for Ha//b most gradually. Therefore, the vortex viscosity is the largest for $H_a//c$ because Abrikosov vortex moves in the superconducting CuO_2 plane. While, the viscosities are smaller for Ha//a, b because Josephson vortex moves between the planes. At a high field of $H_a = 400$ G, S_c shows anomalous Rs-dependence, i.e., Sc decreases with increasing Rs. This implies vortex-flow enhanced melting at the higher fields.

Microwave Absorption in Superconducting/Ferromagnetic YBCO/LCMO Superlattice

H. Zhu, A. Akiba, and **T. Endo**
Mie University, Japan

J. Santamaria
Universidad Complutense de Madrid, Spain

A. Hoffmann
Argonne National Laboratory, U.S.A.

Microwave absorption in high temperature superconductors (HTS) has been an interesting subject in the both viewpoints of practical applications and physical fundamentals. High temperature superconductor microwave filter is one of the promising applications due to very low microwave losses. Meanwhile, microwave absorption in HTS is also a fascinating phenomenon in physics of superconductivity. It is related to some fundamental problems, such as screening current, Josephson junction and vortex dynamics, etc.

Recently, oxide based ferromagnet/superconductor double-layer films and superlattices, as the typical materials in so-called ferromagenet-supreconductor hybrids, have become an interesting topic in fundamental researches, such as vortex pinning and spin-polarized carrier injection, etc.

Here we report the initial results on microwave absorption in $YB_{a2}Cu_3O_{7-\delta}/La_{0.7}Ca_{0.3}MnO_3$ superlattice. The sample, with composition [12 unit cells (u.c.) YBCO/15 u.c. LCMO]$_6$, was grown on (100) $SrTiO_3$ substrate by high pressure sputtering. The magnetically modulated microwave absorption (MA) was measured by means of a standard electron spin resonance (ESR) technique. The first noteworthy result is the diRerence in the signal shape between YBCO single-layer and the superlattice. MA signal of the superlattice for applied magnetic field (H_a) perpendicular to the film layers shows a typical signal corresponding to an absorption at zero field, similar to that in $Bi_2Sr_2CaCu_2O_x$ single crystal for $H_a||c$-axis. However, it is entirely diRerent from that in YBCO single-layer films where it shows a broad peak at low magnetic fields for H_a parallel to c-axis. The second result is that MA signal (including intensity and shape) of the superlattice is highly sensitive to the field configuration. The signal intensity for H_a $\perp$layers is much larger, by 3 orders of magnitude, than that for Haklayers. The signal shape shows obvious diRerence as well. For H_a $\perp$layers, MA signal shows a very sharp peak around zero field, then decreases quickly to baseline at a low field. Whereas in $H_a||$layers, it shows a moderate step at zero field and a visible flat signal remains till higher fields. It indicates that $H_a||$layers is a better field configuration for the superlattice to be used for microwave filters.

Session 3P2
Wave Scattering, Random Media and Wireless Communications II

Scattering of TM Plane Wave from Periodic Grating with Single Defect

K. Hattori and **J. Nakayama**

Kyoto Institute of Technology, Japan

Many authors have studied the wave scattering from periodic grating. However, to find defects in a periodic structure such as metal parallel lines of VLSI, it is necessary to know the effect of defects in the scattering properties. There are two types of periodic grating with defects: one with defects at known positions, and the other with randomly distributed defects. As the simplest case, this paper deals with the scattering of a TM plane wave from a periodic grating with a single defect (see figure below). We assume that the surface of is a superposition of surface profile obtained by displacing a rectangular groove by every integer multiple of the period, but there is a single defect where the grooves is not formed.

The surface z = f(x) is almost a periodic grating with the period L, the width w and the depth d, but has one defect at a known position, x = 0. The wave field above the x axis is represented by a sum of three components: the incident wave, the diffracted wave by periodic grooves without any defect and the scattered wave due to the single defect. The field inside each groove is written by a sum of guided modes. Solving the boundary condition, we will give formulas for the optical theorem and the scattering cross section.

Incident wave is diffracted into the discrete directions by the periodic grating and is scattered into all the directions due to the defect. Scattering cross section and optical theorem will be calculated numerically. The properties of the diffracted and scattered wave field will be discussed, comparing with the scattering properties in the case of TE plane wave incidence [1].

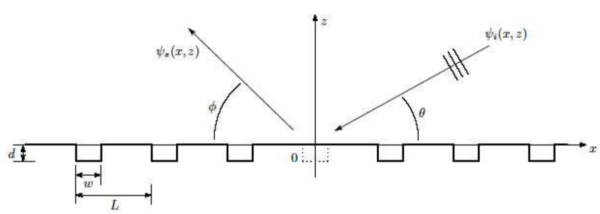

Figure 1: Scattering of TM plane wave from periodic grating with single defect.

REFERENCES

1. K.Hattori, J.Nakayama, "Scattering of TE plane wave from periodic grating with defects", *PIERS2005*, Hangzhou, China.

Determination of Optical Properties of Rectangular Parallelepiped Highly Scattering Media

J. Taniguchi, H. Murata, and **Y. Okamura**

Osaka University, Japan

A frequency domain solution for the photon diffusion equation has been derived for rectangular parallelepiped highly scattering media using the extrapolated boundary and the method of images. The analytical solution showed the measurement light diffusion in sufficient accuracy. Using this method, we can calculate the light diffusion faster than other calculation methods, like Monte Carlo method, Finite element method. We succeeded in determining the absorption and the reduced scattering coefficients of a highly scattering medium by using measurement data. The obtained values were in agreement with those reported by other researchers.

Figure 1 shows a sample cuboid made of an opaque polymer: polyacetal, used in the experimental as a highly scattering medium. The experimental setup is consisted of an amplitude modulated laser diode with the wavelength of 660 nm, a photomultiplier, input and output optical fibers. We measured the diffused light propagated in the highly scattering media changing the source and probe optical fiber position. Figure 2 shows the measured photon fluence amplitude near the edge of the polymer in the plane at z=50 mm. We can see the distortion of the light diffusion by the boundary. The measured result is in good agreement with the calculation. The peak point was shifted away from the source point. Fugure 3 shows the calculated photon fulence amplitude within the polymer by the analytical method for rectangular parallelepiped media. A solution for the slab can not show the light diffusion within 30mm from the interface between the polymer and the air by judging from the relative error of simulated and experimental results. Using the experimental data, we obtained the absorption and the reduced scattering coefficients of polyacetal as follows: absorption coefficient of 0.006 cm^{-1} and reduced scattering coefficient of 8.0 cm^{-1}.

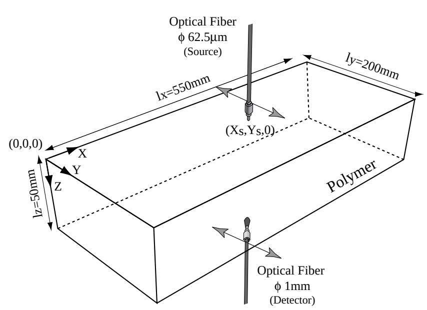

Figure 1: Polymer cuboid for measurement and detection system

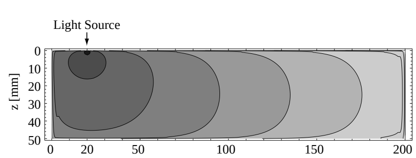

Figure 3: Calculated light intensity distribution within a polymer cuboid(z=252mm)

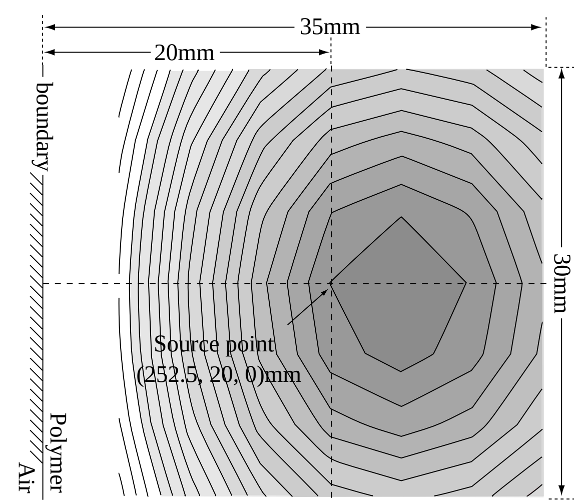

Figure 2: Light intensity measured at the surface near the edge

Numerical and Experimental Investigations of a Tropical Outdoor UWB Channel Characteristics for Short Pulse Transmission

J. Suryana, A. B. Suksmono, Sugihartono, and **A. Kurniawan**
STEI ITB, Indonesia

K. Tanaka and **K. Igarashi**
NICT, Japan

M. Iida
ARIB, Japan

We report the numerical analysis and experimental measurement of a tropical outdoor ultrawideband (UWB) characterizations for short pulse transmissions. The presence of hydrometeor, particularly rain, can produce major impairments to UWB radio links. Rain drops absorb and scatter the UWB signal energy or change the polarization sense of the transmitted signals.

This study addresses the distortion of short pulse shape due to the dispersion of rain scattering media.The transfer function of rain-filled medium was computed using an effective complex of index refraction based on Mie theory for bandwidth transmission 3.1 - 10.6 GHz. Neglegible pulse broadening was noted at rainrate under 50 mm/h, but for rain rate above 100 mm/h, the pulse brodening of the UWB pulse gets larger.

The theoretical performance of short pulse transmission over rain areas are then compared with experimental data which was performed in the campus environment. The bandwidth of the signal used in this experiment is 7.5 GHz and the measurement setup consists of Vector Network Analyzer, an UWB antenna array, metal sheet as reference reflector and raingauge. Our preliminary study, both numerical and experimental results concluded that the rain-fill medium modify the spectrum of UWB signals . This spectrum degradation will impact on pulse broadening of the transmitted monocycles in time domain and cause Intersymbol Interference of the bit streams transmission. Moreover, in the highest intense rain (195-200 mm/h), the synchronization of UWB link will be lost due to high rain attenuation.

Frequency Extrapolation in Terrestrial Microwave Propagation Simulations

M. Grabner and **V. Kvicera**
TESTCOM, Czech Republic

Wideband terrestrial microwave communications are of growing importance today. Quality and availability of microwave communication systems are affected by the propagation characteristics of the tropospheric channel. An electromagnetic wave propagation in troposphere without influence of hydrometeors can be simulated by means of a parabolic equation method [1]. This well established method gives only a single frequency response. Therefore, computationally expensive repeated simulations are needed for wideband propagation channel assessment. In order to speed up the computation of the channel transfer function, a frequency extrapolation method can be used.

We will present in this paper an application of the frequency extrapolation method suitable for terrestrial propagation simulations. In the method, a complex received signal is modeled using the weighted sum of complex exponentials. Hence the transfer function can be written as:

$$H(kf_s) = \sum_{i=1}^{M} R_i z_i^k, \quad k = 0, \dots, N-1.$$

This model is naturally related to physics of clear-air multipath propagation. Here the received signal can be considered as a sum of signals coming from different directions and with different time delays. The extrapolation method uses several single frequency responses calculated via parabolic equation method in the frequency band studied. Complex exponential model parameters z_i and R_i are extracted by means of the matrix pencil method [2]. An extracted model is applied to calculate wideband frequency transfer function of the microwave tropospheric channel that is impaired by an inhomogeneous refractivity distribution between the transmitter and receiver.

Numerical examples of the application of the method are introduced. Results are compared with the channel transfer functions computed using repeated use of parabolic equation method. Computational cost of both methods is compared. Robustness of the extrapolation method is discussed as well as the optimal selection of a model order M and frequency points kf_s used for model extraction.

REFERENCES

1. Levi, M., *Parabolic Equation Methods for Electromagnetic Wave Propagation*, London, The Institution of Electrical Engineers, 2002.
2. Sarkar, T. K., Pereira, O., "Using the matrix pencil method to estimate the parameters of a sum of complex exponentials", *IEEE Antennas and Propagation Magazin*, Vol. 37, No. 1, February 1995, pp. 48-55.

Some Issues in Probabilistic Interpretation of Polarized Wave Scattering in a Random Medium

R. Talhi, A. Lebrere,and **M. Dabernat**
University of Tours and C.N.R.S UMR, France

S. Massaoudi
Catholic University of Louvain, Belgium

It is well known that scattering by random media either discrete (raindrops, atoms) or continuous (atmosphere, ionosphere), induces polarization in an incident unpolarized electromagnetic wave, or modifies an initial polarization. Thus, an exact study of wave propagation in such media must include the complete state of polarization of waves before and after scattering. This representation was initially formulated by Chandrasekhar (but limited to Rayleigh scattering in a homogeneous atmosphere), and was a slight modification of Stokes's vector representation in terms of four parameters (so called Stokes's parameters I, Q, U, V). Polarization has in large part been ignored due to the mathematical complexity it introduced into the Radiative Transfer Equation (RTE) which is an efficient tool for describing the propagation of energy; unfortunately it was often wrongly felt that by neglecting polarization, no significant errors were introduced [1]. Taking into account polarization has led to various applications ranging from better target detection both on-land and in the ocean, to detection of precancerous skin lesions.

The equation describing the electromagnetic wave-energy propagation (or Radiative Transfert Equation, RTE) has no closed-form solution (no analytical solution) and is solved using numerical methods. One has to consider the energy propagation at a certain time (t), at a certain position (X), and in a certain angular direction (K). The scalar RTE admits a probabilistic interpretation which is represented by a Markovian Jump Process -MJP- (Markovian process means a stochastic process whose future evolution at any given time depends only on the state of a system at the present time and not on the states of the system at past times) for the position and direction of a photon (in quantum representation) undergoing scattering in a random medium. The probability density of this process, estimated from a Monte-Carlo simulation, is an approximate solution of the scalar RTE. The probabilistic representation of the vector (or matrix) RTE and some related problems [2], are the main objective of this contribution. For polarized waves, the previous probabilistic representation is no longer valid since incomplete; it is necessary to solve the RTE under its vector (or matrix) form, this is because the variables are not only energies but also polarization parameters (represented by a matrix P) which must be considered as independent variables (namely, each photon will be represented by its jump process (X(t), K(t), P(t))) [3]. Notice that X(t) is continuous in space, while K(t) and P(t) jump at the scattering times. In the simulation of the photons trajectories (or trajectories of elementary polarized waves propagating inside the random medium) corresponding to this MJP , the main steps are : first the computation of the time of the next scattering according to the Poisson (or exponential) distribution, second at the time of a scattering event we compute the probability of the new direction and polarization parameters; finally we calculate the new matrix of the scattered polarization parameters. Then, we consider the forward Kolmogorov equation associated with the previous MJP (i.e. equation of the evolution of the MJP probability density function); this equation is numerically solved by a Monte-Carlo method, that is by averaging the discrete probability density over a large number of independent realizations that simulate the MJP. Consequently, the solution of the vector (or matrix) RTE is then expressed by averaging over the first order moments of the previous discrete probability density with respect to the matrix of polarization parameters. Some examples of this probabilistic approach will be shown; in brief, the agreement with expected results depends on the example complexity. The obtained results and their validity will be discussed. Moreover, concerning the construction of the MJP (and its probability measure), we have to mention some related problems which could be relevant for some applications: for example, the theory of stochastic processes is considered by physicists as a macroscopic theory, and then inconsistent with the quantum mechanics [2,4]; in the same way, if a MJP is only observed at discrete time points, problems of non-existence or non-uniqueness may happen, then care is required [5].

REFERENCES

1. M.I. Mishchenko et.al., "Errors induced by the neglect of polarization in radiance calculations for rayleigh-scatteringatmospheres", *J. Quant. Spectrosc. Radiat. Transfer*, 51, NO.3, 391-510, 1994.
2. D.T. Gillespie, "Why quantum mechanics cannot be formulated as a Markov process", *Phys. Rev.* A49, 1607, (1994).
3. G. Bal et.al, "Probabilistic theory of transport processes with polarization", *SIAM applied mathematics*, (2000)
4. P. Garbaczewski et.al, "Comment on [2]", *Phys. Rev. Comments* A54, (1733-1736), 1996.
5. M.Bladt et.al, "Statistical inference for discretely observed Markov jump processes", *Journal of the Royal Statistical Society*, Series B, Vol. 67, p395, June 2005.

Integrated Gytrotropic Feed Network for Microstrip Phased Array Antennas

S. I. Sheikh
K. F. University of Petroleum and Minerals (KFUPM), Saudi Arabia

Ferrite phase shifters are widely used in phased array antennas for beam scanning purposes. But above 40 GHz, the nonreciprocal gyromagnetic properties of ferrites are limited by its material constraints [1] and processing incompatibilities [2]. A suitable alternative is an externally biased gyroelectric semiconductor material, where interaction between the electromagnetic waves and the free carriers of the media is represented by a tensor permittivity [4]. In this paper, this type of semiconductor substrate is used to theoretically design a microstrip array feeder network with integrated tunable phase shift section. Since, professional softwares cannot simulate gyroelectric (InSb) substrate, a dual gyromagnetic (ferrite) substrate based array feeder is designed and analyzed. This helped in verifying the design process by corroborating the calculated data with the related simulated and experimental results.

Cavity Antenna with Partly Transparent Apertures for Wireless Communications

N. I. Voytovich and **A. V. Ershov**
Southern Ural State University, Russia
N. N. Repin
Open Corporation, Russia
A. N. Sokolov
Chelyabinsk State University, Russia

Cavity antennas with partly transparent aperture are known since the first part of the 20th century. Research of the ones started 42 years ago. Development of high-speed wireless communication systems stimulates the interest in the plane antennas with partly transparent aperture. Several linearly- and circularly-polarized plane antennas are presented in the paper.

Cavity antenna with the partly transparent aperture physical, mathematical, numerical and computational models are presented. Antenna is an open rectangular metal resonant cavity 2 the height $\boldsymbol{H}$ of which is close to half wavelength λ and laterals dimensions a_2 and b_2 are several λ. The resonator upper wide wall of thickness $\boldsymbol{D}$ has a system K_0 rectangular radiating openings 5 with dimensions $l_p \times t_p$ (p=1,..., K_0) and separates the antenna from half space 3 by which an environment external to the antenna is simulated. Cavity antenna is excited by a screened stripline through coupling opening 4 with dimensions $l_0 \times t_0$ in the low wall of thickness d. Region 1 bounded by the stripline screens is considered as a transmission resonator with dimensions $a_1 \times b_1 \times h$, the height of which $\boldsymbol{h}$ is considerably less than λ. Metal pins are arranged around the coupling opening 4 and close the stripline screens. (Metal pins are absent in the picture). An electromagnetic wave source is arranged at the strip bottom. The antenna physical model supposes that the antenna has five areas 1-5 bounded by perfectly conducting resonator walls and opening apertures. General electrodynamics problem is formed for the above regions coupled electromagnetically through opening apertures within the scope of the antenna physical model. The method of equivalent currents is used for the problem definition.

The system of integral equations is received relative to unknown distributions of electric currents on the strip, the pins and the magnetic currents on apertures of the coupling opening and radiating ones. For electric and magnetic field computation Green tensor function method is used. Galerkin method is used for solving the integral equation system. As a result antenna numerical model is received.

Antenna pattern and amplitude-phase distribution of magnetic field on cavity antenna radiating openings are computed for the antenna excited by one, two or four coupling openings. In the paper the relationship of antenna directivity frequency characteristic and dimensions $l_p \times t_p$ (p=1,..., K_0) and radiating openings array as well as a number of radiating openings K_0 in the cavity antenna aperture are discussed. The measured and computed radiation patterns, directivity, return loss, half-power beamwidths and efficiencies of the antenna prototypes will be presented.

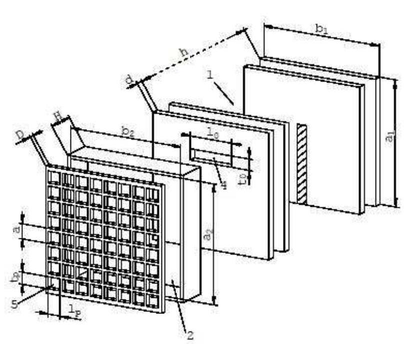

A Study on Relative Backscattering Coefficients of Sea Surfaces in Satellite Altimetry

K. Fukuda, K. Fujisaki, and **M. Tateiba**
Kyushu University, Japan

Satellite altimeters, one of microwave active sensors, are basically a short pulse monostatic radar. In current satellite altimetry, the ocean waveheight is measured by analyzing the leading edge of the mean return waveform of backscattered pulses from ocean surfaces. To observe other parameters of ocean waves and to improve the accuracy of measurements are the central subject of satellite altimetry. To solve these subjects, we proposed the computer simulation method to obtain raw data of scattering[1]. Our first approach was to generate three-dimensional ocean waves numerically and to evaluate the pulse train backscattered from them, ascertaining that the pulse trains have the same statistical properties as the real ones obtained SKYLAB and SEASAT altimeters. That is, we have pursued the raw scattering-data for the known model of ocean waves by computer simulation.

In a recent study, the ocean wave period T is estimated by the following relational expression[2].

$$T \sim (\sigma^0 SWH^2)^{0.25} \tag{1}$$

where σ_0 is the backscattering coefficient of the sea surface and SWH is the significant waveheight. The waveheight is estimated in satellite altimetry with a high accuracy. If the backscattering coefficient is observed by using satellite altimetry, we can estimate the ocean wave period simultaneously. In this paper, in order to show the possibility of detecting the ocean wave period, we relatively estimate the coefficient by surveying the received power for various sea conditions.

We show one example of differences between received powers with various ocean wave heights H and lengths L. Figure 1 shows that the ratio of the received power for some H to that for $H = 5m$ and $L = 35m$ as a function of L. As shown in this figure, different received powers with various H and L are obtained, and we can obtain the ratio of the backscattering coefficients. Furthermore, we show no effects of the ocean wave direction on the backscattering coefficients. By using these results and relational expression (1), we can estimate the ocean wave periods relatively.

REFERENCES

1. M. Tateiba et. al., gA Simple Simulation of the Pulse Train Scattered from Three-Dimensional Ocean Waves in Satellite Altimetry,h *IEICE TRANS.*, vol.e73, no.4, 1990.
2. C. P. Gommenginger et. al., gMeasuring ocean wave period with satellite altimeters: A simple empirical model,h *Geophysical Research Letters*, vol.30, no.22, 2150, 2003.

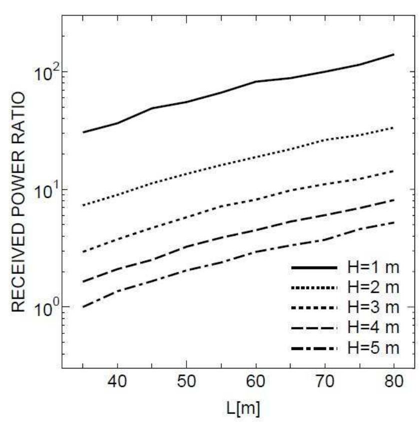

Figure 1: Received power ratio as a function of L.

Soil Multi-Scale Roughness Parameters and Soil Moisture Retrieval from Radar Backscattering Using a Neural Network Technique

L. B. Farah [1], **I. R. Farah** [2], **R. Bennaceur** [3], **Z. Belhadj** [1], and **R. Boussema** [1]

[1]Ecole Nationale d'Ingénieurs de Tunis.Le Belvedere, Tunisie
[2]Ecole Nationale des sciences de l' informatique, Tunisie
[3]Faculté des Sciences de Tunis, Tunisie

The retrieval of information related to physical surface parameters is a major objective of many studies in remote sensing investigations especially SAR applications. In that context, modeling radar backscattering through natural surfaces has become an important theme of research and active remote sensing has shown its utility for many applications in hydrology, geology and other fields.

Most traditional electromagnetic models consider natural surfaces as single scale zero mean stationary Gaussian random processes. Roughness behavior is characterized by statistical parameters like the rms height s and the correlation length l. Recent studies have shown that in natural conditions the agreement between experimental measurements and theoretical values is usually poor due to the large variability of the correlation function and as a consequence backscattering models have often failed to predict correctly backscattering. Many mathematical works dealing with natural surfaces description have shown that they are better described as self-affine random processes than as stationary processes.

Because the classical description of roughness using statistical parameters like the correlation length doesn't lead to satisfactory results to predict radar backscattering, we used a multi-scale roughness description using the wavelet transform and the Mallat algorithm. In this description, the surface is considered as a superposition of a finite number of one-dimensional Gaussian processes each one having a spatial scale. A second step in this study has consisted in adapting a direct model simulating radar backscattering namely the small perturbation model to this multi-scale surface description. We have investigated the impact of this description on radar backscattering through a sensitivity analysis of backscattering coefficient to the multi-scale roughness parameters.

Although significant progress has been made in the ability to acquire remotely sensed data, extracting soil moisture and roughness parameters of natural surfaces from this data has been problematic for many reasons. In fact, many previous studies have dealt with model-based retrieval algorithm and have encountered many problems like the lack of information about the characteristics of natural surface roughness as well as the range of roughness parameters to use in one hand. In another hand, the uncertainties concerning the validity of the scattering models when applied to natural roughness conditions reduces the accuracy of the retrieval procedure. In addition, the relation-ship between the backscattering coefficient is non linear and the problem of retrieving parameters may be ill-posed and it may be not possible to separate the contributions from different mechanisms making the retrieval of several parameters simultaneously necessary.

To perform the inversion of the small perturbation multi-scale scattering model (MLS SPM) we used a multi-layer neural network (NN) architecture trained by a backpropagation learning rule. The inversion leads to satisfactory results with a relative uncertainty of 8%.

Session 3P3
Periodic Structures II

Formation of the Light Localization in a Disordered Waveguide System

A. Komiyama
Osaka Electro-Communication University, Japan

From the interest in the crosstalk[1] in an image fiber which is used to transmit directly an optical image, the propagation properties of light in a random waveguide system have been discussed based on the coupled mode theory. In the discussion the propagation constants of modes are random variables and the propagation properties of light depend strongly on the correlation length of the propagation constants. The transfer process of light power between cores changes continuously from a wave process to a diffusive process with increasing the correlation length. The change has been confirmed not only numerically but also theoretically[2,3]. When the correlation length tends to infinity although the structure of the system becomes uniform along the waveguide axis random geometrical imperfections remain in the cross section. In the disordered system the localization phenomenon of mode waves has been known[4]. The localized mode waves are eigenstates of the system and the amplitude distribution in the cross section is kept unchanged. When a core is illuminated at the input end of the system localized modes are excited and propagate. The average power of light concentrates in a narrow region of the cross section and the distribution is also kept unchanged. The propagation phenomenon of the localized light differs completely from the diffusive transfer of light power between cores. So far, we have no theoretical framework to describe the change from the diffusion to the localization.

In this paper the light localization in a disordered waveguide system composed of randomly different cores is treated based on the coupled mode theory. The propagation constants of modes are generated by using a series of normal random numbers and an initial value problem of the coupled mode equation is numerically solved. By averaging the amplitude and the power of light over a large number of sample waveguides the coherent part and the incoherent part of the light power are obtained. The coherent part propagates in a certain direction in the waveguide system like a beam wave. The direction depends only on the mode coupling coefficient κ. The coherent part is transformed into the incoherent part and decreases exponentially with increasing distance. Only the incoherent part gives rise to the localization. When the total coherent part is transformed into the incoherent part the localization of light is completed and the power distribution of light in the cross section is independent of position along the waveguide axis. The extent of the localized light in the cross section depends only on one parameter $\delta\beta/\kappa$, where $\delta\beta$ is the fluctuation of the propagation constants. The damping factor is estimated from the distance dependence of the coherent part, which is a measure of the distance needed to complete the localization. The damping factor depends on two parameters, $\delta\beta$ and κ.

REFERENCES

1. A. Komiyama, M. Hashimoto, *IEICE Trans.*, E77-C, pp.1808- 1813, 1994.
2. A. Komiyama, 28th GA-URSI, BP.13, 2005.
3. A. Komiyama, Proceedings of 2004 URSI EMT-S, pp.260-262, 2004.
4. A. Komiyama, *Opt. Comm.*, 151, pp.25-30, 1998.

Radiation Characteristics of a Finite Periodic Slot Array in a Parallel Plate Waveguide Filled with a Transversely Magnetized Ferrite

K. Nishimura
Ryukoku Univesrsity, Japan

Recently, research on RF electronic controllable high frequency devices and circuits has been paid attention to [1]. Research on microwave ferrite devices is a kind of the research on the RF electronic high frequency devices. Until now, the vigorous development and research on the microwave devices such as isolators, circulators, phase shifter, delay lines, magnetically tunable resonators has been carried out by using anisotropy and frequency dependence of the permeability of ferrite that can easily be controlled by an external dc magnetic field [2]. On the other hand, research on antenna applications of ferrite materials has not been carried out extensively.

As research on antenna applications using ferrites, elecronic scanning of the radiation pattern of an open-ended retangular waveguide filled with ferrite [3], elecronic scanning of an antenna loaded with circularly arrayed ferrite bars [4], electronic scan of a millimeter-wave leaky wave antenna with a periodic structure loaded with ferrite [5, 6], and microstrip antennas on a ferrite substrate [7] have been researched. Of these, the periodic ferrite structure can work not only as a leaky-wave antenna but also as a magnetically tunable Bragg re ection filter. So, reseach on propagation in the periodic ferrite structure is very interesting. The Bragg re ection characteristics and leaky-wave antenna characteristics have been characterized theoretically by means of the improved perturbation method, the singular perturbation method, and spectral domain [5, 6, 8, 9]. As long as the author knows, the analytical research on ferrite waveguides with a finite array structure has been carried out little. So, the author have theoretically explained the radiation characteristics of a slotted parallel plate waveguide filled with a transversely magnetized ferrite by means of the method of moments. Then, the author have discussed the magnetic tunability of the radiation bandwidth of the slotted parallel plate waveguide filled with ferrite and radiation pattern control by an applied dc magnetic field [10].

In this paper, radiation characteristics of a finite periodic slot array installed on a upper plate of a parallel plate waveguide filled with a transversely magnetized ferrite are analyzed by means of the method of the moments in the case which only the TE_1 mode propagates in in the unperturbed parallel plate waveguide. At millimeter-wave frequencies, the dependence of the characteristics on the applied dc magnetic field is estimated numerically. It is theoretically explained how the chacteristics can be tunned and the radiation patterns can be controlled by varying the dc magnetic field applied to the ferrite.

REFERENCES

1. Special Session on Microwave Analog Smart Devices and Circuits, I*EICE Trans. C*, vol. J87-C, no. 1, Jan. 2004.
2. "SPECIAL SECTION ON MICROWAVE MAGNETICS," *Proc. IEEE*, vol. 76, no. 2, Feb. 1988.
3. G. Tyras and G. Held, IRE Trans. *Microwave Theory & Tech.*, vol. MTT-6, pp. 268-277, July 1958.
4. N. Okamoto and S. Ikeda, *IEEE Trans. Antenna Propagat.*, vol. AP-27, no. 3, May 1979.
5. K. Araki and T. Itoh, *IEEE Trans. Microwave Theory & Tech.*, vol. MTT-29, no.9, Sept. 1981.
6. S. Erkin et al., *IEEE Trans. Microwave Theory & Tech.*, vol. MTT-36, no.3, pp.568-575, March 1988.
7. D. Pozar, *IEEE Trans. Antennas Propagat.*, vol. 40, no.9, pp.1048-1092, Sept. 1992.
8. C. Surawatpunya et al., *IEEE Trans. Microwave Theory & Tech.*, vol. MTT-32, no. 7, pp. 689-695, July 1984.
9. M. Ozaki,M. Asai, J. Yamakita, S. Sawa, *IEICE Trans. C*, vol. J75-C, no. 11, Nov. 1992.
10. K. Nishimura, *IEICE Trans. C*, vol. J84-C, no. 11, Nov. 2001.

A Hybrid Trefftz Element Solution to Plane Wave Scattering Problems of Multilayered Gratings

K. Hasegawa and **S. Sato**
Muroran Institute of Technology, Japan

Numerical approaches based on the finite element method (FEM) are attractive for analysis of plane wave scattering by a periodic structure because of its capability to represent a complex composite structure. Several solutions based on FEM for this problem have been developed. Since the electromagnetic waves scattered by an obstacle are propagating into far away, auxiliary techniques for evaluating infinite half spaces above and below the structure have been introduced.[1, 2, 3] When we employ these solutions based on FEM to analyze a multilayered grating, we must generate a lot of elements in the homogeneous spaces between gratings.

In the previous paper, we introduce a hybrid Tr- efftz finite elements(HTFEs) for infinite half spaces to analyze TE- or TM-plane wave scattering prob- lems by infinite gratings[4]. In this paper, we ap- ply HTFEs to the homogenious spaces between the stacked gratings. Because the interpolating functions of HTFEs satisfy Maxwell equations and are composed of superpositions of space harmonics, the functional can be evaluated by the inte- grations along those boundaries. This fact implies that a homogenious space can be replace an HTFE and reduce the number of total unknowns of the matrix equations derived from conventional FEM procedures. In addition, we change the line elements for HTFEfs boundary from nodal elements to edge elements[5] for electric fields with three componets to consider an oblique incident plane wave on the gratings. We will demostrate validity and usefulness of HTFEs by computed results. For an example, we consider an infinite thin strip grating with embeded in the dielectric with its permittivity $\epsilon_d = 3.4$ as shown in Fig. 1, where $d_1 = 0.25p, d_2 = 0.125p, w = 0.25p$, and N = 4. Here ϵ_0 and μ_0 are the permittivity and the permeability of free space, respectively and λ is the wavelength of the incident plane wave. All of regions $\Omega_0 \sim \Omega_4$ can be divided into Trefftz elements with the interpolat- ing functions composed of lower 40 space harmonics. The boundaries of Trefftz elements are divided into 40 line elements along the x directions. Figure 2 shows diffraction characteristics for TE mode incidence. The results computed by HTFEM (the solid lines) agree well with those computed by the method based on the integral equation[6](●).

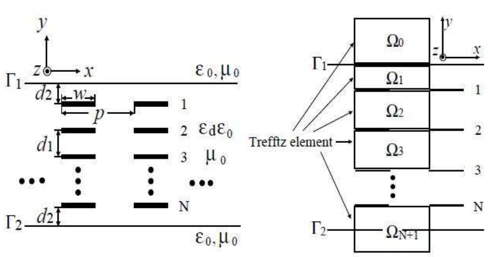

(a) Multilayered strip gratings. (b) Mesh.

Figure 1: Geometry of problems.

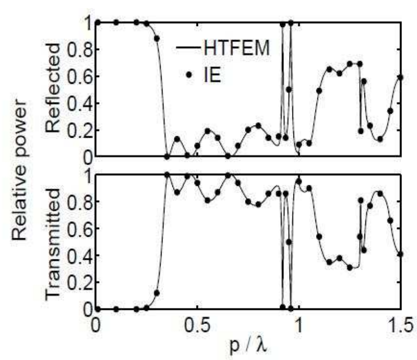

Figure 2: Frequency dependence of relative powers for perfect conductor strip gratings

REFERENCES

1. J. Jin, J. L. Volaski, and J. D. Collins;*IEEE Antennas Propagat. Mag.*, vol. 33, no.3, p. 22, 1991.
2. D. Gedney and R. Mittra:*IEEE Trans. Antennas Propagat.*, vol.39, no.11, p. 1605, 1991.
3. Y. Ohkawa, Y. Tsuji, and M. Koshiba;*IEEE Trans. Magn.*, vol.33, no.2, p.1440,1997.
4. S. Sato and K. Hasegawa:Proc. 10th Int. Symp. Microwave and Optical Tech., p. 91, 2005.
5. X. Q. Sheng ans S. Xu;IEEE Trans. Microwave Theory Tech., vol.45, no.7, p.1009, 1997.
6. T. L. Zinenko, A. Matsushima, and Y. Okuno:*IEICE Trans. Electron.*, E82- C, p.2255.

Mode Analysis of Coupled Cavity Waveguides Consisting of Dielectric Rectangular-Rods

H. T. Jia and **K. Yasumoto**

Kyushu University, Japan

Photonic crystals are discrete periodic structures of dielectric materials in which any electromagnetic wave propagation is forbidden within a fairly large frequency range. A photonic crystal waveguide is formed by surrounding a dielectric space by photonic crystal materials. The guided fields are strongly confined because any electromagnetic energy can not escape through the surrounding materials. Such a waveguide has received a growing attention in view of their promising applications to new integrated optical devices[1]. The mode propagation in two-dimensional photonic crystal waveguides consisting of a lattice of circular and rectangular rods has been studied, using a plane wave expansion method[2]. Although these methods can be widely applied to various configurations of photonic crystal waveguides, the accuracy of solutions and computation cost need more challenging efforts. Recently, Yasumoto et al. has proposed a rigorous semi-analytical method[3] for analyzing a two dimensional waveguide bounded by photonic crystals consisting of layered periodic arrays of circular cylinders. This is a very effective method. The convergent speed is very fast and the calculated precision is very high. However, this method can not analyze loss properties of photonic crystal waveguides.

In this paper, we use an improved Fourier serices method to investigate the guideing properties of coupled cavity waveguides consisting of dielectric rectangular-rods. This work is an extension of our previous studies[4, 5]. Since the photonic crystal waveguide consists of multilayed periodic-arrays, for each array, the electromagnetic properties may be described using the reflection and tranmission matrices by an improved Fourier serices method[4]. The generalized reflection and transmission matrices of multi-layered arrays are obtained by concatenating the reflection and transmission matrices for each of isolated arrays in the layered direction using a simple recursion algorithm. The dispersion equations for TM and TE guided modes are obtained in compact form in terms of two generalized reflection matrices viewed from the guiding region bounded by multilayered periodic arrays. The mode-field distribution inside the homogeneous strip regions of background dielectric are calculated using the space-harmonic wave expression, whereas those inside the inhomogeneous gating regions including the arrayed rods are calculated using Fourier series expression. Numerical examples of the dispersion characteristics and field distributions are presented for several lowest TM and TE modes in photonic crystal waveguides consisting of rectangular rods.

REFERENCES

1. A. Schere, T. Doll, E. Yablonovich, H.O. Everitt, and J.A. Higgins, ed., "Special section on electromagnetic crystal structures, design, synthesis, and applications," *J. Lightwave Technol.* 17, pp.1928-2207(1999).
2. H. Benisty, "Modal analysis of optical guides with two-dimensional photonic band-gap boundaries," *J. Appl. Phys.*, 79, pp.7483-7492(1996).
3. K. Yasumoto, H. Jia, and K Sun "Rigorous analysis of two-dimensional photonic crystal waveguides," *Radio Science,* 40, Art. no. RS6S02, pp.1-7(2005).
4. H. Jia and K. Yasumoto, "A novel formulation of the Fourier model method in S-matrix form for arbitrary shaped gratings," *Int. J. Infrared Millim. Waves,* 25, pp.1591-1609(2004).
5. H. Jia and K. Yasumoto, "Modal analysis of two-dimensional photonic-crystal waveguides formed by rectangular cylinders using an improved Fouries series method," *IEEE Trans. Microw. Theory Tech.*, 54, pp.564- 571(2006).

Scattering of Electromagnetic Waves by Inhomogeneous Dielectric Gratings Loaded with Three Perfectly Conducting Strips

T. Yamasaki, T. Ujiie, and **T. Hinata**
Nihon University, Japan

The scattering and guiding problems of inhomogeneous dielectric gratings have been of considerable interest such as optical fiber gratings, photonic bandgap crystals , frequency selective devices, and other applications by the development of manufacturing technology of optical devices. Recently, many analytical and numerical methods which are applicable to the arbitrarily dielectric gratings have been proposed. However, most theoretical and numerical studies have considered the periodic structures in which the material forming grating was either metallic or dielectric.

In this paper, we proposed a new method for the scattering of electromagnetic waves by inhomogeneous dielectric gratings loaded with three perfectly conducting strips using the combination of improved Fourier series expansion method and point matching method.

In the inhomogeneous dielectric region S_2(0¡x¡D) , the permittivity profile ϵ_2(x,z) and ϵ_3(x,z) is generally not separable with respect to the x and z variables. Main process of our methods are as follows: (1) The inhomogeneous layer is approximated by a stratified layers of modulated index profile with d,(D-d) (2) Taking each layer as a modulated dielectric grating, the electromagnetic fields are expanded appropriately by a finite Fourier series. (3)In the perfectly conducting strip and gap regions at C_1(or $\bar{C}_1$) and C_3(or $\bar{C}_3$) for the boundary, the electromagnetic fields are matched using an orthogonality relation. (4)In the perfectly conducting strip and gap regions at C_2(or $\bar{C}_2$) for the boundary, it makes the matrix relation on both sides using point matching method. (5) Finally, all stratified layers include the metallic regions are matched using appropriate boundary conditions to get the inhomogeneous dielectric gratings loaded with three perfectly conducting strips.

Numerical results are given for the transmitted scattered characteristics for the case of incident angle and frequency for TE waves.

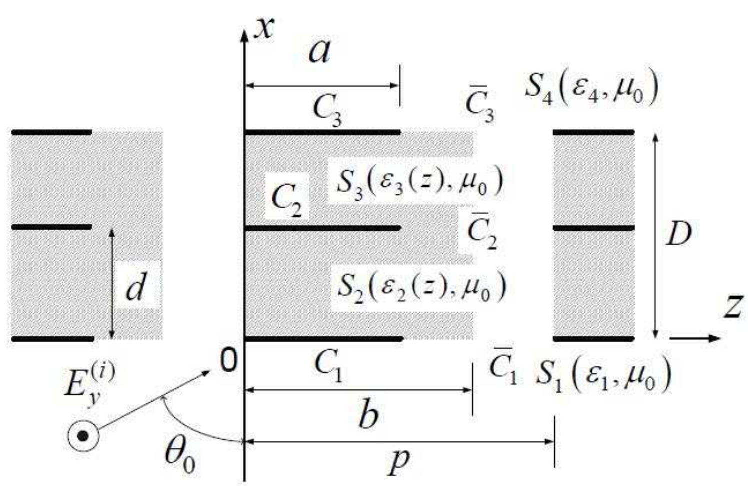

Figure 1: Structure of inhomogeneous dielectric gratings loaded with perfectly conducting strips

Characteristics of Poly-Silane Optical Waveguides with Long Periodic Grating

S. Watanabe, H. Murata, and **Y. Okamura**
Osaka University, Japan

Poly-silane is a polymer material whose refractive index is controlled by UV light radiation and thermal process, the method of which is referred to as gphoto-bleachingh. Using this feature, we can easily and cheaply fabricate poly-silane optical channel waveguides with index-modulated long periodic gratings (LPG) without any development and/or etching procedures. LPG used in optical waveguides of interest has a period of ranges from $100\mu m$ to $500\mu m$, and is employed to couple a core mode to other co-propagating cladding modes at various wavelengths [1]. We analyzed the characteristics of the poly-silane optical waveguides with LPG by a pseudospectral time-domain (PSTD) method, which is available to analyze large scale fields due to use of the fast Fourier transform (FFT) for the spatial derivatives of Maxwellfs equations[2]. Based on the analytical result, we decided the waveguide structure operating as a 1.55m wavelength wideband filter as shown in Fig.1, and fabricated it by the conventional photolithography. We used the experimented setup shown in Fig.2 to measure the transmission characteristics of the waveguide with LPG. Wavelength tunable LD laser light (1520nm-1620nm) was launched into a lensed single mode fiber and the light coupled out was detected with a photo detector. Figure 3 shows the wavelength dependence of the transmission. We can confirm that LPG caused a filtering operation with 20nm bandwidth in the$1.52 - 1.62\mu m$ wavelength region.

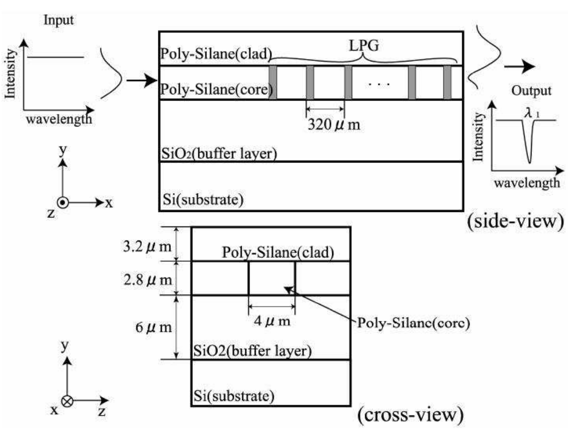

Figure 1: Proposed UWB CMOS LNA topology

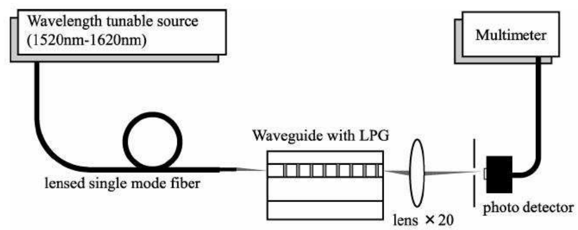

Fig. 2 Experimental setup for measurement of transmission

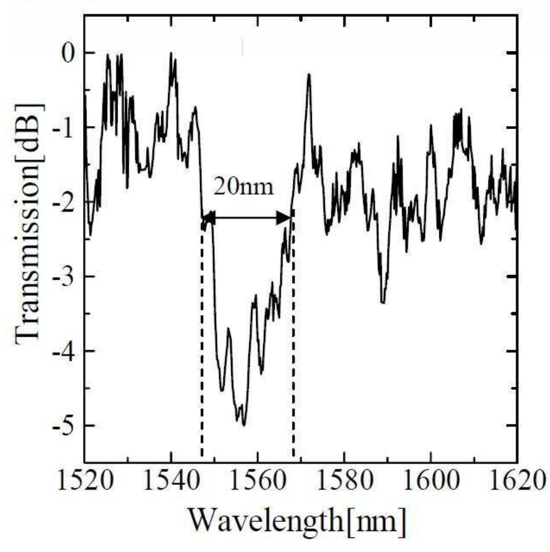

Fig. 3 Experimental result of transmission

REFERENCES

1. V. Rastogi, K. S. Chiang, gLong-period gratings in planar optical waveguidesh, *Appl. Opt. 41*, 6351-6355 (2002).
2. Q. H. Liu, gLarge-Scale Simulations of Electromagnetic and Acoustic Measurements Using the PSTD Algorithmh, *IEEE Trans on GRS. 37*, 919-926 (1999).

Experimental Evaluation of EM Wave Suppressions by Lattice Array of Conductive Wires.

A. Saito, T. Saito, K. Aizawa, and **H. Echigo**

Tohoku Gakuin University, Japan

Considering that electromagnetic(EM) wave scattering is one of the causes of unwanted EM environments, we have been studying on scattering phenomena by conductive rods. In the analyses of EM wave scattering, the results gave the idea that the strip can cause the shade of EM wave or that it can reduce the EM wave strength in the area behind the conductive rods or strips.

We had tried to estimate theoretically the reducing effectiveness (or rejection effectiveness) by the multiple layers of conductive stripes, each of which was made of a few of conductive thin rods or wires. The calculation result gave the effect of almost 20 dB for appropriate frequency band.

In this report, some results of the experimental evaluations for the real EM wave screen which was developed by authors recently. The results shows the suppression effect of about 20dB for 2GHz 3GHz for the constructed arrays.

Scattering of TM Wave from Conductive Rough Surface: Low Grazing Limit of Incidence

J. Nakayama, K. Hattori, and **Y. Tamura**

Kyoto Institute of Technology, Japan

When an electromagnetic plane wave is incident on a conductive flat surface, the reflection takes place. For any angle of incidence, the reflection coefficient is -1 in case of the TE polarization but becomes 1 in case of TM polarization. However, these properties of the reflection coefficient does not hold when the surface gets rough. Several theoretical works state that, when the angle of incidence becomes low grazing limit, the reflection coefficient for TM case changes its sign and becomes -1. This behavior of the reflection coefficient is pointed out for a random surface with infinite extent by a stochastic functional approach[1]-[3] and by the method of statistical Green's function[4]. Introducing the grazing perturbation[5], Charnotskii demonstrates that such a limiting property of the reflection coefficient is true for a periodic surface. However, these thoreticl works are all restricted to a slightly rough case with gentle sloping. However, we give an expectation such that the reflection coefficient for TM wave always approaches to -1 at low grazing limit of incidence for any rough surface, regardless of the surface roughness and surface shape. Because such an expectation for general case seems to be difficult to prove, this paper discusses the periodic case. First, we will present numerical examples for several periodic surfaces with moderate or large roughness, all of which support our expectation. Second, we will give a simple mathematical description to show that such an expectation is true for any periodic surfaces. Third, we will give physical processes that yield such a limiting property of the reflection coefficients for TM case.

REFERENCES

1. J. Nakayama, M. Sakata, and H. Ogura, Radio Sci., VOl. 16, No. 5, pp. 847-853,(1981).
2. J. Nakayama, Radio Sci., Vol 17, No3, pp. 558-564,(1982).
3. Y. Tamura and J. Nakayama, Waves in Random Media, Vol. 9, pp. 341-368, (1999).
4. S. Ito, Radio Sci., Vol. 20, pp. 1-12,(1985).
5. M. I. Charnotskii, Progress in Electromagnetic Research, PIER 26, pp, 1-42,(2000).

Parameter Optimization of Wavelength Selective Gratings Using Genetic Algorithm

K. Higa and **K. Watanabe**

Fukuoka Institute of Technology, Japan

Grating is an optical element that has periodic distribution of refractive index on the surface, and diffracts an incident wave into particular directions. Figure 1 shows an example of geometry under consideration. The grating structure with the period d is uniform in the z-direction, and the x-axis is parallel to the direction of periodicity. We consider a plane incident wave propagating in the direction of polar angle θ and azimuth angle ϕ. Then, the propagation direction of diffraction wave is characterized by the propagation constants corresponding to the x and the z directions:

$$\alpha_n(\lambda) = k(\sin\theta\cos\phi + n\frac{\lambda}{d}), \qquad \gamma = k\sin\theta\sin\phi \tag{1}$$

where n is the order of diffraction wave, λ is the wavelength, and k is the wavenumber in the cover region. The x-directional propagation constant α_n is dependent on the order of diffraction wave and the wavelength though the z-directional propagation constant γ is independent. This property makes gratings famous in many spectroscopic applications.

In this study, we try to obtain a monochromatic wavelength λ using the -1st-order diffraction wave. There is a difficulty to obtain a desired monochromatic light from a light source with wide wavelength range. Trouble comes from the coincidental propagation direction of the desired wavelength and undesired harmonic wavelengths because of the relation: $\alpha_{-1}(\lambda) = \alpha_{-2}(\lambda/2) = \alpha_{-3}(\lambda/3) = \cdots$. To suppress the undesired harmonic components, we optimize the grating parameters and the incident wave conditions with the use of the genetic algorithm. We consider the suppression of the second and the third harmonic components only, and examine two fitness functions:

$$F_1 = (1 - P_{-1}) + P_{-2} + P_{-3}, \qquad ; \tag{2}$$

where P_{-1} denotes the efficiency of -1st-order diffraction wave for the desired wavelength λ, and P_{-2} and P_{-3} are the efficiencies of -2nd- and -3rd-order waves for the undesired harmonic wavelengths $\lambda = 2$ and $\lambda = 3$, respectively. Surely, the ability of present approach is limited by the computation costs. We choose the differential theory to calculate the diffraction efficiencies, because of its fast and accurate evaluation and wide applicability. Also, we use the micro-mutation and seeding techniques on the genetic algorithm to accelerate the convergence. Numerical experiments show the possibility of the grating optimization.

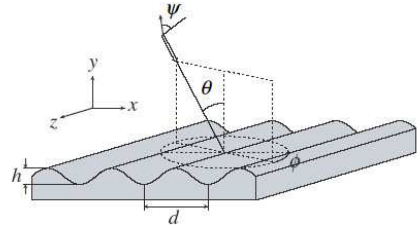

Figure 1: Grating under consideration.

REFERENCES

1. K. Watanabe, "Fast Converging and Widely Applicable Formulation of the Differential Theory for Anisotropic Gratings," *Progress In Electromagnetics Research,* Vol. PIER 48, pp. 279-299, 2004.
2. Z. Q. Meng and H. Misaka, "Fast Genetic Algorithm for Optimization of Inverse Scattering Problem," *T. IEE Japan,* Vol. 122-A, pp. 1005-1010, 2002 (in Japanese).

Session 3P4
Plasmonic Nanophotonics II

Holographic lithography and Defect Engineering for Photonic Crystals

H. B. Sun [1,2] **S. Shoji** [2], and **S. Kawata** [2]

[1]Jilin University, China
[2]Osaka University, Japan

Holographic lithography is promising approach for rapidly fabricating of large-volume three-dimensional photonic crystals (PhCs). However, the lattice constants of PhCs are in principle determined by the wavelength of the laser used for fabrication, as limits the broad use of the delicate laser micro-nanofabrication technology. Here we solve the problem by using two-step exposure, by which not only the more lattice types become available, the lattice constant is arbitrarily adjustable. In addition, by secondary two-photon exposure and laser ablation, donor and acceptor type defects are readily produced. This is an important step toward functional PhC devices. Figure 1 is the scanning electronic microscope image of the scaffold-type fcc PhCs. (a) a brid eye view; (b,c) magnified images of (b) top surface of the structure, and (c) cross-section of a crack in the rim of the structure; (d,e) simulated cross section of fcc lattice in (d) <111> and (e)<11,-1>

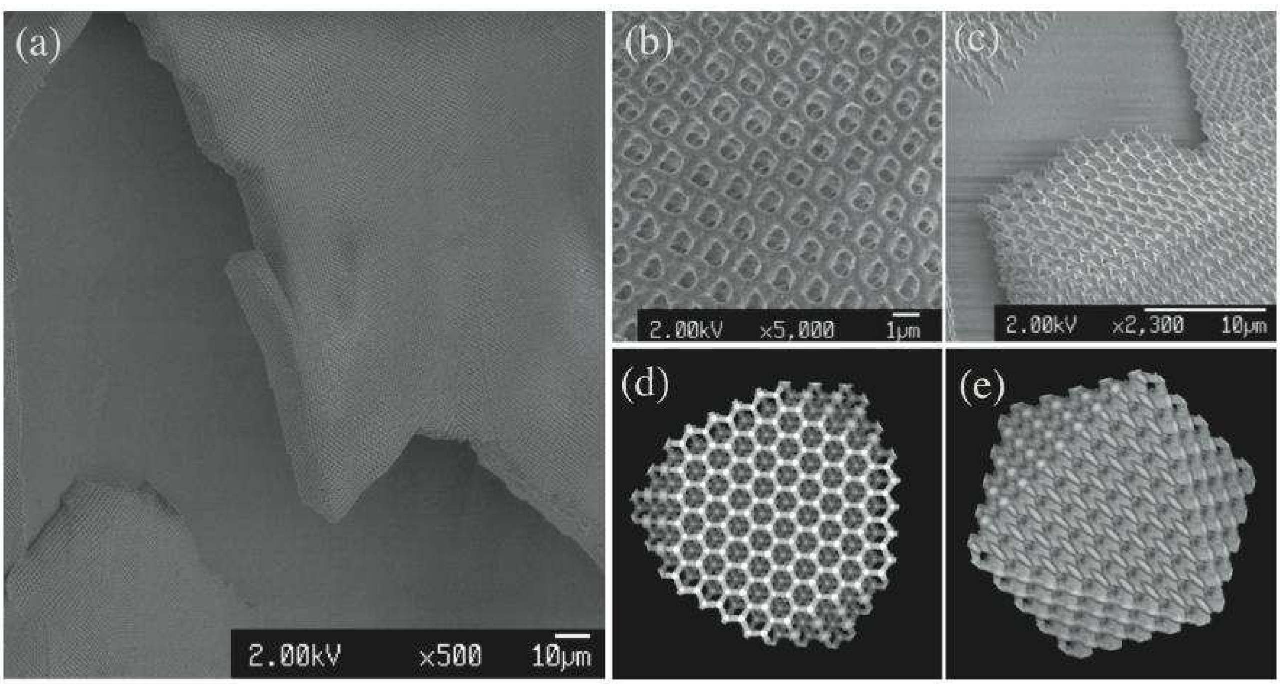

Plasmonic Metamaterials and Its Application to Novel Optical Devices in the Visible Light Frequency Region

T. Tanaka, A. Ishikawa, and **S. Kawata**
RIKEN, Japan

Negative permeability of plasmonic metamaterials is theoretically investigated in the visible light frequency region [1, 2]. To estimate magnetic responses of metallic elements precisely, we determined internal impedance by considering the delay of the current inside the metal structure. In our calculation, the surface resistivity saturates at the inherent frequency of each metal as the frequency increases. For the silver case, the saturation value is 0.4 ohms/m2 and this value is remarkably smaller than that of gold and copper. On the other hand, the internal reactance is increasing as the frequency increases independently of metal. We concluded that the internal reactance is dominant factor to realize the negative magnetic permeability in the optical frequency region. We also show the frequency dependence of the magnetic permeability of Split-ring resonators (SRRs). In the case of SRRs made of gold, only on the filling factor was 11%, the minimum value of the magnetic permeability takes negative value in the entire visible range. On the other hand, the silver SRR exhibits negative magnetic permeability in the visible range even under the low filling factor condition of 3%. Therefore, we concluded that reducing the geometrical capacitance and using silver for SRR are necessary to realize the negative magnetic permeability in the visible light range. In addition, we talk about an application of the plasmonic metamaterials to the novel optical device that can eliminate the unwanted light reflection at the interface between two materials with different indices of refraction [3]. The fabrication techniques of the plasmonic metamaterials are also presented [4, 5, 6].

REFERENCES

1. A. Ishikawa, T. Tanaka, and S. Kawata, *Phys. Rev. Lett.* 95, 237401 (2005).
2. A. Ishikawa, T. Tanaka, and S. Kawata, *Phys. Rev. Lett.* 95, 237401 (2005).
3. T. Tanaka, A. Ishikawa, and S. Kawata, *Phys. Rev. B* (accepted for publication).
4. T. Tanaka, A. Ishikawa, and S. Kawata, *Appl. Phys. Lettt.* 88, 81107 (2006).
5. F. Formanek, N. Takeyasu, T. Tanaka, K. Chiyoda, A. Ishikawa, and S. Kawata, Optics Express 14, pp. 800-809 (2006).
6. F. Formanek, N. Takeyasu, K. Chiyoda, T. Tanaka, A. Ishikawa, and S. Kawata, *Applied Physics Letters* 88, 83110 (2006).

Simulation Study of Optical Properties for Metallic Nanoparticle Ring

Y. C. Lan, W. L. Chen, and **L. Y. Wang**

National Cheng Kung University,Taiwan R. O. C.

The closely spaced metallic nanoparticle arrays can transfer energy and acts like nanosale optical waveguides [1]. The energy transmission is attributed to the evanescent coupling of the localized surface plasmon excited on the surface of the nanoparticles [2]. The linear chain of nanoparticles also displays some collective waveguide modes [3]. If the nanoparticles are arranged to form a square or circular ring, the constructive or destructive interference between the evanescent couplings will occur for different input frequencies. Then, the nanoparticle ring may behave like a ring resonator in the nanoscale [4].

In this work, the optical properties of the nanoparticle ring will be studied via computer simulation. The finite-difference time-domain (FDTD) method with the Drude dispersive model for the metal nanoparticle will be used. The wave propagating in this square ring with square nanoparticles will be simulated in the two-dimensional Cartesian coordinate (therefore, the nanoparticles are actually the nanorods with infinite length). The dispersive relation for the collective plasmon modes will be calculated and showed. The transmittance spectrum for the ring will be computed and analyzed. And the field pattern for the resonant condition will be displayed.

REFERENCES

1. L. A. Sweatlock, S. A. Maier, H. A. Atwater, J. J. Penninkhof, and A. Polman, *Phys. Rev. B* 71, p. 235408, 2005.
2. J. R. Krenn, A. Dereux, J. C. Weeber, E. Bourillot, Y. Lacroute, J. P. Goudonnet, G. Schider, W. Gotschy, A. Leitner, F. R. Aussenegg and C. Girard, *Phys. Rev. Lett.* 82, p. 2590, 1999.
3. S. A. Maier, M. L. Brongersma, P. G. Kik, S. Meltzer, A. G. Requicha and H. A. Atwater, *Adv. Mater.* 19, p. 1501, 2001.
4. S. C. Hagness, D. Rafizadeh, S. T. Ho and A. Taflove, *J. Lightwave Technol.* 15, p. 2154, 1997.

Plasmonic Imaging: a Novel Function of Metallic Nanostructures

J. Kato and **A. Ono**
RIKEN, Japan

S. Kawata
Osaka University, Japan

Metallic nanostructures with a distinct shape and arrangement exhibit particular optical properties and have potential for a variety of applications in imaging, lithography, optoelectronic devices, and biosensors [1]. For example, metallic nanoparticles and nanoshells in dielectrics show intrinsic spectral responses, which are applied to various sensors for biological or chemical applications [2,3]. A sharpened metallic tip is used as a unique probe for an apertureless near-field scanning optical microscopy in nanoimagings and spectroscopy [4,5]. Moreover periodically arranged nanoholes or corrugations on metal film exhibit an extraordinary light transmission and a beaming effect as founded by Ebbesen [6]. In all cases, the surface plasmon polaritons (SPPs) or its localized excitations on bounded metallic surfaces or features play important roles for the field enhancements and the transffers of nearfield light. The plasmonic responses of metallic rods, pillars or rings are also extensively investigated to realize the negative-index metamaterials [7-9].

Recently, Pendry has added a novel function to the plasmonic nanostructures that is the near-field imaging with silver thin slab [10], in which the SPP field is amplified through the negative permittivity of the slab to generate the quasi-perfect replica of the input field near the exit surface. This 'superlens' effect was experimentally demonstrated with the nanolithography technique [11]. The multilayered version is expected to show the better performances in nanoimaging. Thus, in this paper, we have numerically investigated the plasmonic responses of the metallic slab layed system ($\sim$ four layers of 10 nm silver slabs) in the 'image relaying' phenomena. As another interesting property of a metallic nanostructure, we have also proposed a subwavelength imaging scheme for nearfield in which a metallic nanorod array is used as a plasmonic image-transfer device [12]. In both cases, the image resolution of several tens nm was found to be obtained for dipole sources placed near the entrance surfaces. The role of the propagating SPP and the localized SPP in these structures are revealed and their various imaging features are investigated and compared with each other through the three-dimensional FDTD (finite-difference time-domain) simulations.

REFERENCES

1. Near-field and surface plasmon polaritons, S. Kawata, ed. (Springer, Berlin, 2001).
2. T. Okamoto and I. Yamaguchi, *J. Phys. Chem.* B, 107, 10321 (2003).
3. E. Prodan, C. Radloff, N. J. Halas, and P. Nordlander, *Science,* 302, 419 (2003).
4. Y. Inouye and S. Kawata, *Opt. Lett.* 19, 159 (1994).
5. T. Ichimura, N. Hayazawa, H. Hashimoto, Y. Inouye, and S. Kawata, *Phys. Rev. Lett.* 92, 220801 (2004).
6. T. W. Ebbesen, H. J. Lezec, H. F. Ghaemi, T. Thio, and P. A. Wolff, *Nature(London)*, 391, 667 (1998).
7. D. R. Smith, W. J. Padilla, D. C. Vier, S. C. Nemat-Nasser, and S. Schultz, *Phys. Rev. Lett.* 84, 4184 (2000).
8. V. M. Shalaev, W. Cai, U. K. Chettiar, H.-K. Yuan, A. K. Sarychev, V. P. Drachev, and A. V. Kildishev, *Opt. Lett.* 30, 3356 (2005).
9. A. Ishikawa, T. Tanaka, and S. Kawata, *Phys. Rev. Lett.* 95, 237401 (2005).
10. J. B. Pendry, *Phys. Rev. Lett.* 85, 3966 (2000).
11. N. Fang, H. Lee, C. Sun, and X. Zhang, *Science,* 308, 534 (2005).
12. A. Ono, J. Kato, and S. Kawata, *Phys. Rev. Lett.* 95, 267407 (2005).

Dynamics of Enhance-Transmitted Light Beam Through Sub-Wavelength Slit

K. R. Chen, J. Y. Lai, T. H. Tsai, and **J. S. Hong**

National Cheng Kung University, Taiwan

The enhancement of light transmission through sub-wavelength slit is studied with our newly developed two dimensional simulation code of finite-difference time-domain method. The simulations verify the enhanced transmission that far exceeds the diffraction limit; the dynamics are helpful to understand in-depth the resultant beaming of light. Instead of one beam with a specific angle for a given wavelength [3-6], one additional beam with a different angle excited by the induced surface charge can be seen for the same wavelength from the electric field of different polarized direction. In additional to the interference of the scattered light with the transmitted light, the spatial de-coherence and coherence between the magnetic and electric fields is shown to be important for the transmitting process and the beaming mechanisms of the light. Thus, the dynamics will be illuminated in detail for deep understanding. The effect of different width of the exit groove on the enhanced transmission is also studied and explained as an application of above findings.

Plasmonic Nanorod Array for Optical Nanoimaging

A. Ono, J. Kato, and **S. Kawata**
RIKEN, Japan

Nanoplasmonics, plasmonic phenomena induced on metallic nanostructure, is very attractive research field [1]. Metallic nanoprobe, metallic nanoshell, and metallic nanospheres have been developed for the local field enhancement and the optical properties are utilized for plasmonic nanoimaging, plasmonic nanospectroscopy, plasmonic laser, and so on [2, 3].

In this presentation, we propose a plasmonic nanorod array provides two-dimensional near-filed images with nanoresolution [4]. Although the spatial resolution focused by conventional lens is limited to the wavelength of light, plasmonic nanorod array overcame this diffraction limit. We demonstrated that near-field sources in nanometer scale were plasmonically imaged through the array using threedimensional finite-difference time-domain algorithm. Figure 1 shows the configuration of the plasmonic nanorod array and the cross sectional intensity field distribution for nanoimage transfer of a character pattern 'λf. It is constructed by the silver nanorods of 20 nm diameter and 50 nm height hexagonally arranged with 40 nm array pitch. Localized surface plasmon polaritons of nanorods contribute to the nanoimaging. Our simulations show that color information with subwavelength resolution is acquired by well-designed metallic nanostructure. The spatial resolution was 40 nm which was determined by the array pitch. Plasmonic nanorod array is applicable to optical nanoimaging, nanobiosensor, nanolithography, and nanocommunication.

REFERENCES

1. Near-field and Surface Plasmon Polaritons, edited by S. Kawata (Springer, Berlin, 2001).
2. T. Ichimura, N. Hayazawa, M. Hashimoto, Y. Inouye, and S. Kawata, Phys. Rev. Lett. 92, 220801 (2004).
3. T. Okamoto, F. HfDhili, and S. Kawata, Appl. Phys. Lett. 85, 3968-3970 (2004).
4. A. Ono, J. Kato, and S. Kawata, Phys. Rev. Lett. 95, 267407 (2005).

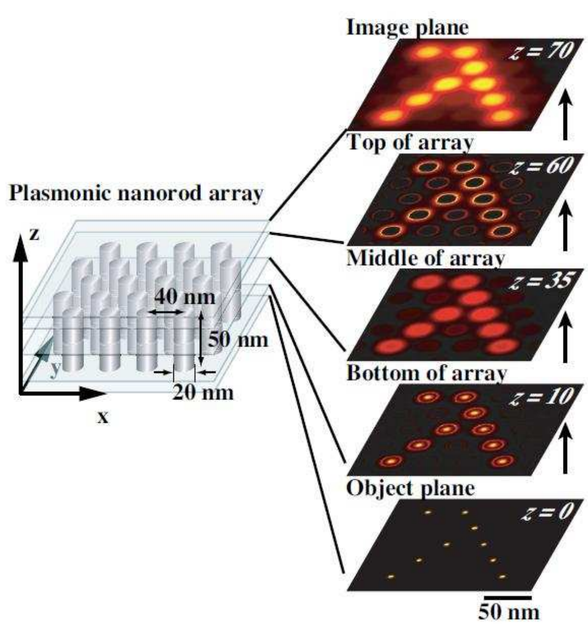

Figure 1: Optical nanoimaging by plasonic nanorod array.

Perturbative Behavior of Surface plasmon Modes

W. C. Liu
National Taiwan Normail University, Taiwan R. O. C.

Surface plasmon mode of a plain metallic surface has been well understood and has many applications. Periodic or isolated structures on a metallic surface can modify the resonant condition and the surface plasmon mode. In this research, we study perturbative behavior of the surface plasmon mode in a metal surface with small distortion and investigate the mode properties of plasmonic structures. The coordinate-transformation differential method [1, 2] is used to calculate surface plasmon modes in a weakly distorted air-silver surface at wavelength of 650 nm. With TM polarization (the magnetic-field vector is perpendicular to the plain), it is found that the Bloch wave numbers and field distributions of the surface plasmon modes are highly sensitive with the distortion of only a couple nanometers for periods much smaller than the wavelength.[3]

Fig. 1 shows the deviation of surface plasmon modes of a sinusoidal surface profile with period d = 500 nm, 100 nm, and 20 nm, respectively. For cases in which period d =500 nm, the deviation of Bloch wave number from that of a plain silver surface is proportional to square of the distortion height h2 and agrees very well with the analytical results describing a weakly, periodically modulated metal film.[4, 5] However, for cases with period d = 100 nm and 20 nm, the agreement becomes worse. The large Kd must break the approximations leading to the analytical result. The exploration of the perturbative behavior of surface plasmon modes will result in a better understand of the fundamental characteristics of surface plasmon and will help to manipulate the surface plasmons in metallic nanostructures.

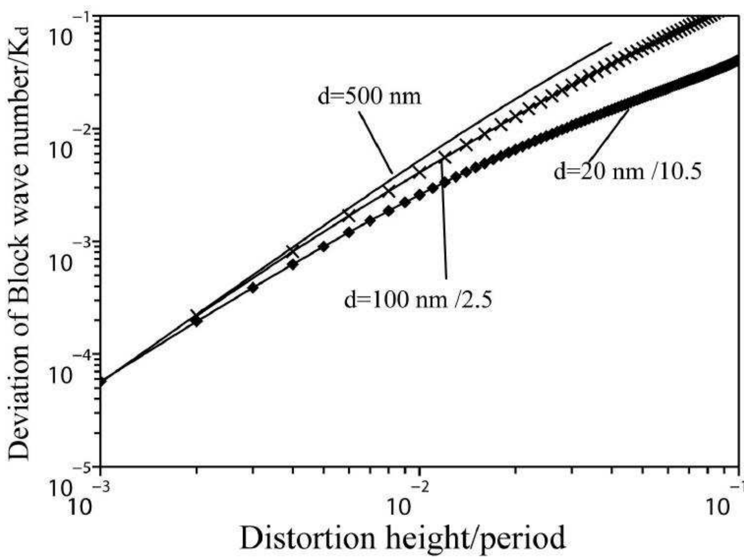

Figure 1: Perturbative deviation of surface plasmon modes of a sinusoidal surface profile. The periods are 500 nm, 100 nm, and 20 nm, respectively. The distortion heights are normalized to the period d and the deviation of Bloch wave number from that of a plain surface are normalized to $K_d = 2\pi/d$. The d=100 and d=20 curves are multiplied by extra normalization constants for comparison.

REFERENCES

1. J. Chandezon, M. T. Dupuis, G. Cornet, and D. Maystre, *J. Opt. Soc. Am.* 72, 839 (1982).
2. L. Li, J. Chandezon, G. Granet, and J.-P. Plumey, *Appl. Opt.* 38, 304 (1999).
3. W.-C. Liu, *Opt. Express* 13, 9766 (2005).
4. S. A. Darmanyan and A. V. Zayats, *Phys. Rev. B* 67, 35424 (2003).
5. A. M. Dykhne, A. K. Sarychev, and V. M. Shalaev, *Phys. Rev. B* 67, 195402 (2003).

Theoretical Analysis of Volume Integral Equation Method and Subhierarchal Parallel Algorithm for Solving Electromagnetic Diffraction Problem on a Dielectric Body in a Layer

Y. G. Smirnov
Penza State University, Russia

We consider a three-dimensional problem of the electromagnetic wave diffraction by a bounded dielectric body of arbitrary shape in the layer shielded by perfectly conducting planes. The problem is reduced to the volume singular integral equation (VSIE) and solved numerically by the Galerkin method. We have proved the convergence and obtained estimation of the rate of convergence for the method.

The main difficulties in the VSIE method are (a) very large time of calculations of the matrix elements when computations are performed with sufficiently high accuracy, and (b) occurrence of large and dense matrices in systems of linear algebraic equations obtained after discretization of the problem.

We demonstrate that when one uses VSIE method for the problem discretization, the matrix elements may be calculated independently. A natural way to calculate the matrix elements is utilization of parallel computations using supercomputers or clusters. Note in addition that in the diffraction problems, the structure of matrices is not arbitrary: we have the so-called structured matrices with O(n) different elements, where n denotes the matrix dimension.

We have created and elaborated efficient solvers for several types of diffraction problems on the basis of subhierarchal algorithms of parallel computations [1] that take into account the matrix structure. We solved 3D vector diffraction problems on bounded dielectric (or magnetic) bodies in a layer by this method.

REFERENCES

1. M.Yu. Medvedik and Yu.G. Smirnov. Subhierarchal Parallel Computational Algorithm and Convergence of Galerkin Method in Electromagnetic Diffraction Problem on Plane Screen. Izvestiya Vyzov. Povolzsky Region. Estestvennye Nauki, 5, pp. 3-19 (2004) (in Russian).

The Quantum Yield of a Metallic Nanostructure of Dimer

J. W. Liaw
Chang Gung University, Taiwan

Using a nanostructure (e.g. nanophotonics, or nanocavity) to enhance the fluorescence of molecules attracts considerable attention recently. In particular, several metallic nanostructures, e.g. metallic colloid, nanoprobe, or nanoantenna, were proposed to enhance the local electric field for the excitation of molecules, because of the effect of the surface plasmon resonance. However some of the results are the quenching, instead of the enhancement, for the fluorescence. The phenomena could be attributed to the poor quantum yield of the nanostructure on the fluorescence. In this paper, a dimer structure is studied, which consists two nearby metallic nanoparticles, to find the possibility for the enhancement. We use a simple-model, a dipole interacting with a dimer, to simulate an excited molecule within a gap of the dimer by solving a set of surface integral equations. The results of the boundary-element method show that the quantum yield of a metallic dimer is better than a single nanoparticle. In addition, the behavior of a dimer is like a low-pass filter which allows most of the fluorescence's energy of longer wavelength radiate to the far field. In contrast, for the short-wavelength ones, the nonradiative part is dominant; i.e. most of the fluorescence is dissipated into Joule's heat inside the metallic nanostructure.

Local-Field Enhancement in Open Cavities of Metallic Nanocylinder Pairs

M. Y. Ng and **W. C. Liu**
National Taiwan Normail University, Taiwan

Confinement of light in nano-scale region of metallic nanoparticles is one of the major challenges for nano-integrated optical devices, near-field optical research and plasmonic devices. Strongly local-field enhancement can be generated by metallic nanoparticles due to excitation of surface plasmon resonances [1]. For single metallic nanoparticle, plasmon resonance strongly depends on the shape and the size of the nanoparticle [2]. Several studies have been made on local-field enhancement by near-field coupling between close-spaced metallic nanoparticles with simple geometric shape. For example, plasmon resonance of two interacting silver nanocylinders exhibits strongly local-field enhancement in the gap between the nanocylinders when the polarization direction of incident light is parallel to the axis joining the nanocylinders and additional plasmon resonances are observed by changing the polarization direction of incident light and the separation distance between the nanocylinders [3].

Based on previous results about near-field properties of metallic nanoparticle pairs, local-field enhancement in the gaps of linear arrays of two or more silver nanocylinder pairs is studied by finitedifference time-domain (FDTD) simulation to obtain a better understand of particle-particle and pair-pair interactions. Fig. 1 shows the TM-mode near-field distributions of two, three and four interacting nanocylinder pairs with radius r=33, 36 and 38 nm, respectively, at λ= 460 nm. For multi-pair systems, high local fields appear not only in the gaps between pairs of nanocyliners but also in the gaps between two closely spacing pairs due to strong pair-pair interaction. Localized surface plasmon resonance of multi-pair nanocylinder systems can be tuned by illuminating wavelength, radius of nanocylinders, and the separation distance between the pairs. An open cavity model is proposed to understand the resonance behaviors of the multi-pair arrays. Our research suggests a simple and practical way to control local-field enhancement in a few metallic nanoparticles and this simple configuration can be applied to plasmonics devices, biological science, waveguide nanostructures, and near-field optical microscopy.

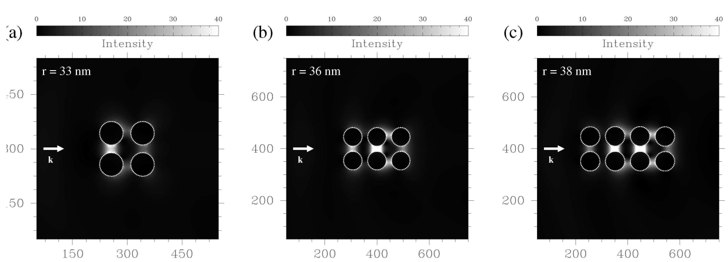

Figure 1: TM-mode near-field distributions of (a) two, (b) three and (c) four interacting nanocylinder pairs with radius r = 33, 36, 38 nm respectively. The wavelength of incident light is 460 nm and direction is normal to the major axis of the pairs. The intercylinder distance of each pair and interpair distance are 20 nm both.

REFERENCES

1. C. Bohren and D. Huffman, "Absorption and Scattering of Light by Small Particles", (Wiley, New York, 1983).
2. J. J. Mock, M. Barbic, D. R. Smith, D. A. Schultz, and S. Schultz, *J. Chem. Phys.* 116, 6755 (2002).
3. J. Kottmann and O. Martin, *Opt. Express* 8, 655 (2001).

Session 3P5
Recent Trends on Microwave Application Technologies

Five-Band Microwave Radiometer System For Non-Invasive Measurement of Deep Brain Temperatures In Newborn Infants : First Phantom Measurement Study

T. Sugiura, S. Hoshino, Y. Sawayama, H. Hirata, and **S. Mizushina**
Shizuoka University, Japan

Introduction

Clinical studies of hypothermal therapy for new-born infants who have suffered hypoxia-ischaemia is currently hindered by difficulty in measuring deep brain temperature. Microwave radiometry has been proposed for non-invasive monitoring of the temperature during the therapy. In the last 10 years, a five-band microwave radiometer system (MWR) has been developed and a calibration result of the system with a contacting waveguide antenna has also been reported. This paper describes the first measurement result in a normal room, not in a shielded room, using a phantom by the MWR.

Method and Results

Several countermeasures for external electromagnetic noise and thermal fluctuation have been done for the system. The system was calibrated and the temperature resolutions for five receivers, which correlate with a 2- confidence interval, were obtained. Temperature distribution phantom within a head was made using water and agar. Based on the model and antenna reciprocal theory, SAR distributions were calculated by an FDTD method and microwave weighting functions were finally obtained. Using the five-band radiometer system, we made a temperature measurement experiment on the phantom for the first time. Temperature resolutions for each receiver were 0.28 (1.2 GHz), 0.32 (1.65 GHz), 0.16 (2.3 GHz), 0.11 (3.0 GHz) and 0.12 K (3.6 GHz receiver). The estimated temperature at 5 cm depth from the surface was 35.72 K while that measured by a thermocouple was 35.89 K. The measurement error was 0.17 K. The confidence interval at the same position was 1.6 K which was a little bit larger than 1 K, which is an immediate goal desired by clinical application.

Conclusions

We have shown the first measurement result using a five-band microwave radiometer system operated in a normal room under ordinary temperatures. The estimation error was only 0.17 K at 5 cm depth. However, the confidence interval of 1.6 K was a bit larger than 1 K which is an immediate target. Further improvement of the system stability is now under consideration.

The Design of Multi-Beam Smart Antenna Arrays for Long Range RFID System

T. Y. Shih, C. C. Chang, and **S. F. Chang**
National Chung Cheng University, Taiwan R. O. C.

A design of multi-beam smart antenna arrays for use in radio frequency identification (RFID) systems with significantly enhanced performance has been newly proposed in this work. The system consists of 1×4 microstrip-feed planar monopole antenna arrays, followed by a 4×4 Butler matrix and then a digitally-controlled 1P4T RF switch circuit. The feeding port of the beam-forming network can be automatically switched, which consequently changes the direction of the beam.

A Butler matrix, which serves as beam-forming network, is the most commonly employed element; however, a particularly severe limitation is caused in system integration due to its large circuit size. In this research, a novel multilayer Butler matrix has been newly designed. The circuit size is reduced nearly 80% comparing to the reported work.

Array beam switching capabilities have been experimentally demonstrated by utilizing a commercial RFID system. This switched-beam arrays functioning as transmitting antennas of RFID reader show that the tag detecting range is increased dramatically from 1.55 m to 8.39 m. Four individual beams with $\sim 19^o$ 3-dB beamwidth are switched within 100^o scanning area in the space. Furthermore, the tag position can be indicated more accurately.

Design of Planar Antenna For Glottal Motion Sensor

J. C. Lin, C. C. Chang, and **S. F. Chang**
National Chung Cheng University, Taiwan R. O. C.

A design of 900 MHz, close coupling antenna, which interacts with human vocal organs, has been proposed in this work. The motivation of this research is to develop a glottal motion detection sensor. This sensor technique is to detect the millimeter-scale vibration of the trachea walls caused by the subglottal pressure variations during phonation. Based on this information, a more accurate voice model can be built for various applications including speaker verification or speech recognition.

Different dielectric properties of human tissues result in multiple reflection when the electromagnetic waves propagate. The main task in this work is to design a close coupling antenna that can efficiently transmit as well as receive the EM wave energy from the human body with minimum reflection loss. The antenna needs to be placed close the neck to ensure the signal quality. Unlike the far-field operation concept, the close coupling effect has been taken into consideration. Additionally, to reduce the impedance mismatch, especially at the interface between the air and the skin, several dielectric materials have been investigated for the antenna surface coating.

It has been known that the glottal cross-section varies during phonation, and consequently influences wave behaviors. A 3-D larynx model has also been established to simulate numerous folding conditions. The analytical and experimental data will be presented.

Study of Appropriate Number of Receivers in Microwave Radiometry Based on the Change of Tissue Electric Constants

Y. Sawayama, S. Hoshino, H. Hirata, M. Kimura, and **T. Sugiura**
Shizuoka University, Japan

Introduction

Multi-frequency microwave radiometry has been proposed as one of the promising methods for non-invasive monitoring of deep brain temperatures. Temperature profile in a head can be retrieved using measured brightness temperatures and radiometric weighting functions (RWF). RWF is calculated by tissue SAR and thus, is a function of tissue electric constants. The accuracy of temperature measurement could, therefore, be influenced by the estimation error of tissue electric constants. On the other hand, it has been pointed out that almost the same accuracy is possible using less number of radiometer receivers by repeated temperature profile simulations. This paper confirms the influence of estimation error of tissue electric constants and the possibility of smaller radiometer system based on temperature retrieval simulations with $2-\sigma$ confidence interval.

Method and Results

Since the electric constants (conductivity and dielectric constant) of living brain tissues in new-born infants can not be measured, the extrapolated values have been obtained by using those of adult's brain taking account of the difference of moisture content between babies and adults. We regard those extrapolated values as the "standard" values in a baby's head. Those constants were varied to the standard10, 20 % and SAR distributions in the babyfs head were calculated by FDTD method. Radiometric weighting functions were obtained and temperature retrieval simulations were made for each condition using the method we have previously reported. The estimation error and 2-σ confidence interval at 5 cm depth (center of baby's head) were 0.88 K and 1.06 K for three-band system while those for five-band system were 0.6 K and 0.46 K, respectively when conductivity estimation error was -20 %.

Conclusion

The results show that three-band system is not satisfactory in the case of the estimation error of tissue electric constants (standard$\pm$ 20 %). Temperature measurement seems to remain nearly unaffected by the variation of dielectric constant.

A Compact Multi-Transmission-Zero Bandpass Filter Using Three-Coupled-Line Resonators for UWB-OFDM Systems

W. C. Lo, Y. M. Chen, C. C. Chang, and **S. F. Chang**
National Chung Cheng University, Taiwan R.O.C.

The UWB systems have been rapidly developed in diverse areas such as high-speed local area networks, position location searching, advanced microwave imaging. The broad bandwidth of UWB systems requires that the band-selection filter in typical UWB transceivers must have large bandwidth percentage (greater than 50% or 2 GHz bandwidth) and high stopband rejection. In addition, the compact form factor is necessitated for future system-on-a-chip (SOC) or system-in-a-package (SiP) implementation. In this paper a compact ultra-wideband (UWB) bandpass filter, as illustrated in Fig. 1, with multiple transmission zeros is presented. This filter uses three-coupled-line resonator where the response is analyzed by using the multiple-coupled-line theory. The derived equations give the precise prediction of passband characteristics and transmission-zero locations. Then an electromagnetic simulator IE3D is performed to include the layout discontinuity and dielectric, radiation and conductor losses. As a result, an optimized performance of flat and low passband insertion loss and transmission zeros on both lower and higher stopbands are obtained. The simulation results, as shown in Fig.2, indicate that 0.3 dB insertion loss, 15 dB return loss over 3.1 to 5.1 GHz are obtained. Transmission zeros are generated at 1.5 GHz and 6.3 GHz. A prototype circuit was fabricated on the RO4003 substrate with the dielectric constant of 3.38, loss tangent of 0.002 and thickness of 31 mils. The measurement results agree very well with the simulation, showing great potentials of the proposed filter in UWB applications.

Index-symmetrical parallel coupled line, ultra wideband bandpass filter, step-impedance resonator, uniform-impedance resonator.

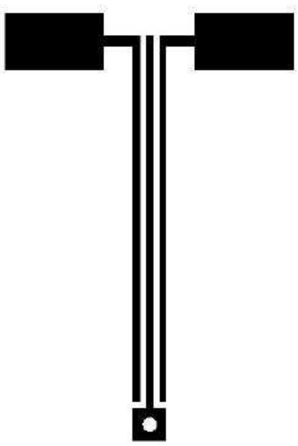

Figure 1: Configuration of the three-line UWB bandpass filter, composed of open-circuited and short-circuited

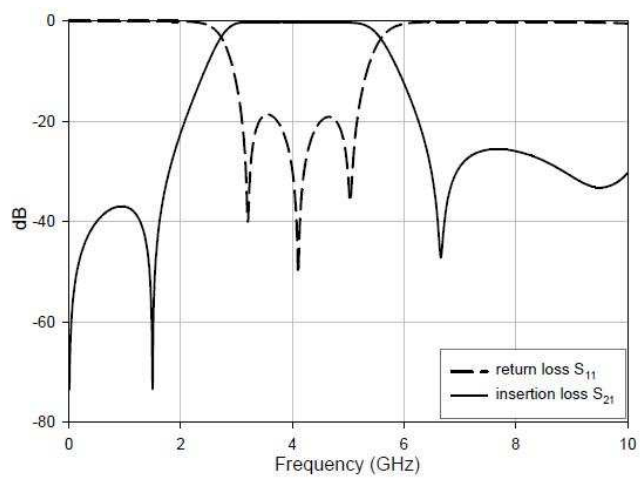

Figure 2: Simulation results of the three-line UWB bandpass filter

A CMOS Fully-Differential Programmable Gain Amplifier for MBOA-UWB System

M. D. Wei, S. F, Chang, and **C. C. Chang**
National Chung Cheng University, Taiwan R.O.C.

This paper presents a wideband fully-differential programmable gain amplifier (PGA) for Multi-Band Orthogonal- Frequency-Division-Multiplexing Ultra-Wide-Band (MB-OFDM UWB) systems. The programmable gain amplifier performs amplitude equalization of the demodulated signal to optimize the dynamic range of the MB-OFDM UWB receiver. The gain tuning of PGA is digitally controlled by the close-loop automatic gain control (AGC) circuitry and all gain settings must have constant settling time over the MB-OFDM UWB channel bandwidth, i.e. 240 MHz. To achieve this constant settling time requirement over the broad 240 MHz range, a linear-in-dB gain control manner of PGA is designed by using a current amplifier and a feedback resistor array. The resistor array is employed to keep high linearity, especially needed for the OFDM signal. The resistor array is realized with high-resistance implant (HRI) polysilicon resistors and N-channel MOSFET switches. The dimension (W/L) of the MOS-switch is carefully selected based on the consideration on linearity and bandwidth. A commonmode feedback (CMFB) circuit is required to stabilize the common mode voltage of the fully differential programmable gain amplifier. The PGA was fabricated with a standard 0.18μm 1P6M CMOS technology, which consumes less than 6.0 mW from a 1.8-V supply and has chip area (excluding pad) of 0.09 mm^2. The chip layout is illustrated in Fig. 1. The PGA has a voltage gain varying from 0 to 20 dB in 2.5 dB steps over 240MHz, as shown in Fig.2. The gain setting of PGA is linear in dB scale, as shown in Fig.3. The differential output swing is 0.5Vp-p with the total harmonic distortion below -65 dB at 10 MHz over the whole gain setting range.

Index-programmable gain amplifier, UWB, current amplifier.

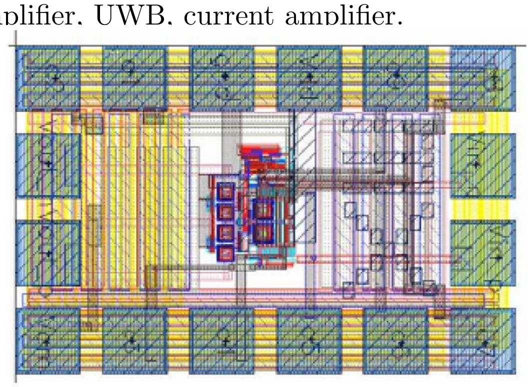

Figure 1: The layout of the CMOS PGA.

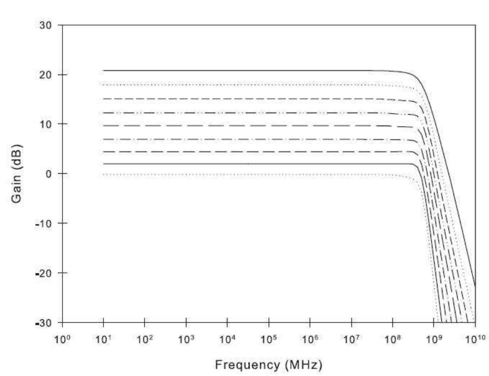

Figure 2: Frequency response of gain tuning

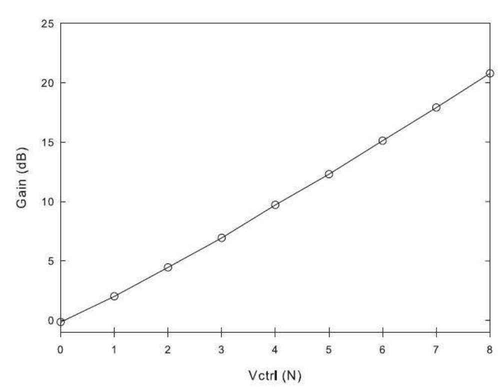

Figure 3: Gain (dB) relation with the control bits

Non-Invasive Measurement of Blood Sugar Level in Millimeter Wave Using Resonant Applicator

Y. Nikawa
Kokushikan University, Japan

I. Introduction

In recent years, diabetes is one of the most increasing diseases. According to the WHO, the number of diabetics in the world is predicted about 130 millions, it is estimated to grow about 300 millions in 2025[1]. To control the diabetes, it is vital to measure the blood sugar level. The available technique of the measurement is now only invasive method, which is to collect the blood sample from the patients. It is not a light burden for them. Therefore it is strongly demanded to develop non-invasive measurement[2], [3].

The complex permittivity of blood relates to the glucose concentration in millimeter waves. Therefore, the change of the reflection coefficient of human tissue can be related to the change of the blood sugar level[4], [5]. Nevertheless, high loss of cutaneous tissues hide the change of complex permittivity of blood in non-invasie measurement.

In this paper, to apply millimeter waves to obtain blood sugar level, reflection coefficient for the human tissue are simulated and the improvement of sensitivity is considered for the measurement. The technique is applied in vivo and the result can be applied to measure blood sugar level non-invasively.

II. Method

To develop practical method for the measurement, electromagnetic (EM) coupling applicator with circular patch has been developed. The patch is fed by waveguide. The center frequency of the measurement is 35.0 GHz. The patch radiator is on the substrate with the thickness of 0.90 mm.

III. Results

The change of reflection coefficient in millimeter wave was measured using simulated model as changing the glucose contents along the resonant frequency. It is found that the resonant frequency of applicator is sensitive to the glucose contents. Also, the change of reflection coefficient was measured in vivo and observed the changing the resonant frequencies. The experimental results agreed well with the simulated ones. From the in vivo measurement, the sensitivity of the reflection coefficient as a function of blood sugar rate was 3.7 [kHz/(mg/dl)]. It is confirmed that by such the measurement technique, blood sugar level can be measured.

IV. Conclusions

Millimeter wave has a great potential to apply to the field of medicine. Simulated and experimental evaluations measuring reflection coefficient in millimeter-waves show the possibility of the non-invasive measurement of blood sugar level. The obtained value is sensitive enough and it is confirmed that the resonant type applicator is very useful to measure blood sugar level non-invasively.

REFERENCES

1. Homepage related to diabetes; http://www.dm-net.co.jp/index.html.
2. N. Hoshi et al., "Application of Microwaves and Millimeter-Waves for the Characterization of Teeth for Dental Diagnosis and Treatment," *IEEE Trans. Microwave Theory tech.*, Vol. 46, No. 6, pp. 834-838, June 1998.
3. Y. Nikawa et al., gStudy on Dental Diagnosis and Treatment Using Millimeter Wavesh, *IEEE Transactions on Microwave Theory and Techniques*, Vol. 48, No. 11, pp. 1783-1788, Nov., 2000.
4. T. Matsushita et al., "Basic study on Non-invasive Monitoring of Blood Sugar Level by Measuring Transmission Coefficient in Millimeter Wave" *IEICE Trans. Electron.*, Vol. J84-C, No.6, pp.527-530, June 2001.
5. Yong Guan et al., gMeasurement of Transmission and Reflection Coefficient in Human Model to Blood Sugar Level by Millimeter Wavesh, 2002 Asia-Pacific Microwave Conference Proceedings, pp. 889-892, Nov. 2002.

Rapid Variations in Atmospheric Refractivity Revealed by an S-Band Phased Array Weather Radar

B. L. Cheong, R. D. Palmer, and **T. Y. Yu**
University of Oklahoma, USA
C. D. Curtis
National Severe Storms Laboratory, NOAA, U.S.A.

Backscattered radar echoes are dependent upon the atmospheric conditions in which the radio waves propagate and the electromagnetic characteristics of the targets. For echoes reflected from stationary targets, the phase of the received signal is approximately constant assuming the refractive index of the air mass between the radar and the target remains unchanged. Temporal variations in humidity and temperature can cause subtle, yet measurable, phase changes in the backscat- tered signal. Pioneering work in the use of this technique for near-surface studies of atmospheric moisture/temperature fields has been conducted by *Fabry et al. [J. Atmos. Oceanic Technol., 14, 978-987, Aug 1997]*, where he used an S-band scanning radar for his experiments. Scanning radar typically have update times on the order of several minutes. As a result, measurements of phase change are limited to a temporal resolution on the same order. Here, we will investigate the possi- ble advantages of the use of a phased array radar system, which can produce rapid updates on the order of seconds. The S-band Phased Array Radar (PAR), which is the centerpiece of the National Weather Radar Testbed (NWRT) located in Norman, Oklahoma, will be used for this study. The NWRT is the nation's first research facility dedicated to phased array radar meteorology and became available to the community in May 2004. It operates at 3.2 GHz and utilizes a modified version of the Klystron transmitter used on the WSR-88D radar network and thus shares many of the same characteristics. PAR employs the SPY-1A phased array antenna used on Aegis-class cruisers and destroyers and can perform a sector scan of 90^o in both azimuth and elevation through electronic scanning. Its 4,352 elements produce a beamwidth of 1.5^o at broadside and 2.1^o at the maximum off-broadside pointing angle of 45^o . Possible advantages of the use of phased array technology may be the mitigation of smearing of clutter targets due to antenna motion, adaptive mapping of clutter targets, and rapid update times, for example. Results will be presented from recent experiments and comparisons made with a closely spaced array of surface meteorological stations, which are used to provide in-situ validation measurements of refractivity.

Refractivity Retrieval Using X-Band Radars: Mitigation of Rapid Phase Wrapping

R. D. Palmer and **B. L. Cheong**
University of Oklahoma, U.S.A.

Modern Doppler weather radars, such as the S-band WSR-88D network in the USA, provide estimates of reflectivity, radial velocity, and spectrum width. These parameters are related to signal strength, atmospheric motion, and turbulent intensity, respectively. Until recently, weather radars were not capable of estimating any parameter directly related to humidity or temperature. Over the past several years, however, *Fabry et al. [J. Atmos. Oceanic Technol., 14, 978-987, Aug 1997]* have developed a method which uses subtle changes in ground clutter signal phase to estimate corresponding changes in atmospheric refractivity. Since refractivity is dependent upon humidity and, to a lesser extent, temperature, a new radar method has emerged which may have a significant impact on the meteorological community. Previous work on this technique has focused on measurements using S-band radar. It is well-known, however, that long-range, S-band radars have a limitation due to the earth curvature effect. At long ranges, this effect eliminates the possibility of lower tropospheric observations, except under extreme ducting conditions. So-called gap-filling radars have been developed at shorter wavelengths (e.g., X-band), which would have much shorter range, and would not be as susceptible to the earth-curvature effect. A significant problem with shorter wavelength radars, however, is seen with the implementation of refractivity retrieval. The technique relies on a phase difference calculation between the so-called reference phase map and the measurement phase map. The time difference between these two maps can be on the order of days, or even months. Given a typical change in atmospheric refractivity over such a time period, a shorter wavelength radar would produce significant phase wrapping problems. At S-band, the problem is less significant and can be circumvented using standard image processing methods. Here, we propose an algorithm called *Differential Refractivity Retrieval* (DRR), which would accumulate phase differences from scan-to-scan. As a result, typical atmospheric changes over such a short time (less than 5 min) would not cause a significant change in signal phase, thus, mitigating phase wrapping. Results will be presented using an advanced radar simulator, which prove its effectiveness. In addition, we will present data from the X-band radar network in southern Oklahoma, which will be deployed in Spring 2006 as part of the project *Collaborative Adaptive Sensing of the Atmosphere* (CASA). This large-scale project is supported by the National Science Foundation of the USA and has several important goals, including the sensing of the gap region created by the earth-curvature effect.

Design and Evaluation of System for Microwave Drying of Textile

J. Vrba, M. Pourová, O. Žák, and **J. Vrba (jr.)**
Czech Technical University, Czech Republic

In this paper we describe our new results dealing with design and evaluation of microwave industrial applicators used for drying of textile materials. We have designed and evaluated two different types of these applicators: open-resonator-type and waveguide-type one. We describe here basic analytical models of the discussed applicators, results of numerical modelling and experimental evaluation as well. Prototype of microwave drying machine working with microwave power of 17 kW at frequency 2.45 GHz is reported.

In this contribution we would like to describe our new results dealing with microwave industrial applicators used for drying of textile materials. We have designed and evaluated two different types of these applicators: open-resonater-type and waveguide-type one. We would like to present theoretical models of the discussed applicators, results of numerical modeling and experimental evaluation as well. Protype of microwave drying machine working with microwave power of 17 kW at frequency 2.45 GHz will be reported.

Session 3P6
Metamaterial and New Material Applications to EMC

Complex Permeability Spectra of Ferromagnetic Metal Composite Materials and EMC Applications

T. Kasagi
Beppu Mizobe Gakuen College, Japan

T. Tsutaoka
Hiroshima University, Japan

K. Hatakeyama
University of Hyogo, Japan

Complex permeability spectra ($\mu^* = \mu^{'} - i\mu^{"}$) of ferromagnetic metal composite materials have been studied in the microwave frequency range. Figure 1 shows complex permeability $\mu^*(a)$ and permittivity $\epsilon^*(b)$ spectra of permalloy ($Ni_{47}Fe_{53}$) composite materials containing the non-treated and heat-treated particles, in which its surface is oxidized in air using a furnace at 300^oC for 5 hours. The $\mu^{'}$ at GHz region increases by heat treatment and the frequency at which the $\mu^{"}$ shows a maximum, shifts higher frequency. These tendencies are owing to the suppression of the eddy current effect in composite materials; the contact electrical resistance between particles increases by heat-treatment of particles. Meanwhile the $\epsilon^{'}$ decreases and the dispersion frequency of ϵ^*, which is observed in several GHz, shifts higher frequency byheat-treatment of particles. Figure 2 shows the μ^* of Ni45Fe55,$Ni_{47}Fe_{53}$ and cobalt composite materials containing the heat-treated particles. For 79 vol.% cobalt composite, the $\mu^{'}$ shows zero at 6 GHz. Further 70 vol.% $Ni_{45}Fe_{55}$ composite has negative permeability above 5 GHz. The construction of the single-layer microwave absorber using these composite materials is also presented.

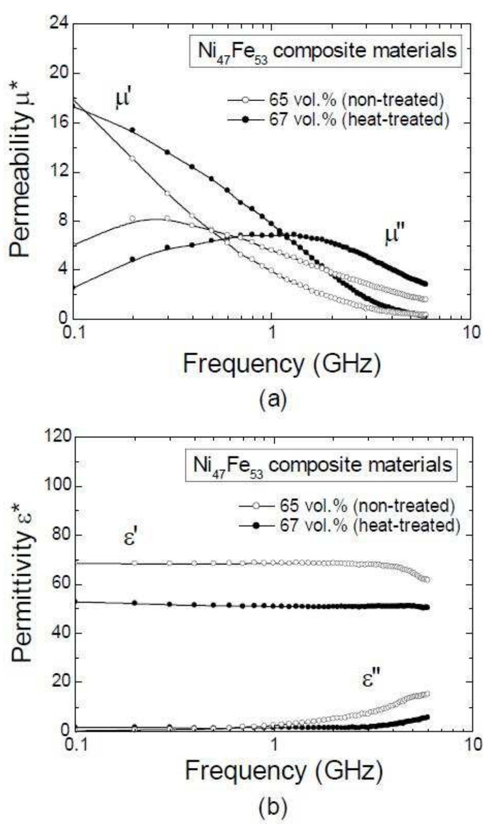

Figure 1: Complex permeability $\mu^*(A)$ and permittivity $\epsilon^*(B)$ spectra of$Ni_{47}Fe_{53}$composite materials.

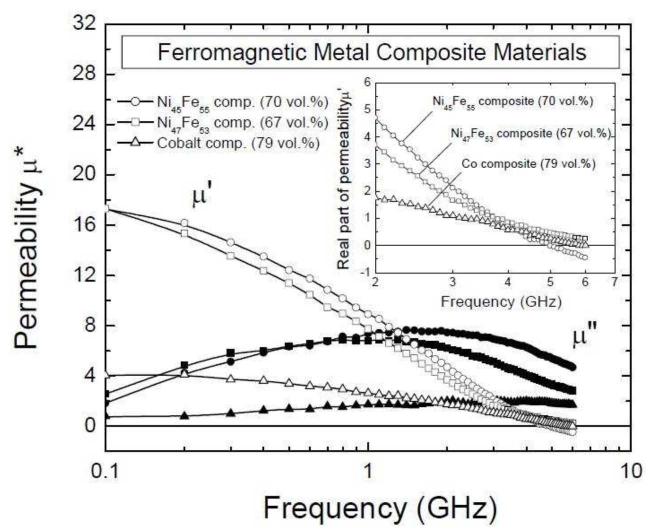

Figure 2: Complex permeability spectra of ferromagnetic metal ($Ni_{45}Fe_{55}$, $Ni_{47}Fe_{53}$ and cobalt) composite materials containing the heat-treated particles.

Permeability Spectra of Substituted Barium Ferrite BaFe12-x(Ti0.5Co0.5)xO19 in Microwave Frequencies and its Use as EMC Devices

T. Tsutaoka and **N. Koga**
Hiroshima University, Japan
T. Kasagi
Beppu Mizobe Gakuen College, Japan
K. Hatakeyama
University of Hyogo, Japan

Substituted barium hexaferrite $BaFe_{12-x}(Ti_{0.5}Co_{0.5})_xO_{19}$ shows the relatively low magnetic anisotropy and the ferrimagnetic resonance occurs in the frequency range from 1 GHz to 20 GHz [1]. In this study, complex permeability ($\mu = \mu' - i\mu''$) and permittivity ($\epsilon = \epsilon' - i\epsilon''$) spectra of $BaFe_{12-x}(Ti_{0.5}Co_{0.5})_xO_{19}$ (x = 0 to 5) have been investigated in the microwave frequency range under zero magnetic field. Figure 1 shows the complex permeability $\mu(a)$ and permittivity $\epsilon(b)$ spectra of $BaFe_{12-x}(Ti_{0.5}Co_{0.5})_3O_{19}$ (x = 3). The real part of permeability μ' shows the negative value above 2 GHz in the zero magnetic field indicating the natural resonance. Since the natural resonance of Ba ferrite exists around 40 GHz, this data indicates that the natural resonance frequency decreases by the substitution of Fe ion by Ti and Co ions. On the other hand, electrical permittivity spectra shows no frequency dispersion in the measurement frequency range. Combining this permeability spectra of substituted Ba ferrite with the negative permittivity spectra in the metal wire composite structure [2], the possible designs of EMC devices such as electromagnetic wave absorbers and shielding panels will be proposed.

REFERENCES

1. S. Sugimoto et al., *J. Magn. Soc. Jpn.* 23 (1999) 611.
2. T. Iwai, K. Hatakeyama, *IEICE Trans. B* E88 (2005).3294.

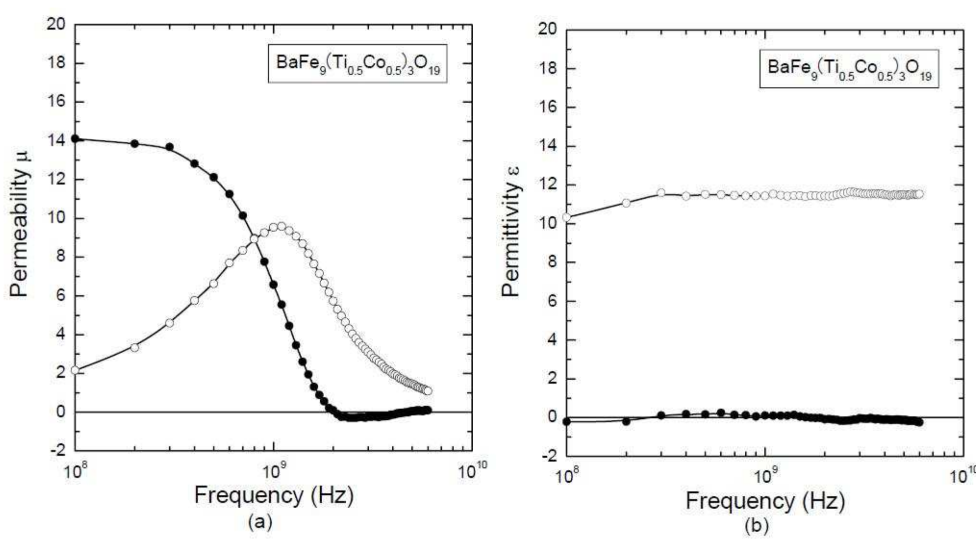

Figure 1: Complex permeability $\mu(a)$ and permittivity $\epsilon(b)$ spectra of $BaFe_{12-x}(Ti_{0.5}Co_{0.5})_xO_{19}$.

Frequency Selective Shielding Screen By The use Of Artificial Media

T. Iwai and **K. Hatakeyama**
University of Hyogo, Japan

Effective permittivity of a three-dimensional strip conductor array and its use as a shielding panel is proposed here. The array shown in Fig.1 is considered as an artificial dielectric material whose effective permittivity shows the resonant type dispersion, having negative value of dielectric constant.

The rectangular-shaped conductors are aligned as shown in Fig.1. The plane waves propagating toward .z direction with electric fields parallel to the strip axis hit the array structure. The calculation was carried out by the Maxwellfs integral form.

The reflection and transmission coefficients can be obtained from the scattered field generated by the conductor array. At the frequencies higher than 9GHz, almost all the incident waves are reflected, and the transmission becomes very small.

When the array structure is considered as a homogeneous dielectric media, effective permittivity can be obtained by reflection or transmission coefficients. The real part of the effective permittivity is shown in Fig.2. The imaginary part is always around null within the calculation error.

Above the resonant frequency, the effective permittivity becomes negative, and the transmission coefficient becomes very small because of the evanescent mode. Fig.3 shows the transmission characteristics calculated from the current distributions. We find that the strip conductor array provides the excellent characteristics as a frequency selective shielding screen compared to the conventional FSS.

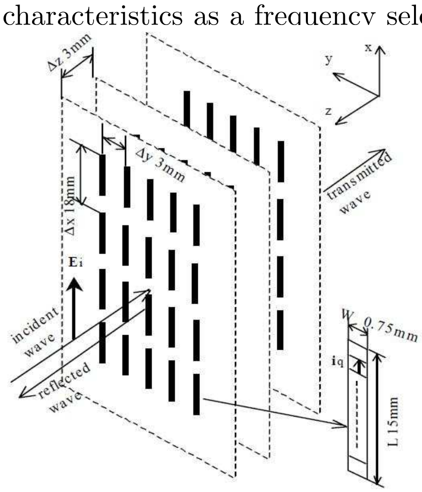

Figure 1: Three-dimensional array of strip conductors

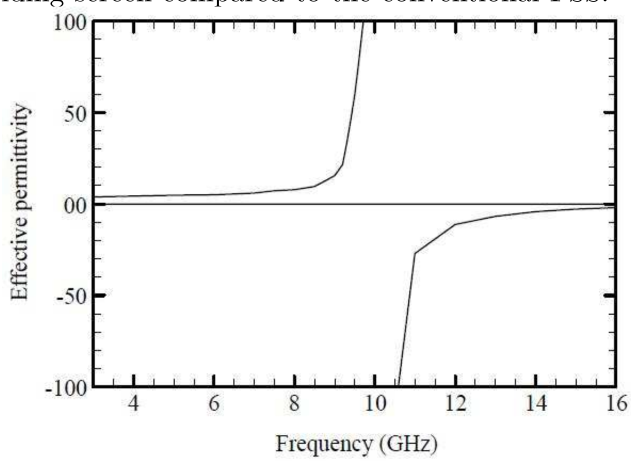

Figure 2: Effective Permittivity (real part)

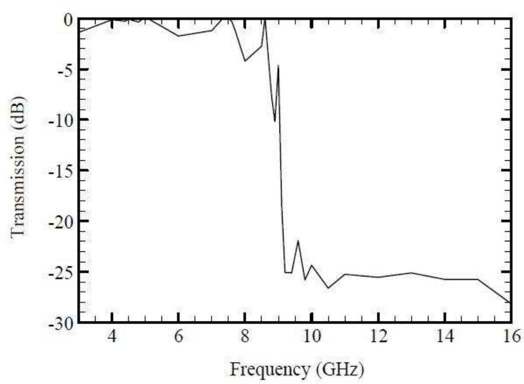

Figure 3: Transmission Characteristics

Study of EM Wave Shielding of Conductive Array Sheet with Ferromagnetic Metal Composite Layer

S. Yamamoto, K. Hasegawa, and **K. Hatakeyama**
University of Hyogo, Japan

Possible designs of EM wave shielding characteristics are discussed here using conductive array sheet, which shows resonant type dispersion in permittivity, with ferromagnetic metal particle composite layer.

Figure 1 shows the measured permittivity ϵ_r of conductive array sheet. Finite length metal wires are aligned periodically on a thin dielectric film. As shown in Fig.1, the array structure shows the resonant type dispersion and the $\epsilon_r^{'}$ becomes negative higher than the resonant frequency f_0 (=9.8GHz).

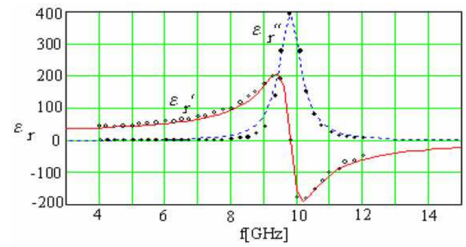

Figure 1: Permittivity ϵ_r of conductive array sheet.

In Fig.2, measured permeability of the permalloy particle composite is shown. The real part of μ_r is almost 0 at wide frequency band higher than 7GHz.

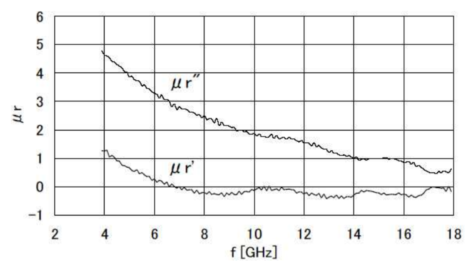

Figure 2: Permeability μ_r of permalloy composite.

Note that ϵ_r in Fig.1 and μ_r in Fig.2 are the constants for different material. Let us assume the imaginary material whose ϵ_r and μ_r are shown in Figs.1 and 2 respectively. The propagation constant $\gamma(= \alpha + j\beta)$ of this material is obtained as shown in Fig.3. The attenuation constant α becomes large value at the k_o which corresponds to f_0 in Fig.1. The phase constant becomes positive for the region lower than f_0 while negative value for the region higher than f_0.

The transmission coefficient or shielding S of this material is obtained from the α, and βin Fig.3. The figure shows the frequency selective shielding characteristics. The maxima of S is obtained at 9.8GHz which is the same f_0 in Fig.1. Figure 4 shows that the high value of shielding is caused due to the resonant permittivity dispersion plus magnetic loss.

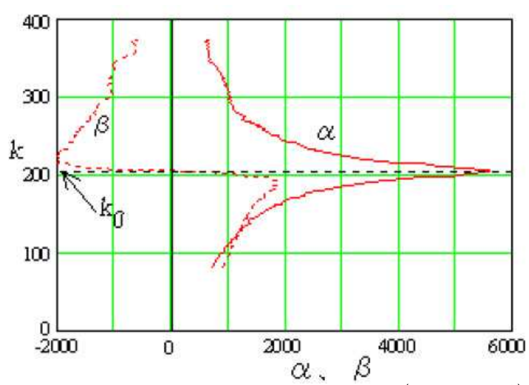

Figure 3: Propagation constant $\gamma(= \alpha + j\beta)$.

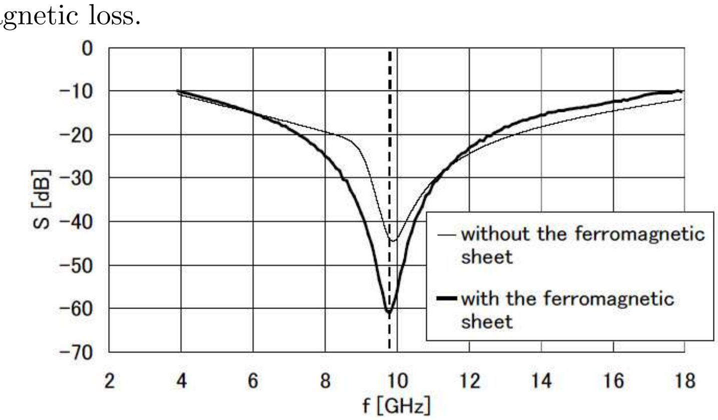

Figure 4: Calculated S with- and without the ferromagnetic sheet.

Broadband EM-Wave Absorber Characteristics Using IC-based Metamaterial

C. Kawamurra and **Y. Kotsuka**
Tokai University, Japan

Matching Characteristics of EM-Wave absorber based on the structural concept of microwave integrated circuit is investigated in this paper. First, the fundamental principle, particularly the method of converting the actual microwave circuit into the integrated circuit type absorber is described. Detailed investigation of the matching characteristics is conducted from FDTD analysis and experimental viewpoint .Fig.1 (a) shows the equivalent circuit of transmission line to a simple EM-wave absorber with space, d and a conductive plate at the back of the absorber. To make this circuit viable on a substrate backed with a conductive plate, the method of arranging a unit circuit element which consists of micro-chip resistors and conductive circuits is introduced as shown in Fig.1 (b). That is, a unit circuit element is composed of a high and a low conductive part to give resistance and inductance as shown in Fig.1 (a). In this construction, the variable function of the circuit constants is also important factor for the present absorber. The resistance and the inductance can be changed by adjusting each area of a high and low conductive part or their occupying areas. As a low conductive part, micro-chip resistors are mounted in the present investigations. Capacitance is given by changing the adjacent space between the tips of the unit circuit elements in a cross shape. By taking the size and the resistivity of the circuit constant as parameters, the matching characteristics are investigated with the aid of FDTD analysis and experiment The problem of finely controlling the resistance value on the resistive section is resolved by the idea of controlling whole size and each section of the cross element without changing the resistivity of the resistive section. Consequently, broadband matching characteristics with an absorption band from 2.62 5.12[GHz] in reflection coefficient of -20 [dB] are obtained. Since all data calculated in this paper are normalized by wavelength, these characteristics can be easily extended to millimeter frequency regions by applying the integrated circuit technology.

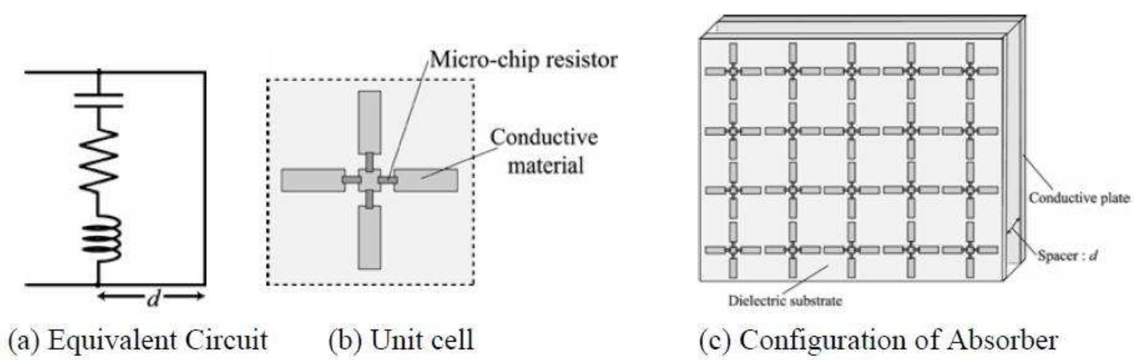

Figure 1: Construction of the present absorber.

Effect of Porosity on Magnetic and Electric Properties of Mg-Zn Ferrites

B. K. Bammannavar and **L. R. Naik**
Karnatak University, India
R. B. Pujar
S. S. Arts College and T. P. Science Institute, India

The use of magnetic materials with specific properties has stressed the need to invoke the role of microstructure on these properties. There are many ferrites that have replaced the conventional magnetic materials in the field of electronic technology. Among them soft poly crystalline nano-ferrites find vide applications from low frequency to radio frequency. Over the last few decades , a number of processing method have been developed to improve the performance of existing materials by reducing their grain size. Hence, an attempt has been made to develop and characterize the nano-crystalline ferrites through chemical route.

The microstructure of ferrites plays a dominant role in determining high power ability as well as low power loss in micro wave devices. In the recent years, much progress has been made in the control of ferrite material properties through chemical composition and preparation techniques. A variety of nano-sized ferrites with the general chemical formula Mg_{1-x} Zn_x Fe_2O_4 where $x = 0.1, 0.2, 0.3, 0.4$ and 0.5 have been prepared from a simple polymer matrix based precursor solution. The solution was composed of metal nitrates with polymer PVA and Sucrose. Thermolysis of the precursor mass at about 500 c resulted in the oxide phase. X-ray diffraction studies confirmed the formation of single phase ferrites while IR studies give the information about absorption bands. SEM studies throw a light on the microstructure of ferrites. While the porosity helps to explain its effect on magnetic and electric properties. The variation of resistivity with temperature shows the break at Curie temp. This indicates the transition from ferrimagnetism to paramagnetism, where as hysteresis studies confirm the presence of MD particles in the samples.

Key words : Nano, feerites, Sucrose, PVA, SEM and MD.

A Sequential Short-Circuited Patches Antenna with Parasitic Elements

P. Y. Lau, H. Wong, and **E. K.N Yung**
City University of Hong Kong, China

Small circularly polarized patch antenna is very attractive in this commercial life owning to their low-profile, ease of fabrication and light weight. For mobile communications, the antenna with good radiation performance such as wide axial ratio, low back loop and symmetric patterns are important. However, the conventional CP patch antennas are suffering from narrow axial ratio bandwidth (generally is 1-2%) [1]. Sequential rotation of antenna elements owns the advantages of wide axial ratio band and symmetry radiation [2]. But the overall size will be comparable large due to the existing of 4-elements patch. To reduce the antenna size, short-circuited (quarter-wavelength patch) technique can be employed. However, this technique will cause the poor radiation pattern with large cross polarization. Figure 1 shows the radiation pattern with short-circuited sequential arrangement patches antenna.

Thus, we shall present a small size short-circuited circularly polarized (CP) patch antenna in sequential rotations with an L-shape parasitic post top loaded on the patch in this paper. The function of the L-shape parasitic post on the patch is for cross-polar and back loop suppression. The four short-circuited patch elements are arranged in sequential rotation with phases of 0^o, 90^o, 180^0 and 270^o and the radiation patterns in both the principle planes (at $\phi = 0^o \& \phi = 90^o$).

Later on, we shall give the analysis on the parasitic elements$'$ effect to the antenna gain, radiation patterns and impedance. Figure 2 shows the antenna radiation patterns after adding the L-parasitic posts. The feed network is built by three Wilkinson power dividers is placed underneath the ground plane. The proposed antenna is operated in the center frequency of $5.8GHz$ with a $-30dB$ back loop compare to $0dB$ main beam. The impedance bandwidth ($SWR < 2$) is 33% from $5GHz$ to 7GHz and the axial ratio bandwidth is around 10% from 5.2GHz to 6GHz. The total area of reduction is 50% in comparison with the conventional sequential fed patch antenna. All results shown below are simulated by commercial EM software IE3D, version 10.0. Experimental results will be illustrated in the presentation during the conference.

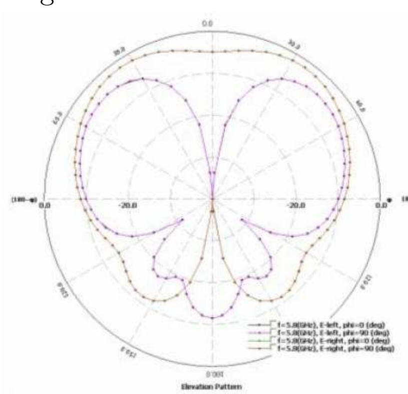

Figure 1: Radiation pattern without L-parasitic post (at 5.8GHz)

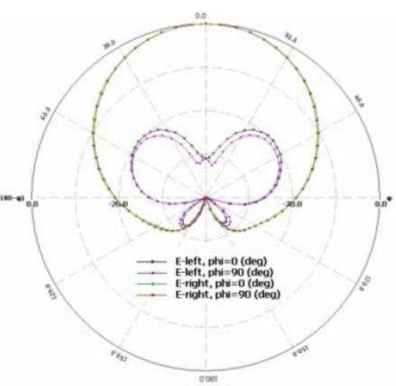

Figure 2: radiation pattern with L-parasitic post (at 5.8GHz)

REFERENCES

1. Wong, M.L., Wong, H., and Luk, K.M., "Small circularly polarized patch antenna", *Electron. Lett.*, Vol. 41, No.16 4th Aug, 2005
2. Huang, J.John., "A technique for an array to generate circular polarization with linear polarized elements", *IEEE Trans. Antennas Propagat.*, Vol. Ap-34,pp.1113-1124, Sept.1986

Suppression of Electromagnetic Radiation Noise from Wireless Module in Millimeter-Wave Band by Using Lid Made of PPS Resin Containing Titanium Oxide

Y. Takase[1], **T. Soh**[2], and **O. Hashimoto**[1]

[1]Aoyama Gakuin University, Japan
[2]The Yokohama Rubber Co., Ltd, Japan

With the practical application of communications equipments in millimeter-wave band, the electromagnetic(EM) radiation noise and the coupling are frequently generated, which cause malfunction and performance deterioration. In this paper, a protection lid with wave absorption capability is attached to a substrate for suppressing the EM radiation noise from a wireless module at 60GHz. The lid made of PPS(Polyphenylene Sulfide) resin containing titanium oxide is dielectric loss material($\dot{\epsilon}_r = 8.8 - j1.7$). When the lid is not attached, the lid is attached or the lid with upper back metal is attached, the various electric power is examined by FDTD method. Figure 1 shows the analytical model used by FDTD method. Figure 2 shows the analytical result of the electric power of the lid loss(dielectric loss), the reflection and the radiation. It is confirmed that the radiation is suppressed by the effect of the lid loss by attaching the lid and the metal with the lid. Figure 3 shows the electric power distribution that transmitted in each cell of inside(a) and outside(b) of the lid for confirmation of the suppression effect of the EM radiation noise. In this figure, h shows height from the substrate. In figure 3(a), it is clarified that the influence on the inside was small by arranging the lid. In figure 3(b), it is also confirmed that the shape of waves changed by the effect of the lid, so even in the case only with the lid, strong attenuation in center of the substrate was obtained. Consequently, the effective data for suppressing the EM radiation noise in millimeter-wave band are provided.

Acknowledgements

This work was financially partly supported by the Grant-in-Aid for 21st COE Program from the Ministry of Education, Culture, Sports, Science and Technology(MEXT) of the Japanese Government.

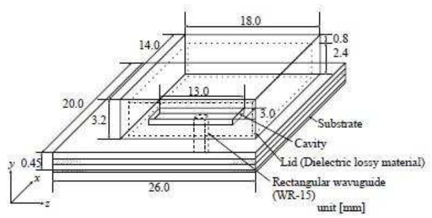

Figure 1: Analytical model.

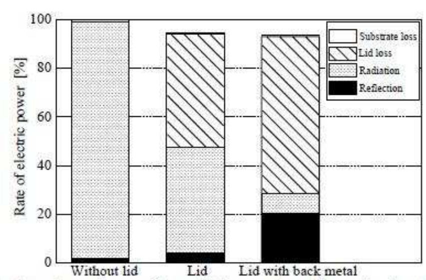

Figure 2: Analyzed results of the rate of each electric power.

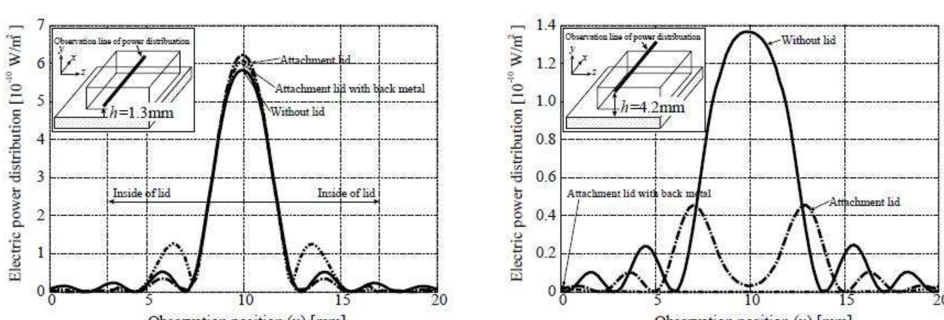

(a) In the case of h =1.3mm(Inside of lid) (b) In the case of h=4.2mm(Outside of lid)

Figure 3: Power distributionin.

EMC Simulations by the Finite-Difference Time-Domain Method with the Surface Impedance Boundary Condition

J. H. Lin, and **W. C. Chen**
National Taiwan Ocean University, Japan

Sievenpiper [High-impedance electromagnetic surfaces, Ph.D. dissertation, 1999, Electrical Engineering Dept., UCLA] proposed the high electromagnetic impedance surface structure which is a cycling structure and has suppression of frequency. Both characteristics make the surface current very small on this band of frequency possible. Therefore, the tangent magnetic can be close to zero. Because the thickness of the high impedance structure usually is much smaller than our target. This structure is the same as coating a thin layer on the object. In ordinary FDTD, if we want to simulate this kind of structure, a very small grid is required to accommodate the surface thickness, and hence more computer memory and computing time are needed.

Incorporation of the surface impedance boundary condition (SIBC) in FDTD is to simulate problems with a high impedance structure, which is called artificial magnetic conductor (AMC).This AMC structure is characterized by a high surface impedance and a suppression bandgap. An AMC structure is shown in Fig. 1 and its characteristic can be explained by the capacitance and inductance in Fig. 2. On the AMC surface, $\bar{E}$ is related to $\bar{H}$ by the equation, $\bar{E}(w) = Z(w)\hat{n} \times \bar{H}(w)$, where $Z = jwL/(1 - w^2LC)$. Convert the above equation into that in the time domain and discretize it into:

$$\bar{E}^{n+1}(t) = \frac{\Delta t}{C}\hat{n} \times [\bar{H}^{n+\frac{1}{2}}(t) - \bar{H}^{n-\frac{1}{2}}(t)] - [\frac{(\Delta t)^2}{LC} - 2]\bar{E}^n(t) - \bar{E}^{n-1}(t).$$

In this study, we compare the original model with the SIBC model with original FDTD method, and observe that computer memory and computing time are saved in a great amount.

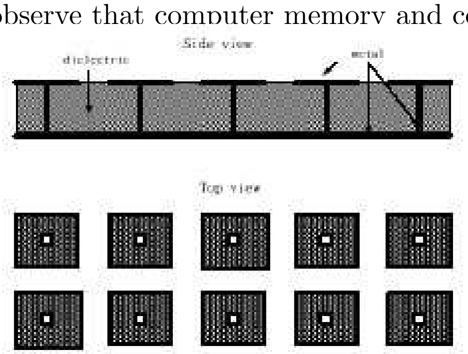

Figure 1: AMC structure

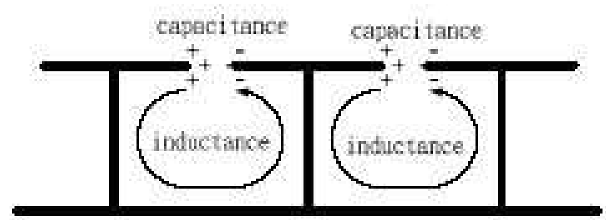

Figure 2: Origin of the equivalent circuit elements

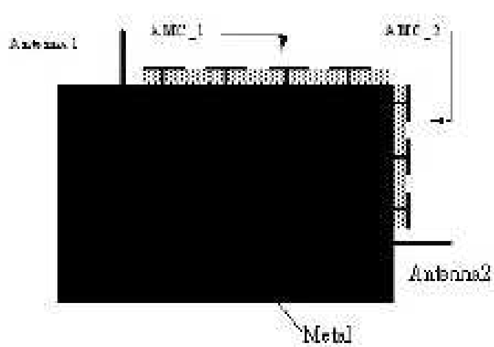

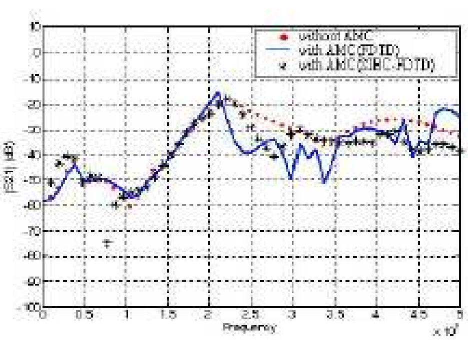

Mitigation of 16 2/3 Hz Magnetic Fields Originated from a Railway System Using Scaling Rules and 3D-Propagation of Eddy Currents

E. Salinas [1], **J. Atalaya** [2], **Y. Hamnerius** [2], **D. G. Chávez** [3]
C. Contreras [3], **C. L. Chinchay** [3], **M. A. Sumari** [3] and **M. Rezinkina** [4]

[1]London South Bank University, UK
[2]Chalmers University of Technology, Sweden
[3]Universidad Nacional de Ingenieria, Perú
[4]Polytechnic University of Kharkov, Ukraine

A study is presented of a novel technique to mitigate magnetic fields in a large architectural complex consisting mainly of two joint buildings to be constructed above a railway station. The magnetic fields are originated from a system of trains which are powered by an alternate current of 200A (rms) and a frequency of 16 2/3 Hz.

The motivation for this study is twofold, firstly there is a growing concern on suspected harmful effects of extremely low frequency (ELF) magnetic fields; and secondly, this type of field produce an interference on electronic equipment driven by electron beams (e.g. TV and computer monitor screens, electron microscopes). This interference becomes evident at field values above the range 0.5-1 ?T. The magnetic field values on various floors of the building compound were predicted, reaching 6.8?T on the floor nearest to the trains.

The technique uses the propagation of induced currents in a 3D-configuration which enhances the properties of the shielding structure. This is achieved by the addition of conductive ribbons (made of aluminium) to a combination of flat shields. In order to design this structure and due to the extremely high aspect ratios involved (e.g. 100metres/5mm), numerical analysis was complemented with experimental validation applying scaling rules for electromagnetic quantities such as frequency, current and magnetic fields. A most useful property is the scale invariance of the shielding factors. The scaling factor used for performing the experiments is 1/10, which implies a working frequency of 1.67 kHz.

Two results of the application of this technique are: 1) the high reliability of the field mitigation values obtained and 2) the cost-effective use of the shielding material in comparison to standard techniques, which is vital considering the large structure involved. The initial unshielded values computed in the building compound were successfully mitigated down to the sub-microtesla level.

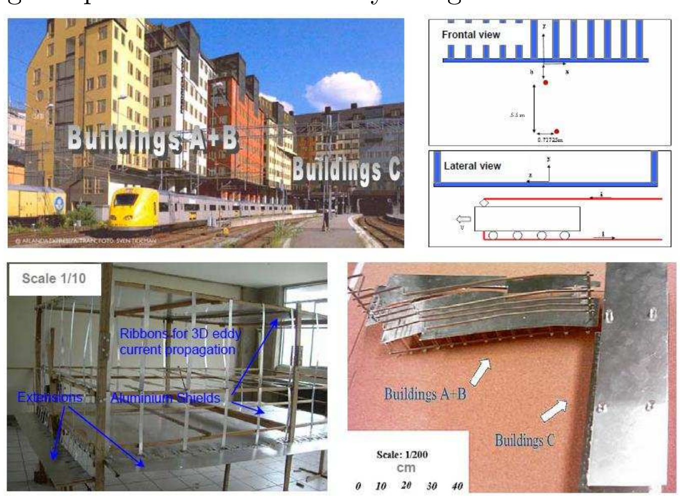

Session 3P7a
Novel Mathematical Methods in Electromagnetics II

An Exploration About Possibly Levitating Magnets Using Nonvertical Configurations

J. N. Ho and **W. C. Wang**

University of Washington, U.S.A.

Previous papers about diamagnetic levitation describe using vertical magnet configurations. At least one paper has mentioned a horizontal configuration using two permanent or electromagnets. However, none gives any quantitative analysis for the horizontal configuration. In addition none seems to have considered levitating a magnet at other angles, cases between these two configurations. The existence of these two extremes suggests that one possibly could levitate a magnet at other angles between 0 (vertical) to $\pi/2$ radians (horizontal). This paper explores one a configuration of two permanent suspending magnets for levitating a magnet using a horizontal configuration as well as another configuration using a permanent and electromagnet combo (allows variable field strength) for levitating magnets at angles not equal to $\pi/2$. This was done numerically by evaluating the basic equations and looking for equilibrium points where net forces and moments on a levitating magnet are zero. For all cases considered here, the two axes of the two suspending magnets were always directly aligned with each other. For a range of angles near $\pi/2$ radians, one can stably levitate a magnet parallel to the suspending magnets by using a permanent and electromagnet combo.

Mollifier and a Boundary Integral Equation on an Open Boundary-I. A Case of a Three Dimensional Scattering

Y. Hayashi

Japan

A scattering problem of waves by an open boundary is usually reduced to that of solving a boundary integral equation considered on the boundary. In a three dimensional case, a boundary is an open surface S of a finite area, and an integral equation is a linear functional equation of the form $T(\tau) = g$ considered on S, where g is an element of a Hilbert space L_2(S) composed of functions which are square integrable on S. Since it is known that a solution for an open boundary problem has a singularity in the vicinity of the periphery ∂S of S, τ is not necessarily square integrable on S, hence $\tau \notin L_2(S)$ but only $\tau \in L_1(S)$. Therefore, L_2-theory which is the most powerful tool of solution is not available to solve $T(\tau) = g$. In order to avoid this trouble, we refer to "mollifier" $R_\delta u$ known in a theory of function spaces, which is an operator that transforms a function to a more smooth function, and create a function $J_\delta(P)$ to which we give the same name "mollifier". Then, it can be proved that $J_\delta(P) = 0$ when $P \in \partial S$, that $J_\delta(P) = 1$ when $P \in S_{2\delta}$ where $S_{2\delta}$ is a part of S composed of points of S whose distance from ∂S is larger than 2δ, and that $J_\delta(P)$ is piecewise infinitely many times differentiable on S. As a consequence, $J_\delta\tau(P)$ becomes to belong to $L_2(S)$ and vanishes on ∂S, and therefore, by the authors method named MEC to solve a linear functional equation considered in a $L_2(S)$-space, an equation $T(J_\delta\tau) = g$ can be solved, obtaining approximate solutions $J_\delta\tau(P) = \sum_{n=1}^{N} c_n\tau_n$, that surely converge to the true solution with the smallest residual error, where $\{c_n\}$ is a set of given constants, and $\{\tau_n\}$ is a given set of functions which is complete in $L_2(S)$. Thus, a solution of $T(\tau) = g$ is shown to be $\tau(p) = 1/J_\delta(P)\sum c_n\tau_n(P)$ when $P \in S - S_{2\delta}$, and $\tau(P) = \sum c_n\tau_n(P)$ when $P \in S_{2\delta}$. Since $\tau(P) = O(1/J_\delta P)$, it may holds that $\longrightarrow \infty$ when $P \longrightarrow \partial S$.

[Note 1] More precisely, $J_\delta(P)$ should be denoted as $J_\delta(\alpha; P)$ because it depends on a parameter α also, where $1 < \alpha < 2$ in a three dimensional case, which indicates that $J_\delta(P)$ tends to 0 when P approaches to ∂S with the order of α, that is $J_\delta(\alpha; P) = O(\rho^\alpha)$ when $\rho \longrightarrow 0$, where ρ is the distance of P from ∂S.

[Note 2] It is obvious that $\tau(P) = \tau_\delta(\alpha; P)$ diverges when$\rho \longrightarrow 0$ with order of $O(\rho^{-\alpha})$. We call $\tau_\delta(\alpha; P)$ a "diverging mode" of order α.

Mollifier and a Boundary Integral Equation on an Open Boundary-II. A Case of a Two Dimensional Scattering

Y. Hayashi

Japan

As a continuation of Part I, we shall study in this paper a two dimensional scattering problem where a boundary is an open line segment of a finite length l on a plane. In this case also the scattering problem is reduced to that of solving a boundary line integral equation considered on l, which is a linear functional equation of the form $T(\tau) = g$ where g is an element of a Hilbert space $L_2(S)$ composed of functions which are square integrable on l. Because a solution of the integrl equation is supposed to have a singularity at the end points A, B of l, τ is not necessarily square integrable on l, hence $\tau \notin L_2(S)$ but only $\tau \in L_1(S)$. Therefore, L_2-theory is not available in this case too. In order to avoid this trouble, we again refer to hmollifierh in a theory of function spaces, and create a function $J_\delta(P)$ to which we give the same name a hmollifierh. Then, it can be proved that $J_\delta(P) = 0$ when $P = A$ and $P = B$, that $J_\delta(P) = 1$ when $P \in l_{2\delta}$ where $l_{2\delta}$ is a part of l composed of points of l whose distance from A and B is larger than 2δ, and that $J_\delta(P)$ is piecewise infinitely many times differentiable on l. As a consequence, $J_\delta(P)\tau(P)$ belongs to $L_2(l)$ and vanishes at $P = A$ and $P = B$. Therefore, an equation $T(J_\delta\tau = g$ is solved in $L_2(l)$ by MEC, and approximate solutions $J_\delta(P)\tau(P) = \sum_{n=1}^{N} c_n\tau_n$ are obtained, where c_n is a set of given constants, and τ_n is a given set of functions which is complete in $L_2(l)$. Thus, similarly to the three dimensional case, we have a solution of $T(\tau) = g$ which are $\tau(P) = 1/J_\delta(p)\sum c_n\tau_n(p)$ when $P \in l - l_{2\delta}$ and $\tau(P) = \sum c_n\tau_n$ when $P \in l_{2\delta}$. Since $\tau(P) = O(1/J_\delta(P))$, it may holds that $\tau(P) \to \infty$ when $P \to A, B$. (See Note 1 below.)

[Note 1] It is shown that $J_\delta(P) = J_\delta(\alpha; P)$ depends on a real number α, that $1/2 < \alpha < 1$, and that $J_\delta(\alpha; P) = O(p^\alpha)$ where $\rho = \bar{A}P$ and $\rho = \bar{B}P$. Consequently, $\tau(P) = tau_\delta(\alpha; P)$ diverges when $\rho \longrightarrow 0$ with order of $O(p^{-\alpha})$. Such a solution is called a diverging mode of order α.

[Note 2] If a line $\bar{A}B$ is defined by $a < x < b$, then a funtion $J(P)$, say, $J(P) = \sqrt{(x-a)(b-x)}$, may often be employed to make $J(P)\tau(P)$ belong to $L_2(l)$. However, such "mollifier" is insufficient in comparison with our mollifier. For example, a solution derived with the help of $J(P)$ does not converge to the true solution, since it does not depend on any parameter such as δ and no limiting operation is possible.

Investigation of Electromagnetic Diffraction by a Dielectric Body Using the Volume Singular Integral Equations

A. Tsupak
Penza State University, Russia

The three-dimensional time-harmonic problem of diffraction of electromagnetic field by an anisotropic dielectric body Q in the rectangular resonator P is examined. The surface of resonator is perfectly conducting.

A three-dimensional body Q with a constant magnetic permeability μ_0 and a positive 3-by-3 matrix (tensor) permittivity $\hat{\varepsilon}(x)$ is placed in the resonator. The components of $\hat{\varepsilon}$ are bounded functions in $\bar{Q}$, $\hat{\varepsilon} \in L_\infty(Q)$, and also $\hat{\varepsilon}^{-1} \in L_\infty(Q)$.

The outside media $(P \setminus Q)$ is characterized by constant permittivity ε_0 and constant permeability μ_0. The components of tensor have a jump at the boundary of Q. The surface of body Q is piece-wise smooth, i.e. conical and corner points are available.

The diffraction problem is stated in terms of generalized boundary-value problem for the system of Maxwell's equations. Fields $\vec{E}$ and $\vec{H}$ are found in space $L_2^3(P)$. Maxwell's equations as well as boundary conditions on perfectly conducting surfaces are considered in distributional sense. For nonresonance frequencies the existence and uniqueness of solutions of the boundary value problem are proved.

The method of volume integral singular equations is applied to solve the problem. Using the tensor Green function of parallelepiped

$$\hat{G}_E(r) = \frac{e^{ik_0 r} - 1}{4\pi r} \cdot \hat{I} + diag\{g^1, g^2, g^3\}\,. \tag{1}$$

the following integral equation is acquired:

$$\begin{aligned} &\vec{E}(x) + \frac{1}{3}\left[\frac{\hat{\varepsilon}(x)}{\varepsilon_0} - \hat{I}\right]\vec{E}(x) - v.p.\int_Q \hat{\Gamma}_1(x,y)\left\{\left[\frac{\hat{\varepsilon}(y)}{\varepsilon_0} - \hat{I}\right]\vec{E}(y)\right\}dy - \\ &\quad - \int_Q \hat{\Gamma}(x,y)\left\{\left[\frac{\hat{\varepsilon}(y)}{\varepsilon_0} - \hat{I}\right]\vec{E}(y)\right\}dy - \int_Q \hat{\Gamma}_2(x,y)\left\{\left[\frac{\hat{\varepsilon}(y)}{\varepsilon_0} - \hat{I}\right]\vec{E}(y)\right\}dy = \vec{E}^0(x). \end{aligned} \tag{2}$$

Tensors $\hat{\Gamma}, \hat{\Gamma}_1, \hat{\Gamma}_2$ are defined by formulas:

$$\begin{aligned} &\hat{\Gamma}(x,y) = k_0^2 \hat{G}_E(r) + (\cdot, grad\ )grad\ G_0(r), \\ &\hat{\Gamma}_1(x,y) = (\cdot, grad\ )grad\ G_1(r), \quad (\hat{\Gamma}_2(x,y))_{ij} = \frac{\partial^2 g^j(r)}{\partial x_i \partial x_j}, \end{aligned} \tag{3}$$

where

$$G_0(r) = \frac{e^{ik_0 r} - 1}{4\pi r}, \quad G_1(r) = \frac{1}{4\pi r} \cdot . \tag{4}$$

The equivalence of differential and integral problems is proved. The existence and uniqueness of solutions of the volume integral singular equations in $L_2^3(Q)$ are proved.

Galerkin method is used for numerical solution of integral equation. Splines of low order are applied as basic and test functions in Galerkin method. The explicit expressions for augmented matrix are written. The convergence of Galerkin method is proved for a wide class of diamagnetic bodies.

Numerical and graphical results for dielectric bodies with real and complex permittivity $\hat{\varepsilon}$ will be presented.

The Lateral Displacement of a Gaussian Beam at an Anisotropic-Isotropic Dielectric Interface

H. Sakurai

Gunma College of Technology, Japan

M. Ohki

Shonan Institute of Technology, Japan

S. Kozaki

Gunma University, Japan

When a bounded light beam is totally reflected at an isotropic dielectric interface, a lateral shift (Goos-Hanchen shift) of the reflected beam is occurred. This effect seems possible to be measured directly in the transmitted near-field region using a scanning tunneling optical microscope. On the other hand, it is reported that the direction of the displacement becomes negative in the case of a total reflection at an uniaxial-isotropic interface. On these points, the transmitted field distribution is studied in relation to the lateral shift at an anisotropic- isotropic dielectric interface.

We study nonspecular phenomena occurred by three-dimensional ordinary and extraordinary beams propagating in a uniaxial crystal and reflected at a uniaxial-isotropic interface. The anisotropic medium has the optical axis of arbitrary direction. First, the Fourier transform is applied to the wave equation in the incidence plane. The incident beam expression is obtained by inverse-Fourier transform of the transformed field. The reflected beam and transmitted beam satisfying the radiation condition are obtained similarly by using the boundary condition and phase matching condition.

Using the Fast Fourier Transform, solutions of reflected and transmitted fields are obtained. The backward Goos-Hanchen shift is observed in the images of the reflected beams. The variations of the shift are studied versus various parameters such as the optical axis and the incident angle. The distributions of the near-transmitted field are also examined in detail.

Numerical Simulation of Ultrasonic Guide Waves Propagation in Architectural Structures

A. Musolino, M. Raugi, F. Turcu, and **F. Turcu**
University of Pisa, Italy

The knowledge of the morphology of the building section is an essential datum both for the study of the answer of the masonry to the vertical and horizontal strengths and for the choice of specific consolidation techniques. Such knowledge is necessary in order to know if the masonry is stone made, bricks or mixed, and if it is composed by one ore more components; in this last case it is important to know their thickness and connections, the form and dimension of stones and bricks, the thickness of the mortar joints. All these parameters influence the local and/or global behaviour of the masonry. Then, in order to design a possible consolidation action by means of some mortar injections, it is also opportune to know the percentage of voids in the section, their dimension and distribution [1 3].

Since in the case of cultural monuments destructive testing is prohibited, it is not possible to use the core borings or cut and compression tests of the structures. For this reason the Non Destructive approaches, like sonic methods, ultrasounds and georadars, are the commonly used methods [4], [5].

In this paper we will address the feasibility of a non destructive test methodology based on the physical principle of the propagation of ultrasounds.

The Ultrasonic tests use a frequency range between 20 kHz and 1000 MHz. Since gaseous media do not transmit such waves, they are used to identify micro-cracks that are able to reflect the wave's front; on the contrary, the ultrasonic signal is highly attenuated because of its small wavelength in comparison to the dimensions of the masonry components [6], [7].

Besides the propagation velocity, others measurable quantities are: the energy content and its distribution in the frequencies domain, the damping phenomena etc.

Techniques based on ultrasounds have been introduced in the non destructive analysis in different engineering fields; in particular, in the case of plants with systems of pipes, ultrasonic waves guided by the pipes' walls have been used. The eventual reflected signals point out the presence of defects or other pipe's features. The ultrasonic guided waves are generated via a piezoelectric, magnetostrictive or magnetomechanical transducer system [8], [9].

In order to extend the procedure to the masonry, typically characterized by a slab shape, a number of numerical experiments have been performed by using codes for the simulation of the propagation of elastic waves.

In particular the model has been created considering a point in the structure where the perturbation has been imposed by a proper transducer. A number of material discontinuities in the examined region have been introduced and the various reflections have been studied. The presence of cracks has also taken into account.

The different wave modes have been compared in order to individuate the mode that presents the greater sensitivity with respect the defect to be individuated. A wide range of frequency has been considered too. The preliminary results obtained by the described analysis show that ultrasounds represent a promising technique in the NDT of masonry.

REFERENCES

1. O. Buyukozturk, "Imaging of concrete structures," NDT & E International 1998, Vol. 31, No.4 pp. 233-243.
2. M. J. Sansalone, W.B. Streett, "The Impact-Echo Method," NDTnet 1998 February, Vol.3 No.2
3. I. D. Hall, A. McNab et al. "Improved Ultrasonic Image Generation through Tomographicc Image Fusion," Ultrasonics 1998; 37, pp. 433-443
4. L. Cartz "Nondestructive Testing: Radiography, Ultrasonics, Liquid Penetrant, Magnetic Particle, Eddy Current," Materials Park: ASM international 1995.
5. C. Colla et al. "Sonic, Elecromagnetic and Impulse Radar Investigation of Stone Masonry Bridges," NDT&E International 1997; 30(4), pp. 249-254
6. M. C. Forde., N. McCavit, "Sonic NDT and radar testing of masonry," NDT&E International 1995; 28(6)
7. M. Shuller et al. "Acoustic Tomography for Evaluation of Unreinforced Masonry. Costruction and Building," Matherials 1997; 11(3), pp. 199-204
8. Alleyne, D.N. and Cawley, P. "The excitation of Lamb waves in pipes using dry coupled piezoelectric transducers", J NDE, Vol 15, pp11-20, 1996.
9. H. Kwun and A. E. Holt , "Feasibility of Underlagging Corrosion Detection in Steel Pipe Using the Magnetostrictive Sensor Technique," NDT&E International 28, pp. 211-214 (1995)

Session 3P7b
Statistical Analysis of Remotely Sensed Data

Detection of Aircraft Embedded in Ground Clutter

S. G. Hwang, S. Sayama, S. Ishii, and **M. Sekine**

National Defense Academy, Japan

It is reported that various radar clutter obey a Weibull distribution under certain conditions. To suppress such Weibull-distributed clutter and detect targets such as aircraft or ships embedded in such clutter.

We propose a Weibull CFAR from Weibull to Rayleigh distribution.

For example, a modified LOG/CFAR(Weibull CFAR),LOG/CFAR with transformation Weibull to Rayleigh distribution, CAFR with control threshold level moment method, and so on.

In this paper, We applied the Weibull CFAR to practical problems observed by an X-band radar at Niigata airport in Japan. The shape parameter c and scale parameter b of the Weibull-distributed clutter were determined by using average clutter amplitudes before a logarithmic amplifier.

Then we transformed Weibull distribution to Rayleigh distribution with the obtained parameters. The threshold level was determined from the computer simulation which has been made to evaluate the detection probability and the false alarm probability.

Thus, we applied the obtained threshold level to the real Weibull- distributed ground clutter and performed a LOG/CFAR processing with transformation from Weibull distribution to Rayleigh distribution.

Finally an improvement value of target-to-clutter ratio 26.4dB was obtained for the detection of an aircraft embedded in ground clutter. This method is superiorto the conventional detection method of 20dB.

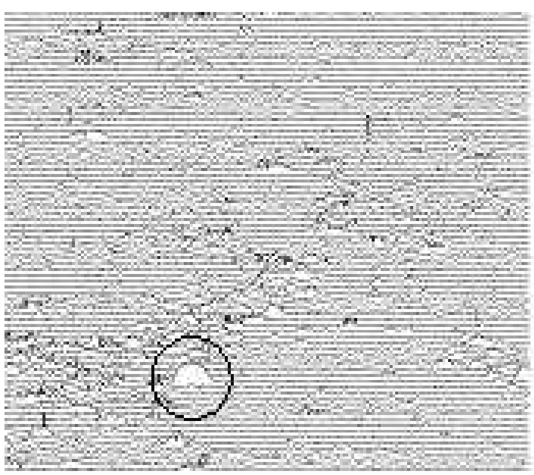

Figure 1: Before processing(A circle is a aircraft)

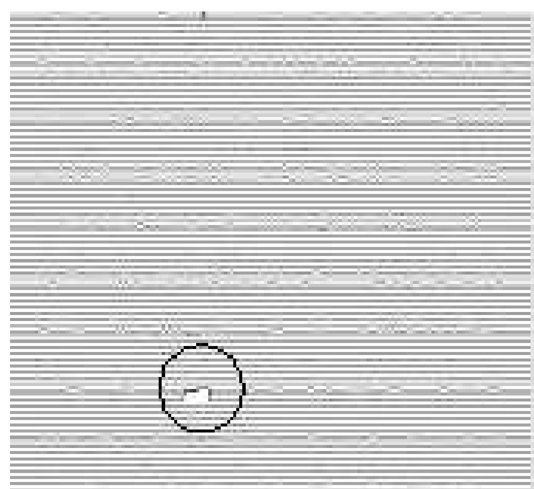

Figure 2: After processsing(A circle is a aircraft)

Amplitude Statistics of Sea Clutter Observed by an X-Band Radar Analyzed by MDL Principle

S. Sayama, S. Ishii, and **M. Sekine**

National Defense Academy, Japan

Introduction In radar signal processing, an important problem is the suppression of the various clutter reflected from the ground, sea, and rain clouds and the detection of targets, such as aircraft or ships embedded in such clutter. It has been long-believed that sea clutter amplitude obey a Rayleigh distribution. From this assumption, a logarithmic constant false alarm rate (LOG/CFAR) technique has been devised which keeps the receiver output level constant against this type of clutter and effectively suppresses the clutter to the receiver noise level [1]. However, recently, because of rapid advances in radar technology, non-Rayleigh sea clutter has been observed with relatively high-resolution radars [2].

Observations of Sea Clutter Sea clutter was observed using an X-band radar with a frequency 9,380MHz, a horizontal beamwidth 0.6°, a vertical beamwidth 20°, a horizontal polarization, an antenna scan rate 18rpm, a pulsewidth $0.25\mu s$, a pulse repetition frequency 1kHz, and a transmitted peak power 53kW. This radar is located on the top of Mt. Yahiko with the height of 630m in Niigata prefecture.

Sea Clutter Amplitude Analyzed by MDL Principle To analyze the sea clutter amplitude, we introduce the Minimum Description Length (MDL) principle [3], which is more rigorous fit of the distribution to the data than the Akaike Information Criterion (AIC) [4] and five probability distribution models, the log-normal, Weibull, log-Weibull, K- [5], and generalized gamma function [6] distributions.

In general, return signals have strong correlation and the same properties within the beam width of an antenna. Thus we divide the observed data into data within the beam width of an antenna. The size of data is 256 range bins corresponding to a range interval of 2.4km and 6 range sweeps corresponding to an azimuth interval of 0.6°. The number of data points is 1,536. The observed data is divided into 42 data within the beam width of an antenna.

Conclusion The numbers of the smallest MDL of the log-normal, log-Weibull, K-, and generalized gamma function distributions are 1, 6, 12, and 23, respectively, from 42 range sweep numbers. It is discovered that the sea clutter amplitudes obey the log-normal, log-Weibull, K-, and generalized gamma function distributions with the shape parameters of 0.515, 1.94 to 2.49, 1.15 to 12.59, and 3.43 to 5.86, respectively. Therefore, it is concluded that suppression of such sea clutter will require new log-normal/CFAR, log-Weibull/CFAR, K/CFAR, and generalized gamma function/CFAR processors.

REFERENCES

1. J. Croney, *Wireless Eng.*, 33, pp. 83-96, (1956)
2. M. Sekine, et al., *Weibull radar clutter*, IEE, (1990)
3. J. Rissanen, *Automatica*, 14, pp.465-471, (1978)
4. H. Akaike, *IEEE Trans. on Autom. Control*, AC-19, pp.716-723, (1974)
5. E.Jakeman et al., *IEEE Trans. on Antennas & Propag.*, AP-24, pp.806-814, (1976)
6. E. W. Stacy, *Annals of Mathematical Statistics*, 33, pp.1187-1192, (1962)

Statistical Analysis of Airborne SAR Images over a Forest Region

S. Fukuda and **S. Nakamura**

Japan Exploration Agency(ISAS/JAXA), Japan

A high resolution airborne SAR system has great potential for information extraction from distributed targets such as forest. Especially the system promises a new era of the statistical texture analysis. While in a moderate resolution radar image the radar cross section (RCS) of forests can be regarded to be constant, RCS fluctuation originating from intrinsic spatial variability of the scene becomes important in the high resolution images.

When considering statistical characteristics of textured SAR images, radar echoes are represented as the product of texture and speckle noise. If a gamma distribution is assumed for the texture component of the product model, the probability density function of the observed intensity images is given by the K-distribution, which is widely recognized as a good description of the high resolution SAR images. The smaller the order parameter of the K-distribution, the stronger the non-Gaussian property of data statistics. The order parameters are estimated based on a sub-optimal logarithmic method.

In this presentation, the results of texture analyses over the coniferous forests concerning the following items, accompanied with field experiments, using the Japanese polarimetric airborne sensor, Pi-SAR, are shown. Since strength of the texture effect generally depends on mixture of different scattering mechanisms, the L-band Pi-SAR images over the forests are appropriate for investigation of the fluctuation behavior.

- Relation between physical characteristics of the forests and the non-Gaussianity of the SAR data
- The forest texture's dependency upon the direction of the incident wave
- Polarimetric variation of the forest texture and its application

Biomass Estimation Algorithm of Coniferous Forests Based on Statistical Texture Analysis Approach of High-Resolution Polarimetric SAR Data and Its Evaluation

H. Wang [1], **K. Ouchi** [1], **M. Watanabe** [2], and **M. Shimada** [2]

[1]Kochi University of Technology, Japan

[2]Japan Aerospace Exploration Agency/Earth Observation Research and Application Center, Japan

RCS(Radar Cross Section) is first analyzed and it saturates easily for our data (40 tons/ha for L-band data). One new biomass estimation algorithm is presented based on the statistical texture analysis of high-resolution polarimetric SAR (synthetic aperture radar) data, which can be used to estimate the biomass beyond RCS saturation level. To develop this approach, amplitude distribution is analyzed, and it is found that K-distribution fits the data best among Rayleigh, log-normal, Weibull and K-distributions by using AIC (Akaike Information Criterion). Then, the regression curve is developped by plotting the relation between biomass and the order parameter of K-distribution. Further, the correlation coefficient of cross-polarization data is higher than those of co-polarization data.

To evaluate this algorithm, the ground-truth data of 23 stands in the test sites were collected in August and September, 2005, and the biomasses were computed using an experiential formula for the Hokkaido forests. Comparison is then made between the ground-truth biomass and the biomasses computed from the proposed algorithm. Among all 23 stands, there are 4 stands of which the biomass is underestimate by more than 20 tons/ha. The source of this underestimation is that there are several tall broadleaf trees to yield large biomass, while these trees, when imaged by SAR, decrease the order parameter to give smaller biomass estimation. The other factors may yield estimation error are:

• Species: the regression curve shows that one species has higher correlation coefficient. However, there are considerable broadleaf trees as undergrowth in each stand, and some stands are mixed conferious.

• Measurement erros: there are two groups carried out the measurement. One experiment was done: two groups measured the biomass in the same stand but different places twice, and it is found that the biomass difference between the two measurements in the same stand were 5.4% and 7.7%.

The result shows the measurement accuracy of 85%. It can be concluded that, at least for the Hokkaido forests on relatively flat ground, this approach can be a good algorithm to estimate forest biomass using polarimetric SAR data.

Statistical Deforestation Models Due to Human Population and Relief Energy in East Asia

S. Tanaka
Shimane University, Japan

R. Nishii
Kyushu University, Japan

Deforestation is a result of complex causality chains in most cases. But identification of limited number of factors shall provide comprehensive general understanding of the vital phenomenon at a broad scale, as well as projection for the future.

Only two factors – human population size (N) and relief energy (R: difference of minimum altitude from the maximum in a sampled area) – are known to give sufficient elucidation of deforestation by our previous studies with nonlinear regression models, whose functional forms were suggested by step functions fitted to one-kilometer square high precision grid-cell data in Japan (n=8697).

In this study, likelihood with spatial dependency was derived, and several deforestation models were selected for the application to East Asia by calculating relative appropriateness to data. For the measure of appropriateness, Akaike's Information Criterion (AIC) was used. The logit-transformed models were also employed so as to avoid anomaly in asymptotic lower and upper bounds with homoscedastic error, and to know whether the two terms of N and R are interrelated with a multiplicative form or not.

To formulate East-Asian dataset, landcover dataset estimated from NOAA observations available at UNEP, Tsukuba for F, gridded population of the world of CIESIN, US for N, and GTOPO30 of USGS for R, were used. The resolutions were matched by taking their common multiple of 20-minutes square.

Estimated coefficients of the models common in all four test fields in East Asia were examined whether they are useful as environment indicators. The values tangibly showed regional differences in terms of man-forest relationship.

Session 3P8
Poster

Designs of 1/8-Wavelength Shorted-Patch Antennas in Multilayered Structures

H. H. Chen, S. H. Lee, C. F. Liu, C. C. Yeh,
R. C. Hsieh, and **Y. H. Chou**

Huafan University, Taiwan, R.O.C.

In this work, two $\lambda/8$ shorted-patch antenna designs in multilayered structures are developed and analyzed for possible applications to the miniature antenna designs in wireless communication technologies. The design concept of the proposed antennas is based on the mechanism of a $\lambda/4$ shorted-patch antenna. Fig. 1 shows the proposed antenna designs, in which the metal patch of a $\lambda/4$ shorted-patch antenna is divided into the upper and lower patches. These patches and the ground plane are then connected by the shorting posts and the connecting posts. Under such an arrangement, the antennas are implemented in a multilayered structure. Meanwhile, the lengths of the upper and lower patches, thus the length of the antennas, can be reduced to be $\lambda/8$ approximately. The proposed antenna designs not only has the merits of miniature antenna size and easy fabrication in multilayered structures, but also can be easily analyzed by an appropriate equivalent transmission line model. To analysis the proposed antenna designs, the characteristics of the shorting posts and the connecting posts will be first investigated. The design considerations and the equivalent circuit models of the posts are then developed. By the obtained results, the $\lambda/8$ shorted-patch antennas in a multilayered structure are designed. The performances of the proposed antennas will be then analyzed by EM numerical simulations. Also, the equivalent transmission line models for such antenna designs will be developed. Finally, the $\lambda/8$ shorted-patch antennas designed at the 2.4GHz are carried out for the experimental verification.

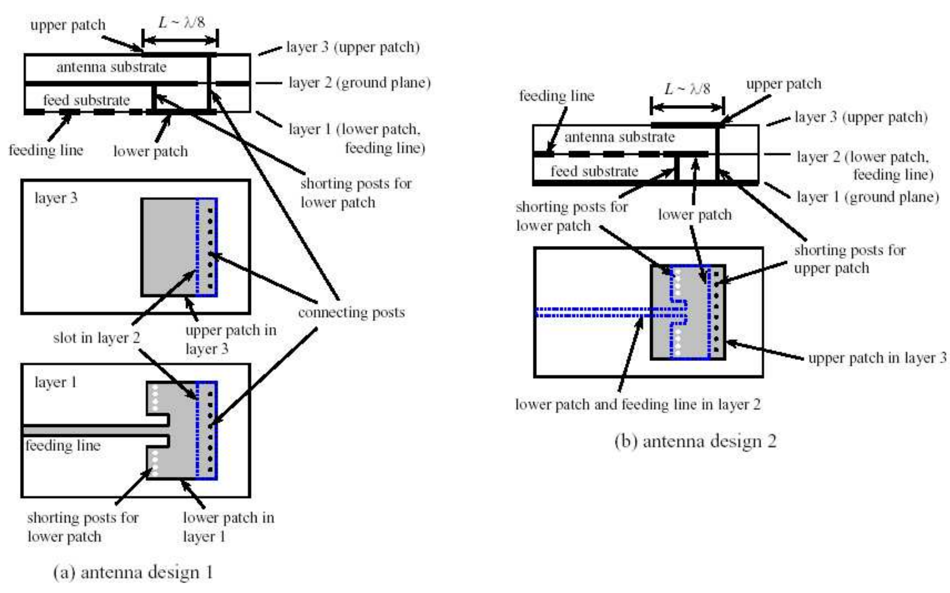

Figure 1: Two $\lambda/8$ shorted-patch antenna designs in multilayered structures.

Bandwidth Enhancement of a Microstrip Antenna with a Loaded Chip-Resistor

C. Y. Huang, P. Y. Chiu, and **C. C. Lin**

National Kaohsiung Normal University, Taiwan

Microstrip antennas are popular planar antennas due to their low cost, low profile, ease of design and manufacturing. Unfortunately, microstrip antennas exhibit low bandwidth and limit these antennas to narrowband applications. In this paper, a chip-resistor loading of a half-wave patch antenna is implemented by introducing a slit to the non-radiating edge of the patch antenna and loaded the open end of the slit with a chip-resistor. Adjusting the slit length and resistance allows the amount of current flowing through the resistor and hence the bandwidth characteristic can be broadened. The resistance can be made to have less effect by mounting it at the centerline of patch where current density is less, improving efficiency while still providing the bandwidth-enhancing effects of resistive loading. Measured impedance bandwidth in this study can be increased to 7.74 while conventional one has merely 1.9. Details of the antenna design are described and typical experimental results are presented and discussed.

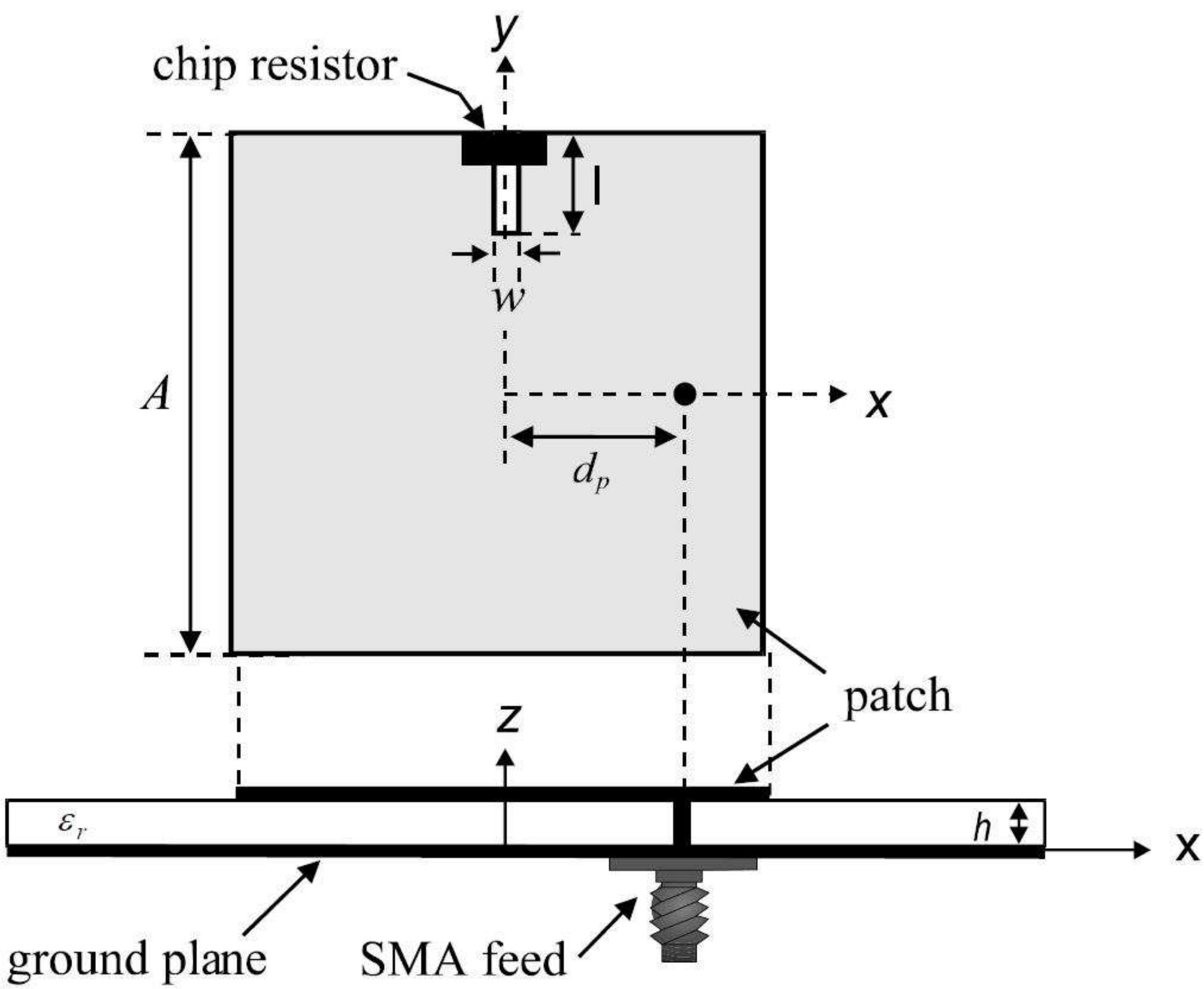

Figure 1: Geometry of a chip-resistor loaded microstrip antenna.

Design and Fabrication of a Novel V-Band Tapered Slot Antenna

N. W. Chen and **C. T. Chuang**
National Central University, Taiwan

Endfire tapered slot antennas (TSAs) have found wide applications from communication systems, automotive radars to imaging arrays for remote sensing due to their planar design, high bandwidth, symmetrical pattern, and low sidelobe level (SLL). It appears the low manufacturing cost, low sensitiveness to manufacturing error at millimeter (mm)-wave frequency, and high compatibility with integrated circuits make the TSAs well-suited for mm-wave applications, especially for mm-wave communication systems. However, the substrate thickness limit of the TSAs renders their design somewhat complicated. Specifically, the electrically very thin substrate ($t_{eff} < 0.03\lambda_0$, where t_{eff} is the effective thickness of the substrate and λ_0 is the free space wavelength at the operating frequency) is required to avoid deterioration of the radiation patterns. Here, a novel V-band (50-75 GHz) TSA that can be fabricated on an electrically thick silicon substrate ($t_{eff} = 0.05\lambda_0$ at the center frequency of the band) without pattern deterioration is proposed and developed. Specifically, the length and width of the proposed TSA are $2.9\lambda_0$ and $1.4\lambda_0$ at the center frequency of the band, respectively. A portion of the substrate is sculptured. Meanwhile, periodically arranged metallic strips are imprinted on the back of the sculptured substrate. The proposed TSA is analyzed using a commercial full-wave electromagnetic solver HFSS. The directivity and gain of the antenna are 12dB and 11dB, respectively. Compared with the design without aforementioned treatment, the E- and H- plane radiation patterns are greatly improved by the sculptured substrate. The SLL in the E and H planes is -19dB and -16dB, respectively. In addition, the front-to-back (F/B) ratio in the E and H planes is further improved by the metallic strips. The F/B ratio in the E and H planes is respectively 19dB and 18dB. The developed antenna is expected to find applications in mm-wave wireless systems. The numerical and experimental results of the proposed TSA will be presented at the conference.

Dual-Broadband Y-Shaped Monopole Antenna with Shorted Strip-Sleeves

H. M. Hsiao, J. H. Lu, and **J. W. Wu**

National Kaohsiung Marine University, Taiwan R.O.C.

Owing to tremendous growth in wireless communication technology, especially for the IEEE 802.11 a/b/g WLAN standards in the 2.4 GHz (2400.2484 MHz), 5.2 GHz (5150.5350 MHz) and 5.8 GHz (5725.5825 MHz) bands, dual-band operations of the printed monopole antennas (MA) are required. For the proposed antenna designs, the printed inverted-F or shorted MA apply a shorting pin for ground connection, which makes the antenna complexity increased to promote the fabrication cost. For the double-T or modified inverted-L MA, more antenna parameters are required to make the design procedures complicated for dual-band operation. In addition to the designs using the printed MA, the parasitic strip-sleeve had been introduced to generate a resonant mode for operating in the 2.4 and 5.2 GHz bands. However, this monopole antenna needs a relatively larger space occupied than that required for the printed monopole antenna design. In this article, we propose a novel dual-broadband design of the printed MA with dual shorted strip-sleeves. Simply by shorting the conducting strips with the ground plane and imaged from the MA, the upper resonant mode can be easily excited to obtain dual-broadband operation for a printed monopole antenna.

As shown in Fig. 1, dual I-shaped strip-sleeves are shorted with the ground plane of the proposed dual-broadband Y-shaped monopole antenna, respectively. Fig. 2 shows satisfactory agreement for the proposed dual-broadband monopole antenna operating at the 2.4 and 5 GHz bands. The proposed monopole antenna provides much greater bandwidths for two operating bands to meet the 802.11a/b/g specifications. Peak antenna gains for both two operating bands are measured to be, respectively, 4.8 and 3.5 dBi and the gain variations for both two bands are within 1.0 dBi. Probably due to the shorted strip-sleeves introduced, the antenna peak gain across the lower operating band for the proposed antenna design has 1 dB larger than that of the convetional monopole antenna.

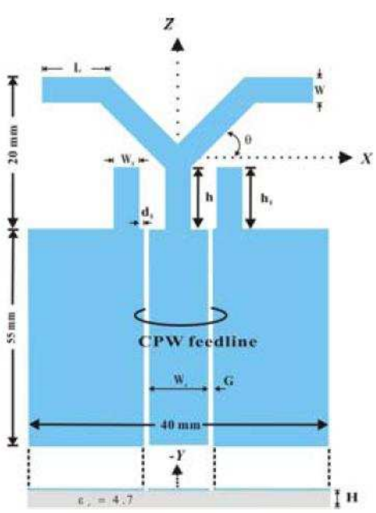

Fig. 1

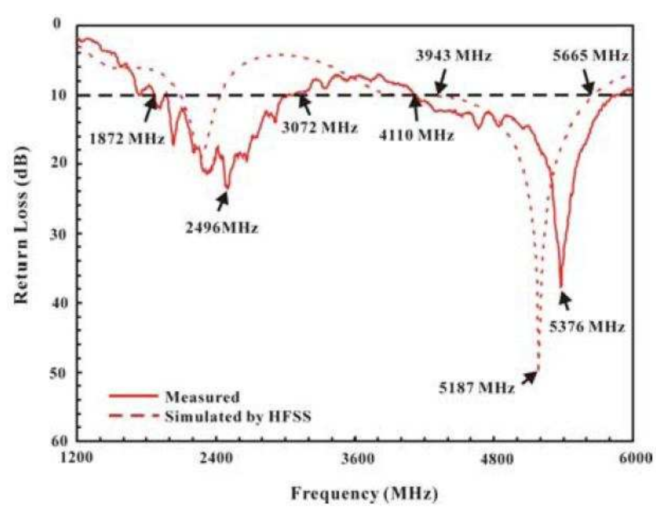

Fig. 2

Investigation of CPW-Fed Triangular-Ring Slot Antennas and Triangular-Ring Slot Coupled Patch Antennas

J. S. Chen and **W. F. Chang**

Cheng Shiu University, Taiwan R.O.C.

Designs of coplanar waveguide (CPW)-fed equilateral triangular-ring slot antennas with tuning-stub and triangular-ring slot coupled patch antennas are proposed and experimentally investigated. The impedance matching of the resonant frequency can be obtained only by adjusting the tuning-stub length for the proposed triangular-ring slot antenna with tuning-stub. For the design of ring-slot coupled patch antenna, slightly changing the patch size causes the tunable frequency-ratio f_2/f_1 between the first two operating frequencies to fall in the range of about 1.1-1.42. Details of the proposed designs are investigated by experimental as well as theoretical studies.

CPW-Fed Notched Annular-Ring Slot Antenna for Suppression of Harmonic Mode

Y. F. Lin and **H. M. Chen**

National Kaohsiung University of Applied Sciences, Taiwan R.O.C.

The dual-frequency properties of an annular-ring slot antenna (without notch) fed by coplanar waveguide (CPW) is presented and experimentally studied. The excited dual modes of the annular-ring slot antenna are fundamental mode TE_{11} and the second mode TE_{21}. The frequency ratio of the two modes (TE_{11}/ TE_{21}) is about 2.0. The radiation patterns of the two frequencies are alike to the dipole antenna. The H-plane patterns are entire omnidirectional. The impedance matching and the radiation characteristics of the annular-ring slot antenna were studied using the software HFSS. The simulated and measured results are in good agreement. The characteristics of different ground plane size and slot widths are also discussed in this paper. The structure of the CPW-fed notched annular-ring slot antenna with a tuning stub is shown in Fig. 1, and is printed on an FR4 substrate of thickness h = 1.6 mm and relative permittivity ϵ_r= 4.2. This slot antenna has a simple structure with one layer of dielectric and metal. The 50-Ω CPW feeding structure is composed of a center strip width W = 6.0 mm and gap width G = 0.5 mm. In addition, a tuning stub of length of S and width W terminates the CPW feed. In order to achieve a better impedance matching, the tuning stub should be lengthened and that causes the inner ring section of the annular-ring slot to be etched outwards with a length of S_d and width of W + 2G. A pair of notched slot is etched at the rim of the inner ring patch, which slot has a length of L_d and width of W_s. By carefully adjusting the notched slot, the simple printed slot antenna can operate in the lower band compared with the regular annular-ring slot antenna and the higher mode TE_{21} is suppressed for the current path changed.

A novel simplified miniature CPW-fed notched annular-ring slot antenna has been proposed and tested at 2.4 GHz. The prototype has been designed and fabricated and found to have the bandwidth of 18%, and the radiation pattern measured at resonance is very close to omnidirectional in the H-plane. Good impedance matching for the operating frequency can easily be obtained. HFSS simulation software was used and measurements were conducted to verify the simulation results. The proposed antenna has a simple and effective feeding structure has adequate operational bandwidth, and has radiation patterns such that it is suitable for use in WLAN applications.

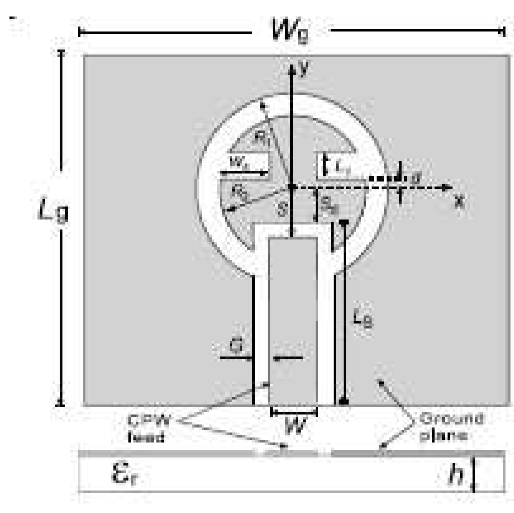

Figure 1: Geometry of CPW-fed notched annular-ring slot antenna.

Compact Folded Monopole Antennas

C. Y. Huang, P. Y. Chiu, and **C. C. Lin**
National Kaohsiung Normal University, Taiwan

An investigation of broadband folded monopole antennas with shorting pins is proposed. The proposed antennas are compact in size, and can provide sufficient bandwidths for DCS (1710-1880 MHz), PCS (1850-1990 MHz), 3G (1920-2170 MHz), and WLAN (2400-2484 MHz) bands. The method to realize the compact in size is introducing a folded monopole antenna. Folded monopole is difficult to be accomplished with planer substrate. Here, we introduce the shorting pin and find its optimal position to approaching as folded antenna. Details of the antenna design and experimental results are presented and discussed.

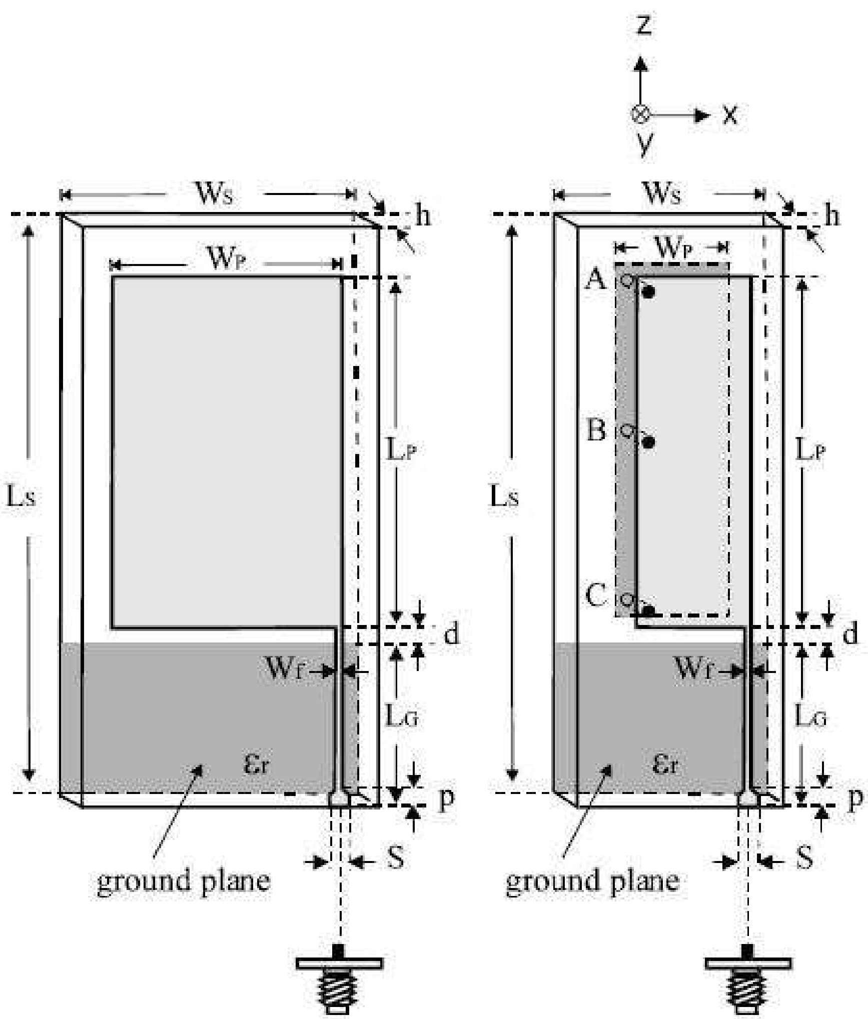

Figure 1: Geometry of the simple monopole antenna and the proposed folded monopole antenna with shorting pins.

A Miniaturized Phased Array Aperture Antenna Based On Bulk Ferroelectric Material

L. Peng[1], **J. T. Huangfu**[1], **L. X. Ran**[1], **Y. K. Zou,**[2] and **J. A. Kong**[1,3]

[1]The Electromagnetics Academy at Zhejiang University, China
[2]Boston Applied Technologies Inc., U.S.A.
[3]Massachusetts Institute of Technology, U.S.A.

A novel miniaturized phased array aperture antenna using a voltage-controllable ferroelectric material with high dielectric constant is proposed. This antenna system combines the phase shifters and the radiating elements in a single structure, which could significantly simplify the complexity and the cost of the conventional phased array antenna systems. Simulation results on such structure are given, which agrees well with the theoretical analysis.

Figure 1 shows the configuration of an aperture antenna system consisting of a bulk BST block with a rectangular cross section, a grounded plane and multiple electric poles connected to computer-controlled DC driver. The incident surface of the BST could be connected with a matched aperture, such as a horn or a rectangular waveguide. The electric poles could be applied by different DC voltages, such that the parts of the BST block sandwiched between different poles and the grounded plane will have different permittivities, yielding different phase shifts at the outgoing surface of the BST block for a plane wave incidence.

Figure 2 shows the simulated horizontal radiation pattern (dotted line) as well as that directly calculated by antenna theory (solid line). In subfigure (a), (b) and (c), the radiation pattern for equals to 0, -15 and -30 degree are shown, respectively. We see that all the simulation results, both the direction of the main lobe and the beam widths of the main lobe and the side lobes, agree fairly well with the theoretical ones.

A novel miniature phased array aperture antenna system utilizing an electrically controlled bulk ferroelectric BST ceramic is proposed. Such scheme combines the phase shifters and the radiating elements in a single structure, which could significantly simplify the complexity and decrease the cost of the conventional PAA systems.

Acknowledgement

This work is supported by the Key Project of National Science Foundation of China (NSFC) under Contract No. 60531020.

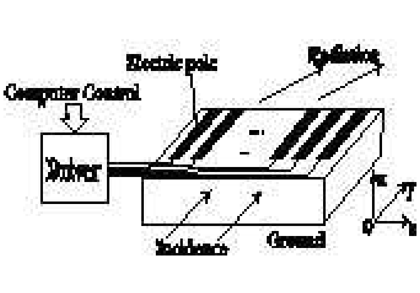

Figure 1: Configuration of the BST based aperture antenna system

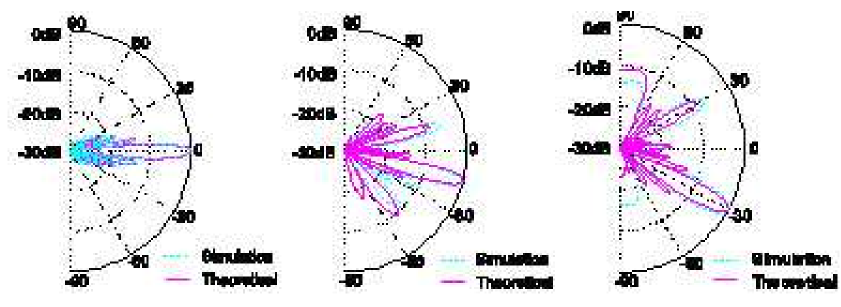

Figure 2: Radiation pattern in H-plane for $a = 0.4\lambda_0$ and $d = 0.45\lambda_0$ (a) 0 degree radiation; (b) -15degree radiation; (c) -30 degree radiation.

The Effective Permittivity of Metal Rod Arrays In Thz Band

S. Xi[1,2], **L. F. Shen**[1], **J. T. Huangfu**[1,2], **L. X. Ran**[1,2], and **J. A. Kong**[1,3]

[1]Electromagnetics Academy at Zhejiang University, China
[2]Zhejiang University, China
[3]Massachusetts Institute of Technology, USA

Until recently, the expected negative permittivity is usually obtained from a periodic array of metallic rods. J. B. Pendry has shown the effective permittivity of this structure in the GHz frequency band. In this work, considering the aluminum rods, we calculate the fields distribution in such a structure for a TE wave incidence in the THz band, and give the effective permittivity utilizing the plane wave expansion method.

In the THz band, metals can no longer be treated as perfect conductors, for the frequency is much closer to the plasmon frequency of metals than in the GHz band. The permittivity of metal is of the form

$$\epsilon(\omega) = 1 - \frac{\omega^2}{\omega(\omega + i\Gamma)}$$

Making use of this equation, the fields distribution can be obtained throw the plane wave expansion method. Figure 1 shows the electric fields distribution of each unit. The effective permittivity can be derived from the ration of electric displacement flux and electric flux of each unit. The effective permittivity is shown in figure 2.

Compared with the result with Pendry's equation, the effective plasma frequency is shifted to a larger one.

Acknowledgement

This work is supported by the Key Project of National Science Foundation of China (NSFC) under Contract No. 60531020.

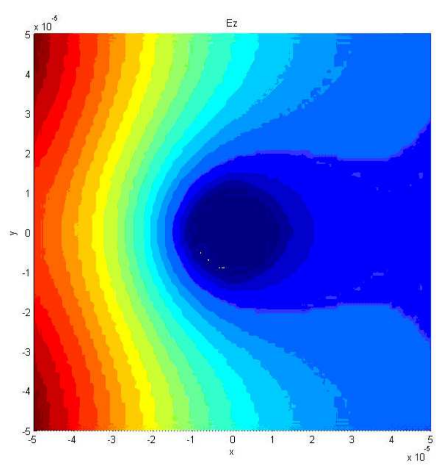

Figure 1: The electric fields distribution

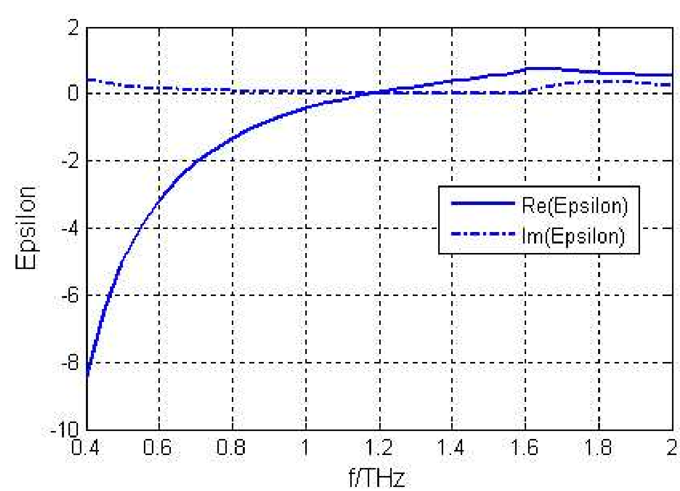

Figure 2: The effective permittivity

Multi-Frequency Resonator Based on Dual Bands S Shaped Left-Handed Material

D. X. Wang[1,2], **J. T. Huangfu**[1,2], **L. X. Ran**[1,2], **B. I. Wu**[3], **T. M. Grzegorczyk**[1,3]
H. S. Chen[1,2], and **J. A. Kong**[1,3]

[1]Electromagnetics Academy at Zhejiang University, China
[2]Zhejiang University, China
[3]Massachusetts Institute of Technology, U.S.A.

In this paper, we experimentally realize a 1D RHM (Right-handed Material)-LHM (Left-handed Material) multi-frequency resonator based on LHM with dual negative bands. The resonator consists of dual negative bands LHM and air, which are arranged in an X-band waveguide. Multi-resonant frequencies for the resonator are observed within two left-handed bands of the LHM. For the case that the resonator has two resonant frequencies, the two resonance happen in the two negative bands respectively as shown in Fig. 1. The prism experiment and estimated μ_{1y} from the experimental data show that the multi-resonant frequencies are caused by the left-handed properties of the LHM sample. The incorporation of LHM into the resonator design allows more flexibility to realize multi-resonance. The dual bands S shaped LHM offers a simple way to design the expected negative bands for the desired resonance frequencies. It is easier to change the size of the rings of the dual band S shaped LHM to realize the expected double negative bands than to find a specific dispersive RHM. Once the expected negative bands are achieved, one can simply realize the resonance within the bands. Compared to normal RHM, the dual band S shaped LHM demonstrates the feasibility to realize the expected multi-resonant frequencies within the 1D RHM-LHM resonator.

Acknowledgement
We acknowledge the support by the Chinese National Science Foundation under Contract No. 60531020.

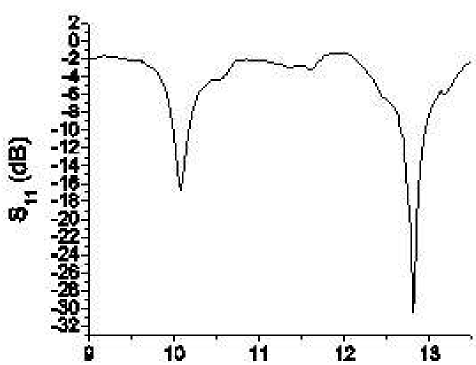

Figure 1: The measured S11 curve of the RHM-LHM resonator from 9GHz to 13.5GHz. The total length of the resonator is 11mm. We can find two resonant frequencies, 10.1GHz and 12.84GHz.

Experimental Realization of A Wide-Band Backward Coupling Waveguide Coupler Using Left-Handed Material

J. J. Zhang[1,2], **J. T. Huangfu**[1,2], **H. S. Chen**[1,2], **L. X. Ran**[1,2], and **J. A. Kong**[1,3]

[1]Electromagnetics Academy at Zhejiang University, China
[2]Zhejiang University, China
[3]Massachusetts Institute of Technology, USA

Recently, Left-handed metamaterial is more and more used in EM appliances such as antenna and filter. In this paper, we use two kinds of LHM to realize a wide-band backward couping waveguide coupler in X-band. Slab-like LH samples are inserted in the waveguide to form backward wave, and then lead to backward coupling.

Firstly, a LHM sample composed of periodically arranged dual-band extended S-shaped resonators is filled in the primary waveguide and the EM wave is backward edge-coupled into the secondary waveguide filled with a right-handed material. At the interface between the LH and the RH material, the wave vectors of the EM waves transmitted in the primary and the secondary branches have the same directions due to phase matching conditions, while the Poynting vectors are contra-directional, which leads to a backward coupling. The experimental results of the compared output power are shown in Fig.1, which indicates a backward coupling. In order to get a wider coupling band, we change the RHM stuffed in the secondary waveguide for another kind of LHM, which is composed of periodical Ω-shaped resonators. Since the pass-band of one LHM is the other's forbidden-band, the Ω-shaped material acts as a LHM while the dual-band S-shape one acts as a RHM, and vice versa.As a result, by combining the bands of the two kind of LHM, we finally get a wide band of 8-14GHz (Fig.2).

Acknowledgement

We acknowledge the support by the Chinese National Science Foundation under Contract No. 60531020.

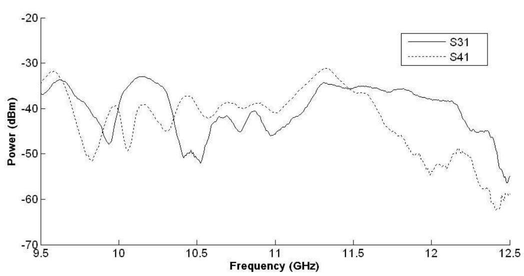

Figure 1: Experimental results of a dual-band coupler

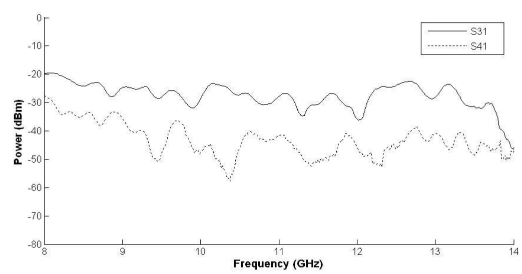

Figure 2: wide-band coupling using Ω shaped LHM and dual-band S-shaped LHM samples.

A Miniaturized Microstrip Dual-Mode Filter for Spurious Suppression

C. J. Wang, S. Y. Chen, and **Z. C. Ker**

Feng-Chia University, Taiwan

A miniaturized microstrip dual-mode open-loop filter with defected ground structures is presented in this paper. The proposed filter has the characteristics of wide stopband, reduced size, and high selectivity. The combination of dual-mode loops and defected ground structures successfully eliminates the nearest two spurious harmonics. The simulated and experimental results show that the transmission coefficients are -30 and -25 dB at 2^{nd}- and 3^{rd}-harmonic frequencies.

Key Words :microstrip band-pass filter; spurious suppression; dual-mode; defected ground structure (DGS)

Near-Field Scanning Dielectric Probe Millimeter-Wave Microscopy

E. Kume and **S. Sakai**

National Institute of Advanced Industrial Science and Technology, Japan

Recently developed is the near-field scanning optical microscopy which is expected to be employed in various areas such as Nanoelectronics, Biochemical applications and so on. Little attention, however, has been given to near-field scanning probe microscopies in the millimeter-wave and submillimeter-wave regions. The millimeter-wave field has the potential of penetrating into the bulk of samples such as plastics, paper and so on, so that near-field scanning millimeter-wave microscopy is expected to contribute to nondestructive testing applications.

The characteristics of a dielectric probe for scanning near-field millimeter-wave microscopy are presented, and both transmission and reflection type microscopy systems using this dielectric probe are shown. The dielectric probe was fabricated from Teflon and shaped like a cone. The beam profile of the millimeter-wave radiated from the tip of the Teflon probe was measured by three-dimensional scanning using a different Teflon probe. The 93.5 GHz millimeter-wave was focused on the tip of probe at the wavelength level, and the millimeter-wave power was found to decrease exponentially with distance from the tip.

A transmission near-field scanning millimeter-wave microscopy system which consisted of two Teflon probe and scanning system was demonstrated. The sample was a glass microscope slide to which metals were deposited, having a cross-slit pattern of which the width was 3 mm near the wavelength. The millimeter-wave radiated from the tip of the Teflon probe was transmitted through the cross-slit of the sample, and detected using a different Teflon probe. The slit width primarily agreed with the actual slit width of the sample, though the millimeter-wave was diffused around the edge of the slit.

A reflection near-field scanning millimeter-wave microscopy system using a Teflon probe was also constructed. The resolution of this microscope was evaluated measuring the aluminum board which was ditched at even intervals. The ditches to 1.4mm pitch could be observed clearly. A contactless IC card was measured for demonstrating the nondestructive testing. Internal structures such as the leaf-shaped antenna coil and IC chips were able to be observed by penetrating a plastic outside cover.

Electromagnetic Scattering of Three-Dimensional Objects Solved by Parallel Generalized Method of Moments with Multilevel Fast Multipole Algorithm

J. H. Lin, K. J. Wu, and **I. H. Huang**
National Taiwan Ocean University, Taiwan R.O.C

In this paper, based on the generalized method of moments (GMoM), we develop a parallel program (PGMoM) for solving scattering problems of conducting, dielectric objects or objects characterized by the impedance boundary condition (IBC). In addition, this parallel program contains three formulations for conducting objects: electric field integral equation (EFIE), magnetic field integral equation (MFIE), and combined field integral equation (CFIE). We observe that CFIE for closed conducting objects exhibits much better convergent performance than EFIE. PGMoM is implemented both on PC cluster in our laboratory and on those at National Center for High-performance Computing (NCHC). The efficiency of parallel GMoM is examined for various cases.

Large scattering objects are our problem targets. The iterative method such as conjugate gradient method (CGM) is applied to solve the large-sized problems. To speed up the matrix-vector multiplications in CGM at each iteration, MLFMA (Multi-Level Fast Multipole Algorithm) is implemented to this end and is also parallelized to take advantage of parallel computing architecture.

Scattering objects		4λ conducting sphere (EFIE)	4λ conducting sphere (CFIE)	4.5λ conducting sphere (EFIE)	4.5λ conducting sphere (CFIE)
Unknowns(N)		15093	15093	19026	19026
Memory (MB)	rank0	171	167	258	253
	rank1	153)	153	250	249
	rank2	154	151	253	251
	rank3	169	169	248	245
Memory (single) (MB)		536	536	732	732

Table. 1: Comparison of memory consumption between GMoM and PGMoM for EFIE and CFIE.

Machines	1	2	3	4
Memory(MB)	536	280	201	169
One-iteration Communication time(sec)	0	1	1.63	2.45
One-iteration time(sec)	149	76	54	41
Real one-iteration computing time(sec)	149	75	52.37	38.55

Table. 3: The maximum memory consumption, one-iteration time, one-iteration communication and total one-iteration computing time versus machines for a 4λ conducting sphere of 15093 unknowns.

Scattering objects	4λ conducting sphere (EFIE)	4λ conducting sphere (CFIE)
Unknowns(N)	15093	15093
GMoM	14893 (sec)	1639 (sec)
PGMoM	3944 (sec)	464 (sec)

Table. 2: CPU time comparison between GMoM and PGMoM for EFIE and CFIE.

Machines	2	4	8
$S_{relative}$	1	1.766	2.976
$E_{relative}$	1	0.883	0.744

Table. 4: The relative efficiency and relative speedup versus machines at NCHC for a 4λ conducting sphere of 15093 unknowns.

Inverse Scattering by Local Shape Function with Total Variation Method

J. H. Lin and **B. H. Pong**

National Taiwan Ocean University, Taiwan R.O.C.

In recent years, the total variation method applied in inverse scattering [P.M. van den Berg and R.E. Kleinman, *Inverse Problems,* vol. 11, 5-10, 1995] or data de-blurring gains much attention in that it is capable of reconstructing piecewise constant profile objects. This method leads to images of better resolution and clearly exhibits the object sharp boundary, for which previous works utilizing the Tikhonov regularization fail to reconstruct satisfactorily and always give rise to oscillating structures.

In this work, we apply the local shape function with total variation method in a two-dimensional TM and TE electromagnetic problems in microwave regime. A cost function is defined as the difference between the measured data and the simulated one under current γ function standing for scattering amplitude of each small cell. A total variation penalty term is included to emphasize the piecewise-constant profile characteristics. The cost function is minimized to a specified tolerance by iteratively updating γ. Each iteration calculates the gradient to find the conjugate direction, and the step size along the direction via the Hessian of the cost function. The most computationally intensive part for the iterative algorithm lies in calculating the gradient and Hessian, which involves forward scattering problems for all transmitters and receivers. The forward solver such as CG-FFT once invoked to efficiently solve many forward scattering problems.

Local shape function method is used to model scattering problems due to dielectric objects or metallic ones. No a priori information about the unknown object is required. We shall investigate several aspects of this algorithm applied for TM and TE cases including the image quality; reconstructions from real measurement data; parallel efficiency analysis; frequency hopping scheme in the larger object reconstruction.

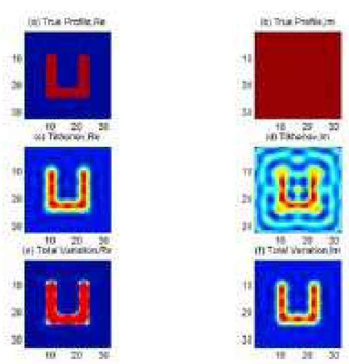

Figure 1: U-shaped object images by Tikhonov and total variation method

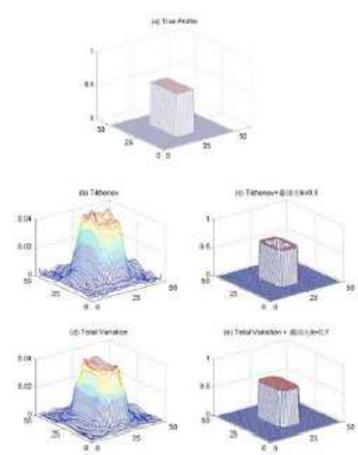

Figure 2: Reconstructed images of a conducting object by Tikhonov and total variation method

Dual Patch Butterfly Shape Stacked Structure Wide Band CP Microstrip Antenna

H. C. Lien and **H. C. Tsai**

Wu Feng Institute of Technology, Taiwan, R.O.C

This paper investigates the design measurement and characteristics of a dual patch Butterfly Shape Configuration Antenna (BSCA), which is formed by equilateral triangle slot dual patch with a mixed vertically stacked dielectric substrate structure. Make use of a special impedance transformer that is less than quarter-wave length to improve the impedance bandwidth of the antenna. Tune by a differences dielectric and spacing each other to achieve the desired of a larger impedance/axial ratio bandwidth. The experimental results verify that the antenna has an impedance bandwidth (VSWR< 2) more than 30% and a 3-dB Axial Ratio (AR) bandwidth of 28%. Simulation and measurements results on CP gain and polar patterns are presented and compared.

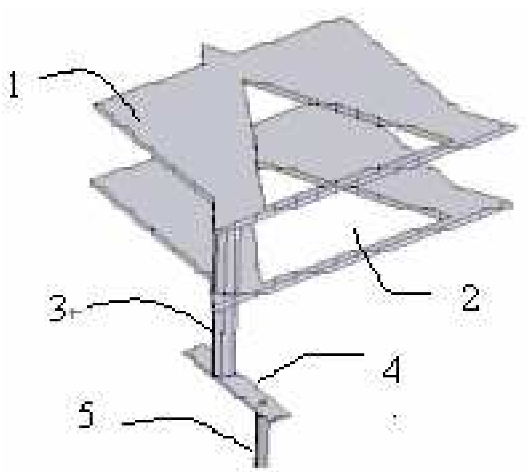

1	Butterfly Shape radiating element
2	Equilateral triangle slot
3	Cylindrical conductor
4	Rectangular feed line
5	SMA connector

Figure1. Geometry of the proposed antenna

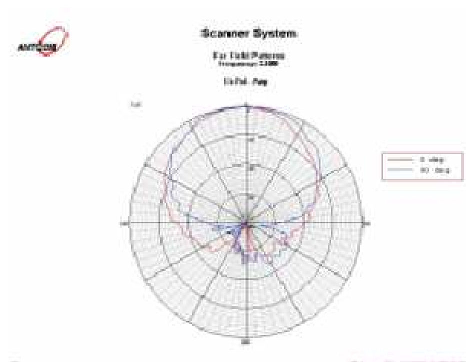

Figure.2 depicts the LHCP far field patterns of the antenna.

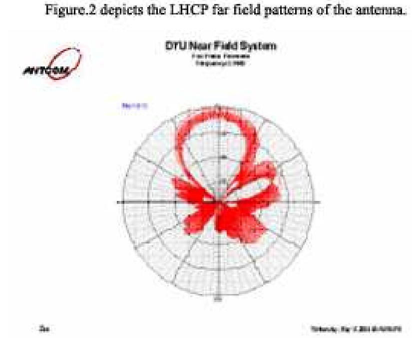

Figure.3 The AR results from experiment.

Using Nonlinear Universal Blocks with Floket Channels for Accurate Electromagnetic Modeling of Nonlinear Microwave Semiconductor and Ferrite Devices

G. S. Makeeva[1], **O. A. Golovanov**[2], and **M. P. Horvath**[3]
[1]Penza State University, Russia
[2]Penza Military Institute of Artillery, Russia
[3]The George Washington University, U.S.A.

Commercially available FEM and FTDT software packages use to design nonlinear microwave devices (NMD) are adequate of the technology level of the present day, but do not include the deep physical processes upon which NMD of the near future will be based.

The goal is to develop a new approach using universal autonomous blocks with Floket's channels filled by nonlinear media (NUBF) for rigorous mathematical modeling of NMD, containing gyromagnetic or semiconductor medium insertions with a "strong" nonlinearity, on the design of prospective NMD. The NUBF descriptors are determining in the form of system of nonlinear differential equations, connecting magnitudes of incident and reflected modes on cross-sections of multimode Floket's channels. The methods of a recomposition of NUBF were developed using a linearization of the descriptors of NUBF.

The NUBF method is different from known numerical methods by solving nonlinear Maxwell's equations complemented by the equations of motion in nonlinear media with the non-asymptotic radiation boundary conditions [1] on NUBF bounds and input sections of NMD (without a simplification of nonlinear Maxwell's equations and boundary conditions).

Using the NUBF method the mathematical models of NMD, containing bounded ferrite or semiconductor medium with a "strong" nonlinearity, were created. The nonlinearity functions (the dependences of the drift velocity on the electric field intensity or the magnetization on the magnetic field intensity in a ferromagnet) are described approximately by using the uniform approximation by the high order polynomials.

The methodology of determining of NUBF descriptors is based on solving 3D-nonlinear diffraction boundary problem at electrodynamical accuracy level. In the goal to determine the NUBF descriptors the non-stationary nonlinear Maxwell's equations complemented by the equation of motion of charge-carriers in semiconductors or the equation of motion of the magnetization vector in a ferromagnet were reduced to the systems of the stationary nonlinear Maxwell's equations for each of combination frequencies. Using the cross-section method the 3D-nonlinear diffraction problems are reduced to boundary problems for the system of nonlinear ordinary differential equations solved together with the system of nonlinear algebraic equations.

The effective computational algorithms for the numerical realization of NUBF descriptors were created using the iterative computational process or the Nuwton's iterations in combination with projecting models (the alternative computational process for an authenticity of results of mathematical modeling).

The developed numerical NUBF method permits to create convergent algorithms for solving of nonlinear stationary Maxwell's equations, to alleviate numerical problems, connected with the instability of computing processes (the nonlinear media is divided on NUBF in the goal to exclude cumulative round-off errors), to make a quick transition from one geometry of problem to other ones.

Using the NUBF method a methodology of accurate electromagnetic modeling of the semiconductor and ferrite NMD was developed and the results of mathematical simulation of frequency multipliers were obtained.

Acknowledgement
The work of G. S. Makeeva and O. A. Golovanov was supported by THE RUSSIAN FOUNDATION FOR BASIC RESEARCH, Grant N 05-08-33503-a.

REFERENCES

1. O.A. Golovanov. Radiotekhnika i elektronika, 35 (1990), 1853.

Design of the Miniaturized Noise Suppression Filters Using Multilayer Inductors

Y. H. Chou, J. L. Lai, C. C. Yeh
H. H. Chen and **R. C. Hsieh**

Huafan University, Taiwan, R.O.C.

Recently, the embedded functions of handsets for mobile communications are increased significantly for satisfying the personal convenience and entertainment requirements. In order to isolate the interference between RF signal and these functional digital devices, the compact noise suppression filters are needed to attenuate the RF power around frequency bands of GSM/DCS/PCS to prove the normal operations of these devices, and also prevent the RF signal feedback to antenna to keep the sensitivity of the original receiving path better (Fig.1(a)). In this work, a miniaturized noise suppression filter with higher cut off frequency, higher rejection rate, and lower capacitance will be implemented for the applications mentioned above. The multilayer coil configuration will be adopted in the design which possesses the benefits of the compact size, simple feature, and easy to fabricated. Fig. 1(b) shows the structure of multilayer coil inductor which is bounded in the region of two grounded planes with the ports located at the top region of the substrate. According to this structure, the effects of inherent parasitic capacitors as shown in the figure will be investigated firstly. It can be shown that these components construct two zeros effectively in the transmission path of signal at the frequency bands of mobile used. By choosing the suitable ceramic material and proper layer stacking, the transmission zeros can be controlled precisely to locate at the frequencies of 900MHz and 1800MHz respectively which were achieved by designing the specific values of parasitic components and the extra tuning capacitors. The performance of the overall design will be evaluated by the 3D EM simulation. Finally, the finished filter will then be manufactured by the process of low temperature cofired ceramic (LTCC) with the size of $2.0mm \times 1.2mm$ for four channels applications.

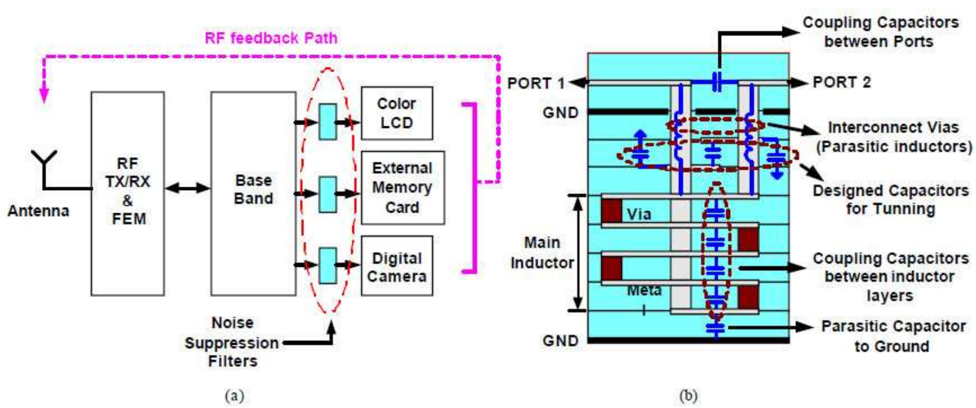

Figure 1: (a) Mobile system with noise suppression filters (b) Multilayer structure for inductor with parasitic and extra designed components specified.

Algorithmic System for Identifying Bird Radio-Echo and Plotting Radar Ornithological Charts

L. Dinevich and **Y. Leshem**

Tel-Aviv University, Israel

The proposed algorithmic system for identifying bird radio-echo against the background of reflectors of other types was developed within a novel approach based on the analysis of echo movement characteristics. A long-term implementation of the previously designed algorithm (Dinevich et al. 2004) has demonstrated its ability for identifying bird echo with high confidence. At the same time, this work enabled to determine the directions of further research, aimed at: a) significant reduction of computation time; b) increasing echo identification accuracy in cases of weak echo and of large dense bird masses; c) plotting radar ornithological charts on-line.

In the course of the present study, a comparative analysis was carried out of radio-echo typical of different categories of reflectors. As a result, a set of characteristics was obtained that distinctly specify bird echo and distinguish it from echoes of other types of reflectors. The algorithmic system based on this set of characteristics enables to determine whether a radio-echo movement belongs to one of the four patterns: a) straightforward at non-uniform velocity; b) straightforward at uniform velocity; c) significant deviation from a straight line, nonuniform velocity and d) chaotic undirected shifts. The data on echo movement pattern were used for plotting bird (bird group) flight vectors. In order to filter off false vectors, a special algorithmic procedure was devised based on a number of additional echo characteristics, including the threshold value, the extent of chaotic status in the direction of closely located vectors, the maximum and minimum velocities etc. Another proposed algorithmic procedure enables to make a prompt and accurate (at least 80% confidence) decision on the bird-not birdEorigin a particular echo on the basis of its fluctuation pattern. The system enables on-line plotting of operational ornithological charts every 12-15 min, including charts that combine meteorological and bird monitoring data, and thus is as an efficient means of maintaining air traffic safety in complicated meteorological and ornithological conditions. In view of the fact that MRL-5 radars are located in many countries and cover an extremely vast territory, it appears expedient to connect them into a network. Using the algorithmic system for bird echo identification by means of MRL-5 radar, such a network could perform intercontinental bird monitoring in the real-time mode, contributing to providing collective air traffic safety.

Key words: radar ornithology, bird echo identification, radio-echo, birds, bird migration, air traffic safety, meteorological radar.

Resonant Scattering by Layered Dielectric Structure with Weakly Kerr-Like Nonlinearity

V. V. Yatsyk
Nat. Acad. of Sci. of Ukraine, Ukraine

The transverse inhomogeneous, isotropic, nonmagnetic, linearly polarized, weakly nonlinear (a Kerr-like dielectric nonlinearity) dielectric layer is considered. The algorithms for the solution of nonlinear diffraction problems (with use of approaches developed in [1-3]) and the results of a numerical analysis of the diffraction problem of a plane wave on the weakly nonlinear object with positive and negative value of the susceptibility are shown. The effects: non-uniform shift of resonant frequency of the diffraction characteristics of a weakly nonlinear dielectric layer, i.e. its reduction when positive value of the susceptibility and increase at negative value of the susceptibility; itself the channeling of a field; increase of the angle of the transparency of the nonlinear layer when growth of intensity of the field (at positive value of the susceptibility); de-channeling of a field (at negative value of the susceptibility) are found out. These effects are connected to resonant properties of a nonlinear dielectric layer and caused by increase at positive value of the susceptibility or reduction at negative value of the susceptibility of a variation of dielectric permeability of a layer (its nonlinear components) when increase of intensity of a field of excitation of researched nonlinear object, see [4].

The principal fields where the results of our numerical analysis are applicable are as follows: the investigation of wave self-influence processes; the analysis of amplitude-phase dispersion of eigen oscillation-wave fields in the nonlinear objects, see [5]; extending the description of evolutionary processes near to critical points of the amplitude-phase dispersion of nonlinear structure; new tools for energy selecting, transmitting, and remembering devices; etc.

REFERENCES

1. Akhmediev N. N., Ankiewicz A., "Solitons," Moscow, Fizmatlit, 2003.
2. Schurmann H. W., Serov V. S., Shestopalov Yu. V., "TE-polarized waves guided by a lossless nonlinear three-layer structure", *Physical Review E,* vol. 58, no. 1, 1998, pp. 1040-1050.
3. Shestopalov V. P., Sirenko Yu. K., "Dynamic Theory of Gratings," Kiev, Naukova Dumka, 1989.
4. Yatsyk V. V., "The Numerical Simulations and Resonant Scattering of Intensive Electromagnetic Fields of Waves by Dielectric Layer with Kerr-Like Nonlinearity", *E-print: Computational Physics, http://arxiv.org/pdf/physics/0412109,* no. 12, 2004, pp. 1-11.
5. Yatsyk V. V., "Diffraction Problem and Amplitudes-Phases Dispersion of Eigen Fields of a Nonlinear Dielectric Layer", *E-print: Computational Physics, Optics, http://arxiv.org/pdf/physics/0503089,* no. 3, 2005, pp. 1-13.

Analysis of Current Density Distribution Induced by ELF Magnetic Fields Utilizing Fast-Multipole Surface-Charge-Simulation Method for Voxel Data

S. Hamada and **T. Kobayashi**

Kyoto University, Japan

This paper describes an application of the FMM(fast multipole method[1])-SCM(surface charge simulation method) for voxel data[2] to analyses of current density distribution in a voxel model induced by ELF magnetic fields. The FMM-SCM for voxel data treats a square surface of a voxel that has different inside and outside conductivities as a surface element of the SCM that caluculates three-dimensional Laplacian field. The main features of the method are as follows. (I) The diagonal form FMM provides $O(D^2)$ performance in the memory-capacity and operation-cost, when the number of voxels is about D^3. (II) The MoM (method of moment) strictly imposes the continuity of the flux passing through each boundary element, therefore the solution globally satisfies the Gauss' law. These features make it high-speed, high-capacity, and high-stability calculation method.

This method is applied to analyses of induced current in a numerical human model called 'Taro'. Taro, a Japanese adult male model, was developed by NICT (National Institute of Information and Communications Technology), Kitasato Univ., Keio Univ., and Tokyo Metropolitan University[3]. He consists of 7,977,906 voxels except the air region around him, and the cubic voxel size is 2mm. Applied 50Hz magnetic fields are three kinds of homogeneous 1μT field, B_x (case i-x), B_y (case i-y), and B_z (case i-z), and three kinds of magnetic dipole (0.5π μWb m) field generated by M_x (case ii-x), M_y (case ii-y), and M_z (case ii-z). Figs. 1 and 2 show the calculated current density distributions of the cases i-y and ii-y, respectively. The calculation times on 32bit PC (Pentium IV, 3GHz, 2Gbyte-RAM, Windows 2000) listed in Table 1 demonstrate good performance of the FMM-SCM for voxel data.

Fig. 1. Calculated **J in the case i-y.**

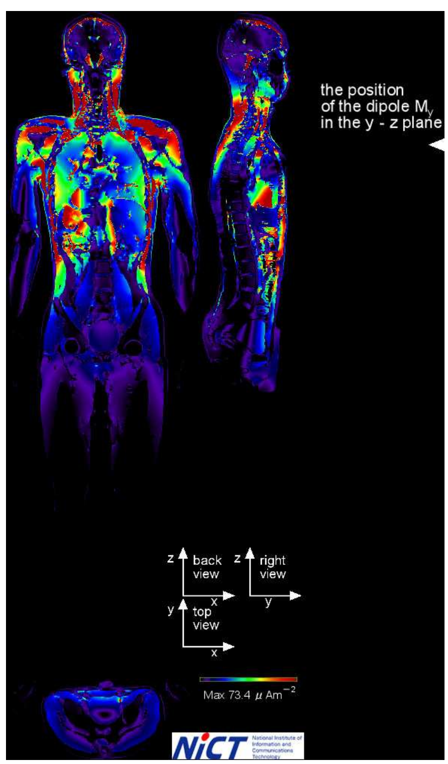

Fig. 2. Calculated **J in the case ii-y.**

Table 1. Calculation time.

case i-x	6h 23min.
case i-y	5h 53min.
case i-z	6h 06min.
case ii-x	6h 16min.
case ii-y	6h 42min.
case ii-z	6h 33min.

References

(1) L. Greengard, V. Rokhlin, Acta Numerica, **6**, 229-269 (1997)

(2) S. Hamada, T. Kobayashi, Proc. 2005 annual conf. FM, IEE Japan, II-4, 148-153 (2005)

(3) T. Nagaoka, et al., Phys. Med. Biol. **49**, 1–15 (2004)

An Analysis of the Transfer Matrix Method on Band Structure of One Dimension Graded-Index Photonic

I. C. Tsai and **J. J. Wu**
Chung Hua University, Taiwan R.O.C
T. J. Yang
National Chiao-TUng University, Taiwan R.O.C

Abstract - The characteristics of guide wave scattered by graded-index photonic crystal are systematically investigated with the use of an equivalent network method. By carefully modulate the width of uniform layer, the higher order band gaps can be eliminated.

Stucture

A one dimension photonic crystal, a two-dimensional space (x z) with one dimension guiding (x), is considered by this letter. The unit cell is depicted in Fig. 1(a). The structure of unit cell which include two layers: one is the uniform layer with the width W_1 and the other is graded index layer with the width W_2 .

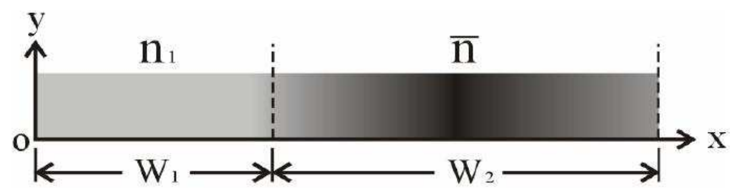

Fig.(1) a unit cell: a homogeneous layer in left side and a graded-index layer in right side

$$n_1 = 1.38,\ W_1 = 89nm,\ \overline{n} = 2.00,\ W_2 = 121nm$$

Numerical Analysis

Assume W_1 is 89nm. By using transfer matrix method, we illustrate the electromagnetic dispersion and reflection index diagrams. From Fig. 1(a)(b), the interest is that there is no bandgap in $2\omega_o$.

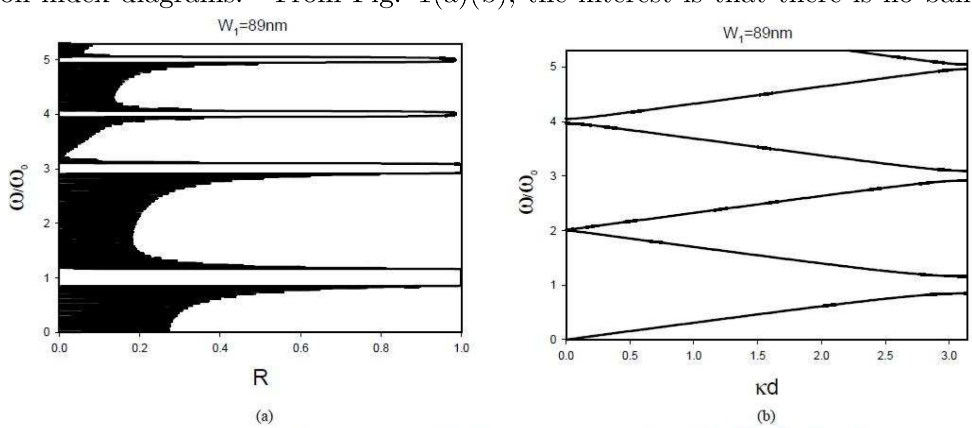

Figure 2 (a) reflection index diagram (b) electromagnetic dispersion diagram: Second band gap is erased

First band Gap=0.3080, Second bandgap=0.0080, Third bandgap=0.1760, Forth bandgap=0.0840, Fifth bandgap=0.0840 , their reflection index are R1=1.0000, R2=0.0988, R3=0.1.0000, R4=0.9846, R5=0.9846. The fundamental frequency , ω_o , is 2583.7 (THz).

This phenomenon can be understood by harmonic suppression. We can calculate the input impedance to give the physical explains. If W_1 is 40nm, the third bandgap will be erased. If W_1 is 13nm, the forth bandgap will be erased. If W_1 is 22nm, the fifth bandgap will be erased. Therefore this type of periodic structures may provide another degree of freedom to design optical-frequency selector.
Notices: The refraction index of 1.38 is M_gF_2 . The refraction index of 2.35 is ZnS

Cavity Antenna with Partly Transparent Apertures for Wireless Communications

N. I. Voytovich and **A. V. Ershov**
Southern Ural State University, Russia
N. N. Repin
Open Corporation, Russia
A. N. Sokolov
Chelyabinsk State University, Russia

Cavity antennas with partly transparent aperture are known since the first part of the 20th century. Research of the ones started 42 years ago. Development of high-speed wireless communication systems stimulates the interest in the plane antennas with partly transparent aperture. Several linearly- and circularly-polarized plane antennas are presented in the paper.

Cavity antenna with the partly transparent aperture physical, mathematical, numerical and computational models are presented. Antenna is an open rectangular metal resonant cavity 2 the height $\boldsymbol{H}$ of which is close to half wavelength λ and laterals dimensions a_2 and b_2 are several λ. The resonator upper wide wall of thickness $\boldsymbol{D}$ has a system K_0 rectangular radiating openings 5 with dimensions $l_p \times t_p$ (p=1,..., K_0) and separates the antenna from half space 3 by which an environment external to the antenna is simulated. Cavity antenna is excited by a screened stripline through coupling opening 4 with dimensions $l_0 \times t_0$ in the low wall of thickness d. Region 1 bounded by the stripline screens is considered as a transmission resonator with dimensions $a_1 \times b_1 \times h$, the height of which $\boldsymbol{h}$ is considerably less than λ. Metal pins are arranged around the coupling opening 4 and close the stripline screens. (Metal pins are absent in the picture). An electromagnetic wave source is arranged at the strip bottom. The antenna physical model supposes that the antenna has five areas 1-5 bounded by perfectly conducting resonator walls and opening apertures. General electrodynamics problem is formed for the above regions coupled electromagnetically through opening apertures within the scope of the antenna physical model. The method of equivalent currents is used for the problem definition.

The system of integral equations is received relative to unknown distributions of electric currents on the strip, the pins and the magnetic currents on apertures of the coupling opening and radiating ones. For electric and magnetic field computation Green tensor function method is used. Galerkin method is used for solving the integral equation system. As a result antenna numerical model is received.

Antenna pattern and amplitude-phase distribution of magnetic field on cavity antenna radiating openings are computed for the antenna excited by one, two or four coupling openings. In the paper the relationship of antenna directivity frequency characteristic and dimensions $l_p \times t_p$ (p=1,..., K_0) and radiating openings array as well as a number of radiating openings K_0 in the cavity antenna aperture are discussed. The measured and computed radiation patterns, directivity, return loss, half-power beamwidths and efficiencies of the antenna prototypes will be presented.

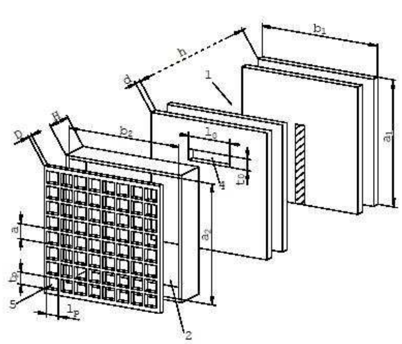

Improvement of Surface Resistance Property of $ErBa_2Cu_3O_7$- Films with $BaTiO_3$

Y. Shingai [1,8], **M. Mukaida** [1,8], **R. Teranishi** [1,8], **K. Yamada** [1], and **N. Mori** [1], **A. Ichinose** [5,8]
R. Kita [3,8], **S. Horii** [7,8], **Y. Yoshida** [6,8], **K. Matsumoto** [4,8], **T. Abe** [2,8], **A. Saito** [2,8]

[1]Kyushu University, Japan
[2]Yamagata University, Japan
[3]Shizuoka University, Japan
[4]Kyoto University, Japan
[5]CRIEPI, Japan
[6]Nagoya University, Japan
[7]University of Tokyo, Japan
[8]CREST-JST, Japan

We have improved surface resistance (RS) properties of $ErBa_2Cu_3O_{7-\delta}$(ErBCO) films by using $BaTiO_3$(BTO) doping (BTO+ErBCO). The as-grown BTO+ErBCO films did not have enough carriers. We solve this problem by using O3+O2 as background gas during the growth of BTO+ErBCO films. Then, O3+O2 gas is useful to grow BTO+ErBCO films with superior superconducting properties. The RS of a 2wt%BTO+ErBCO film is the lowest in BTO+ErBCO films grown in this study. This value is equal to that of a 1.5wt%BZO+ErBCO film. The microstructures of the 2wt%BTO+ErBCO film are observed by transmission electron microscopy (TEM). In the image, the BTO+ErBCO films did not have nanorods as the observed in BZO+ErBCO films against our expectation. However, the precipitates what BZO+ErBCO films do not have, are observed.

Session 4A1
Numerical Techniques I

Sine Transform Based Preconditioner for the FDFD Method Inside a Parallel Plate Waveguide

A. Chabory, B. P. de Hon, and **A. G. Tijhuis**
Eindhoven University of Technology, The Netherlands

The FDFD method (Finite Difference Frequency Domain) is a versatile and accurate tool to solve Maxwell's equations in the presence of inhomogeneous regions. This method leads to large, sparse linear systems for which iterative methods based on Krylov subspaces constitute suitable solvers. However, this approach is inherently limited by slow convergence, leading to long computation times. In this paper, a method is presented to overcome this limitation for a two-dimensional waveguide configuration. We propose a preconditioner that involves the discrete sine transform and is based on a physical approximation.

We consider a parallel-plate waveguide section filled by dielectric scatterers and excited by TE incident modes. The problem is reduced to the Helmholtz equation and is discretized with finite differences. The extent of the computational domain is limited to the waveguide section where the scatterers are located. At the transverse boundaries that limit the waveguide section, the modal representation of the solution is used to obtain an exact formulation for the absorbing boundary conditions. These absorbing boundary conditions combined with the discretizion of the Helmholtz equation yield a linear system involving a sparse block matrix.

The preconditioner is defined such that it approximates the linear system by decoupling the mutual influences of all the modal components propagating inside the waveguide. This preconditioner can be associated with a matrix, the blocks of which are diagonalizable by means of the discrete sine transform. That corresponds to an approximation of the initial two-dimensional problem by several one dimensional problems, each one associated with an effective dielectric permittivity that is invariant along the transverse coordinate.

Simulations show that this preconditioner produces a significant decrease in the number of iterations required by Krylov-subspaces methods. This preconditioner outperforms the ILU preconditioner (incomplete LU factorization). Typically, for a computational domain of size $2\lambda \times 2\lambda$ discretized on 64×64 points, the decrease in the number of iterations is about a factor of 20 with no preconditioning and about a factor of 5 with ILU. Moreover, this preconditioner yields almost the same number of iterations regardless of the grid size. By contrast, if no preconditioner or an ILU preconditioner are used, then the number of iterations increases significantly when the grid size is decreased.

Total-Field/Scattered-Field Boundary Condition for CIP Method

Y. Ando and **M. Hayakawa**
The University of Electro-Communication, Japan

Total-field/Scattered-field (TF/SF) boundary condition is used in the finite-difference time-domain (FDTD) method to simulate incident plane waves in scattering and diffraction problems. The condition can be imposed to add or subtract a presumed incident wave at the neighbouring nodes of the boundary in order to satisfy the Maxwellfs equations for the total or scattered fields.

Recently, the constrained interpolation profile (CIP) method has been developed as a numerical solver for problems including different phases, and the extension to electromagnetic problems has been performed. The method is based on the upwind scheme with the profiles between two grid points, interpolated in terms of cubic polynomials which allow us to calculate fields at the next time step with good precision. Although CIP method provides us many advantages for electromagnetic field computation, particular techniques are not developed, for example, TF/SF boundary. In this study, we present the implementation of TF/SF boundary to CIP scheme.

The advection equation $\partial f/\partial t + c\partial f/\partial x$ with the constant velocity c, can be solved by CIP scheme with the spatial and temporal discretization by $i\Delta x$ and $n\Delta t$, respectively, as follows.

$$f_i^{n+1} = (1+2\zeta^3-3\zeta^2)f_i^n + (3\zeta^2-2\zeta^3)f_{i-s}^n + s\Delta x(2\zeta^2-\zeta^3-\zeta)g_i^n + s\Delta x(\zeta^2-\zeta^3)g_{i-s}^n, \tag{1}$$

$$(\frac{\partial f}{\partial x})_i^{n+1} = (1+3\zeta^2-4\zeta)g_i^n + (3\zeta^2-2\zeta)g_{i-s} + s\frac{6}{\Delta x}(\zeta-\zeta^2)(f_i^n - f_{i-s}^n) \tag{2}$$

where s takes +1 or -1 corresponding to the sign of the velocity c, and $\zeta = c_0\Delta t/\Delta x$

We consider that the incident field p (p_i^n in the discretized representation) illuminates the analysis region. Suppose that in the TF region the variables f and g take the total field which is equal to the scattered field plus the incident field, and they take the scattered field in the SF region. The above updating formulas are valid if the both of i and $i-s$ belong to the same region, TF or SF, and are not valid at the interface. Consider that the TF region is extended in the right-hand side of the position i as shown in Fig.1. In the case of $c>0$, the above equation must be modified because the TF profile to get f_i^{n+1} cannot be correctly interpolated between i and $i-1$ because the value f_{i-1}^n is not the total field. In order to get the correct profile, the values at $i-1$ need to be replaced with the total field by adding the incident field p_{i-1}^n. Therefore, the modified formulas are given by

$$f_i^{n+1} = (1+2\zeta^3-3\zeta^2)f_i^n + (3\zeta^2-2\zeta^3)(f_{i-1}^n + p_{i-1}^n) + \Delta x(2\zeta^2-\zeta^3-\zeta)g_i^n + \Delta x(\zeta^2-\zeta^3)(g_{i-1}^n + q_{i-1}^n), \tag{3}$$

$$g_i^{n+1} = (1+3\zeta^2-4\zeta)g_i^n + (3\zeta^2-2\zeta)(g_{i-1}^n + q_{i-1}^n) + \frac{6}{\Delta x}(\zeta-\zeta^2)(f_n^i - f_{i-1}^n - p_{i-1}^n), \tag{4}$$

where q_i^n indicates the discrezed representation of $\partial p/\partial t$. Similarly, the incident field at i must be subtracted to obtain the scattered field at $i-1$ if $c<0$:

$$f_{i-1}^{n+1} = (1+2\zeta^3-3\zeta^2)f_{i-1}^n + (3\zeta^2-2\zeta^3)(f_i^n + p_i^n) + \Delta x(2\zeta^2-\zeta^3-\zeta)g_{i-1}^n + \Delta x(\zeta^2-\zeta^3)(g_i^n - q_i^n), \tag{5}$$

$$g_{i-1}^{n+1} = (1+3\zeta^2-4\zeta)g_{i-1}^n + (3\zeta^2-2\zeta)(g_i^n + q_i^n) + \frac{6}{\Delta x}(\zeta-\zeta^2)(f_n^{i-1} - f_i^n - p_i^n). \tag{6}$$

For the case of multi-dimensional electromagnetic field analyses, we need to invoke the directional splitting technique to derive advection equations from Maxwellfs equations. In the x-advection phase, the incident fields are added or subtracted at the interface between TF and SF regions as described in one-dimensional case. In the following y-advection phase, the incident field cannot be added or subtracted formally in the same manner as above because the fields are shifted to ±x-direction, which causes errors due to the difference. Therefore, the incident fields added or subtracted need to be modified into the ones after the x-advection.

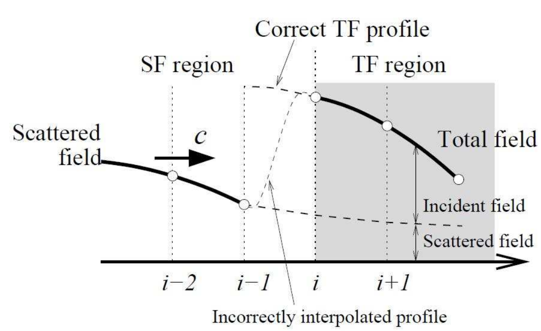

Figure 1: Interpolated profile at the TF/SF interface. The circles stand for the values at the position.

REFERENCES

1. T. Yabe, F. Xiao, and T. Utsumi, gThe constrained interpolation profile method for multiphase analysis,h J. Comp. Phys., vol.169, no.2, pp.556-593, 2001.

A Study of Topology Optimization for Built-in Antenna Loaded with Magnetic Material

A. Matsuzaki [1], **H. Morishita** [1], **T. Nomura** [2], **K. Sato** [2]
K. Taguchi [3] and **T. Kashiwa** [3]

[1]National Defense Academy, Japan
[2]Toyota Central R&D Labs., Aichi, Japan
[3]Kitami Institute of Technology, Japan

With the recent rapid progress in handsets, the design of their antennas is acquiring great importance. In particular, built-in antennas are required. A downsizing technique of antennas for handset by utilizing a magnetic material has been studied [1]. It was found that magnetic materials have an effect on lowering resonance frequency of a planar inverted-F antenna (PIFA) instead of changing the radiation characteristics at both 900MHz and 2GHz bands. However, the optimum configuration and arrangement of magnetic materials have not yet been studied. Recently, the topology optimization method is applied for a structure design problem of dielectric materials, which has already been reported [2]. This method is considered as an efficient approach to obtain optimum configuration and arrangement of magnetic materials.

In this study, we apply uniquely the topology optimization method to optimize the configuration and arrangement of the magnetic materials, which is inserted in the PIFA, by using adjoint variable method (AVM) [3] and the FDTD method. In the application of topology optimization to this problem, the magnetic material is divided into the design cell, and material properties of each cells are perturbed in each iteration step and updated to reach for the optimal design. The density method is used to determine magnetic permeability values in each cell.

First, in order to confirm the validity of using AVM approach, the sensitivities of design parameters are estimated using AVM approach and central differences for a sweep of magnetic permeability. Secondly, topology optimization method is applied to lower the reflection coefficient in the frequency band of the incident wave. As a result, it is found that the topology optimization approach is successfully applied to design the structure of magnetic materials.

REFERENCES

1. Y. Kawano, S. Hayashida, H. Morishita, K. Koyanagi, gA study on miniaturization of 900MHz and 2GHz band antenna by utilizing magnetic material,h 2005 IEEE AP-S International Symp., vol. 3B, pp. 347-350, July 2005.
2. G. Kiziltas, J. L. Volakis, N. Kikuchi, gTopology design optimization of dielectric substrates for bandwidth improvement of a patch antenna,h *IEEE Trans.*, vol. 51, No. 10, pp. 2732-2743, Oct. 2003.
3. N. K. Nikolva, J. W. Bandler, M. H. Bakr, gSensitivity analysis with the FDTD method on structured grids,h *IEEE Trans.*, vol. 52, No. 4, pp. 1207-1216, April 2004.

A Low Cost Hybrid FDTD Algorithm to Compute Optical Propagation in Dispersive Media

J. B. Cole, S. Banerjee, and **T. Plewe**
University of Tsukuba, Japan

The recursive convolution (RC) algorithm is widely used to solve Maxwell's equations in dispersive media and in metamaterials, but it is complicated, and computationally costly. Unless a model of the dispersion is used, the electric field at all time steps must be stored memory.

We introduce a low-cost model-independent hybrid version of the Yee algorithm for monochromatic radiation which requires the value of the permittivity at only a single frequency.

Taking the magnetic permeability, μ, to be constant, but allowing the electical permittivity, ε to be a complex function of frequency (which incorporates the conductivity), Maxwell's equations become

$$\begin{aligned} \mu\partial_t \mathbf{H}(\mathbf{x},t) &= -\nabla\times\mathbf{E}(\mathbf{x},t) && (1)\\ \partial_t\int_0^t \varepsilon(\mathbf{x},t')\mathbf{E}(\mathbf{x},t-t')dt' &= \nabla\times\mathbf{H}(\mathbf{x},t). && (2)\end{aligned}$$

where $\mathbf{H}$, the magnetic intensity, $\mathbf{E}$ the electric field, and $\mathbf{x} = (x, y, z)$.

Replacing the derivatives of eqn. (1) with finite-difference (FD) approximations, the update of $\mathbf{H}$ in the Yee algorithm is given by

$$\mathbf{H}(\mathbf{x}, t+\Delta t/2) = \mathbf{H}(\mathbf{x}, t-\Delta t/2) - \frac{1}{\mu}\frac{\Delta t}{h}\mathcal{D}\times\mathbf{E}(\mathbf{x},t), \tag{3}$$

where $\nabla \cong \mathcal{D}/h$, $\mathcal{D}$ is a FD operator, and h is the grid spacing. Thus The update of $\mathbf{E}$ is complicated by the integration in (2). In the RC algorithm the integral is numerically evaluated by assuming the time variation of $\mathbf{E}$ to be small compared to that of ε. The $\mathbf{E}$ update beomes a function of not only $\mathbf{H}$ but also of a new quantity $\mathbf{\Psi}$, called the the accumulation field, which is a function of $\mathbf{E}$ at all time steps up to the current one. By using a physical model of the dispersive effects, such as the Drude model, it is possible to construct a recursion relation connecting $\mathbf{\Psi(t+\Delta t)}$ with $\mathbf{\Psi(t)}$.

In this way memory and computation requirements can be reduced, but they are still substantial, especially in three dimensions because $\mathbf{\Psi}$ is a three-dimensional vector field. Furthermore, the parameters of the dispersion model must be known.

Using the fact that the displacement field is given by $\mathbf{D} = \varepsilon\mathbf{E}$ in the frequency domain, Haftel [1] has derived a Yee-like hybrid algorithm for monochromatic radiation in which $\mathbf{E}$ can updated without using an accumulation field. Knowing ε at only one frequency, the propagation of electromagnetic radiation in a dispersive medium can be computed. Since only the $\mathbf{E}$ and $\mathbf{H}$ fields are computed, the computational cost is no higher than that of the Yee algorithm. In addition we can improve the accuracy on a coarse grid by using [2] nonstandard finite difference methods.

We have calculated propagation a dispersive material, and compared our results with the RC algorithm and with experimental data.

REFERENCES

1. M. I. Haftel, pp. 171-185 in "Advances in the Applications of Nonstandard Finite Difference Schemes," R. E. Mickens, ed., World Scientific (Singapore, 2005).
2. J.B. Cole, *High Accuracy Yee Algorithm Based on Nonstandard Finite Differences: New Developments and Verifications*, IEEE Trans. Antennas and Propagation, vol. 50, no. 9, pp. 1185-1191 (Sept., 2002).

Numerical Characteristics of Integro-Difference Time-Domain (IDTD) Method

S. T. Chun, M. Kragalott, and **R. S. Schechter**
Naval Research Laboratory, U.S.A.

An integro-difference time-domain (IDTD) algorithm, which is based on the integral form of Maxwell's equations, has recently been developed for the higher-order time domain analysis of electromagnetic waves [1]. It achieves fourth-order accuracy in space and time by taking into account the spatial and temporal variations of electromagnetic fields within each computational cell. We analyze dispersion and stability properties of the IDTD method and compare them with those of the Yee and other higher order FDTD methods. While IDTD is a fourth-order algorithm, the Courant-Friedrichs-Lewy (CFL) stability criterion is shown to be the same as that of the Yee's second order conventional FDTD method. It is also shown that the IDTD method possesses superior dispersion properties relative to other fourth order FDTD methods.

REFERENCES

1. S.T. Chun, and J.Y. Choe, "A Higher Order FDTD Method in Integral Formulation," IEEE Trans. Antennas & Propagation, 53(7), pp. 2237-2246, July 2005.

This work was supported by the Office of Naval Research, Washington, DC.

Fast MoM Calculation With/Without Magnetic Boundary Condition

K. Takei and **M. Ikegaya**
Hitachi Cable Ltd., Japan

To improve portability of wireless apparatus, recently their shapes have been required thinner and thinner. A built-in antenna is suitable for the apparatus. The design of such antenna requires EM calculation of the scattering object, which consists of a circuit board and the antenna. For antenna design, only small parts of this scattering object, i.e. the antenna, can be changeable. Method of moment (MoM) is quit attractive for this EM calculation, because this method requires less unknown than other method, ex. FEM, FDTD. In this article we propose novel calculation techniques, which can reduce unknowns comparing to conventional MoM calculation. Supposing that S is the full region, where conductors can exist, designing antenna with circuit board is equal to defining the small area Sa, where conductors were absent. Our techniques introduce new unknowns on Sa instead of induced currents on $\neg S \cap Sa$. The matrix equation of MoM consumes computation time proportioning to the triple power of the number of unknowns. In the case of a practical design of built-in antenna, Sa occupies very small area in S, therefore the proposed technique successfully reduced time consumption by one several tenths. One of these techniques use voltages v on Sa as unknowns by using only electric boundary condition. The matrix equation is directly derived from the conventional one of MoM [1,2].

$$\begin{bmatrix} J^{se} \\ J^{\neg Sa\cap\neg Se\cap S} \\ 0 \end{bmatrix} = [Y] \begin{bmatrix} V^{Se} \\ 0 \\ V^{Sa} \end{bmatrix}, -[Y^{Sa}_{Sa}][\nu^{Sa}] = [Y^{Se}_{Sa}][V^{Se}]. \tag{1}$$

Where Y and Se are admittance matrix and the area, on which exciting sources exist respectively.

The other technique introduces magnetic current K on Sa by using field equivalence theorem. Assuming an ideal 0-volume cavity attaching to Sa, both electric and magnetic boundary condition derived the other matrix equation. Expanding the volume of cavity to finite, this equation can be applied for the objects including dielectric.

$$[T_{Sa}]\left([Y]\begin{bmatrix} V^{Se} \\ 0 \\ 0 \end{bmatrix} - [Y][Q]\begin{bmatrix} 0 \\ 0 \\ K^{Sa} \end{bmatrix}\right) + [W_{Sa}]\begin{bmatrix} 0 \\ 0 \\ K^{Sa} \end{bmatrix} = -[T_{Sa}][Y][Q]\begin{bmatrix} 0 \\ 0 \\ -K^{Sa} \end{bmatrix} + [W_{Sa}]\begin{bmatrix} 0 \\ 0 \\ -K^{Sa} \end{bmatrix},$$

$$-2\left([W^{Sa}_{Sa}] - [T^{Se}_{Sa}\, T^{\neg Sa\cap\neg Se\cap S}_{Sa}][[Y^{\neg Sa\cap S}_{\neg Sa\cap S}]\begin{bmatrix} Q^{Sa}_{Se} \\ J^{Sa}_{S\neg Sa\cap\neg Se\cap S} \end{bmatrix}\right)[K^{Sa}] = [T^{Se}_{Sa}\, T^{\neg Sa\cap\neg Se\cap S}\begin{bmatrix} Y^{Se}_{Se} \\ Y^{Se}_{S\neg Sa\cap\neg Se\cap S} \end{bmatrix}[V^{Se}] \tag{2}$$

Where Q,T, and W are defined as [Q][K]=[E], [T][J]=[H], and [W][K]=[H] respectively.

The matrix equation of first technique, which is available for the scattering objects consisting of only conductors, has possibility to deliver spurious solutions due to lack of magnetic boundary condition. Nevertheless, these undesirable solutions can be remove experiment with manufactured samples. Actual example of antenna designs of PCfs WAN antenna, PDA's GPS antenna, and HPfs DVB-H antenna, which includes numerical EM calculation, making sample and testing sample, shows the simpler matrix equation without magnetic boundary condition successfully reduces total tern around time of the practical design of built-in antenna for mobile apparatus.

REFERENCES

1. K. Takei and T. Ogawa, gIncrement-Decrement Algorithm for Compact Circular Polarized Antennah, ICEcom, Dubrovnic, 2005. [2] K. Takei, Proc. PIERS, Singapore, 2003, p. 154.

Multiple Region Finite-Difference Time-Domain Simulation Accelerated by Plane-Wave Time-Domain Techniques

J. H. Lin [1], **G. J. Mon** [2], **S. G. Lin** [3], and **M. Y. Lu**
[1]National Taiwan Ocean University, Taiwan
[2]Acrosser Technology Co., Taiwan
[3]Quanta Computer Inc., Taiwan

Using FDTD method to solve electromagnetic wave problems requires gridding the whole space, even including the free space where field quantities are of no particular interest. This results in a waste of computer memory and execution time. In previous works, a multiple region FDTD (MR-FDTD) method is proposed to only grid the interested regions and calculate $\overline{\mathbf{E}}$ and $\overline{\mathbf{H}}$ in these regions by FDTD. As for the interaction among regions, Kirchhoff integral formula or equivalent current approaches are applied. Although this MR-FDTD method can avoid gridding the free space and updating EM fields in the free space, these approaches involve surface integrals for each node on surfaces of sub-regions. This process incurs additional computations and also requires additional storage at previous times.

Recently a time domain counterpart of the fast multipole method (FMM) in the frequency domain, the plane wave time domain (PWTD) method can alleviate the computational cost. We tailor PWTD to suit the setting of Kirchhoff integral formula by rephrasing the formula as follows

$$\overline{E}(\overline{r},t)=\frac{1}{8\pi^2c^2}\int\int d^2\Omega[\delta(t-\frac{\hat{k}\cdot(\overline{r}-\overline{r}^c_m)}{c})]*\{-[\partial_t^2\delta(t-\frac{\hat{k}\cdot\overline{R}_c}{c})]$$
$$*[\oint ds^{'}(\hat{n}\cdot\hat{k})\delta(t-\frac{\hat{k}\cdot(\overline{r}-\overline{r}^c_m)}{c})*\overline{E}(\overline{r},t)]+[c\partial_t\delta(t+\frac{\hat{k}\cdot\overline{R}_c}{c})]*(\hat{n}\cdot\Delta^{'})\overline{E}(\overline{r},t)]\}$$

The gist of this new formula lies in the three convolutions:

1. The rightmost convolution stands for projections of source contributions onto outgoing waves in various directions, i.e. plane wave expansions of sources.
2. The second convolution represents the translation from the source region to the field region for each direction. Notice that this translation process is characterized by plane-wave inherent diagonal property, which implies that a plane wave propagating in some direction does not interact with other plane wave in another direction.
3. The leftmost convolution contrast to the rightmost one projects incident plane waves onto field points.

This three-stage approach can accomplish the Kirchhoff integral in $\mathrm{O(N^{1.5}logN)}$ operations as detailed in [Arif Ergin et.al., *IEEE Ant. Propag. Mag.*, vol. 41, 39-52, 1999] instead of $\mathrm{O(N^2)}$ operations if by direct calculation. In our simulation, we examine the accuracy of PWTD in calculating E due to distant sources. It is observed that the error can be controlled by adjusting parameters in the PWTD algorithm. The computing time and memory requirement by MR-FDTD with PWTD are in comparison with those by direct calculations. It shows that this approach indeed has better computing efficiency. Furthermore regions in MR-FDTD setup are not necessarily characterized by same parameters as required by ordinary FDTD. Instead, each region can have its own grid size, time increment step and even the axis orientation. With this flexibility and freedom in choosing suitable parameters, MR-FDTD exhibits much more efficiency in contrast to ordinary FDTD. To demonstrate the applicability of the new algorithm, we simulate problems with regions of different orientation or grid density. Both results indicate satisfactory accuracy and low computational demand.

Radiation-Pattern Synthesis Based on Quadratic Programming for Multimode Circular Horns

H. Deguchi and **M. Tsuji**
Doshisha University, Japan

Introduction

To suppress both sidelobe level and cross-polarization component while shaping a pencil beam or a sectral beam with high gain, we have applied quadratic programming approach to radiation pattern synthesis of multimode horns. The taper configuration of such horns can be obtained by an optimization design procedure using the mode coefficients which are pre-calculated by the quadratic programming as one of the design goal. We present a design example of the multimode horn with spline-profile taper, which provides high circular-coverage gain with low sidelobe of about -30dB.

Design principle

Let us consider an axially symmetrical horn with an arbitrary taper profile. An aperture distribution of such a horn can be expanded by TE_{1n} and TM_{1m} modes. Its radiation pattern is obtained by linear combination of their radiation patterns. The mode coefficients can be solved by an optimization with equality/inequality constrains for achieving specified radiation characteristics, for example, coverage gain, sidelobe level and peak cross-polarization level which are formulated by linear equations. In case of the sectral beam horn for covering a circular area uniformly, the objective function which is defined by a gain at the edge of the coverage is written as a quadratic equation. Since far-filed radiation patterns of circular-waveguide modes with flat wavefront are given by real function, their mode coefficients that are unknown real value can be solved by the quadratic programming approach. Finally, the spline profile of the horn can be determined by non-linear optimization technique based on the pre-calculated mode coefficients. The concept of the proposed pattern synthesis can be also applied to various types of taper configuration with irises and/or coaxial cavities inside the circular-aperture horn.

Design example and evaluation

We now design a sectral beam horn with sidelobe of -30dB and peak cross-polarization level of -40dB, and VSWR¡1.065, where angular diameter of the circular coverage is 40 degrees and center frequency is 10GHz. Table 1 shows the mode coefficients determined by the quadratic programming. We confirmed that both the measured far-field radiation patterns and the VSWR of the fabricated horn agree with the predicted ones. The designed horn achieves approximately uniform gain over the coverage with low sidelobe of about -30dB and excellent VSWR characteristics. We will numerically and experimentally discuss the frequency characteristics of the designed horn in detail at the talk.

Table 1. Mode coefficients at horn aperture used as one of the design goal.

	TE_{11}	TM_{11}	TE_{12}	TM_{12}	TE_{13}	TM_{13}
Amplitude [dB]	-5.8	-4.1	-5.4	-12.4	-30.0	-33.7
Phase [deg]	0	0	0	0	0	180

Numerical Analysis of an Elliptical Core Optical Fiber with Arbitrary Refractive Index Profile

S. Furukawa[1], **T. Hinata**[2], **N. Shimizu**[3], and **W. Satou**[2]

[1]Sano College, Japan
[2]Nihon University, Japan
[3]Nippon Light Co.,Ltd., Japan

As an analysis method of a fiber with the radial and the angular inhomogeneous core, circular Fourier expansion method (CFEM) proposed by Vassallo[1] is useful. The analysis area of CFEM is separated in S_0(homogeneous area to simplify an analysis at $r = 0$, refractive index of n_0), S_1(inhomogeneous area with refractive index profile of $n(r, \theta)$), andS_2 (homogeneous area with refractive index n_c) as shown Fig.1. Electromagnetic components of all area and refractive index profile of S_1 are expanded to Fourier series. Simultaneous differential equations which are obtained by substituting those to Maxwellfs equations are computed by a difference method such as 4-th order Runge-Kutta method. Then the calculation of Fourier coefficients for a given refractive index profile and its inverse is required with the number of step size for a difference method. Fourier coefficients are calculated by a numerical integration method for cases except simple refractive index profile[2]. This process will be spent a lot of time to keep an accuracy of analysis.

This paper gives a method which can be analytically computed the Fourier coefficients by dividing the refractive index profile of an inhomogeneous area into homogeneous layers along angular orientation (see Fig.2). An accuracy of this method is examined for propagation characteristics of an elliptical fiber with α-power refractive index profile. It is found that this method can be computed in good accuracy by adequately selecting division number of homogeneous layers to angular orientation, step size of 4-th order Runge-Kutta method, and truncation number of Fourier series.

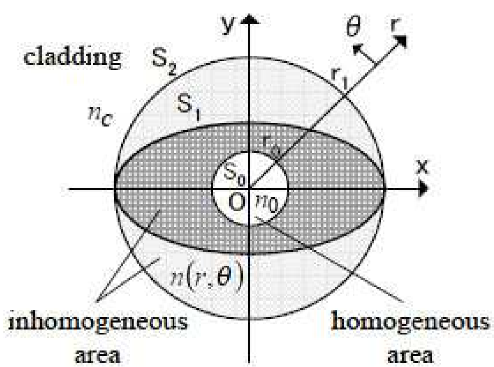

Figure 1: Cross section and coordinate system

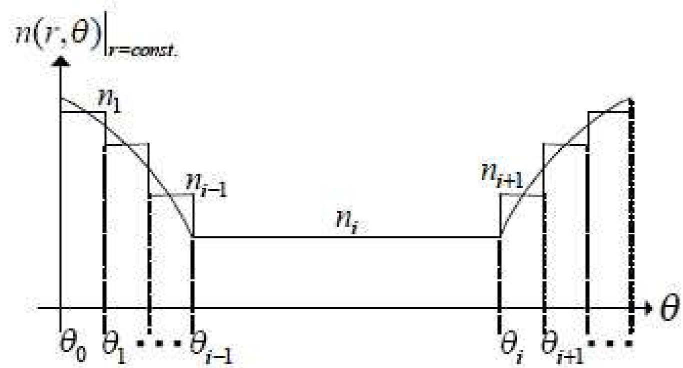

Figure 2: Homogeneous layer division along angular direction of refractive index profile

REFERENCES

1. C.Vassallo: J.Lightwave Technol., vol.8, no.1, pp.1723-1729, 1990.
2. G.Trommer: ntzArchiv, Bd.9, pp.121-125, 1987.

Session 4A2
Induced Current in a Human Body by ELF/Intermediate Electric or Magnetic Fields

Simple Dosimetry for Human Exposure to Non-Uniform ELF Magnetic Field

K. Yamazaki, T. Kawamoto, and **T. Shigemitsu**

Central Research Institute of Electric Power Industry, Japan

Regarding recent concerns on the health effects of ELF (extremely low frequency) magnetic fields, compliance testing in accordance with guidelines in highly non-uniform magnetic field has been a critical issue. In these cases, when the measured maximum magnetic fields on the surface of the human body exceed the reference level, the basic restriction should be investigated in a different way. However, this requires numerical calculation of the induced current or electric field, which is not readily achievable. Therefore, a simple method of investigating the conformity with a guideline, particularly one applicable to practical situations, is strongly desired. In this paper, a simplified method that can be used to estimate the maximum induced current from magnetic field measurements in practical complex situations was proposed. This method is based on the reduction rate of the magnetic field within a spherical model. The relationship between the reduction rate of magnetic field and the rate of maximum induced current to that of uniform field exposure was approximated using a simple regression curve. The validity of the proposed method was verified by comparing it with data by numerical calculation for anatomically correct human model, which was obtained from a literature. This study has practical values for assessing compliance with guidelines.

Calculation of Induced Current Inside a Human Body near an IH Cooker by SPFD Method

Y. Kamimura, K. Ito, and **Y. Yamada**

Utsunomiya University, Japan

Recently, it is concerned about the effect of the electromagnetic field on the human body. The basic restrictions for exposure to electromagnetic fields in each frequency band are determined by ICNIRP (International Commission on Non-Ionizing Radiation Protection). At the frequency of 20 kHz (internal frequency of the IH cooker used in this study), the basic restriction for the exposure to the induced current density is 40 mA/m^2 (for the general public exposure) and 200 mA/m^2 (for the occupational exposure).

In this study, magnetic field exposure of human body near an IH cooker is evaluated using Scalar Potential Finite Difference (SPFD) method. The maximum induced current densities are compared among three kinds of anatomy human body models of the Japanese adult male/female and the American adult male. Moreover, the induced current densities are averaged by one square centimeter in the area, and compared with the guideline of ICNIRP. As a result, in the case with the portable type IH cooker and a pan designed for the IH cooker, it is found that the maximum induced current densities are considerably different among these three models of the human body, and the induced current exceeding the guideline of ICNIRP may not flow inside of human body. In addition, decreasing the computation load and the computer resource by dividing the model is considered. As a result, the difference of calculation result by dividing the model is almost negligible and computation load is decreased.

Analysis of Induced Electric Field within Eccentric Multi-Layered Sphere

Y. Suzuki and **M. Taki**
Tokyo Metropolitan University, Japan

Membrane structures within organism effect on distributions of induced electric field and induced current caused by external electromagnetic field. There are several scales of membrane in biological body. For example, retina is tissue level membrane, and plasma membrane is cell structure level membrane. The eccentric multi-layered spherical model is useful to clarify the essential nature of effect of those membrane structures on internally induced electric field.

Numerical methods such as finite difference method have difficulty to deal with the membrane model, because mostly shapes of membrane are much thinner than these of other tissues or organs. A suitable calculation mesh size is restricted by the thickness of membrane. Therefore, these types of numerical calculation make calculation costs, which mean spending cpu time and using memory size, higher.

In this study, quasi-analytical approach is applied to save calculation costs. Solutions of internal electric field distribution within eccentric multi-layered spherical model are derived from the extended method of Mie theory. In this technique, additional theorem for spherical vector wave function is applied to realize extremely eccentric inner sphere with thin membrane. The advantage of this method is not only saving calculation costs but also applying wide frequency range from ELF to high frequency electromagnetic field.

As an application of this technique, we performed induced electric field analysis for an eyeball within spherical head model exposed to time varying magnetic field at 20Hz. Spatial distribution of incident magnetic field is uniform for this analysis. A preliminary result of this analysis indicates that maximum electric field strength with retina and sclera is 1.8 times larger than that without membrane. As mentioned above, this technique is useful for dosimetory to investigate magnetophosphene phenomenon.

Analysis of Current Density Distribution Induced by ELF Magnetic Fields Utilizing Fast-Multipole Surface-Charge-Simulation Method for Voxel Data

S. Hamada and **T. Kobayashi**

Kyoto University, Japan

This paper describes an application of the FMM(fast multipole method[(1)])-SCM(surface charge simulation method) for voxel data[(2)] to analyses of current density distribution in a voxel model induced by ELF magnetic fields. The FMM-SCM for voxel data treats a square surface of a voxel that has different inside and outside conductivities as a surface element of the SCM that caluculates three-dimensional Laplacian field. The main features of the method are as follows. (I) The diagonal form FMM provides $O(D^2)$ performance in the memory-capacity and operation-cost, when the number of voxels is about D^3. (II) The MoM (method of moment) strictly imposes the continuity of the flux passing through each boundary element, therefore the solution globally satisfies the Gauss' law. These features make it high-speed, high-capacity, and high-stability calculation method.

This method is applied to analyses of induced current in a numerical human model called 'Taro'. Taro, a Japanese adult male model, was developed by NICT (National Institute of Information and Communications Technology), Kitasato Univ., Keio Univ., and Tokyo Metropolitan University[(3)]. He consists of 7,977,906 voxels except the air region around him, and the cubic voxel size is 2mm. Applied 50Hz magnetic fields are three kinds of homogeneous 1μT field, B_x (case i-x), B_y (case i-y), and B_z (case i-z), and three kinds of magnetic dipole (0.5π μWb m) field generated by M_x (case ii-x), M_y (case ii-y), and M_z (case ii-z). Figs. 1 and 2 show the calculated current density distributions of the cases i-y and ii-y, respectively. The calculation times on 32bit PC (Pentium IV, 3GHz, 2Gbyte-RAM, Windows 2000) listed in Table 1 demonstrate good performance of the FMM-SCM for voxel data.

Fig. 1. Calculated **J in the case i-y.**

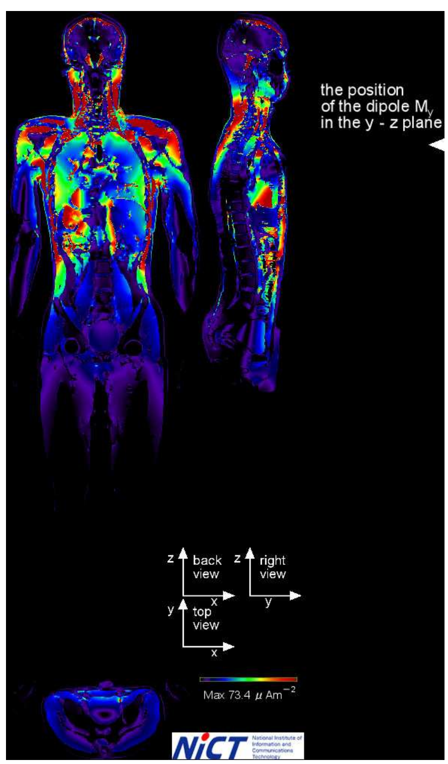

Fig. 2. Calculated **J in the case ii-y.**

Table 1. Calculation time.

case i-x	6h 23min.
case i-y	5h 53min.
case i-z	6h 06min.
case ii-x	6h 16min.
case ii-y	6h 42min.
case ii-z	6h 33min.

References

(1) L. Greengard, V. Rokhlin, Acta Numerica, **6**, 229-269 (1997)

(2) S. Hamada, T. Kobayashi, Proc. 2005 annual conf. FM, IEE Japan, II-4, 148-153 (2005)

(3) T. Nagaoka, et al., Phys. Med. Biol. **49**, 1–15 (2004)

Induced Currents in Realistic Japanese Models Due to Power-Frequency Electric Fields

A. Hirata and **O. Fujiwara**
Nagoya Institute of Technology, Japan

In recent years, there has been an increasing public concern about adverse health effects due to electromagnetic (EM) wave exposures. According to the ICNIRP (International Commission on Non-Ionizing Radiation Protection) guidelines [1], induced current density is used as a dosimetric metric in quantifying interactions between humans and power-frequency fields. Therefore, induced current density in an anatomically realistic human body model [2, 3], including female [4] and child [5] models, for exposure to power-frequency electric and magnetic fields has been investigated extensively. The models used in these works were developed based on the European and the American. Namely, no study has been conducted using a realistic model based on the Asian.

We first review the above studies, and then explain briefly our project, which investigates induced currents and fields in Japanese models [6].

REFERENCES

1. International Commission on Non-Ionizing Radiation Protection (ICNIRP), gGuidelines for limiting exposure to time-varying electric, magnetic, and electromagnetic fields (up to 300 GHz),h *Health Phys.*, vol.74, pp.494-522, 1998.
2. M. A. Stuchly and T. W. Dawson, gInteraction of low-frequency electric and magnetic fields with the human body,h *Proc. IEEE*, vol.88, pp.643-664, 2000.
3. P. J. Dimbylow, gCurrent densities in a 2 mm resolution anatomically realistic model of the body induced by low frequency electric fields,h *Phys. Med. Biol.*, vol.45, no.4, pp.1012-1022, 2000.
4. P. Dimbylow, gDevelopment of the female voxel phantom, NAOMI, and its application to calculations of induced current densities and electric fields from applied low frequency magnetic and electric fields,h *Phys. Med. Biol.*, vol.50, no.6, pp.1047-1070, 2005.
5. A. Hirata, K. Caputa, T. W. Dawson, and M. A. Stuchly, gDosimetry in models of child and adult for low-frequency electric field,h *IEEE Transactions on Biomedical Engineering*, vol.83, no.9, pp.1007-1012, 2001.
6. T. Nagaoka, S. Watanabe, K. Sakurai, E. Kunieda, T. Watanabe, gDevelopment of realistic high-resolution whole-body voxel models of Japanese adult male and female of average height and weight and application of models to radio-frequency electromagnetic-field dosimetry, h *Phys. Med. and Biol.*, vol.49, pp.1-15, Jan. 2004.

Electric and Magnetic Field Distributions along High Voltage Power Lines

Q. W. Pan
Manukau Institute of Technology, New Zealand

It has long been a concerning issue . that extremely-low -frequency electromagneticfields (ELF/EMF) generated by high voltage power transmission lines may be harmful to our health, perhaps even initiating cancer. However, solid evidence has yet to be found, although there are quite a number of weakly proven claims published. For those who are living underneath these unsightly lines , it is worthwhile to have a clear picture about the field distributions. A comprehensive measurement in a residential area next to a sub-station is being conducted . taking into account building material, landscaping, street traffic, etc. Preliminary records show that along a power transmission line, the electric field is maximal under the droop (midway between two pylons) and minimal at the pylon. For the same voltage, a double -circuit line generates lower level surrounding electric fields than a single-circuit line. Trees, houses and tall objects act as electric field shields on the ground. Figs. 1 is an example of electric field distributions of 220 kV lines. Based on the measured fields, induced currents are calculated, compared and discussed.

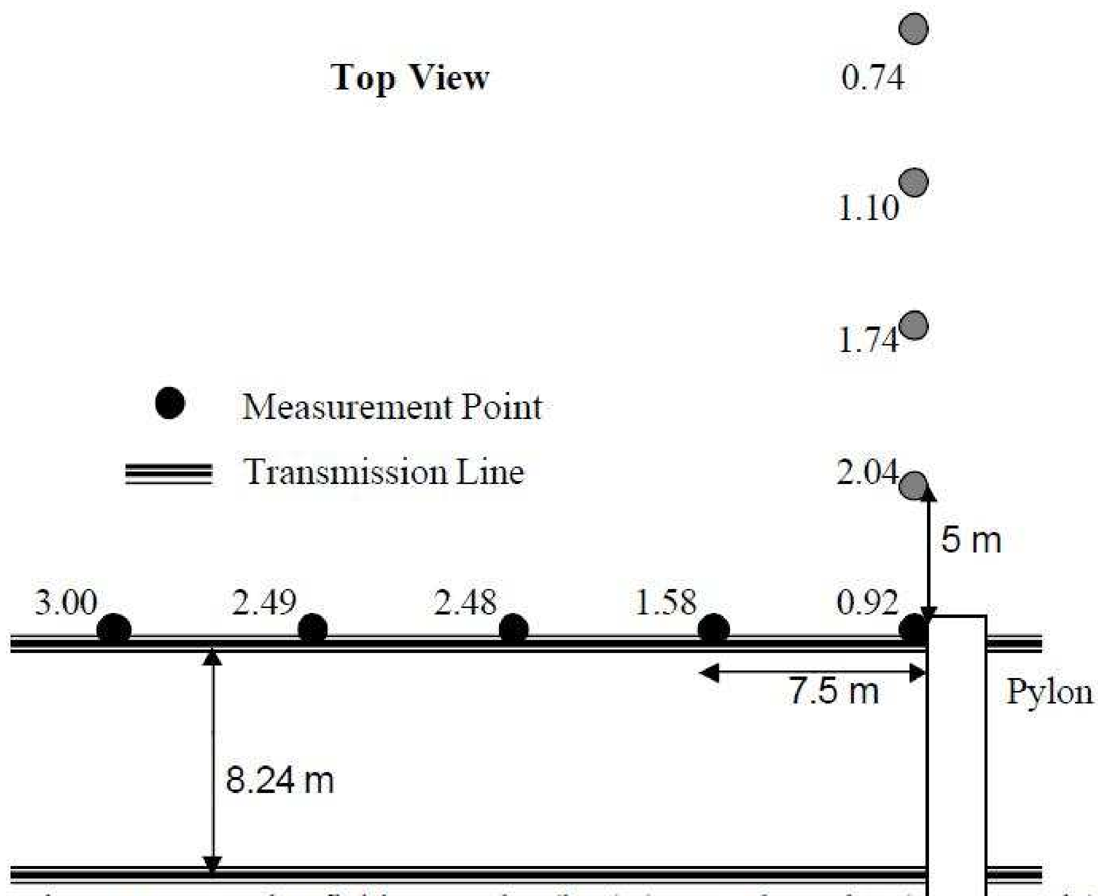

Fig. 1 Measured E field strengths (kV/m) near the pylon (not to scale)

A Transfer Function Method for Determination of MRI Heating of an Implanted Medical Lead Wire

S. M. Park, R. Kamondetdacha, A. Amjad, and **J. Nyenhuis**
Purdue University, U.S.A.

The RF magnetic field in Magnetic Resonance Imaging (MRI), which has a frequency of 64 MHz for a 1.5 T MR system, induces an electric field in the patient. The intensity of the RF field is quantified through the specific absorption rate (SAR) in W/kg. For routine MRI, the whole body average SAR may be as great as 4 W/kg. The electric field induces current in an implanted lead wire that is used, for example, with an implanted cardiac pacemaker or a neuronal stimulator. Some of the current induced in the lead will flow into the tissue near the electrode at the end of the lead wire, potentially resulting in dangerous heating. [1]

In this work, the method of moments is used to calculate the current induced in a simulated implanted lead. The lead is modeled as a solid wire with insulation and the electrode is modeled by removal of insulation from the end of the wire. The electric field in the tissue at point r near the electrode, $\mathbf{E}_{electrode}(\mathbf{r})$, is calculated as the integral along the length t of the lead of the product of a transfer function $\mathbf{S}(\mathrm{t}, \mathbf{r})$ and the tangential component Et of the electric field.

$$\mathbf{E}_{electrode}(\mathbf{r}) = \int_{Lead} \mathbf{S}(\mathrm{t}, \mathbf{r}) E_t dt$$

From the knowledge of the transfer function, the electric field in the tissue around the electrode and hence the temperature rise for a given electric field distribution in the body can be calculated. The figure shows the calculated magnitude —S_r(t,P)— of the transfer function for the radial electric field magnitude —Er— for simulated leads of lengths 40, 60 and 80 cm with wire diameter $\Phi = 1$ mm, insulation thickness 0.4 mm, and 6 mm of metal exposed at one end. The evaluation point P is 0.5 mm below the end of the electrode and 0.5 mm from the surface, as illustrated in the graph. The different shapes of transfer functions indicate different sensitivities to the electric field in the body. It is noteworthy that the sensitivity is not necessarily greatest near the electrode. The phase of the transfer function was also calculated. For a lead with effective length greater than approximately half wavelength, the variation in phase exceeds π, resulting in non-resonant behavior. The temperature rise at the electrode was measured in a phantom to test the predictions of the calculations. These results can be used to help predict the heating of an implanted lead by the RF magnetic field in MRI.

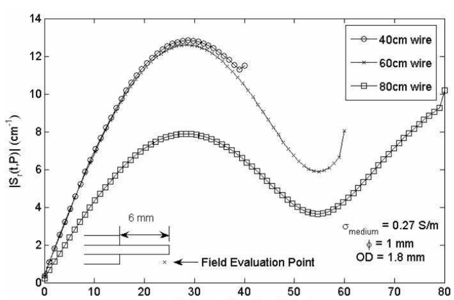

Calculated —S_r(t,P)— for three lead lengths. t=0 corresponds to the end of the lead that is opposite the electrode. The field evaluation point P is near the end of the electrode, as indicated.

REFERENCES

1. Nyenhuis JA, Park SM, Kamondetdacha R, Amjad A, Shellock FG, and Rezai AR, MRI and Implanted Medical Devices: Basic Interactions With an Emphasis on Heating, *IEEE Transactions on Device and Materials Reliability*, vol. 5, 467-480, 2005.

Session 4A3
Electromagnetic Wave Scattering from Atmospheric Irregularities

High Resolution Atmospheric Profiling Using Range Imaging

T. Y. Yu and **P. Chilson**
University of Oklahoma, U.S.A.
W. O. J. Brown
National Center for Atmospheric Research, U.S.A.
S. Frasier
University of Massachusetts, U.S.A.

The range resolution of a pulse radar is determined by the receiver bandwidth and pulse shape. For profiler radars, typical range resolution is on the order of a few tens of meters to a few hundreds of meters. Although resolution can be improved by transmitting a shorter pulse, sensitivity is degraded due to less energy contained within one pulses. Many efforts have been made to mitigate the fundamental limitation with the goal of improving range resolution, such as pulse compression, oversampling, etc. Recently, a technique which exploits frequency agility has been developed to image the profile of atmospheric structure at fine scale. The technique is termed Range IMaging (RIM) (Palmer et al, 1999) or Frequency domain radar Interferometric Imaging (FII) (Luce et al. 2000). Signals from multiple close-spaced frequencies can be optimally combined to estimate the range distribution of echo power within the conventional range gate. The RIM/FII problem has been solved by the approaches used in spectral estimation such as Fourier method, Capon method, MUSIC, and maximum entropy. Moreover, Doppler spectra can be obtained at each sub-gate by RIM's Doppler sorting capability. By implementing RIM/FII on spatially spaced receivers, high resolution profile of 3D wind fields can be obtained using spaced antenna method on the synthesized data generated by RIM. This technique is termed RIM-SA (Yu and Brown, 2004). As a result, a profile of the horizontal wind and the three spectral moments can be obtained at enhanced range resolution.

In this work, an overview of RIM/FII will be presented and the progress will be reported. The feasibility and application of RIM/FII and RIM-SA to atmospheric observations will be demonstrated using various systems including the NCAR's Multiple Antenna Profiler Radar (MAPR), NOAA's Platteville 915-MHz Tropospheric Profiler, and conventional 915 MHz boundary profiler. Examples of fine layer structure, Kelvin-Helmholtz (KH) waves, bore, and other interesting cases will be presented. In addition, some of the high resolution results will be compared with in-situ measurements and the S-band Frequency modulation continuous wave (FMCW) of the University of Massachusetts. Finally, comments on the future RIM/FII development will be provided.

REFERENCES

1. Luce, H., M. Yamamoto, S. Fukao, D. Helal, and M. Crochet, 2001: A frequency domain radar interferometric imaging (FII) technique based on high resolution methods. *J. Atmos. Sol.-Terr. Phys.*, **63**, 221–234.
2. Palmer, R. D., T.-Y. Yu, and P. B. Chilson, 1999: Range imaging using frequency diversity. *Radio Sci.*, **34**, 1485–1496.
3. Yu, T.-Y. and W. O. J. Brown, 2004: High-resolution atmospheric profiling using combined spaced antenna and range imaging techniques. *Radio Sci.*, **39**, RS1101, doi:10.1029/2003RS002907.

Radar Imaging of Troposphere and Stratosphere Echoes with new Middle and Upper Atmosphere Radar (MUR)

G. Hassenpflug, **M. Yamamoto,** and **S. Fukao**
Kyoto University, Japan
H. Luce
Toulon University, France

The horizontally layered structure of the atmosphere dictates that study of vertical processes and inter-layer interactions requires much finer vertical resolution than studies of horizontal processes require of the corresponding horizontal resolution. In the troposphere, convective processes and turbulence caused by wind shear are among the important processes leading to significant vertical mixing.

VHF-band radar observations contribute to studies of atmospheric physics, particularly inertio-gravity waves, turbulence, climatology and meteorology, over scales ranging from small-scale (3-m) to mesoscale (100-km). Requirements for more detailed observations led to radar imaging, a group of techniques using multiple frequency interferometry to improve range resolution, and multiple receiver antennas to improve angular resolution.

The Middle and Upper Atmosphere Radar (MUR) at Shigaraki, Shiga, Japan ($34.85^o N$, $136.10^o E$) is a VHF-band radar with a center frequency of 46.5 MHz and the flexibility to change beam direction pulse-to-pulse. In 2004 the system was upgraded to fully digital with support for up to 5 transmit frequencies in a 1 MHz bandwidth, and up to 25 receiver channels, whereby the total antenna area is divided into 25 individual antenna groups which can be digitally combined flexibly into the available receiver channels.

In this paper we present results using this imaging platform in range imaging (1-D), angular imaging (2-D) fully 3-D imaging; we apply data-adaptive processing algorithms, notably the Capon method, and are able to detect Kelvin-Helmholtz instabilities clearly, as shown in Figure1 , as well as convective events. We discuss the value of such high-resolution imaging for studies of small-scale turbulence, layer structures, and physics of the troposphere and stratosphere.

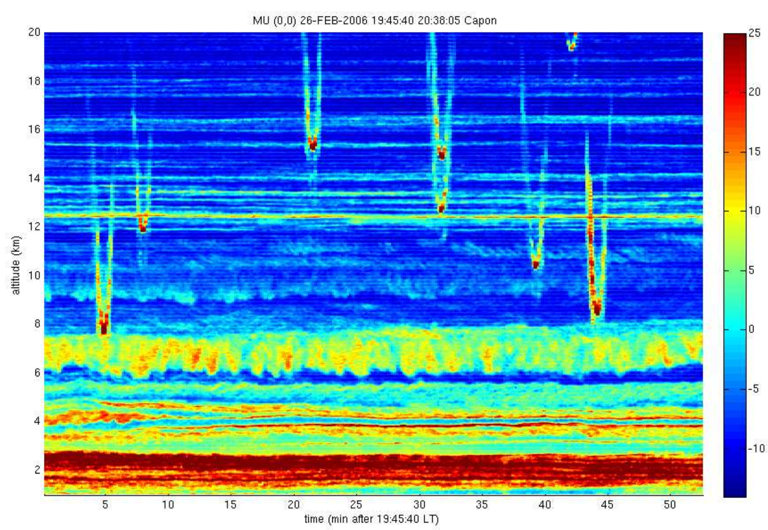

Figure 1: Height-Time plot of Capon method imaging brightness (dB) for a 1-hour period on 28th February 2006, showing clearly KHI signatures from {2-12 km}. Aircraft echoes are seen as parabola-shaped interference.

Review of Atmospheric Boundary Layer Observations Using the Turbulent Eddy Profiler

R. D. Palmer and **B. L. Cheong**
University of Oklahoma, U.S.A.

Over the past several years, Coherent Radar Imaging (CRI) has become an accepted technique for high-resolution observations of the atmosphere. The method has been successfully applied from the atmospheric boundary layer (ABL) to the thermosphere. By vertically transmitting over a wide conical region and sampling the backscattered signal on the ground using spatially separated receive antennas, it is possible to estimate the angular structure and dynamics of the observed atmosphere with unprecedented resolution and simultaneity. CRI uses a wide transmit beam and is essentially a digital beamforming technique and thus can be implemented with a variety of optimization criteria. From our experience, data-dependent methods offer high-resolution and improved clutter rejection capabilities, which are particularly important for ABL observations. In the present work, we review results from our experience over the last several years with the sophisticated *Turbulent Eddy Profiler* (TEP), developed by researchers at the University of Massachusetts in the 1990s. The TEP system is a unique 915 MHz boundary layer radar consisting of 64 independent receivers. Elements of the array are easily reconfigurable allowing studies of optimized array configurations, for example. Our observations include a complete diurnal cycle showing the growth and decay of the convective boundary layer, mixed turbulence-precipitation interaction, and various forms of biological clutter. A system overview will be provided but emphasis will be placed on observational results.

Fine Scale Multistatic Wind Field Observations with EAR

K. Nishimura, E. Gotoh, T. Harada, and **T. Sato**
Kyoto University, Japan

Conventional monostatic atmospheric radar, which can only obtain the radial component of the wind velocity, is restricted in its spatial resolution. This is because this radar must estimate a wind vector by using, at least, three Doppler velocity components measured at spatially separate targets under the assumption of horizontal homogeneity of the wind field.

In this paper, a multistatic radar observation technique, which uses two receiver arrays together with a high-gain rapid scanning monostatic wind-profiler, is presented. Multistatic receiver arrays obtain non-radial components of the wind velocity; hence, the technique enables us to determine 3D wind velocity at each minimum resolution volume. Consequently, it eliminates estimation errors caused by horizontal inhomogeneity of the wind field and improves spatial resolution.

Applying this technique, we made a series of tropospheric observations in September 2004, utilizing digital receiver systems at the Equatorial Atmosphere Radar, West Sumatra, Indonesia. Each receiver antenna is equipped with this digital receiver and recording system, which is constructed with a cost-effective ready-made digital receiver PCI board and a PC. By using this structure, the receiver array can arbitrarily swing the beam after observations.

First, the importance and the effectiveness of ground clutter rejection using an adaptive spatial filter, which is another advantage of digital receiver systems, is demonstrated. Then profile of a 3D wind velocity field with a high horizontal resolution is presented. Considering the accuracy of the multistatic radar system, the resulting wind field shows the existence of significant perturbation that previously would have beobservations (Fig.1).

From November to Dece en averaged in conventional monostatic radar mber, 2006, we made another 3-week observation at the EAR employing Spano's code, which provides high SNR while it has no blind region caused by code truncation. As the Spano codes require a real-time identification of the transmitted code, we newly developed an online signal processing software in order to compress the data. We furthermore utilized a computationally generated aperiodic receiver array that does not have grating-lobes under the constraint that each adjacent antenna should not be closer than 0.7 wavelengths. More precise analyses are made by using the data observed in this observation.

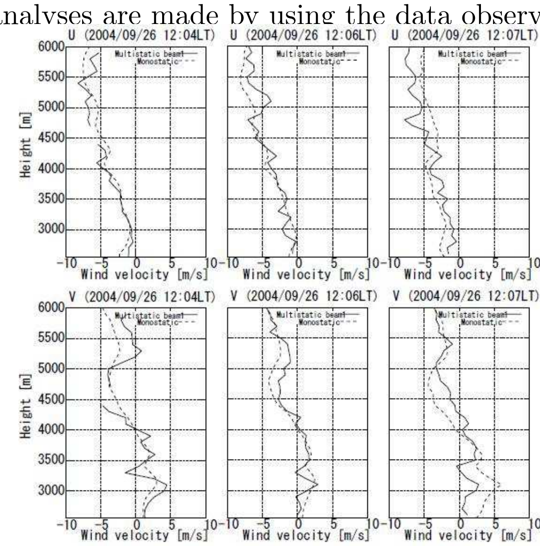

Figure 1: Zonal (top row) and meridional (bottom) components of observed wind velocities measured with the monostatic (dashed) and the multistatic (solid) systems.

Multi-Sensor Ground-Based Remote Sensing Measurements of Turbulence and Microphysical Parameters in Marine Boundary Layer Clouds at Palau in the Tropical Western Pacific Ocean

K. K. Reddy [1], **R. Shirooka** [1], **T. Ushiyama** [1], **H. Kubota** [1], and **H. Uyeda** [1,2]

[1]Institute of Observational Research for Global Change (IORGC), Japan
[2]Nagoya University, Japan

The main objective of the PALAU (Pacific Area Long-term Atmospheric observation for Understanding of climate change) project is to understand (cloud-precipitation processes, land-atmosphere and air-sea interactions and also focusing on seasonal and intra-seasonal variations) importance of the atmospheric processes over Aimeliik Observatory in the Western tropical Pacific Ocean region. At Aimeliik observatory (7.45^{o}N, 134.47^{o}E) several ground based remote sensors [Wind profiler radar (WPR) with Radio acoustic sounding system (RASS), Ceilometer, Micro Rain Radar (MRR), JW Disdrometer (JWD), and Automatic Weather Station (AWS)] are operated continuous since 2003. Upper air sounding is carried out by National weather service (NWS) which is (located about 10 km south of Aimeliik observatory) confided by National Oceanic and Atmospheric Administration (NOAA) located at Koror (7.33N, 134.48E) the capital of Palau. The desire turbulence and microphysical information is obtained from the radar reflectivity and other elements of the Doppler velocity spectra. At Aimeliik, the precipitating cloud observed near wind profiler shows a diurnal variation during westerly wind regime and increases from afternoon to evening and decreases in the nighttime. During the westerly wind regime the precipitating cloud systems are mostly associated with convection activities. These cloud systems are short lived about couple of hours with high intensity of the rain. Whereas in Easterly wind regime more often shallow convective clouds are observed. JWD, MRR and wind profiler derived raindrop size distributions characteristics show significant seasonal dependence of rain integral [Rain drop size distribution (DSD)] parameters. The intensity of precipitation strong and duration was short during westerly wind phase. On the other hand, weak intensity and long duration was observed during easterly wind phase. The difference of DSD parameters between westerly and easterly monsoon is large.

Additionally, combining information of ceilometer aerosol backscatter data with the WPR, MRR and JWD allows us to investigate how the relative effects of aerosol correspond to changing meteorological events (easterly and westerly or/during inactive and active phase of MJO) and regional regimes. The details of the analysis procedure and results will be presented during the conference.

Observations and Analysis in Long-Distance Propagations of VHF Waves Transmitted from Oversea TV Broadcasting Stations

T. Takano, K. Sakurai, H. Nakata, H. Akaike, S. Ujigawa
I. Nagashima, A. Hirai, Y. Kawamura, and **S. Shimakura**
Chiba University, Japan

We have observed broadband spectra in VHF band in Chiba, Japan, to investigate anomaly of propagation of broadcasting waves from distant Asian TV broadcasting stations. Broadband observations from 47 to 76 MHz are done with a log periodic dipole-array antenna at Tateyama, which locates about 150km southeast from Tokyo. The altitude of the position of the antenna is about 64m above the sea level. Received signal with the antenna was amplified with a pre-amplifier attached right under the antenna and transferred to an observation house by coaxial cable. A spectrum analyzer is used to obtain spectral characteristics of the observed signal. No commercial radio and TV stations are allocated in this observing band in Japan except for Japanese army and emergency broadcastings of local governments.

We found that TV broadcasting waves from China, Philippines, Thailand and Malaysia can sometimes propagate and there are three types of propagations. Seasonal and daily variations of received broadcasting waves were investigated.

Propagation Type A has upper frequency limit of around 60MHz and the frequency boundary shows fluctuation in time scale of few tens minutes. This type of propagation can be seen in daytime (8:00-20:00 JST) in spring and fall. Broadcasting stations which show Type A propagation are in Malaysia and Thailand. Type B shows many TV frequencies in 50 to 75 MHz and propagate in midnight 20:00-24:00 JST in spring and fall. Broadcasting stations are also in mainly Malaysia, Thailand and Philippines. Propagation Type C is shown in daytime (8:00-16:00 JST) in summer and corresponding stations are mainly in China.

The distance from the observation point to Chinese, Malaysia, Philippines TV stations are about 800km, 5200km, and 2800km, respectively. Supposing that a broadcasting wave is reflected with one-hop by the ionosphere, it calculated that the Es layer altitude is required to reflect the China-TV waves, and the F2 layer altitude is required for reflection of the Malaysia and Philippines TV waves. The profiles of electron density in ionosphere show seasonal and daily variation. Es layer becomes active mainly in summer and F2 layer has higher electron densities in spring and fall. These characteristics seem to fit with observed characteristics of Types A, B, and C.

We are also performing a simulation of propagations of VHF waves with the ray tracing method. In results, F2 layer from daytime to evening in spring and fall refracts 50MHz electromagnetic wave. Moreover, changes of the maximum frequency with time are also obtained that corresponds to characteristics of Type A propagation. These facts suggest that Type A is mainly Malaysia broadcasting wave reflected by F2 layer, and Type C is mainly Chinese broadcasting waves reflected by Es layer. We also conclude with both observations and simulations that Type B propagation is caused by scattering by equatorial plasma bubbles.

Performance of the Developed Low-Power and High-Sensitivity Cloud Profiling FM-CW Radar at 95 GHz

T. Takano [1], **K. Akita** [1], **H. Kubo** [1], **H. Abe** [1], **J. Yamaguchi** [1]
K. Futaba [1], **Y. Kawamura** [1], **H. Kumagai** [2], **T. Takamura** [1], and **Y. Nakanishi** [2]

[1]Chiba University, Japan
[2]The National Institute of Information and Communications Technology, Japan

It is getting more important to know the global environment and the global change of climate for the human beings. One of the most significant features to know them is cloud. Information on 3-dimensional structures of clouds, sizes and distribution of cloud particles, dependence on size of optical characteristics of cloud particles, motions of particles in clouds, and so on are all desirable to solve role of clouds. Observations of clouds with radars would be most powerful method to derive such information. Conventional microwave radars canAhowever, detect precipitation particles but are not able to detect particles in clouds because their sizes, less than a few tens microns, are much smaller that the wavelengths and, therefore, their cross sections are quite small. Radar observations of cloud particles at millimeter waves, which have realized recently, have much more sensitive. Several groups have reported the development and observational results that demonstrate powerful performances to investigate cloud particles.

We have designed and developed a cloud profiling radar at 95GHz. We adopt a frequency- modulated continuous wave (FM-CW) radar rather than a pulse radar because the former can achieve more sensitive system than the latter if comparing with same instantaneous output power of transmitted millimeter wave. We designed the facility to observe clouds between 0.3 and 20km in height with a resolution of 15 m. The velocities measured as Doppler shift would be less than 1 m/sec. Consequently, a low-power of 0.5W and high-sensitivity of -32 dBZ at 5 km were realized for the developed FM-CW cloud profiling radar at 95 GHz.

Using the developed millimeter-wave FM-CW radar, we observed clouds on cruises on Mirai, a Japanese scientific research vessel, in 2004 in the Arctic Ocean and in 2005 in the northern half of the Pacific Ocean. On each cruise, which lasted 5 months, the facility run well and present good observational data. The observed data with our cloud profiling radar are compared with the lidar data of the National Institute for Environmental Studies operated by Nobuo Sugimoto and his coworkers. This shows that the radar data can reveal interior structures in heavily obscured clouds which cannot be seen with lidar data because of heavy extinction in visible light. Precise comparison of these data will be presented.

Session 4A4
Microwave Materials for Functional Devices

2-10 GHz-Range Surface Acoustic Wave Filters Using Zero-TCFESuper High Coupling Substrates

K. Yamanouchi and **Y. Satoh**
Tohoku Institute of Technology, Japan

The development of GHz-band surface acoustic wave (SAW) devices has become necessary because of the increasing volume of information and communication media, such as mobile telephone, satellite broadcasting, spread spectrum communications. Especially, zero TCF, wide band and low loss filters with an ultra-small size and high performance are required for mobile communication systems. We show the SAW resonators and ladder type SAW resonator filters using high coupling $SiO_2/5^oY$-X $LiNbO_3$ with Zero Temperature Coefficients of Frequency (TCF). The theoretical analysis of 5-10GHz ladder type filters including the propagation attenuations and resistive loss of interdigital transducers are shown. Finally the experimental results below 2.0dB insertion loss with a wide band and zero TCF at 2-10GHz-range are shown, using submicron fabrication technology.

Carbon Nanotube Electronics

T. Mizutani
Nagoya University, Japan

Carbon nanotubes (CNTs) are seamless hollow cylinders with honeycomb lattice composed of carbon atoms with diameters as small as 1 nm and lengths of several microns [1]. They are attracting much attention because of their unique electrical properties. The saturation velocity of the electrons is expected to be 3-5 times larger than that of Si and GaAs materials [2]. A large transconductance of 17.6 S/mm has been realized [3], which is about 20 times larger than that of the state-of- the-art Si-MOSFETs technology. Ballistic electron transport with no scattering is also expected. Considering these features, CNT-FETs are expected to be one of the most promising candidates for a future nanoelectronics technology. In order to fully develop the potential of the CNTs, there are several issues which should be addressed such as controlling of CNT position, chirality, polarity of the channel and doping. In this talk, we will present recent results on the position-controlled CNT-FETs and discuss the method to control the electrical properties of the CNT channel.

CNT FETs were fabricated on a $SiO_2/p^+ - Si$ wafer by using the position-controlled CNT growth technique, in which CNTs were grown on the patterned catalysts [4]. The FETs usually show p-type conduction. A large transconductance of 1 S/mm was obtained even for the device with 5-μm-long gate and 100-nm-thick SiO_2 gate insulator. The FET operation is explained by the Schottky barrier transistor model, in which the drain current is controlled by the modulation of the Schottky barrier at the source and drain contacts by the gate voltage [5, 6]. This is quite different from the conventional FETs, in which the current is controlled by the potential modulation in the channel under the gate. Based on this model, we have realized the n-channel FETs by using the source/drain contact metal with small work function without any impurity doping in the CNT channel [7]. This indicates the tunability of the channel polarity by the contact metal and paves the way to the complementary circuits.

The CNTs can exhibit metallic as well semiconducting characteristics depending on the chirality. It is very important to grow preferentially the semiconducting CNTs. Using plasma enhanced CVD growth, preferential growth of semiconducting CNTs have been confirmed by the measurement of I-V characteristics of the CNT-FETs [8].

Finally, we will discuss the possibility of optoelectronic devices based on the CNT technology. When the CNT-FETs was illuminated, photocurrent increased linearly with increasing the input power. A large dynamic range of 4 orders of magnitude was confirmed [9]. Photoemission modulation has also been confirmed [10]. These results indicate the potentatial of CNT-FETs as optoelectronic devices.

REFERENCES

1. S. Iijima, Nature 354 (1991) 56.
2. V. Perebeinos et al., *Phys. Rev. Lett.* 94 (2005) 86802.
3. A. Javey et al., *Nano Lett.* 4 (2004) 1319.
4. Y. Ohno et al., *Jpn. J. Appl. Phys.* 42 (2003) 4116.
5. S. Heinze et al., *Phys. Rev. Lett.* 89 (2002) 106801.
6. T. Mizutani et al., *Jpn. J. Appl. Phys.* 44 (2005) 1599.
7. Y. Nosho et al., *Appl. Phys. Lett.* 86 (2005) 73105.
8. H. Ohnaka et al., *Jpn. J. Appl. Phys.* 45 (2006), to be published.
9. Y. Ohno et al., *Jpn. J. Appl. Phys.* 44 (2005) 1592.
10. Y. Ohno et al., Nanotechnology 17 (2006) 549.

A Liquid Crystal Beam Former for Two-dimensional Millimeter-Wave Steering

H. Kamoda, T. Kuki, H. Fujikake, and **T. Nomoto**
NHK(Japan Broadcasting Corporation), Japan

A liquid crystal beam former is a device that can electrically steer and/or form a millimeter-wave beam utilizing a feature of liquid crystal (LC).The permittivity of LC can be varied by an applied control voltage, so that the delay time during which a millimeter-wave propagates through the LC can be electrically varied.The liquid crystal beam former we had developed previously was constructed by stacking LC layers and electrodes alternately so as to control the permittivity of each LC layer, and was able to steer in one dimension [1]. This paper presents a new structure and the experimental results for two-dimensional steering.

The structure of the newly fabricated beam former is outlined in Fig.1 (a). An incident wave propagates through the beam former, being affected by a permittivity distribution that can be created across the stacked LC layers by applying control voltages to them through the electrodes. The permittivity distribution along the y-axis is created by adjusting the control voltages layer by layer, as can be done by the conventional beam former [1]. In order to control the permittivity distribution along the x-axis as well as the y-axis, several strips of control electrode run along the z-axis, and each strip is connected to a control voltage source independently, as shown in Fig.1(a).

In the experiment, we firstly measured the phase shift of a 60-GHz wave passing through the LC layers in order to verify the beam steering capability. A maximum phase shift of 330° was observed, which is a reasonable value considering the permittivity variation of the LC. Then, the two-dimensional beam steering capability was examined by measuring the radiation patterns. Fig.1 (b) shows the result of E-plane (yz-plane) steering, indicating successful beam steering up to 10°. In the case of H-plane (xz-plane) steering, which had not been possible using the previous conventional beam former, we applied control voltages strip by strip to the control electrodes, which caused steering of the main beam up to 5°. Fig.1 (c) shows that H-plane steering can be achieved as designed.

Consequently, two-dimensional steering can be performed by the strip-shaped control electrodes to make a two-dimensional permittivity distribution across the aperture of the beam former.

REFERENCES

1. H. Kamoda, T. Kuki, H. Fujikake, and T. Nomoto, "Millimeter-wave beam former using liquid crystal," Proc. 34th European Microwave Conf., Amsterdam, pp. 1141–1144, Oct. 2004.

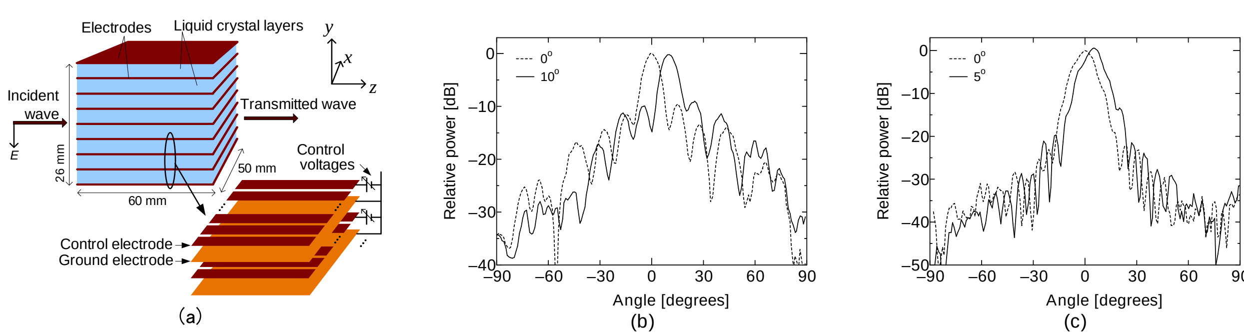

Figure 1: (a) Structure of the liquid crystal beam former. (b) and (c) show the radiation patterns showing E-plane and H-plane steering respectively. They were measured using a pyramidal horn to feed a 60-GHz wave into the LC device. The dotted lines represent the patterns for a 0° main beam. The solid lines represent the patterns for maximum main beam deflection for each plane.

Response Time of Microwave Liquid Crystal Devices

Y. Utsumi and **T. Kamei**

National Defense Academy, Japan

The decay time of a liquid crystal device increses in proportion to the square of the layer thickness, so with a liquid crystal layer (nematic liquid crystal BL011) thickness of about 50mm as used in the configuration of most microwave liquid crystal devices, the decay time (20s) ends up being about 2000 times greater than the rise time (10ms). It is thus hoped that a way can be found to substantially reduce the decay time even if this entails a slight increase in rise time and deterioration of the dielectric properties.

The first promising means of achieving this involves substituting the liquid crystal layer with a so-called polymer dispersed liquid crystal (PDLC) consisting of a polymer (NOA65) dispersed into a nematic liquid crystal (BL011) at a suitable concentration. With a layer thickness of 50μm, an applied voltage of 100V and a polymer concentration of 9wt%(weight percent), we obtained that the decay time (650ms) could be reduced to about 1/30th that (20s) of a plain liquid crystal at the expense of an increase in rise time (28ms) of about 2.8 times and a deterioration of dielectric birefringence $\Delta\varepsilon'$(0.28) of about 50%.

As the second promising method, with the aim of controlling the decay time by a bias field in the same way as the rise time, thereby reducing the decay time, we propose a high-speed variable phase shifter where a coplanar waveguide with a floating electrode (CPW-FE) is filled with a plain liquid crystal (BL006) without rubbing in an effort to control the orientation of the liquid crystal molecules by only changing the direction of the bias field.

Fig.(a) shows the case where the bias field is applied between the CPW center conductor and gland plane, and Fig.(b) shows the case where it is applied between FE and center conductor, the ground plane. By switching between the bias voltage application methods shown in Fig.(a) and (b), it is possible to use bias field in two directions to control the liquid crystal molecules so that they are aligned parallel with or perpendicular to the high-frequency electric field of the CPW device.

In the 18GHz band variable phase shifter we developed, we obtained a rise time of 75ms and a decay time of 200ms with a 500μm wide CPW center conductor, a gap of 20μm between the center conductor and ground plane, and a liquid crystal layer thickness of 50μm. Under these conditions, the birefringence $\Delta\varepsilon'$ of the liquid crystal was 0.23.

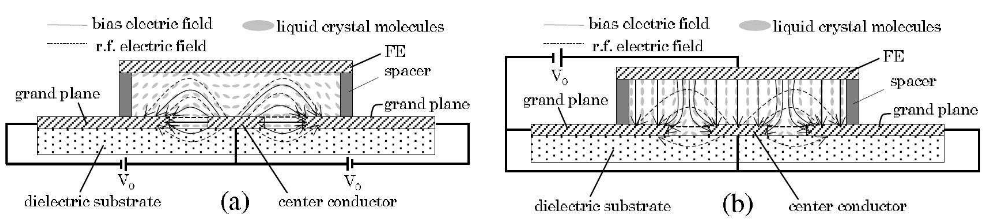

Figure 1: Liquid crystal molecules' alignment in a CPW-FE device.

Microwave Variable Phase Shifter Using Ferroelectric Liquid Crystal

H. Moritake, S. Morita, R. Ozaki, T. Kamei, and **Y. Utsumi**

National Defense Academy, Japan

Microwave tunable components, such as filters and phase shifters, have attracted considerable attention for use in satellite broadband applications. Nematic liquid crystals have already been used to realize microwave phase shifters. On the other hand, ferroelectric liquid crystal possesses spontaneous polarization and has fast switching speed. In this study, we discuss the microwave variable phase shifter fabricated with the ferroelectric liquid crystal material.

Figure 1 shows a schematic of the device construction in microstrip type used in this study. A microstrip line is deposited on a dielectric substrate, and another brass substrate is to enable it to be used as a ground plane. Both surfaces of the glass and brass substrates were coated with polyimide because the initial molecular orientation is parallel to the substrate. The dc voltage was applied to the microstrip line using a function generator and a power amplifier for applying the voltage to the liquid crystal layer.

In the ferroelectric liquid crystal, a helical structure forms in the absence of applied voltage and the helical structure unwinds under application of the voltage higher than a certain voltage The dielectric permittivities perpendicular to the substrate are different in the wound and unwound states. Therefore, the phase delay of the microstrip line changes under applying the dc voltage to the liquid crystal layer. Figure 2 shows the applied voltage dependence of the phase shift in the case of an offset voltage of 20 V. The phase shift increased with the voltage and was saturated above 100 V. This result indicates that the phase shift can be controlled by the application of appropriate voltage. The phase shift response with and without the application of stepwise voltage was measured. The response times depend on the voltage and were less than 30 ms under application of sufficient voltage. In particular, the decay time of this device is much less than that using nematic liquid crystal. The phase shifter fabricated with a coplanar waveguide using ferroelectric liquid crystal is also discussed in this presentation.

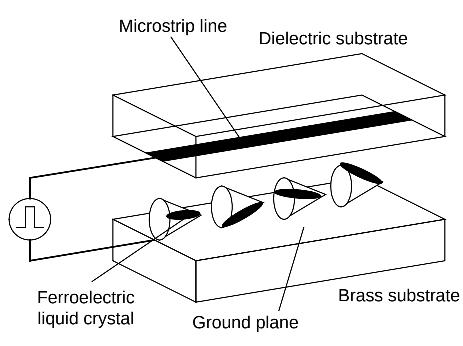

Figure 1: Schematic of microstrip device structure.

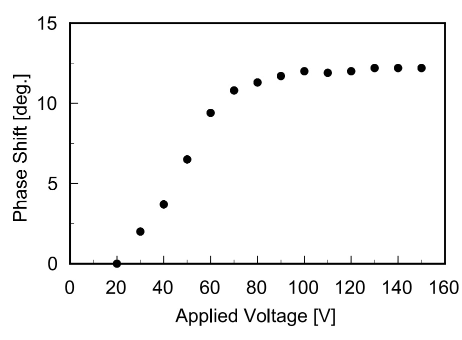

Figure 2: Applied voltage dependence of phase shift in microstrip type device.

Preparation of Aluminum Nitride Thin Films for Film Bulk Acoustic Resonator Devices

K. Nagao, K. Nishimura, and **T. Yamada**
Ube Industries, Ltd., Japan

Film bulk acoustic resonator (FBAR) devices are appropriate for mobile communication systems operating at high frequencies between 1-10 GHz. Aluminum nitride (AlN) has been studied as piezoelectric thin film material used for FBAR devices because of their low acoustic loss, high ultrasonic velocity and fairly large piezoelectric coupling constant. We have investigated the influence of the electrode materials and the sputtering conditions on the crystal orientation and the internal stress of AlN thin films in order to develop FBAR devices. AlN thin films were prepared on Mo, Mo/Ti, Mo/Au/Ti electrode materials using DC magnetron reactive sputtering method. The crystal orientation of the AlN thin films was evaluated using the full wide at half maximum (FWHM) of the x-ray diffraction (XRD) rocking curves of AlN (002) peaks. The internal stress of the AlN thin films was estimated from the difference of curvature of the substrate induced by the film growth.

All the XRD patterns from the films deposited on these electrodes revealed only hexagonal AlN(002) peak in addition to the peaks caused by electrode materials. However the orientation of the AlN thin films strongly depends on the electrode materials. The FWHM of AlN thin films deposited on Mo, Mo/Ti and Mo/Au/Ti electrodes were 8.1, 4.0 and 2.0 degree, respectively. The FWHM of AlN thin films was strongly dependent on that of Mo(110) peak. The surface roughness of electrode materials decreases as decreasing the FWHM of Mo (110) peak. These results suggest the smooth surface of electrode material is beneficial for highly oriented AlN thin film growth.

A steep transition of internal stress from a tensile state to a compressive state was observed with decreasing the sputtering pressure. This behavior is attributed to the bombardment of the growing layer by energetic plasma species. Stress-free AlN thin films, which was necessary to make FBAR devices, were obtained by controlling the sputtering pressure. In this study, the fabricated FBAR based on AlN thin film deposited on Mo/Au/Ti electrode achieved an effective electro-mechanical coupling constant (keff2) of 5.0% and a quality factor (Q) of 1,090 at a resonant frequency of 1.9GHz.

In addition, the fundamental characteristics of the FBAR duplexer which is under development for the WCDMA handsets will be also presented.

A Broadside-Coupled Interdigital Resonator

I. Awai and **T. Nishimura**
Ryukoku University, Japan

1. Introduction

Artificial dielectrics have a huge equivalent permittivity due to the large displacement of electrons in the constituting metal strips, which contributes to miniaturization of resonators. There are two opposing limits in the construction of resonators , one of which is to decrease the number of metal strips to the limit, two, and the other is to increase it as many as possible. The present resonator is made of two metal strips. We will report on its small size, strong suppression of spurious frequencies and reasonable loss property.

2. Resonant frequency

Expecting use of the LTCC (Low Temperature Cofired Ceramics) technology, the structure of the resonator is basically of shielded stripline as shown in Fig.1. The strong broad-side coupling of two interdigital resonators splits the resonant frequency widely, resulting in a very low first mode and upward-expelled second mode. The resonant frequency varies according to the gap between two metal strips as shown in Fig.2. The narrow gaps would give small resonator size if the resonant frequency is kept constant, and good spurious property at the same time.

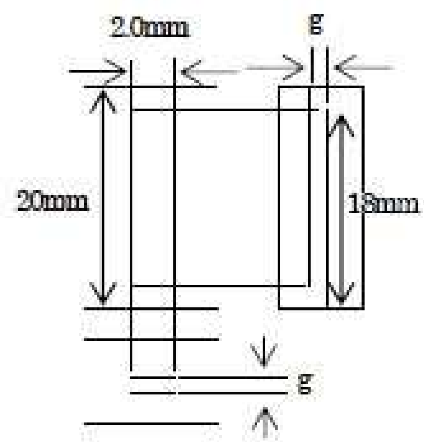

Figure 1: Structure of proposed resonator.

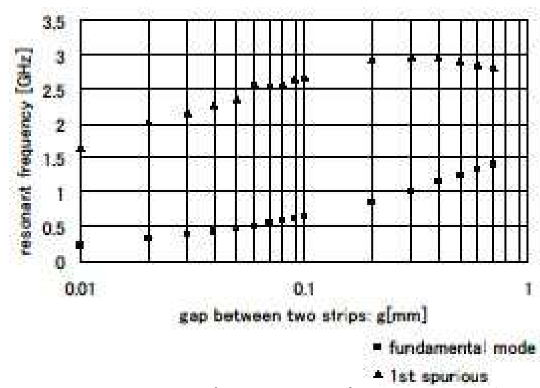

Figure 2: Resonant frequency of 1st and 2nd modes versus gap of metal strips.

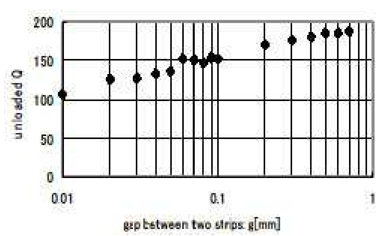

Figure 3: Unloaded Q versus gap of metal strips.

3. Unloaded Q

Conductor loss should increase with a narrower gap between two interdigital metal strips, since the current density on the surfaces facing each other increases. The simulated result is described in Fig.3, which predicts degradation of the unloaded Q (Qu) into 60% for the narrowest case. But the current density could be decreased by wider or thinner metal strips, inducing the recovery of Qu.

4. Conclusion

We have designed a small-sized bandpass filter using the present resonator and prepared to fabricate it with lamination of printed circuit boards. The plating technology we are now training in will finish the fabrication.

Session 4A5
UXO/Landmine Detection

Landmine Detection Radar Using Circular Small Loop Antenna Array

T. Miwa, K. Kimura, and **Y. Yamakoshi**
Gunma University, Japan

1. Introduction

GPR is promising technique to distinguish mines into other reflectors because of high imaging resolution. This paper presents mine detection radar with circularly arraigned small loop antennas. This radar can reduce the signal-to-clutter ratio by optimization of the antenna orientation through FDTD simulation. The validity of this radar is demonstrated by experiments.

2. FDTD simulation

The antenna orientation is important factor to reduce the SCR in this system. The optimum antenna orientation is evaluated by 3D-FDTD simulations considering surface roughness and medium inhomogenety. In the simulation result, the optimum orientation of loop axis is obtained when the loop axis is oriented for around specular reflection points of averaged surface both transmitter and receiver. When the antenna height and separation is 5cm and 15 cm, respectively, the optimum tilt angle is around 45 degree. Moreover, theorthogonal angle combinations between transmitter and receiver axis is almost high SCR. It improves the SCR by more than 5dB comparative to the conventional parallel antenna arrangements. Therefore, we select 1 transmitter and 4 circularly arraigned receiving antenna array system, whose axis have vertical direction and direction to transmitter, respectively.

3. Experimental results

This measurement system is consists of vector network analyzer and RF switching system which are controlled by GPIB through a personal computer. A mock plastic mine (TYPE 72) is buried at 7 cm depth in gravel under rough surface. The antenna separation between each receiver and transmitter is 15cm. The antenna array is scaned over the square region of the side of 40 cm with the interval of 2.5cm. Fig. 1 shows that the imaging results obtained in the frequency range between 1 and 5 GHz. We can find that the surface clutter is significantly reduced. Fig. 2 shows the 3D contour imaging result of metal reflectors such as cylinder 1 (radius=65mm, height= 10mm), cylinder 2 (r=50mm, h=4cm) and rectangle 1 (100mm*5mm). This system can also reconstruct the target shape.

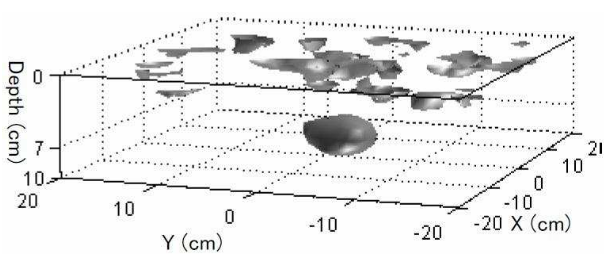

Figure 1: Imaging result of a mock land mine buried at 7cm below rough surface

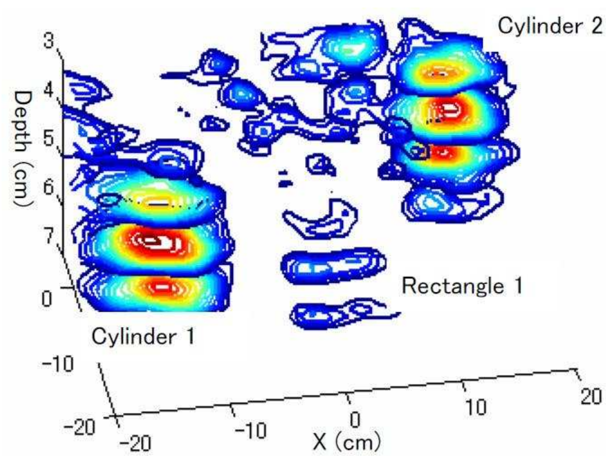

Figure 2: 3D contour image of metal targets.

4. Conclusion

A small loop antenna array based landmine detection radar was developed. This system can reduce the surface clutter by 5dB and also extract the target shape information.

Plastic Landmine Imaging with Integrated Walled LTSA Handset

S. Masuyama and **A. Hirose**
The University of Tokyo, Japan

Ground penetrating radars (GPRs) are expected to become a powerful technique to detect non-metallic landmines. However, it is still difficult to detect plastic landmines because of the low reflectance of plastics and the influence of ground surface. We previously proposed a multiple-frequency radar imaging system using a complex-valued self-organizing map (CSOM) to visualize plastic mines. It observes complex amplitude (amplitude and phase) of the reflection in both the spatial and frequency domains. The three dimensional data (two spatial and one frequency dimensions) are fed to a CSOM so that we obtain a segmented image to indicate landmines. However, our previous system takes long time for observation because a pair of transmitting and receiving antennas is mechanically scanned over the ground surface.

In this paper, we propose and design a wideband and compact walled linearly tapered slot antenna (Walled LTSA) and integrate them. We report that we can find plastic landmines using this hanset with a reduced observation time.

The handset is composed of two parts, namely, integrated antennas and switching circuit which switches transmitting antennas and receiving ones. The integrated antenna is composed of 144Walled-LTSA elements (12×12 in space). The Walled LTSA is an LTSA surronded on its four sides by alminium plates. Intervals of the alminium plate is determined to realize a singe-mode (TE_{10}) operation in the 8-12GHz frequency band. The aperture size of the Walled LTSA is determined to be 14mm $\times$28mm, resulting in the whole aperture size of approximately 18cm$\times$36cm for the 144-integrated antenna. On the other hand, switching circuit is to select one or two antennas as transmitting and/or receiving antenna. Switching circuit is composed of three types of mechanical switches (12pin-type$\times$12, 6pin-type$\times$2 , transfer-type$\times$6), i.e., 20 switches in total.

We observed a plastic landmine using the handset. The depth of the buried landmine is about 1cm. In this experiment, we used a double-ridged horn antenna for transmission while the switched Walled LTSA elements for detection. Through the observation, the transmitting antenna is fixed, and the receiving antenna is switched electrically one by one to take data at 144 spatial points. The handset and the transmitting antenna are faced to the ground at the height of about 30cm. A vector network analyzer (VNA) measures the transmitting coefficient S_{21} from 8 to 12GHz. Then, the obtained multiple-frequency complex amplitude image is segmented by a CSOM .

Fig.1 shows the amplitude, phase and CSOM output images. As we can see from the figure, the landmine part is clearly classified into a single class. Furthermore, measurement time is reduced to 62s for 144 sampling points in space at 51 frequency points. It is approximately 1/10 of the observation time in the previous system in which we scanned a pair of antennas mechanically.

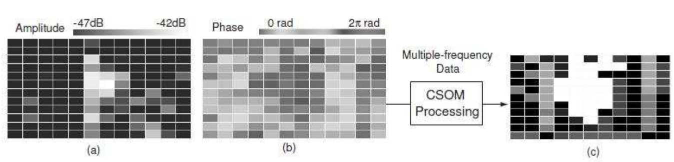

Figure 1: (a)Amplitude, (b)phase, and (c)classification result for the plastic landmine buried in the ground.

Test and Evaluation of Japanese GPR-EMI Dual Sensor Systems at Benkovac Test Site in Croatia

J. Ishikawa and **M. Kiyota**
Japan Science and Technology Agency (JST), Japan
N. Pavković
Development and Training (HCR-CTRO), Japan
K. Furuta
Tokyo Denki University (TDU)/JST, Japan

The objective of Croatia-Japan joint test at Benkovac test site is to evaluate abilities of dual sensor systems compared with existing electromagnetic inductive (EMI) sensors, that is, metal detectors (MDs). The test is designed so as to clear differences between dual sensors and MDs in discriminating landmines from fragments and expanding detectable range in the depth direction, which contribute to increasing probability of detection (PD) and decreasing false alarm rate (FAR). Devices to be evaluated here are 4 prototypes of anti-personnel landmine detection systems using both ground penetrating radar (GPR) and EMI sensor developed under a project of the Japan Science and Technology Agency (JST), the competent authority of which is the Ministry of Education, Culture, Sports, Science and Technology (MEXT).

The developed prototypes make no explicit alarm and the final decision whether or not a shadow in the image is a real landmine is left to operators. This is similar to the way that medical doctors find cancer by reading CT images. Since operators' pre-knowledge of the locations of buried targets significantly influences the test results in these kinds of works, three lanes are designed to be suitable for blind tests. This article presents an experimental design and evaluation results for the project.

Objective of the test and evaluation is to confirm performance of GPR+EMI dual sensor systems in comparison with existing metal detectors (MDs) and to provide reliable data as a basis for future work. By using the data from which general principles can be established on the relative value of different equipment, techniques, the trial aims at clearing differences of performance between dual sensors and MDs, especially in terms of discriminating landmines from fragments and expanding detectable range in the depth direction. Improvement of the performance will contribute to increasing probability of detection (PD) and decreasing false alarm rate (FAR).

Keywords: Test and evaluation, dual sensor system, electromagnetic induction (EMI) sensor, ground penetrating radar (GPR), experimental design.

Remote Sensing of Explosives in a Landmine by Nuclear Quadrupole Resonance

G. Ota, H. Itozaki, J. Barras, and **K. Sakuta**
Osaka University, Japan
M. Tachiki
National Institute of Material Science, Japan

The nuclear quadrupole resonance (NQR) detection is, similar to the nuclear magnetic resonance (NMR), a kind of the resonance technique between radio frequency (RF) wave and the nucleus, and can detect the chemical structure of explosives directly. The advantage of the NQR in the landmine detection is the low rate of misidentification. The NQR detects radio frequency (RF) wave with a specific frequency unique to an explosive material and has a few chance to misidentify different material as an explosives. We confirmed the NQR's detectability of several materials including trinitrotoluene (TNT) and cyclotrimethylenetrinitramine (RDX), which mainly consists of the explosives inside a landmine. Especially, we succeeded the remote detection of RDX from 30cm away.

TNT has a specific problem about the NQR detection. Though the NQR signal of TNT decays in some milliseconds as the directions of the nuclei generating the NQR signal falls apart, each spin doesn't get back to the stable state for some seconds. In this case, the adjustment of the transmitting pulse sequence to regenerate the NQR signal by rephrasing the nucleus during one relaxation period resulted in the drastic reduction of detection time without the decrease of the signal to noise ratio. One of such sequence is called spin locked spin echo (SLSE). We adopted p-nitrotoluene, which has a similar chemical structure and NQR property as TNT, as an alternative and demonstrated the 900 times of improvement of measurement time by using the SLSE sequence.

It is also important for the field operation of a NQR detector to prevent the environmental noise from disturbing the measurement of weak NQR signal. One of the large noise sources is the injection of radio transmission signal including amplitude modulated (AM) wave since the NQR frequencies of explosives lie in the range of 500kHz to 6MHz. We developed the active noise control (ANC) system in AM frequency range to cancel out this injection of radio transmission signal. The ANC system consists of an environmental noise detector, an automatic anti-phase signal generator, and a canceling wave radiator. The canceling wave radiator produces anti-phase wave with the same amplitude and inverted phase against the environmental observed by the noise detector. We reduced AM radio wave up to -40dB by our ANC system in the field test.

We integrated the technologies described into a prototype of an NQR landmine detector and luggage screener to demonstrate the performance of the NQR sensors.

Classification of Mine-Like Objects under Rough Ground Surface Using GPR Data

M. Nishimoto, S. Ueno, K. Nagayoshi, and **Y. Kimura**

Kumamoto University, Japan

Detection and identification of small and shallowly buried landmines is a very challenging problem. Compared with the metal detector that is widely used for landmine detection, a ground penetrating radar (GPR) based approach would appear to offer many advantages, particularly for the detection of plastic landmines with little or no metal content. However, reliability of the GPR system applied to detection and identification of shallowly buried landmines is not sufficient because the GPR also receives returns from other subsurface objects such as rocks, tree roots, or metal fragments in the ground, which yields high levels of false alarms. Accordingly, development of highly reliable algorithms for target detection and identification that are applied to GPR data is highly desired.

In the process of target identification, it is required to discriminate between targets and clutter objects using features extracted from reference data prepared through prior experiments and/or numerical simulations. In general, the selection of the features plays a key part in target classification, because classification performance strongly depends on the features. In this study, we employ a time interval between two pulses reflected from top and bottom sides of mine-like objects as a feature and examine the classification performance. Since the time interval is closely related to the thickness and permittivity of the objects, we can expect that this feature is available and suitable for target classification. Through laboratory experiments and Monte Carlo simulations using data set generated by a two dimensional finite difference time domain (FDTD) method, we show the time interval is a good feature for classifying between the landmines and confusing clutter objects.

Hand-Held GPR MD Sensor System (ALIS) and Its Evaluation Test in Croatia

X. Feng[1,2], **Q. Lu** [1], **T. Kobayashi** [1,3] , **K. Takahashi** [1], and **M. Sato** [1]

[1] Tohoku University, Japan
[2] Jilin University, China
[3] Japan Science and Technology Agency, Japan

Currently for landmine detection, metal detector (MD) is the most popular sensor. Another popular sensor is ground penetrating radar (GPR). Both of the sensors are based on the electromagnetic field.

ALIS (Advanced Landmine Imaging System) is a novel hand-held sensor system combined with MD and GPR and can offer subsurface visualization information, and can show the MD sensor output in real time. The system has a sensor position tracking system that needs only one CCD camera attached on the sensor handle. The GPR of the system is stepped frequency radar system whose RF component is a newly developed compact vector network analyzer.

Based on the diffraction electromagnetic waves of subsurface targets, we combined migration algorithm into GPR system that can improve signal-clutter ratio and can image buried objects clearly. Considering the effects of ground surface and inhomogeneous soil to diffraction field, we optimize the migration aperture based on the comparison between migration trajectory and diffraction surface of the electromagnetic waves. Also we can directly use the migration to do the interpolation for building the grid 3D data set to solve the problem of the random data position that is always a problem for hand-held system to offer visualization information.

Some field test for landmine detection sensors including ALIS had been carried out in 2006 from February to March at Benkovac test site in Croatia. The evaluation tests are organized by the Japan Science and Technology Agency (JST) and the Croatian Mine Action Center - Center for Testing, Development and Training (HCR-CTRO). It is in the frame of the International Test and Evaluation Programme (ITEP) project.

Session 4A6
Basic and Applied Concepts of Electromagnetic Vector Imaging: Polarimetry in Radar and SAR Remote Sensing

Fully Polarimetric L- and X-Band Pi-SAR Observation of Tomakomai Forested Area

Y. Yamaguchi, Y. Yajima, and **H. Yamada**

Nigata University, Japan

A fully polarimetric airborne synthetic aperture radar, named Pi-SAR, had numerous data-take flights over Japan during 1997-2005. The system has a dual-frequency mode (X- and L- band) and has the resolution of 1.5 m and 3 m, respectively. One of the important target areas is Tomakomai, Hokkaido, Japan, because the area is planted forest with pine trees and broad-leaf trees. The temporal data employed here are taken in Aug., Nov., Feb. 2005.

This paper shows the decomposition result of polarimetric SAR image using a four-component decomposition based on covariance matrix[1]. The four components represent surface, double bounce, volume, and helix scattering power. The volume scattering power is mainly caused by oriented dipoles with a best-fit probability distribution function.

It is shown that the volume scattering power dominates other powers in all season in the L band, however, the fraction ratio of the volume scattering power in the X-band changes according to season, i.e., season dependent. This fact seems to be caused by the X-band wavelength and the corresponding polarimetric scattering characteristics by tree canopy. Color compsite image of the decomposed power clearly indicates the change of forest scattering season by season. Therefore, the four-component decomposition of POLSAR image may serve to understand the situation of forest.

REFERENCES

1. Y. Yamaguchi, M. Ishido, T. Moriyama, H. Yamada, "Four-Component Scattering Model for Polarimetric SAR Image Decomposition," *IEEE Trans. Geoscience Remote Sensing*, vol. 43, no.8, pp.1699-1706, Aug. 2005

Polarimetric Analysis of Radar Signature Of A Manmade Structure

J. S. Lee
Naval Research Laboratory, U.S.A.

E. Krogager
Danish Defence Research Establishment, Denmark

W. M. Boerner
UIC-ECE Communications, Sensing and Navigation Laboratory, U.S.A.

Identification of manmade structures from radar images has always been a difficult task, especially for single-polarization radar. Fully polarimetric radar, however, can provide detailed information on scattering mechanisms that could enable the target or the structure to be identified. Complexity remains stemming from overlaps of single bounce scattering, double bounce scattering and triple and higher order bounce scattering from various components of manmade structure that makes physical interpretation a challenge. In this paper, we will present an interesting example using polarimetric SAR data of the Great Belt Bridge, Demark, to illustrate the capability of polarimetric SAR in analyzing radar signatures. Polarimetric target decomposition is used to differentiate the multiple bounce scatterings contained in the polarimetric SAR images. Two C-band Danish EMISAR data takes, the first obtained during the bridge's construction and the second after its completion, are used to extract the scattering characteristics of the bridge deck, bridge cables and supporting structures.

Implementation of Differential Repeat-pass Sar Interferometry For (i) The Search For Earthquake Precursory Land-Cover Deformation In Taiwan In Coordination With The Integrated Search For Taiwanese Earthquake Precursors Istep Taiwanese Program For Promoting Research Excellence; And (ii) The Assessment Of Land-Cover Subsidence By Ground-water Withdrawal And/or Sea-Water Infusion By Coastal Erosion

C. T. Wang
NCU-CSRSR, Taiwan

W. M. Boerner
UIC-ECE Communications, Sensing and Navigation Laboratory, U.S.A.

Worldwide, medium- to short-term earthquake prediction is becoming ever more essential for safeguarding man due to an un-abating population increase, but hitherto there have been no verifiable methods of reliable earthquake prediction developed - except for a few isolated examples of earthquake prediction in China and in Greece. This dilemma is a result of previous and still current approaches to earthquake prediction which are squarely based on the measurement of crustal movements, observable only after a tectonic stress-change discharge (earthquake) has occurred. The prediction models were derived from past histories of measurements, mainly carried out during the past 30 - 40 years, although initiated soon after the San Francisco Earthquake of 1906. During the past decade it was proved and shown that it is not possible to derive reliable models for earthquake predictions from crustal movement measurements alone, and that an entirely new approach must be taken and rigorously pursued over years and decades to come.

In support of this conclusion, there have been reported throughout the history of man anecdotal historical up to scientifically verifiable earthquake precursor or "seismo-genic" signatures of various kind - biological, geological, geo-chemical and especially a rather large plethora of diverse electromagnetic ones on ground, in air and space, denoted as "seismo-electromagnetic" signatures. The existence of all of these signatures can no longer be denied even by the fiercest seismological expert opponents; and it is absolutely high noon that those signatures be more rigorously assessed in order to develop a strategy for designing and carrying out controlled "seismo-genic" and "seismo-electromagnetic" studies on how to set up world-wide a network of measurement sites for conducting a holistic set of measurements for providing an improved understanding on why and how such precursor signatures are generated, and how and where those may best be observed subject to the rather poor signal-to-noise ratio (SNR), requiring much improved digital instrumentation as time goes on due to the ever increasing man-made electromagnetic noise generation.

A number of pilot studies had been initiated, had been supported for a few years, and then aborted because of the high operating costs involved, the poor SNR making signal detection tedious if not impossible with the current state of the art in instrumentation, and because earthquakes don't appear upon demand. For example such major studies as the USGS/NSF NEHER Program of the early 1990's after the Loma Prieta M 7 earthquake of 1987; in Japan the ERSFP after the Kobe Earthquake of 1995; in Greece the ongoing electro-potential methods of Varatsov; in China, and in various regions as well as independent states of the former Soviet Union. There exists a rather large number of fiercely competing groups in Russia coming up with their own diversified yet highly incomplete modeling approaches seeking support from the West for unfortunately all too low-cost scientific mercenary services. No clear picture has evolved and should not be expected; and a much wider internationally coordinated investigation is required, which may well last for several decades before a unified approach and with it a solution to this vital problem may be found - if ever.

In this overview a systematic analysis of main historical records, a summary of pertinent "seimo-genic" as well as observed "seismo-electromagnetic" effects and modern ground-based to air- and space-borne metrological signature investigations are presented. Specifically, remote sensing techniques not yet conceived but in urgent need - such as the remote sensing of the groundwater table - for advancing our understanding of this highly interdisciplinary complicated geophysical problem are being identified, and input is sought from participants for possible active future involvement.

How Infrasonic Imaging And Hf-Othr Technology Can Favorably Be Implemented For Detecting The On-Set Of Tsunamis And The Real-Time Imaging Of Its Spreading

W. M. Boerner
UIC-ECE Communications, Sensing and Navigation Laboratory, U.S.A.

Worldwide, medium - to short-term tsunami prediction is becoming ever more essential for safeguarding man due to an un-abating population increase within low-lying coastal regions. But hitherto there have been no verifiable methods of reliable tsunami prediction developed - except for a few isolated examples of placing arrays of costly short-lived sensors along the ocean bottom. This dilemma is a result of not yet having identified the proper approaches to tsunami prediction.

The question on whether there do exist reliable prediction methods was answered long ago by the fauna living within the coastal littoral zone that are affected by tsunamis. Especially during the last devastating "Boxing Day - 050426 Tsunami" many verifiable episodes on how fish escaped the affected coastal region in time, elephants and other non-domesticated animals rushing for higher ground locations well in time before the tsunami crest approached, and so on provide proof that some electromagnetic or more likely infrasonic local warning signatures are received by these creatures relatively long before the approaching tsunami strikes. We presume that the signatures could be infra-sonic waves traveling at high speeds as under-water surface waves that could be detected by marine fauna as well as coastal animals and birds observing such precursors and acting instinctively without delay. Tsunamis have existed for millions of years and fauna of the affected coastal region has developed instinctive warning mechanisms that we need to explore. One such method, it is here surmised is the role infrasonic signatures must play.

Various infrasonic imaging and wave reception methods will be discussed, and some viable solutions will be proposed for further in-depth consideration.

Whereas such infrasonic signatures may - and may not - explain local hazard warning mechanisms that affected fauna in a long evolutionary process has developed,; those yet unexplained sensor mechanisms are of little relevance for obtaining an overall understanding of the on-set and the rapid spreading of the tsunami across entire oceans and from one into the other, occasionally. Ideally, it would be desirable to have a huge fleet of distributed, equally spaced satellite altimeters roaming over the oceans like the GPS satellites, but that is currently only a dream.

We require a more far-reaching ocean mapping technique which covers the affected wider region of for example the entire Indian Ocean - for now excluding satellite observations - from Sumatra around India to the African Coast from Somali down to the Cap. Such a device exists in principle, and it is based on the high-energy transmission and reception capabilities of the HF-OTHR (High Frequency - Over-The-Horizon-Radar) which makes use of the Ionosphere as a reflector. The HF-OTHR can detect minute disturbances in the atmosphere via troposphere to lower mesosphere but also minute changes of the relative ocean surface height at the order of several centimeters. Although major ionospheric disturbances may impact high resolution ocean surface imaging, it is however possible to detect instantaneously the initiation, the rapid spreading of ocean-height and density changes generated by tsunamis and its impact on close to distant coastal shores.

How such a HF-OTHR wide-area mapping and ocean-surface imaging system can be used, will be demonstrated by examples using open-literature information of the DSTO HF-OTHR at Jindalee near Alice Springs which covers most of the East Indian Ocean and beyond. Thereupon, a proposal is made on the future mission-oriented development of such mega-billion dollar facilities for covering all of the known Oceanic regions that have been affected in the past by tsunamis which are generated by sea-quakes along ocean submerged fault lines. Major attention will be paid to the regularly re-occurring tsunamis within the Indian Ocean, initiated along the outer coastal region of Sumatra, and so on.

Recent Developments of Radar Remote Sensing: Air- and Space-Borne Multimodal SAR Remote Sensing in Forestry and Agriculture, Geology, Geophysics (Volcanology and Tectonology): Advances in P0L-SAR, IN-SAR, POLinSAR and POL-DIFF-IN-SAR Sensing and Imaging with Applications to Environmental and Geodynamic Stress-change Monitoring

W. M. Boerner
UIC-ECE Communications, Sensing and Navigation Laboratory, U.S.A.

Worldwide, medium- to short-term earthquake prediction is becoming ever more essential for safeguarding man due to an un-abating population increase, but hitherto there have been no verifiable methods of reliable earthquake prediction developed - except for a few isolated examples of earthquake prediction in China and in Greece. This dilemma is a result of previous and still current approaches to earthquake prediction which are squarely based on the measurement of crustal movements, observable only after a tectonic stress-change discharge (earthquake) has occurred. The prediction models were derived from past histories of measurements, mainly carried out during the past 30 - 40 years, although initiated soon after the San Francisco Earthquake of 1906. During the past decade it was proved and shown that it is not possible to derive reliable models for earthquake predictions from crustal movement measurements alone, and that an entirely new approach must be taken and rigorously pursued over years and decades to come.

In support of this conclusion, there have been reported throughout the history of man anecdotal historical up to scientifically verifiable earthquake precursor or "seismo-genic" signatures of various kind - biological, geological, geo-chemical and especially a rather large plethora of diverse electromagnetic ones on ground, in air and space, denoted as "seismo-electromagnetic" signatures. The existence of all of these signatures can no longer be denied even by the fiercest seismological expert opponents; and it is absolutely high noon that those signatures be more rigorously assessed in order to develop a strategy for designing and carrying out controlled "seismo-genic" and "seismo-electromagnetic" studies on how to set up world-wide a network of measurement sites for conducting a holistic set of measurements for providing an improved understanding on why and how such precursor signatures are generated, and how and where those may best be observed subject to the rather poor signal-to-noise ratio (SNR), requiring much improved digital instrumentation.

A number of pilot studies had been initiated, had been supported for a few years, and then aborted because of the high operating costs involved, the poor SNR making signal detection tedious if not impossible with the current state of the art in instrumentation, and because earthquakes don't appear upon demand. For example such major studies as the USGS/NSF NEHER Program of the early 1990's after the Loma Prieta M 7 earthquake of 1987; in Japan the ERSFP after the Kobe Earthquake of 1995; in Greece the ongoing electro-potential methods of Varatsov; in China, and in various regions as well as independent states of the former Soviet Union. There exists a rather large number of fiercely competing groups in Russia coming up with their own diversified yet highly incomplete modeling approaches seeking support from the West for unfortunately all too low-cost scientific mercenary services. No clear picture has evolved and should not be expected; and a much wider internationally coordinated investigation is required, which may well last for several decades before a unified approach and with it a solution to this vital problem may be found - if ever.

In this overview a systematic analysis of main historical records, a summary of pertinent "seimo-genic" as well as observed "seismo-electromagnetic" effects and modern ground-based to air- and space-borne metrological signature investigations are presented. Specifically, remote sensing techniques not yet conceived but in urgent need - such as the remote sensing of the groundwater table - for advancing our understanding of this highly interdisciplinary complicated geophysical problem are being identified, and input is sought from participants for possible active future involvement.

Whereas the electromagnetic precursor are observed for earthquakes and volcanic eruptions those seem to be less applicable to the detection of approaching tsunamis, instead HF OTHR radar imaging as well as infrasonic surface pressure imaging seem to provide the most promising method of approach and will be discussed.

Microwave Radiometry Technology for the Nature-Society System Biocomplexity Assessment

V. F. Krapivin and **F. A. Mkrtchyan**

Russian Academy of Sciences, Russia

Biocomplexity refers to phenomena that result from dynamic interactions between the physical, biological and social components of the Nature/ Society System (NSS). The investigations of the processes of interaction between the Society and Biosphere are, as a rule, targeted at understanding and estimating the consequences of such interactions. The reliability and precision of these estimations depend on criteria founded on conclusions, expertise and recommendations. At present, there is no unified methodology for selection between the set of criteria due to the absence of a common science-based approach to the ecological standardization of anthropogenic impacts on the natural environment. After all, the precision of the ecological expertise for the functioning and planning of anthropogenic systems, as well as the representativeness of the global geoinformation monitoring data, depend on these criteria.

We are introducing the scale of biocomplexity ranging from the state where all interactions between the environmental subsystems are broken to the state where they correspond to natural evolution. In this case, we have an integrated indicator of the environmental state including bioavailability, biodiversity and survivability. It reflects the level of all types of interactions among the environmental subsystems. In reality, specific conditions exist where these interactions are changed and transformed. For example, under the biological interaction of the type consumer/producer or competition-for-energy-resources there exists some minimal level of food concentration where contacts between interacting components cease. In the common case, physical, chemical and other types of interactions in the environment depend upon specific critical parameters. Environmental dynamics is regulated by these parameters and the main task is in the parametrical description of it. Biocomplexity reflects these dynamics.

This report is oriented on the development of biocomplexity indeces basing on the remotely measured environmental characteristics. Microwave radiometry is used as effective technique to assess the land cover parameters. Other ranges help to form input information for the NSS Biocomplexity Model that will be developed in the framework of this work.

Keywords: biocomplexity, nature-society system, remote observations, microwave radiometry

An Adaptive Poliarization Optics Technology for Ecological Monitoring of the Aquatic Enviroment

F. A. Mkrtchyan, V. F. Krapivin, V. I. Kovalev,
V. V. Klimov, and **S. P. Golovachev**

Russian Academy of Sciences, Russia

Spectroellipsometry is a peak of polarization optics. The creation of multichannel polarization optical instrumentation and use of spectroellipsometric technology are very important for the real-time ecological control of aquatic environment. Spectroellipsometric devices give us high precision of measurements. Spectroellipsometric multichannel measurements in an aquatic environment provide an information basis for the application of modern algorithms for the recognition and identification of pollutants.

This report is aimed to describe

- A technology of combined use of spectroellipsometry and algorithms of identification and recognition that allowed the creation of a standard integral complex of instrumental, algorithmic, modular and software tools for the collection and processing of data on the aquatic environment quality with forecasting and decision - making functions
- A compact measuring - information multichannel spectroellipsometric system (device) for monitoring the quality of aquatic environment, that is based on the combined use of spectroellipsometry and training, classification, and identification algorithms .

This spectroellipsometric system will differ from modern foreign analogues by the use of a new and very promising method of ellipsometric measurements, an original element base of polarization optics and a complex mathematical approach to estimating the quality of a water object subjected to anthropogenic influence.

Unlike foreign analogues, the system has no rotating polarization elements. This allows one to increase the signal-to-noise ratio and the long-term stability of measurements, to simplify and reduce the price of multichannel spectroellipsometers.

The technology of combined use of spectroellipsometry and the algorithms of detection and classification will allow the creation of an original system of instrumental, algorithmic, modular and software tools for the collection and processing of data on the aquatic environment with forecasting and decision-making functions.

Session 4A7
High Frequency Micromachined Circuits

An Integrated Transmitter Circuits Design for Ultra-Wideband System

T. Y. Tzou and **F. C. Chen**
National Chiao Tung University, Japan

This paper presents a novel integrated transmitter design incorporating a transmit-receive (T/R) switch, a new higher order derivative Gaussian pulse generator and a pulse position modulator (PPM) for use in an impulse radio ultrawideband (IR-UWB) system. A fully integrated UWB transmitter is designed using standard 0.18-um CMOS technology.

Our proposed single chip UWB transmitter can produce the effective higher order pulse shape whose spectrum is occupied under FCC limitation floor, and this pulse can be transmitted without any extra filtering. Our proposed pulse transmitter has two main function blocks: a PPM modulator and a pulse generator. The modulator consists of delay elements and a 4 to1 multiplexer. The time shifted pulse is then selected according to two bits control data by using the 4 to 1 multiplexer. In the input stage, the oscillator has a 2V and pulse repetition frequency of 100MHz (up to 500MHz) sinusoidal wave. The PPM modulator's output signal drives the pulse generator. Then the signal passing through a simple RC differentiator will produce an approximate Gaussian pulse at the rising edge of the square wave. In order to shrink the pulse from nanosecond to picosecond level duration, several inverters are adopted to perform the function of pulse shaping. We employ a PMOS transistor as a common-gate amplifier acting as a differentiator. The monocycle pulse can be obtained by taking the derivative of the previous Gaussian pulse. Then we utilize the third-order RLC differentiator to differentiate the impulse to become a higher order Gaussian pulse in the output stage. Finally the pulse would go through a T/R switch and radiate through an UWB antenna. The T/R switch is a key building block of a transceiverfs front end for time-division duplexing communications. Our switch is a single-pole doublethrow (SPDT) architecture with the body-floating technique which improves the insertion loss and increases the power handling capability. Additionally, the developed switch exhibits low insertion loss, high isolation and good linearity with operating bandwidth needed for UWB applications. The simulation results show that the output waveform indeed complies with FCC indoor mask without any filtering and has a bandwidth from 3.1GHz to 10.6GHz, demonstrating the transmitterfs function work. Furthermore all circuits are ready to be integrated with the other components to form an on-chip transceiver for low cost, low power, and system integration potential with other digital circuits. The detail simulation results will be presented in this talk.

Wideband Diode Linearizer for RF Amplifier with Adaptive Bias Stabilization

K. W. Lau, Q. Xue, and **C. H. Chan**
City University of Hong Kong, China

Due to the popularity of wireless communications, a reconfigurable/multi-band module is being aroused. Power amplifiers, which possess inherently nonlinear characteristics, are the indispensable components. It is well-known that there is always an approximately inverse relationship between efficiency and linearity. The price paid for higher efficiency is that serious nonlinearity causes both out-of-band emissions and in-band distortions. Intermodulation products not only interfere the adjacent channel users, but also degrade the signal-to-noise ratio. Therefore, linearization of amplifier has been intensively investigated for past few decades. Most approaches focus on compensating intermodulated products with identical RF signals but 180 degree out of phase or using an additional nonlinear device to maintain constant impedance at operation frequency. Impedance matching as well as the ability of linearization make those techniques operate in narrow-band applications.

In this paper, we propose a linearizer integrate both suppression of the spectral regrowth and an adaptive current (I_C) with a stable DC bias voltage (V_{BE}) biasing for the BJT amplifiers. The stabilizer utilizes a forward-biased diode in shunt connection with the base-emitter (BE) junction, which is well isolated from RF signals, therefore the amplifying transistor is biased with the same forward-biased voltage of the diode. In addition, the linearizer provides a low impedance return path for the low frequency even-order distortions, and hence, suppressing the intermodulation distortions. Adopting this approach, the amplifier is biased with a nearly constant VBE under small- and large-signal amplification and more than 15dB improvements are achieved for adjacent channel power ratio (ACPR) of WCDMA modulation at 1.9, 2.1 and 2.4GHz. By connecting different resistances in serious with the diode, the dynamic range of adaptive current can be controlled. With the advantages of low frequency operation, low cost, simple and compact circuitry, this approach is useful for portable devices.

A Microstrip Dual-Band Spiral Filter with Spur-Line Structure and Defected Ground Structure

Z. C. Ker, J. H. Yao, S. Y. Chen, and **C. J. Wang**
Feng-Chia University, Taiwan R. O. C.

A microstrip filter with dual-band frequency response is demonstrated in this paper. A dual-spiral resonator is incorporated with spur-line structures and defected ground structures (DGSs) are etched on the ground plane. The spur-line structures are embedded to improve the skirt effect and the stopband characteristic of the dual-band microstrip bandpass filter such that good frequency selectivity and out-of-band rejection can be achieved. The DGSs have not only the advantage of fast attenuation rate at the edges of the passband, but they also decrease the insertion loss at 5-GHz band. The measured results show the fractional bandwidths of 11.3 % and 8.3 % centered at 3.95 GHz and 4.7 GHz, respectively.

Amplitude Modulation Using Injection Locking Oscillator Under Strong Envelop Variation Injection

C. Thongsopa and **C. Saetiaw**
Suranaree University of Technology, Thailand
A. Intarapanich
National Electronics and Computer Technology Center, Thailand

Injection locking oscillators exhibit some properties which are useful for many applications. Most applications of injection locking oscillator, such as power combining [1] and beam forming [2], utilize the phase variation of oscillator output when the oscillator is in locking condition but the eRect of injected signal amplitude has not been exploited.

In this research, we investigate the eRect of strong amplitude variation of injected signal to the output amplitude of injection locking oscillator and show that amplitude modulation (AM) can be obtained by an injection locking oscillator. We have derived the relationship between injected signal amplitude and output amplitude of the oscillator when it is in locking condition. We have found that the amplitude of oscillator output is directly controlled by the amplitude of the injected signal. To obtain AM signal at the oscillator output, the injected signal envelope must satisfy

$$A_{inj} = [2Qm\omega_s A_{EN}\cos(\omega_s t + \alpha)]/\omega_0 \tag{1}$$

where m is the modulation index, Q is the quality factor of the oscillator, and A_{EN},ω_s,ω_0, and α are amplitude, frequency of injection signal, oscillating frequency and phase of the injected signal envelope respectively.

To verify the result, an active antenna with an injection locking oscillator has been built using a dual gate MESFET from NEC (NE25139) as shown in Fig 1. When a signal, satisfying the condition above, is injected into the 2nd gate of the MESFET, the AM signal is evident at the output , as shown in Fig 2.

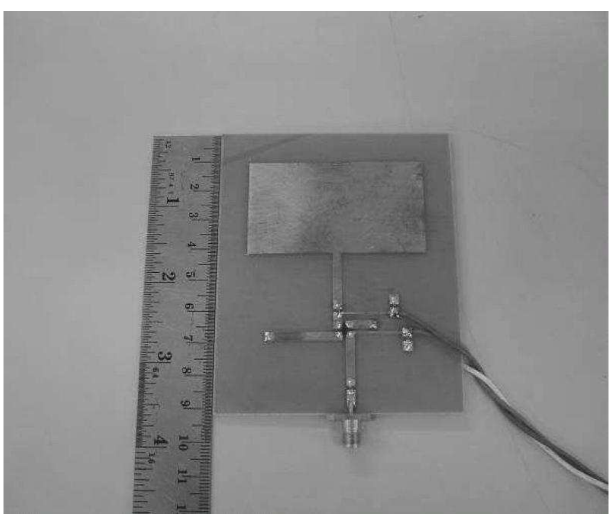

Figure 1: The injection locking oscilla- tor with a patch antenna.

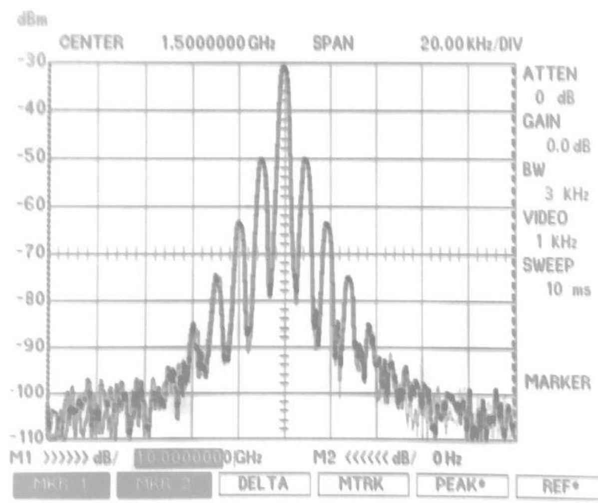

Figure 2: AM signal at the oscillator output.

REFERENCES

1. J. Harvey, E. R. Brown, D. B. Rutledge, and R. A. York, "Spatial power combining for high-power transmitters," *IEEE Microwave Mag., vol.* 1, no. 4, pp. 48-59, Dec. 2000.
2. P. Liao and R. A. York, "A new phase-shifterless beam scanning technique using arrays of couple oscillator," *IEEE Trans. Microwave Thoery and Tech.*, vol. 41, no. 10, pp. 1810-1815, Oct. 1993.

A Broadband Microstrip-to-Coplanar Stripline Transition

C. H. K. Chin, Q. Xue, and **C. H. Chan**
City University of Hong Kong, China

Radio-Frequency (RF) circuitries employing coplanar stripline (CPS) structure, which possesses uniplanar and balanced characteristics, have been becoming a trend for solid-state device integration lately. In most CPS-based circuitry applications, transitions are always required to couple the RF energy from CPS lines to microstrip lines such that CPS measurements can be achieved conveniently with conventional microstrip lines. Several methods of designing microstrip-to-CPS transitions have been proposed. With the aid of the mode-conversion concept [1], a transition with a 3-dB back-to-back insertion loss bandwidth of 49% was introduced. By employing symmetric T-junction [2], a better transition with a 3-dB bandwidth of 68% was developed. Utilizing broadside-coupled strips [3], a wideband design with 1-dB insertion loss bandwidth attained 72% was proposed, however a relatively large structure is required for the transition. Recently, using composite right/left handed transmission line technology [4], a transition with a 3-dB insertion loss bandwidth of 85% was developed. Size reduction was realized in the design, yet the complexity is increased due to the mounting of lumped elements.

In order to deal with the impasse, a via and coupling strips are adopted to provide an easier field transformation from microstrip to CPS so as to obtain a broadband transition with size reduction. To demonstrate the performance of the transition, a balanced and an unbalanced back-to-back structure are fabricated and measured. The proposed microstrip-to-CPS transition attains a 3-dB insertion loss bandwidth of 84% and 85% for the unbalanced type and balanced type back-to-back connection, respectively. The measured 1-dB insertion loss bandwidth for the unbalanced type is 74%, while 79% is achieved for the balanced type. The proposed design can be exploited in feeding antennas and other CPS-based integrations.

REFERENCES

1. N. I. Dib, R. N. Simons and L. P. B. Katehi"New uniplanar transitions for circuit and antenna application," *IEEE Trans. Microwave Theory Tech.*, vol. 43, pp. 2868-2873, Dec. 1995
2. Y. Qian and T. Itoh, "A broadband uniplanar microstrip-to-CPS transition," *Microwave Conf. Proc. APMC* '97, vol. 2, pp. 609-612, 1997.
3. T. Chiu and Y. S. Shen, "A broadband transition between microstrip and coplanar stripline," *IEEE Microwave and Wireless Components Letters*, vol. 13, no. 2 pp. 66-68, Feb. 2003.
4. C. J. Lee, K. M. K. H. Leong and T. Itoh, "Abroadband microstrip-to-CPS transition using composite right/left-handed transmission lines with an antenna application," 2005 *IEEE MTT-S Int. Microwave Symp. Dig.*, June 2003.

Microstrip Ring Resonator Filter Miniaturization Using Vias

M. E. S. Mostafa and **H. B. E. Shaarawy**

Cairo University, Eygpt

Bandpass filters of high performance, compact size, low insertion-loss, sharp rejection, wide-band, and low cost are highly desirable to enhance the overall performance of any communication system. Miniaturization of microstrip filters may be achieved by using many techniques, but very often for specified substrates, a change of geometry of filters is required and therefore numerous new filter configurations become possible. Since microstrip resonator filters have compact size, low radiation loss and they are easily fabricated, they are used in satellites, mobile phones and other wireless communication systems.

In this paper we present a new compact, low insertion-loss, sharp rejection, wideband bandpass filter. This filter may be considered as a modification of a previously published bandpass filter using ring resonators [1] which in turn was developed from a previously published band stop filter [2]. In these papers, the equivalent ring circuit is divided by the input and output ports to form a shunt circuit, the circuit takes into account the mitered bend, the T-junction effect between the feed line and the ring resonator and two orthogonal stubs.

The main approach of this paper is to reduce the filter size while enhancing other filter properties such as insertion-loss, bandpass bandwidth, and keeping constant group delay along the passband.

It was found that for a ring resonator filter with two orthogonal stubs operating at Bluetooth frequency on RT Duroid Teflon 6006, of dielectric constant 6.15, dielectric thickness 0.025 inch and loss tangent 0.0025, the simulated results using the ready-made software package Zeland IE3D show two attenuation poles surrounding the center frequency, forming a wide passband. The complete filter area is 30.67×30.67mm. The filter has a 3-dB fractional bandwidth of 66% starting from 1.6GHz to 3.2GHz, with a center frequency of 2.42GHz and insertion loss of 0.17dB. The filter has very sharp rejection due to the presence of two attenuation poles at 1.55GHz and 3.4GHz of -62dB and -68dB, respectively. The filter also has a very good return loss value.

It was observed that the presence of the two orthogonal stubs increases the size of the filter by about 75%, while the ring resonator only occupies 25% of the total area of the filter. Since our main aim is to reduce the filter size, so, we remove the two orthogonal stubs and replaced them by via holes in certain locations.

A filter was designed, fabricated and measured using two vias of radius 0.25mm. The filter is fabricated on Duroid Teflon 6006, with the same previously mentioned specifications. The filter size is 16.27×16.27mm, which corresponds to size reduction of 71.86%. The filter 3-dB fractional bandwidth has increased to 95.8%, keeping the sharp rejection and enhancing the filter performance. This filter also has a linear phase response along its passband.

In order to study the effect of via's radius on the overall performance of the filter, three different radii (0.15mm, 0.25mm, and 0.4mm) were tested. It was found that the effect of changing the via's radius is very small.

REFERENCES

1. Hsieh, L. H. and Chang, K., "Compact, Low Insertion-Loss, Sharp-Rejection and Wide-Band Microstrip Bandpass Filter", *IEEE Trans. Microwave Theory Tech.*, Vol. MTT-51, April 2003, pp.1241-1246.
2. Chang, K., Microwave Ring Circuits and Antennas. New York: Wiley, 1996.

Session 4P1
Numerical Techniques II

Coupling Characteristics of Optical Fibers with Two Elliptical Cores

K. Kameda and **S. Furukawa**
Sano College, Japan

T. Hinata
Nihon University, Japan

The fiber type devices are utilized in the coherent optical communication system and/or the optical sensor system. The optical fiber with an elliptical core is desirable as a constituent device of the polarization maintaining directional coupler and the mode filter which actively use polarization characteristics. Such devices have been investigated by a manufacturing experimentation and an analysis. As in the design of the fiber type devices with circular cores, the design of the fiber type devices which couple elliptical cores must be exactly analyzed the coupling characteristics. As the analysis method of the fiber type devices with elliptical cores, the perturbation analysis method replacing elliptical cores by rectangular cores, the method based on the mode coupling theory, and the boundary element method is reported. However, there is still room to study for the higher accurate analysis method and the detail of the coupling characteristics.

In this letter, an optical fiber with two elliptical cores (Fig.1) is formulated by IPMM (Improved Point Matching Method) and is discussed for the accuracy of the coupling length and the coupling characteristics in case where the structure parameter is varied. The feature of our IPMM is to be able to analyze the propagation characteristics in high accuracy because electromagnetic fields are completely expanded by the Mathieu functions for all region of two elliptical cores and those common cladding. Therefore, even if two elliptical cores are the strong coupling and/or the large ellipticity, the coupling length of high precision can be calculated.

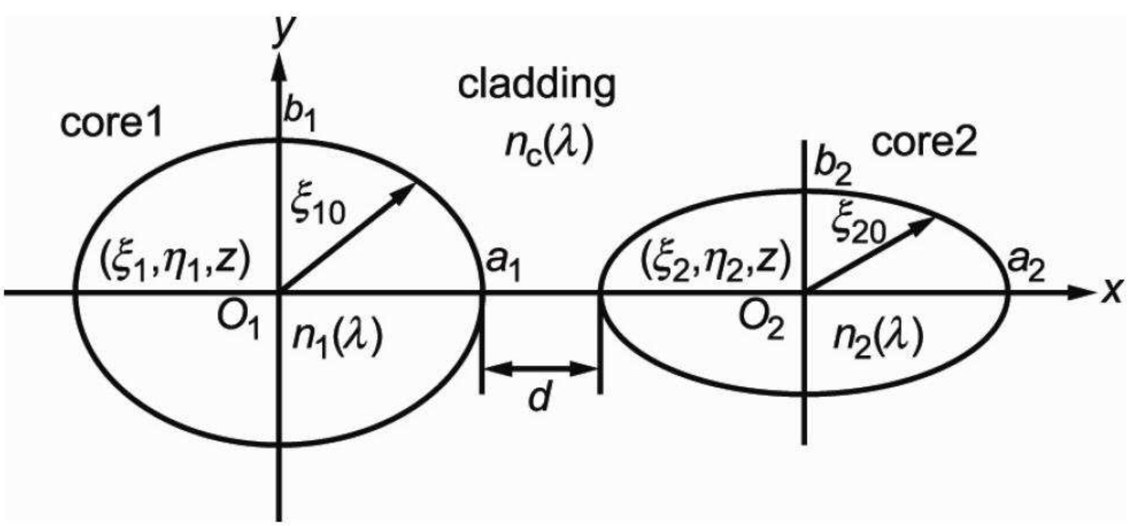

Figure 1: Cross section and coordinate system.

Numerical Analysis of the Pulse Response for an Anisotropic Medium

T. Yamaguchi, T. Yamasaki, and **T. Hinata**
Nihon University, Japan

In the finite-difference time-domain (FDTD) analysis of electromagnetic wave scattering from a linear-passive-anisotropic medium, the following equation of electron motion should be combined with Maxwell's equations.

$$m\frac{d^2\mathbf{u}}{dt^2} + mv\frac{d\mathbf{u}}{dt} + m\omega_0^2\mathbf{u} = e(\boldsymbol{E} + \boldsymbol{B}_0 \times \frac{d\mathbf{u}}{dt}) \tag{1}$$

m: the mass of electron, $\mathbf{u}$: the displacement vector of electron, ν: the collision frequency ($\nu \geq 0$), ω_0: the resonance frequency, e: the charge of electron, $\boldsymbol{B}_0$: the external static magnetic field. For $\boldsymbol{B}_0 = \mathbf{u}_z B_0$ in eq.(1), the constitutive parameter $\bar{\bar{\epsilon}}(s)$ for the complex frequency $s = \sigma + i\omega, \sigma > 0$, are given by

$$\boldsymbol{D}(\boldsymbol{r}, s) = \bar{\bar{\epsilon}}(s)\boldsymbol{D}(\boldsymbol{r}, s), \tag{2}$$

$$\bar{\bar{\epsilon}}(s)/\epsilon_0 = \bar{\bar{\epsilon}}(s) = \begin{pmatrix} \epsilon_{xx} & \epsilon_{xy} & 0 \\ \epsilon_{yx} & \epsilon_{yy} & 0 \\ 0 & 0 & \epsilon_{zz} \end{pmatrix}, \epsilon_{xx} = \epsilon_{xy} = 1 + \frac{(s^2 + s\nu + \omega_0^2)\omega_p^2}{(s^2 + s\nu + \omega_0^2)^2 + s^2\omega_c^2},$$

$$\epsilon_{xy}(s) = -\epsilon_{yx}(s) = \frac{s\omega_p^2\omega_c}{(s^2 + s\nu + \omega_0^2)^2 + s^2\omega_c^2}, \epsilon_{zz}(s) = 1 + \frac{\omega_p^2}{s^2 + s\nu + \omega_0^2}$$

ω_p: the plasma frequency, ω_c: the cyclotron frequency.
To be a passive medium, the matrix $\boldsymbol{W}(\mathrm{s}) = s\bar{\bar{\epsilon}}(s)$ must be a positive-real matrix (PRM). We can prove that the tensor permittivity $\bar{\bar{\epsilon}}(s)$ in eq.(2) is PRM. To simplify the FDTD analysis for the anisotropic medium, $\bar{\bar{\epsilon}}(s)$ is often used as a constant matrix for the incident frequency ($s = i\omega$). For example, substituting $\omega = 2.9 \times 10^{15}$rad/s (wavelength C$\lambda = 650$nm), $\omega_p = 1.5 \times 10^{15}$rad/s, $\omega_c = 3.0 \times 10^{15}$rad/s, and $\omega_0 = \nu = 0$rad/s into eq.(2), then we get $\epsilon_{xx} = \epsilon_{yy} \simeq 4.81$, $\epsilon_{xy} = -\epsilon_{yx} \simeq 0.28i$, and $\epsilon_{zz} \simeq 0.73$. $\bar{\bar{\epsilon}}(s)$ for these parameters satisfies the positive-real property. However, they cannot be implemented directly into the FDTD method since $\bar{\bar{\epsilon}}(s)$ is complex. If the oR-diagonal elements have a real number with the opposite sign, they do not satisfy the positive-real property.

Fig.1 shows the responses of Gaussian pulse incident for the anisotropic medium $\bar{\bar{\epsilon}}_1$ satisfying the positive-real property and $\bar{\bar{\epsilon}}_2$ not satisfying it.

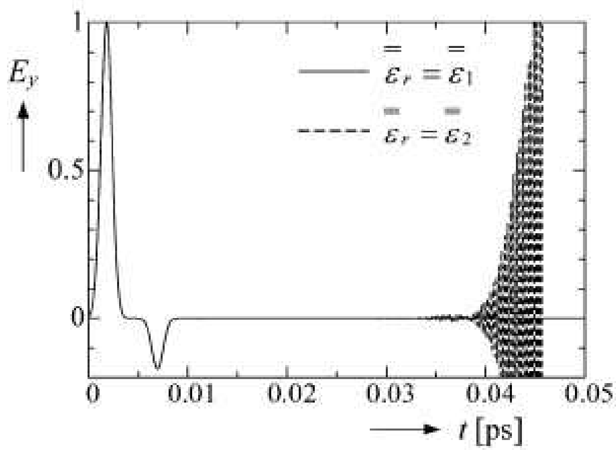

$$\bar{\bar{\epsilon}}_1 = \begin{bmatrix} 2.0 & 0.1 & 0 \\ 0.1 & 2.0 & 0 \\ 0 & 0 & 0 \end{bmatrix} \in \text{PRM}$$

$$\bar{\bar{\epsilon}}_2 = \begin{bmatrix} 2.0 & 0.1 & 0 \\ -0.1 & 2.0 & 0 \\ 0 & 0 & 2.0 \end{bmatrix} \notin \text{PRM}$$

Figure 1: Pulse responses at 800 nmdistance fromthe boundary between free space and the anisotropic medium.

Error Control of the Multilevel Fast Multipole Algorithm

S. Ohnuki
Nihon University, Japan

W. C. Chew
University of Illinois at Urbana-Champaign, U.S.A.

The electromagnetic scattering problem with a large number of unknowns is one of the challenging issues in EM community. Among many proposed algorithms, the multilevel fast multipole algorithm (MLFMA), a hybrid of the fast multipole method and the multilevel multigrid algorithm, is a promising one which can handle over 10 - 20 millions of unknowns.

The error control of MLFMA is important, since three error sources exist in the computational process. The error due to the interpolation/anterpolation and quadrature can be fully controlled because of the bandlimited property of the radiation pattern. The other one arises in the truncation process on which we mainly focus.

In this presentation, we will discuss two essential issues concerning the truncation error of MLFMA. First, the worst-case interaction for the multilevel box implementation will be clarified. This information is crucial in predicting and controlling the error, since the worst-case interaction determines the upper bound. We will show that the computational errors for all the possible interactions are bounded by that for the worst-case interaction in the nearest box pair at the finest level. Secondly, the boundary between the large and small buffer cases will be clarified. The error for large buffer cases is fully controlled by using the conventional selection rules. However, the small buffer cases have a different scenario; the recently developed new approach is needed and the achievable minimum error is subject to the number of buffers. We will show that the new approach is the powerful formula for general element distributions and gives the definition of the boundary between two cases.

Monte Carlo Simulation of Phosphor-Screened Ultraviolet Light in a White Light-Emitting Device

C. Chung Chang and **Chien C. Chang**
Academia Sinica, Taiwan ROC

R. L. Chern
National Taiwan University, Taiwan R.O.C.

We study the optical properties of phosphor-screened ultraviolet light emitted by a quantum well through a chamber. The chamber contains randomly distributed red, blue and green phosphors, and is top-covered with a layer of omnidirectional photonic bandgap material. A Monte Carlo ray tracing method is developed to model the absorption, reflection and transmission for the excited radiation of the ultraviolet light as well as the visible light by the individual phosphor particles. The efficiency of emitting white light by synthesizing the visible light through the top substrate is investigated with respect to the weight ratio, the size of phosphor particles, the dimension of the chamber and the reflectivity of the side wall and the bottom substrate.

The phosphor particles considered here have a radius ranging from $2\mu m$ to $6\mu m$. These are substantially larger than the wavelengths of the visible light, and therefore visible light as well as ultraviolet light can be modelled as rays of photons, each of which carries a photon energy with itself. By tracing a large number of rays of photons, the optical properties of phosphor-screened light can be obtained by counting the number and directions of the photons at the outlet of the chamber. Ray tracing includes free travelling of light, collisions of light photons with phosphors (reflection, transmission, absorption: emission and dissipation), reflection of light by the side wall and bottom substrate, as well as total reflection of ultraviolet light by the top superstrate. All the optical processes are required to follow Snell's law for plane waves incident on a flat surface, while the orientation of each collisional process, scattering direction of emitted light, and the chances of light to be reflected, refracted, transmitted or absorbed, emitted or dissipated are determined by sampling a set of appropriate random numbers.

In previous studies, Monte Carlo ray tracing methods have been developed for calculating the destinations and intensities of luminescent emission in a phosphor screen, modelling the optical properties of fluorescent powders, and investigating the optical emission properties of a fluorescent display. *Unlike these studies which deal with phosphors with fixed positions, the presently proposed Monte Carlo ray tracing method is mainly developed for randomly distributed phosphor particles, which means that the size, location, density, and even the shape of the phosphors can be arbitrarily distributed.*

Numerical Study on Waves from Particles Composed of Bunches of Helices

M. Asai
Kinki University, Japan

J. Yamakita
Okayama Prefectural University, Japan

Artificially-constructed materials such as chiral media composed of electrically small conducting helices as the analogues of chiral molecules [1] and double negative materials made of e.g. thin metallic wires with resonant metallic rings [2] etc. have been of interest in recent years. In theoretical research work, they have been considered not only as continuum characterized by constitutive equations but also as aggregations of particles with structural parameters. Considering the particles' structures helps to design the particles and the mixing conditions and to explain detailed phenomena. As for the chiral media, the method of determination of effective medium constants based on the structural parameters of inclusions and mixing mannar such as quasi-static approach e.g. Maxwell-Garnett method [3], methods of calculation of polarizability of inclusions by thin-wire moment method (MoM) [4] and scattering cross sections [5], a method based on wave equations for randomly-distributed particles [6], methods of inverse scattering [7] etc. have been reported. Direct analyses of the whole structures made of hundreds of helices have also been tried [8]. Such brute force approach also would help to a certain extent to know phenomena of the real structures which experimental measurements hardly give, although the whole physical dimensions and numbers of particles are limited to some extent because of the tough requirements of computer resources. Researchers on carbon microcoils (CMC) have been interested in such media because of the fine absorption properties of CMC at frequencies of tens through hundreds GHz [9]. The bulk of CMC synthesized for a large amount is usually composed of racemic mixture of coils and in experiments of absorption they are often embedded into polymetylmetacrylate(PMMA) beads or PMMA foams where CMC is distributed in the forms of particles made of bunches of coils. In this work, thin-wire MoM is used to analyze electromagnetic waves scattered from a particle composed of a bunch of conducting helices in free space to predict the characteristics of media realized by distribution of the particles, where the effective medium constants are determined from the scattering cross sections [5].

REFERENCES

1. I. V. Lindell, A. H. Sihvola, S. A. Tretyakov and A. J. Viitanen, "Electromagnetic Waves in Chiral and Bi-Media", Artech House (1994) pp. 1-18, 193-243.
2. *IEEE Trans. Antennas Propag., Special Issue on Metamaterials*, **51** [10] (2003).
3. A. H. Sihvola and I. V. Lindell, *J. Electro. Waves and Applic.*, **6** [5/6] (1992).
4. C. R. Brewitt-Taylor, P. G. Lederer F. C. Smith and S. Haq, *IEEE Trans. Antennas Propag.*, **47** [4] (1999).
5. F. Guerin, P. Bannelier, M. Labeyrie, J. Ganne and P. Guillon, *J. Phys. D*, **28** (1995).
6. Y. Nanbu, T. Matsuoka and M. Tateiba, *IEEJ Trans. FM*, **123** [3] (2003).
7. K. W. Whites, *IEEE Trans. Antennas Propag.*, **43** [4] pp. 376-384 (1995).
8. M. Asai, J. Yamakita, *IEEJ Technical Meeting on EMT*, **EMT-04-119** (2004).
9. S. Motojima, Y. Noda and S. Hoshiya, *J. Appl. Phys*, **94** (2003).

Combined RWG-Orthogonal Polynomial Expansion for MoM Analysis of Patch Antenna on Finite Dielectric Substrate

A. Saeedfar, H. Sato, and **K. Sawaya**
Tohoku University, Japan

The calculation of the electromagnetic scattering from arbitrarily shaped three-dimensional dielectric bodies has been of considerable current interest owing to the wide range of applications such as analysis of printed antennas on finite size substrate dielectric materials. In this article, an integral approach with a new solution method is used by MoM to obtain coupled currents inside a dielectric body and on the surface of a patch antenna, which are required for computation of antenna and field parameters. For this purpose, a coupled tensor-volume/surface integral equations is employed to obtain the polarization current inside the dielectric and the surface current on the patch antenna. For the tensor-volume integral equation, we use a mixed-domain expansion using Legendre polynomial basis function and cubic modeling. In mixed-domain MoM, a combination of entire-domain and subdomain basis functions, including three-dimensional modified Legnedre polynomial basis functions with different degrees is utilized for field expansion inside dielectric bodies. This hybrid formulation bridges the limitations of entire-domain and subdomain expansions in some problems and combines the geometric flexibility inherent in subdomain expansion with computational efficiencies of entiredomain formulation. In mixed-domain expansion method, we use polynomials with higher degree for some macro-blocks located in the internal part of the dielectric object and polynomials with lower degrees (pulse function as a special case), which behave as subdomain basis function are used for smaller blocks at corners and boundaries of the dielectric body. Also, the analytical nature of the polynomial functions improves the field representation in near field problems due to the non-uniform behavior of fields in this case. Furthermore, we use a modified Legendre polynomial basis function, which leads to a semi-orthogonal expansion of the unknown polarization current inside the dielectric body. This basis function is derived from the orthogonal Legendre polynomial, which is modified to impose the continuity condition of the currents between neighboring elements in sub-sectioning procedure of MoM. This allows the use of high-order basis functions without introducing ill-conditioning of the resulting MoM matrix. We have already examined the accuracy of this method for far filed scattering problems and in the case of thin-wire antenna in close proximity of a three-dimensional dielectric body in [1]-[4] and here, we apply it for the case of patch antenna on a finite substrate. For current modeling on the patch antenna, we apply Rao-Wilton-Glisson (RWG) basis function and calculate its coupling with volume blocks through the Galerkinfs method. Accuracy and efficiency of the proposed method is confirmed by comparing it with different methods such as conventional MoM, point matching method and FDTD method.

REFERENCES

1. A.Saeedfar, K.Sawaya,, hAccuracy Improvement in Moment Method Solutions of the Tensor-Volume Integral Equation for Three-Dimensional Dielectric Scatterersh, Proceedings of the tenth International Symposium on Antennas and Propagation (ISAP f05), August 2005, Seoul, Korea
2. A.Saeedfar, K.Sawaya, hMixed-Domain Moment Method Solution of the Tensor-Volume Integral Equation for Three-Dimensional Dielectric Scatterersh, Proceedings of the International Conference on Electromagnetics in Advanced Applications (ICEAA05), September 2005, Torino, Italy
3. Amin Saeedfar, Kunio Sawaya, h Mixed-Domain Galerkinfs Method for Tensor-Volume Integral Equation Using Legendre Polynomial Expansion and Efficient Numerical Integrationh, submitted to the 2006 IEEE AP-S /URSI Symposium[4].Amin Saeedfar, Hiroyasu Sato, and Kunio Sawaya, hNumerical and Experimental Impedance Analyses of a Thin-Wire Antenna in the Presence of a High-Permittivity 3D Dielectric Bodyh, submitted to the 2006 IEEE AP-S /URSI Symposium.

Hybrid Numerical Simulation of Electrostatic Force Microscopes in 3D

U. B. Bala, M. Greiff, and **W. Mathis**
University of Hannover, Germany

For modeling and simulating micro-electro-mechanical systems (MEMS), multi physics aspects must be taken into consideration. From the numerical point of view additional problems arise since frequently we are confronted with multi-scale problems. Therefore advanced numerical methods have to be applied. At the same time the coupled mechanical and electrical behavior have to be taken into account. This can be achieved by dividing the model into an electrical part and a mechanical part. The interaction between them can conveniently be realized by using a staggered simulation approach. An interesting example of MEMS is the so-called electrostatic force microscope (EFM) which can be used for scanning samples with nearly atomic resolution. An EFM is used to scan surfaces holding an electric potential or a charge distribution. In the present model a more detailed description is given on the electrical part.

For developing a model of the EFM diRerent eRects have to be considered. For example long distance interaction, charge distribution and non-linearity of the material properties, singularity etc. In order to take into consideration these eRects the simulation region is divided into three regions as shown in Fig. 1. As high values of the electric field will occur at the pick of the tip, a special numerical method is needed to calculate these electric field more eRectively. For this reason an augmented FEM method will be applied to region 1. Since charge distribution and nonlinearities of the dielectric properties may have to be considerd, a versatile numerical method such as finite element method (FEM) should be applied to region 2. As boundary element method (BEM) works well when the boundary is infinite or semi-infinite, the large distance interaction between the tip and the cantilever can be conveniently treated by using BEM in the region 3. Later all these three numerical methods will be coupled with each other.

In this paper a coupled simulation will be presented in 3D. A typical potential distribution in the cut plane through the middle of the cantiliver is shown in Fig. 2 and the high value of the electric field at the pick of the tip is shown in Fig. 3. In the present paper a detailed description is given on the 3D coupling methods together with several simulation results of the EFM.

Since the scanning process of EFM is dynamic, one has to deal with a moving sample and moving boundaries. As a result the mesh has to be updated at each time step. This can be done by recalling the mesh generator at each time step. But this is a time consuming process. The approach presented here is based on an arbitrary Lagrangian Eulerian (ALE) algorithm in 3D. In this work the mesh is modeled as massless elastic which is deformed by the cantilever and the sample. Since there is no time derivative in the governing equation, no modification is needed and the ALE is reduced to a mesh updating met

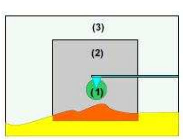

Figure 1: 2D EFM model

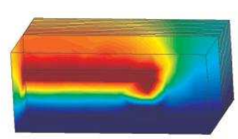

Figure 2: Potential distribution

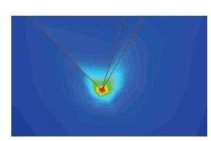

Figure 3: Electric field distribution

Pulse Propagation Characteristics of Multilayer Printed Circuit with Via Structures

D. Kobayashi [1], **S. Furukawa** [2], and **T. Hinata** [1]

[1]Nihon University, Japan
[2]Sano College, Japan

This article presents the pulse propagation characteristics through the via structures(via, pad, and clearance hole as shown in Fig.1) by using the FDTD method. We investigated the size of the via structures so as to maximize the peak value of pulse responses for the Gaussian pulse incident with the pulse-width from 0.2 ps to 20.0ps. We showed that the pulse width is limited by the radius of via and the radius of pad. Numerical accuracy is investigated from the points of the sell size, the terminal conditions of microstrip line, and the distance between the exciting point (OP-1 in Fig.1) and PML.

The peak value of responses becomes smaller as the pulse width is reduced. When the via radius avia is enlarged, the peak value becomes smaller. For example, if the normalized peak value of the response is demanded more than 0.5, the pulse width should be assumed larger than 2.0ps for avia=15m.

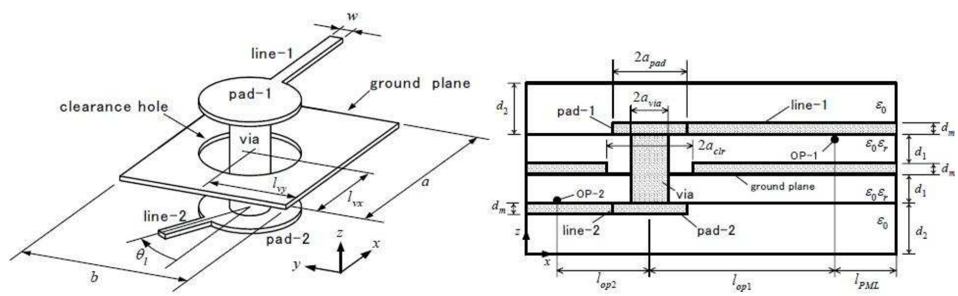

Figure 1: Configuration of a multilayer circuit board with via structures and microstrip lines.

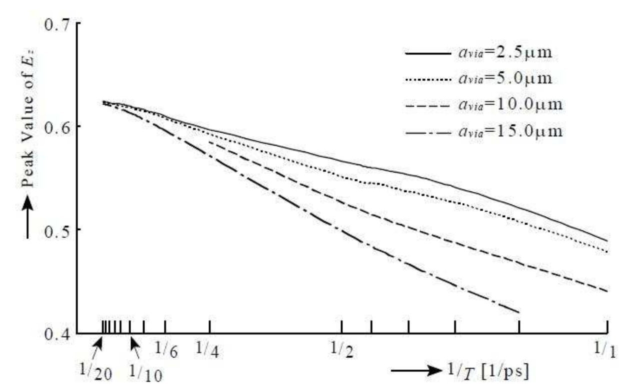

Figure 2: Normalized peak values of pulse response at OP-2 versus the inverse of the pulse width T when the via radius. avia is changed from 2.5μm to 15.0μm(θ_l=90deg., a_{pad}= a_{clr}= 30μm)

Electromagnetic Scattering from Polygonal Geometry

S. Ohnuki, N. Ohtaka, and **T. Hinata**

Nihon University, Japan

Analysis of electromagnetic scattering plays an important role in target identification and radar cross section reduction. Among many types of targets, polygonal geometry can be considered as one of the canonical structures to study the scattering mechanism which involves the edge diffraction, coupling, and resonance.

The authors have developed a numerical technique called the point matching method (PMM) which can be widely applied for electromagnetic scattering and propagation problems. The method is based on a kind of mode matching technique for which the whole physical space is divided into sub-regions. The electromagnetic field in each sub-region can be expanded by using the separation-of-variables solution of wave equation in the local coordinate system. Therefore, the computational results are very accurate and considered as reference solutions.

In this presentation, a unique field decomposition is introduced for various polygonal geometries. We perform the convergence test for varying the truncation mode number and show that the relative error can be controlled under 10^{-8}. The bistatic RCS is investigated in terms of target identification. Compared with the RCS of two scatterers which have the same geometry in the illuminated region, we will clarify the contribution of the geometry in the shadow region to the scattered wave in the far field.

Spectral-Element Discontinuous Galerkin Methods for Waveguiding Structures

M. Min
Argonne National Laboratory, U.S.A.

We will present a higher-order numerical technique with phase-preserving nature. This method is based on multidomain body-conforming spectral-element discretization approach, and we use exponential integrators for time integration. Within this regime boundary and interface conditions are imposed weakly through penalty terms with numerical fluxes. We will show exponential convergence in both space and time without stair-stepping phenomena for the problems with sharp discontinuities along the surfaces between different media.

Numerical simulations of light propagating through photonic band gap structures and interacting with metallic nanoparticles will be demonstarated.

Computational performance for three dimensional structures and practical implementation will be discussed provided with comparison to lower order FDTD methods.

Energy and Signal Indices of a Negative Index Medium

H. Hosono and **T. Hosono**

Nihon University, Japan

The energy index of Lorentz medium was defined by Brillouin. However, so far we have no such definition for non-Lorentzian media. In this report we give the energy index of a negative index medium, and show that it is equall to the inverse signal velocity. We assume the following permittivity ϵ and permeability μ:

$$\epsilon(s) = \mu(s) = 1 + 2/(s^2 + 0.25s + 1)) \tag{1}$$

where $s := i\omega$ is the imaginary frequency.

Let us consider a unit-step-modulated sine-wave of frequency ω_c propagating in the z-direction:

$$E(s) = \omega_c/(s^2 + \omega_c^2)e^{st - sn(s)z} \tag{2}$$

where

$$n(s) := \sqrt{\epsilon(s)\mu(s)} = 1 + 2/(s^2 + 0.25s + 1)$$

is the complex refraction index.

Then the energy index (inverse velocity) is given by

$$n_e = \bar{U}/\bar{S} = 1 + |2(1 - s^2)/(s^2 + 0.25s + 1)^2| \tag{3}$$

where $\bar{U}$ is the mean energy density, and $\bar{S}$ the mean energy flow density.

If $[z, t_s]$ is the space-time at which the frequency ω_c arrives, then the main-signal velocity is defined by z/t_s.

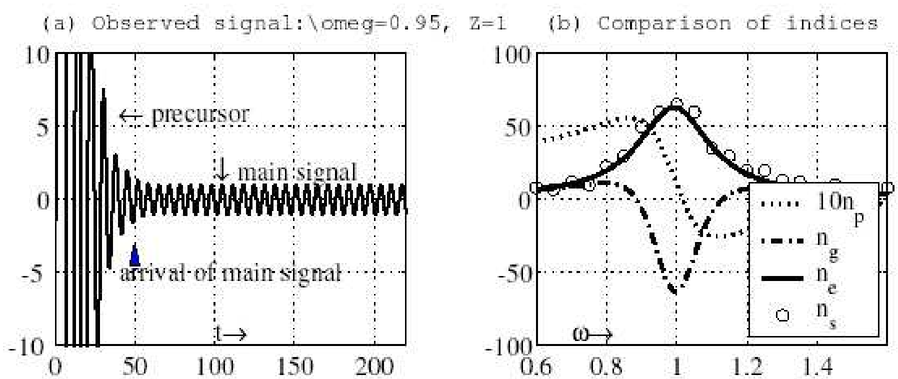

Figure 1: Main-signal velocity is equal to the energy velocity

Fig.1(a) is an example of signal with $\omega_c = 0.95$ observed at $z = 1$. The arrival time $t_s = 50$ and the distance $z = 1$ give the main-signal velocity $V_s = 1/50$ or the index $n_s = 50$.

By carrying out similar processes for various carrier frequencies, we obtain Fig.1(b). This clearly shows that the signal index is equal to the energy index, not to the group index $n_g := \Re[d(sn(s)/ds]$ or the refractive (phase) index $n_p := \Re[n(s)]$ which takes negative values over $1 < \omega < 1.6$.

Ray-Tracing Acceleration Techniques to Compute Diffraction and Double and Triple Effects in Rcs Prediction Methods Based on Physical Optics

L. Lozano, F. S. de Adana, and **M. F. Catedra**
Universidad de Alcalá, Spain

Several improvements in ray-tracing acceleration techniques to compute the diffraction, double and triple effects in the RCS (Radar Cross Section) prediction using Physical Optics (PO) based methods are presented. The approach reduces considerably the CPU time requirements without an important increase of the memory resources necessary. The approach is based on the application of Angular Z-Buffer (AZB) algorithm together with the SVP algorithm (Space Volumetric Partitioning), for electrically large and complex bodies modeled by a high number of flat and/or curved surfaces. Once the surfaces have been stored in the appropriate AZB and SVP matrices, the process to obtain the RCS is as follows:

1. The procedure starts taken a voxel of the SVP matrix of the geometrical model.

Given a direction of RCS analysis, the surfaces candidates to contribute to each effect are selected. The selection is made considering the matrices associated to the AZB anxel where is located of the direction under study. These surfaces are called active surfaces.

3. For each one of the active surfaces it is found the potential surfaces that can shadow the active surface in the observation direction. The surfaces that potentially can shadow the active surface are all those that are contained in the SVP matrices of the voxels that are cut by the incident ray.

4. The process will end when the active surface is shadowed, in other case its contribution to the RCS is computed.

5. The steps 2-4 are performed for all the active surfaces.

6. The steps 1-6 are repeated for all directions in which the RCS should be computed.

The methodology explained above is repeated for each voxel in which the total space has been divided.

The new technique developed presents a great advance computing the RCS of complex targets modeled using parametric surfaces. The CPU-time is reduced with this approach because the AZB algorithm selects the potential contributor surfaces. And the computer memory required is reduced because the SVP algorithm splits gthe greath problem in smaller problems. Several examples will be included in the paper to probe the considerable reduction of computation time obtained from the application of this method.

Session 4P2
Electromagnetic Modeling and Inversion and Applications

Microwave Surface Impedance of a Nearly Ferroelectric Superconductor

C. J. Wu and **C. M. Fu**

National University of Kaohsiung, Taiwan

The microwave surface impedances of a nearly ferroelectric superconductor (NFE-SC) in the dielectric-like response are calculated based on the electrodynamics of a nearly ferroelectric superconductor. Surface impedances for two model structures are calculated. Firstly, the intrinsic surface impedance for a bulk material such as a structure of a semi-infinite superconductor is calculated. The calculated frequency-dependent surface resistance decreases with increasing frequency. Secondly, we calculated the intrinsic surface impedance for a superconducting thin film of a finite thickness. It is found that the frequency-dependent surface resistance is strongly dependent on the film's thickness. It is seen a comb-like shape in the surface resistance for a film with thickness being equal to $10\lambda_L$, where λ_L is the London penetration length. However, the comb-like behavior is strongly suppressed when the thickness of film is lowered to.

Calculations of Optical Properties of an Annular Dielectric Mirror

C. J. Wu and **S. Gwo**

National University of Kaohsiung, Taiwan

In this work we theoretically study the optical properties of the annular dielectric mirrors. Optical wave properties are investigated from the reflection response calculated based on the transfer matrix method in cylindrical coordinate. Numerical analyses have been made on the wavelength-dependent reflectance for an InN/Air annular mirror. The results are then compared with those of parallel dielectric mirrors. The dependences of reflection response on the number of periods, azimuth number, initial radius and thickness ratio of bilayer are also illustrated. In addition, we further demonstrate the reflection spectrum for an annular dielectric resonator.

A Model of Porous Medium Magneto-Hydro-Dynamics and Its Inverse Problem

Y. Guo
Chinese Academy of Science and Wuhan Institute for Industrial and Applied Mathematics, China

In this paper, we propose a new model for dynamics of porous solid medium saturated with compressible magneto-fluid, directly coupled the stress, flow and electromagnetic fields, studied their interactions and propagation regularity of waves and proved that there exist various P and S waves, and also their mixture, which generally possess damping and frequency scattering effects. In magnetic (geomagnetic and bio-magnetic etc) field, conductive fluid (seawater, oil and blood etc) flows to induce electric current thus changes the magnetic field; whereas electric current flows in magnetic field producing mechanical force, which influences the deformation of solid skeleton and the fluid, the deformation of solid skeliton and Darcy osmosis in the interstitial passage in true changing the flow of the fluid. After the linearization of the model, the general decompositions of the displacement vectors on solid and flow fields as well as magnetic field are given. In the diphase medium, we have theoretically shown the existence of six types of various forms of waves and their behaviors. The difficulties and abundant anticipated contents of the new model come right from the complicated interactions.

In this paper, some mistakes on magneto-hydrodynamics have been corrected, the (Micro-)Bermuda Effect, the possible mechanism of the luminescence in earthquake and a iterative method for solving its inverse problem of Xie Ganquan Type are presented. Various inverse problems, mathematical research on conservation laws, similarities of the Transmission Wire Theory, concentrations of dynamical stress, nonlinear waves, variational principles and many other inverse problems related to the model will be presented later.

Further study of this model is undoubtedly important in geophysics, oceanography, life science and the science of energy resources.

The Propagation of an Elastic Wave in Half-Infinite Space a in Magnetic Field

H. T. Cai
Central South University, China

In this paper we assume the system of co-ordinates for the half-infinite space and the neighboring vacuum, and make the following assumption:

1. The load on the surface of the half-infinite space depends on the time t only and is independent of x only.
2. The conduction is perfect.
3. $H_2 = H_3 = 0$, $H_1 = H$.
4. $\mu \approx 1$ for the medium in the half-infinite space.
5. Displacement currents are disregarded in the equations of coupled fields for a perfect conductor.
6. Lagrangean co-ordinates are used.

Thus, we will obtain a solution to the elastic one-dimensional problem of the perfectly conducting half-infinite space bordered by a vacuum, assuming the existence of a primary constant magnetic field and any increasing and then decreasing pressure on the surface of the half-infinite space. Solutions of this type will contain a moderate range of mechanical pressures. The problem of high pressures in magnetic fields may be considered on the basis of the theory of plastic gas as a model of a solid body in the range of very high pressures.

Non-Contact Bias Voltage Measurement on Analog Circuits that Uses the Electro-Optic Probing Technique

W. K. Kuo
National Formosa University, Taiwan R.O.C.

The electro-optic (EO) probing technique has many applications, such as characterization of micro-antennas and antenna arrays, verification of electromagnetic compatibility (EMC), and failure diagnosis of microelectronic integrated circuits. Therefore, this technique plays an increasingly important role for the future design and fabrication of high-speed and high-integrated circuits. However, in some practical testing requirement, DC bias voltage also can provide very useful information for fault detection of analog circuits. Therefore, if the EO probing technique can be extended to measure the DC bias voltage, this EO failure diagnosis tool becomes more flexible and powerful. Though a metal probe tip can be used for the DC bias voltage measurement, the metal tip may make indentations on the probe pad or conductor line of microelectronic circuits, which may cause subsequent reliability problems. Besides, the metal probe tip only can contact the pad without passivation on the circuit. The non-contact EO probing is an ideal tool to perform the bias voltage measurement.

We propose a novel method to measure bias voltages on analog circuits by the non-contact EO probing technique. An electro-optic probe tip with a side metal electrode is proposed to perform this measurement. This probe tip can be placed near the edge of the metal line of the circuit under test to sensing the electric field between the side metal electrode and the circuit metal line. This approach makes the measurement system is less sensitive to the probe tip height. For traditional approach, the system is very sensitivity to the height and is less accurate. The static vector electric field distribution sensed by the EO probe tip is simulated by Maxwell 2D simulator. The simulation results are consistent with the real measurement results. Besides, for the proposed system, a low-frequency sine wave signal is used as the power supply of the circuit under test and all bias voltages are modulated at a frequency. The modulated quasi-DC bias voltage on the circuit can be sensed by an EO probe tip using a high sensitivity lock-in amplifier. An example circuit is tested by this method and the resulted voltage error between the measured value and actual value less than 3% is demonstrated.

Markov Skeleton Processes and Their Applications

Z. Hou and **H. T. Cai**
Central South University, China

A stochastic process $X(t)$ is called a Markov skeleton process(MSP) if it has the Markov property on a sequence of stopping times $\tau_n \uparrow \infty$. The usual Markov process, semi-Markov process, deterministic Markov process and semi-regenerative process can be regarded as special cases of MSP. In this paper, first, backward and forward equations with which we can compute one-dimensional distribution is derived, and then formulas to compute finite-dimensional distribution and the existence and computation of limit distribution are also obtained. Based ourselves upon the above the results, we give a tentative study of queueing system, reliability system, and storage system. Transient distribution and formulas to compute limit distribution of the stochastic processes introduced for studying these system are presented in the latter half the paper.

A Power Line Communication (PLC) System

Y. Watanabe
Musashi Institute of Technology, Japan

In this report, we focused attention on a Power Line Communication (PLC) system used the MHz band, and calculated balance-unbalance conversion factor and leaked electric field in the power line with branch in high frequency, such as 2MHz- 30MHz.

In order to understand the characteristics of an actual electric power line, first, we studied very simplified model, and next, we studied a little complex model. To confirm the validity of the calculation, we measured these characteristics of the same model beforehand, and compared the measurement value with the calculation value. In calculation, we used the method of moments that was one of the electromagnetic field analysis methods as the calculation method, and calculated these characteristics. And we calculated both a simple model and a little complex model.

The simplified power line model without the branch is gate form arranged on ground plane, and one of pair line in the model is grounded at far end side of signal impression. In case of the power line with branch, we studied two typical branch models, such as outlet branch model, in which both two lines of the pair line diverge in the same length, and switch branch model, in which only one line of the pair line become long so as to set on a lamp switch. And we assumed the actual power line model, expanded the model to the about one room model based on a simple model as a little complex model.

As a result of the comparison with the measured and calculated values, they are approximated well in balance-unbalance conversion factor, common mode current and leaked electric field. Therefore, it was confirmed that the calculation model using the method of moments was effective to calculate the characteristics of PLC.

3D GL Method for the Electromagnetic Field in the Nanometer Materials

G. Xie, F. Xie, and **J. Li**
GL Geophysical Laboratory, U.S.A.

We proposed Macro . Macro, Macro-Micro, and Micro-Micro approaches to compute the electromagnetic (EM) field in the nanometer materials. In this paper, we propose a 3D GL method for the EM field in the nanometer materials. We account EM field energy, quantum energy in nanometer materials, and interaction energy into Lagrangian density. The Green functions of the Euler equations are constructed. We use 3D GL method to solve the Euler equation. The EM field in the nanometer materials is calculated. Our 3D GL method for EM field in nanometer materials is useful for interpreting the material properties. In our methods, there is no big matrix is needed to solve. There is no any error reflection on the boundary. The EM wave and quantum properties in the materials are presented.

REFERENCES

1. New GL method and its advantages for resolving historical difficulties, 2006, Progress In Electromagnetics Research Symposium 2006, Cambridge, USA March 26-29, P. 306-311

A Filter Analysis for Local Internet System Using SAGILD Modeling

B. H. Xie
New York Industries Inc., U.S.A.
J. Li and **G. Xie**
GL Geophysical Laboratory, U.S.A.

There are random noise in the public electric system and internet system. The noises will contaminate and disturb the local internet system in the office and family, In particular, it converts to unknown virus. We are designing a new filter by using SAGILD modeling to prevent and reduce the random noise. Using SAGILD modeling, we simulate our filter designing schemes. We run SAGILD modeling for the public electric system environment without the filter. Then we simulate our public electric system environment with our filter parameter and configuration The significant difference and main noise sources are found. Our company is close near New York Empire Building. Many traveler customs are visiting to our center to use out internet. The noise and unknown virus are occurring in the peak time. After the filter simulation, we change our new internet parameter configuration. Our internet cafe system become to very smooth, stable, and fast. By using SAGILD modeling, we clearly analyzes the scattering interaction and influence between the global and local internet system. The SAGILD modeling tool helps us to find the main noise and designing the special filter to reduce the noise and obtained very good filtering efficiency. The filter will be useful for wide internet system.

REFERENCES

1. Li, Jianhua, Xie, Ganquan, Xie, L., Xie, F., 2006, New Stochastic AGILD EM modeling and inversion, Progress In Electromagnetic Research Symposium 2006, Cambridge, USA, P.490-494

The 3D AGILD EM-Flow Coupled Modeling

G. Xie, J. Li, and **F. Xie**
GL Geophysical Laboratory, U.S.A.

In this paper, we proposed 3D AGILD Electromagnetic (EM) and flow coupled modeling. We use a strip differential integral equation on the boundary zone and differential equation in the internal domain to construct EM and flow coupled modeling. In our Method, there is no any error boundary reflection error. The coordinate singularity in the =0 is removed. Our method is useful for EM stirring in the steel caster and magnetic dynamic. The simulations show that our 3D AGILD EM-flow coupled modeling is fast and accurate.

REFERENCES

1. Xie, Ganquan, Li, Jianhua, Xie, Feng, 2006 New GL method and its advantages for resolving historical difficulties. PIERS 2006, Cambridge, P 306-311.
2. Xie, Ganquan, Li, Jianhua, Xie, Feng, 2006 2.5D AGILD electromagnetic modeling and inversion. PIERS 2006, Cambridge, P 390-394.
3. Li, Jianhua, Xie, Ganquan, Xie, L. Xie, Feng, 2006 New stochastic AGILD modeling and inversion. 2006, Cambridge, P 490-494
4. Li, Jianhua, Xie, Ganquan, Xie, L. Xie, Feng, 2006 New stochastic AGILD modeling and inversion. 2006, Cambridge, P 490-494

A Metro Carlo AGILD EM Inversion

G. Xie, J. Li, and **F. Xie**
GL Geophysical Laboratory, U.S.A.

In this paper, we present a new Metro Carlo AGILD inversion to recover the random the EM parameter media. We construct Markov chains and quasi Markov chains. By using Metro Carlo AGILD modeling strategy simulation, we can find the conditional probability density distribution. According to the Bayes translate theorem and Markov chain and quasi Markov chain properties, we can find the probability density distribution $\mathrm{P}(\sigma, \epsilon, \mu)$—$(\mathrm{E}(\mathrm{r_d}), \mathrm{H}(\mathrm{r_d}))$. We can find the assemble mean $< \sigma >$, $< \epsilon >$, $< \mu >$ and their correlation covariance, cross covariance images. Our Metro Carlo AGILD Markov simulation is very fast. Our Metro Carlo AGFILD EM inversion has high and reasonable inference resolution. Our Metro Carlo AGFILD EM inversion is useful for material sciences, nanometer materials, surface physics, rough surface, medical sciences, biology, geophysical exploration and finance. Our Metro Carlo AGFILD inversion method can be extended to the seismic, acoustic and their coupled inversion for anisotropic EM, mechanics, thermotics, and quantum random media.. Our new Metro Carlo GL and AGILD inversion algorithm and software are developing.

REFERENCES

1. Li, Jianhua, Xie, Ganquan, Xie, L. Xie, Feng, 2006 New stochastic AGILD modeling and inversion. 2006, Cambridge, P 490-494
2. Xie, Ganquan, Li, Jianhua, Xie, Feng, 2006 New GL method and its advantages for resolving historical difficulties. PIERS 2006, Cambridge, P 306-311
3. Xie, Ganquan, Li, Jianhua, Xie, Feng, 2006 2.5D AGILD electromagnetic modeling and inversion. PIERS 2006, Cambridge, P 390-394.
4. Xie, Ganquan, Li, Jianhua, Li, Jing, Xie, Feng, 2006 3D and 2.5D AGILD EMS stirring modeling in the cylindrical coordinate system

A 3D AGILD Forest Modeling

G. Xie, J. Li, and **F. Xie**
GL Geophysical Laboratory, U.S.A.

In this paper, we proposed a 3D AGILD Forest Modeling. We consider Earrth, Forest, and Air three layered media. The Forest layer include inhomogeneous EM parameters. We use 3D strip EM differential integral equations on the boundary strip zone and Garlekin differential EM equations in the internal domain to construct the 3D AGILD forest modeling. Our 3D AGILD Forest Modeling is useful for the forest exploration.

REFERENCES

1. Xie, Ganquan, Li, Jianhua, Xie, Feng, 2006 New GL method and its advantages for resolving historical difficulties. PIERS 2006, Cambridge, P 306-311.
2. Xie, Ganquan, Li, Jianhua, Xie, Feng, 2006 2.5D AGILD electromagnetic modeling and inversion. PIERS 2006, Cambridge, P 390-394.
3. Li, Jianhua, Xie, Ganquan, Xie, L. Xie, Feng, 2006 New stochastic AGILD modeling and inversion. 2006, Cambridge, P 490-494
4. Xie, Ganquan, Li, Jianhua, Li, Jing, Xie, Feng, 2006 3D and 2.5D AGILD EMS stirring modeling in the cylindrical coordinate system.

Session 4P3
UWB Antennas for Radar and Telecommunication

An Omnidirectional UWB Printed Dipole Antenna with Small Waveform Distortion

M. Ameya, M. Yamamoto, and **T. Nojima**
Hokkaido University, Japan

In impulse-based UWB communications, if correlation detection is used as the demodulation scheme, waveform distortions of transmitted and received pulses caused by antennas induce degradations of the communication performance. In order to avoid these degradations, it is necessary that radiation characteristics of the antenna be constant over the wide frequency range.

In this paper, we propose a novel UWB printed dipole antenna as shown in Fig.1. This antenna has omnidirectional radiation patterns over the frequency range of 3.0 to 10.7 GHz. The realized gain of the antenna is between -1 dBi and 3 dBi in the UWB band of 3.1 to 10.6 GHz. From calculations of cross-correlation between template and received waveforms, it is observed that the waveform distortion caused by this antenna is very small.

Fig.2 shows radiation patterns in the azimuthal plane (xy-plane). For each frequency, an omnidirectional pattern is achieved. The variation of the gain in the xy-plane is less than 6 dB at all frequencies. The correlation coefficient and the received energy are shown in Fig.3. For comparison purposes, the results of a thin printed dipole antenna are also shown in this figure. The proposed antenna has high correlation coefficient of 0.92-0.96 at any direction in the xy-plane. The waveforms of the template pulse and the received pulses are shown in Fig.4. It is clear that the waveform distortion of the received pulse by the proposed antenna is very small.

Based on these results, the proposed antenna can be a suitable candidate for the antenna for impulse-based UWB communication system using correlation detection. This antenna can be very useful because of its omnidirectional radiation patterns, especially in mobile situation.

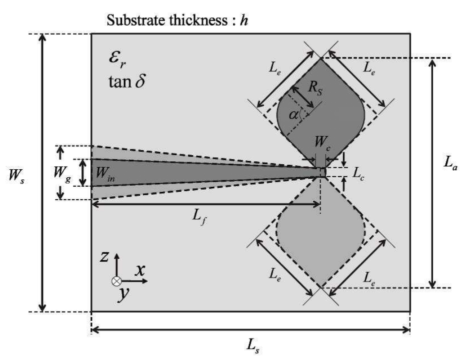

Figure 1: Geometry and coordinate system.

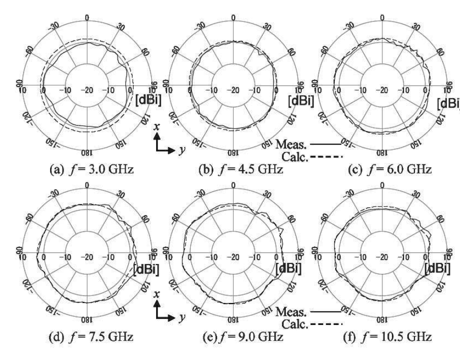

Figure 2: Radiation patterns in xy-plane.

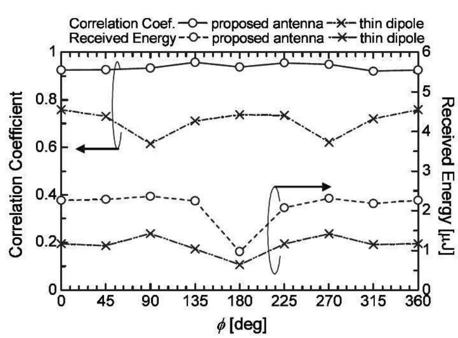

Figure 3: Correlation coefficient and received energy.

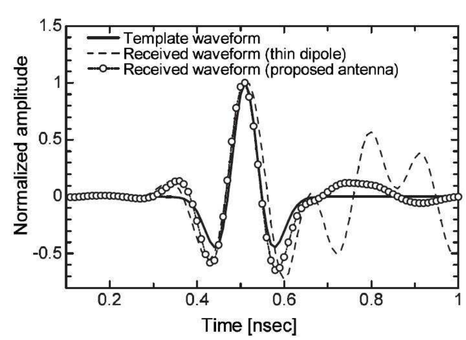

Figure 4: Template pulse waveform and received pulse waveform at $\Phi = 135^o$

Optimization of Conical Helix Antenna Using Particle Swarm Method

A. A. L. Neyestanak
Jahad Daneshgahi, Iran

Earlier work has shown the particle swarm to be a useful choice to more recognized evolutionary algorithms for certain kinds of problems [1, 2]. Furthermore, the PSO algorithm retains the conceptual simplicity of the genetic algorithm while being much easier to realize and apply to design problems with both discrete and continuous design parameters [3].

In this paper, conical helix antenna over ground is optimized using particle swarm optimization (PSO) algorithm. The optimization is used to increase the BW and Gain of the antenna to make it applicable to wireless communication using the MOM analysis. Parameters used for the optimization are the number of turns, turns space and radius of the helix antenna in the top and bottom.

Important objects will be discussed to publicize the person who reads with the fundamental concepts that make the PSO a viable optimization method for antenna optimization problems. The PSO randomly initializes the position and velocity of each particle within the swarm at the beginning of the optimization. Each position corresponds to a possible solution to the problem, and is specified as the matrix where M is the number of particles in the simulation and N is the number of dimensions of the problem. Figure 1 shows a typical Flow chart of the PSO process.

REFERENCES

1. D. Gies and Yahya Rahmat-Samii, "Particle Swarm Optimization for Reconfigurable Phase Differentiated Array Design", *MICROWAVE AND OPTICAL TECHNOLOGY LETTERS*, Vol. 38, No. 3, August 5 2003.
2. M. Clerc and J. Kennedy, The particle swarm: Explosion, stability, and convergence in a multidimensional complex space, *IEEE Trans Evolutionary Computation* 6 (2002), 58-73.
3. J. Robinson and Y. Rahmat-Samii, "Particle Swarm Optimization in Electromagnetics," *IEEE Trans. Antennas Prop.* vol. 52, no. 2, pp. 397-407, Feb. 2004.

Analysis and Optimization of a New Ultra Wide Band Microstrip Antenna

A. A. L. Neyestanak and **S. A. Hosseini**
Islamic Azad University, Branch of Rey, Iran

In this paper a novel design approach of the familiar E-shaped patch antenna is presented [1- 2]. In the presented approach, by using the simulated annealing, some modifications have been implemented to the incorporated slots and feed position, which lead to even more enhancement in the antenna bandwidth. Details of the antenna design approach and experimental results are presented and discussed.

This Antenna has a novel feed structure that eliminates the above limitations of probe-fed E-shaped patch antennas [1]. The feed structure consists of a standard 50-printed microstrip feed line and a metal feed strip that connects the antenna to a microstrip feed line. During the production, the E-shaped patch and the feed strip are cut out of a single sheet of metal, and then the strip is twisted away from the antenna. Finally, the feed strip is connected to the microstrip feed line by connecting or other means. This way, the antenna can be made-up and integrated to the microstrip circuit very easily, at low cost. The feed structure does not add to the height of the antenna because it is located between the ground plane and the E-shaped patch. There is no important weakening in the antenna bandwidth, due to the use of the new feed structure instead of a coaxial probe feed.

Variety of simulated annealing method is proposed to increase the bandwidth as well as to access ultra wideband antennas. Simulated Annealing is resulted from the physical process of annealing metals, in which a metal is heated and then little by little cooled in order to form strong crystalline bonds within the structure [3-4].

Choices of simulated Annealing are proposed in this paper are:
1) Original Simulated Annealing: The original simulated annealing uses a random number generator with a uniform distribution to produce the new configurations (within the step size). 2) Boltzmann Annealing: Boltzmann annealing uses a random number generator with a gaussian distribution. 3) Fast Annealing: In fast annealing the temperature decreases at a quicker rate than the other annealing methods described beyond. 4) Very-Fast Re-Annealing.

Antennas geometry and the VSWR of a wide-band microstrip antenna (optimized by simulated annealing) are presented in Fig. 1. In table 1 a comparison between optimized antenna using simulated annealing and antenna discussed in [1] and measurement result is accessible.

Table 4P3.2: Comparison Results

	S11 Lower Frequency(dB)	S11 Higher Frequency	Fractional bandwidth
Ref[1]	-21 @5.3 (GHz)	-13.5 @5.95 (GHz)	19%
This paper	-27.5 @5.25 (GHz)	-17 @5.90 (GHz)	22.5%
Measurement	-23.5@5.23(GHz)	-15.5 @5.85 (GHz)	21.2%

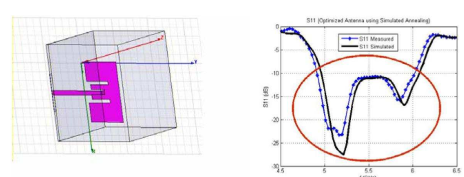

Figure 1: a. Geometry of wide-band microstrip antenna antennas b. VSWR vs. Frequency

REFERENCES

1. Yuehe Ge, Karu P. Esselle, and Trevor S. Bird, gA Broadband E-Shaped Patch Antenna with a Microstrip Compatible Feedh, *MICROWAVE AND OPTICAL TECHNOLOGY LETTERS* / Vol. 42, No. 2, July 20 2004
2. Y. Ge, K.P. Esselle, and T.S. Bird, Broadband E-shaped patch antennas for 5.6-GHz wireless computer networks, 2003 IEEE Antennas Propagat Soc Int Symp 2003, Columbus, OH, pp. 942.945, 2003.
3. Kamal, gA brief note on Simulated Annealingh, http://aurora.physics.uwo.ca/stockwel/sim_ann.html, Aug 2001.
4. Thompson, M., and Fidler, J.K., gFast Antenna tuning using transputer based Simulated Annealingh, *Electronics Letters*, Vol.36, No.7, pp603.605, Mar 2000.

Time Domain Characterization of 1-2 GHz Circular-Ended Bowtie Antenna with Coaxial Balun Using the Normalized Impulse Response

J. Suryana, A. B. Suksmono, Sugihartono, and **A. Kurniawan**
STEI ITB, Indonesia

K. Tanaka and **K. Igarashi**
NICT, Japan

M. Iida
ARIB, Japan

Frequency domain analysis is a powerful and compact tool for characterizing the antenna parameters such as gain, radiation pattern and the impedance as a function of frequency. However, if time or space is a major concern, such as in the GPR application, the time domain analysis would be a very important tool due to their unique capability for determining the echo delay and range profile of target image.

In this paper, we will describe the classical theory of system characterization in time domain, and then also propose the mathematical model for characterizing the 1 - 2 GHz circular-ended Bowtie antenna with simple coaxial balun. From the measurement results, we concluded that the implemented Circuler-ended Bowtie antenna with coaxial balun has good normalized impulse response with very small ringing, so it is suitable for GPR applications.

A Modified UWB Bow-Tie Antenna for Impulse Radio

A. A. Lestari and **A. G. Yarovoy**
Delft University of Technology, The Netherlands
E. T. Rahardjo
University of Indonesia, Indonesia
L. P. Ligthart
Delft University of Technology, The Netherlands

The 3.1 - 10.6 GHz frequency range allocated for UWB radio applications by the FCC in 2002 has attracted much attention in the industry and academia due to the advantages of UWB communication, which include large channel capacity, low spectral density of transmitted power, high immunity against EMI, and fading robustness. One of the realizations of UWB telecommunication is the so-called impulse radio, in which information is sent by transmitting very short EM pulses. Transmission of such pulses requires antennas especially designed for this purpose. This paper presents a UWB antenna especially developed for impulse radio.

The proposed UWB antenna is adopted from an impulse ground penetrating radar (GPR) antenna which operates in the frequency range 0 - 3 GHz. This GPR antenna, which is a modified UWB bow-tie antenna [1], has been scaled down to be suitable for pulse radiation within the 3 - 10 GHz range. The resulting antenna has a small planar geometry with dimensions of 7 cm by 1.5 cm and was realized as a printed antenna on a dielectric substrate. The antenna geometry is optimized for excitation with a monocycle of 0.2 ns duration. This pulse has a central frequency of around 5 GHz and its spectrum essentially covers the 3 - 10 GHz bandwidth.

An effective resistive loading profile for suppression of antenna ringing has been determined for this antenna by means of the FDTD method. The loading is realized with a number of chip resistors soldered along the antenna. The resistors closest to the feedpoint serve at the same time as secondary sources of radiation in addition to the main source of radiation at the feedpoint. The distance between the main and the secondary sources of radiation is chosen in such a way that radiations coming from those locations combine constructively in the broadside direction of the antenna. In this way one practically improves the antenna radiation efficiency.

The transmit waveform of the proposed antenna has been compared with that of a conventional bow-tie antenna with comparable size and it has been found that taking mismatch losses into account the waveform peak of the proposed antenna is substantially higher, indicating improved antenna efficiency. Furthermore, it was shown that the antenna ringing is adequately suppressed after less than 3 times the pulse duration. This will set the potential limit of data rate at more than 1 Gbit/s.

The input impedance of the UWB antenna has been computed by means of the FDTD method and the method of moments. The results agree with measurements and indicate that the input impedance is relatively stable in the 3 - 10 GHz range and furthermore its VSWR is smaller than 1.5 for nearly the whole 3 - 10 GHz range. In addition, we computed and measured its radiation patterns and it has been found that within the 3 - 10 GHz range the antenna exhibits omni-directional H-plane patterns, which generally is preferred for telecommunication. The antenna also shows adequately flat gain within this range.

A UWB balun for feeding the antenna is currently under development. This balun has a small planar (2-D) structure for convenient implementation of both the antenna and balun in compact devices.

REFERENCES

1. A.A. Lestari, Y.A. Kirana, A.B. Suksmono, A. Kurniawan, E. Bharata, A.G. Yarovoy, L.P. Ligthart, "Compact UWB Radiator for Short-Range GPR Applications," Proceedings of the 10th International Conference on Ground Penetrating Radar (GPR 2004), vol. 1, pp. 141-144, Delft, The Netherlands, June 2004.

Design Optimization of UWB Printed Antenna for Omnidirectional Pulse Radiation

N. Fortino, G. Kossiavas, and **J. Y. Dauvignac**
Université de Nice, France

The use of Ultra Wide Band technology in telecommunications implies the study of appropriated radiating structures. In UWB devices, antenna impulse response alters the shapes of transmit pulses and then make the antenna as a much more important component than in narrowband systems. Thus, besides the standard specifications (impedance matching, efficiency, and integration), the UWB antenna must maintain almost constant radiation patterns and phase center position over the entire bandwidth. In this paper, we present the design and the optimization of a coplanar printed antenna. Time domain measurements have been performed to characterize the antennas and validate these evolutions.

A novel triangular CPW-fed-printed-antenna with specific ground planes is presented. This shape allows a 50 Ω impedance matching, an omnidirectional radiation pattern in perpendicular plane to the substrate, a limited size and a low cost [1]. A triangular slot and capacitive effects are introduced inside the triangular patch to confer a better matching over a wider bandwidth ([3,1- 10,6]GHz), and a smaller overall size to the structure. A second work is carried out to obtain a better stability of radiation patterns and lower directivity along frequency range. The arms of the ground planes are tilted to control the diagram. Then, an optimized antenna with double folded arms is presented. The measurements of several antenna prototypes matched from 3 to more than 10 GHz validate the simulated results (performed by ADS and HFSS software tools). All these design improvements lead to a size reduction of 70 % from the initial structure.

Time domain measurements are also necessary to characterize the antennas. Measurements facility and data processing are first presented and validated. The antenna under test is measured using a pre-calibrated tapered slot antenna [2]. Transfer functions of transmitting and receiving antennas are differentiated considering the derivation effect [3]. Transmit transfer functions (magnitude and group delay) are plotted versus frequency and radiation direction in the principal planes. These characterizations allow us to compute the radiated pulses when a reference synthesized pulse is applied at the input of the transmitting antenna. Also, the dispersion is compared for the different antennas. In conclusion, we highlight the interest of working on the antenna design in order to decrease the pulse distortion.

REFERENCES

1. N. Fortino, G. Kossiavas, J.-Y. Dauvignac, and R. Staraj, Novel antennas for ultra-wideband communications, *Microwave and Optical Technology Letters*, V.41, N.3, pp.166-169, May 2004.
2. E. Guillanton, J.-Y. Dauvignac, C. Pichot, and J. Cashman, A new design tapered slot antenna for ultrawide-band communications, *Microwave and Optical Technology Letters*, V.19, N.4, pp.286-289, 1998.
3. J. Kunish, J. Pamp, Consideration regarding the correlation between UWB antenna transmit and receive responses, URSI EMST, 2004.

Optimization and Evaluation of Antenna Elements Attached to the Optical Electric Field Sensor

N. Hayashi and **M. Sato**
Tohoku University, Japan

We are developing a GPR system using an Optical Electric Field Sensor(OEFS) as a receiver to be used for detecting landmine. Laboratory measurement showed that not only targets in air are detected clearly, but also buried objects can be detected using this GPR system. For further improvement, developing antenna element attached on electrode of the OEFS was focused on in this study.

The dipole antenna has been used as an antenna element. In this study, we proposed a new type of antenna element that is based on the Vivaldi antenna. Vivaldi antenna has wide frequency bandwidth, but disturbs the E-field on the surrounding area a lot. So, we tried to optimize the new type of antenna that has wide frequency bandwidth and less disturbance to the E-field by using Method of Moment(MoM). And, then, we discovered optimal antenna element by resizing the Vivaldi antenna. By resizing the Vivaldi antenna to small, a new type of antenna element (small Vivaldi) that has wide frequency bandwidth and less disturbance to the E-field was proposed.

Moreover, we carried out measurements for the evaluation of the small Vivaldi. First, we evaluated the receiving characteristic. From that result, we confirmed better receiving characteristic of small Vivaldi antenna than previous one. Compared with the dipole antenna, the spectrum of the small Vivaldi antenna is flat and smooth, and receiving voltage is higher from a few dB to 10dB. Next we conducted another measurement for the evaluation of the disturbance to the E-field. From result, we confirmed less disturbance to the E-field by the small Vivaldi antenna. And from those experiment, good agreement between the results of MoM and measurement was observed, so availability of MoM became apparent.

In this study, the antenna element that is small, but has wide bandwidth and high receiving voltage is proposed and demonstrated. As future work, we will carry out the measurement to get image of the target for evaluation the small Vivaldi antenna comprehensively, then, will demonstrate the availability of the small Vivaldi antenna.

The Design of a Wideband TEM Horn Antenna with Balloons

S. Norouzi and **C. Ghobadi**

An exponentially tapered wideband TEM horn antenna having balloons is designed. The balloons are used to improve the impedance characteristic of the TEM horn antenna. The measured bandwidth for VSWR less than 2.0 ranges from 50 MHz to 1100 MHz. The designed antenna can be used not only for EMC measurement but also for broadband communication system.

Broadband TEM Horn Array for FOPEN Radar

S. Norouzi

This paper describes the analysis, design and test of a broadband TEM horn array for airborne Foliage Penetrating (FOPEN) Radar. Measured results are shown for a 2×26 prototype array mounted on a l/l6Ih scale model of a DeHavilland DASH-7 aircraft. A detailed evaluation of the array performance including platform multipath is discussed.

A New Design of TEM Horn Aintennas for Pulse Radiation

S. Norouzi

For the convenience of practical applications, the pulse radiation antennas; used in ground penetrating radar should not only be directive, efficient and distortionless on radiation, but also be as small as possible in size. In this paper, we present a new design of a TEM horn antenna that can meet the above requirements.

A Planar UWB Triangular Monopole Antenna with Bandwidth Enhancement

C. C. Lin and **H. R. Chuang**
National Cheng Kung University, Taiwan, R.O.C.

This paper presents a novel and simple technique to increase the bandwidth of a planar UWB triangular monopole antenna (PTMA). Compared with other configurations of planar monopole antennas, such as square or circular, the bandwidth of the PTMA is relative narrow. In order to improve the bandwidth of the printed PTMA, the means of ridging the conventional rectangular ground plane is employed. The function of the ridged ground plane keeps the input impedance maintaining constant and more than 3:1 bandwidth can be achieved. The HFSS 3-D EM solver is employed for design simulation. The parametric study on the ridged ground plane is also investigated. A printed PTMA is fabricated on the FR-4 PCB substrate, and the measured VSWR is less than 2 from 3 to 10 GHz. The proposed antenna also maintains the monopole-type omni-directional radiation patterns.

Self-Compensating Antennas For A Dispersionless Uwb Channel

J. S. Tyo, C. J. Buchenauer, and **M. Dogan**

University of New Mexico, U.S.A.

It is a well-known fact that the transmit and receive responses for antennas in the time domain are related by a time derivative. The presence of this differentiation operation therefore makes it difficult to have an UWB communications channel that does not need some compensation. The compensation can come in the form of pulse shaping or postprocessing. The most common types of UWB antennas are based on modifications of monopole-type designs or TEM horns, which means that they will roughly replicate on transmit over some range of frequencies and will roughly integrate on receive, leading to a channel that integrates for some finite clear time.

Since the transmit and receive responses are related by a derivative, an antenna the "half"-differentiates on transmit will "half"-integrate on receive, and therefore be self compensating. The frequency-domain Green's function for the electric field for a 3- dimensional point source (i.e. a point electric dipole) contains a (jw) term in the numerator. We know well that this corresponds to to a differentiation in the time domain. The Green's function for a 1-dimensional source (i.e. a plane of current) is constant as a function of frequency, meaning that it replicates in the time domain. However, the 2- dimensional source (i.e. a line source) has a Green's function that varies like (jw)^(1/2), which corresponds to a half derivative. The receive response will vary like (jw)^(-1/2), leading to a dispersion-free channel. In this paper, we will present models and experiments showing how this class of antenna can be approximated in practice.

Array Geometry for Real-Time Ultra Wideband Systems

N. Y. Soltani
Iran University of Science and Technology, Iran

M. Asgari
IRIB Faculty, Iran

F. H. Kashani
Iran University of Science and Technology, Iran

In this paper we want to focus on finding appropriate array geometry for DOA of wideband sources. Although there are many wideband DF algorithms for wideband systems, we cannot rely on this kind of algorithms. This is because they are not real-time and therefore applicable, especially when the number of sources increases. That's why, we prefer to concentrate on using a narrowband DF algorithm and try to eliminate the errors of these algorithms for DOA of wideband sources, by determining the array configuration constraints. In fact, we will prove that frequency independent array geometry can help us avoid of using a complex wideband algorithm. Here, a typical array is introduced to show the problem of using narrowband DOA for a wideband signal, so array pattern and algorithm behavior to this array configuration will be compared. Then to solve the problem, a frequency independent array geometry will be investigated and some typical results are shown.

Indoor Propagation Property and Its Application to MIMO-OFDM Systems

Y. Ohwatari, H. Nishimoto, H. P. Bui, Y. Ogawa, T. Nishimura, and **T. Ohgane**
Hokkaido University, Japan

INTRODUCTION

Multiple-input multiple-output (MIMO) systems using multiple antennas at both of the transmitter (TX) and receiver (RX) can increase transmission rate in multipath-rich environments without additional frequency spectra. When channel state information (CSI) is available also at the TX side, the maximum throughput of the MIMO channel is achieved by using eigenbeam-space division multiplexing (E-SDM) which is also called the singular value decomposition (SVD) algorithm. When the uplink and downlink channels are not reciprocal as in a FDD system, we need to feed back the CSI from the RX side to the TX side. However, system throughput can be limited by the feedback information in MIMO-OFDM systems because the transmitter needs the CSI for all the subcarriers. The number of subcarriers is 52 for the IEEE802.11a wireless LAN standard. In OFDM systems, we can assume that multipath signals with larger delay than a guard interval (GI) are negligible. The authors have proposed a scheme that we feed back time-domain CSI, namely an impulse response. The GI in the IEEE802.11a standard is 800 nsec (16 sampling point interval). We can reduce the feedback amount to less than 1/3 compared to the feedback of all the subcarrier channels. In this paper, we propose a new CSI feedback method based on indoor propagation property. The method can reduce drastically the CSI feedback amount.

INDOOR PROPAGATION MEASUREMENT

The measurement campaign was carried out in a conference room in a building of Hokkaido University. A line-of-sight (LOS) condition was taken as the absence of an obstructing object between the TX and RX. A nonline-of-sight (NLOS) condition was created by placing a metal partition between the TX and RX. The measurement band was from 5.15 GHz to 5.4 GHz. We obtained 78,449 different MIMO channel matrix data using a network analyzer. Examples of time-domain channels are shown in Fig. 1. We can see that the amplitude of multipath signals decays almost exponentially with respect to time, and that dominant multipath components exist in the region much shorter than the GI (800 nsec) for the IEEE802.11a standard.

CSI FEEDBACK IN MIMO-OFDM SYSTEMS

We propose the CSI feedback of only dominant time-domain components whose amplitude is within 10 dB from the peak value for each channel. The time-domain components are estimated by the minimum square error algorithm. At the TX side, channels for all the subcarriers are calculated applying the FFT to the 0 padded time-domain data, and TX weights are determined for the E-SDM transmission. Fig. 2 shows the average bit error rate (BER) of the E-SDM transmission using a 4×4 MIMO system. The solid curves show the BER performance of the proposed method, and the dotted ones show that in a case where all the 16 time-domain CSI components in the GI are fed back. It is seen that the performance degradation of the proposed method is very little. The average number of feedback sample points per channel is 3.5 and 6.3 for the LOS and NLOS cases, respectively. From these results, it is concluded that we can reduce drastically the amount of CSI feedback.

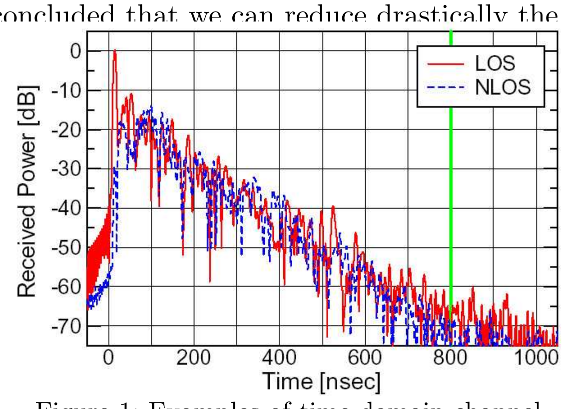

Figure 1: Examples of time-domain channel.

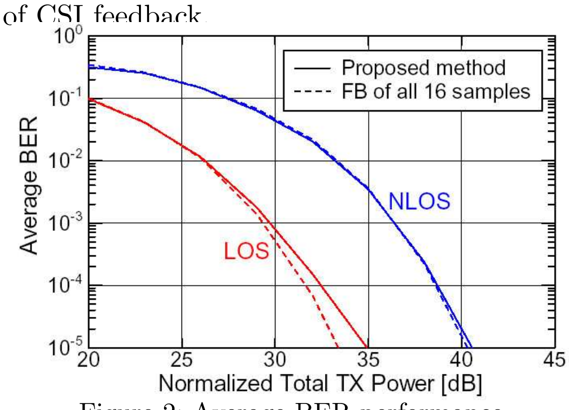

Figure 2: Average BER performance.

Transmit and Receive Timing Control in LOS MIMO-UWB Environments

M. Takanashi, T. Nishimura, Y. Ogawa, and **T. Ohgane**
Hokkaido University

Introduction

We conducted propagation measurement of multiple-input ultra wideband(MIMO-UWB) systems in Line-of-Sight(LOS) environments, and evaluated bit error rate(BER) performance using the measured data. We discovered that the arrival time of direct waves from different tranmit antennas differs for MIMO configuration and affects the BER performance. In this paper, we show the measurement results and propose performance improvement with the transmit(Tx) and receive(Rx) timing control.

Wideband Propagation Meaurement

In this measurement, we obtained MIMO propagation data in a frequency domain with a vector network analyzer. We used a broadband dipole antenna employing self-complementary radiationg element and microstrip line feed as Tx and Rx antennas. We examined three types of MIMO configuration as shown in Fig.1 and obtained 2100 data changing the position of Tx and Rx antenna array pair along x-axis and y-axis for each configuration. The Tx and Rx arrays weew fixed 1[m] apart. The direct wave arrived at each Rx antenna, that is, it was a LOS environment. The measurement was conducted in a shield room, and we did not have interference from other radio systems. We measured transmission of each Tx and Rx antenna pair from 50[MHz] to 12.05[GHz] with a frequency interval 7.5[MHz]. We wil show the behavior only for "Pos1" and "Pos2" due to limitations of space.

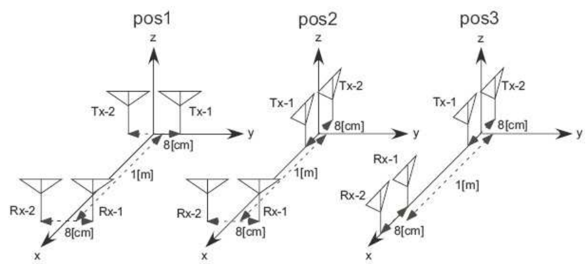

Fig. 1: MIMO configuration.

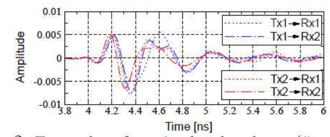

Fig. 2: Examples of received pulse shape ("pos1").

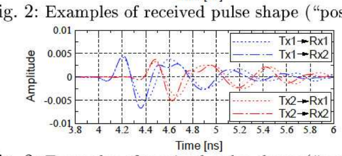

Fig. 3: Examples of received pulse shape ("pos2").

We assumed a Tx monocycle pulse given by $p(t) = [1-4\Pi(t/\tau)^2]exp[-2\Pi(t/\tau)^2](\tau = 0.2877[ns])$. In Figs.2 and 3, we show examples of received pulses for "pos1" and "pos2" in the MIMO environments, respectively. They were calculated using the measured transmission data. We can see that the arrival time of pulses differs for antenna configuration because of the difference of propagation distance.

Transmit and Receive Timing Control

Because the arrival time differs for antenna configuration, we examined three cases as shown in Fig4. In each case, the timing of direct waves is different. This can be done by controling the Tx and Rx timing. The Rx timing is controlled by adjusting the sampling instant. We receive both the transmitted direct waves at the first sampling time for "type1". We receive only on transmitted wave at the first sampling time for "type2". We receive one transmitted wave by a Rx antenna at the first sampling time, and another transmitted wave by the other Rx antenna at he second sampling time for "type3".

We used frequency domain equalization for inter-symbol interference and co-channel interference suppression. The BER performance is shown Fig.5. We can see that the BER performance differs for antenna configuration and timing control. From the simulation results, we can see that the performance using the timing control "type3" is the best among the three control schemes. It is conjectured that the correlation was the lowers for"type3", and that co-channel interference suppression was best in this case.

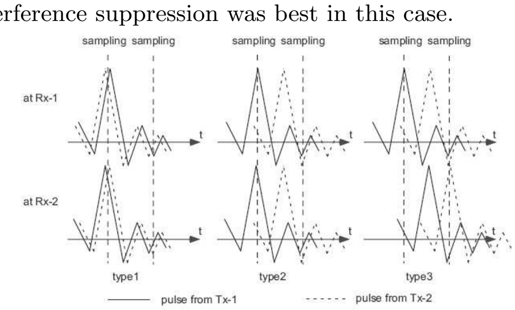

Fig. 4: Reception of direct waves.

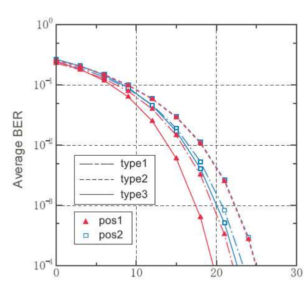

Fig. 5: The BER performance.

Session 4P4
Remote Sensing of Ocean/Forests

Performance Evaluation of Ku-Band Airborne Interferometric SAR

Y. Hara, T. Horiuchi, M. Higuchi, M. Tsuchida, and **M. Iwamoto**

Mitsubishi Electric Corporation

M. Furuhata

Japan Resources Observation System Organization

Interferometric SAR is an active research area, in which many researchers have involved, and has become a promising tool for operational DEM (Digital Elevation Model) measurement. This paper describes a Ku-band interferometric SAR system developed for LBS (Location Based Service) by Mitsubishi Electric Corporation and its evaluation results by flight test.

Laser profiler has been commonly and widely used to obtain DEM from an aircraft. However, laser profiler has drawbacks as shown below:

-Laser profiler cannot be operated in bad weather. Even a small amount of cloud has a bad effect to DEM measurement by the laser profiler.

-The beam spot of the laser profiler is small, and then an aircraft to carry the laser profiler has to fly over the observation area many times. This makes the cost to obtain DEM very expensive.

On the other hand, interferometric SAR has the capability to acquire the DEM data at any time (day and night) and with any weather. And the cost is less than that needed by the laser profiler, because the beam spot of the interferometric SAR is much larger than that of the laser profiler.

We have developed a Ku-band airborne interferometric SAR, which has a capability to acquire DEM of high accuracy as well as high resolution SAR imagery. The system has a capability to obtain SAR image with the resolution of 0.3m. The system has de-chirp-on-receive architecture for high resolution ranging to reduce the bandwidth of the signal processor. The DEM is obtained by interferometric SAR processing, which utilizes the data taken from two antennas. We have developed a precise motion compensation algorithm, a noise tolerant phase unwrapping algorithm, and a precise geometric correction algorithm to obtain accurate DEM. The final goal of the DEM accuracy is 0.5m with 0.5m horizontal resolutions. The system is installed on a Cessna 208 aircraft. The characteristics and the parameters of the system will be shown in the final paper.

The flight test was conducted, and field data was obtained in the area of different terrain types. The terrain types include mountain, flat field, and city. Then, the DEM taken by interferometric SAR were compared with those taken by the laser profiler, and it was proved that the accuracy of the DEM taken by interferometric SAR comparable to that by the laser profiler and is less than 0.5m in most of the terrain types.

L-Band SAR Coherence Map over a Forest, and Relation to Biomass

M. Watanabe, M. Shimada, and **R. Furuta**

Japan Aerospace Exploration Agency/Earth Observation Research and Application Center,Japan

L-band SAR coherence map over a well-managed national forest were derived from Japanese Polarimetric and Interferometric Airborne SAR (PiSAR) data with special resolution of a few m. Several observations were performed over the forest within a day and coherence maps for HH, HV, and VV were made from two flight data, whose observation interval was within an hour. The coherence values in this site are ranging from 0.5 to 0.8 and high coherence values of $0.7 \sim 0.8$ are appeared at the lower sigma-0 areas, which corresponds to very young stands. On the other hands, a variety of coherence value is appeared at mature forest stands. Our previous study shows the one of four species planted in the site revealed higher saturation value in a biomass-sigma_HH curve than the others and a possible cause of the characteristics are discussed in this paper.

Analysis of Bragg Scattering Phenomenon Observed in L-band SAR Images of Machine-Planted Rice Paddies

H. Wang [1], **K. Ouchi** [1], **N. Ishitsuka** [2], **G. Saito** [3], and **K. Mohri** [4]

[1]Kochi University of Technology, Japan
[2]National Institute for Agro-Environmental Sciences, Japan
[3]Tohoku University, Japan
[4]Okayama University, Japan

This article presents the analysis of the Bragg scattering phenomenon which has been observed in the images of machine-planted rice paddies acquired by the JERS-1 L-band synthetic aperture radar (SAR). The simultaneous measurements of rice plants were made at the SAR data acquisition times. Large differences of 20-25 dB in image intensity between the transplanting and ripening stages are found to be dependent on the planting direction and bunch separation. This selective image enhancement is a result of the Bragg resonance backscatter due to the double-bounce of incident L-band microwave between the flooded water surface and periodically planted bunches of rice plants. A support to the double-bounce scattering is provided by the decomposition analysis of L-band and X-band polarimetric Pi-SAR data; and a simple numerical simulation based on the physical optics model shows fairly good agreement with the JERS-1 SAR data.

Results and discussions are presented on the enhanced radar backscatter observed in the JERS-1 L-band SAR images of machine-planted rice fields. The ground-truth, decomposition analysis of airborne Pi-SAR data and a simulation study based on the physical optics scattering model have shown that the selective enhanced backscatter is a result of the Bragg resonance scattering from the double-reflection between regularly spaced bunches of rice plants and irrigated water surface. The present paper is mainly of academic interest, but it is reconfirmed that L-band SAR is less suitable for monitoring rice plants, in particular, machine-planted rice plants, in comparison with X-band or C-band SARs.

A Generic Multi-Agent System for Analyzing Spatial-Temporal Geographic Information

I. R. Farah, K. S. Ettabaa, I. Hamdi, and **M. B. Ahmed**
Ecole Nationale des sciences de l informatique, Tunisie

In a lot of theoretical and practical applications of different geographical disciplines, the use of Geographical Information Systems (GIS) is by now a more or less common issue. Visualization, presentation, administration and analysis of geographical relevant data are a main feature of scientific research and teaching. Furthermore, in commercial contexts like advertisement, marketing, navigation, administration, project management and planning becomes crucial.

The retrieval and location of geographic information will require a significant amount of time and effort. In addition, different users usually have different views and interests in the same information. In order to resolve such problems, this paper proposes a generic geographic information model system based on multi-Agent (MA) architecture. By paralyzing tasks and offering more efficiency and flexibility, this approach seems to be fruitful in order to construct flexible and extensible system improving more capability and efficiency of GIS services. We further illustrate the design and implementation of the multi-agent system that uses image analysis agents for generating and processing parallel programs by calling the available method. In a first time, we validated our approach on satellite images of SPOT4 representing a north Tunisian region for different dates in order to detect changes for a possible prediction and a better decision making and in a second time we represent how to model and represent geographic data.

Potential Estimation of Heat Flux Through Sea Ice and Cover Snow by Remote Sensing

Y. Sasaki and **S. Iwasaki**
National Defense Academy, Japan
S. Kakuta
apan Agency for Earth-Ocean Science and Technology, Japan
V. K. Pavlov
Norwegian Polar Institute, Norway
T. J. Weingartner
University of Alaska, U.S.A.

We have discussed the potential estimation of heat flux through sea ice and snow layer by remote sensing. A series of extensive observations were made in the Sea of Okhotsk and the Arctic Ocean, since both areas show a great contrast in thickness of ice and snow. Authors have derived some dependences of the heat flux in ice and snow on each thickness, physical properties, and meteorological parameters. The most fundamental parameters in above flux estimation are the thickness and surface temperature of snow layer whose thermal conductivity is only one tenth of that of sea ice. It has been known from our observation that the microwave radiometry at lower frequency like 6GHz is useful to estimate the thickness (less than 1m) of snow with uniformity, however, the thickness is very highly variable in many ice seas, especially in summer season, and this variability, in turn, affects the heat conduction. Authors have then derived a probability density function of snow thickness from the occurrence observation of snow thickness in the Chukuchi Sea. This function enabled us to estimate the antenna temperature which considers the variability in snow thickness. This function also gave us a perspective of the effect of variability in snow thickness on heat flux in ice and snow. The brightness temperature of snow showed an increasing multiple scattering effect with thickness in the ground-based measurement in the Sea of Okhotsk, however, the satellite measurement showed quite a similar pattern in the mid-Alaskan area.

Another important parameter is the surface temperature of snow, however, a correction must be applied to its remote observation. We compared the measurements between thermometer and infrared radiometer in the Sea of Okhotsk and found that the former showed eight to ten W/m2 (approximately 1.5^{o}c) higher radiations than the latter.

Dependency of the Normalized Radar Cross Section of Ocean Surface on Polarizations

A. Nadai, T. Umehara, and **S. Uratsuka**
National Institute of Information and Communications Technology, Japan

Recent years, many satellites with polarimetric synthetic aperture radar (SAR) have been launched. The polarimetric analysis will be applicable for the earth surface including the ocean. However, the knowledge of polarimetric feature of normalized radar cross section (NRCS) is little on the ocean surface. In this paper, the NRCS of ocean surface are measured using an airborne SAR and the dependency on the polarization is analyzed.

The NICT and the JAXA has been developed an airborne SAR (Pi-SAR) that is a dual-frequency polarimetric SAR with L-band and X-band. The range of incidence angle is enough wide to acquire the dependency of NRCS on incident angle from one observation, because the swath is more than 10km. Moreover, the time interval of observation of one target is able in less than several minutes. The NRCS of ocean surface depends strongly on the wind over the ocean. The airborne SAR is able to observe same area in enough short time to be ignore the change of wind.

The NRCS for parallel polarizations (VV, HH) is much stronger than that for cross polarizations. The large difference represents the ability of Pi-SAR to measure the NRCS for parallel polarizations. The dependency of NRCS on incident angle is different between the radar frequencies and the polarizations. Many observations have done with various weather conditions. The dependency of NRCS on ocean wind will be presented.

Directional Characteristics of Wind-Wave Development Under High-Resolution Wind Fields

T. Shimada and **H. Kawamura**

Tohoku University

We investigate fetch-limited wind-wave development under alternating coastal wind jets and wakes induced by orographic effects. Synthetic Aperture Radar and scatterometer resolve wind jets and wakes with widths of 10-40 km. Using the wind field and a third-generation wave model, we simulate the nearshore wave field. As a result, broader directional wave spectra are seen in wakes while we can find evolution of the directional wave spectrum with offshore distance in both wind jets and wakes. Especially within the offshore distance of 40 km, directional wave spectra have two peaks. These characteristics are well reflected in the overall directional spreading field. The overall directional spreading closely corresponds to the wind speed distribution, and is small/large in wind jet/wake region. The results mean that wave energies that come from neighboring wind jet regions cross in wake regions and combine with wave energy generated by local wind in wake regions.

The characteristics of wind-wave developments are revealed due to high-resolution winds derived by SAR and wave simulation with high spatial resolution for the first time. The results cast the orographic modification of wind as the ultimate cause of the directionality of wave spectra in coastal seas. The characteristic directionality of ocean surface wave fields brings better understanding of high individual wave occurrences, spectrum shapes, sea surface slopes, and wave energy transfer.

Automatic Detection Approach of Ship using RADARSAT-1 Synthetic Aperture Radar

C. S. Yang
Korea Ocean Research and Development Institute, Korea

K. Ouchi
Kochi University of Technology, Japan

Background:

During the period of every summer to early autumn seasons, ships have been wrecked or grounded from effect of a typhoon in the waters around Korean Peninsular. For marine structures, in addition to that, ocean wave data during typhoons pass are very important to guide ships safe navigation and to determine design waves.

Methodology:

1. Data : QuickSCAT and SAR data during typhoon
2. Data Analyses: WindWave Spectra and Wave height
3. Validation with field data of Ieodo Ocean Research Station, located 149 km southwest of Marado, the southernmost island of Korea.
4. Investigation of Ship Accident during typhoon

Predicted Results:

1. Results of wind and wave fields under typhoon in the South Sea of South Korea
2. Relationship of extreme wave and ship casualty

Measurement of Ocean Waves by Synthetic Aperture Radar Using Cross-Track Interferometry

A. Nadai, T. Umehara, and **S. Uratsuka**
National Institute of Information and Communications Technology, Japan

N. Sudo
Tokai University, Japan

The continuous monitoring of ocean waves in wide area is difficult by any in-site method. The synthetic aperture radar (SAR) is one of powerful tools to monitor the ocean waves continuously in wide area. The measurement technique of ocean waves using SAR is investigated using the analysis of the spatial pattern in the intensity image. The intensity method has some disadvantages like that the radar cross section is not related to the ocean wave directly, that the intensity relation between the measured wave components depends strongly on the geometry of observation, and that the wave height is not able to measure. The cross-track interferometry is a technique to measure the topographic information of the earth surface. In this study, the cross-track interferometric technique is applied to the measurement of ocean waves.

The National Institute of Information and Communications Technology has been developed a dual-frequency airborne SAR system named Pi-SAR, in corroboration with the JAXA. The cross-track interferometric function of X-band radar of Pi-SAR can measure the topography with accuracy of 2m. The ocean wave components measured using the interferometric method agrees well with those using the intensity method. The intensity relation between the measured wave components using the interferometric technique is independent to the observation geometry. The results by the interferometric method also agree with the in-situ data measured by the buoy and the supersonic wave meters.

Directional Spectrum Estimation from HF Ocean Radar

Y. Hisaki
University of the Ryukyus, Japan

HF ocean radar can estimate wave spectrum by analyzing the Doppler spectrum of backscattered radio waves radiated to the sea surface. It is possible to estimate wave directional distributions of Bragg wavelength from the first-order Doppler spectrum. Wave directional spectrum can be also estimated from first- and second-order Doppler spectra.

The radar-estimated directional distributions of Bragg wavelength are estimated from the ratio of observed first-order scattering. These short-wave directional distributions are estimated for the 2-parameter model and 4-parameter model. The short-wave directional distributions are compared with model predictions from the wave energy balance equation. The parameterization of the source function in the energy balance equation is investigated. In particular, the effect of the nonlinear source function on the prediction of short-wave directional distributions is investigated. The nonlinear source function is calculated from both the exact computation and the Discrete Interaction Approximation (DIA).

The agreement between radar-estimated short-wave directional distributions and model predictions is good. The 4-parameter model is better than the 2-parameter model to estimate short-wave directional distribution from HF ocean radar. The short-wave direction change associated with a sudden wind shift can be reproduced both from the exact computation and the DIA. The short-wave directional distributions calculated from the exact computation are narrower than those calculated from the DIA and estimated from the HF radar. These parameterizations are also important for wave spectrum estimation developed by Hisaki (2005) and Hisaki (2006).

REFERENCES

1. Hisaki, Y.: Ocean wave directional spectra estimation from an HF ocean radar with a single antenna array: Observation. Journal of Geophysical Research, Vol. 110, C11004, doi:10.1029/2005JC002881, 2005.
2. Hisaki Y.: Ocean wave directional spectra estimation from an HF ocean radar with a single antenna array: Methodology. Journal of Atmospheric and Oceanic Technology Vol. 23, No. 2, 268-286, 2006.

Long Range Ocean Radar for Surface Current Measurement in the Southern Part of the East China Sea

S. Fujii
University of Ryukyu, Japan
S. Kojima, K. Sato, and **T. Matsuoka**
National Institute of Information and Communications Technology, Japan

The High-frequency (HF) ground-wave Doppler radar is a useful technique for monitoring the ocean-surface conditions; accordingly, it has become a powerful tool in the oceanographic research. The HF ocean radar can obtain the data of ocean surface cover a wide range at a time from the shore-based radar.

We designed the new long range ocean radar (LROR) to observe ocean surface currents up to 200km from the shore. The radar system is composed of the two radars which is set with the baseline distance of 120 km, so the current vectors within a 200 x 200-km area can be measured. The LROR system uses a 9.2-MHz radio wave with a maximum transmission power of 1kW. It uses the FMICW (frequency modulated interrupted continuous wave) technique with a frequency sweep of 22 kHz, which corresponds to a range resolution of about 7km. The radio waves are transmitted with a broad beam formed by a three-element Yagi antenna, and the backscattered signals are received by a phased-array antenna. Each element antenna of the array is followed to individual receiver to compose DBF (digital beam forming) network. Angular resolution, which corresponds to the recieving beam width, is provided by the aperture of the phased-array antenna. The antenna aperture is about 200 m long, producing a minimum beam width of eight degrees. The total angular coverage of the transmitting and receiving antennas ranges over a 120-degree swath; thus the radial components of the ocean-surface current are obtained within this sector-shaped area. The velocity resolution along the radial direction is 2.5 cm/s. The two radial velocities, which is along the different directions made by two radars at the minimum, is necessary for estimation the current vector.

Ishigaki Island and Yonaguni Island were selected as the radar sites for monitoring the Kuroshio current. Both islands are located south-west end of the Ryukyu Islands, forming the archipelago between Kyushu and Taiwan. The Kuroshio current flows into the East China Sea through the strait between Taiwan and the Ishigaki Islands. So the observation area of LROR covers the upper-stream region of the Kuroshio current in the southern part of the East China Sea.

The LROR is operated from July 2001. A set of current vectors in the observation area are obtain at 30 minutes interval. Figure 2 shows the averaged current vectors over one day (Nov. 5, 2004). In this vector map, it is clearly shown that the Kuroshio current is flowing into the observation area from southwest and turns eastward near the continental shelf. The maximum velocity of the measured currents is over 200 cm/s. And the width of the Kuroshio current is estimated to be about 70 km in this observation.

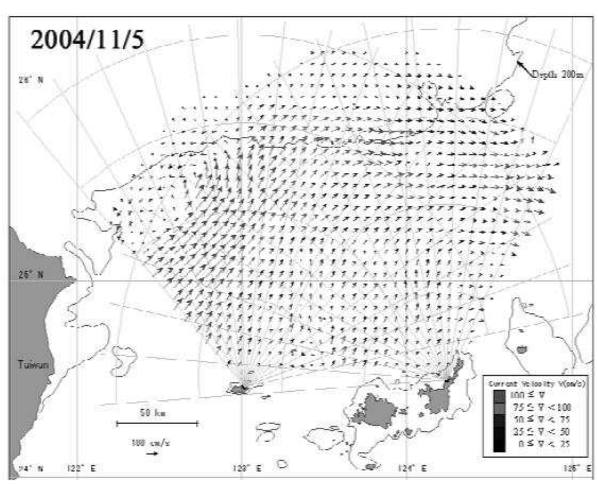

Wavelet Analysis for Internal Wave Detection in ERS SAR and ASTER Image Data

Y. Arvelyna and **M. Oshima**
Tokyo University of Marine Science and Technology, Japan

On this paper, wavelet analysis has been used for internal wave detection in ERS SAR and ASTER images data over Tsushima Strait, Southwest of Japan, during 1993-2004 period. Various wavelet transforms, e.g. Haar wavelet, Symlet wavelet, Biorthogonal wavelet, Coif wavelet and Daubechies wavelet, are tested comparably with different level of synthesize image on horizontal, diagonal, and vertical detail, and approximation to study the internal wave characteristic in image. Internal wave features were detected as elongated pattern in image with higher wavelet coefficient (¿36) than sea surface (¡10) on horizontal and vertical detail coefficient of image transforms at level 2-5. The decomposition image shows the tendency that the decomposition of internal wave feature using wavelet transform tends to follow the wavelet function. This may reduced the height of leading wave. Smoother result of internal wave shape can be formed using higher scale resolution of image at level 5 and higher number of vanishing moments such as Daubechies wavelet-db5, Symlet wavelet-sym5, and Discrete Meyer wavelet. The compactly supported wavelet function with orthogonal basis with scale function and FIR filter, such as discrete Meyer function is proposed for smoothness of feature, space save coding, and to avoid depashing in image.

So far, the detection processes were performed well on the internal waves data that occurred at north coast off Kitakyushu and NW/W/SW/E coast off Tsushima Island on June to September period whose lengths were detected between 6-28 km and wavelength between 120m-1.28km. The directions of internal wave propagation were varied between NW-SW at eastern channel and N-SW at western channel of Tsushima Strait.

Keywords: wavelet analysis, SAR image, optical image, internal wave.

Gim-Technology for the Classification and Qualitative Interpretation of the Data of Remote Sensing for Water Surface

F. A. Mkrtchyan, V. F. Krapivin, and **S. M. Shapovalov**

Russian Academy of Sciences, Russia

The basic scheme of collection and processing of the information in geoinformation monitoring system(GIMS) recognizes that effective monitoring researched object is possible at complex use of methods of simulation modeling, collection and processing of the information.

From the position of system analysis, the system of collection and processing of the information in geoinformation monitoring represents the structure uniting the computers of various classes, databases and the advanced problem-oriented software. Creation of such system demands the development of formalized description of the information flows and unique methodology of its processing.

Development of geoinformation monitoring systems requires the decision of a set of problems related to the formation of data measurements flows to be solved. The problem of classification of aquatories using the remote sensing measurements is one of important among them. Various algorithms of the theory of images recognition, statistical decisions and cluster analysis are used to solve this problem.

The feature of remote measurements is information acquisition, when the data of measurements, acquired during tracing of flying system along routes of survey, are directed to input of the processing system. As result the two dimensional image of investigated object is registered. Statistical model of spottiness for investigated space is one of models for this image.

In real conditions, the study of spots, the acquiring of their statistical characteristics and their using in a problem of detection is enough a complex problem. It is necessary to develop the criteria allowing the distinguishing the spots from other phenomena. For example, it is necessary to determine such threshold the exceeding of which is the spot indicator. Also it is necessary to develop model presentation of processes of spots detection.

The mathematical model describing the background characteristics of water surface spottiness is proposed. Operative software for this model is realized. The results of the software application to the satellite data processing for the Atlantic, Pacific and Arctic regions are given.

Session 4P5
Design of Complex Transmitters in Changing Enviroments by Simualtions: Recent Advances and Future Requirements

Circularly Polarized Antennas for Realizing In-Vivo Whole-Body Exposure

J. Q. Wang and **O. Fujiwara**
Nagoya Institute of Technology, Japan

K. Wake, H. Kawai, and **S. Watanabe**
National Institute of Information and Communications Technology, Japan

Base stations of mobile communications are being installed in our daily environment, which has raised a public concern about the possible health hazard against their emitting radio-frequency (RF) waves, and triggered the development of various in-vivo exposure system for bio-effect test. The realization of a whole body exposure from base stations, however, is not easy because the coupling between the RF fields and humans varies with life patterns. Nevertheless, the whole body exposure setups developed so far employ a waveguide structure or a transverse electromagnetic (TEM) cell structure in which the field polarization is linear, although the RF coupling between a base station antenna and a human body does not always have a single linear polarization.

To simulate a great variety of coupling between the RF fields and free constraint exposed subjects, we proposed a new method of employing circularly polarized antennas for an in-vivo whole body exposure setup. We realized approximately the circular polarization using two dipole antennas that intersect at a right angle and have a phase shift of 90o. This structure allows the antennas to induce a circularly polarized RF field in the far-field region. We further extend the two dipole antennas to 3/2 wavelength in order to shape a broad exposure area with a relatively uniform field level. We designed the antennas at 2.14 GHz, and assumed four exposed rats to be with a distance of 1.4 - 1.8 wavelengths (20 cm - 26 cm) under the antenna.

We first investigated the electric field distribution in the rat area using the finite difference time domain (FDTD) method. The result showed that, in the absence of the four rats, more than 80% of the relative electric field levels were within 0.75 $\pm$15% in each of rat cage area. This result exhibited a fair uniformity for the field distribution. A uniform field distribution is expected to cause smaller variation in the specific absorption rate (SAR). We also checked the ratio of the antenna axes. It was found to be about 1 dB towards the direction of rats. A ratio of antenna axes ranging from 1 to 3 dB is usually considered as a circularly polarized antenna.

With the employment of anatomical rat models, we calculated the variation in the whole-body average SAR due to the ratsf free movement and growth. We simulated 40 situations of the four rats inside the cages under the antenna for each stage of growth. As a result, it was found that the whole-body average SAR varies within $\pm$50%, which is a reasonable and acceptable quantity in view of the actual variation in a human body for RF exposure from a base station. Moreover, we also made a quantitative analysis for the SAR in fetuses inside pregnant rats, and the SARs in new-born rats just after the mother rats had. The results demonstrated a three times higher SAR in a new-born rat compared to that in the mother rat.

The basic performance of the proposed antenna has also been investigated experimentally. The comparison between the FDTD-calculated and measured electric field distributions will be shown at the presentation.

SAR Calculation in Immature Rats Exposed by an 8-Shaped Loop Antenna in 1.5 GHz Band

S. Tanaka and **T. Uno**
Tokyo University of Agriculture and Technology, Japan
K. Wake, H. Kawai, and **S. Watanabe**
National Institute of Information and Communications Technology, Japan
H. Masuda and **A. Ushiyama**
National Institute of Public Health, Japan
M. Taki
Tokyo Metropolitan University, Japan

Rapid spread of cellar phones has raised a public concern about possible health effects of electromagnetic field (EMF). However, the EMF dosimetry inside infants is not enough detailedly investigated. Therefore, the priority of dosimetry in immature animals, which simulate the infants, is also increasing (WHO, The International EMF Project, June 2004). Until now, our group proposed an 8-shaped loop antenna, which can realize the local EMF exposure inside 4-, 8-, and 12-week-old rats in 1.5 GHz band (Watanabe et al, BEMS2004, pp. 52.53, 2004). However, the validity of antenna for immature ratsf exposure has not been evaluated yet. In this paper, the localization of SAR inside 1-, 2-, and 3-week-old rat models is calculated using the finite-difference time-domain (FDTD) method in 1.5 GHz band.

Immature rats grow very quickly after their birth. Therefore, three numerical rat models of 1-, 2-, and 3-week-old based on their X-ray CT images were developed. Spatial resolution of models was $0.25^3 mm^3$. Six types of tissues were classified. In the numerical simulation, the 8-shaped loop antenna was placed above ratsf heads with the distance of 4.5 mm. The analytic region is $641 \times 521 \times$ 851 cells. The absorbing boundary conditions are the perfectly matched layer (eight layers).

First, the SAR distribution inside the 1-, 2-, and 3-week-old rat models is calculated. As a result, the maximum SAR always appears on the top of their heads. In addition, the high SAR also appears around their mandibles. This is remarkable in the younger-aged rat models. Next, brain and whole-body average SARs in the models are also calculated and compared between the average values, to evaluate the localization of exposure. The result indicates that the localization of 1-week-old model is about the half value of 3-week-old model. From the results, the improvement of localization is necessary.

In the actual exposure, the adjustment of distance between the antenna and rats is difficult. The uncertainty estimation of localization caused by the distance will be shown at the presentation.

Movement of the Peak SAR Location in Close Proximity to the Surface of a COST244 Phantom Exposed to a Dipole Array Antenna

S. Kajiwara
Matsushita Electric Industrial Co., Japan

In recent years, many types of array antenna techniques (T_x Diversity or Adaptive Array Antenna or MIMO) have been proposed for cellular phone terminals. These antennas include two or more EM sources for numbers of transmitters, so that the radiation characteristics can be improved significantly. However, it is expected that such sources could produce many SAR peaks and complex SAR distribution patterns near the phantom surface. So the SAR measurement method which is predicted by an extrapolation method from the SAR data inside a phantom might cause large error.

In this paper, we conduct a basic study of the movement of the peak SAR location in close proximity to a COST244 phantom exposed to a half-wavelength dipole array antenna at 2GHz. Some array antenna models fed various phase deference X_ω are compared using FDTD method (Fig.1). Furthermore, we experimentally confirm the calculated results by the thermo-graphic and E-probe methods. Consequently, an abrupt movement of the peak SAR location can be confirmed in the $X_\omega = 0$ model. The peak SAR area which located near the feed point on the surface moved to the center of the element, so it was not always the same as that of a few mm inside the phantom (Fig.2). The result also revealed that the average value of SAR measured from the center of the element was highest, so an E-probe method could give us true location of the maximum peak in the SAR estimation.

FDTD Analysis for propagation Characteristics of Wireless LAN Equipped in a Jumbo Aircraft

M. Hirono, Y. Kawahara, T. Hikage, T. Nojima, and **M. Omiya**
Hokkaido University, Japan

Electromagnetic field (EMF) distributions inside an airplane excited by the wireless LAN terminal are analyzed and propagation characteristics are evaluated based upon the analysis results. We employed the FDTD technique and a supercomputer to estimate the EMF distributions excited inside the cabin. Moreover, large-scale parallel computing based upon several node partitions was used because of its memory and speed capabilities. It could give us a good perspective within a reasonable computation time. In Addition, a simplified histogram estimation method for electric field strength in whole area of the cabin were employed to deal with the complicated electromagnetic field (EMF) distributions. The obtained results implied that FDTD computer simulation could be used for estimating complicated EMF excitation problems precisely. This paper discusses effects of the loss due to passenger's body in the cabin. We use a typical airplane now in active service, and 2.45 GHz band wireless LAN simulators. Fig.1 shows FDTD analysis model. We examine the EMF histograms of inner space of cabin when the 54 passengers occupy the cabin. Figure 2 presents the histograms derived from analyses of electric field distributions. In this case, the relative electric field distributions are about 5 dB lower than one of the case of no one existing in the cabin. Further investigations that estimate the EMF of whole area of jumbo jet are being conducted.

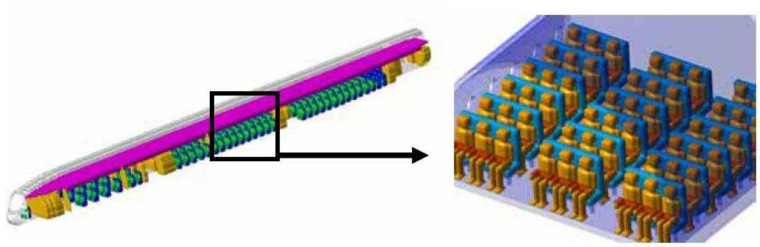

Figure 1: FDTD model

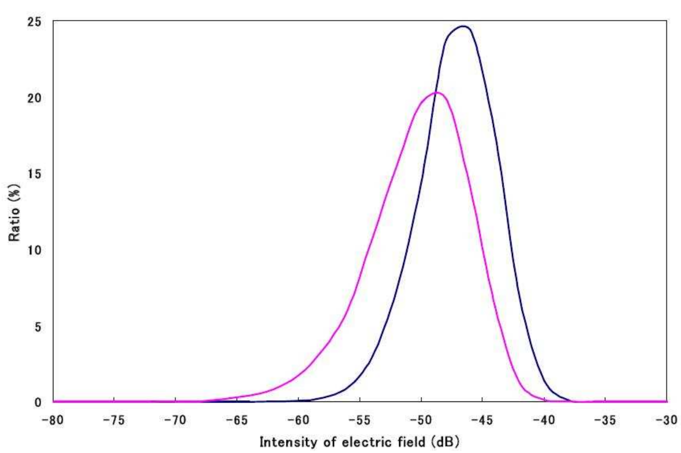

Figure 2: Histograms of electric field intensity in the cabin.

Evaluation of Indoor Propagation of the Medical Implant Communication System (MICS) by FDTD Simulations.

A. J. Johansson
Lund University, Sweden

The Medical Implant Communication System (MICS) is a standard set for use to communicate with medical implants such as heart pacemakers. It uses a frequency band of 402-405 MHz, and is standardized by ETSI [1] and FCC [2], as well as other countries. As MICS shares the frequency allocation with the weather balloon service, the system has a limit on the EIRP from both the body with the implant, and from the external base station, of 25 microwatts. The instantaneously used bandwidth is restricted to 300 kHz. Together this gives a usable range in the order of meters. The downlink to the implant is further restricted by the limited power available to run the receiver and the LNA within it. The same power limit also restricts the uplink as it will in practice reduce the EIRP to a lower level than the maximum. The signal will further be heavily attenuated by losses in the body tissue, and from reflections against the body surface due to the impedance mismatch versus the air.

The communication link will typically be used for diagnostic use in a consultation room at a hospital, and in the patientfs home. In order to verify the functionality of the implant, and to set the correct operating parameters in it, the link must also be used at the time of implantation in the operating room. The communication distance is typically 1 to 3 meters, which equals distances less than 4 wavelengths in air. This makes the classical propagation models unusable as they are dependent on the devices being in the far-field of each other.

The operating room is a challenging environment to characterize the radio wave propagation in, especially if done by measurements. The room itself is typically filled with metal furniture and instruments which influence the wave propagation. It is hard to do the measurements during an actual operation, due to risks of infection for the patient, and that a number of electronic devices are used which both can influence the measurement, and that can be disturbed by it. Additionally, as we would like to include the effects of the human body in the channel, which would make it necessary to make measurements inside the patient. One alternative is to use a full-size human phantom. These are heavy, expensive and the measurements would need extended access to the operating room. A more practical strategy is to do the study by electromagnetic simulations.

We have used FDTD simulations to characterize the wave propagation in indoor environments. Initial investigations were done in an ordinary room, modelling a consultation room at a hospital. The wave propagation in the same room was also measured using two dipole antennas. The results showed that the correspondence between the FDTD simulations and the measurements was very high [3]. An operating room at Lund University Hospital was then modelled in the FDTD tool Semcad. (Figure 1). The model accurately represent the existing operating room as the dimensions all the furniture and instruments were taken at the site. A patient was modelled by placing a homogenous human phantom on the operating table. By placing a dipole in the simulation at the position of the base station, the field dtrength at the implant position could now be calculated. We also investigate different placements and polarizations of the base station antenna, and different positions of the implant in the body.

REFERENCES

1. *ETSI EN 301 839-1*, European Telecommunications Standards Institute, 2002.
2. *47 CFR 95.601-95.673 Subpart E*, Federal Communications Commission, 1999.
3. *Wireless Communication with Medical Implants:* Antennas and Propagation, PhD-thesis, Anders J Johansson, LUnd University, 2004

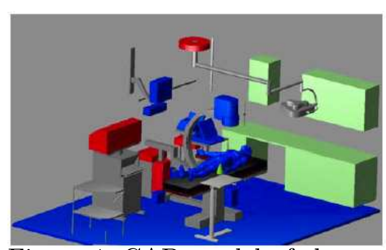

Figure 1: CAD model of the operating room.

Printed Quasi-Yagi Antennas for Switched-Beam WLAN Applications

K. F. Hung and **Y. C. Lin**
National Taiwan University, Taiwan

Smart antenna technologies are widely recognized as a promising solution for addressing the increasing demand of the future wireless network capacity. Switched beam antennas and adaptive arrays are two approaches to implement the smart antenna function. In general, switched-beam antenna systems offer a robust construction against multi-path propagation effects and a reduced complexity that is inherent with fully adaptive implementations. The switched beam system generates overlapping radiation beams that cover the surrounding area. When an incoming signal is detected, the base station determines the optimal setting aligned in the direction of the signal of interest and automatically switches to that beam to form a communication link. By narrowing the beamwidth, the switched beam antennas have an increased gain that in turn may reduce the transmitted power or increase the effective range. The antenna of narrow beam also mitigates the multipath interference coming from other directions beyond the main beam.

In this paper, an array of printed quasi-Yagi antennas is proposed for switched-beam WLAN applications. The switched beam antenna system consists of four printed quasi-Yagi antenna elements, four dihedral corner reflectors, a circular base ground plane. A switch network is built on the back of the ground plane feeding the antenna element through the vertical transition. The pattern of each antenna covers a sector of 90 degrees in the horizontal plane. The full omni-directional coverage is then implemented by employing the four-element array that is fed with the switch network controlled by the system circuitry underneath the base ground plane of the array module. The design is illustrated in the 5-6 GHz band and the promising performances are achieved, including the impedance bandwidth of 30%, the front-to-back ratio of better than 20 dB, the polarization isolation of 30 dB, and antenna gain between 7-9 dBi in the band.

Virtual Prototyping and Failure Synthesis: RF Design and Optimization of Mobile Device Terminals

R. Tay [1], **N. Chavannes** [2], **P. Futter** [3], **N. Guan Hong** [1], and **N. Kuster** [2]

[1]Motorola Innovation Centre, Singapore
[2]Foundation for Research on Information Technologies in Society (IT'IS), Switzerland
[3]Schmid & Partner Engineering AG (SPEAG), Switzerland

Introduction and Objectives

During the design phase of mobile telecommunications equipment it is essential to assess and predict potential failures of the device at an early stage and in particular prior to the production phase. Possible sources include design related elements (e.g., contacts between LCD bezel and PCB, loose shields, etc.) or component related issues (e.g., amount of metallic content in plastic, variation of metallic thickness due to process changes, etc.). Being an effective means for EM investigations, numerical simulation has previously demonstrated its suitability for mobile phone analysis.

The objective of this study, however, was to investigate if enhanced TCAD environments can act beyond common EM simulation and proof its value as a virtual prototyping platform. Embedded into a regular design process/environment, a latest quad-band phone was thus rigorously numerically examined regarding failures, synthesis and prediction capabilities of RF performance for mobile device terminals.

Methods

Simulations were conducted by using the FDTD based platform SEMCAD X which provides 3-D ACIS based modeling and OGL rendering, furthermore, enriched by method enhancements and FDTD hardware acceleration. The original detailed CAD dataset of the commercial phone from Motorola Inc. consisted of $> 1'000$IGES parts which were directly imported into the TCAD platform and processed without major simplifications. Minimum spatial grid resolutions of 100 μ m were used to resolve critical details via the automated grid generation. The availability of hardware accelerated FDTD providing computation speeds up to $300 - 400$MCells/s, enables a simulation of the described device structure in < 15 minutes.

Initial simulations were run to ensure an accurate representation of the phone whereas thorough comparisons to experimental data from the DASY4 scanners and from the anechoic chamber was performed. Subsequently, the availability of accelerated simulations allowed to build up a failure synthesis matrix, concentrating on the design and component related items of interest.

Results and Discussion

After initial numerical results of the phone by inclusion of matching networks from the physical model were validated by measurements of impedance and radiation performance, the failure synthesis table was built up. The analysis of manufacturing defects of various connectors (LCD brackets, keypad connectors, etc.) revealed that certain underestimated connections have a significant influence on the RF performance of the device. Numerous conditions were assessed by measurements; in all cases the simulations were able to predict the experimental findings. Finally, the influence of composite materials and metal coatings was investigated for certain shielding and housing parts. The study concluded that speed and feature enhanced TCAD tools exceed the use as a common simulation tool and revealed its value as a virtual prototyping platform being embedded within industrial environments.

Solutions for Computational Dosimetry of Tomorrow

A. Christ, G. del Castillo, and **N. Kuster**
Swiss Federal Institute of Technology, Switzerland
N. Chavannes and **E. Cherubini**
Schmid Partner Engineering AG, Switzerland

INTRODUCTION The last years of progress in numerical simulation software and increased computational performance enable the electromagnetic modelling with computational domains of 10 - 30 million mesh cells (Finite-Difference Time-Domain method), which is sufficient, e. g., for an anatomical whole body model with a resolution of 1 mm. Nevertheless, simplified models or hybrid techniques are required if the environment of the exposed body or a remote antenna has to be included in the simulation. During the development of a wireless device and for the optimization of its RF performance, a large set of different usage positions, antenna types and device configurations need be considered and SAR characteristics showing the demand for highest computation speed and automatic optimization.

OBJECTIVE The goals of this study are:

- to overcome the current limitations of existing FDTD technology by making use of latest hardware developments and optimized algorithms
- to develop a scripting interface (based on the scripting language Python) for the efficient evaluation of parameterized simulations and for automatic optimization
- to apply the developed methods on computationally intensive applications

REQUIREMENTS and METHODS For many dosimetric applications, such as whole body simulations in the 5-6 GHz range, a mesh resolution in the submillimeter range is required leading to a mesh size of approximately 1 billion cells. The simulation of a complete Ferris Wheel setup including anatomical high-resolution models of the exposed animals poses similar demands on the mesh size. This lead to the development of a high-performance FDTD kernel making use of the extended memory range of 64-bit systems thereby allowing to treat problems of over 1 billion of mesh cells.

The ongoing miniaturization of RF devices and the high number of components to be considered in the model (often more than 1000) does not only pose highest demands on the modeling environment, but also requires a very fine mesh, which is strongly overdiscretized with respect to the wavelength and which in turn increases both the memory requirements and the simulation time. This can only partially be compensated by parallelization or vectorization techniques of today's standard microprocessors. ADI methods can yield a certain improvement for a particular application range. However, a tremendous gain in computational speed (approximately a factor of 10) could be achieved by using graphics processors to execute the FDTD algorithm. This also enables the efficient evaluation of problems with a large parameter space and automatic optimization techniques. The performance of the developed methods is demonstrated with the numerical evaluation of the SAR and temperature increase caused induced by an MRI scanner in an anatomical model of a patient wearing a medical implant.

CONCLUSION The developed methods allow to significantly increase the numerical accuracy of the FDTD algorithm by using higher grid resolution and by including more details into the anatomical model. The enhanced capabilities of the algorithm to treat large problems, such as MRI applications, without any trade-offs due to loss of fine details of the model greatly increases the accuracy and realibility of the computational results.

Acknowledgements: Schmid & Partner Engineering AG, Zürich, Switzerland

Reliable Prediction of Mobile Phone Performance for Different Daily Usage Patterns by Numerical Methods

N. Chavannes [1], **P. Futter** [2], **R. Tay** [3], **K. Pokovic** [1], and **N. Kuster** [2]

[1]Foundation for Research on Information Technologies In Society (IT'IS), Switzerland
[2]2Schmid & Partner Engineering AG (SPEAG), Switzerland
[3]Motorola Innovation Centre, Singapore

Introduction and Objectives

The objective of this study was to evaluate whether the performance of mobile phones can be reliably predicted by numerical methods. It has previously been demonstrated that performance can be accurately assessed for standardized testing positions at the head. In this study, the requirements were extended to actual usage patterns such as different positions at the head and especially for different ways to hold the phone with the hand. The latter is of particular importance because fingers placed at certain locations could strongly affect the antenna.

Methods

The study was performed using one of the latest commercial quad-band mobile phones from Motorola Inc. Different antenna types were evaluated for this phone. Simulations were conducted by application of the FDTD based platform SEMCAD X which provides a 3-D ACIS®based solid modeling environment, further enriched by method enhancements and hardware accelerated EM solvers. Through these performance improvements, the CAD dataset generated during the design phase could be directly imported into the simulation platform, without the need for major model simplification. The detailed CAD dataset of the phone consisted of more than 900 distinguished main parts; moreover the PCB was modeled by 5 PEC/dielectric layers. Using resolutions down to 50 m for RF significant parts and by application of the implemented methods, the entire device was computed in less than 15 minutes. All measurements were conducted using the near-field scanning system DASY4 equipped with the latest probes available.

Results and Discussion

The numerical and experimental characterization was conducted in free space and subsequently extended in complexity with various dielectric loads (SAM standard phantom, anatomical human heads). Hand models in different physiological positions were generated in the Poser ®package and enriched by anatomically derived bone/muscle/skin configurations. Depending on the applied antenna, hand configuration and head model, the device efficiency decreased from over 70% (free space) down to less than 15% (head and hand). In particular one antenna type operating in the PCS band showed a strong dependence and detuning of the device under the presence of an adjacent finger; this effect could be successfully reproduced using both methods. The performed analysis led to the incorporation of an optimized antenna which finally allowed improvement of the phones efficiency and reduced the sensitivity to being held. In addition, different parameters were evaluated, such as the impedance, far-field as well as near-field distributions of E- and H-fields and the SAR. Good to excellent agreement between measurement and simulation was obtained for all examined parameters and configurations. For the averaged SAR, deviations from measurements of less than 10% were obtained. The resulting reliable prediction for various daily usage configurations demonstrates the usability of numerical methods in the early design phase of devices as complex as high-end multi-band mobile phones.

Passive Metallic Implants In the Near Field of a Dipole: FDTD Simulation Results for SAR In the MRI-Based Head Model

H. Virtanen[1], **J. Keshvari**[2], and **R. Lappalainen**[1]

[1]University of Kuopio, Finland
[2]Nokia Research Center, Finland

The coupling of EM fields with active and passive implants in the human body is one safety aspect concerning the wide-spread use of RF fields in personal communications. While interactions with active implants have been quite extensively researched, only a few studies have focused on passive implants. The results, however, indicate that the presence of a conductive metallic implant may cause local SAR enhancement in the nearby tissues. This is mainly due to EM flux concentration near the conductive body. In this study the effects of passive metallic head region implants on SAR in the near field of a dipole, were studied numerically using the FDTD method. The implants modeled were authentic common metallic implants like fixtures, bone plates and ear rings and they were chosen on the basis of a literature survey. A MRI-based head model with 27 identified tissue types was used as the phantom. The EM field source was a simple half-wave dipole antenna scaled for 900, 1800 or 2450 MHz frequencies. The set up for modeling was based on our earlier studies of basic implant models (rings and pins) and the aim was to simulate the worst case situations. The implants located superficially in tissues near the dipole and resonance lengths were chosen whenever possible without loosing the practical meaning of the study. Moreover, the implants were considered as perfect electric conductors (PEC) in the simulations although authentic metallic implants are not perfectly conductive. The results indicate that the presence of implants should be taken into account in RF dosimetry because the EM field in tissues may enhance locally near the conductive implant. The highest enhancement of ${\rm SAR}_{1g}{}^{max}$ due to an implant was about 150 percent and for ${\rm SAR}_{10g}{}^{max}$ 60 percent as compared to the same case without an implant. However, generally passive metallic implants should not cause significant enhancement in mass averaged SAR in the near field of a RF source (i.e. mobile phone), unless they are very close to the source and have specific dimensions and orientation.

A Dual-Band Internal Antenna for Mobile Handsets: the Consideration of the Handset Case, Battery, Head, and Hand

Y. J. Cho and **S. O. Park**
Information and Communications University, Korea

This paper proposes a compact internal antenna of the modified planar inverted F antenna (PIFA) type with a parasitic patch. It also considers the influences of the handset case, battery, and head. A low profile design is implemented on both the top and bottom sides of the FR-4 substrate. The proposed antenna, with the small size of $27.5 \times 12 \times 7$ mm^3, can be easily placed in the actual handset. The measured bandwidths of the proposed antenna with handset case and battery (VSWR ¡ 2) can cover 140 MHz (1740 - 1880 MHz) in KPCS (Korean PCS) band and 90 MHz (2400 - 2490 MHz) in Bluetooth band. The shifting of resonance frequency is slightly changed when the proposed antenna installed in the handset case with battery is next to the phantom head. However, the radiation patterns of the far-field characteristics have a strong influence on the phantom head while retaining the slightly variation with VSWR value.

The effects of antenna performance due to the head and hand are also investigated. The hand is located near the phone in handset communication as close as the distance between the phone and head. Therefore, the effects of the hand should not be ignored. The holding pose is wrapping the phone case with all fingers in the vicinity of the lower part of one. It is interesting to note that the maximum peak point of SAR values occurs near and at the nail region of the second finger instead of the right edge region at the head. The edge part of the second finger in the right hand is located between the right hand side of the head and the radiation element of the backside of handset phone. This means that the finger is more susceptible to absorption of the radiation field when wrapping the handset phone. For example, the peak 1g SAR value is about 1.22 W/kg on the finger of hand while retaining the 1g SAR value as 0.8 W/kg inside of the head. We can find that the position of wrapping the handset phone is important to reduce the effect of an electromagnetic wave absorption in head and hand.

Numerical simulation and experiment results of antenna electrical performance are investigated by considering the antenna, phone case, battery, phantom head, and hand. Additionally, the proposed antenna is also considered with a SAR value in case of applying to the head and hand. By investigating the effects of the antenna performance such as the impedance bandwidth, radiation patterns, gains, and SAR value due to human body such as the head and hand in advance, the try and error procedure of mobile phone antenna design in the practical situation can be further reduced.

Session 4P6
Electromagnetic Fields of Nanometer Electromagnetic Waves and X-Ray

Synchrotron Radiation and Free-Electron Lasers-Tutorial Review

T. Shiozawa
Chubu University, Japan

In recent years, synchrotron radiation (SR) and free-electron lasers (FELs) have been playing an important role for the radiation sources in the region of the ultraviolet (UV) and X-ray wavelengths. In synchrotron radiation and free-electron lasers, high-brightness short-wavelength radiation can be produced by directly converting the kinetic energy of electrons, which are moving with relativistic velocities (comparable with the light velocity in vacuum), to electromagnetic wave energy. The electromagnetic waves emitted by synchrotron radiation cover a broad continuous spectrum extending from the far infrared (FIR) through the visible to the ultraviolet (UV) and X-ray wavelengths. On the other hand, free-electron lasers can generate coherent radiation with much higher brightness in the same spectral range, as compared with synchrotron radiation. In recent years, research efforts to realize the X-ray free-electron laser have been made in research facilities in several countries such as the United States and Germany. With its short and coherent pulses with enormous peak power, the X-ray free-electron laser will open a whole new field of scientific research, such as new medical and life sciences or fabrication of nano-scale structures. The present paper briefly reviews the basic principles of synchrotron radiation and free-electron lasers, from the viewpoint of classical electrodynamics. The operation principle of the free-electron laser can be explained purely classically, as opposed to the conventional laser whose operation principle is based upon quantum electrodynamics. In particular, special attention is paid to research efforts in the UV and X-ray free-electron lasers (1). For a more detailed discussion of the basic principles, refer to the reference (2).

REFERENCES

1. http://sbfel3.ucsb.edu/www/fel table.html.
2. T. Shiozawa : Classical Relativistic Electrodynamics - Theory of Light Emission and Application to Free-Electron Lasers, Springer, Berlin (2004).

Present Status and Future Prospect of Saga Synchrotron Light Project

M. Kamada, K. Takahashi, J. Azuma, T. Tanaka, and **H. Ogawa**
Saga University, Japan

Since the first observation of Synchrotron light (SL) in 1947, the science and technology using SL have been grown up to the present. SL has many useful characteristics (wide photon energy range from far-infrared to x-rays, high flux, high brilliance, small divergence, cleanness, polarization, short pulse, and so on), and is powerful and promising tool for nano-technology, bio-technology, material engineering, environmental applications, and so on. The Saga-SL, the first synchrotron light facility in Kyushu Island, is therefore expected to be used for wide variety of industrial applications as well as the academic studies in Kyushu area. Taking account of the limited amount of money and desired performances has optimized the parameters of the Saga-SL. It should be noted that the electron energy of 1.4 GeV, the critical energy of 1.9 KeV, and the emittance of 25.5 nmrad are designed with the straight section of about 2.7 m and 8 cells in the circumstance of 75.6 m. The wiggler of 5 or 7.5 T will also provide hard X-rays with the critical energy of 6.5 or 9.8 KeV.

The accelerator complexes consisting of a 250 MeV linac and an accelerator/storage ring have passed the inspection by the government on December 15, 2005 and now they are operational. Three prefecture open beam lines and one universityfs beam line are also ready for uses after recent efforts in construction. Many users from industries, universities, and institutes are welcome to activate and encourage the economics and young persons in local areas. The Synchrotron Light Application Center of Saga University has been carrying out academic subjects using advantage of SL. The center is interested in the new frontier fields such as non-thermal process and photo-CVD, advanced analyses, creation of combination system between semiconductors and bio-specimens, basic and application in environmental and material science, and so on. The center is also interested in the industrial application with SL as well. The useful and powerful methods with SL may produce wide variety of applications.

X-Ray Waveguides and Waveguide-Based Lens-Less Hard-X-Ray Imaging

C. Fuhse, C. Ollinger, and **T. Salditt**
University of Gottingen, Germany

In 1974, Spiller and Segmüller demonstrated that also X-rays may be confined in waveguides [1]. The complex refractive index for X-rays is usually written as $n = 1-\delta-i\beta$. Away from the absorption edges, δ can be approximated by $\rho_e r_e \lambda^2/2\pi$, where λ is the X-ray wavelength, ρ_e is the electron density, and $r_e \approx 2.818\times 10^{-15}$ m is the classical radius of the electron. Accordingly, X-rays may be guided in a guiding core of low electron density in cladding with a higher electron density. In 2003, Bergemann *et al* have calculated that X-rays may be confined in waveguides down to a fundamental limit of ≈ 10 nm in one or two dimensions [2]. This is significantly below the focal spot sizes achieved with state-of-the-art hard-X-ray focusing devices and waveguides may thus remarkably enhance spatial resolution in X-ray microscopy. In 1997, Lagomarsino *et al* demonstrated lens-less imaging of a nylon fibre with a planar waveguide at a spatial resolution of 140 nm [3]. However, since a planar waveguide was used, high spatial resolution could only be obtained in one direction. Two-dimensional beam confinement was demonstrated in 2002 by Pfeiffer *et al* who coupled an X-ray beam into lithographically prepared polymer channel waveguide [4].

In this paper we give a brief introduction to the propagation of X-rays in waveguides by analytical theory and finite-difference calculations [5]. We show how a very small, divergent, and coherent beam with a monochromatic flux of 10^6–10^7 photons per second may be obtained from two-dimensionally confining waveguides with cross-section dimensions well below 100 nm [6]. These devices may now be applied to various hard-X-ray microscopy techniques.

As a first application we present waveguide-based lens-less hard-X-ray projection imaging. The experimental setup corresponds to Gabor's "new microscopic principle" [7] today known as in-line holography. The sample is placed in the divergent waveguide beam and a magnified Fresnel diffraction pattern is recorded with a CCD detector. The optical transfer function related to the sample may then be deduced from a holographic reconstruction which is carried out numerically. As well known from holography with visual light, the reconstruction of an in-line hologram is drastically disturbed by the "twin-image". However, this problem may be solved by off-axis holography [8] which requires a second coherent reference wave. We demonstrate how X-ray waveguides may provide two coherent beams for off-axis holography and show first experimental results with a spatial resolution far in the sub-micron range.

REFERENCES

1. E. Spiller and A. Segmüller, *Appl. Phys. Lett.* **24**, 60, (1974).
2. C. Bergemann, H. Keymeulen, and J. F. van der *Veen, Phys. Rev. Lett.* **91**, 204801 (2003).
3. F. Pfeiffer, C. David, M. Burghammer, C. Riekel, and T. Salditt, Science **297**, 230 (2002).
4. S. Lagomarsino, A. Cedola, P. Cloetens, S. Di Fonzo, W. Jark, G. Souillié, and C. Riekel, *Appl. Phys. Lett.* **71**, 2557, (1997).
5. C. Fuhse and T. Salditt, Appl. Opt., acccepted.
6. A. Jarre, C. Fuhse, C. Ollinger, J. Seeger, R. Tucoulou, and T. Salditt, *Phys. Rev. Lett.* **94**, 074801 (2005).
7. D. Gabor, Nature **161**, 777 (1948).
8. E. M. Leith and J. Upatnieks, J. Opt. Soc. Am. **52**, 1123 (1962).

X-Ray Nanofocusing Limits for Capillaries and Zone Plates

C. Bergemann
University of Cambridge, U.K.
F. Pfeiffer, C. David, H. Keymeulen, and **F. van der Veen**
Paul Scherrer Institut, Switzerland

There is tremendous interest, and significant current research effort, to focus hard X rays to spot sizes of order 1 nm. Several routes are being pursued in practice, notably capillary waveguide optics and Fresnel zone plates, but also refractive and multilayer Laue lenses, and Kirkpatrick-Baez mirrors.

The propagation of X-ray beams through optical elements is described by the Helmholtz equation. For forward propagation, this is well approximated by a Schrödinger-type equation. We have used the powerful apparatus of quantum mechanics to implement a fast and robust numerical algorithm for the beam propagation through simple optical elements: capillary waveguides and zone plates.

The equivalent of the Heisenberg uncertainty relation leads to a focusing limit of order 10 nm, given by the decay length of the evanescent waves, that depends on the electron density of the optical element, but not on the X-ray wavelength. This limit applies to capillary optics [C. Bergemann *et al.*, Phys. Rev. Lett. 91, 204801 (2003)], and it also applies to Fresnel zone plates (in the standard geometry, i.e. with zones parallel to the optical axis) under plane wave illumination.

In contrast, the limit does *not* apply to zone plates in the one-to-one ($2f$-to-$2f$) focusing geometry. Here, the incoming X-rays provide sufficiently large transverse wavevectors to lead to "unbound" states from the Schrödinger viewpoint, and the Heisenberg uncertainty demands become much less stringent. Under specular reflection conditions, the zone plate focal spot size is found to be limited by the outermost zone width only, as expected classically. The specular reflection condition needs to be fulfilled quite precisely, though. The graph below shows the focal spot size generated from a point source at varying distance from the zone plate, and it is evident that the Heisenberg limit, of order 10 nm, is only overcome for a small range of distances [F. Pfeiffer *et al.*, submitted to Phy. Rev. B].

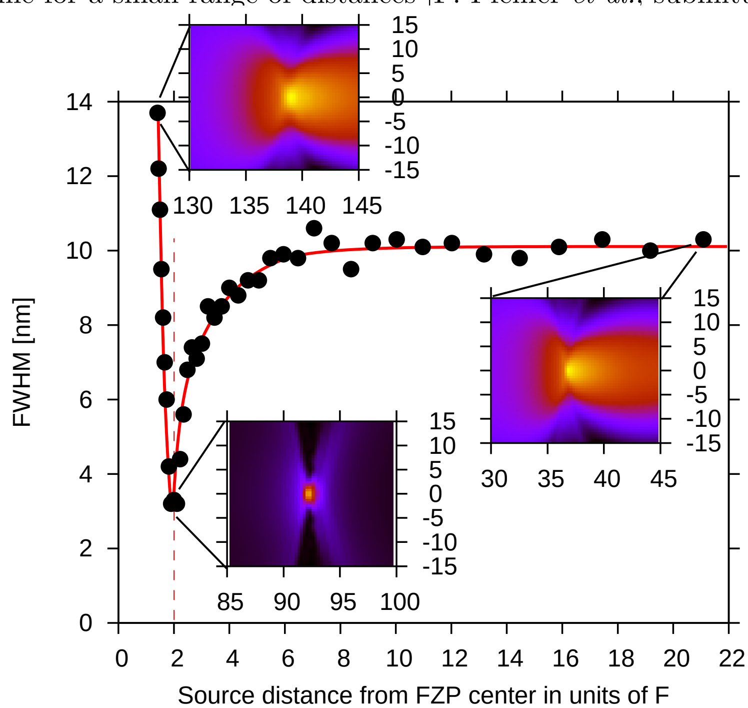

Analysis of Dispersion Characteristics in Photonic Crystal Consisting of Periodic Atoms for Nanometer Waveguides

Y. Miyazaki
Aichi University of Technology, Japan

N. Goto and **T. Innami**
Toyohashi University of Technology, Japan

Nanometer wave waveguide is a basic element for nanometer wave devices, which will be important for measurements, information transmission and processing in the fields of nano-space condensed matter, nano-technologies, bio-engineering, cell membrance and genetics. However, effective nanometer waveguides have not been developed yet. As an effective waveguide structure, we investigated photonic crystal with a lattice constant of the same order as the wavelength of nanometer waves. Although periodic structures are artificially made in optical wavelength region, natural atomic array structure can be regarded as the periodic structure in nanometer wave region. In nanometer wave region, refractive index of materials is smaller than 1, and has characteristics that depend on the frequency of the incident electromagnetic wave. For nanometer waves with the wavelength less than 0.5nm, atomic interval of the medium is the same order as the wavelength, and the material is considered as in a discrete structure. For the wavelength larger than 1nm, a periodic structure of moleculars is effective.

We numerically calculated the photonic band structures and dispersion characteristics for two-dimensional carbon and molybdenum arrays with plane wave expansion method. Although complete bandgaps do not exist in these matters, we found the existence of local bandgaps. For molybdenum crystal, the bandgaps exist between and X for TE wave and between M and and between and X for TM wave. For carbon crystal, the bandgaps exist between M and and between and K for TE wave and between and K for TM wave. The bandwidth for these bandgaps are of the order of THz. Although the two-dimensional model used in this research do not simulate the real periodic atoms, fundamental characteristics of bandgap in nanometer wave region were found.

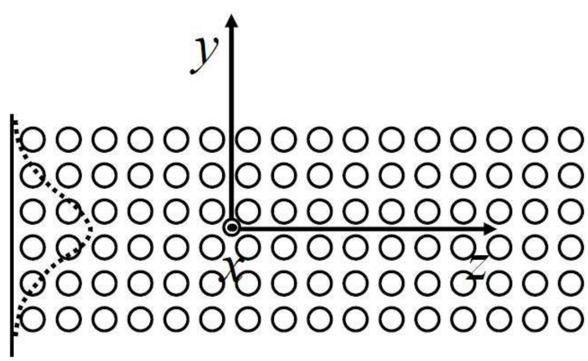

Figure 1: Two-dimensional photonic crystal consisting of circular cylinder array

REFERENCES

1. S. Tsujimoto and Y. Miyazaki: *Trans. IEE Japan*, Vol.119-C, No.1, pp.105-110 (1999).
2. Y. Miyazaki: *Trans. IEE Japan*, Vol.120-C, No.1, pp.68-73 (2000).
3. Y. Miyazaki and R. Fukuo: Proc. ISMOT'2001, pp.461-466, Montreal (2001).
4. T. Innami, Y. Miyazaki and N. Goto: *Trans. IEE Japan*, FM, Vol.124, No.12, pp.1198-1202 (2004).

Electromagnetic Characteristics of Grid Structures for Scattering Fields of Nano-Meter Electromagnetic Waves and X-Rays

Y. Miyazaki
Aichi University of Technology, Japan

X-ray, that is, nano-meter electromagnetic wave is very important physical tool for medical diagnosis and recently automatic image diagnosis using X-ray is rapidly developed[1]. However, image processing for medical diagnosis, based on photo-electric absorption, interactions between electrons and photons of X-ray, Thomson scatterings and Compton scatterings that are physiological and physical phenomena of X-rays in biomedical media are not so much studied[2-4]. The spatial characteristic in the received X-ray image is determined by the intensity of transmitted waves with scattered waves. The characteristics of transmitted waves depend on both the absorption and scattering characteristics. Therefore, for the identification of the characteristics of biomedical media by X-ray transmission, signal to noise ratio of primitive X-ray diagnosis is not so high. Although the use of the grid is efficient to remove the scattering wave from the transmitting wave, the grid has not been studied sufficiently. Also, by using spatial grid filter and the characteristics of scattering, absorption, dispersion and spectroscopy properly, it may be possible to find more accurate new method of X-ray image diagnosis. In this paper, the electromagnetic wave characteristics, primarily, the scattering filter characteristics of X-ray beam using the grid are studied. Based on this analysis, the optimum scattering wave filter may be found.

To obtain the electromagnetic scattering and transmitting fields with X-rays incident on the grid, the electromagnetic boundary value problem is considered using filter grid shown in fig. 1. The grid structure consists of atoms arranged periodically in x- and z-directions in the inner region II with grid material region II^1 and grid space region II^2. In fig. 1, the X-ray incidents on the grid input boundary z=-l_z in exterior region I^- and the characteristics of scattering and transmitting waves in exterior region I^+ are investigated for the nano-meter electromagnetic waves, the grid material (II) has complex dielectric constant due to the periodic structure of the atoms. In this case, the complex dielectric constant is considered to be periodic in x- and z-directions.

In case of y-polarized nano-meter electromagnetic wave, the electromagnetic fields in the grid region II(1) are analyzed by using periodic Fourier expansions in x- and z-directions. The y-polarized plane wave propagating toward z-direction is considered as an incident wave. In each region, the electromagnetic fields are expressed as integral representation with respect to the spectrum α of z-direction using spectral functions. Hence, all the electromagnetic fields can be derived from the spectral functions determined by boundary conditions. The component unit of grid ($2l_x \times 2l_x$) is arranged along x-direction with a period T, the transmitted and scattered field in region I^+ are determined using the boundary condition at the boundary of the grid z=l_z The tangential component of the electromagnetic fields should be continuous at the boundaries $z = \pm l_z$ and $x = \pm l_x + nT$, $|z| < l_z$. Using the periodicity of the grid in x-direction, the spectral function is assumed to be periodic in x-direction. The transmitted and scattered fields can be given by Wiener-Hopf method, as a method of spectral resolution.

The electromagnetic scattering and transmitted characteristics through X-ray grids are shown. X-ray grids have the spatial filter characteristics necessary to signal processing of the receiving characteristics in X-ray diagnosis. Based on this theory, the identification method of transmitting and absorption characteristics may be improved, and also it may be possible to utilize the scattering and spectroscopic characteristics effective for developing more rate X-ray image diagnosis.

REFERENCES

1. H. Aichinger, et al, Radiation Exposure and Image Quality in X-Ray Diagnostic Radiology (2003).
2. Y. Miyazaki, *Trans. IEE Japan*, Vol.83, No.2, pp.132-136 (2000).
3. Y. Miyazaki, The Papers of Technical Meeting on Electromagnetic Theory, IEE Japan, EMT05-77 (2005).
4. Y. Miyazaki, *Jpn. Jour. Appl. Phys.*, Vol.13, No.8, pp.1238-1248 (1974)

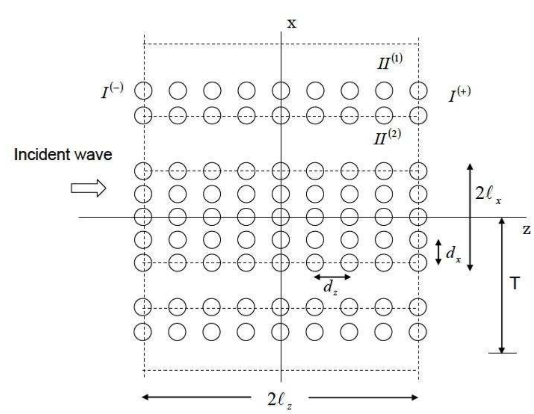

Figure 1: Structure of the grid

FDTD Parallel Computing of Fundamental Scattering and Attenuation Characteristics of X-Ray for Medical Image Diagnosis

[1]**K. Takahashi,** [1]**Y. Miyazaki,** and [2]**N. Goto**
[1]Aichi University of Technology, Japan
[2]Toyohashi University of Technology, Japan

X-ray diagnosis depends on the intensity of transmitting and scattering waves in X-ray propagation in biomedical media. To obtain the precise information on tissues, such as fat, bone and internal organs in biomedical media, the characteristics evaluation of refractive index and absorption depending on X-ray wavelength are indispensable. In this paper, we analyze scattering and absorption characteristics in biomedical media which consists of various atoms, using FDTD method[1,2]. In FDTD simulation, great amount of memory and calculation time are required because in this case, the size of the analysis space becomes larger than the wavelength. Therefore, parallel computing of FDTD method is considered to obtain realistic results in reasonable calculation time[3].

When the wavelength of X-ray is shorter than 0.5 nm, the structure of the material is considered to be discrete. In this study, electromagnetic scattering of X-ray Gaussian beam with 0.05 - 0.2 nm wavelength by random media is analyzed by two-dimensional FDTD method. The random media consists of many atoms whose sizes and positions are given randomly. The shape of atom is assumed to be square. In random media, atoms as random scatterers are generated by giving the length of a side of square a_i, positions of one apex (y_i, z_i), and dielectric constants ϵ_i. Statistical properties of electromagnetic scattering are discussed by using statistical parameters, such as average and variance of a_i and ϵ_i.

In our simulation, X-ray beam is assumed to be incident in the z direction and total analysis space is divided into some subregions along propagating direction z. The size of subregion is 30 nm (3000Δs) along y-direction and 20 nm (2000Δs) along z-direction, where Δs is the cell size of FDTD method and is 0.01 nm. Incident wave is X-ray Gaussian beam with 0.2 nm wavelength and 3 nm beamspot. As parameters for random atoms, a_i is from 0.1 nm to 0.2 nm, the number of atoms N is 3800, and four different values $n_a^{(i)}$ are given to the refractive indices of atoms $n_a^{(i)}$ for the simulations.

Simulation results show that qualitatively, as na becomes smaller than 1.0, the attenuation of the electric field amplitude at the center point of the beam becomes large and the intensity of scattering field becomes relatively strong at the foot of the beam. The presence of scattering fields causes the deterioration in the contrast of X-ray image, precise study of these characteristics can contribute to develop image processing technique to obtain high-quality X-ray images.

We develop a new approach to perform parallel FDTD computation using grid computer network. In FDTD analysis, the electromagnetic fields are calculated by difference equations derived from Maxwell's equations. We transform the difference equations to discrete linear equations. The solution of the difference equation is obtained by the solution of the linear equation. Fig. 1 shows the lattice points of FDTD computation. For the calculation of field intensities $\mathbf{X}^n$(i,j) at point (i,j), repeating the backward substitution, $\mathbf{X}^T$ is obtained by the initial value of the fields, where T is the final time step of the calculation. The advantages of this algorithm are relatively efficient. Relatively, small memory is required comparing with conventional FDTD and no concurrent data communication is occurred.

Based on these evaluations, simulation of X-ray scattering and attenuation characteristics depending on the X-ray wavelength with long-distance ropagation and comparison with experimental results may be shown.

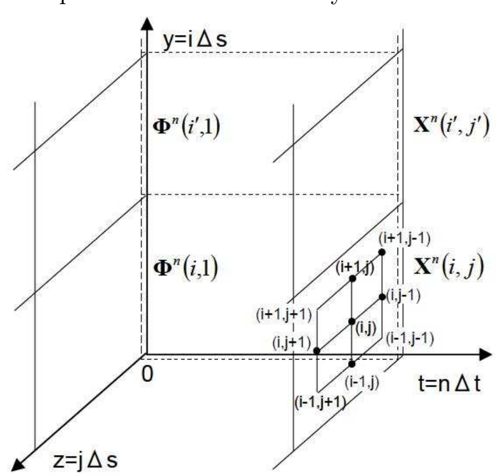

Figure 1: Lattice point for FDTD parallel Computation

REFERENCES

1. Y. Miyazaki, J. Sonoda and Y. Jyonori, *Trans. IEE Japan,* Vol.117-C, No.1, pp.35-41 (1997).
2. K. Takahashi and Y. Miyazaki, Trans. *IEE Japan,* Vol.120-C, No.12, pp.1905-1912 (2000).
3. K. Takahashi, H. Xinmin and Y. Miyazaki, *Digest of ISMOT-2005,* Fukuoka, Japan, B-16, p.109 (2005).

Orthogonal Relations of Electromagnetic Fields Including Evanescent Filed in Dispersive Medium

J. B. Li
Fuji Photo Film, Japan
M. Agu
Fukushima National College of Technology, Japan

Introduction

Intensive studies on evanescent waves have been promoted because of practical applications. As the evanescent electromagnetic field is a spatially localized field, the photon concept plays an important role in the near-field optics[1].

In this paper, with regard to the quantization problem of evanescent filed in dispersive medium, we consider a half-filled space where evanescent field appears when total reflection occurs. Starting from the divergence of the Poynting vector, we derive the orthogonal relations of the electromagnetic filed in different modes, including the evanescent electromagnetic field.

Orthogonal relations of the field in dispersive medium

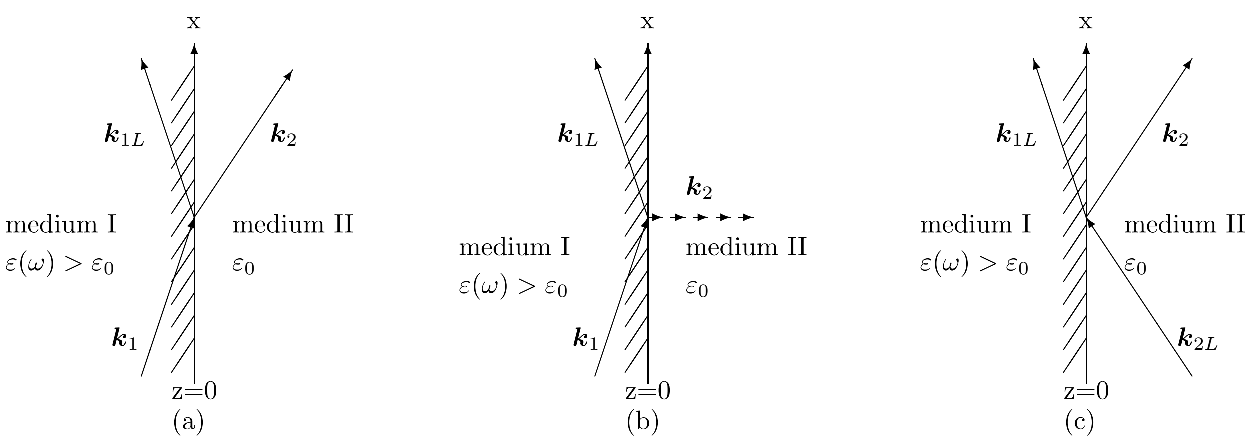

Figure 1: (a)Right-going propagating waves in region I and region II (b)Right-going waves where evanescent wave appears in region II (c)Left-going waves

As shown in fig. 1, the total field consists of right-going field and left-going field, where an evanescent field appears in the region II when total reflection occurs at the boundary. Therefore, the orthogonal relation of the total electromagnetic field in the whole space is expressed as,

$$\int d\boldsymbol{r} \left[\left(\frac{\omega'\varepsilon' - \omega\varepsilon}{\omega' - \omega} \right) \boldsymbol{e}' \cdot \boldsymbol{e}^* + \frac{1}{\mu_0} \boldsymbol{b}' \cdot \boldsymbol{b}^* \right] = 2 \frac{\partial \omega^2 \varepsilon(\omega, z)}{\omega \partial \omega} \delta(\boldsymbol{k}'(z) - \boldsymbol{k}(z)). \tag{1}$$

where $\boldsymbol{e}$ is the total electric field and $\boldsymbol{b}$ is the total magnetic field, the symbol $*$ denotes the complex conjugate and $'$ indicates the fields with the propagation constant $\boldsymbol{k}'$. And $\varepsilon(\omega, z)$ and $\boldsymbol{k}(z)$ are defined as;

$$\varepsilon(\omega, z) \quad = \quad \varepsilon(\omega) U(-z) + \varepsilon_0 U(z), \quad \textit{and}, \quad \boldsymbol{k}(z) = \boldsymbol{k}_1 U(-z) + \boldsymbol{k}_2 U(z), \tag{2}$$

REFERENCES

1. C. K. Carniglia and L. Mandel: *Phys. Rev.* **D3**, (1971) 280.

Structure Dependent Magnetic and Electrical Properties of Nano Ferrites

P. P. Kulkarni, V. R. Bote, and **S. A. Mane**
S. S. Arts College, India
R. B. Pujar
T. P. Science Institute, India

Ferrites are iron oxide based ceramic materials which behave as ferrimagnets. There is a growing need for nano sized ferrites for advanced technological applications. Chemical synthesis routes play a crucial role in designing final products. Chemical processing minimizes the problem of diffusion, impurities and agglomeration. The solution was composed of metal nitrate with polymer PVA and sucrose. Thermolysis of the precursor mass, at an external temperature around 500^oC, resulted in the oxide phase. The exothermic decomposition of precursors helps the material to disintegrate and to dissipate heat of decomposition, inhibiting the sintering of the fine particle. Sucrose being excess to metal ions, works not only as chelating agent but also serves as an efficient fuel for the combustion reaction. The oxide system investigated through this process include Ni-Zn-Cu, Ni-Zn-Mg and Ni-Zn Nano-ferrites.

X-ray diffraction patterns confirm the formation of single phase ferrites. All the samples show face centered cubic structure. IR absorption bands ν_1 and ν_2 are assigned to the vibrations of tetrahedral and octahedral complexes respectively. The presence of Fe^{2+} at octahedral sites results in the spitting of ν_2 band. SEM micrographs indicate the development of porosity at the base of the neck. Metal ion vacancies produce large pores at the boundaries of the crystallites. Hysteresis studies show the small values of Mr/Ms. This suggests that MD particles are present in all the samples. The variation of resistivity with temperature indicates the break at curie temperature. It is due to the transition of the sample from ferrimagnet to paramagnetic region. The electrical conductivity follows VerWey de Bore mechanism.

Key words : Nano, ferrites, Sucrose, PVA, SEM and MD.

Innovation Use of Nano Technology in Magnetic Storage Devices

D. Bajalan

Austria

New and light magnetic devices will be invented to make life in the 21st century more functional and the researchers have to gain more knowledge of quantum effects within nano-meter body size [1, 2]. Nanotechnology will increase its influence in electrical engineering and electrical materials strongly [1]. Our understanding of interatomic and electrostatic interactions have now reached a point where we can quite comfortably explain the macroscopic properties of matter, based on quantum mechanics and electrostatic interactions between electrons and ionic nuclei in the material. The fundamental equations of Maxwell will continues playing its large influence in nano magnetic devices($\nabla \cdot \mathbf{E} = \rho/\epsilon$, $\nabla \cdot \mathbf{B} = 0$, $\nabla \times \mathbf{E} = \partial \mathbf{B}/\partial \tau$, $\nabla \times \mathbf{B} = \mu_o \mathbf{J} + \mu_o \epsilon_o \partial \mathbf{E}/\partial \tau$). Nano-technology is providing a critical bridge between the physical sciences and engineering, on the one hand, and modern molecular biology on the other. Materials scientists, for example, are learning the principles of the nanoscale world by studying the behavior of biomolecules and biomolecular assemblies. In the case of magnetic devices, which are the subject of this work, there will be continued development in nano magnetic structures.Nano magnetic structures are becoming one of the trends in developing the magnetic devices like magnetic recording, storage, and other electronic devices. The industry of magnetic data storage systems will profit from the nano-magnetic structures to produce ultra high density recording media at lower prices. Nano-technology enables new design concepts and opportunities for the information industry . The computer industry will benefit largely from the size change in magnetic structures, which are used in technologies of hard disk drives (HDDs) or magnetic random access memories (MRAMs), and other hardware of computer systems parts. The cost per data bit will decrease year by year. The bit price decrease will give larger chances to store data onto magnetic recording media. With the advent of thin films and lithography techniques it is now possible to prepare nano-structured objects with a well controlled geometry, and the ability of modern lithography to produce arbitrary nano-scaled images on a given substrate [3].

REFERENCES

1. D. Bajalan, H. Hauser, P. L. Fulmek, *Physica B* 343, 384 (2004).
2. D. Bajalan, Progress in Electromagnetic Research Symposium (August 22 to 26), Hangzhou, China: Extended paper (ISBN 1-933077-07-7), 386 (2005).
3. D. Bajalan, Progress in Electromagnetic Research Symposium (March 28 to 31), 2004, Pisa, Italy: Extended paper (ISBN 88 8492 268 2), 667 (2004).

Nano-Beam Production by Particle Channeling

D. Bajalan

Austria

Since 1991, here has been a lot of study on carbon nanotubes to understand their formation and properties. Carbon nanotubes stick out in the field of nanostructures, owing to their exceptional mechanical, capillarity, electronic transport and superconducting properties. Carbon nanotubes are cylindrical molecules with a diameter of order 1 nm and a length of many microns [1]-[2]. They are made of carbon atoms and can be thought of as a graphite sheet rolled around a cylinder. In general NTfs could be manufactured of different diameters - from a fraction of a nm to a few microns, of different lengths - from a micron up to a few millimeters, of different materials. This makes nanotubes a very interesting object for channeling research [1].

REFERENCES

1. S. Bellucci, V.M. Biryukov, Yu. A. Chesnokov, V. Guidi, and W. Scandale, Phy. Rev. special topics -accelerators and beams, 6, (2003) 033502-1 . 033502-4.
2. V.M. Biryukov, Y.A. Chesnokov, S. Bellucci, V. Guidi, W. Scandale, IEEE-Proceedings of the particle accelerator conference, (2003) 986.

Channeling in SWNT and Other Applications of Carbon Nano Tubes

D. Bajalan

Austria

If the DRAM industry is to continue with its exponential rate [1]of density improvement, it seems likely that there will need to be a radical change in the construction of memory devices at some point. Certainly quantum-dot devices have possibilities in this role and significant RD effort has been put forward to develop it. A different possibility is in the construction of a nanometer-sized memory device based on the self-assembly of buckyballs inside of carbon nanotubes. This bucky shuttle memory offers nonvolatility and terahertz switching speeds. Also, each bit could require as little as two square nanometers. Creating efficient channeling structures from single crystals to epitaxial layers to nanotubes might have a significant effect onto the industrial world.

REFERENCES

1. D. Bajalan, Progress in Electromagnetic Research Symposium (August 22 to 26), Hangzhou, China: Extended paper (ISBN 1-933077-07-7), 386 (2005).

Session 4P7
Novel Mathematical Methods in Electromagnetics III

Three-Dimensional Forward Solvers based on improved Formulations of the Extended Born Approximation

D. Franceschini [1], **A. Abubakar** [2], **T. M. Habashy** [2],and **A. Massa** [1]

[1]University of Trento, Italy
[2]Schlumberger-Doll Research, U.S.A.

A wide number of applications, like subsurface detection, medical imaging and non-destructive evaluation and testing, require the modeling of the full three-dimensional scattering in the complex scenarios. Integral equation method is one of the effective and powerful tools for solving such electromagnetic problems. However, their computational cost becomes expensive when a fine discretization of the computational domain is needed. In fact, depending on the frequency, the size and the contrast of the scatterer, a large number of cell might have to be employed and this leads to a full complex system to be inverted. In order to avoid prohibitive computational efforts, many different kinds of approximations have been widely used to develop faster forward solvers. First of all, in [1] Born proposed to replace the internal field with the distribution of the field in absence of the scatterer. Such a method has been shown to be suitable only for weak contrasts [2], limiting its actual range of application. As a matter of fact, the estimation of the field inside the scatterer has been improved by the so-called Extended Born approximation (EBA) [3], without significantly increasing the computational efforts with respect to the Born method. By means of a non-linear localized approximation, the field inside the scatterer is obtained projecting the background field onto a depolarization scattering tensor. Notwithstanding many works have shown the accuracy of the EBA if compared to that of the Born approximation, some lack of accuracy when the scattering medium is in close proximity of the source [4] still remains. In order to overcome this limitation, the source behavior has been taken into account in the scattering tensor, obtaining considerable improvements with respect to the standard EBA approximation. Successively, this approach has been extended [5] to the full three-dimensional case considering the source behavior by means of a Green function formulation. In particular, the Extended Born is applied firstly to the spatial distribution of the Green function tensor, so that the source excitation is taken into account in the scattering tensor. Certainly, such a procedure requires more resources if compared to the standard EBA approximation, but there is still a significant computational saving with respect to the full integral equation methods.

In this context, further numerical results will show that the original EBA has been effectively improved using a Green function formulation. Moreover, an innovative formulation of the EBA based on an higher order approximation will be discussed and compared with the other approaches. The results will show that such techniques may achieve accurate results in many situation of practical interest without requiring the inversion of a huge full complex matrix and thus avoiding the computational requirements of a full integral equation method.

REFERENCES

1. M. Born, Optik, Springer-Verlag, New York, 1933.
2. M. Nieto-Vesperinas, Scattering and Diffraction in Physical Optics, Wiley, New York, 1991.
3. T. M. Habashy, R. W. Groom, and B. Spies, "Beyond the Born and Rytov approximations: a non linear approach to electromagnetic scattering," *J. Geophys. Res.*, vol. 98, pp. 1759-1775, 1993.
4. C. Torres-Verdin and T. M. Habashy, "Rapid numerical simulations of axissymmetric single-well induction data using the Extended Born approximation," *Radio Sci.*, vol. 36, pp. 1287-1306, 2001.
5. A. Abubakar and T. M. Habashy, "A Green function formulation of the Extended Born approximation for three-dimensional electromagnetic modeling," *Wave Motion*, vol. 41, pp. 211-227, 2005.

Characteristics of Diffuse Photon Density Waves in Column-Shaped Media

J. Taniguchi, F. Iwata, M. Hattori, H. Murata, and **Y. Okamura**

Osaka University, Japan

Diffuse optical tomography (DOT) plays an important role in investigating the inside of turbid media such as biological tissues, clouds, turbid plastics, and painted surfaces. Particularly, diffuse photon density waves (DPDWs) excited with a sinusoidally amplitude modulated light source are an essential means to acquire necessary data for recovering objects with different properties in the scattering media. So far there have been reported various analytical and numerical methods to express the propagation of DPDWs in turbid media: Green's function in 3-dimension in an infinite or a slab-shape medium for the analysis, and a Monte-Carlo and a finite-element method for the numerical.

In this report, we analytically and experimentally demonstrated DPDWs in column-shaped scattering media for eventually examining forearms or forefeet interested in orthopedic surgery. As a tested sample we used a turbid crystalline polymer like polyacetal with a diameter of 52mm simulated the forearm. First, we derived a Green's function of DPDW in a column-shaped medium when exciting a sinusoidally amplitude modulated light at a point position. Next, we measured DPDW propagating in the scattering medium by use of an experimental setup consisting of a modulating diode laser operating at 660nm, a photo-multiplier, input and output optical fibers, a heterodyne detecting system, and a rotating sample mounting.

Figures 1 and 2 plot the results obtained from the theory and the experiment: the amplitude and the phase of DPDW as a function of rotating angle. We deduced absorption and reduced scattering coefficients comparing values of amplitudes and phases of DPDW obtained numerically and experimentally: the former coefficient was $0.009cm^{-1}$ and the latter one was $11cm^{-1}$. These values were in good agreement with those measured for the slab-shaped sample. Furthermore, we prepared samples, in which a small hole with a diameter of 7.5mm was drilled to simulate the inside of the forearm. We investigated the distorted DPDWs as changing materials inserted into the hole: air, water, and diluted milk.

Now we are analyzing the last cases and imaging the inserted materials.

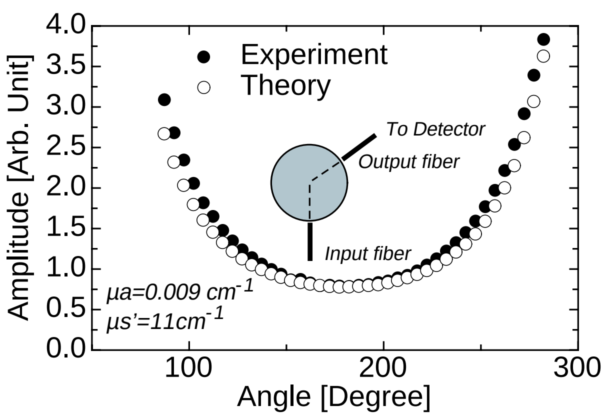

Figure 1: Amplitude of DPDW vs. rotation angle

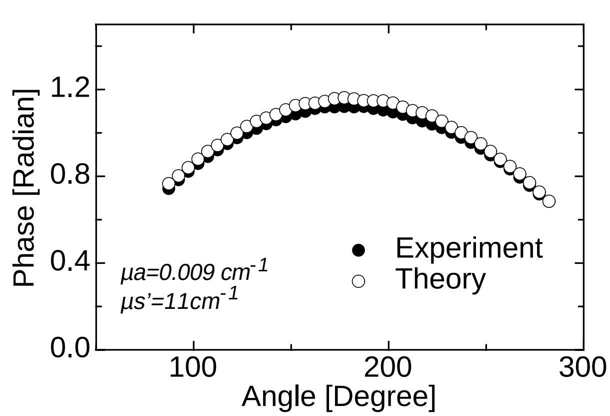

Figure 2: Phase DPDW vs. rotation angle

Computation of the Scattering of Arbitrary Shape Bodies Modeled by Parametric Surfaces Using the Multilevel Fast Multipole Method

I. González, O. Gutiérrez, F. S. de Adana, and **M. F. Catedra**
Universidad de Alcalá, Spain

An application of the MLFMA to the electromagnetic analysis of realistic bodies modeled by NURBS surfaces is presented. The discretization of the geometry is carried out using also NURBS surfaces that permit an exact representation of the body under analysis. The basis and test functions are also conformed to the geometry to take advantage of the exact representation. A dual mesh is used to improve the convergence of the method and to allow analyzing non conducting bodies.

The main advantage of the presented scheme, as mentioned above, is the use of a discretization of the geometry totally conformed to the exact shape of the body under analysis. Each NURBS surface is divided in quadrangular patches, obtaining a lower number of subdomains by comparison of the discretization using triangular patches. Moreover, being the patches completely conformed to the real NURBS, there is an exact correspondence between the geometrical and the electrical representations of the body under analysis, allowing the treatment of complex bodies without any kind of approximation in the electrical representation.

Multilevel Fast Multipole Method (MLFMA) has been implemented over the geometrical discretization described above. The method is implemented in such way, that the number of levels of the multilevel approach can be as high as desired, and it is a parameter that can be chosen by the user. The aggregation and dis-aggregation terms are obtained by the Fast Multipole Method (FMM) formulation, at the lowest level following an interpolation-anterpolation procedure to accomplish the matrix-vector product at the highest levels. The basis functions are the Rao-Wilton-Glisson rooftops and the test functions are the razor-blade functions. Both functions have been modified in the implemented approach to be adapted to the conformed mesh.

A new approach to solve the problem is used. The approach can be an alternative to the Combined-Field Integral Equation (CFIE) formulation and shows better features than the CFIE to calculate the scattering from conducting bodies for ill conditioned problems. The scheme is also useful to analyze, using the Impedance Boundary Condition (IBC) approximation, the scattering from conducting bodies that can be totally or partially coated by dielectric materials. The scheme uses a dual mesh to represent the currents: one mesh represents the electric currents, and its dual mesh represents the magnetic currents.

Illustrative numerical examples will be included in the paper together with validations against measured data for a number of representative test cases.

New Electric Field Integral Equation for Computer Aided Design of 3-Dimensional Waveguide

M. Tanaka and **K. Tanaka**

Gifu University, Japan

It is very important to calculate the transmitted and reflected powers of a waveguide with high accuracy, in order to design waveguide circuits or discontinuities. As a basic theory of computer aided design (CAD), we proposed a boundary integral equation that is called Guided-Mode Extracted Integral Equation (GMEIE) for a 2-dimensional waveguide[1],[2]. GMEIE can be numerically solved by the standard method of moment (MoM). In this paper, we propose a new electric field integral equation (EFIE) that is suitable for basis theory of CAD of a 3-dimensional (3D) waveguide.

We consider a 3D waveguide as shown in Fig. 1. The two waveguides whose cross-sections are rectangle $a_i \times b_i$ $(i = 1, 2)$ are connected by the junction, where the junction is an arbitrary shape. We suppose that $a_i \geq b_i$ and a TE_{10} mode can only propagate in the waveguides 1 and 2. The incident wave that is a TE_{10} mode comes from the left side of the waveguide 2.

The surfaces of the waveguide are denoted by S_0, S_1 and S_2, where S_0 has finite area, and S_1 and S_2 have infinite area. The surfaces S_{10} and S_{20} denote the virtual surface between the junction and the waveguide 1, and between the junction and the waveguide 2, respectively.

We start from a conventional EFIE, which is the same form as that for a scattering object. However, there are two differences between EFIE for a waveguide and that for an object: (1)the surface of a waveguide has infinite area, while that of an object has finite area; (2)the incident field is implicit in EFIE for a waveguide, while that is explicit in EFIE for an object. Therefore, a conventional EFIE can not be directly solved by MoM. We briefly show the procedure to derive a new EFIE.

We decompose the electric and magnetic fields into "guided fields" and "unguided field" that is the sum of cutoff modes. For instance, the electric field $E(x)$ in the waveguide 1 is decomposed as $E = TE^{+(1)} + E^C$, and that in the waveguide 2 is decomposed as $E = RE^{+(2)} + E^{-(2)} + E^C$, where T and R are unknown transmitted and reflected coefficients, respectively. $E^{+(1)}$, $E^{+(2)}$ and $E^{-(2)}$ are the transmitted, reflected and incident guided modes, respectively. E^C denotes unguided field.

Substituting the decomposed fields into a conventional EFIE and applying Green's theorem into guided-modes, we obtain a new EFIE. A crucial point is that the unknown functions on S0 are total field, and those on S_1 and S_2 are unguided fields. Since the unknown functions on S_1 and S_2 in the new EFIE are unguided fields, they vanish at far point from the origin. Therefore, S_1 and S_2 which have infinite area can be treated as finite area. However, the new EFIE can not be numerically solved by MoM, because the coefficients T and R are unknown.

Using an asymptotical express of Green's function, we obtain additional equations. Finally, we can solve the new EFIE by MoM.

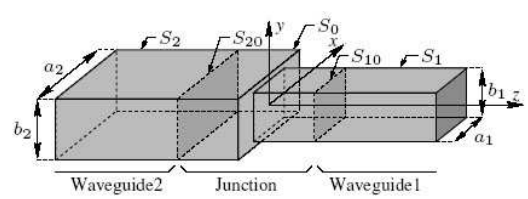

Figure 1: Model of 3D waveguide

REFERENCES

1. K. Tanaka, M. Kojima: *Electron. Lett.* vol. 24, pp. 807-808 (1988).
2. K. Tanaka, M. Nakahara: *IEEE Trans. Microwave Theory Tech.*, vol. 40, pp. 1647-1654 (1992).

Static Stability and Plate Spacing for Diamagnetic Levitating Magnets

J. N. Ho
University of Washington, U.S.A.

W. C. Wang
University of Washington, U.S.A.

This paper analyzes the static stability of a diamagnetic levitating magnet. Balancing forces is necessary but does not guarantee stable levitation. Restoring forces (minimizing potential energy) of a levitating magnetic around the zero force point is also required. An equivalent statement is that any small displacement from the zero force point causes the magnet to return to the zero force point. A derivation using this concept gives a stability criterion for cylindrical levitating magnets. The criterion controls the spacing of the diamagnetic plates needed to stably levitate a magnet. This was verified by experiments using regular graphite and pyrolitic graphite plates. When adjustment for plate thickness is included, theoretical stability requirements and experimental results match well.

Responsibility of Electromagnetism for the Origin of the Rings of Saturn from Superconducting Particles of the Protoplanetary Cloud

V. V. Tchernyi
Russian Academy of Science, Russia

The reason for the coming into being and stable existence of the rings of Saturn has been a mystery and an unsolved scientific problem for 400 years. In 1859 Maxwell deduced that the rings consisted of solid and separate particles. Further experiments proved that the ring particles contain frozen water with inclusions of ammonia, methane, sulphuric and organic compounds, ferrosilicates and other substances. The particles of the rings move as they should according to Kepler laws. Gravitation force compensated by centrifugal force for any particle.

Numerous attempts to explain the origin of the rings with the use of notions about gravitation, particles' interaction with solar wind or emergence from dust plasma have not been successful. Moreover, the existing theories of the rings are characteristically heterogeneous and not united by a single physical nature of their origin. But most importantly they cannot explain a multitude of the phenomena observed. A paradoxical situation has taken shape, where, with the exception of a huge database on the properties of the rings, excellent photographs and radar data obtained by means of expensive devices on board the space probes, no full-value physical picture of the rings of Saturn existed till today.

According to the new understanding, the rings of Saturn took shape from superconductive ice particles of the protoplanetary cloud that initially surrounded Saturn. After the magnetic field of Saturn came into being the superconductive particles of the protoplanetary cloud began drifting to the plane of the magnetic equator, which as a result led exactly to the formation of the highly flattened disk around Saturn. Similar to magnetic particles creating dense and rarefied areas in a nonuniform magnetic field the superconductive ice particles also form their groups, which from outside look like a system of rings. The superconductivity of the ring particles is confirmed by the fact that the ring particles are relics of the early days of the Solar system and were never subject to coalescence and heating. The superconductive particles cannot stick together as the magnetic field emanates from them and pushes the particles apart. Indeed, the Sun heats the rings weakly, the temperature in area of the rings being only around one hundred degrees above the absolute zero. And high-temperature superconductivity discovered in 1986 can already be observed under such temperatures, and in the same 1986 experimentally demonstrated superconductivity of ice.

The discovery of the superconductivity of the matter of the ring particles allows to explain many experimental data on land-based and space research of Saturn: how the rings came into being, how they were grouped into the disk; why the ring particles do not get mixed; why the microwaves of the circular polarization are reflected from the ring as if from a magnetic mirror; why the magnetic field is pushed out from the rings; why the spokes take shape; why non-polarized electromagnetic radiation ranging from kilohertz to megahertz emerges; where from some kind of an atmosphere appears near the rings; how density waves and bended waves take shape; why earth type planet does not have a rings, and a lot more.

Statistical Representative Volume Element for Predicting the Dielectric Permittivity of Random Media

D. Jeulin and **M. Moreaud**
Ecole des Mines de Paris, France

An efficient way to predict the dielectric permittivity of heterogeneousmedia makes use of numerical solutions of the corresponding partial differential solutions, before estimating the effective properties by spatial averaging of the solution. The input image can be a 3D image of the studied medium obtained by various techniques, or simulations of realizations of an appropriate model of random structure. Beside the finite element method, efficient iterative techniques operating by Fast Fourier Transform on periodic media were recently developed for micromechanics problems [6], and for the dielectric permittivity [2, 1]. We use this numerical approach in this paper.

When using numerical simulations, it is of primary importance to know the representativeness of the effective property estimated on a bounded domain of a microstructure. In other words, we need to know the size of a so-called "Representative Volume Element" RVE [4]. A similar question appears for engineering purpose, when working on parts with dimension of the same order as the microstructure, as appears in micro-electronics devices. To solve this problem, we developped a statistical approach involving higher order statistical information than average values. The second order moment of the field over an infinite domain can be worked out when the effective property is known, but it does not provide any information on the fluctuations of the average made over a finite domain. Recent developments use a geostatistical approach based on the experimental determination of the integral range A3 [5] from numerical simulations [4]. It enables us to relate the variance $D^2_Z(V)$ of the effective property as a function of the volume V of the simulation and of A3. For a large specimen (with $V \gg A_3$), we have $D^2_Z(V) = D^2_Z A_3/V$, D^2_Z being the point variance of the random field Z(x). The properties A_3 and D^2_Z are estimated from realizations of Z(x) on domains B with an increasing volume V. Then from D^2_Z is computed an interval of confidence of the effective properties as a function of the volume of the simulations and of the number of realizations, providing a statistical definition of the RVE. This methodology was applied to the case of the dielectric permittivity of various random media [1], and to the elastic properties and thermal conductivity of a Voronoi mosaic [4], and of real microstructures. In this paper, our approach is first validated by integral ranges obtained from the estimation of the dielectric permittivity of 2D autodual random sets (a two phase symmetrical dead leaves model [3], for which the exact effective permittivity is known), and then applied to complex models of 3D multiscale random nanocomposites reproducing the non homogeneous distribution of carbon black or of carbon nanotubes in a matrix. The effective permittivity ... and the corresponding RVE are estimated on images of ..(x) with increasing sizes and for an increasing contrast of permittivity.

REFERENCES

1. Jeulin D., Delarue A. (2002) Numerical Homogenization of Dielectric Properties of Random Media. Application to Nanocomposites, In: Journee doctorale 2002 Saint-Etienne (20 Novembre 2002), Signaux et milieux complexes, ISBN 2-86272-281-2, Th. Fournel et G. Brun (eds), Presses de l'Universite Jean Monnet, pp. 77-87.
2. Eyre, D.J., G.W. Milton (1999): 'A fast numerical scheme for computing the response of composites using grid refinement', *Eur. Phys. J. Appl. Phys.* 6, pp. 41-47.
3. Jeulin, D. (ed) (1997): Proceedings of the Symposium on the Advances in the Theory and Applications of Random Sets (Fontainebleau, 9-11 October 1996) (World Scientific, Singapore).
4. Kanit T., Forest S., Galliet I., Mounoury V., Jeulin D. (2003): 'Determination of the size of the representative volume element for random composites: statistical and numerical approach', International Journal of solids and structures, Vol. 40, pp. 3647.3679.
5. Matheron, G. (1971): The theory of regionalized variables and its applications. (Paris School of Mines publication).
6. Moulinec H., P. Suquet (1994): 'A fast numerical method for computing the linear and nonlinear mechanical properties of composites', C.R. Acad. Sci. Paris, 318, S*rmé*rie II, pp. 1417-1423.

Plane Wave Diffraction by a Finite Parallel-Plate Waveguide with Four-Layer Material Loading: The Case of E Polarization

J. P. Zheng and **K. Kobayashi**
Chuo University, Japan

The analysis of electromagnetic scattering by open-ended metallic waveguide cavities has received much attention recently in connection with the prediction and reduction of the radar cross section (RCS) of a target [1-4]. Various diffraction problems involving two-dimensional (2-D) and three-dimensional (3-D) cavities have been analyzed thus far based on high-frequency techniques and numerical methods. However, the solutions obtained by these methods are not uniformly valid for arbitrary cavity dimensions.

In the previous papers [5], we have considered a finite parallel-plate waveguide with three-layer material loading as a geometry that can form cavities, and solved the plane wave diffraction with the aid of the Wiener-Hopf technique. In this paper, we shall analyze the plane wave diffraction by a finite parallel-plate waveguide with four-layer material loading as an important generalization of the waveguide geometry problem considered in previous paper [5]. We shall present illustrative numerical examples of the RCS to discuss the far field backscattering characteristics. In the following analysis, the case of E-polarization will be treated.

Introducing the Fourier transform for the scattered field and applying boundary conditions in the Fourier transform domain appropriately, this problem is formulated in terms of the simultaneous Wiener-Hopf equations satisfied by unknown spectral functions, which are solved exactly in a formal sense through the factorization and decomposition procedure. Applying a rigorous asymptotics with the aid of the edge condition, we shall derive an efficient approximate solution. The derivation of the scattered field of the whole space will then be discussed by taking the Fourier inverse of the solution and applying the saddle point method.

The time factor is assumed to be and suppressed throughout this paper.

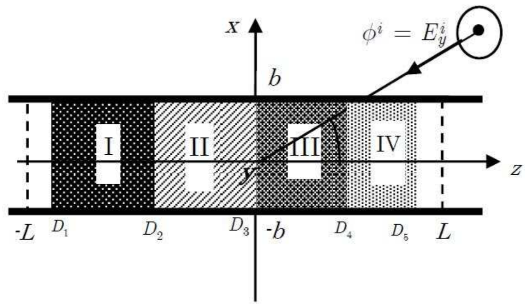

Figure 1: Geometry of the problem.

REFERENCES

1. Stone, W.R., ed., Radar Cross Section of Complex Object. *IEEE Press*, New York, 1990.
2. Lee, S.-W. and Ling, H., Data Book for Cavity RCS: Version 1, Tech. Rep., No. SWL 89-1, Univ. Illinois Urbana, 1989.
3. Lee, S.-W. and Marhefka, R. J., Data Book of High-Frequency RCS: Version 2, Tech. Rep., Univ. Illinois, Urbana, 1989.
4. Bhattacharyya, A.K. and Sengupta, D. L., Radar Cross Section Analysis and Control, Artech House, Boston, 1991.
5. Okada, S., Koshikawa, S., and Kobayashi, K., Wiener-Hopf analysis of the plane wave diffraction by a finite parallel-plate waveguide with three-layer material loading: Part I. the case of E polarization, Electromagnetic Waves & Electronic Systems, 2002, vol. 7, no. 4-5, pp. 41-49.

Plane Wave Diffraction by a Finite Parallel-Plate Waveguide with Four-Layer Material Loading: The Case of H Polarization

E. H. Shang and **K. Kobayashi**
Chuo University, Japan

Analysis of the scattering from open-ended metallic waveguide cavities has received much attention recently in connection with the prediction and reduction of the radar cross section (RCS) of a target [1, 2]. A number of two- and three-dimensional (2-D and 3-D) cavity diffraction problems have been analyzed thus far by means of high-frequency ray techniques and numerical methods, but it appears that the solutions obtained by these approaches are not uniformly valid for arbitrary cavity dimensions.

In the previous papers [3-5], we have carried out a rigorous RCS analysis of 2-D cavities with and without material loading, formed by a parallel-plate waveguide, using the Wiener-Hopf technique . We have also considered a finite parallel-plate waveguide with three-layer material loading as a geometry that can form cavity structures, and carried out the Wiener-Hopf analysis of the plane wave diffraction [6, 7]. As an important generalization to the geometry in [6, 7], we shall consider, in this paper, a finite parallel-plate waveguide with four-layer material loading, and analyze the H-polarized plane wave diffraction by means of the Wiener-Hopf technique. Our final solution is shown to be valid for the waveguide length large compared with the incident wavelength.

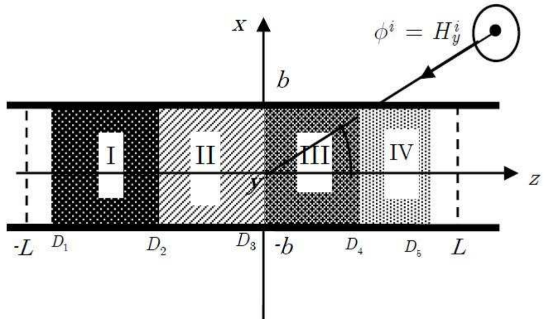

Figure 1: Geometry of the problem

REFERENCES

1. Lee, S.-W. and H. Ling, gData book for cavity RCS: Version 1,h Tech. Rep., No. SWL 89-1, Univ. Illinois, Urbana, Jan. 1989.
2. Lee, C. S. and S.-W. Lee, gRCS of a coated circular waveguide terminated by a perfect conductor,h *IEEE Trans. Antennas Propagat.*, vol. AP-35, no. 4, pp. 391-198, Apr. 1987.
3. Kobayashi, K., and Sawai, A., Plane wave diffraction by an open-ended parallel plate waveguide cavity, *J. Electromagn. Waves Appl.*, vol. 6, no. 4, pp. 475-512, 1992.
4. Koshikawa, S. and Kobayashi, K., Diffraction by a parallel-plate waveguide cavity with a thick planar termination, *IEICE Trans. Electron.*, vol. E76-C, no.1, pp. 142-158, 1993.
5. Koshikawa, S. and Kobayashi, K., Diffraction by a terminated, semi-infinite parallel-plate waveguide with three-layer material loading: the case of H polarization, Electromagnetic Wave and Electronic Systems, 2000, vol. 5, no. 1, pp.13-23.
6. Okada, S., Koshikawa, S., and Kobayashi, K., Wiener-Hopf analysis of the plane wave diffraction by a finite parallel-plate waveguide with three-layer material loading: Part I. the case of E polarization, Electromagnetic Waves & Electronic Systems, vol. 7, no. 4-5, pp. 41-49, 2002.
7. Okada, S., Koshikawa, S., and Kobayashi, K., Wiener-Hopf analysis of the plane wave diffraction by a finite parallel-plate waveguide with three-layer material loading: Part II. the case of H polarization, Electromagnetic Waves & Electronic Systems, vol. 7, no. 4-5, pp. 50-55, 2002.

Algorithmic System for Identifying Bird Radio-Echo and Plotting Radar Ornithological Charts

L. Dinevich and **Y. Leshem**

Tel-Aviv University, Israel

The proposed algorithmic system for identifying bird radio-echo against the background of reflectors of other types was developed within a novel approach based on the analysis of echo movement characteristics. A long-term implementation of the previously designed algorithm (Dinevich et al. 2004) has demonstrated its ability for identifying bird echo with high confidence. At the same time, this work enabled to determine the directions of further research, aimed at: a) significant reduction of computation time; b) increasing echo identification accuracy in cases of weak echo and of large dense bird masses; c) plotting radar ornithological charts on-line.

In the course of the present study, a comparative analysis was carried out of radio-echo typical of different categories of reflectors. As a result, a set of characteristics was obtained that distinctly specify bird echo and distinguish it from echoes of other types of reflectors. The algorithmic system based on this set of characteristics enables to determine whether a radio-echo movement belongs to one of the four patterns: a) straightforward at non-uniform velocity; b) straightforward at uniform velocity; c) significant deviation from a straight line, nonuniform velocity and d) chaotic undirected shifts. The data on echo movement pattern were used for plotting bird (bird group) flight vectors. In order to filter off false vectors, a special algorithmic procedure was devised based on a number of additional echo characteristics, including the threshold value, the extent of chaotic status in the direction of closely located vectors, the maximum and minimum velocities etc. Another proposed algorithmic procedure enables to make a prompt and accurate (at least 80% confidence) decision on the bird-not birdEorigin a particular echo on the basis of its fluctuation pattern. The system enables on-line plotting of operational ornithological charts every 12-15 min, including charts that combine meteorological and bird monitoring data, and thus is as an efficient means of maintaining air traffic safety in complicated meteorological and ornithological conditions. In view of the fact that MRL-5 radars are located in many countries and cover an extremely vast territory, it appears expedient to connect them into a network. Using the algorithmic system for bird echo identification by means of MRL-5 radar, such a network could perform intercontinental bird monitoring in the real-time mode, contributing to providing collective air traffic safety.

Key words: radar ornithology, bird echo identification, radio-echo, birds, bird migration, air traffic safety, meteorological radar.

Interpolating Wavelets on the Interval for Time-Domain Electromagnetics

C. Represa [1], **J. Muñoz** [2], and **S. Amat** [3]

[1]Universidad de Burgos, Spain
[2]Universidad de Murcia, Spain
[3]Universidad Politécnica de Cartagena, Spain

Wavelets bases have been presented as a powerful tool to perform the approximation and the numerical resolution of partial differential equations. Consequently, wavelets have been also applied to the solution of Maxwell's equations in time domain. The development of electromagnetic fields in scale and wavelet functions, has given rise to the techniques known as Multi Resolution in Time Domain (MRTD). These techniques are based on the possibility of increasing the spatial resolution of a signal, from a coarse grid to a fine one, using low-resolution functions (scale functions), combined with others of intermediate resolution levels (wavelet functions). Different functions have been used in this type of analysis: Battle-Lemarie, Haar, Daubechies, or biorthogonal. All these techniques involve series expansions of the fields, and their coefficients are obtained appling moment methods, where integrals of scaling times wavelet functions and it derivatives must be solved.

In contrast to those schemes, some authors make use of the Discrete Wavelet Transform (DWT) in order to compute the wavelet coefficients of the expansions and hence no integrals have to be evaluated. Here, derivative operators based on Beylkinfs derivations are constructed using orthonormal bases of compactly supported Daubechies wavelets and they are applied to the decomposition of the field components. Maxwell's curl equations are then rewritten in matrix form and then, the electric and magnetic field solutions are obtained at some time intervals and at each point on the spatial grid.

Despite all their advantages, orthogonal wavelets have some inconveniences, such as a large support and a very oscillatory behaviour. In this work, multiresolution theory is presented from a different point of view, based on interpolatory schemes. Therefore, new algorithms based on multiresolution analysis are devised. These algorithms are broad enough to include not only orthogonal wavelets as special case, but also non orthogonal wavelets. The freedom to choose the interpolatory functions makes it possible to keep advantages of multiresolution, while eliminating inconveniences of orthogonal wavelets. Another advantage to be considered in this interpolatory multiresolution setting is the possibility of analyzing nonlinear interpolation schemes in a natural way. We propose to investigate a new MRTD scheme for the time domain solution of Maxwell equations. We adopt an interpolatory stencil which is symmetric around a given interval and was considered by Deslauriers and Dubuc. A point-value interpolation scheme is used, with one-sided stencils at intervals where the centered-stencil choice would require function values which are not available. Hence, boundary conditions recieve a simplified treatment. Perfect electric and magnetic walls are modelled utilizing the symmetry conditions for the tangential fields, which are taken into account for the construction of the derivative operators. Maxwellfs curl equations are discretized both in space and time following a leap-frog algorithm and written in matrix form. Following Harten's framework, an Interpolatory Wavelet Transform (IWT) is defined and a derivative opearator written in standard form is applied to the multiresolution decomposition of the electromagnetic field. In order to show the efficiency of this scheme, a plane wave propagating is analyzed, followed by a series of numerical verification on some resonant structures.

Index Terms–Interpolating wavelets, multiresolution analysis, wave propagation.

Session 4P8
Microstrip and Printed Antennas

Compact UHF Band Cavity Backed Microstrip Antenna for Airborne Applications

K. N. Rao
Research Centre Imarat (RCI), India

Microstrip antennae are generally used above L Band especially for air borne applications. Below L Band, the size of Microstrip antenna will be very big. Normally materials, whose dielectric constant is around 2.2, will be used for antenna applications. For UHF band applications, novel micro strip antenna with ground plane will be 300×350mm. this size antenna cannot be mounted on any onboard systems. By using high dielectric constant material ($\epsilon_r = 10$), we can reduce its size to some extent at the cost of its gain and efficiency. The size of antenna with ground plane at UHF Band with dielectric constant 10 will be around 200×250mm. We designed aperture coupled Microstrip antenna with size as low as 100×120mm with ground plane. i.e. almost one third reduction in size. We achieved around 3% impedance bandwidth, -20dB gain, 155^0 (43%) 3dB-beam width. Since, gain of this antenna is very less, we got good beam width. Back radiation is very high in this case. By using cavity and LNA, gain has been increased and back radiation is reduced significantly. 30dB LNA is used. Overall gain achieved is around 7dB and 3dB beam width achieved is 120^0 (33.33%). The design and performance details are given in this paper.

Microstrip antennae are increasingly used for airborne applications like Satellites, Aircrafts, and Missiles because of its low profile and lightweight. Cutout is to be made for the section (Body) to mount the Microstrip antenna to have conformal advantage like minimum drag. This is very important for vehicles moving at a faster rate especially above 2 mach. The cutout size will be slightly more than antenna size (width and length). The size of the antenna, which works in L Band and above will be very less and can be mounted very easily. Antennae at UHF Band and below require huge cutout. Novel antenna requires cutout size of 300×350mm. This may not be possible for airborne vehicles, as structure will become weak. Even with high dielectric constant like 10, the size requires will be around 200×250 mm. The materials having dielectric constant more than 10 cannot be used for antenna applications, as efficiency will be very poor and does not radiate at all.

We designed aperture-coupled antenna with two dielectric substrate materials. One, antenna substrate, with dielectric constant 10 and thickness 1.57mm on which patch is made on one side and other, feed substrate, with dielectric constant 10 and thickness 0.635mm on which feed line is made on one side and ground plane is made on other side. The aperture opening is made for excitation. To match the impedance, feed line is loaded with Microstrip line at suitable places. The dimensions are calculated for patch, feed line and aperture opening. LNA is designed to suit to this application with $30dB$ gain. Cavity is designed to avoid back radiation. The depth is around one fourth of its wave length. The length and width is almost same as antenna dimensions.

The aperture-coupled antenna is made and tested in UHF Band. The minimum VSWR achieved at center frequency is 1.376. The impedance bandwidth for VSWR$\leq 2:1$ achieved is around 3%. The size of antenna is around one third of novel antenna.

Conclusion:

Compact UHF Band cavity backed Micro strip antenna has been realized. It is particularly suitable for airborne applications. Its design and measured performance over the designed band is demonstrated in this paper.

References:

1. I J Bhal and P Bharatia, "Microstrip Antennas", *Artech House*, 1980.
2. R E Munson, "Conformal Microstrip Antennas and Microstrip phased arrays", *IEEE Trans. Antennas and Propagation*, Vol. AP-22, PP. 74-78, Jan. 1974.
3. D M Pozer, "A Microstrip Antenna aperture coupled to a Microstrip line", *Electronics Letters*, Vol. 21, pp. 49-50, Jan. 1985.
4. D M Pozer, "A reciprocity method of analysis of printed slot and slot-coupled Microstrip antennas", *IEEE Trans. Antennas and Propagation*, Vol. AP-34, PP. 1439-1446, Dec. 1986.
5. P L Sullivan and D Schaubert, "Analysis of an aperture coupled Microstrip antenna", *IEEE Trans. Antennas and Propagation*, Vol. AP-34, PP. 977-984, Aug. 1986.
6. K N Rao, "Ultra Low Size Aperture Coupled UHF Band Microstrip Antenna For Airborne Applications", 2nd International Conference on Microwaves, Antenna, Propagation and Remote Sensing (ICMARS-2004) in Nov 2004.

Right Angle-Shaped Slot Antenna for IEEE 802.11b/g/j Applications

C. Jamjank, P. Wiriyacosol, and **N. Anantrasirichai**
King Mongkut's Institute of Technology Ladkrabang, Thailand
T. Wakabayashi
Tokai University

A microstrip-fed Right angle-shaped slot antenna is enhanced to support user demands on wireless LAN applications. This paper presents procedure details on designing a right angle-shaped slot antenna for the conventional IEEE 802.11b/g, Wi-Fi standard, and extensional IEEE 802.11j operating in Japan. Some matching techniques to control the dual-frequency range characteristics are revealed. Effects of the ratio of the right angle-shaped slot arm length, the position and length of the feed line were evaluated. Finite-Difference Time Domain (FDTD) method was adopted to analyze the characteristic of the proposed antenna. Antenna characteristics including electric field, magnetic field, current distribution and radiation patterns are shown. The simulation results show a remarkable microstrip-fed right angle-shaped slot antenna that can be utilized in 2.4 to 2.4835 GHz and 4.9 to 5.091 GHz bands.

A right angle-shaped slot antenna is one of the simplest structures developed from a right angle antenna, referring in [1-2]. The advantages of the proposed right angle-shaped antenna are lightweight, thin profile and easy to be fabricated. The antenna was designed at the perimeter of 0.44 of the guided wavelength. FDTD method software as referring in [3] was used to analyze the proposed antenna.

In this paper, a microstrip-fed Right angle-shaped slot antenna is presented. The design is considered to satisfy IEEE 802.11b/g and IEEE 802.11j covering 2.4 to 2.4835 GHz and 4.9 to 5.091 GHz bands. FDTD method was applied to evaluate the characteristic of the propose antenna. Although a lot of studies though the Right angle-shaped antenna have been done, controlling of dual matching resonant frequency is rarely investigated. This paper presents 3 of matching technique effects which are the effects of the ratio of right angle-shaped slot arm length, the effects on positioning of microstrip

feed line and the effects on of the length of microstrip feed line After a proper adjusting, the ratio of the vertical slot length by the horizontal slot length is 1:1.56. The simulation result antenna can be applied to serve 2.4 to 2.4835 GHz and 4.9 to 5.091 GHz bands, referring to Figure 1 and Figure 2.

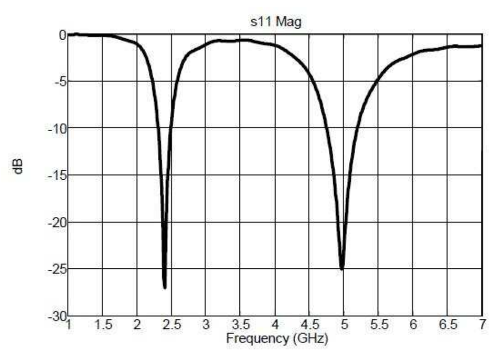

Figure 1: Return Loss

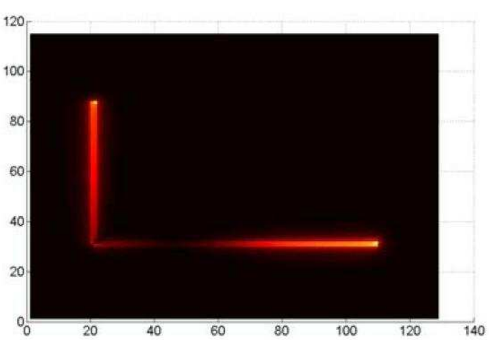

Figure 2: Current Density

REFERENCES

1. Rakluea, P., "Analysis of Right Angle Microstrip Slot Antenna", Tencon 2005 . IEEE Region10, 21-24 November, 2005.
2. Jamjank C., P. Rakluea, N. Anantrasirichai, and T. Wakabayashi, "Right Angle Microstrip Slot Antenna for Dual Frequency Operation", ISIC-2004, 8-10 September, 2004.
3. Qian Youngxi, and Tatsuo Itoh, "FDTD Analysis and Design of Microwave Circuits and Antennas Software and Applications", Realize Inc., 1999.

Particle Swarm Optimization of Dual-Band CPW-fed Antenna for WLAN Operation

W. C. Liu and **C. M. Wu**

National Formosa University, Taiwan, R.O.C.

The growth of wireless local area network (WLAN) communication systems has generated significant interest in the development of various WLAN antenna designs. We propose a novel design of a coplanar waveguide (CPW)-fed monopole antenna with wide dual-band operation simultaneously suitable for use in the WLAN application. A pair of short strips is introduced to the coplanar waveguide (CPW) feeding line to achieve dual-frequency resonance and reduce the antenna size. The evolutionary design process of using a particle swarm optimization (PSO) algorithm in conjunction with the method of moments (MoM) is employed to determine the geometrical parameters of the antenna for optimum dual-frequency operation. Prototypes of the obtained PSO-optimized design have been constructed and experimentally studied. The resulted antenna explores wide dual-band operation with 10 dB impedance bandwidths of 30% and 56.7% at bands of 2.43 and 5.33 GHz, respectively, to cover the 2.4/5 GHz WLAN operating bands, and show good agreement with the numerical prediction. Good radiation performances over the operating bands have also been observed. Also, implementation of the physical PSO and large effects of varying antenna parameters on the antenna resonant frequencies and impedance bandwidths have all been examined and discussed.

RFID Tag Antenna with Relative Humidity Sensing Function

K. H. Chang, Y. H. Kim, Y. J. Kim, and **Y. J. Yoon**

Yonsei University, Korea

A new type of a component, the relative humidity sensing antenna using a modified polyimide is proposed for RFID. The proposed structure can be applied for RFID sensor tag as a physically and functionally combined antenna with the RH sensor. For high sensitivity, a polyimide film was synthesized from aromatic monomers where no hydrophobic element is included, instead of using a commercially available polyimide. The fabricated microwave RH sensors were characterized in view point of sensitivity. To obtain the better sensitivity, the modified polyimide film was formed on the microstrip patch antenna with high quality factor. Furthermore, to enhance the resolution, the patch antenna was designed to have a narrower bandwidth by meandering structure. From the measured results, it is achieved that the sensitivity of the proposed structure was -108 kHz/%RH under 25%-90%RH. This means that the proposed component provides the humidity sensing function as well as the radiation. Therefore, it is apparent that the proposed RH sensing antenna using a modified polyimide can be applicable and useful for the implementation of the compact RFID sensor tag.

Acknowledge

This research was supported by the MIC (Ministry of Information and Communication), Korea, under the ITRC (Information Technology Research Center) support program supervised by the IITA (Institute of Information Technology Assessment) (IITA-2005-C1090-0502-0012)

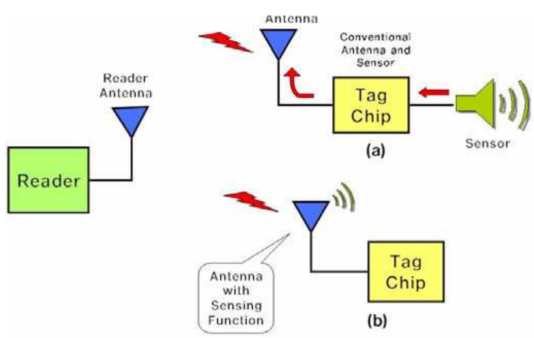

(a) Conventional antenna and sensor
(b) Proposed antenna with sensing function

Figure 1: Configurations of the sensor RFID system

Radiation Characteristics of a Microstrip Patch Antenna with LHM Substrate

A. Kusunoki and **M. Tanaka**
Oita University, Japan

Left-handed material (LHM) with negative permittivity and permeability shows the interesting properties of negative refractive index, negative refraction, and backward wave propagation in some frequency band [1]. In recent years, the LHMs have been of great interest for both basic and practical researches, and considerable attention has been focused on the development of LHM-based microwave devices.

Microstrip patch antennas are widely used in communication systems due to its low cost, light weight, and easy fabrication [2]. However the classical type of the antennas have some shortcomings such as a narrow bandwidth and a low gain and a low efficiency. In order to broaden the bandwidth, several techniques have been proposed. One of the commonly used techniques is to vary the material parameters of the substrate. The general trend toward miniaturization of electronic devices requires the downsizing of a microstrip patch antenna.

It is the purpose of this paper to investigate the radiation characteristics of a microstrip patch antenna with an LHM substrate. Consider a microstrip patch antenna consisting of a rectangular radiating patch and a ground plane on the upper and lower sides of the LHM substrate. Figure 1 shows the geometry of the problem. A microstrip line is located on the substrate and is connected to the patch to feed the antenna. The LHM is assume to be dispersive, and its permittivity and permeability are expressed by the lossy Drude equations [3]: $\epsilon(x, y, z, \omega) = \epsilon_0(1 - \omega_{pe}^2(x, y, z))\{\omega[\omega - j\Gamma_e(x, y, z)]\}$, $\mu(x, y, z, \omega) = \mu_0(1 - \omega_{pm}^2(x, y, z))/\{\omega[\omega - j\Gamma_m(x, y, z)]\}$. Here ω_{pe} and ω_{pm} are the plasma frequencies, Σ_e and Σ_m the collision frequencies, ϵ_0 and μ_0 the permittivity and the permeability of free space. Noting the constitutive relations for the LHM, one can derive differential equations for the polarization and the magnetization vectors. The finite-difference time-domain (FDTD) update equations for the three-dimensional LHM may be obtained by employing the auxiliary differential equation FDTD (ADE-FDTD) method.

Computer simulations are performed for two types of microstrip patch antennas with LHM substrates of the same material parameters. The material parameters of the lossless and homogeneous LHM are $\Gamma_e = \Gamma_m = 0$ and $\omega_{pe} = \omega_{pm} = 9.4248 \times 10^{10}$rad/s. The dimensions of the microstrip patch antennas A and B are $L_{A1} = 2L_{B1} = 12.45mm$, $L_{A2} = 2L_{B2} = 16.00mm$, $L_{A3} = 2L_{B3} = 2.09mm$, $L_{A4} = 2L_{B4} = 2.46mm$, $L_{A5} = 2L_{B5} = 4.00mm$, $s_{A1} = 2s_{B1} = 24.00mm$,$s_{A2} = 2s_{B2} = 23.34mm$, and $s_{A3} = s_{B3} = 0.795mm$. Now the investigation domain containing the microstrip patch antenna and the background free space is divided into $100 \times 120 \times 18$ cells in the x^-, y^-, and z^- directions. The cell sizes are $\Delta x = 0.389mm$, $\Delta y = 0.400mm$, and $\Delta z = 0.265mm$, and the time-step size is $\Delta t = 0.6407ps$. Figure 2 illustrates the radiation patterns of the antennas A and B in the x-z plane at resonant frequencies of f = 5.0950GHz and f = 5.0850GHz. It is seen from Fig. 2 that similar radiation patterns are obtained at almost same resonant frequencies. Note that the volume of the microstrip patch antenna can be reduced to 1/4 by using the LHM substrate.

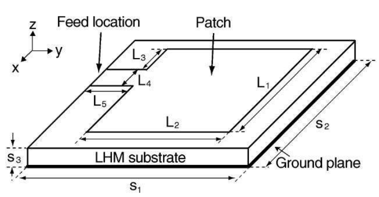

Figure 1: Geometry of the problem.

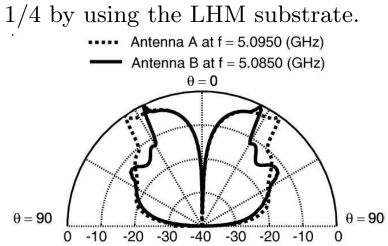

Figure 2: Radiation patterns of antennas A and B in x-z plane at f = 5.0950GHz and f = 5.0850GHz.

REFERENCES

1. V. G. Veselago, "The electrodynamics of substances with simultaneously negative values of and μ," Soviet Physic Uspekhi, vol. 10, no. 4, pp. 509.514, Jan.-Feb. 1968.
2. R. Garg, P. Bhartia, I. Bahl, and A. Ittipiboon, "Microstrip Antenna Design Handbook," Artech House, Boston, 2001.
3. R. W. Ziolkowski, "Pulsed and cw gaussian beam interactions with double negative metamaterial slabs," Optics Express, vol. 11, no. 7, pp. 662-681, April 2003.

Typical Slanted Longitudinal Slot Waveguide Antenna

S. K. Satnoor, R. M. Vani, S. N. Mulgi, P. M. Hadalgi, and **P. V. Hunagund**

Gulbarga University, India

The slotted waveguide antennas have found immense applications in many modern communication systems because of their extensive use in highly sensitive systems. Many researchers have designed different types of slots on the broader wall of waveguide to improve radiation characteristics. From the exhaustive literature survey, it is also learnt that circular polarization can be achieved with corrugated horn[1], sectoral horn with flange technique, microstrip[2] and helical antennas[2] etc. But the achievement of circular polarization with slot configuration on the broader wall of the waveguide is very rare in literature. Iqbal Ahmed Khan et al.[4] have got right circular polarization (RCP) and left circular polarization (LCP) using chirodomes placing infront of the pyramidal horn. This is found to be very tedious, time consuming and costly affair in designing and fabricating the helices. Giorgio Montisci et al.[2] have presented a paper on waveguide slot antenna for circularly polarized radiated field with longitudinal inclined slot (one pair) using HFSS software. In this communication, an effort is made to position these slanted longitudinal slots on the broader wall of the waveguide by trial and error method, and position or location of these slots were optimized for better radiation characteristics and the experimental results are on par with the Iqbal Ahmed Khan et al[4].

From the detailed experimental study it is found that the proposed antennas are quite capable in producing RCP and LCP. The array of slanted longitudinal slots also improves the gain of the antenna without perturbing the VSWR. These antennas may find applications in radar communication. Moreover these antennas are found to be simpler in design and fabrication than that of radomes[4], which have the similar results. This shows the superiority of TSLSWGA over radomes made of chiral material.

REFERENCES

1. Biao Du, Edward Kai-Ning Yung, Ke-Zhong Yang, and Wen-Jing Zhang, "Wide-band linearly or circularly polarized monopulse tracking corrugated horn" *IEEE Trans. Antennas Propagat,* vol. 50, No.2, pp. 192-197, Feb. 2002.
2. Chih-Yu Huang; Jian-Yi Wu; Kin-Lu Wong; "Cross-slot-coupled microstrip antenna and dielectric resonator antenna for circular polarization", *IEEE Trans.Antennas Propagat,* vol. 47,issue 4, pp. 605-609, April 1999.
3. S.H. Zainud-Deen, Hamdy A. Sharshar and K.H. Awadalla, "Synthesis of circular polarized normal mode helical antenna" *IEEE Antenna and Propagation Society International Symposium,* vol. 3, pp. 1608-1611, 13-18 July 1997.
4. Iqbal Ahmed Khan, Raghavendra S C and Kulkrani A B, "Performance characteristics of antenna radomes made of chiral materials",*Proc. International Radar Symposium,* India- 2001, pp. 640-655, Dec, 11-14, 2001.
5. Giorgio Montisci, Michela Musa and Giuseppe Mazzarella, "Waveguide slot antenna for circularly polarized radiated field", *IEEE, Trans. Antennas Propagat.,* vol. 52, pp. 619-623, Feb. 2004.

Compact Stacked Microstrip Antenna with Inverted C-Slot for Wireless Communications

R. M. Yadahalli[1], **R. M. Vani**[1], **S. F. Farida**[2], and **P. V. Hunagund**[1]

[1]Gulbarga University, India
[2]Salt Lake Community College, U.S.A.

Traditionally Microstrip antennas suffer from low impedance BW characteristics. Wideband results have been achieved by employing multilayer substrates, parasitic elements and aperture coupled feeds [1-3]. However, the stacked microstrip antennas occupy considerable space in mobile communication terminals & devices. Hence, the compact design of stacked microstrip antenna is proposed by introducing an inverted C-type slot on parasitic patch with an air gap of 1mm between lower and upper substrates.

The proposed design consists of a driven and parasitic element with an inverted C-slot in the parasitic patch, which is fed by 50Ω co-axial type of feeding as shown in the Fig.1. The configuration is on the glass epoxy substrate ($\dot{a}_r = 4.3$ & $h = 1.59$mm). The commercial software package IE3D V 11.09 [4] is used to model the antenna. The resonance frequency, bandwidth and gain computed with IE3D software are compared in Table I. From the observations, it is amply clear that by introducing an inverted C-slot & air gap between the substrates, the size reduction is achieved. It is further found that by increasing air gap between lower and upper substrates, the bandwidth & gain of the antenna can be improved. The radiation pattern of all antennas remains broadside.

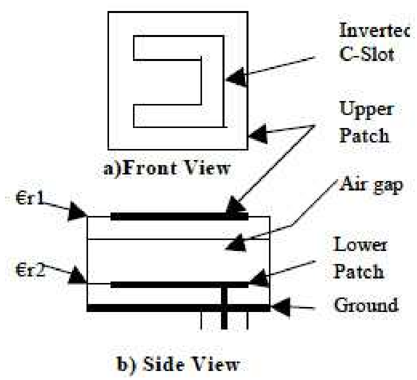

Figure 1: Stacked Microstrip Antenna

TABLE I

Parameters / Antennas	f_r (GHz)	Return Loss (dB)	Band Width (%)	Gain (dBi)
Conventional Stack Antenna	5.75	-29.28	15.65	-11.35
Antenna 1 (Air gap of 1mm)	2.737	-11.61	2.19	3.136
Antenna 2 (Air gap of 2mm)	2.737	-15.38	4.75	3.784
Antenna 3 (Air gap of 3mm)	2.737	-19.1	6.58	4.2

REFERENCES

1. Broadband Microstrip Antennas by Girish Kumar, K.P.Ray, 2003 *ARTECH HOUSE, INC.*
2. Damino, J.P., Bennegueche, and A.Paparnik, "Study of Multilayer Antennas with Radiating Elements of various Geometry", *Proc. IEE, Microwaves, Antennas Propagation,* Pt.4, Vol. 137, No. 1990, PP. 163-170.
3. Sabban A., "A New Broadband Stacked Two Layer Microstrip Antenna" *IEEE AP-S International Symposium Digest*, June 1983, PP. 63-66.
4. IE3D V 11.09, Zeland software, Inc, Fremont, CA.

Enhancement of Bandwidth of Compact Stacked Microstrip Antenna using Air Gap Technique

R. M. Yadahalli[1], **R. M. Vani**[1], **S. F. Farida**[2], and **P. V. Hunagund**[1]
[1]Gulbarga University, India
[2]Salt Lake Community College, U.S.A.

Microstrip antennas are widely implemented in many applications, especially in wireless communication. This is due to attractive features such as low profile, conformal shaping, simplicity of manufacture & easy integration with circuits. However, narrow bandwidth is the main limitation that restricts the scope of microstrip patch antennas technology. It is well known that the typical impedance bandwidth of standard microstrip patch antennas is just a few percent. For this reason, numerous methods have been suggested in order to alleviate this problem. The bandwidth is affected primarily by the antenna thickness and the substrate permittivity. Hence, in this paper, efforts are made in making the antenna of low permittivity, by having both the fed & parasitic substrates in suspended configuration [1-2]. While the BW of microstrip patch antennas is desired to be increased drastically, the size has to be decreased correspondingly due to demands of mobile communications. This is why an inverted C-slot is introduced in the parasitic patch as shown in figure 1.

This paper presents a compact configuration of suspended stacked-square microstrip antenna. The proposed configuration consists of a fed patch and the parasitic patch that has an inverted C-slot along with air gap (of 3mm) between the lower & upper substrates and also an air gap between the fed patch and the ground plane as shown in the figure1. The substrates are using glass epoxy material having a dielectric constant of 4.3 and a thickness of 1.59 mm and coaxial type of feeding is used. To optimize the configuration, the Zeland IE3D EM V 11.09 simulation software package [3] is used.

Resonant frequency, gain and bandwidth computed with IE3D are compared in Table 1. It is observed from the table that with this slot configuration, the frequency reduction can be achieved. Also it is found that bandwidth increases with decrease in air gap & better BW is obtained with antenna3. It is further found that the radiation pattern of all antennas remains broadside.

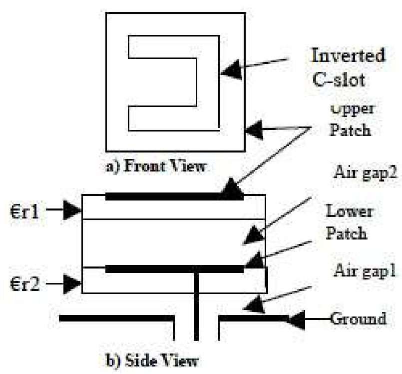

Figure 1: Suspended Stacked-Square MSA.

Table1

Parameters / Antennas	f_r (GHz)	Return Loss (dB)	Band Width (%)	Gain (dBi)
Conventional Stack Antenna	5.75	-29.28	15.65	-11.35
Antenna 1 (airgap 1 of 2.5mm)	3.526	-10.8	2.836	7.68
Antenna 2 (airgap 1 of 2mm)	3.526	-12.32	6.097	7.67
Antenna 3 (airgap 1 of 1mm)	3.368	-14.72	10.99	7.0

REFERENCES

1. Broadband Microstrip Antennas by Girish Kumar, K.P.Ray, 2003 *ARTECHOUSE, INC.*
2. E.Nishiyama, M.Aikawa and S.Egashira, "Stacked microstrip antenna for wideband and high Gain", *IEE Proc.-Microw. Antennas Propagation,* Vol.151, No.2, April 2004.
3. IE3D V 11.09, Zeland software, Inc, Fremont, CA.

Slot Loaded Equilateral Triangular Microstrip Antenna

R. M. Yadahalli[1], **R. M. Vani**[1], **S. F. Farida**[2], and **P. V. Hunagund**[1]

[1]Gulbarga University, India
[2]Salt Lake Community College, U.S.A.

Microstrip antennas (MSAs) are increasingly finding applications in modern days communication systems as they are found to be lightweight, planar configuration and inexpensive to fabricate. However, they possess the intrinsic limitations as the narrow impedance bandwidth. In this study an effort is made to enhance the impedance bandwidth of the proposed antennas by adopting slot loading technique [1]. Further, one of the most attractive features of the equilateral-triangular MSA is that the area necessary for the patch radiator becomes about half as large as that of a nearly square MSA. Accordingly, an equilateral triangular MSA can be installed in a narrower space than a nearly square MSA can [2].

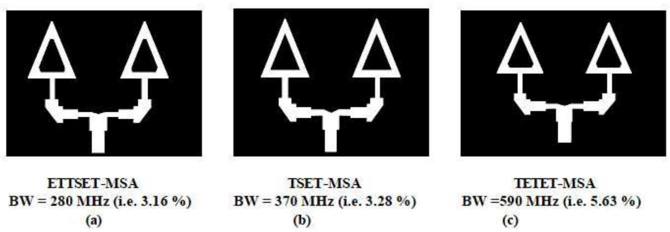

Figure 1: The schematic diagrams of equilateral triangular MSAs.

In this report we are communicating three edge truncated triangular slot equilateral triangular microstrip antenna (ETTSET-MSA), triangular slot equilateral triangular microstrip antenna (TSET-MSA) and two edge truncated equilateral triangular microstrip antenna (TETET-MSA). The schematic diagrams of these proposed antennas are as shown in Fig.1. These antennas have been designed on commercially available glass epoxy material (ϵ_r=4.2 & h=1.6mm). The impedance bandwidth of proposed antennas are studied in detail with vector network analyzer.

The impedance bandwidth of ETTSET-MSA, TSET-MSA and TETET-MSA is 3.16%, 3.28% and 5.63% respectively. The impedance bandwidth of TSET-MSA is 1.32 times and TETET-MSA is 2.11 times more when compared to the ETTSET-MSA.Then the impedance bandwidth of TETET-MSA is 1.59 times more when compared to TSET-MSA. This shows that the superiority of using TETET-MSA.

REFERENCES

1. Jeen-Sheen Row, "Dual-frequency triangular planar inverted-F antenna", *IEEE Trans Antennas & Propag.*, vol. 53, no.2, 874-876, Feb.2005.
2. Y. Suzuki, N.Miyano and T.Chiba, "Circularly polarized radiation from singly fed equilateraltriangular microstrip antenna", *IEE Proceedings*, vol.134, no.2, 194-197, April-1987.

Slotted Rectangular Microstrip Array Antenna for Bandwidth Enhancement

R. B. Konda, G. M. Pushpanjali, S. N. Mulgi, and **P. V. Hunagund**

Gulbarga University, India

The inherent narrow impedance bandwidth of the microstrip antenna (2-3%) is a major barrier for using it in today's communication systems. To enhance the bandwidth of a resonant-type patch antenna, various shapes of microstrip patch antennas have been proposed, such as patch antennas with parasitic elements, multi layered patches and slot antennas [1-3].

In this paper, a technique for enhancement of impedance bandwidth of microstrip array antenna by incorporating a pair of slot and H-shaped slot in the radiating patches in conventional two-element rectangular microstrip array antenna (TRMSA) is presented. The schematic diagrams of these antennas are shown in Fig.1. The antennas have been designed for the frequency f = 9.4 GHz, taking glass epoxy as a dielectric material (år= 4.2 and h = 1.6 mm). The experimental results show that, the proposed antennas i.e., two-element slotted pair rectangular microstrip array antenna (TSPRMSA) and two-element H-shaped slot rectangular microstrip array antenna (THRMSA) have considerably better impedance bandwidths than that of a corresponding conventional (TRMSA). This shows the superiority of slots when put in the conventional TRMSA, which will enhance their bandwidth nearly 2.4 to 3.5 times than that of conventional TRMSA.

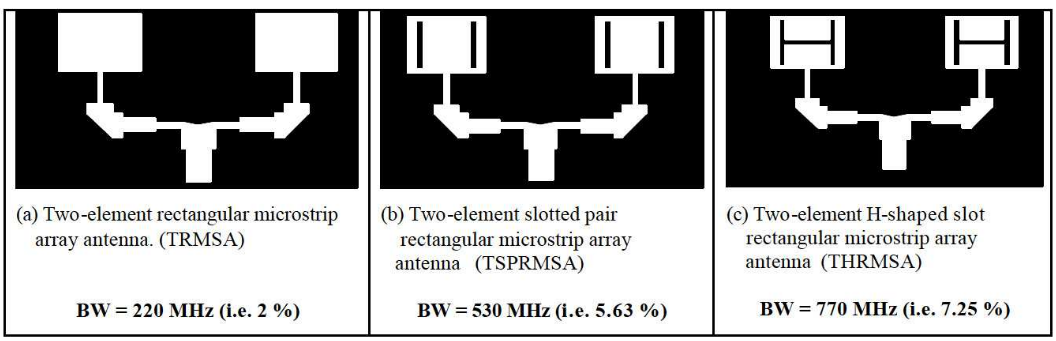

Figure 1: Schematic diagram of different slot antennas of MSAs.

REFERENCES

1. Kai Fong Lee & Wei Chen, *Advances in Microstrip and Printed Antennas* (John Wiley, New York), 1997.
2. Jeen-Sheen Row, "Dual-Frequency Triangular Planar Inverted-F Antenna", *IEEE Trans Antennas & Propag.*, vol. 53, no.2, 874-876, Feb.2005.
3. Sze, J Y and K L Wong, "Single-layer single patch broadband rectangular microstrip antenna", *Microwave and Opt. Tech. Lett.*, vol. 22, no. 4, 234-236, Aug. 1999.

Flange Effect on V-Slot Array on the Narrowwall of a Rectangular Waveguide

G. Jyoti, K. K. Usha, S. K. Satnoor, S. N. Mulgi, and **P. V. Hunagund**
Gulbarga University, India

Flange technique is one of the promising effective methods used in improving the radiation characteristics of a slotted wave-guide array antenna. In the literature, many slotted wave-guide array antenna with flange technique were reported [1-2]. But these studies were carried out on broadwall slotted wave-guide array antennas. The flange effect of narrowwall slotted waveguide arrays are seldom in literature. In the year, 2001 a V-slot array in the narrow wall rectangular waveguide was reported [3].

In this communication we present the flange effect on V-slot array located on the narrowwall of a rectangular waveguide (V-SNWWGA). The proposed design consists of 3-pairs of symmetric and opposite phase V-slots grooved on the narrowwall of a rectangular waveguide. The length of the slot is chosen as $\lambda_0/2$ and angle eθf is limited by the waveguide narrowwall dimensions to a value 15_o for the frequency 10GHz. Further, the metallic flanges are designed and machined for the length 5λ and width 1.5λ. These flanges are fixed to the V-slot antenna with the help of hinges. The measurements were taken for different flange angles. Table 1 shows the experimental results for the optimized flange angle (30_o). It is amply clear from the table that, using flange technique the gain of the antenna has been increased from -15.4 dB to -1.47 dB. It is evident from the table that flanges have predominant effect in reducing the HPBW, increase in the gain and improving the VSWR.

Table 4P8.2: Experimental Results of V-SNWWGA.

Characteristics	With flange	Without flange
VSWR	1.14	1.508
Gain (dB)	-1.47	-15.4
HPBW (deg)	14	19
Position of mainlobe (deg)	20R	35R

R-main lobe shift towards the right side from the common-axis.

REFERENCES

1. P.C. Butson and G. T. Thompson, "The effect of flanges on the radiation patterns of waveguide and sectoral horn", Proc. of the Institution of Electrical Engineers, Vol. 106, Part B, No. 2.28., pp. 422-426, July 1959.
2. K. Yoshitomi and H. Jia, "Slot antenna with lossy flange", Engineering sciences Reports, Kyushu University, Japan, vol. 17, no.1, pp. 41-48, June 1995.
3. M.Auxiliadora Hernandez-Lopez and Mercedes Quinitillan, "Coupling and radiation through V-shaped Narrow slots using the FDTD method", *IEEE. Trans on Antennas and Propagt.*, vol.49. No.10, pp. 1363-1369. Oct. 2001.

Session 4A8
ESD and Transients

Impulsive Fields Caused by Low-Voltage ESD

M. Honda
Impulse Physics Laboratory, Inc., Japan

It is well known that electrostatic discharge (ESD) events emanate strong transient electromagnetic (EM) fields. For example, an AM radio receive click noise when lightning events occur in some distant area. ESD also occur when a charged metal object (a steel piped chair, for example) contacts to adjacent metal objects. This tiny ESD event radiates strong EM fields to surrounding space and possible to interfere hi-tech electronic systems, which include high speed (GHz clock) digital circuits and/or RF devices.

The charge voltage (V) of the metal object is several hundred volts to several thousand volts, which values are strong depend on electrostatic conditions such as amount of static charge (q) and object's capacitance (C) to the ground. $V = q/C[V]$ An ESD occurrence at charge voltage of metal object ($C < 150pF$) around 3kV or less, human body does not feel any electrical shock. However, an electronic system (high speed digital circuits) placed near by the ESD generated object, in this low voltage condition, reacts very sensitive to this phenomenon. The reason is field coupling between the ESD generated objects (act as transmitting antenna) and the electronic systems (receiving antenna). According to a series of ESD experiments by author, the form of ESD fields are impulsive in some cases, specifically in the low voltage ($V < 3kV$), small capacitance ($C < 10pF$) conditions [1]. Understanding of transient fields caused by low voltage ESD between 2-metal objects, following fundamental conditions would be considered.

Electrostatic field strength before discharge

Electrostatic field strength E between the metal objects (electrode + air gap + electrode) to be contact just before the discharge, is defined as a charge voltage V divided by an air gap width g. $E = V/g[V/m]$ In high voltage conditions, such as $V = 20kV$ (gap width $g \approx 6mm$), the electrostatic field strength E is on the order of $10^6 V/m$. This is based on the Paschen's law with regard to the critical air breakdown strength 3kV/mm in normal atmospheric condition [2]. On the contrary, in low voltage conditions, such as V=1kV, the electrostatic field strength E is on the order of $107V/m$. As for the "Paschen-minimum" condition ($V \approx 350V, g \approx 6\mu m$), the E is about$6x107V/m$. Therefore, in low voltage conditions, strong E fields are exist in the gap.

Rise time of discharge current

In the gap, the charge q (mass, m) is accelerated by electrostatic field E, $F = qE[N]$. This value is equivalent to $md^2 \times /dt^2$. Then, charge velocity v at distance x is defined as $v = (2qE \times /m)1/2$ [m/s]. (assumed to be the initial velocity is zero) If the gap width (distance) g is $6\mu m$, the final velocity of the charge will be $1.05x10^7 m/s$. (about 1/30 of the light speed in vacuum) Therefore, quick discharge would occur in low voltage (or small gap) ESD. The discharge current i (dq/dt) is strong dependent on transferable charge Q at the gap within a very short time window Δt (as spark gap "ON" time). This current value can be used to explain ESD's induction fields. The rise time of discharge current (di/dt) or charge acceleration component ($d2q/dt2 = di/dt$) is also very important parameter to determine the ESD's radiated fields.

REFERENCES

1. M. Honda, "A New Threat EMI Effect by Indirect ESD on Electronic Equipment", *IEEE/IAS, trans*, Vol.IA-25, pp939-944, 1989.
2. W.D. Greason, "Electrostatic Discharge in Electronics", John Wiley & Sons Inc. Electrostatics and Electrostatic Applications Series, #12, 1992.

Wideband Measurment of Voltage and Current Rise Time Due to Micro Gap Discharge as Low Voltage ESD Using the 12 GHz Experimental System

K. Kawamata

Hachinohe Institute of Technology,Japan

S. Minegishi and **A. Haga**

Tohoku Gakuin University,Japan

O. Fujiwara

Nagoya Institute of Technology,Japan

Very fast transition durations are arisen from the micro gap discharge as low voltage ESD. These transients are occurrence the very wide band electromagnetic noise source. Over the past few years a considerable number of studies have been made on electromagnetic noises of the ESD and the electrical contacts from the viewpoint of EMC. The electromagnetic noise characteristics of the gap discharge are clearer by degrees. However, there has been only a little amount of information about voltage and current waveforms of the transition duration due to a starting of the discharge. Very little is known about the transition duration measured the low voltage ESD in very wide band system. The main purpose of this paper is to clarify an aspect of the transition duration due to low voltage gap discharge below about 1500V as the EMI (electromagnetic interference) source.

In the first, a measurement system using the distributed constant line system was established to observe the transition duration, because the transients are very rapid.. It is desirable to observe the voltage waveform and current waveform of transition duration in very wide band. The voltage waveform, and the current waveform is measured by an electric field sensor (infinitesimal monopole antenna), and a magnetic field sensor (infinitesimal loop antenna) respectively. The insertion loss of the coaxial electrode system was within about -3dB in frequency range below 12GHz.

It was confirmed that the distributed constant experimental system enables to measure the very fast transients of about 40 ps in 12 GHz bandwidth. As a consequence of the experiment using the system, voltage and current rise time of transition duration were shown 40 ps or less. Besides, the rise times were changed in configuration of electrodes, source polarity and discharging voltage.

Key words: wideband measurement, ESD, gap discharge, transition duration, rise time, distributed constant line.

Relationship between Gap Breakdown Field and Rise Time of Discharge Current Due to Collision of Hand-Held Metal Piece Electrified with Low Voltage

Y. Taka, I. Mori, and **O. Fujiwara**

Nagoya Institute of Technology, Japan

Electrostatic discharge (ESD) events due to charged metal objects cause electromagnetic interference (EMI) to high-tech information equipment. For the EMI of this kind, it is well known that the lower voltage ESD gives the stronger EMI. This is due to ESD currents with very short rise-time, which produce electromagnetic fields having wideband frequency spectra. To understand the ESD current behavior, with a 6-GHz digital oscilloscope, we previously measured discharge currents through the collision of a hand-held metal piece from a human body electrified with low voltages below 900 V, and examined the dependence on the charge voltage of the peak and rise time of the discharge current. As a result, it was found that for the charge voltage from 200 V to 600 V, the current peak increases with the charge voltage, while the rise time is almost kept constant. In the present study, we investigated effects on the gap breakdown field of the rise time of the discharge current waveform. Based on the current calculation model we previously proposed for human ESD events, we derived a formula to determine the rise time of a discharge current through the hand-held metal piece from a charged human body as a function of gap breakdown field, which could quantitatively explain results measured with a 12-GHz digital oscilloscope.

Wideband Measurement of Discharge Current Injected through Air Discharge of an ESD-gun

I. Mori[1], **O. Fujiwara**[1], and **S. Ishigami**[2]

[1]Nagoya Institute of Technology, Japan
[2]National Institute of Information and Communications Technology, Japan

In conjunction with high speed and low voltage operation of ICs, the electromagnetic (EM) immunity of electronic devices has been degrading. Especially it is well known that transient EM fields due to electrostatic discharge (ESD) events have broadband frequency spectra, which cause a serious failure to high-tech information equipment. From this perspective, an ESD-immunity test is being prescribed in the IEC 61000-4-2, which consists of two types methods of testing, contact and air discharges of the ESD-gun. The former is the way that the current is injected onto equipment under test (EUT) by contact of the gun, and the latter is the way that the current is injected through air discharge that occurs, when the charged gun approaches the EUT. Normally contact discharge is conducted because of high-reproducibility of the injected current waveform.

We previously measured with a 6GHz digital oscilloscope discharge currents for both contact and air discharges of an ESD-gun charged with various voltages. As a result, we found that for charge voltages below 1 kV approaching speed of the ESD-gun does not almost affect the discharge current waveforms, and also that current peak and rise time become higher and shorter, respectively, in comparison with those for contact discharge. This indicates that if the test voltages are set below 1 kV, there exists a possibility that air discharge provides a more severe immunity test than contact discharge. It was also found that the rise time of measured current waveforms reaches a measuring limit due to the bandwidth of the digital oscilloscope we used (70 ps).

In this study, we have measured with a 12GHz-digital oscilloscope discharge currents for the air discharge of an ESD-gun with charge voltages from 200 V to 1 kV, and have examined the dependence of peak current and rise time on charge voltages. As a result, we have found that the same tendency was observed between our results previously measured with a 6GHz oscilloscope and this study with a 12GHz oscilloscope with respect to the dependence of peak current and rise time on charge voltages. We have also found that for charge voltages below 600 V, the rise time of measured waveforms is close to 35 ps corresponding to the measuring limit of a 12GHz digital oscilloscope. This implies that air discharges of the ESD-gun with low charge voltages could produce an ESD current with a few ten pico-seconds rise time.

Our future task is to elucidate the factors that determine rise time limit of the current waveform for air discharge of an ESD-gun with low charge voltages.

Effects of the Non-linear Heating of the Ionosphere Due to Lightning Discharges

S. S. De, S. K. Adhikari, M. De, and **A. Guha**

University of Calcutta, India

B. K. De

Tripura University, India

Wide-band electromagnetic pulses radiated from the lightning strokes initiate the process of heating. In this presentation, the heating effect at the lower edge of the ionosphere (D-region) due to the incidence of electromagnetic pulses coming from lightning discharges has been investigated theoretically. Variation of temperature increase is also estimated.

The electromagnetic radiation from lightning discharges introduces variation in electron temperature, ionizing frequency and effective collision-frequency of electrons. The magnitude of temperature changes of electrons has been estimated through some model calculation. Due to incidence of lightning pulses in the weakly ionized D-region of the ionosphere, the effective electron collision frequency and ionizing frequency vary with the electron temperature because of their dependence on the average electron velocity. The ionization frequency represents the net change in the ionization due to production and loss processes.

For wide energy range of electrons, the collision frequency would be averaged over the Maxwellian distribution of electron velocities. Within the lower ionosphere, the collision between N_2, O_2 and A_r are important for the determination of effective collision frequency. Electron-neutral particle collisions are strongly dependent on electron temperature.

Following some algebraic simplifications, the expressions of normalized electron temperature has been obtained. The heating effects have been considered by horizontal lightning strokes with specific temporal and spatial variations of temperature increases. Numerical analysis reveals that the waves are in temporal domain with short intense pulse having a peak around 4.6 μsec. After that, it decays exponentially thus giving a broad weak negative pulse with the maximum around tens of μsec. The first positive pulse provides the heating of the lower ionospheric electrons. The nature agrees with previous works.

For the long-time model, the ionospheric plasma is taken to be sharply bounded at height h = 50 km, where the ambient temperature T = 272 K. The peak velocity of the streamer is assumed as 9×107 msec^{-1}. 50 km height is chosen as the height of the lower edge of the ionosphere where the heating effects occur due to the incidence of electromagnetic pulses from lightning discharges. The calculation shows substantial heating from a single median stroke of cloud-to-ground discharge. The position of lightning discharge is taken at a height of 4 km from the ground. The direct and ground reflected pulses have been considered. For horizontal discharge, the temporal variation of electron temperature above the stroke produced by the same source has been evaluated. The enhancement of temperature due to lightning discharge field maintains correspondence with the effective collision-frequency growth.

When the incident electric field in the lower ionosphere is very high, the energy gained by the free electrons from such fields cannot be readily transferred to the heavy particles. Hence the average energy of the electrons, i,e., the electron temperature is raised by the electric field.

Simulation of Creeping Discharge Dynamics

A. Adalev and **M. Hayakawa**
The University of Electro-Communications, Japan
N. V. Korovkin
Saint-Petersburg State Polytechnical University, Russia
D. I. Iudin
Radiophysical Research Institute, Russia
V. Y. Traktengerts
Institute of Applied Physics, Russia

Despite the fact that the discharge over a dielectric surface is a widely observed and used phenomenon, the methods of its mathematical description and simulation are not sufficiently evolved. Rare papers related to creeping surface discharge use models which are similar to that proposed in [1] for modelling streamer evolution in gas. They treat just a single streamer stem and, moreover, all the attention is payed to the move of the streamer head. However, since streamer phase in the surface discharge development is rather short [2] and is replaced by the leader one very fast, a nonlinear conductance of a streamer channel behind the head plays the main role in the surface discharge.

In the present work the initially complex and nonlinear problem of creeping discharge modelling is divided into several problems of less complexity that may be solved separately at some time step. The discharge area (above a dielectric sheet separating a metal needle from a ground plain electrode) is presented as a system of gas sphere cells covering the dielectric. The discharge tree (conducting cluster) is represented by a nonlinear circuit consisting of capacitances, nonlinear conductances, and controlled sources. The latter simulate field potential of the needle electrode and of the free charge located in the neighbouring cells. The coefficients for the controlled sources and cell capacitances are determined from the results of static field calculation.

In the present model, cell conductance is strongly correlated to the density of electrons in the cell. The effects of electron drift, impact ionization, and photoionization are involved into the conductance model. The physical parameters of the latter two processes are deduced from the experimental data available in the literature. Further improvement of the conductance model is discussed in respect to plasma heating up to the temperatures that enough for the streamer-to-leader transition.

Cell initiation (attaching to the existing cluster) is performed if the initiation threshold of 26 kV/cm is reached in the cell. This ensures a gradual rise in the cell conductivity due to electron multiplication in air. Competition strategy is used for cell initiation when the probability of the latter depends not only on the potential of the cell but also on the potentials of the other candidates for initiation. Following the models of irreversible growth" (e.g. [3]), the power law of probability dependence on electric field intensity was chosen.

In addition to discharge patterns which created to be very similar to experimental Lichtenberg figures, the model allows us to determine such local properties of the discharge as current, voltage drop, loss, field and charge distribution. This allows us to determine characteristics of electromagnetic radiation which is very important for EMC and also gives us an additional instrument for studying discharge physics. Moreover, the model may also easily take into consideration geometric features of electrodes and dielectric, so that we can examine their effect on the discharge as well.

REFERENCES

1. I. Gallimberti, A computer model for streamer propagation," *J. Phys. D: Appl. Phys.*, vol. 5, pp. 2179–2189, 1972.
2. E. M. Bazelyan and Y. P. Raizer, *Spark discharge*. New York: CRC Press LLC, 1998.
3. N. Femia, L. Niemeyer, and V. Tucci, Fractal characteristics of electrical discharges: experiments and simulation," *J. Phys. D: Appl. Phys.*, vol. 26, pp. 619–627, 1993.

Alternative Method of Measuring Current Distribution in Telecommunication Sites

A. H. Samad
Malaysia

Aim :

This paper explains the alternative technique to measure current distribution during lightning strike at telecommunication station. Investigation of current distribution at a working site using surge generator is impossible since it will exposed the working telecommunication system to large current and possible induced voltage. By using signal generator in place of surge generator, the current distribution is investigated and rectification can be made.

Content :

Lightning current travel from one grounding point to another grounding points because of ground potential rise. The path is via the dedicated copper tape, which acts as bonding between two ground points. This cable is located underground.

However, there is another connection, through screen of coaxial cables and reference ground wire of the 48V DC system. These wires connected to switching equipment and rectifier respectively. Large part of this wire is inside the telecommunication exchange. The typical installation is as figure 1. A lightning current from grounding point 1 to grounding point 2 will travel using three paths; bonding wire, coaxial cables and reference DC. The current distribution will be determined by total impedance of the cables. It is impossible to measure the impedance.

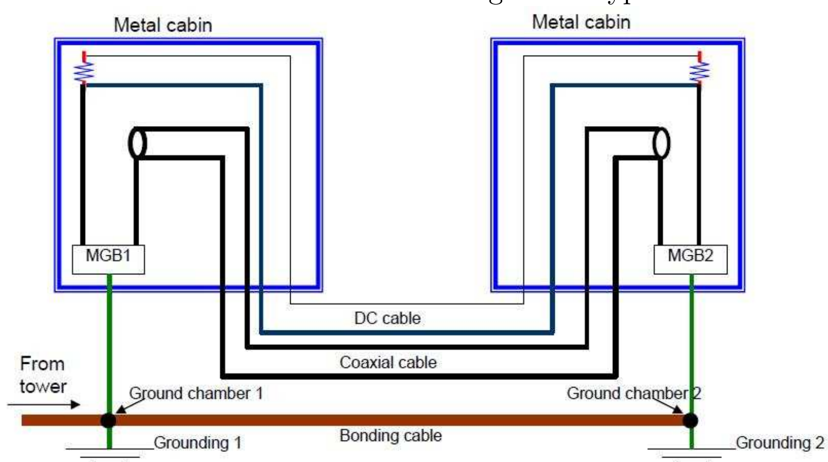

Figure 1: Typical installation of bonding cable, coaxial cable and DC cable

By using signal generator, the current distribution from ground chamber 1 to ground chamber 2 is measured at individual cable. Frequency from 1 kHz to 1MHz is chosen, which typical frequency spectral of lightning current is.

A measurement at site shows large percentage (75%) of total current actually flowing through coaxial cables and reference DC. This explains the damages of telecommunication system inside the cabin.

A laboratory set-up resembles the site was build to investigate the current distribution. Experiment using surge generator was also conducted. The current distribution results using signal generator (frequency domain) and surge generator (time domain) is compared. Comparison of percentage using peak value did not show any agreement. A better comparison, using Fast Fourier transform on the time domain data shows better agreement with the frequency domain technique.

This technique is applicable to facilitate improving current distribution on bonding wiresof working telecommunication sites.

Author Index